PIERS 2008 Cambridge

Progress In Electromagnetics Research Symposium

Abstracts

July 2–6, 2008
Cambridge, USA

www.emacademy.org
www.piers.org

PIERS 2008 Cambridge Abstracts

Published by

The Electromagnetics Academy
777 Concord Avenue, Suite 207
Cambridge, MA 02138

www.emacademy.org
www.piers.org

ISSN: 1559-9450
ISBN: 978-1-934142-05-9

Progress In Electromagnetics Research Symposium

July 2–6, 2008
Cambridge, USA

PIERS 2008 CAMBRIDGE ORGANIZATION

PIERS Chair

J. A. Kong, MIT, USA

PIERS 2008 General Chairman

Ram Shenoy, Schlumberger-Doll Research, Cambridge, Massachusetts, USA

PIERS 2008 General Co-Chairman

Tarek Habashy, Schlumberger-Doll Research, Cambridge, Massachusetts, USA

PIERS 2008 Technical Chairmen

Aria Abubakar, Schlumberger-Doll Research, Cambridge, Massachusetts, USA
Tarek Habashy, Schlumberger-Doll Research, Cambridge, Massachusetts, USA

PIERS 2008 Cambridge International Advisory Committee

L. C. Botten	J. Brady	C.-H. Chan	W. C. Chew
H.-T. Chuah	S. T. Chun	S. Cummer	O. Dorn
N. Engheta	J.-M. R. Fournier	A. K. Fung	Z.-H. Gu
L. Gurel	M. Hallikainen	Y. Hara	H.-C. Huang
A. Ishimaru	D. Lesselier	L.-W. Li	I. V. Lindell
S.-G. Liu	K.-M. Luk	S. Mano	A. Massa
G. D. McNeal	Y. Miyazaki	P. Pampaloni	A. Priou
K. Senne	R. Shin	E. Slob	T. Takenaka
M. Tateiba	A. Tijhuis	L. Tsang	P. van den Berg
D. Watts	K. Yasumoto	J. Zehentner	W.-X. Zhang

PIERS 2008 Cambridge Technical Program Committee

A. Baghai-Wadji	G. Berginc	W.-M. Boerner	H. Braunisch
K.-S. Chen	Y.-H. Chen	T.-J. Cui	V. Druskin
A. Elsherbeni	H. C. Fernandes	M. Gianinetto	J. Goswami
W. Hu	K. Kobayashi	Q.-H. Liu	S. Lucyszyn
R. Mackie	E. Marengo	P. Meaney	E. L. Miller
M. Moghaddam	Z.-P. Nie	D. Omeragic	M. Rajarajan
R. Ramer	C. Rappaport	N. Seleznev	C. Seo
A. Sihvola	D.-P. Tsai	G. Uslenghi	J. Volakis
J. Vrba	G. Xie	A. Yaghjian	M. Zaslavsky

PIERS 2008 Cambridge Symposium Committee

J. J. Bao	H. S. Chen	Y. Du	Z. Y. Duan
W. Feng	H. Huang	J. T. Huangfu	Q. Jiang
F. M. Kong	M. Lai	S. Lee	Z. Y. Li
D. R. Liu	B. I. Wu(Chair)	P. L. Xie	L. Ye
L. Y. Yu	B. L. Zhang	P. H. Zhou	

PIERS 2008 CAMBRIDGE SESSION ORGANIZERS

A. Abubakar
G. Bonmassar
W. C. Chew
J. C. Goswami
H. Jeong
D. Lesselier
L. Menon
E. Recami
J. Vrba
G. Xie
L. M. Zurk
S. Alyones
S. V. Boriskina
V. K. Devabhaktuni
T. M. Habashy
S. Kar
J. Li
G. A. Newman
Y. V. Shestopalov
H. G. Wang
T. J. Yang
G. Berginc
H. Braunisch
Y. A. Eremin
G. R. Hadley
H. Kikuchi
V. A. Markel
M. Oristaglio
Y. M. Strelniker
M. T. Wnuk
M. Zamboni-Rached
D. J. Bergman
H. C. Chaves Fernandes
F. A. Fernández
H. E. Hernández-Figueroa
K. Kobayashi
A. McGurn
K. Radhakrishnan
R. Talhi
C.-J. Wu
A. Zaoui

PIERS 2008 CAMBRIDGE SPONSORSHIP

- ☐ Schlumberger-Doll Research (SDR)
- ☐ MIT Center for Electromagnetic Theory and Applications/Research Laboratory of Electronics
- ☐ The Electromagnetics Academy at Zhejiang University
- ☐ Zhejiang University
- ☐ The Electromagnetics Academy

PIERS 2008 SESSIONS

Session 2A1
Efficient Electromagnetic Solvers for Large Problems

Parallelization — Key to Solving Real-world Radiation, Scattering and EMI/EMC Problems Described by Large Number of Degrees of Freedom (DoFs)

Raj Mittra
Electromagnetic Communication Laboratory, Penn State University, USA

Abstract— In this paper we identify some challenges in real-world EM-simulation problems, which we have recently encountered in the process of designing complex systems for computers, communication and radar, that are beyond the capabilities of present day commercial computer codes that they are typically designed to run on single processors. We then go on to describe some frequency as well as time domain approaches, that are based on parallel algorithms, and are designed to handle large problems in a computationally efficient manner.

Some example problems that provide us such challenges are: (i) arrays comprising of many elements that may be multiscale, complex and inhomogeneous: (ii) two large antennas, typically phased arrays, each of which may involve thousands of elements, mounted on a complex platform involving RAM materials, with the antennas separated by 100's or 1000's of wavelengths; (iii) conformal antennas mounted on complex platforms, e.g., aircrafts or automobiles; (iv) antenna array mounted on the topside of a helicopter that must communicate through its rotating blades; (v) a multi-layer computer chip with hundreds if not thousands of interconnects and other structures with fine details and micron-size features; (vi) small antenna in a cellphone sharing the platform with power supply and other systems such as cameras. While not all of the problems mentioned above are large in terms of the wavelength, they do share one attribute that is common to them, namely that the number of DoFs (degree of freedom) required to accurately describe the problem often exceeds 10E+9-obviously well beyond the capability of most existing codes that are available today that are designed to run on serial machines. Another factor that adds to the challenge we encounter when tackling these problems is that they are multiscale in nature and are inhomogeneous as well. Thus many approaches that might work for PEC objects that are large but smooth, cannot be used to handle these type of problems.

While a multitude of CEM (Computational Electromagnetics) methodologies for modeling and simulation abound-that are based on the Method of Moments (MoM), Finite Element Method (FEM), and Time Domain techniques, e.g., the Finite Difference Time Domain Method (FDTD-and while most commercial code developers claim that they can tackle arbitrary problems with ease, fundamental roadblocks do surface when attempting to use them for very large problems that cannot be accommodated on a single processor. Sometimes, the run-times of these codes can be shortened, very effectively, by parceling off different parametric studies to different processors, each one handling a different set of parameters, e.g., frequencies or incident angles of the impinging waves. However, following such a strategy does not obviate the basic difficulty that arises when one attempts to solve a problem with DoFs that are so large that one cannot fit it on a single CPU, even for a single set of chosen parameters. This often forces us to introduce simplifications and to solve the downsized versions of the problem that can be run on a single processor. However, the caveat in following such a strategy is that it is difficult to estimate the errors introduced in the process of downsizing the problem, and one is always unsure about the level of accuracy of the solutions generated in this manner.

In this paper we will first describe some novel techniques for parallelizing both the time and frequency domain techniques for solving large problems of the type described above. We'll then go on to present some examples of large problems that have been solved using the parallelized versions of FDTD, FEM, and MoM algorithms. Finally, we will discuss a novel time-domain approach for embellishing the parallel FDTD code, which enables us to solve very large problems that cannot be accommodated, even on parallel platforms available to the user, because the problem size is much too large for the available memory, despite the use of multiple processors providing increased storage in their RAMs.

Fast CEM Solvers Based on Volume and Surface Integral Equations

Qing Huo Liu[1], **Yun Lin**[1], **Chun Yu**[1], **Jun Ho Lee**[2], **Jianguo Liu**[2], **and Ergun Simsek**[3]

[1]Department of Electrical and Computer Engineering, Duke University, USA
[2]Wave Computation Technologies, Inc., Durham, NC, USA
[3]Schlumberger-Doll Research, Boston, MA, USA

Abstract— In this presentation, we will give an overview of recent fast methods developed at Duke University for electromagnetic forward simulation using volume and surface integral equations for large-scale problems.

For the volume integral equation method, we continue our earlier work on the stabilized biconjugate-gradient fast Fourier transform (BCGS-FFT) algorithm for 3-D inhomogeneous objects embedded in general multilayered media. With this method, the layered medium Green's function is calculated rapidly through a singularity subtraction technique. The volume integral equation is formulated with a weak form. The stabilized biconjugate-gradient method is used to solve the discretized system equation iteratively, where the FFT algorithm is utilized to speed up the matrix-vector multiplication. We demonstrate that our simulator can solve a system with 21 million unknowns on a single processor.

For the surface integral equation, we recently have developed an exact radiation boundary condition for an unbounded domain based on a Toeplitz matrix structure, which significantly reduce the memory and CPU time in the traditional boundary element method. We call this surface integral equation method the spectral integral method (SIM) because it uses the fast Fourier transform for the computation. To further improve the capability of this technique, we have combined this SIM with the spectral element method (SEM) so that the interior domain can be arbitrarily inhomogeneous and can contain perfect conductors. The hybrid SIM/SEM technique can be viewed as an improvement over the traditional boundary-element/finite-element hybrid technique. In the presentation we will demonstrate the high-accuracy and efficiency of the hybrid SIM/SEM technique for 3-D scattering problems.

Fast Solvers for 3D Finite-difference Modeling EM Logging Tools

Sofia Davydycheva[1], **Vladimir Druskin**[2]
Mikhail Zaslavsky[2], **Tarek Habashy**[2], **and Leonid Knizhnerman**[3]

[1]Schlumberger, SPC, Sugar Land, TX, USA
[2]Schlumberger, SDR, Cambridge, MA, USA
[3]CGE, Moscow, Russia

Abstract— We apply a 3D finite-difference (FD) modeling approach to simulate the response of electromagnetic logging tools in general 3D formations with arbitrary anisotropy. To decrease the computational cost of the forward modeling, we employ three different iterative solvers. They all give identical answer, up to 5–6 significant digits. However, the convergence rate of each solver depends on the frequency, spacing and the formation conductivity. Comparison of efficiency of the three solvers is provided:

(I) Spectral Lanczos Decomposition Method (SLDM). The problem is solved in the electric field formulation. Solution is obtained as a matrix function of the operator of the problem. There is no preconditioning, and convergence may be slow at low frequencies or at low conductivities. However, it is a multi-frequency solver. If the tensor conductivity is real (quasi-static approximation: dielectric constant $\varepsilon = 0$), the field at all frequencies can be computed with no extra cost.

(II) SLDM with inverse operator. We calculate the matrix function as an expansion on inverse powers of the operator of the problem. It allows pre-conditioning that significantly reduces the condition number of the stiffness matrix. The method converges very fast at low frequencies. It is also a multi-frequency solver for quasi-static problems.

(III) Recently, a new pre-conditioned solver has been developed, with a divergence free pre-conditioned operator. The problem is solved in the magnetic field formulation. It is fast single-frequency solver, which allows arbitrary complex tensor conductivity of the medium.

The high efficiency of the software, due to the use of the optimal FD grid and material averaging within the grid cells, allows one to use it routinely for modeling and inversion of complex 3D media with arbitrary conductivity anisotropy.

The software is benchmarked against other independent software and is used to model triaxial induction logging tool response in various 3D geometries.

A Mode-matching/Finite Element Hybrid Strategy for Analyzing Waveguide Discontinuities and Resonant Cavities

Alejandro Díaz-Morcillo[1], **Ivan A. Mantilla-Gaviria**[2], **and Juan V. Balbastre**[2]

[1]Universidad Politécnica de Cartagena, Spain
[2]Universidad Politécnica de Valencia, Spain

Abstract— In the last decades, different analytical and numerical techniques has been applied in solving structures composed of microwave devices as corrugated filters, horns, irises or ovens. Analytical methods, due to the constraints imposed on the problem geometry, have a limited application, and general numerical methods, as the finite difference-time domain (FDTD) or the finite element method (FEM), have a high computational cost.

In this work, different waveguiding structures have been analyzed by means of a domain decomposition and a combined use of the mode-matching (MM) technique and the FEM in order to improve the computational efficiency of the overall solution. A typical structure that can take profit of this strategy is a microwave heating applicator containing a non-rectangular object, as shown in Figure 1.

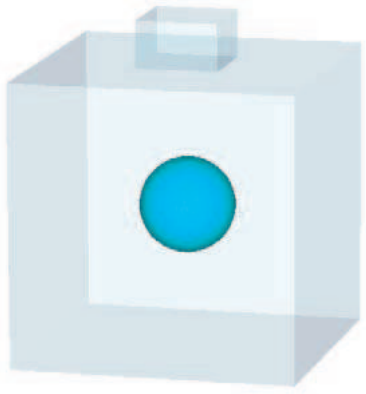

Figure 1: Microwave heating applicator.

In Figure 1, the structure can be analyzed as a set of cascaded two-port networks. In the regions with a waveguide structure the MM method is applied, reducing the domain of the FEM application to the zone of non-rectangular geometries. After obtaining the generalized scattering matrix (GSM) of each subdomain, the global GSM, which characterizes the device, is obtained. In this case the waveguide structure is rectangular, simplifying the computation of the transverse electric and magnetic fields and the integrals involved in the MM technique. Nevertheless, the generalization for arbitrary waveguiding structures is straightforward, obtaining the different modes of the waveguide by means of the application of the FEM over the section of the waveguide and solving the corresponding eigensystem.

In MM regions the GSM is obtained directly. In order to improve its computacional efficiency, in the FEM regions the generalized admittance matrix (GAM) is obtained, and later the GSM can be calculated from it. The use of GAM instead of GSM in the formulation of the FEM have four main advantages:

- For a given set of modes in the structure, the matrix of the linear system is unique, whilst the use of the GSM formulation generates a different matrix for each mode.
- Imposing boundary conditions at ports yields a sparser linear system matrix.
- Imposing the boundary condition of electric wall is natural. Therefore, it is not necessary a compression/decompression of the linear system.
- The computation of the GSM from the GAM is almost immediate, with a computational cost depending only on the number of the employed modes.

Moreover, in order to optimize the solution of the multiple FEM linear systems a parallelized version of direct method based on a left-right looking factorization is used instead of an iterative method. This work was supported in part by Fundación Séneca (Región de Murcia) under grant 05840/EE1/07.

On Improving Computation Efficiency of Finite Element Method in Designing Sensor for Geophysical Applications

Jaideva C. Goswami, **Gerald Minerbo**, **and Betty Rong**
Schlumberger Technology Corporation
110 Schlumberger Dr., Sugar Land, TX 77478, USA

Abstract— In sensor design, especially for geophysical applications, one often comes across sensor dimensions that are smaller than the operating wavelength and the probed volume. However, the sensor geometry usually contains multiscale features that need to be accurately modeled along with the surrounding medium which is considerably larger than the sensor. The finite-element modeling of such problem is complicated by the fact that the computation volume is large — even after using suitable absorbing boundaries — and that the high aspect ratio of some elements, especially in the sensor, can lead to slow and premature convergence. Ill-conditioning can also be caused by the wide range of conductivities present in the model. The degrees of freedom can easily be in millions. Signal levels measured by such sensors are comparable to background noise. In addition to multiscale features, sensors may also contain nonlinear materials that further slow down the convergence. Given certain specifications of the sensor, the design process may require 100 s of execution of forward model. Each forward nonlinear FEM model can take few hours of computation time. Accurately designing these sensors is thus very challenging. In this paper some numerical schemes are described that use linearization, suitable preconditioner, and linear solver in combination with a numerical noise removal method to improve the computation efficiency. Examples of electrical dipole in layered medium in the vicinity of other metallic objects are presented. Commercial FEM software is used to compute magnetic field. To remove the numerical noise caused by coarse discretization, the forward model is run twice — with and without the external object. Difference of the two results gives the magnetic field due to the external objects. Accuracy of the results is verified by solving the problem with fine discretization as well as with other available FEM software.

Design of Frequency-domain EM Finite Elements for Geophysical Applications

D. Pardo, C. Torres-Verdín, M. Paszynski, and M. J. Nam
The University of Texas at Austin, Austin, TX, USA

Abstract— Currently, two major applications drive the simulation of EM measurements for geophysical applications: resistivity borehole logging, and marine controlled-source EM. Both applications are based on frequency-domain measurements because accurate time-domain measurements are, in general, difficult to acquire.

Simulation of geophysical EM measurements in general 3D geometries is CPU-time and memory intensive. However, several techniques (e.g., Fourier analysis) can be utilized to reduce the dimensionality of the problem to 2.5D, 2D, 1.5D or 1D, either in terms of cylindrical or Cartesian coordinates.

After deriving proper variational formulations for 3D, 2.5D, 2D, 1.5D, and 1D, the main component of this paper focuses on selecting proper discretizations. The latter step involves two choices: First, selection of proper continuous finite element spaces that guarantee a correct solution of Maxwell's equations. While in 3D such a selection is based on the usual $H(\text{curl})$-Nédélec spaces, dimensionality reductions typically give rise to mixed spaces of the type $H(\text{curl}) \times H^1$, with possibly additional non-trivial finite energy conditions. The second part of the discretization process consists of selecting adequate discrete spaces, that is, adequate grids. We propose the use of goal-oriented adaptive higher-order techniques, as opposed to more traditional *a priori* 'optimal' grids. While the latter gridding techniques provide excellent results in simple geometries, adaptive techniques are more flexible, and enable reliable and more accurate simulation results in the presence of complex geometries. In particular, we present an hp goal-oriented strategy (where h indicates the element size, and p the polynomial order of approximation) that provides exponential convergence in terms of the error in the quantity of interest vs the CPU time independently of the number, location, or strength of field singularities.

We also propose a parallel implementation of the EM simulator based on a hybrid approach (where the logical information of the grid is stored in all processors), compared to the more traditional domain-decomposition approach. Additionally, we describe several direct and iterative solvers (including multi-grid) of linear equations, and we analyze their main advantages and disadvantages in the context of EM geophysical applications.

Results from our work indicate that (1) It is essential to implement goal-oriented based gridding techniques, which make unnecessary the use of variational formulations based on the secondary field. (2) The proposed paralellization strategy enables reasonable performance (scalability) and, more importantly, it can be easily implemented with any existing FE code. (3) The use of spectral methods is essential to improve performance and accuracy, and they should be used in the directions where EM fields are expected to be smooth. (4) Current state-of-the-art (and commercial) iterative solvers may provide inaccurate solutions in many situations. Direct solvers should be used for verification purposes.

An Efficient 3D Integral Equation Method for Computation of Electromagnetic Wavefields in a Layered Configuration Containing Inhomogeneous Objects

P. M. van den Berg[1], **A. Abubakar**[2], **and T. M. Habashy**[2]

[1]Delft University of Technology, The Netherlands
[2]Schlumberger-Doll Research, Cambridge, USA

Abstract— This paper is concerned with the source type of integral equation to compute the electromagnetic scattering by an inhomogeneous 3D object in a planar layered medium in the frequency domain. By decomposing the scattered field into a particular and a general constituent, the structure of the integral operator of the integral equation is constructed. The particular constituent represents the scattered field inside the layer that embodies the contrasting object, due to the presence of virtual contrast sources inside the inhomogeneous object, while the general constituent represents the interaction with the other layers due to the presence of source distributions on each side of the layer that embodies the contrasting object. The part due to the particular constituent has a convolution structure in all spatial directions. The part due to the general constituent consists of two terms; one has again a convolution structure with respect to all spatial coordinates, while the other has a convolution structure with respect to the horizontal coordinates and a correlation structure in the vertical coordinates. These properties facilitate a fast and efficient computation of the integral operator with the help of Fast Fourier Transforms. Hence, the total computational time of this approach will be equal to $2N_{\text{iter}}N\log(N)$, where N_{iter} is the total number of iteration of the CG-type solver and N is the total number of unknowns.

The Green tensor is obtained as an inverse Fourier-Bessel integral with respect to the horizontal radial coordinate. In view of numerical efficiency, it is desirable to keep the spatial derivatives outside the Fourier integral, rather than to consider them as spectral multiplications with the wave vector inside the Fourier integral. Furthermore we show that since the integral operator acts as a filter for the product of the fields and the contrast, the number of Fourier components that are needed to accurately calculate the integral operator, can be reduced.

The method is applied to simulate the geophysical low-frequency electromagnetic problem, i.e., the controlled-source electromagnetic (CSEM) method.

A Parallel, Fourier Finite-Element Formulation with an Iterative Solver for the Simulation of 3D LWD Measurements Acquired in Deviated Wells

D. Pardo[1], **M. J. Nam**[1], **C. Torres-Verdin**[1], **and M. Paszynski**[2]

[1]The University of Texas at Austin, USA
[2]AGH University of Science and Technology in Krakow, Poland

Abstract— A number of 3D simulators of borehole resistivity measurements have been developed during the last two decades for oil-industry applications. These simulators have been successfully used to study and quantify different physical effects occurring in 3D geometries. Despite such recent advances, there are still a great many 3D effects for which reliable simulations are not available. Furthermore, in most of the existing results only partial validations have been reported, typically obtained by comparing solutions of simplified model problems against the corresponding solutions calculated with a lower dimensional (2D or 1D) numerical method. The lack of 3D simulation results (as opposed to 2D results) is due to major difficulties encountered when solving geometrically challenging problems. Namely, for mesh-based methods (Finite Elements, Finite Differences, Boundary Elements, etc.), the size of the system of linear equations becomes excessively large to be solved in real (logging) time.

To overcome this problem, we developed a new geometry-based formulation for simulating 3D resistivity borehole measurements employing a mix of 2D and 1D algorithms. In so doing, we utilize a 2D self-adaptive goal-oriented *hp*-adaptive strategy (where h indicates the element size, and p the polynomial order of approximation) combined with a Fourier series expansion in a non-orthogonal system of coordinates. This combination naturally generates a spatial domain decomposition that is used as building block for the construction of an efficient iterative solver, thereby making unnecessary the use of algebraic domain-partitioning algorithms. Moreover, the 2D self-adaptive refinement strategy enables accurate simulations of problems that include high material contrasts (occurring, for example, when simulating a metallic mandrel in an oil-based mud) and high dynamic ranges of electrical conductivity that include presence of electrical anisotropy.

The above method has been implemented in parallel computers for faster execution in multiple core processors as well as in large parallel distributed memory machines.

We simulate 3D wireline and logging-while-drilling (LWD) electromagnetic measurements to study prominent effects in a borehole environment penetrating invaded and anisotropic formations, such as those occurring in deviated wells. Numerical results confirm the reliability, accuracy, and efficiency of the method. Moreover, we are able to quantify the relative accuracy of the simulations as a function of the number of Fourier modes used to represent the solution. The new method enables a substantial reduction in the CPU time and memory requirements compared to conventional methods. In particular, the simulation time of a single logging position is reduced from over an hour (when using a 3D *hp*-FEM) to only a few (1–3) minutes, without sacrifice of accuracy.

Session 2A2
Remote Sensing

Dielectric Properties of Carbonate Rocks

Nikita Seleznev[1], **Tarek M. Habashy**[1], **Austin Boyd**[1]
Mehdi Hizem[2], **and Ollivier Faivre**[2]

[1]Schlumberger-Doll Research, Cambridge, MA, USA
[2]Schlumberger-Riboud Product Center, Clamart, France

Abstract— During the past few decades, carbonate oil reservoirs have become increasingly important for the oilfield industry. Approximately one-half of the world's oil is produced from limestone and dolomite reservoirs, and that proportion is expected to increase. Carbonates contain more than 60% of the world's remaining oil in place. The giant carbonate oil fields, particularly in the Middle East, are expected to dominate world oil production in the 21st century.

Compared to siliclastic rocks, carbonates are often simpler in terms of mineralogy but far more complex in terms of pore structure. This complex pore structure is due to diverse biological and chemical origins often combined with a complex diagenetic history. Not only may carbonate differ greatly from one place to the other, but within one sequence considerable variations may occur.

Understanding and predicting the effect of pore structure on electrical and dielectric properties represent both a theoretical and experimental challenge. However, a sound physical model may have a major impact on the estimation of oil in place and, therefore, we propose in this paper such a model that is able to explain dielectric and permittivity dispersion curves at full and partial saturations for carbonates with greatly varying microgeometries.

The new dispersion model is based on laboratory experiments below 1 GHz for a variety of samples that are considered representative of oilfield reservoirs and that also span a wide range of texture types found in carbonates. The model response to parameters such as the aspect ratios of grains, pores and hydrocarbons, as well as water saturation, is realistic and well understood. Correlation of the Petrographic Image Analysis results with the model parameters and the rock dielectric dispersion strongly support the new dispersion model.

Evaluation of the Sacttering Matrix of Flat Dipoles Embedded in Multilayer Structures

S. J. S. Sant'Anna[1, 2], **J. C. da S. Lacava**[2], **and D. Fernandes**[2]

[1]Instituto Nacional de Pesquisas Espaciais, Brazil
[2]Instituto Tecnológico de Aeronáutica, Brazil

Abstract— Interest in retrieving parameters from natural targets out of microwave remote sensing data has increased lately. Full polarimetric SAR data make the analysis feasible, especially when polarimetric decomposition techniques are utilized. These techniques are based on the characterization of radar scattering from complex targets in terms of a linear combination of scattering from simpler ones, consisting in an effective tool for the analysis of polarimetric data. From this point of view, knowledge of the scattering matrix from simpler targets is crucial for the interpretation of polarimetric SAR data. Besides, the closer to the exact solution the determination of the scattering matrix is, the more precise the scattering analysis will be. The purpose of this work is the evaluation of the scattering matrix of flat dipoles embedded in a multilayer planar structure illuminated by an elliptically polarized plane wave at oblique incidence.

The structure under investigation is composed of four isotropic, linear, homogenous layers stacked up in the z direction, that is: two confined layers located between free space (the upper layer) and ground (the lower layer). The lower layer of complex permittivity ε_g and complex permeability μ_g occupies the negative-z region. Each of the two confined layers is characterized by thickness ℓ_n, complex permittivity ε_n and complex permeability μ_n, where $n = 1, 2$. Perfect electric and magnetic conductors of infinitesimal thickness, that act as scattering elements are printed on each layer interface. The layers are assumed to be infinite along the transversal x and y directions. The development is based on a global rectangular coordinate system located on top of the ground layer (interface $z = 0$) lying on the xy-plane.

The analysis is carried out by means of the full-wave technique in the spectral domain. According to this methodology, the structure is treated as a boundary value problem, where electric and magnetic currents located on each interface act as virtual sources of the scattered fields. The corresponding spectral Green's functions can be obtained analytically in a closed, simple form. Expressions for the far-zone electromagnetic fields scattered by the multilayer structure are derived by asymptotical evaluation of the Fourier transform using the method of stationary phase. From these expressions and the knowledge of the current densities (that can be estimated through the method of moments, for example), the scattering matrix components are then established for any incident and scattering direction.

Following this approach, the scattering matrices for planar electric and magnetic dipoles printed on the interface $z = \ell_1$ are obtained and evaluated. The results for a particular case (normal incidence on an electric dipole surrounded by free space) are in accordance with those presented in the literature. A similarity measure between the scattering matrices of planar electric and magnetic dipoles shows that both matrices are non-similar in the polarimetric SAR decomposition context.

Radio Frequency Metrology for Mobile Atmospheric Pressure Plasma Devices

V. J. Law, **N. O'Connor**, **and S. Daniels**
National Center of Plasma Science and Technology, Dublin City University
Collins Avenue, Glasnevin, Dublin 9, Dublin, Ireland

Abstract— Within the last decade the atmospheric pressure plasma-jet, needle, pencil and torch have all demonstrated a potential for direct impact on society in the guise of surface modification of engineering materials, and the destruction of microbial pathogens on contaminated surfaces. The advantages of these plasma devices are their ability to be mobile (hand-held), and hence take the plasma chemistry to the treatment surface, rather than bringing the surface to the plasma. Additionally the low electrical power consumption of these plasma devices allows them to be deployed in large numbers.

At Dublin City University, we have applied the developments in low pressure plasma radio frequency metrology [1, 2] to mobile atmospheric pressure plasma devices. In particular, to the semiconductor power switching circuitry and Flyback transformer that drive an atmospheric discharge and it's climatically controlled expanding plume [3].

This paper describes the application of non-invasive real-time passive and active radio frequency (RF) metrology to atmospheric pressure dielectric barrier argon and helium discharges. The active RF metrology uses frequency-domain reflectometry deployed on the main power-line. The electrical length between the plasma and test plane determines the frequency position of the plasma signal. In the case of the passive RF metrology, time-domain and frequency-domain measurements on the power-line are used to capture the discharge power density, and the power spectral density. Diplexers, directional couplers and capacitive probes act as front end probes and their out of band properties used to protect the measurement equipment from drive power level of typically 1.5 kV and pulse repetitions rate of 10 to 100 kHz. It is shown that oscillator frequency pulling and phase noise are deterministic measures of changes in the plasma power density and expanding plume interaction with the treated surface. It is also shown for sinusoidal excitation; pulse width modulation of the carrier is a measure of the discharge current.

REFERENCES

1. Law, V. J., J. Lawler, and S. Daniels, "Non-invasive VHF injected signal monitoring in atmospheric plasma and axial DC magnetron," Vacuum 82, doi:10.1016/j.vacuum 2007.08.007.
2. Law, V. J., "Process induced oscillator frequency pulling and phase noise within plasma systems," Vacuum 82, doi:10.1016/j,vacuum.2007.10.001.
3. Aranda-Gonzalvo, Y., D. L. Seymour, C. L. Greenwood, J. A. Rees, T. D. Whitmore, S. Daniels, and V. J. Law, "Dielectric barrier discharge driven by a flyback circuit: Analysis using energy resolved molecular beam mass spectrometry," *18th ISPC*, poster 30P-59, abstract number 137, Kyoto, Japan, 2007.

Monitoring of Satellite Thermal Pattern in Ocean Front Evolution

S. Nakamura
Kyoto University, Japan

Abstract— Monitoring of satellite thermal pattern of ocean front evolution is studied. The author has obtained a set of satellite thermal pattern on the ocean to find spacial structure of ocean front and its time evolution. A typical pattern is introduced in order to get a dynamical understanding of the ocean front evolution.

A New Approach to Mars Ionosphere Characterisation

M. Iorio[1], **F. Fois**[1], **R. Mecozzi**[1], **G. Picard**[2], **R. Seu**[2], **and E. Flamini**[3]

[1]Thales Alenia Space Italy, BU Observation Systems & Radar
Via Saccomuro 24, Rome 00131, Italy
[2]Infocom Department, University of Rome "La Sapienza", Via Eudossiana 18, Rome 00184, Italy
[3]ASI, Agenzia Spaziale Italiana, Viale Liegi 26, Rome 00189, Italy

Abstract— Presently two different instruments are operative in order to investigate the distribution of water, liquid and solid, in the upper portions of the crust of Mars, the Mars Advanced Radar for Subsurface and Ionosphere Sounding (MARSIS) and the SHAallow RADar (SHARAD) respectively on board the Mars Express and MRO missions. A secondary objective of the MARSIS instrument is the Mars Ionosphere characterisation through the Active Ionosphere Sounding (AIS) sensor. This operative mode presents a frequency agility capability in order to estimate the Mars ionosphere spectral properties. This method allows the sounding of the first ionosphere layer only. However another method used to characterise the Mars ionosphere, is the estimation by the ground penetrating data. The AIS mode allows the measure of the plasma frequency shape in the first layer of the ionosphere and the determination of the maximum plasma frequency value; an indirect approach respect to AIS mode is the use of the sounder data. The sounder signal passes thorough the ionosphere layer and after the surface reflection is received by the instrument. During this path the signal is distorted by the propagation through the ionosphere. To optimise the sounder data this distortion shall be estimated to compensate the signal. The information of the compensation function coefficients can be used to extrapolate the ionosphere property. Here will be presented a new ionosphere data inversion approach using the ground penetrating data in order to remove the data instability and the solutions uncertainly of the method. After the analytical data inversion formulation is done, the performance of the method and its applicability will be evaluated. Finally, an application to the experimental data, in order to test the proposed ionosphere data inversion method, will be presented.

Application of Modular Artmap for Landuse Image Classification

Chue-Poh Tan[1], **Ka-Sing Lim**[2], **Chen-Change Loy**[1], **and Weng-Kin Lai**[1]

[1]Centre for Advanced Informatics, MIMOS Berhad, Technology Park Malaysia
Kuala Lumpur 57000, Malaysia
[2]Faculty of Engineering, Multimedia University, Persiaran Multimedia
Cyberjaya 63100, Selangor, Malaysia

Abstract— This paper presents the development of Synthetic Aperture Radar (SAR) image classifier based on the Modular ARTMAP (MARTMAP) for landuse classification. The prediction of class membership is made collectively by combining outputs from multiple novelty detectors. In this paper, this novel classifier has been applied on San Francisco data with multi-polarization data for landuse classification. Distancebased familiarity discrimination is introduced to improve the robustness of MARTMAP in the presence of noise. The effectiveness of the proposed architecture is analyzed and compared with popularly used Maximum Likelihood and one-against-one Support Vector Machine (OAO-SVM). Experimental results show that MARTMAP is able to retain effective familiarity discrimination in noisy environment, and yet less sensitive to class imbalance problem as compared to its counterparts.

The potential of SAR in discriminating among different landuse environment has been demonstrated in several studies [1–16]. Previously, AIRSAR data over Sydney had been considered, and the potentials for characterizing different building clusters by extracting single, double and triple bounce effects have been presented. A segmentation-based classification was proposed, which utilized a decomposition technique on a data to improve the polarimetric discrimination capability in suburban areas [17]. Besides, E. Costamagna et al. [18] proposed a different statistical properties of built aggregates in an urban area using SIR-C measurements to provide an efficient classification result.

REFERENCES

1. Gamba, P. and B. Houshmand, "An efficient neural classification chain for optical and SAR urban images," *International Journal of Remote Sensing*, Vol. 22, No. 8, 1535–1553, May 2001.
2. Carpenter, G. A., M. N. Gjaja, S. Gopal, and C. E. Woodcock, "ART neural networks for remote sensing: Vegetation classification from LANDSAT TM and terrain data," *IEEE Trans. Geosci. Remote Sensing*, Vol. 35, 308–325, 1997.
3. Mannan, B., J. Roy, and K. A. Ray, "Fuzzy ARTMAP supervised classification of multispectral remotely sensed images," *International Journal of Remote Sensing*, Vol. 19, No. 4, 767–774, 1998.
4. Tan, C. P., J. Y. Koay, H. T. Ewe, H. T. Chuah, and S. Bahari, "Applications of remote sensing in the monitoring of rice crops," *IEM Journal*, Vol. 67, No. 4, Dec. 2006.
5. Tan, C. P., J. Y. Koay, K. S. Lim, H. T. Ewe, and H. T. Chuah, "Classification of multitemporal SAR images for rice crops using combined entropy decomposition and support vector machine technique," *Progress In Electromagnetics Research*, PIER 71, 19–39, 2007.
6. Tan, C.-P., H.-T. Ewe, and H.-T. Chuah, "A hybrid entropy decomposition and support vector machine method for agriculture crop type classification," *PIERS Online*, Vol. 3, No. 5, 620–624, 2007.
7. Lim, K.-S., C.-P. Tan, J.-Y. Koay, V. C. Koo, H.-T. Ewe, Y.-C. Lo, and A. Ali, "Multitemporal C-band radar measurement on rice fields," *PIERS Online*, Vol. 3, No. 1, 44–47, 2007.
8. Lim, K. S., S. Bahari, C. P. Tan, J. Y. Koay, M. Y. Chua, V. C. Koo, H. T. Ewe, A. Halim. and M. Safid, "Rice field measurement using C-band scatterometer," *4th National Microwave Remote Sensing Seminar*, MACRES, Kuala Lumpur, November 28, 2006.
9. Tan, C. P., J. Y. Koay, K. S. Lim, H. T. Teng, H. T. Ewe, H. T. Chuah, and S. Bahari, "Image classification of rice growth stages using combination of entropy decomposition and support vector machine (EDSVM)," *Proceedings for PacRim AIRSAR Significant Results Symposium*, MACRES, Kuala Lumpur, June 26–28, 2006.
10. Koay, J.-Y., C. P. Tan, S. Bahari, H.-T. Ewe, and H.-T. Chuah, "Theoretical modeling and measurement comparison of season-long rice field monitoring," *PIERS Online*, Vol. 1, No. 1, 25–28, 2005.

11. Ulaby, F. T., R. K. Moore, and A. K. Fung, *Microwave Remote Sensing: Active and Passive*, Norwood, Artech House, MA, 1986.
12. Bouman, B. A. M. and D. H. Hoekman, "Multi-temporal multi-frequency radar measurements of agricultural crops during the Agriscatt-88 campaign in The Netherlands," *Int. J. Remote Sens.*, Vol. 14, 1595–1614, 1993.
13. Tran, T. N., R. Wehrens, D. H. Hoekman, and L. M. C. Buydens, "Initialization of Markov random field clustering of large remote sensing images," *IEEE Trans. Geosci. Remote Sensing*, Vol. 43, No. 8, 1912–1919, 2005.
14. van Zyl, J. J., "Unsupervised classification of scattering behavior using radar polarimetry data," *IEEE Trans. Geosci. Remote Sensing*, Vol. 27, No. 1, 36–45, Jan. 1989.
15. Cloude, S. R. and E. Pottier, "An entropy based classification scheme for land applications of polarimetric SAR," *IEEE Trans. Geosci. Remote Sensing*, Vol. 35, No. 1, 68–78, Jan. 1997.
16. Yahia, M. and Z. Belhadj, "Unsupervised classification of polarimetric SAR images using neural networks," *IEEE International Conference Information and Communication Technologies 2004*, 335–337, 2004.
17. Lombardo, P., T. M. Pellizzeri, and A. Tomasuolo, "Classification of polarimetric SAR images of suburband areas using joint annealed segmentation and H/A/α decomposition," *Proceedings IEEE/ISPRS Joint Workshop Remote Sensing & Data Fusion over Urban Areas*, 117–121, Rome, Italy, 2001.
18. Costamagna, E., P. Gamba, P. Lombardo, and G. Chinino, "Statistical analysis and neuro-fuzzy classification of polarimetric SAR images of urban areas," *Proceedings of the ERS/ENVISAT Symposium*, Sweden, 2000.

A Millimeter-wave Vibrometer for Remote Acoustic Measurement

John A. Scales[1], **Brian J. Zadler**[1], **Manoja D. Weiss**[1], **and Martin L. Smith**[2]

[1]Colorado School of Mines, Golden, CO, USA
[2]New England Research, White River Junction, VT, USA

Abstract— There are many applications for remote vibration measurement, including land-mine detection and the monitoring of large-scale engineering structures such as bridges and dams. While laser Doppler vibrometers are widely available and have high sensitivity, they are relatively expensive and their performance degrades in the presence of rough surfaces, foliage and low-reflectivity surfaces. In order to overcome some of these limitations we have built a millimeter-wave vibrometer using mostly low-cost off-the-shelf components, operating at 40 GHz. Our vibrometer is able to measure sub-millimeter per second vibrations from diffuse reflectors at several meters distance. We use a highly stable 10 MHz oscillator to provide phase locking for multiple down-conversion steps. Currently the system operates in mono-static mode (since we have only one horn lens), but with separate source and receiver oscillators it could also be used bi-statically. The final down-conversion step is a 10 MHz IQ mixer with which we mix with our RF and clock signals to produce a final DC IF. The quadrature components can then be digitized with high dynamic range using low-cost audio A/D converters. We will show preliminary tests of this system and discuss some possible extensions and comparisons with other receiver configurations.

About Methods of Classification and Qualitative Interpretation of the Data of Remote Sensing of Water Surface

F. A. Mkrtchyan and V. F. Krapivin

Institute of Radioengineering & Electronics RAS
1 Vvedensky Sq., Fryazino, Moscow reg. 141190, Russia

Abstract— The problem of classification of terrestrial landscapes and aquatories basing on the remote measurements is one of important among them. Various algorithms of the theory of images recognition, statistical decisions and cluster analysis are used to solve this problem. At present time there are many methods of recognition which are caused appreciably by variety of statements of specific tasks. The problem of recognition consists in the divide of some group of objects by classes with the certain requirements. The objects having objectively general properties are related to one class. Feature of remote measurements is collection of the information when the data of measurements achieving the data processing system belong to the traces of flying system. As result the two dimensional image of investigated object is registered. Statistical model of spottiness for investigated space is one of models of this image. In real conditions, the research of spots, the reception of their statistical characteristics and their use in a problem of detection is enough a complex problem. It is necessary to develop the criteria allowing to distinguish the spots from other phenomena. For example, it is necessary to determine such threshold the exceeding of which is the spot indicator. Also it is necessary to develop modeling representation of processes of spots detection. The mathematical model parametrizing the phone characteristics of water surface spottiness is proposed. From the aforesaid follows, that statistical characteristics for "spottiness" of brightness temperatures in microwaves can be used for detection and classification of the phenomena on a surface of the ocean, that was caused by a degree of sea roughness.

The analysis of empirical histograms for "spottiness" of "brightness temperatures in microwaves" shows, that in most cases (l^+, l^-) — characteristics will be coordinated with exponential distribution, and amplitude characteristics will be coordinated with normal distribution. Therefore for detection and classification of the phenomena on a surface of ocean it is necessary to apply optimal algorithms for the COMPUTER training to taking statistical decisions for the aforesaid distributions.

Relative software is realized. The results of the software application of the satellite data processing for the Arctic, Atlantic and Pacific regions are given.

Remote Sensing of a Multiple Scale Sea Surface Using a Variational Technique

Ezekiel Bahar
Electrical Engineering Department, University of Nebraska-Lincoln, Lincoln, NE 68588-0511, USA

Abstract— Scattering from typical multiple scale sea surfaces accounts for contributions from stationary phase-specular points on the larger scale rough surface, as well as diffuse scattering contributions from the smaller scale rough surface that rides upon the larger scale surface. The standard hybrid two scale physical optics-small perturbation model of the sea surface depends critically upon the specific decomposition of the total surface height spectral density function and the Raleigh roughness parameter $k^2\langle h^2\rangle$ associated with the smaller scale surface, is restricted such that the product of the wave number times the root means square height is of order one.

Using a variational method to decompose, in a smooth continuous manner, the total surface height spectral density function into larger and smaller scale surfaces, a unified full wave solution is expressed as a weighted sum of two cross sections. The first is a physical optics type cross section that is reduced by a factor equal to the characteristic function squared of the smaller scale surface. The second is a perturbation type cross section that is modulated by the slopes of the larger scale surface. Unlike the standard small perturbation solution, the full wave solution is not restricted to rough surfaces with small Raleigh roughness parameters. Upon decreasing a variational parameter, equal to the ratio of the mean square heights of the larger scale surface and the total surface, from one (the total surface is regarded as the larger scale surface) to zero (the total surface is regarded as the smaller scale surface), it is shown that the unified full wave solution for the total cross section is stationary over a very wide range of the variational parameter (usually between 0.8 and 0.2). Thus for typical sea surfaces the variational parameter can be chosen to be 0.5. For this choice of the variational parameter, the Raleigh roughness parameters for the larger and smaller scale surfaces are equal and significantly larger than one.

Session 2A3a
Interaction of Waves and Media

Tellegen Particles

Peer Fischer and Ambarish Ghosh

Rowland Institute, Harvard University, Cambridge, MA 02142, USA

Abstract— An isotropic medium made of particles that have coupled permanent electric and magnetic moments has first been considered by Tellegen, when he conceived of a fifth circuit element of an electrical network, the "gyrator" [1, 2]. Remarkably, Tellegen's proposal to make orientable microscopic magnets coupled to electrets has never been realized before [1, 3]. A few experimental studies consider Tellegen's proposal, but none of these are based on particles with permanent coupled electric and magnetic dipole moments. Here we show that 'Tellegen particles' can be made using a technology that was used to make electronic paper (Gyricon) [4, 5]. Moreover, we show that the Tellegen particles, which have a diameter of 50 to 100 microns, can be dispersed randomly in a polymer matrix to make a disordered material that exhibits a sizeable magneto-electric response, and that they can be used to make a switcheable soft-matter magneto-electric.

The symmetry of the Tellegen particles will be discussed in some detail. It will be shown that the particles are a special 'metamaterial', since an electric-dipolar ferromagnet can at present not been realized at the molecular level.

Tellegen assumed that the particles with coupled permanent electric and magnetic moments should behave linearly, as this is advantageous for a network element [1]. Such a medium has been discussed in the electromagnetics literature as a "Tellegen medium", or a "non-reciprocal bi-isotropic medium". A gas of Tellegen particles in which collisions randomize the orientation of the particles may be described by linear constitutive equations. However, the interactions between the dipolar particles and their surroundings will in general result in a response that is nonlinear. The dynamics of the particles in the present system will be discussed.

REFERENCES

1. Tellegen, B. D. H., *Philips Res. Rep.*, Vol. 3, 81, 1948.
2. O'Dell, T. H., *The Electrodynamics of Magneto-electric Media, Series Monographs on Selected Topics in Solid State Physics*, Vol. 11, North-Holland, 1970.
3. Raab, R. E. and A. H. Sihvola, *J. Phys. A-Math.*, Vol. 30, 1335, 1997.
4. Crowley, J. M., N. K. Sheridon, and L. Romano, *J. Electrostat.*, Vol. 55, 247, 2002.
5. Sheridon, N. K., *Flexible Flat Panel Displays*, edited by G. P. Crawford, Wiley, 2005.

Group Velocity in Lossless Bianisotropic Dispersive Media

Arthur D. Yaghjian
S4 Inc., Massachusetts, USA

Abstract— It seems reasonable to expect that the group speed of a classical wave packet in lossless, homogeneous, temporally dispersive, bianisotropic media is less than or equal to the free-space speed of light (c). Such a media has constitutive relations in the frequency domain given by

$$\mathbf{B}(\mathbf{r},\omega) = \overline{\boldsymbol{\mu}}(\omega)\cdot\mathbf{H}(\mathbf{r},\omega)+\overline{\boldsymbol{\nu}}(\omega)\cdot\mathbf{E}(\mathbf{r},\omega) \quad (1)$$

$$\mathbf{D}(\mathbf{r},\omega) = \overline{\boldsymbol{\epsilon}}(\omega)\cdot\mathbf{E}(\mathbf{r},\omega)+\overline{\boldsymbol{\tau}}(\omega)\cdot\mathbf{H}(\mathbf{r},\omega) \quad (2)$$

where $\mathbf{B}$ is the magnetic induction, $\mathbf{H}$ is the magnetic field, $\mathbf{E}$ is the electric field, and $\mathbf{D}$ is the electric displacement. The $\overline{\boldsymbol{\mu}}$ and $\overline{\boldsymbol{\epsilon}}$ are the permeability and permittivity dyadics, respectively, and $\overline{\boldsymbol{\nu}}$ and $\overline{\boldsymbol{\tau}}$ are the magnetoelectric dyadics. Although a literature search produced a proof of the result that the group speed is less than or equal to the speed of light only in isotropic media, it is possible to prove the same result for bianisotropic media as well in a reasonably straightforward manner. The proof begins by deriving the $\mathbf{v}_g = \nabla_k\omega$ expression for group velocity $\mathbf{v}_g$ from an analytic-signal representation of a wave packet in $\mathbf{k}-\omega$ space (so as to involve positive ω only and thus have a unique ω for each $\mathbf{k}$). A textbook derivation of $\mathbf{v}_g = \mathbf{S}/U$ for anisotropic media, where $\mathbf{S}$ is the Poynting vector and U is the electromagnetic internal energy density, is then generalized to hold also for bianisotropic media. Lastly, upper bounds on $|\mathbf{S}|$ and lower bounds on U are found that can be used to prove that $|\mathbf{v}_g| \le c$ in lossless, homogeneous, temporally dispersive, bianisotropic media.

Applications Based on Space Transformation Method by Using Bi-layered Isotropic Material

Jiangtao Huangfu[1], **Dongxing Wang**[1], **Hongsheng Chen**[1]
Bae-Ian Wu[2], **Lixin Ran**[1], **and Jin Au Kong**[1,2]

[1]The Electromagnetics Academy at Zhejiang University
Zhejiang University, Hangzhou 310058, China
[2]Research Laboratory of Electronics
Massachusetts Institute of Technology, Cambridge, MA 02139, USA

Abstract— Coordinate transformation method paved a way for community to realize various useful applications, such as invisible cloaking and so on. However, the constitutive parameters derived by this method have commonly to be anisotropic and vary in space. In this paper, such anisotropic constitutive parameters are equivalent achieved by utilizing bi-layered homogeneous isotropic materials with subwavelength periodicities. A thin compressed horn antenna filled with layered media is verified in simulation. Compared to traditional ones, our antenna design has dramatically reduced sizes and good directivity. It is also easy to realize. As another example of application, a right-angle bent waveguide with low reflection based on layered media are realized and verified in numerical simulation. Our results show that method of using bi-layered isotropic materials is a good candidate for realizing anisotropic parameters derived from coordinate transformation method and can be used widely in practical applications.

Electromagnetics in Minkowski Spacetime with Geometric Algebra: Applications to Moving Media

Marco A. Ribeiro and Carlos R. Paiva
Instituto de Telecomunicações and Department of Electrical and Computer Engineering
Instituto Superior Técnico, Av. Rovisco Pais 1, Lisboa 1049-001, Portugal

Abstract— Bianisotropic media were introduced to electromagnetic theory through the study of moving media [1]. A coordinate-free approach to this topic, using dyadic analysis, can be found in [2]. Clifford's geometric algebra, namely through its version in Minkowski spacetime commonly known as STA (spacetime algebra) [3], presents a new insight to electromagnetics within the framework of special relativity. For instance, Thomas rotation in the composition of boosts [4] and a covariant description of the constitutive relation for isotropic media [5] have been developed using STA. In this work we use STA to present a general approach to electromagnetic theory in special relativity especially focused on the study of moving media. We begin our study by restating the approach to special relativity without the second postulate on the speed of light [6] through STA. Then, using a similar approach to [5], we present the spacetime constitutive relation of isotropic media in $C\ell_{1,3}$ [7] and show how this concise formalism can be readily translated into the more usual setting of three-dimensional space corresponding to $C\ell_3$ [8]. By introducing what we call the vacuum form reduction, we show how the covariant description of the constitutive relation in $C\ell_{1,3}$ for isotropic media which uses rotors as a fundamental algebraic tool [3] — can be reduced to the more tractable form of the spacetime constitutive relation for vacuum. This enables a straightforward approach to a coordinate-free treatment of such topics as wave vectors and normal surfaces in moving media which circumvents the cumbersome calculations of three-dimensional dyadic analysis [2]. Furthermore, with our approach, we present a new perspective on the equivalence between the so-called topological and materials interpretation [9, 10] that leads to such new exciting applications as perfect invisibility devices or artificial black holes.

REFERENCES

1. Kong, J. A., *Electromagnetic Wave Theory*, 879–952, EMW Publishing, Cambridge, Massachusetts, 2005.
2. Chen, H. C., *Theory of Electromagnetic Waves*, 299–339, McGraw-Hill, New York, 1985.
3. Hestenes, D., "Spacetime physics with geometric algebra," *Am. J. Phys.*, Vol. 71, 691–714, July 2003.
4. Paiva, C. R. and M. A. Ribeiro, "Doppler shift from a composition of boosts with Thomas rotation: A spacetime algebra approach," *Journal of Electromagnetic Waves and Applications*, Vol. 20, No. 7, 941–953, 2006.
5. Puska, P., "Covariant isotropic constitutive relations in Cliffordss geometric algebra," *Progress In Electromagnetics Research*, PIER 32, 413–428, 2001.
6. Lévy-Leblond, J.-M., "One more derivation of the Lorentz transformation," *Am. J. Phys.*, Vol. 44, 271–277, March 1976.
7. Lounesto, P., *Clifford Algebras and Spinors*, Cambridge University Press, Cambridge, 2nd ed., 2001.
8. Matos, S. A., M. A. Ribeiro, and C. R. Paiva, "Anisotropy without tensors: a novel approach using geometric algebra," *Opt. Express*, Vol. 15, 15175–15186, November 2007.
9. Schurig, D., J. B. Pendry, and D. R. Smith, "Calculation of materials properties and ray tracing in transformation media," *Opt. Express*, Vol. 14, 9794–9804, October 2006.
10. Leonhardt, U. and T. Philbin, "General relativity in electrical engineering," *New J. Phys.*, Vol. 8, 247, 2006.

Soliton Transverse Instabilities in Nonlocal Nonlinear Media

Yuan Yao Lin[1], **Ray-Kuang Lee**[1], **and Yuri S. Kivshar**[2]

[1]Institute of Photonics Technologies, National Tsing-Hua University, Hsinchu 300, Taiwan
[2]Nonlinear Physics Center, Research School of Physical Sciences and Engineering
The Australian National University, Canberra, ACT 0200, Australia

Abstract— Symmetry-breaking instabilities have been studied in different areas of physics, since they provide a simple means to observe the manifestation of strongly nonlinear effects in nature. One example is the transverse instabilities of spatial optical solitons in Kerr nonlinearity associated with the growth of transverse modulations of quasi-one-dimensional bright and dark soliton stripes in both focusing and defocusing nonlinear media. In particular, this kind of symmetry-breaking instability turns a bright-soliton stripe into an array of two-dimensional filaments and bends a dark-soliton stripe creating pairs of optical vortices of opposite polarities. Consequently, the transverse instabilities set severe limits on the observation of one-dimensional spatial solitons in bulk media. Several different physical mechanisms for suppressing the soliton transverse instabilities have been proposed and studied, including the effect of partial incoherence of light and anisotropic nonlinear response in photorefractive crystals, and the stabilizing action of the nonlinear coupling between the different modes or polarizations. In this article we demonstrate that significant suppression of the soliton transverse instabilities can be achieved in nonlocal nonlinear media. First we employ numerical treatment to solve and analysis the soliton transverse instability based on a nonlinear Schödinger equation in focusing nonlinearity with diffusion nonlocality. Then we construct analytical models to describe transverse instability by asymptotic expansion in the long-scale and short-scale regime with the help of variational approximation method and investigate its effect under nonlocal response. Numerically the evolution of the soliton stripe are performed to verify the predictions.

Modulation Instabilities of Elliptical Solitons

Yuan Yao Lin and Ray-Kuang Lee
Institute of Photonics Technologies, National Tsing-Hua University, Hsinchu 300, Taiwan

Abstract— The modulation instabilities of two-dimensional (2D) optical solitons have been studied in radial and azimuthal directions for circularly symmetric solitons and vortices. Recently, elliptical soliton is proposed in strong nonlocal media, in fact which support similar solutions as linear Ince-Gaussian beams. Experimental observations of elliptical solitons in photorefractive materials are also reported recently. In this report, elliptical bright solitons are studied numerically with a more generalized formulation. The corresponding modulation instability spectrum indicates the existences of dipole and quadrupole modes, which are totally suppressed in circularly symmetric solitons. We consider the propagation of an optical beam in a nonlinear medium described by the normalized two-dimensional nonlinear Schodinger (NLS) equation in elliptical coordinates with semifocal separation of elliptical cylinder coordinate. We employ separation of variables and varational approach to obtain soliton solution by minizing the averaged Lagragian of NLS in elliptical coordinates by which we solve with self-consistency numerically. The modulation instabilities are subsequently analyzed by conventional linear stability analysis with perturbed solutions. Consequently, a soliton in a cylindrical asymmetrical system loses its radial symmetry and turns its shape into an elliptical one due to a strong modulation in the azmuthal direction. The bifurcations demonstrate that elliptical solitons increase their power as the semifocal separation increases. The modulation instability spectrum reveals that in an elliptical coordinate one can suppress the instability of radial symmetric eigen mode with a cutoff semifocal separation. Nevertheless, the elliptical coordinate also introduce higher excitation modulation modes both in x-direction and y-directions.

Session 2A3b
Electromagnetic Theory

Representation of Einstein's Relativity by Smith's Chart

C. F. Chen[1] and Y. F. Tung[2]

[1]Department of Electronic Engineering, The Chinese University of Hong Kong
Shatin, N. T., Hong Kong, China
[2]Department of Translation, The Chinese University of Hong Kong
Shatin, N. T., Hong Kong, China

Abstract— The first author is an engineer (Ph.D. Cambridge, 1971) and the second a humanist (Ph.D. Harvard, 1994). They co-author this paper starting from two completely different points of view: one through mathematical reasoning, the other the pictorial approach on the Smith Chart.

P. A. M. Dirac's well-known book *General Theory of Relativity* uses

$$x^{\mu},\ \mu = 0,\ 1,\ 2,\ 3 \tag{1}$$

which is the four coordinates of the time t and three space coordinates, while Einstein's original work is to use

$$t = t,\ x = x,\ y = 0,\ z = 0 \tag{2}$$

He deliberately assumed $y = 0$, $z = 0$, just for simplicity.

Einstein states that the space-time continuum of the special theory of relativity considered as a Euclidean continuum introduces Minkowski's work for description of the four-dimensional space-time continuum known as "Galilean Coordinate Systems" which determine events.

The validity of the Lorentz transformation follows from the following condition

$$\mathrm{d}s^2 = \mathrm{d}x_1^2 + \mathrm{d}x_2^2 + \mathrm{d}x_3^2 + \mathrm{d}x_4^2 \tag{3}$$

This belongs to two adjacent points of the four-dimensional space-time continuum and has the same value for all selected reference-bodies.

Following Einstein's simplified version, that is $y = z = o$, we have

$$S^2 = (ct)^2 - X^2 \tag{4}$$

We call the magnitude $\mathrm{d}s$ the distance apart of the two events in the complex-plane.

The Smith Chart was originally designed for using in impedance matching in Transmission-line, and then has been applied to Waveguides studies, and later on, with some modification, to feedback systems design and other applications by the first author of this paper.

The second author, however, simply sees Smith's Chart as a picture without knowing anything about its mathematic background. She is very knowledgeable about non-mathematic literature on Einstein because she has translated many books and written one concerning Einstein. When, incidentally, the first author was working on the subject of relativity on the Smith Chart, she asked: "Is the Smith Chart the whole universe of time-space of Einstein's relativity?"

Surprisingly inspired by her question, the first author answered: "You can look at the Chart in that way. In fact, Bertrand Russell's explanation of Einstein's relativity in his *Relativity ABC* is very similar to what you are saying although Russell did not know the existence of the Smith Chart. If your idea gets translated back to mathematics; that means a bilinear transformation on which the Smith Chart is based."

Taking Russell's point of view, she argued that the surface of the Smith Chart maybe a good device to explain the theory of relativity. In the full paper, we will try to show the derivation of the various coefficients of the bilinear transformation in order to construct a chart better representing the theory of relativity.

Fundamental Properties of DC Field Sensors

B. Z. Kaplan[1], **A. Sheinker**[1], **and U. Suissa**[2]

[1]Department of Electrical and Computer Engineering, Ben-Gurion University of the Negev
P. O. Box 653, Beer-Sheva 84105, Israel
[2]Department of Electrical Engineering, Sami Shamoon College of Engineering
P. O. Box 45, Beer-Sheva 84100, Israel

Abstract— The uniqueness of dc field sensors can be made explicable by imagining a simple experiment of measuring dc magnetic fields. The simplest sensor that jumps to mind, when mentioning magnetic fields, is a search coil. A search coil, however, is not capable of measuring static fields. It is usually employed for measuring varying fields, which induce a measurable voltage in the coil. Is there, nevertheless, a way around, where a search coil can be employed for static magnetic fields? The answer is yes. One may rotate the search coil in the field and measure the generated voltage. One has thus created a system that resembles a generator, whose output ac amplitude is proportional to the sensed dc field. Connection of a measuring device to the coil terminals (it is usually attained through slip-rings) causes the coil to be loaded. The load consumes power. It thus means that the rotation of the search coil would be possible only if a mechanical power is supplied to the system. The lesson that can be learned is probably of two folds: 1. Certain ways of measuring DC fields involve mechanical movement. 2. The measurement of DC fields appears to be power consuming.

It is also interesting to notice that in the past there used to be what we may call mechanical fluxgates. They were constructed of two collinear relatively long wound ferromagnetic cores with a gap between them. An asymmetrical ferromagnetic object used to be forced to rotate in the gap. This caused modulation of the flux passing in the cores, and caused ac voltage proportional to the measured field to be generated between the coils terminals. The similarity between this system and a conventional fluxgate is evident. This is due to the fact that the flux modulation in a conventional fluxgate is attained by periodically varying the magnetic susceptibility of a region in the core by an auxiliary perpendicular periodic flux.

The present work is applicable also for electric dc field sensors. There also the sensing procedure in many of the sensors involves mechanical motion. It can in addition be shown that the related sensing procedure is also power consuming.

A Toroidal Harmonic Representation of the Yukawa-potential Kernel for a Circular Cylindrical Source

J. P. Selvaggi, **S. J. Salon**, **and M. V. K. Chari**
Rensselaer Polytechnic Institute, Troy, NY 12180-3590, USA

Abstract— A true cylindrical series expansion of the Yukawa- or screened Coulomb-potential kernel is developed for a finite circular cylindrical source through the application of a toroidal harmonic expansion. The Yukawa kernel is separated into a singular and nonsingular part. The singular part is expanded in terms of the associated toroidal harmonics and the nonsingular part is expanded in terms of an elementary binomial expansion.

Cerenkov Radiation in the Waveguide Filled with an Anisotropic Double-negative Medium

Zhaoyun Duan[1], **Bae-Ian Wu**[2], **Jie Lu**[2], **Jin Au Kong**[2], **and Min Chen**[3]

[1]Vacuum Electronics National Lab, School of Physical Electronics
University of Electronic Science and Technology of China, Chengdu 610054, China
[2]Research Laboratory of Electronics, Massachusetts Institute of Technology
Cambridge, MA 02139-4307, USA
[3]Department of Physics, Massachusetts Institute of Technology
Cambridge, MA 02139-4307, USA

Abstract— A charged particle uniformly moving in a medium with a speed faster than the phase velocity of light in the medium emits Cherenkov radiation. The physical properties of the Cerenkov radiation are investigated theoretically for a particle traveling along the axis of a cylindrical waveguide filled with an anisotropic double-negative medium(DNM). In this paper, the inversed Cerenkov radiation, Cherenkov radiation condition and Cherenkov radiation angle can be founded by analytical analysis. The effects of the different particle velocity, different constitutive parameters of the anisotropic DNM are discussed. It is shown that the total radiated energy increases with increasing the particle velocity, the maximum radiated energy spectral density appears at the frequencies which correspond to those modes in the lossless case for different DNM when the loss of the anisotropic DNM is smaller, and becomes much smoother as the loss is bigger, and the total radiated energy is a decreasing function of the loss, the expected maximum radiated energy per unit length can be realized by choosing suitable DNM. The obtained conclusions illustrated by a numerical example offer a theoretical basis for possible experimental research of Cherenkov radiation in the DNM, and potential applications such as detectors and wave oscillators or amplifiers. For example, the Cherenkov radiation based on the DNM may be one of the most promising approaches for the high power terahertz radiation sources.

ACKNOWLEDGMENT

This work was supported by the Office of Naval Research under Contract N00014-06-1-0001, the Department of the Air Force under Air Force Contract F19628-00-C-0002, National Natural Science Foundation of China (Grant Nos 60601007, 60532010 and 60531020), Youth Science and Technology Foundation of UESTC (Grant No JX05018) and Chinese Scholarship Council.

Scatterer's Geometry Influence on 'Power-Law' Formula in Random Mixing Composites

Peiheng Zhou[1,2], **Bae-Ian Wu**[2], **and Jin Au Kong**[2]

[1]State Key Laboratory of Electronic Thinfilms & Integrated Devices
University of Electronic Since and Technology of China, Chengdu, China
[2]Research Laboratory of Electronics
Massachusetts Institute of Technology, Cambridge, MA, USA

Abstract— In this paper, a widely used class of mixing models, formed by the 'power-law' approximation is studied for the design of random dispersing absorbers. It is found that scatterer's geometry has an influence on the decision of formula's power parameter in spite of random orientation.

The general power-law model applied to the effective permittivity of a two phase mixture is $\varepsilon_{eff}^{\beta} = f\varepsilon_i^{\beta} + (1-f)\varepsilon_e^{\beta}$, where f is the volume fraction of inclusion scatterers, subscript i and e represent the inclusion and matrix component respectively. Different β value indicates distinguishing application background. Based on the effective medium method, the power-law approximation has already been analytically proved. However the application of this model with various power values in a single background is rarely reported. Our simulation shows that the formula fits to the effective permittivity of randomly orientated and located spherical and flake like scatterers with $\beta = 1/3$ and $1/2$ respectively, where they are under the same mixing conditions. This kind of results can be achieved in a wide range of volume fraction of inclusion and frequency band in both spherical and flake like case. In a general case of power-law coherent with effective medium method, β is defined as the shape factor of a beta distribution function for dipoles dispersion. Our analysis further introduced a geometric influence on the solution of the special beta distribution function which determines the value of β relating to the shape dependence of depolarization factors. It is clear that the geometric feature of scatterers contributes to the mean depolarization through the integral of the whole composite in an arbitrary direction. By this approach, a mixing law is figured out for the design of random dispersed composite in absorbing application.

Session 2A4
Electromagnetic Modeling, Inversion and Applications 1

GL Electromagnetic and Mechanical Uniform Coupled Modeling

Ganquan Xie, **Jianhua Li**, **and Feng Xie**
GL Geophysical Laboratory, USA

Abstract— The Electromagnetic (EM) equation was derived by Faraday and Maxwell. In particularly, Maxwell introduced the displaced current term and completed the EM Maxwell equation. The Maxwell equation was derived from experiments, instead of Newton's principle. The elastic mechanical (ME) equation was derived partly from Newton mechanical principle, partly from experiment. In this paper, an EM and ME uniform equation system and coupled equation are presented. We propose GL EM and ME uniform and coupled modeling for mechanical electric or mechanical magnetic materials. Also the GL EM and ME modeling can be used in the geophysical exploration and earthquake exploration.

Modal-based Tomographic Imaging of Electrically Large Cells from Far Zone Observations

Ersel Karbeyaz and Carey M. Rappaport
The Bernard M. Gordon Center for Subsurface Sensing and Imaging Systems (Gordon-CenSSIS)
360 Huntington Avenue, Stearns Center, Suite 302, Northeastern University, Boston, MA 02115, USA

Abstract— Non-invasive assessment of the health of an embryo or a single cell is an open issue of critical importance for the success of certain procedures like in vitro fertilization (IVF). A three dimensional (3D) understanding of the investigated structure, such as how various organelles are distributed within the cell, is necessary to achieve this goal. Advanced microscopy techniques can provide both amplitude and phase information from multiple views, but obtaining detailed volumetric information is still challenging. In particular, imaging mitochondria is usually quite difficult since there may be tens of thousands of these tiny, low-contrast scatterers overlapping each other within the cell.

When the inhomogeneities in an investigated object are comparable in size to the wavelength of the probing signal, as is the case of a cell being illuminated by a laser operating in or near the visible spectrum, techniques based on straight ray assumptions suffer from the effects of diffraction and refraction. In this case, diffraction tomography techniques considering wave propagation and diffraction phenomena must be employed.

Although the electromagnetic properties of cellular structures exhibit slight variations relative to the background, classical optical diffraction tomography (ODT) techniques based on the Born or Rytov approximations are not suitable to image these objects since their overall electrical sizes are quite large when probed in or near the visible spectrum, and the observed scattered light is in the far zone.

In this work, we present a novel method to image these objects in two dimensions (2D), which is based on the expansion of the target object function in terms of Fourier-Bessel basis functions with corresponding, unknown expansion coefficients, and an alternative approximation for the total fields within the scatterer. Unlike the Born and Rytov approximations, this new approximation satisfies the continuity of the total tangential fields along the object support-background boundary for each circular mode using the known incident and observed scattered fields, and takes into account the fact that the refractive index distribution along structures being investigated varies slightly around a known mean value. The resulting ill-posed linear system of equations is solved via truncated singular value decomposition (TSVD) for the unknown expansion coefficients. This approach can be readily extended to more realistic 3D cases.

To validate the proposed method and compare its performance with that of the existing ODT techniques, a number of simulations involving plane wave scattering through various 2D objects, such as radial cylinders, random phantoms, and finally cell models with miscellaneous mitochondrial distributions, are performed. Except for the radial cylinders for which an iterative, analytical forward solution is available, Finite-Difference Time-Domain (FDTD) method is used in the simulations. Basic principles of the FDTD method, such as total-field scattered-field formulation, near to far field transform, PML absorbing boundary condition are employed in these simulations. The far zone scattered fields obtained with these simulations are then utilized to reconstruct the probed objects via both the proposed method and the conventional ODT techniques. Qualitative and quantitative superiority of the proposed technique is demonstrated.

Diagnostic of Non Uniform Multi-conductor Transmission Lines

Marc Olivas Carrion, **Nicolas Ravot**, **Adrien Lelong**, **and Fabrice Auzanneau**
CEA LIST, Gif-Sur-Yvette, F-91191, France

Abstract— Nowadays a vehicle harness represents more than three kilometers of cables with twisted pairs, coaxial cables, simple wires and many different connectors. The reliability of the system depends on the health and quality of the cables used for communication or power supply. The sensitivity of the network to failures depends on the design and the complexity. It is essential to monitor each transmission between embedded systems inside a car to avoid problems such as communication or DC network breakdown.

Currently, many diagnosis methods based on Time- or Frequency Domain Reflectometry (TDR or FDR) are used for complex wiring, such as those developed for aeronautics [1]. These methods can also be used in the automotive domain for interconnections such as the CAN network (twisted pair).

Recently, several studies were dealing with the wideband analysis of the response of the channel formed by complex networks [2, 3]. In the first reference a theoretical model was developed for a network made of uniform lines to help understand and explain reflectometry measurements results. In the second reference, the global architecture of the harness was described and the characteristics of in-vehicle power line were deduced from measurements and from extensive parametric studies based on a deterministic propagation model.

In this paper we adapt these methods to fault detection and localisation based on channel characterization in the frequency domain. The propagation model is used as a reference for a given topology to assist the diagnosis of complex networks formed by NUMTL (Non Uniform Multi-Conductor Transmission Lines).

In order to illustrate this work, a first example will present the case of a ten wires NUMTL and a second case study will apply this method to real harness architecture.

REFERENCES

1. Furse, C., Y. C. Chung, C. Lo, and P. Pendayala, "A critical comparison of reflectometry methods for location of wiring faults," *Smart Structures and Systems*, Vol. 2, No. 1, 25–46, 2006.
2. Auzanneau, F., M. O. Carrion, and N. Ravot, "A simple and accurate model for wire diagnosis using reflectometry," *PIERS Proceedings*, 232–236, Prague, Czech Republic, August 27–30, 2007.
3. Carrion, M. O., M. Lienard, and P. Degauque, "Communication over vehicular DC lines: Propagation channel characteristics," *IEEE ISPLC 2006*, 2–5, March 26–29, 2006.

An Improved Forward Scattering Simulation Technique for Microwave Breast Imaging

B. Babu and M. Condon

RINCE, School of Electronic Engineering, Dublin City University, Dublin 9, Ireland

Abstract— Microwave imaging is a promising alternative to conventional mammography methods. At microwave frequencies, normal and malignant tissues show high contrasts in their electrical properties. Microwave Imaging (MWI) systems can be used to construct three-dimensional profiles of the electrical properties of the body part that is being examined. MWI systems illuminate the body part with electromagnetic radiation of a suitable frequency. Using the measured scattered field at the surface of the body, inverse scattering algorithms reconstruct profiles of the electrical properties of the target. It is therefore of the uttermost importance that the forward scattering set-up is correct so that an inversion algorithm can create accurate profiles of electrical properties. We propose an improvement over the existing integral equation based forward scattering simulation techniques for microwave breast cancer imaging. Early detection of breast cancer is crucial. At this stage, the size of malignant tissue can be in the order of millimeters. For imaging involving such a small malignancy, one must use high-frequency radiation. At such frequencies, in order to overcome the relaxation effect of complex permittivity, we use the Debye model. For solving the forward scattering problem, we use the stabilized bi-conjugate gradient fast Fourier transform method (BI-CGSTAB-FFT). For the scattering domain, we apply the so-called cyclic boundary condition. This reduces the number of FFTs involved thus saving time and memory. For the BI-CGSTAB-FFT iteration method, we choose the initial value of the total field to be the incident electric field. This choice yields better convergence than a random selection of initial condition.

Semi-analytic Mode Matching (SAMM) Algorithm Used to Compute Nearfield Scattering in Rough Lossy Ground from Dipole Sources

Ann Morgenthaler, **He Zhan**, **and Carey Rappaport**
Gordon-CenSSIS, ECE Department, Northeastern University, Boston, MA 02115, USA

Abstract— The 3D Semi-Analytic Mode Matching (SAMM) algorithm is used to determine nearfield scattering from underground targets in modestly rough lossy soil, where a dipole source (either below ground in a borehole or above ground) is used. Scattering is described by moderately low-order superpositions of spherical modes placed at multiple user-specified coordinate scattering centers (CSCs). These CSCs are placed both within the underground targets and their images as well as within the rough surface layer as needed. Mode coefficients are found numerically by least-squares fitting all boundary conditions at discrete points along the relevant interfaces while at the same time obeying radiation conditions. SAMM results are compared with the completely different Half-Space Born Approximation (HSBA) method.

Choosing the appropriate number and location of the CSCs is the crux of the SAMM method. Using large numbers of scattering centers and/or high-order spherical mode superpositions allows too many degrees of freedom, which can result in a non-optimal local minimum solution to the singular value decomposition. This problem can be reduced by "steering" the SAMM solution towards the correct global solution using low order modal solutions initially and adding high order modal corrections iteratively.

Another important means of reducing the problem size is to "decouple" the original problem into smaller pieces by standard equivalence theory, each piece of which may be solved with its own set of CSCs. The resulting multi-step/few CSC analysis will generally be faster and more accurate than a one-step/many CSC calculation. Additionally, symmetries inherent in each subset of the problem may be exploited. As SAMM is not a perturbative algorithm, decoupling the problem does not introduce any level of approximation into the algorithm. SAMM is primarily a nearfield method, modeling the fields best near the scatterer. As in ray tracing, SAMM obeys Maxwell's equations in the region of interest but may not be accurate outside that region. Unlike conventional Born approximation methods, however, SAMM does not require uniform backgrounds or specialized Green's functions, and it maintains accuracy for large or strong dielectric contrast scatterers, including metal scatterers.

Modeling Millimeter-wave Detection of Body Worn Explosives

Carey M. Rappaport, **José A. Martínez Lorenzo**, **Richard Sullivan**, **and Amanda Angell**
The Gordon CenSSIS, Northeastern University
360 Huntigton Ave, Suite 302 Stearns Center, Boston, MA 02115, USA

Abstract— Millimeter-wave radar (MMR) has been proposed to detect concealed body worn explosives at distances up to 50 meters. Operating in the 50 to 350 GHz frequency range, MMR is particularly effective at resolving small target features and has the advantage of requiring physically small antennas to generate sharp interrogating beams. The wave interaction with realistic body cross sections is modeled showing the complexity of the nearfield scattering phenomena for both transverse magnetic (TM) and transverse electric (TE) cases in a full wave two-dimensional computational geometry.

A human body cross section is illuminated with thirteen plane waves, working at 77 GHz (wavelength of 3.89 mm), in order to simulate narrow beams produced by an array of reflector antennas, located at 50 m range and distributed along a 4 m aperture. The explosives targets are simulated with an array of vertically-oriented metal pipes loaded into a canvas vest.

Near-Field to Near/Far-Field transformations are performed to compare the scattering from bodies with and without this array of pipes, which shows that simple threshold analysis will not detect the threat when a single plane-wave illumination is used. Detection is reliable when illuminating with an array of reflectors using digital beamforming in transmission and reception modes.

Extending MAS/TSA Technique for Conducting Environments to Enhance Underwater UXO Discrimination

D. Kakulia[1], **G. Ghvedashvili**[1], **and F. Shubitidze**[2]

[1]Chavchavadze Ave. 3, Tbilisi State University, Tbilisi 0128, Georgia
[2]Thayer School of Engineering, Dartmouth College, HB 8000, Hanover, NH 03755, USA

Abstract— There are approximately one million acres of underwater lands at DoD and Department of Energy (DOE) sites that are highly contaminated with unexploded ordnance (UXO) and land mines. The detection and disposal of Underwater Military Munitions are more expensive than excavating the same targets on land. Therefore, innovative detection and discrimination systems with 0% false alarm rate that can reliably discriminate between hazardous UXO and innocuous items are required. Recently, electromagnetic induction sensing has been considered as a potential candidate for underwater detection. In order to explore the potential of various EMI sensing technologies for underwater detection and discrimination and to achieve a high ($\sim 100\%$) probability of detection, and to distinguish UXO from non-UXO items accurately and reliably, first the underlying physics of the EM scattering phenomena in underwater environment needs to be investigated in detail. This understanding can then be used to development innovative EM sensors with improved discrimination capabilities.

The main objective of the paper is to extend the combined Method of auxiliary sources and thin skin depth approximation procedure for underwater environment and to investigate how marine environments change EMI sensor performance and associated processing approaches for detecting highly conducting and permeable metallic objects underwater. The numerical results will be designed to for illustrating the underlying physics of EMI scattering phenomena for metallic objects that are placed inside a conducting medium, and the interaction effects between the object and it surrounding conducting medium will be analyzed.

Inverse Scattering by Signal Subspace and Level Set Methods

E. A. Marengo and F. K. Gruber

Northeastern University, Boston, MA 02115, USA

Abstract— The signal-subspace-based imaging of spatially extended scatterers from the scattering matrix has been investigated for scalar fields in the linearizing framework of the Born approximation in [1] and [2] and in the more general multiple scattering case in [3–5]. These methods are part of the modern focus on so-called "qualitative methods" in inverse scattering [6]. In this talk new theory and algorithms are presented for signal-subspace-based imaging of penetrable extended scatterers (characterized by a scattering potential function) using scalar and electro- magnetic fields. The focus of past work by our group in this area has been on non-iterative sampling and enclosure approaches. In the present research, reconstruction of the shape of the scatterer is achieved by exploiting the geometrical information about the scatterer that is contained in the singular system of the scattering matrix, which directs the evolution of a test shape by means of the level set method [7]. The scatterers are assumed to be embedded in a known but rather general linear and reciprocal background medium. The developments hold within exact scattering theory; thus no linearizing approximations are involved in the associated forward model, and the imaging or support inversion of the scatterers holds not only for the special case of sub-wavelength or point targets but also for the more general case of objects of rather arbitrary shape and dimensions including objects having simply or not simply connected support regions such as collections of targets plus clutter in disjoint domains. While for a scalar point target there is a single Green function vector or propagator per target (a "Green function vector"), and while for an electromagnetic point target there can be 6 such propagators (3 electric dipoles and 3 magnetic dipoles), for an extended target one must associate a countably infinite number of communicable modes or propagators per target. For a given SNR the space of such communicable modes becomes (within ϵ-approximations of linear mappings detailed in two of the references above) essentially a finite-dimensional one. Then one can consider imaging functions or pseudo-spectra $P(D'_o)$, where D'_o represents a given support, with D_o being the actual scatterer support, which render images by exploiting signal subspace properties of the scattering or data matrix K and of linear propagation mappings based on the known background Green function and parameterized by the assumed support D'_o. One example is provided by the following receive-mode pseudospectrum:

$$P(D'_o) = \left[\sum_{p=N(D_o)+1}^{N_{\text{tot.}}} \sum_{q=1}^{N(D'_o) \le N(D_o) < N_{\text{tot.}}} \left| \left(\Psi_p,\, \psi_{r,\,q}^{(D'_o)} \right) \mathcal{Y}_{\text{eff.}} \right|^2 \right]^{-1}$$

where: $N_{\text{tot.}}$ is an essential number of degrees of freedom; $(\Psi_p,\, Q_p,\, \sigma_p)$ is the singular system of the scattering matrix K as measured with the given remote sensing system, so that $K = \sum_p \sigma_p |\Psi_p\rangle\langle Q_p|$ in Dirac bra-ket notation, and for which $p > N(D_o)$ represents negligible singular values σ_p; , $(\psi_{r,\,q}^{(D'_o)},\, J_q^{D'_o},\, \lambda_q^{D'_o})$ is the singular system of the radiation mapping from the sources induced within the scatterer support D'_o to the measured scattered fields at the receiver system, and for which $q > N(D'_o)$ represents negligible singular values $\lambda_q^{(D'_o)}$; and $(\cdot,\, \cdot)\mathcal{Y}_{eff.}$ represents the non-weighted L^2 inner product for L^2 fields $\in \mathcal{Y}_{eff.}$ measured within the receiver support. If $D'_o \subseteq D_o$ then $P(D'_o)$ peaks which provides an image of the object. This property of the singular functions of the scattering matrix is exploited in the above-provided signal-subspace-based imaging scheme and in alternative variations of the algorithm to direct the evolution of the shape by means of the level set method. The performance of the non-iterative sampling of our past work in this area (where the test shape is a small, point-like region) versus the level set approach of the present research are comparatively explored. We have validated the proposed imaging approaches via computer simulations, and these and related computational results will be reported at the conference talk

ACKNOWLEDGMENT

This research was supported by US AFOSR under Grant No. FA9550-06-01-0013.

REFERENCES

1. Zhao, *SIAM J. Appl. Math.*, Vol. 64, 725–745, 2004.

2. Hou, et al., *J. Comp. Phys.*, Vol. 199, 317–338, 2004.
3. Marengo, et al., *IEEE T. Image. Process.*, Vol. 16, 1967–1984, 2007.
4. Marengo, *Proc. 2007 IEEE Stat. Signal Process. Workshop*, 304–306, Madison, Wisconsin, August 26–29, 2007.
5. Hou, et al., *Inverse Probl.*, Vol. 22, 1151–1178, 2006.
6. Cakoni and Colton, *Qualitative Methods in Inverse Scattering: An Introduction*, Springer, Berlin, 2006.
7. Santosa, *ESAIM: COCV*, Vol. 1, 1733, 1996.

Early Detection and Characterization of Breast Tumors from Microwave Data Using a Level Set Technique

N. Irishina, **O. Dorn**, **and M. Moscoso**

Universidad Carlos III de Madrid, Avda de la Universidad 30, Leganes 28911, Madrid, Spain

Abstract— We present a novel reconstruction algorithm for the early detection of breast cancer from frequency domain microwave data. The goal is to detect, locate and characterize a tumor in its early stage of development. The breast model is composed of four different tissue types which are separated by sharp interfaces. These are skin, fibroglandular tissue, fatty tissue and the tumor. In the inverse problem, the interfaces need to be reconstructed from the data together with certain characteristic properties of each of the individual regions. A level set technique is used for representing the boundary of the tumor and the interfaces between fatty and fibroglandular tissue. A Debye model is used for the electromagnetic parameters for taking into account dispersion in the medium. The algorithm consists of four stages of increasing complexity. In each succeeding stage more details are recovered from the data. The final stage performs a search for the correct size and permittivity value of the detected tumor. An evolution strategy is employed in each stage of the algorithm for evolving the level set function(s) representing the interfaces between different tissue types as well as the internal profiles. For finding the correct contrast value for the detected tumor we employ a special probing technique in order to avoid local minima. We show that our method is able to correctly detect and locate very small hidden tumors. Moreover, in most cases a good approximation of the correct size and permittivity value is provided by the algorithm which might be useful in practical applications as one component for correctly characterizing a tumor as 'benign' or 'malignous'. Numerical examples are presented in 2D which demonstrate the performance of our technique.

ACKNOWLEDGMENT

The presented work is financed by the Spanish Ministery of Education and Science, grant No. FIS2007-62673, and by the Autonomous Region of Madrid, grant No. S-0505/ENE/0229 (COMLIMAMS).

Microwave Subsurface Sensing and Imaging Using Matlab-based FDFD Method

Qiuzhao Dong and Carey M. Rappaport
Center for Subsurface Sensing and Imaging Systems, Northeastern University
Boston, MA 02115, USA

Abstract— We have developed a new algorithm for the electromagnetic inverse scattering problem in inhomogeneous media using Matlab sparse matrix routines implementing the finite difference frequency domain (FDFD) model [1], referred as the FDFD-based inversion method. The key issue of this method is to build a linear expression for the inverse problem from the FDFD forward model by using the vector-based Born approximation of single scattering of incident field. The advantage of the FDFD-based approach it that no Green's function is required, so it can be readily applied to strongly layered or discontinuous backgrounds. This inversion algorithm is tested for microwave subsurface object detection by comparing with the conventional inversion procedure using an integral equation Green function based Born Approximation (GFBA). This electromagnetic scattering inverse algorithm is easily implemented and robust to the heterogeneity of the background.

Numerical experiments have been conducted for two types of 2-dimensional applications: 1) Multiple borehole antenna source and receiver configurations for the detection of buried objects in soil; and 2) Microwave breast tumor detection. In the former, the contrasting permittivity of dielectric contaminant pools near the ground interface scatterers the uniform background half-space field. In the latter, the antennas are immersed in coupling fluid surrounding an inhomogeneous dielectric breast model based on MRI measurements. This case tests the applicability of the inversion method in highly inhomogeneous background media.

REFERENCES

1. Dong, Q., H. Zhan, and C. Rappaport, "Efficient 3D finite difference frequency-domain modeling of scattering in lossy half-space geometries," *IEEE Antenna and Propagation Conference Proceedings*, 1789–1792, June 2007.

3D Microwave Imaging Utilizing Two Interleaved Antenna Arrays: Initial Phantom Results

Paul M. Meaney[1], **Qianqian Fang**[2], **Sherri D. Geimer**[1]
Margaret W. Fanning[1], **Tian Zhou**[1], **and Keith D. Paulsen**[1]

[1]Thayer School of Engineering, Dartmouth College, Hanover, NH, USA
[2]Martinos Center for Biomedical Imaging, Massachusetts General Hospital
Charlestown, MA, USA

Abstract— For several decades, researchers have been investigating near field microwave imaging for a variety of non-invasive applications where the recovered dielectric properties of a target under test can provide valuable diagnostic information such as breast cancer detection and temperature monitoring during thermal therapy. While numerous approaches that have involved important approximations have been attempted over the years, the ultimate goal is to provide full 3D renderings of the target zone. The previous approximations have included 2D imaging strategies and other algorithm approximations such as the Born and Rytov approximations and were often used because of various practical restrictions such as fixed amounts of measurement data and computational limitations. Regardless of these barriers, progress has still been achieved to the point where full 3D imaging is becoming viable.

We have developed a data acquisition system that is a hybrid of a multi-channel microwave measurement system with a monopole antenna array mechanical motion device to acquire a full complement of 3D data from around a target. The antennas are arranged on two separate, interleaved arrays which can move independently. This allows for the full complement of in-plane data at all of the vertical positions, but also allows for a substantial amount of cross-plane data, especially for cases where the separate arrays are at different heights. Previous studies have shown that the addition of this cross plane data is important to the overall image quality. Advances in the data acquisition hardware make it possible to acquire the data in only a few minutes with this hybrid approach. In addition, we have also implemented a full 3D, Gauss-Newton reconstruction algorithm which utilizes both the FDTD approach for the forward problem solution at each iteration and the adjoint method for constructing the Jacobian matrix as techniques for substantially reducing the overall computational expenses. While the current computations now require a few hours on a 4-node multi-processor machine, these costs are already quite reasonable and will certainly come down with further algorithmic improvements and hardware advances such as the use of GPU processors and larger processor clusters.

Finally, we present initial 3D imaging results from real measured data from our new system. In general the recovery of the multi-target object is quite good with a considerable reduction in artifacts above and below the planes of the targets compared with those for our 2D algorithm. These had previously been attributed to 3D effects that could not be accounted for in the 2D approximations. Overall the results are encouraging and bode well as we work towards applying microwave imaging to other medical and commercial applications.

ACKNOWLEDGMENT

This work was sponsored by NIH/NCI Grant # PO1-CA080139.

Session 2A5
Poster Session 1

An Analysis of the Landau-Lifshitz Reaction Term in Classical Electrodynamics

G. Ares de Parga
Dpto. de Física, Escuela Superior de Física y Matemáticas
Instituto Politécnico Nacional
U.P. Adolfo López Mateos, Zacatenco, C.P. 07738, México D.F., México

Abstract— Since Dirac obtained the so named Lorentz-Dirac equation [LD] as the equation of motion for a charged point particle, it has generated many discussions about its validity. Indeed, the runaway solutions, the preaccelerations, the renormalization of the electron's mass and the violation of physical causality by the use of the advanced solutions of the Maxwell equations, are the main reasons for the long historical discussion about the LD equation. This unsatisfactory situation is evidenced by the continued appearance of new equations of motion in the literature.

By using a first order approximation of the LD equation, Landau and Lifshitz obtained an equation within the frame of classical electrodynamics, the Landau-Lifshitz equation [LL]. Spohn has claimed that the LL equation can be obtained with the same degree of accuracy than the LD equation. Rohrlich has noticed that LL equation is a second order differential equation which doesn't permit runaway solutions or preaccelerations. It is important to note that Ares de Parga has proposed a physical deduction of the LL equation which implies a change in the concept of the radiation rate of energy; that is: the regular LD reaction term is substituted by the LL reaction term. In the present work, we analyze the different situations where the LL reaction term vanishes. In these cases, the LL equation of motion coincides with the Lorentz equation. We propose some physical interpretations in order to understand the absence of radiation rate of energy in such situations.

Electrical Resistivity Measurements and Behavior of High T_c Super Conductor by Using Bi-Pb-Sr-Ca-CuO System

M. M. Ahmed, **Mumtaz Humayun**, **N. M. Memon**, **and I. Sajid**
Department of Electronic Engineering, Mohammad Ali Jinnah University, Islamabad, Pakistan

Abstract— Two batches of Bi-based Superconductor samples were prepared by solid-state reaction method. All samples were cooled slowly in air. Samples were sintered for 120 hours. The samples were quenched in liquid Nitrogen. The Electrical resistivity measurement showed that the sample sintered at (77) °C for 72 hours had the best T_c. The T_c was found near 144 K. But the sample Sintered at (800±5) °C for 92 hours had lower T_c as sintered at (870) °C, and show the semiconductor behavior. *X-ray* diffraction study showed that the samples were multi-phased.

Analytical Method for Strip Line and Coplanar Waveguide on Compound Substrate

N. Ishimaru[1], **T. Fukuda**[1], **K. Wakino**[1], **Y. D. Lin**[2], **C. W. Kuo**[3], **and T. Kitazawa**[1]

[1]Department of Electrical & Electronic Engineering, Ritsumeikan University, Japan
[2]Institute of Communication Engineering, National Chiao Tung University, Taiwan, R.O.C.
[3]Department of Electrical Engineering, National Sun Yat-sen University, Taiwan

Abstract— An efficient analytical method is presented for the shielded strip line and coplanar waveguide (CPW) on a compound substrate (Fig. 1). The method is based on the extended version of spectral domain method [1, 2]. Fields in the inhomogeneous compound substrate are expanded in terms of the specific eigen functions, which ensure the continuity conditions between the constituent dielectrics of substrate and satisfy the biorthogonal relation over the whole compound substrate region. Then fields in the compound substrate as well as air region can be transformed into spectral domain, where Green's functions are derived easily and fields can be related to the source aperture fields. The line parameters of strip line and CPW are derived in the stationary expressions [3], and the numerical values are insensitive to the deviation in the unknown aperture fields. The accurate numerical values can be obtained by expanding the aperture fields in terms of a small number of basis functions. Fig. 2 shows the effective dielectric constant of strip line on the dielectric substrate of finite width.

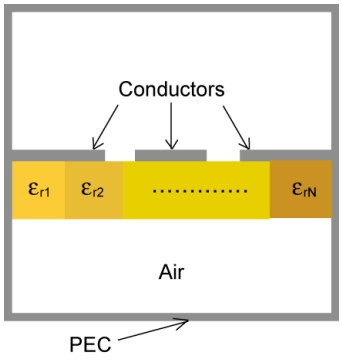

Figure 1: Coplanar waveguide on compound substrate.

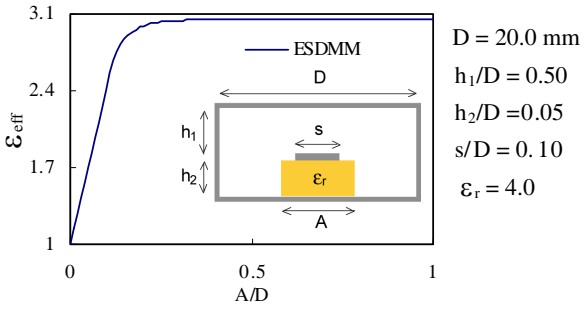

Figure 2: Effective dielectric constant of strip line on the dielectric substrate of finite width.

REFERENCES

1. Kariya, N., Y. Uematsu, and T. Kitazawa, "An efficient full-wave analysis of lossy transmission lines with anisotropic media," *28th European Microwave Conference Proceedings*, 283–288, Feb. 1998.
2. Shiraishi, T., K. Wakino, T. Nishikawa, and T. Kitazawa, "An efficient analysis of lossy discontinuities in waveguide by using extended spectral domain approach combined with mode matching method," *2002 Asia Pacific Microwave Conference Proceeding*, Vol. 1, 73–76, Nov. 2002.
3. Kitazawa, T., "Metallization thickness effect of striplines with anisotropic media: Quasistatic and hybrid-mode analysis," *IEEE Trans. Microwave Theory Tech.*, Vol. 37, 769–775, Apr. 1989.

Variational Method of Strip Lines on an Inclined Substrate

T. Fukuda[1], **N. Ishimaru**[1], **K. Wakino**[1], **Y. D. Lin**[2], **C.-W. Kuo**[3], **and T. Kitazawa**[1]

[1]Department of Electrical & Electronic Engineering, Ritsumeikan University, Japan
[2]Institute of Communication Engineering, National Chiao Tung University, Taiwan, R. O. C.
[3]Department of Electrical Engineering, National Sun Yat-sen University, Taiwan

Abstract— A variational method is presented for the analysis of strip lines on an inclined substrate (Fig. 1). The effective dielectric constant of the transmission line was analyzed by using the method of lines [1]. The stationary expressions of the line parameters, C and L, are derived in the present manuscript for the first time based on extended spectral domain approach (ESDA). The procedure is quite versatile, and is applicable to the various structures. Eigen functions are introduced in the combined region of air and dielectric substrate, and they satisfy the biorthogonal relation which opens the way for the spectral representation of the fields in the inhomogeneous region. The basis functions for the unknown aperture fields take the edge singularities into consideration, and the accurate numerical values can be obtained by using a small number of basis functions. The numerical results are verified by comparing the values by finite element method (FEM) for different dielectric constants of substrate (Fig. 2). The effect of the inclined substrate on the characteristic impedances and phase constants can be investigated numerically.

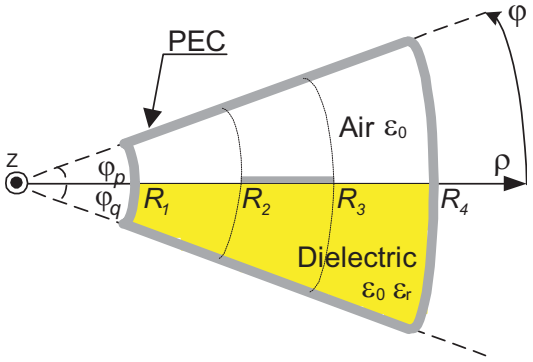

Figure 1: Strip lines on an inclined substrate.

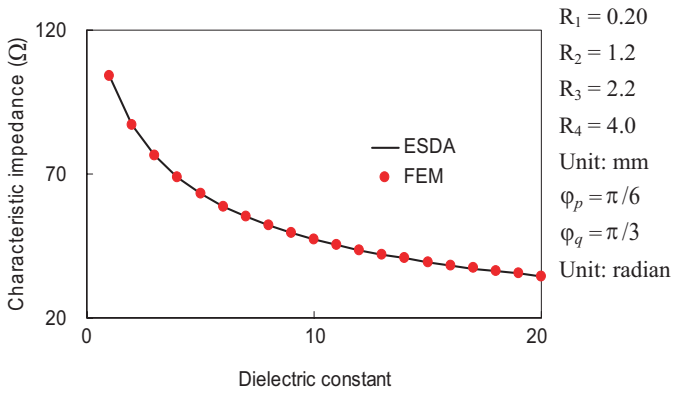

Figure 2: Characteristic impedances of strip lines on an inclined substrate.

REFERENCES

1. Tripathi, A., et al., "Method of lines for the analysis of microstrip structures on inclined plane," *Electronics Letters*, Vol. 32, No. 2, 123–125, January 18, 1996.

Propagation, Time-reversal and Gain-removal Stabilization in Dispersive Media

Maryam Jalalinia and Carey M. Rappaport
Gordon Center for Subsurface Sensing and Imaging
Department of Electrical and Computer Engineering
Northeastern University, Boston, MA, USA

Abstract— Propagation in dispersive media has been a research subject of interest for many years. Time reversal in these kinds of media is an interesting subject in a variety of inverse problems such as biomedical or environmental applications. The first thing in addressing these problems is defining an accurate model for dispersive material which is valid in a wide range of frequency.

In our work, a new accurate parametric rational Z-transform conductivity model, called Four-zero, is developed and implemented in FDTD to solve both forward and reverse propagation problems in dispersive media. One of the challenging issues in developing a new propagation model is its stability. In FDTD algorithm, all media, lossless or lossy, are subjected to Courant stability condition which determines the lower bound on spatial grid spacing in terms of time steps. In dispersive media, we are faced with a more restricted stability condition of Von-Neumann type, which should be solved analytically in z-plane and plays a significant role in choosing the model parameters with optimized stability. We address this issue by a comprehensive stability analysis.

We develop a time-reversal method to predict the propagation in dispersive media modeled by our Four-zero conductivity model. The inherent instability in the reversal algorithm necessitates a stabilization technique. A novel comprehensive gain-removal method is developed for implementation in various media, lossless or lossy, non-dispersive or dispersive, for forward propagation as well as time reversal. This technique removes the requirement to satisfy the stability condition.

The gain-removal method is based on the fact that in any medium (lossless or lossy) with spatial and temporal gridding parameters exceeding stability condition, we can enforce gain-removal (amplitude attenuation) to the traveling wave to stabilize the propagation. This results in a new set of stable wave equations for electric and magnetic fields which can be solved computationally. At the last step, removed gain can be inserted directly by multiplying the amplitude by the gain.

The numerical results indicate the successful application of the new Z-transform modeling of dispersive materials by Four-zero rational formulation in implementation of forward and reverse FDTD algorithm with gain-removal stabilization technique.

Validation and Calibration of a 3D Deterministic Simulation Software for Indoor Electromagnetic Propagation

Marco Allegretti, **Claudio Lucianaz**
Riccardo Notarpietro, **and Giovanni Perona**
Electronics Department, Politecnico di Torino
C. so Duca degli Abruzzi 24, Torino 10129, Italy

Abstract— Accurate and validated electromagnetic simulation tools are nowadays needed in order to plan third generation cellular telecommunication services. In particular, some applications require an highly reliable radio coverage even inside buildings, with an eye to emission levels imposed by national laws and electromagnetic compatibility problems.

This work shows the results of indoor measurement campaigns carried out at UMTS frequency band with a cheap and automated measurement chain. Measurements were then used to validate a deterministic simulation software based on 3D ray tracing and were performed both in a furnished apartment built up by brick walls and concrete structure and in a new and still unfurnished office characterized by light and sound isolating walls.

The environments above described characterize the typical ones that engineers face out when they are planning new networks; in addition, pieces of information about the electromagnetic properties of wall, ceiling and floor materials are required by the simulation software.

So, measurement campaigns were performed in order to characterize the electromagnetic propagation in indoor environment and were then compared to the output obtained by the simulation software.

In both measurement environments a continuous wave transmitter, tuned at 2 GHz, equipped with an omnidirectional antenna was used. The receiver was realized with an inexpensive solution: a discone antenna connected to a Spectrum Analyzer controlled via GPIB interface, a notebook used as automated data logger and an optical mouse (with an ad hoc mechanical support and dedicated software based upon modified operating system drivers) to acquire the exact position for every measurement points starting from a known location.

Such inexpensive solution allows a measurement speed of 10 cm/second, adequate for an indoor environment, and measurements are directly associated via software to the positions acquired by the optical system (mouse).

Measurements highlighted sensitive differences in propagation characteristics on the base of the different materials used in building up the internal walls (as a matter of fact, penetration losses are quite susceptible with respect to the wall materials and the ray tracing approach is based on such feature to estimate the reflected signals ray by ray). So, since different characteristics of building materials impact on propagation phenomena, the consequences were immediately evident when comparing measurements and simulations.

The environment characterized by brick and concrete walls pointed out higher reflection levels and the trends of simulations followed well enough the measurements. Instead, since the newest building techniques create walls characterized by a low penetration loss, simulations weren't so accurate since the simulation software doesn't take into account eventual direct contribution got by transmission through walls: a systematic, almost constant, underestimation of simulations was put into evidence in such cases and simulations needed to be at least unbiased in order to get an acceptable agreement with measurements.

Finally, it was put into evidence that the contributions of pieces of furniture is not so important as one can think at a first approach.

Convergence of Krylov Solvers and Choice of Basis and Weighting Set of Functions in the Moment Method Solution of Electrical Field Integral Equation

G. Angiulli and S. Tringali
DIMET, Univ. Mediterranea, 89100 Reggio Calabria, Italy

Abstract— In Computational Electromagnetics, iterative techniques for solving algebraic linear system of equations are of fundamental importance, since actual problems give rise to linear systems too large to be practically solved by direct methods. There exists much study regarding the numerical aspects of such problems, but it's not clear at all how the efficiency of iterative solvers are conditioned by the choosing of the basis and weighting functions in the Moment Method (MoM) [1, 2]. In this work we investigate as performances of some major Krylov subspace iterative solvers, i.e., GMRES and LSQR, and CG-like techniques, namely MINRES and BiCG, are affected by different choice of these set of functions, pointing out as their convergence is highly dependent on this choice, which actually distinguish a particular implementation of the MoM from all the (theoretically) innumerable others. Specifically, we consider the algebraic linear system of equations $\mathbf{ZI} = \mathbf{V}$ obtained by reducing the integral equations from the TM_z scattering of a plane wave by an ideal metallic body using MoM exploiting subdomain basis and weight functions of varying amplitude [3]. It can be observed that exists a critical threshold δ_0 such that, whenever either the basis or the weight pulses are given with an amplitude greater than δ_0, then the total number of internal loops necessary for taking the relative residual under a definite tolerance $\epsilon > 0$ increases all of a sudden, in such a dramatic way that it can even prevent the convergence of the selected Krylov solver. Finally, we try to explain this numerical behavior by inquiring into the spectral properties of both the starting integral equation and the impedance matrix $\mathbf{Z}$.

REFERENCES

1. Klein, C. A. and R. Mittra, "The effect of different testing functions in the moment method solution of thin-wire antenna problems," *IEEE Trans. on Antennas and Propagation*, 258–261, March 1975.
2. Peterson, A. F., C. F. Smith, and R. Mittra, "Eigenvalues of the moment-method matrix and their effect on the convergence of the conjugate gradient algorithm," *IEEE Trans. on Antennas and Propagation*, Vol. 36, No. 8, 1177–1179, 1988.
3. Harrington, R. F., *Field Computation by Moment Methods*, Krieger, Malabar, FL, 1982.

An Improved Finite-difference Scheme for Parabolic Partial Differential Equations by Localized Conduction Coefficients

Y.-P. Chiou[1,2] and C.-H. Du[1]

[1]Graduate Institute of Photonics and Optoelectronics
National Taiwan University, Taipei 10617, Taiwan
[2]Department of Electrical Engineering
National Taiwan University, Taipei 10617, Taiwan

Abstract— We propose an improved finite-difference scheme to enhance the accuracy of parabolic partial differential equations (PDE) by using localized conduction coefficients. The scheme is applied to laser beam propagation in free space under paraxial approximation. Our results shows the accuracy are greatly improved when the conduction coefficients are predicted or estimated. The accuracy enhancement is obtained with minor modification in the implementation. Such scheme can easily be applied to parabolic PDE with location dependent properties. We will demonstrate several applications based on this scheme in our poster.

Simulation of Relevant Process Variables for Electrochemical Etching

R. Neugebauer, **H. Knüpfer**, **K. Wolf**, **and H.-J. Roscher**
Fraunhofer Institute for Machine Tools and Forming Technology IWU
Chemnitz, Germany

Abstract— The process of electrochemical etching requires the existence of an electrolytic bath and two electrodes with a certain distance in between, which is called the gap width. For an intensive etching process the gap between the electrodes should vary over short periods. The increase of the gap provides the possibility to rinse the removed material.

Material which is ablated by the process of electrochemical etching in an electrolytic bath must be removed by rinsing. A periodic expanding of the working gap between electrode and work piece is essential for an intensive etching process. The duration of the rinsing process should be kept short for the reason of efficiency. Small working gaps lead to high contour accuracy during the etching process itself. The arising process forces reach to kilo Newton range. Thereby, a short circuit between electrode and work piece must be avoided. By the usage of new high dynamic actuators instead of powered drive solutions a profile of the electrode movement could be realized, which is better adapted to the process requirements. This article introduces a Simulink® model (under simplifying assumptions) for the determination of relations between the movement of the electrode and the arising forces in the working gap. The results are fundamental input data for dimensioning of actuating elements.

State-of-the-art for the adjustment of the gap size is to use a powered drive. A motor-driven tappet provides a sinusoidal curve of the gap width over time. A rectangular-shaped gap over short periods would be optimal. Moreover, the motor-driven approach requires large electrical engine power and high effort for the positioning accuracy of the tiny etching gaps. To overcome these problems high dynamic actuators, for example piezo-stacks, can be used because they can act with relatively high frequency and high accuracy while providing high reaction forces and the necessary stroke.

To prove the usability of different actuators simulations were done, which are introduced in the first section. This section also introduces the physical model of the system from which the differential equations and the Simulink® model are derived. The behavior of the system and conclusions concerning dimensioning of certain input parameters are discussed in the following section. Finally, the last section provides conclusions and an outlook.

As the simulations show, the realization of a piezo-based vibration drive is very promising. Since the estimated spring stiffness of the piezo actuator as well as the electrode mass are realistic values, they are retained. The working gap can be forced to be relatively constant caused by the nonlinear system properties and by applying a drive frequency which is advantageous to the resonance frequency. Additionally, a trapezoid excitation performed by the piezo actuator is reasonable to achieve the desired gap shape. The large reaction forces limit the minimal working gap to approximately 10 micrometer at relatively small electrode shell areas. The resulting opened gap should be large enough for the rinsing.

The next step is to verify the simulation results by doing measurements of the system. On basis of the results the model can be improved by considering the masses of the actuator and the linear drive as well as its stiffness. Additionally, the shell area can be calculated depending on the gap width and the real dynamic viscosity of the liquid should be used.

Using Cavity Complexity to Reduce the Number of Traced Tubes Required in Predicting Backscatter

Saeed M. Khan
Kansas State University at Salina, 2310 Centennial Avenue, Salina, KS 67401, USA

Abstract— When the geometrical optics aperture integration (GO-AI) is used to study cavity backscatter, ray tubes are traced from the opening through the cavity and back to the opening. This procedure is commonly known as shooting and bouncing (SBR) requires that the incident field be collimated into tubes of equal cross section on entry. The field distribution on the exiting ray tubes will depend on the divergence or convergence of the rays surrounding the tube (2 rays for 2-D and a minimum of 3 rays for 3-D tracing) and also the material properties of the coating inside the cavity. The aforementioned field distributions are used to find backscattered fields using an aperture integration technique. The monostatic backscatter from the cavity is the sum of the contributions from all exiting tubes. The number of ray tubes used increases drastically with the size of the inlet. Computational efficiency of such a scheme can be greatly enhanced by reducing the numbers of ray tubes that need to be traced. A 2-D GO-AI [1] investigation has revealed that fewer numbers of tubes need to be traced for cavities which have been defined to be simpler (or less complex) based on the divergence average of the rays that surround each tube. By shooting a small number of tubes through a cavity at randomly spaced intervals (at an arbitrarily selected angle of incidence), the average divergence can be calculated. Using this technique, a single offset bend (8.7λ opening) can be shown to have less average divergence than a double offset bend (8.7λ opening as well). It can also be shown that the single bend requires less number of tubes per wavelength to correctly predict backscatter from the cavity. This paper will investigate further the effectiveness of the technique described by studying curved cavities and offset bend cavities coated with dielectric materials on the inside. All GO-AI RCS data will be verified by comparing the results obtained from a hybrid modal technique.

REFERENCES

1. Khan, S. M., "Reducing the numbers of ray tubes used in cavity backscatter studies," *IEEE AP-S International Symposium on Antennas and Propagation and USNC/URSI National Radio Science Meeting*, Albuquerque, New Mexico, USA, July 9–15, 2006.

Singular Analytical Integration for Efficient Volume Integral Equation Implementation

F. J. Pérez Soler[1], **F. D. Quesada Pereira**[1], **A. Alvarez Melcon**[1], **and L. Peregrini**[2]
[1]Technical University of Cartagena, Campus Muralla del Mar s/n, Cartagena 30202, Spain
[2]University of Pavia, Strada Nuova 65, Pavia 27100, Italy

Abstract— The volume integral equation technique is a widely used formulation for the analysis of a large class of problems containing dielectric objects of finite dimensions and complex shapes. In this type of problems, Green's functions can not account for the dielectric objects in a semi-analytic fashion, and one has to resort to the use of the well known free-space Green's functions. With this formulation the dielectric objects are modeled with the aid of polarization currents defined on their volumes. The subsequent application of the Method of Moments (MoM) requires the computation of overlapping integrals between the free space Green's functions and the basis and testing functions. An interesting feature when developing this approach, is that surface charge distributions appear at the outer surfaces of homogeneous bodies. As a result, several combinations of surface and volume integrals need to be computed, before filling up the complete MoM matrix system.

One of the main difficulties in the implementation of this formulation is the integration of the coincident basis and testing cells. This is because of the well known singularity of the potential Green's functions. To overcome this problem, integration techniques based on polar and spherical coordinates have been developed in the past [1]. Also, singularity extraction techniques have been applied. They are mainly based on the extraction of the singular behavior of the Green's functions, splitting the whole contribution in static and dynamic parts. The dynamic part thus obtained is not anymore singular, and it can be integrated numerically without effort. What remains, then, is the calculation of the static terms, containing the singular behavior of the Kernel.

In this contribution we have derived an efficient implementation of the volume integral equation approach. The technique is based on applying a Taylor series expansion to the free-space Green's functions. Following this procedure, we demonstrate that not only the singularity is extracted, but also the discontinuities in the spatial derivatives are eliminated. In this way, the integration of the dynamic term is further simplified. Second, analytical integration is applied for the static singular terms. This increases accuracy, and reduces considerably the computational cost. The analytical integration is based on the dyadic identities reported in [2], which are extended for the first time to account for volume integration, and mixed surface-volume interactions, in rectangular and hexahedral domains.

In order to show the efficiency of the new analytical approach, let us consider an example case of the electric scalar potential contribution in the analysis of a shielded microstrip line. The substrate has been discretized using rectangular prisms (a total of 2220 unknowns are used in

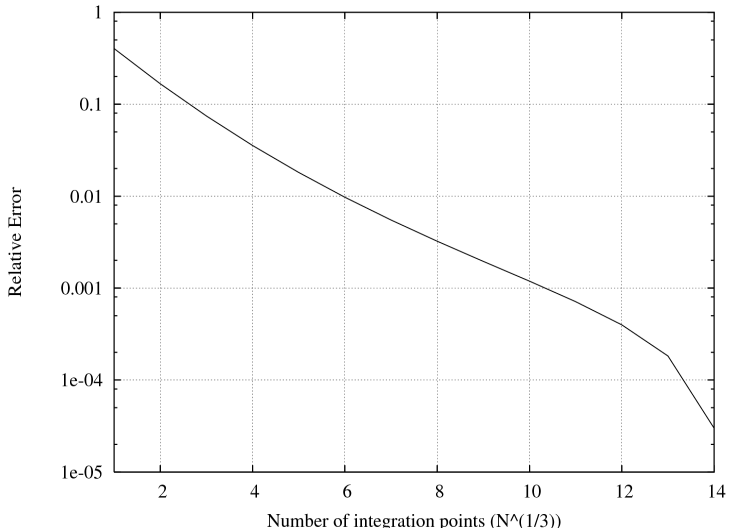

this problem). We present in the Figure the error obtained for the volume interactions computed by the spherical transformation algorithm, as compared to the closed-form solution obtained with the analytical expressions derived in this work. It can be noticed in the figure that errors below 10^{-3} are obtained when more than 10^3 points are used in the numerical integration. When 14^3 points are used, the total static MoM matrix needs 7.2 minutes to be computed, whereas only 17.1 seconds are needed when using the proposed analytical approach.

REFERENCES

1. Pereira, et al., "Analysis of finite microstrip structures...," *Radio Science*, Vol. 40, RS1004, January 2005.
2. Arcioni, et al., "On the evaluation of the double surface integrals...," *IEEE Trans. Microwave Theory and Techniques*, Vol. 45, No. 3, 436–439, March 1997.

A Study on the Interference in Single Frequency Network and On-Channel Repeater

Sung-Woong Choi and Heon-Jin Hong
ETRI-Radio & Broadcasting Technology Lab., Radio Technology Department
161 Kajong-Dong, Yusong-Gu, Taejon 305-350, Korea

Abstract— In digital TV, SFN (Single Frequency Network) and OCR (On-channel Repeater) are often considered for the efficiency of frequency allotment. Both of them broadcast using the same frequency. In this paper, we discuss the performance and evaluate some coverage criterions for SFN and OCR. Also, we propose method and simulation for coverage planning and estimation.

A Novel Ultra-wideband Bandpass Filter

I-Tseng Tang[1], **Ding-Bing Lin**[2], **Chi-Min Li**[3], **and Min-Yuan Chiu**[3]

[1]Department of Environment and Energy, Nation University of Tainan, Tainan, Taiwan
[2]Institute of Computer and Communication Engineering
National Taipei University of Technology, Taipei, Taiwan
[3]Department of Communications and Guidance Engineering
Nation Taiwan Ocean University, Keelung, Taiwan

Abstract— A novel and compact ultra-wideband band-pass filter with a fractional bandwidth (FBW) of about 110% is proposed. The filter is based on a circuit model using hybrid bended microstrip and five quarter-wavelength short-circuited stubs, and using double reverse U-shaped defected ground structure (DRU-DGS) provides attenuation pole to suppress the second spurious harmonic. The proposed filter had a good performance, including an ultra-wideband bandpass (3.1–10.6 GHz), a small size and sharp rejection. The filter also demonstrated an UWB reject band from 12.2 GHz to more than 20 GHz at −20 dB.

Introduction: In early 2002, the U.S. Federal Communications Commission (FCC) approved the unlicensed use of ultra-wideband (UWB) (range of 3.1–10.6 GHz) for commercial purposes. Recently, the development of new UWB filters has increased via different methods and structures. Although most of these ultra-wide-band band-pass filters are suitable for use in practice, existing radio signals such as wireless local-area network (WLAN) that operate at high frequencies may interfere with the ultra-wideband radio system within the range defined by the FCC.

Design Concept and Improvement: Figure 1(a) shows the conventional filter using hybrid microstrip and quarter-wavelength short-circuited stubs. To reduce the size of the conventional filter, the microstrip line was bent as a hexagon, and also these quarter-wavelength short-circuited stubs are all connected to one common via-hole, as shown in Fig. 1(b).

(a) (b)

Figure 1: (a) Traditional quarter-wavelength shorted-circuited stubs filter circuit model, (b) Structure of the proposed UWB filter.

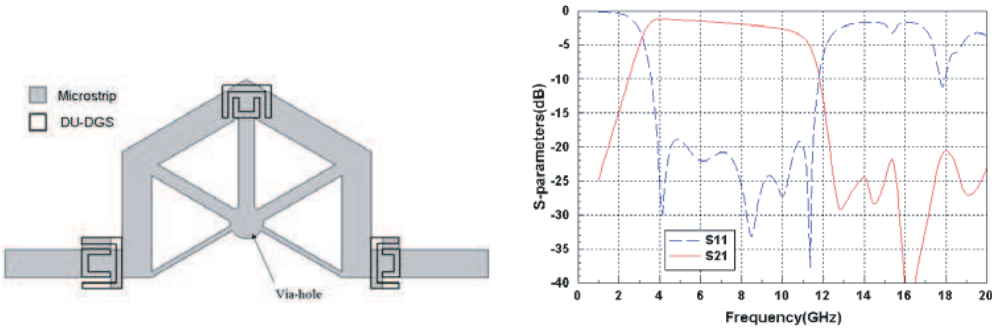

(a) (b)

Figure 2: (a) Structure of the proposed UWB filter with DRU-DGS, (b) Simulation of the proposed UWB filter.

In view of in the harmonic suppression design of the microwave bandpass filters, some many forms were proposed. From the defected construction equivalent circuit, we may know the band-

rejectional frequency of a defected construction mainly is controlled by the inductance and capacitance values. The double reverse U-shaped defected ground structure (DRU-DGS) was employed effectively for suppressing the harmonic resonance of the bandpass filters, since it can be implemented with a small dimension and controllability of the provided band-rejection. Fig. 2(a) shows the novel proposed UWB bandpass filter with the DRU-DGS. This structure has a good performance in passband and a wide stopband in the out-of-band. Fig. 2(b) shows the simulated S-parameters performances of the novel proposed UWB bandpass filter with the DRU-DGS.

REFERENCES

1. Hong, J. S. and H. Shaman, "An optimum ultra-wideband bandpass filter with spurious response suppression," *IEEE Wamicon*, 1–5, Dec. 2006.
2. Ting, S.-W., K.-W. Tam, and R. P. Martins, "Miniaturized microstrip lowpass filter with wide stopband using double equilateral U-shaped defected ground structure," *IEEE Microw. Wireless Compon. Lett.*, Vol. 54, No. 6, June 2006.

Design of the Broadband Filter Using Dual-mode Resonator

Jin-Sup Kim, **Se-Hwan Choi**, **and Kyu-Bok Lee**
Wireless Communication Research Center, Korea Electronics Technology Institute, R. O. Korea

Abstract— The broadband suspended substrate filter is proposed and implemented using dual-mode resonator, aiming at transmitting the signals in the passband of 10–18 GHz. It is composed of two quarter-wavelength resonators and shunt inductance. The shunt inductance is introduced to establish a strong magnetic coupling between two quarter-wavelength resonators. After optimization of this filter, a good bandpass behavior with transmission poles is theoretically realized and experimentally confirmed. Within the whole bandpass filter passband, the return loss is found higher than 11 dB, and the insertion loss is less than 1.9 dB.

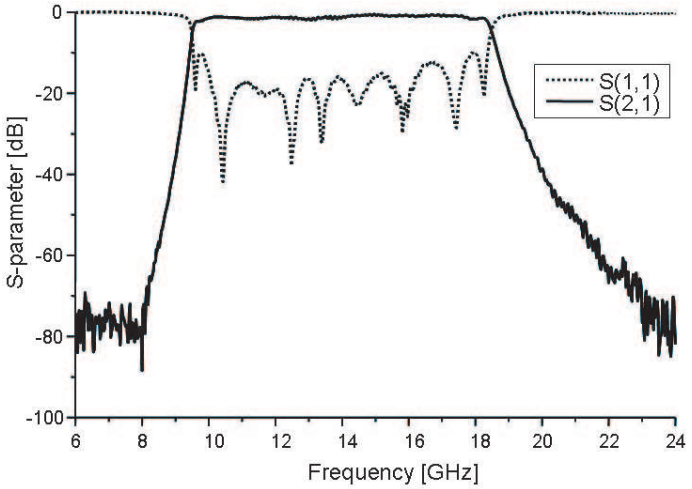

Figure 1: Measured results of suspended substrate filter.

REFERENCES

1. Rhodes, I. D., "Suspended substrate filters and multiplexers," *Proceedings of 1986 European Microwave Conference, 16th EuMc*, 8–18, 1986.
2. Kim, J. S., N. S. Kim, W. G. Moon, S. G. Byeon, and H. S. Shin, "A novel broadband suspended substrate stripline filter using resonators with T-shaped open-circuited stubs," *IEEE MTT-S Int. Microw. Symp. Dig.*, 917–920, June 2007.

The Non-homogeneity of Permittivity in Microwave Dielectric Resonator

Victor N. Egorov
Eastern-Siberian branch of FSUE "VNIIFTRI", Russia

Abstract— The high precision measurements of permittivity were performed for thermostable ceramic microwave dielectric resonators on frequency range 3–10 GHz. The "dielectric post resonator" method [1, 2] was applied for measurements by using scalar network analyzer with frequency resolution 1 Hz. In measurements the cylindrical specimen (dielectric resonator) was placed closely between two flat copper mirrors with diameter 116 mm. The excitation of H_{0mp} modes was performed by semirigid coaxial cables with loop on end. Resonator transmission coefficient $\log|S_{12}|^2$ has been tuned to meaning less -30 dB. The ceramic specimens ♯1, 2, 3, 4, 5 with permittivity ε about 9.7, 30, 39, 58, 98 and single crystal of sapphire has been measured by this method. The results of measurements with expanded uncertainty are given in paper. Measured mean ε of the each ceramic specimen has the different values for operating resonance modes H_{0mp} with different radial index m and axial index p, which have different value of filling factor $K_{1E} = W_{1E}/W_{\Sigma}$, where W_{1E}, W_{Σ}-electrical energy in specimen and complete energy of resonance. The value of K_{1E} was limited as $0.992 < K_{1E} < 0.9999$ in this measurements.

On each resonance frequency of H_{0mp} modes the expanded uncertainty of ε for each ceramic specimen is less than difference between max and min measured value ε or this specimen. The dependence $\varepsilon(K_{1E})$ for specimens 1 ($\varepsilon \approx 9.7$), 2 ($\varepsilon \approx 30$), 3 ($\varepsilon \approx 39$), 4 ($\varepsilon \approx 58$) and 5 ($\varepsilon \approx 98$) is given in paper. For these specimens the dependence $\varepsilon(K_{1E})$ may be explained, if specimens is not homogeneous and ε increase from the periphery to central part of specimen, especially, in radial direction. The dependence of measured value ε versus filling factor K_{1E} (Table 1) confirm that, because the increase of K_{1E} yields the decrease of strength E on cylindrical surface of specimen. The function $\varepsilon(K_{1E})$ is closely to linear and has the different relative slope for different specimens, what is correspondence to different power of radial dependence $\varepsilon(r)$. For example, the dependence $\varepsilon(K_{1E})$ for specimen 3 is more strong, than one for specimen 2 with closely sizes and for specimen 4, which has the less sizes. For the homogeneous single crystal of sapphire the dependence $\varepsilon(K_{1E})$ is absent.

Table 1: Measured ε on the modes H_{0mp} and filling factor K_{1E} for specimen 3 ($\varepsilon \approx 39$).

Index		$p = 1$	$p = 2$	$p = 3$
$m = 1$	ε	39.373	39.436	39.446
	K_{1E}	0.99647	0.99916	0.99969
$m = 2$	ε	39.291	39.389	39.412
	K_{1E}	0.99364	0.99803	0.99916
$m = 3$	ε	39.256	39.355	39.390
	K_{1E}	0.99199	0.99718	0.99864

REFERENCES

1. IEC 61388-1-3, Waveguide Type Dielectric Resonators — parts 1–3 General Information and Test Conditions — Measuring Method of Complex Relative Permittivity for Dielectric Resonator Materials at Microwave Frequency.
2. Egorov, V. N., "Resonance methods for microwave studies of dielectrics (review)," *Instruments and Experimental Techniques*, Vol. 50, No. 2, 143–175, 2007.

Genetic Algorithms Applied to Microwave Filters Optimization and Design

M. F. Jiménez Nogales, J. Pascual García, J. Hinojosa, and A. Alvarez-Melcón
Universidad Politécnica de Cartagena, Spain

Abstract— In [1], a group of experts estimated the state of microwave computer-aided design (CAD) in the year 2010. In a panel discussion, M. Mongiardo predicted much of the emphasis will shift to an optimization and design environment that allows integrated design. In this sense, we propose an alternative approach for the optimization of microwave filters based on Genetic Algorithms. It is known that the definition of a proper fitness function is essential to assure success in the Genetic Algorithm. Consequently, several fitness functions have been studied, as related to this convergence. First, we have used fitness functions defined with discrete target specifications (cut-off frequencies, rejection frequencies). In this case the distances from the target specifications and the real response have been defined using linear, exponential and sigmoid functions. We have observed that convergence can be improved with the sigmoid functions, if a proper slope constant is selected. Secondly, another class of fitness functions can be defined, if the target response is known at all frequency points. In the case of filters, this is possible using synthesis techniques for elliptic transfer functions, as for instance those reported in [2]. In this situation, we propose a new fitness function that has proven to be very robust. The new fitness function (F) is defined as:

$$F = a\Delta_{11}(PB) + b\Delta_{11}(RB) + c\Delta_{21}(PB) + d\Delta_{21}(RB) \tag{1}$$

where (a, b, c, d) are weighting coefficients, and $\Delta S_{11}(PB)$ is an average distance from the target and the real response, at all frequency points lying within the passband (PB) (the other parameters are defined in a similar way, with RB meaning the rejection band). For each frequency point, the distance is defined again using a sigmoid, which showed to exhibit the best convergence rate in the first part of the work.

To demonstrate the usefulness of the new fitness function, we present the evolution of the fitness for a population of 120 individuals and for a second order filter. We can observe the well behavior of the population, which does not saturate, presenting, along the whole population, a steady increment of the fitness.

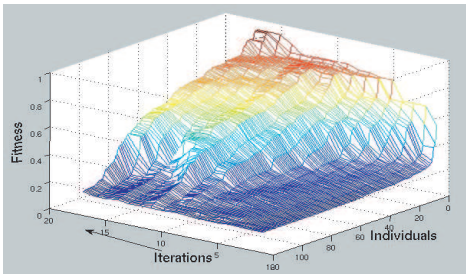

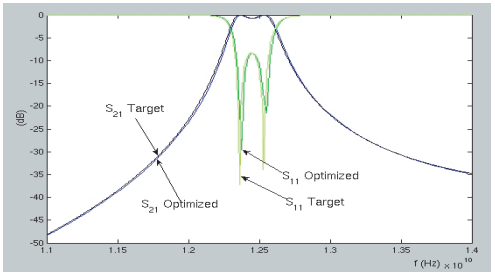

REFERENCES

1. Bootin, R. C., et al., "Microwave CAD in the year 2010 — A panel discussion," *Int. J. of RF and Microw. Comp.-Aided-Eng.*, Vol. 9, No. 6, 439–448, 1999.
2. Cameron, R. J., "Advanced coupling matrix synthesis technique for microwave filters," *IEEE Trans. Microw. Theory and Tech.*, Vol. 51, No. 1, 1–10, 2003.

Design of LTCC UWB Antenna with Band Notch Characteristic

Se-Hwan Choi, **Ho-Jun Lee**, **and Jong-Kyu Kim**
Korea Electronics Technology Institute, Republic of Korea

Abstract— The frequency range of UWB system is from 3.1 GHz to 10.6 GHz. However, there are several narrow band services that already occupy some parts of UWB band. In order to solve this problem, UWB antennas had better have a built-in band-pass filter. This structure can reduce interferences from near by WLAN standard 802.11a, which its frequency range is 5.725–5.825 GHz. Recently, the Ministry of Information and Communication (MIC) of Korea announces the frequency range of UWB systems that consists of low band (3.1–4.8 GHz) and high band (7.2–10.2 GHz). In this paper, we propose a compact UWB antenna with band-notch characteristic. To create the band-notch characteristic, the spoon-shaped slots are added in the monopole antenna. The proposed antenna is made by using low temperature co-fired ceramic (LTCC) process and fed by 50 ohm coplanar waveguide (CPW). This antenna is operating in the UWB spectrum from 3.1 to 10.6 GHz and has the stop band from 4.8 GHz to 6.3 GHz where VSWR is higher than 3. The size of this antenna is 15 mm∗15 mm∗1 mm.

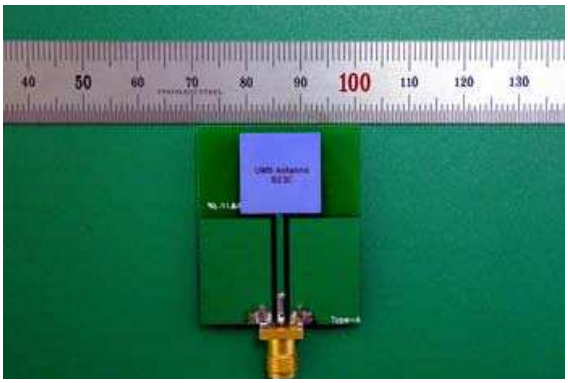

Figure 1: A fabricated antenna.

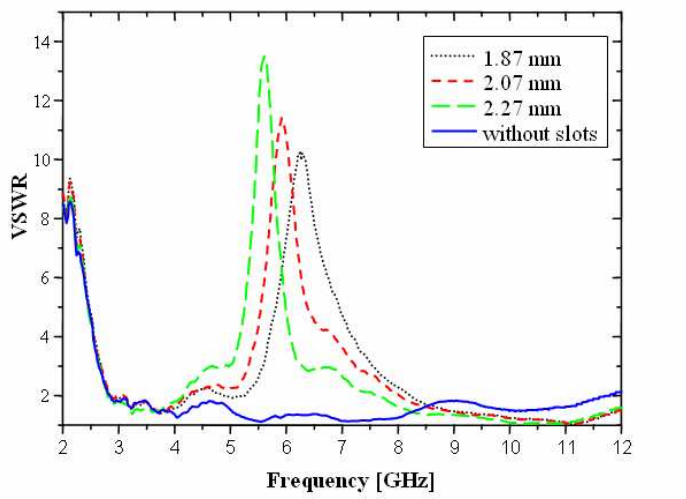

Figure 2: Measured VSWR for various length of slot.

Multi-scale Triangular Patch High Impedance Ground Planes to Improve the Bandwidth of Conformal Bow-tie Antennas — Fabrication

Bora Cakiroglu[1], **Peter J. Collins**[1]
Michael J. Havrilla[1], **Kubilay Sertel**[2], **and Andrew J. Terzuoli**[1]

[1]Air Force Institute of Technology
2950 Hobson Way WPAFB, OH 45433-7795, USA
[2]ElectroScience Laboratory, The Ohio State University
1320 Kinnear Rd., Columbus, OH 43212, USA

Abstract— Broadband, low-profile antennas, such as spirals, log-periodics, and bow-ties, substantially suffer in gain and bandwidth performance when they are brought close to a conducting surface. Thus, when standard broadband antenna designs are conformally placed on vehicle bodies, they can no longer achieve the high data rates required by modern communication and networking scenarios. A simple remedy for this has been to place an absorber lined cavity behind the antenna to preserve some bandwidth, at the expense of reduced gain. However, recently introduced high impedance ground planes (HIGPs) have novel electromagnetic features that have been shown to improve conformal antenna performance without the detrimental effects of absorber losses. In [1], thin metamaterial HIGP designs were incorporated into the antenna substrate to replace the lossy absorber layers, maintaining broadband characteristics and avoiding losses.

In this paper, we present a thin triangular-patch mushroom structure HIGP designed as a meta-substrate for a broadband bow-tie antenna. Specifically, two different-scale triangular-patch mushroom HIGP samples were analyzed and optimized using Ansoft's commercial full-wave solver (HFSS v.10). The sizes and periodicities were designed such that the two samples have band-gaps that appear success in frequency. Subsequently, we incorporated both designs into a single, multi-scale periodic HIGP, along with the active bow-tie antenna printed directly onto a RT/Duroid 5880 substrate to form the HIGP-antenna combinations. As seen in the figure, these designs were realized using the T-Tech Quick-Circuit system, and were characterized using an Agilent E8362B network analyzer.

We discuss the results of this characterization, and specifically show the advantages of the multi-scale HIGP in increasing the bandwidth of the conformal bow-tie designs.

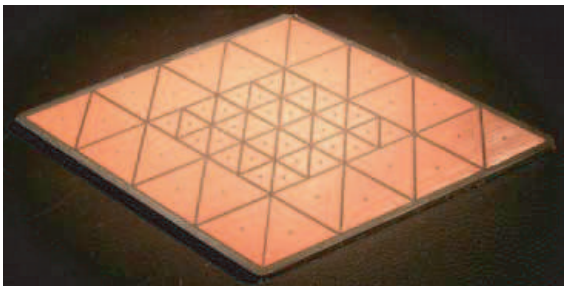

Figure 1: Conformal bow-tie antenna on a multi-scale triangular-patch HIGP.

REFERENCES

1. Sievenpiper, D. F., L. Zhang, R. F. J. Broas, N. G. Alexopolus, and E. Yablonovitch, "High-impedance electromagnetic surfaces with a forbidden frequency band," *IEEE Transactions on Microwave Theory and Techniques*, Vol. 47, 2059–2074, November 1999.

Improved Bandwidth Conformal Bow-tie Antennas Printed on Multi-scale Triangular-patch High-impedance Ground Planes — Simulation

Murat Dogrul[1], **Peter J. Collins**[1]
Michael Saville[1], **Kubilay Sertel**[2], **and Andrew J. Terzuoli**[1]

[1]Air Force Institute of Technology, Dayton, OH 45433, USA
[2]ElectroScience Laboratory, The Ohio State University, Columbus, OH 43212, USA

Abstract— Gain and bandwidth metrics of broad-band low-profile antennas severely deteriorate when they are placed conformally onto the conductive skins of air, sea, and ground platforms. This detrimental effect is primarily due to out-of-phase reflections from the conductive body interfering with the antenna's self radiation. Furthermore, lateral waves launched by the antenna couple into the thin substrate placed between the antenna and the platform, giving rise to surface waves resulting in significant diffraction from the edges of the substrate.

To remedy these two major mechanisms degrading antenna performance, high impedance ground planes (HIGP) were proposed in [1]. HIGPs made of a 2-dimentional periodic arrangement of a mushroom structure not only provide perfect-magnetic-conductor (PMC)-like reflection but also suppress the surface waves within the stop-band of the substrate modes. Thus, when the antenna is conformally placed over the HIGP, its gain is expected to double from the free-space value, due to in-phase reflections. Additionally, its bandwidth is expected to be as large as the band-gap of the mushroom structure, provided the original design has sufficient bandwidth to cover the band-gap of the HIGP.

Previously considered HIGPs were made of square-patch mushroom structures having a single periodicity. Here, we consider a multi-scale triangular-patch HIGP design. Element sizes can be chosen such that the band-gap of each periodic subsection is placed successively in frequency. The final multi-scale composite HIGP structure has increased band-gap, thus providing increased bandwidth for the conformal antenna. Furthermore, triangular mushroom elements provide a natural platform for the particular broadband antenna used in the bow-tie antenna design as shown in the figure.

We investigate the performance of the bow-tie antenna in free-space, on a conducting ground plane, on a PMC, and on the multiscale HIGP. Three HIGPs are considered, two having uniform periodicities with different scales, and one having the multiscale design. We present our simulation results (using Ansoft-HFSS v.10) and demonstrate the performance of the broadband, conformal bow-tie antenna placed over the multiscale HIGP.

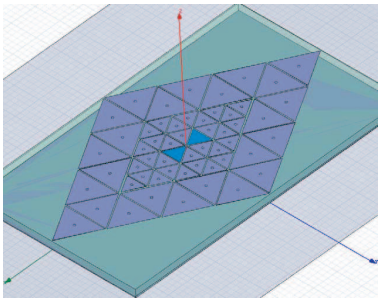

Figure 1: Bow-tie antenna inside multi-scale HIGP.

REFERENCES

1. Sievenpiper, D., L. Zhang, R. F. J. Broas, N. G. Alexopolous, and E. Yablonovitch, "High-impedance electromagnetic surfaces with a forbidden frequency band," *IEEE Trans. on Microwave Theory Tech.*, Vol. 47, No. 11, 2059–2074, November 1999.

Design of Wideband Antenna with Resistive and Capacitive Loading

Sangbong Jeon and Chang-Hoi Ahn
Yeungnam University, Korea

Abstract— The ground penetrating radar (GPR) has been employed in a wide range of applications such as detection of landmine or shallowly buried object in ground. It means short-range radar systems. As targets are mostly located in the near of intermediate zone, the near-field characteristics of the antenna are important. A GPR that operates in the time domain make produce the late-time ringing because it should be able to transmit in ultra-wide bandwidth. The late-time ringing is oscillations that follow the transmitted pulse. The oscillations are caused by the internal reflections between the feed and the open ends of the antennas. To transmit the pulse without late-time ringing, the resistive loading is a useful technique to suppress late-time ringing [1]. However this technique drops radiation efficiency because of dissipating currents. Also to avoid this drawback the use of non-dissipative reactive loading has been proposed which is capacitive loading realized on a planar structure such as a bow-tie antenna with a slot perpendicular to the current direction [2]. However in the case of a microstrip antenna with a narrow strip, the slot has low capacitance. As an alternative we introduce strip fingers to load high capacitance. The geometry of the antenna under consideration is depicted in Fig. 1. The resistive graphite strips suppresses the late-time ringing and the capacitive loading technique using strip finger improves the radiation efficiency.

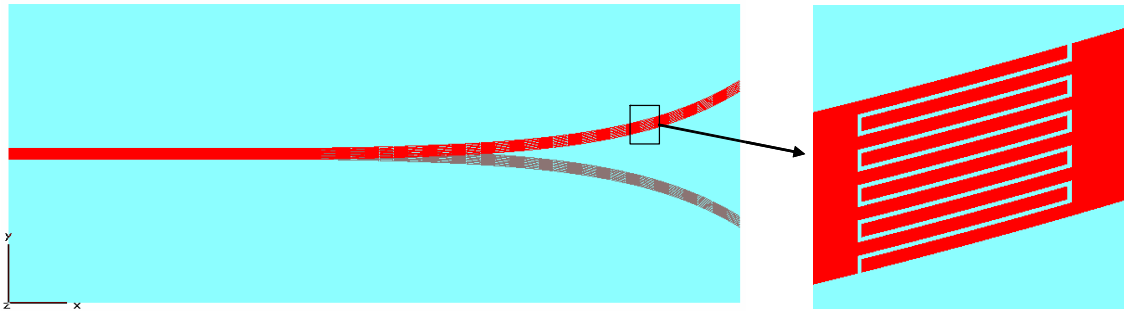

Figure 1: Geometry of the proposed microstrip antenna.

REFERENCES

1. Wu, T. T. and R. W. P. King, "The cylindrical antenna with nonreflecting resistive loading," *IEEE Trans. Antennas Propag.*, Vol. 13, 369–373, 1965.
2. Lestari, A. A., A. G. Yarovoy, and L. P. Ligthart, "R-C loaded bow-tie antenna for improved pulse radiation," *IEEE Trans. Antennas Propag.*, Vol. 52, 2555–2563, 2004.

Session 2A6
Electromagnetic Compatibility 1

Novel Fractal Electromagnetic Bandgap Structures to Suppress Simultaneous Switching Noise in High Speed Circuits

Kuo-Chiang Hung[1], **Ding-Bing Lin**[2], **Chin-Sheng Chang**[3]
Chun-Te Wu[4], **and I-Tseng Tang**[5]

[1]Institute of Computer and Communication Engineering
National Taipei University of Technology, Taipei, Taiwan
[2]Department of Electronic Engineering, National Taipei University of Technology, Taipei, Taiwan
[3]Institute of Microelectronics, Department of Electrical Engineering
Advanced Optoelectronic Technology Center, National Cheng-Kung University, Tainan, Taiwan
[4]Department of Electrical Engineering, Da-Yeh University, Changhua, Taiwan
[5]Department of Environment and Energy, Nation University of Tainan, Tainan, Taiwan

Abstract— A fractal low-period coplanar electromagnetic bandgap power/ground planes for suppressing simultaneous switching noise is presented. The effective suppressing bandwidth of fractal low-period coplanar electromagnetic bandgap and meander-bridge structure is from 264 MHz to 20 GHz. The results show the presented structure is superior to other structure for suppressing simultaneous switching noise.

Introduction: In recent year, the exceptional configurations to mitigate the simultaneous switching noise (SSN) in printed circuit board (PCB) were discussed by etching low-period coplanar EBG (LPC-EBG) structures on the power/ground planes to provide a wider bandgap bandwidth [1]. The LPC-EBG structure is chosen as the reference design in this paper. Although the LPC-EBG can isolate wide-band SSN, but the bandwidth and the cut-frequency does not enough. In order to create the multiple transmission zeros at higher frequency band, the fractal structures had been used in [2]. However, it still lack to have a good isolation in the lower frequency band. Therefore, this paper proposed the novel fractal LPC-EBG (FLPC-EBG) which were designed and measured. In addition to possessed lower cut-frequency, the higher inductance of meander-bridge to connect each FLPC-EBG cells.

Design Concept and Improvement: Figure 1(a) shows the dimensions of unit cell FLPC-EBG structure which is applied on a two-layer FR-4 PCB substrate. The thickness of substrate is 0.4 mm and the dielectric constant is 4.4. The excitation port 1 is at (15 mm, 75 mm) and the receiving port 2 is at (45 mm, 75 mm). The FLPC-EBG and meander-bridge structure as shown in Fig. 1(b). The detail parameters of meander-bridge are illustrates in Fig. 1(c). Fig. 2 shows the measurement results of proposed structures and the measurement range from 50 MHz to 20 GHz. The bandwidth is defined by $|S_{21}|$ lower than -20 dB. From this table, the suppressed SSN range of FLPC-EBG and meander-bridge structure is from about 264 MHz to 20 GHz (19.736 GHz bandwidth).

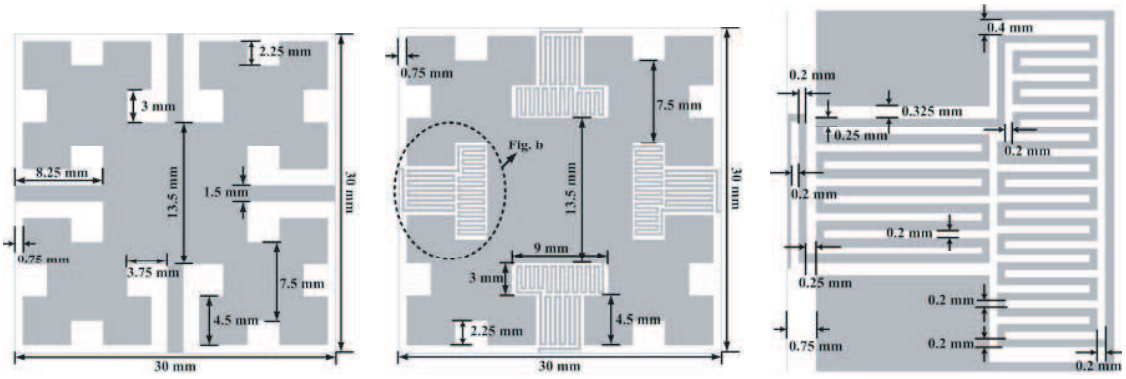

(a) (b) (c)

Figure 1: The proposed testing board. (a) FLPC-EBG structure. (b) FLPC-EBG and meander-bridge structure. (c) Meander-bridge structure.

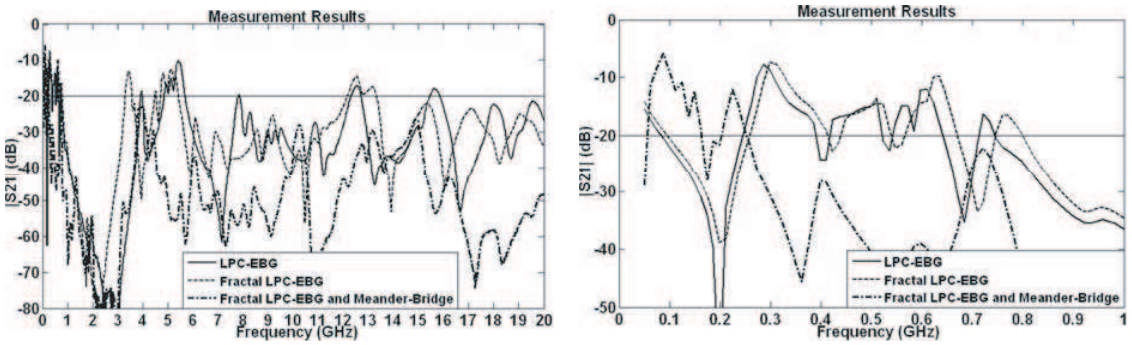

(a) (b)

Figure 2: Measurement results of testing board. (a) Measure range from 50 MHz to 20 GHz. (b) Lower frequency range of the proposed structures.

Table 1: Bandwidth and the suppressed frequency ranges.

Cases	Frequency range (B.W.) (GHz)
LPC-EBG	0.746∼3.918 (3.172)
FLPC-EBG	0.808∼3.309 (2.501)
FLPC-EBG and meander-bridge	0.264∼20 (19.736)

REFERENCES

1. Wu, T.-L., Y.-H. Lin, T.-K. Wang, C.-C. Wang, and S.-T. Chen, "Electromagnetic bandgap power/ground planes for wideband suppression of ground bounce noise and radiated emission in high-speed circuits," *IEEE Microwave Theory and Techniques*, Vol. 53, 2935–2942, Sept. 2005.
2. Kern, D. J., D. H. Werner, A. Monorchio, L. Lanuzza, and M. J. Wilhelm, "The design synthesis of multiband artificial magnetic conductors using high impedance frequency selective surfaces," *IEEE Transactions on Antennas and Propagation*, Vol. 53, 8–17, Jan. 2005.

Assessment of Possible Health Risk from Electromagnetic Fields of Portable Radio Station Devices

Roman Kubacki and Jaromir Sobiech
Military Institute of Hygiene and Epidemiology, Poland

Abstract— Radio frequency communication device, so called radio station, could be used in a variety of configuration, e.g., as vehicular mounted, rack mounted, transit case element or as manpack. The manpack radio station is contained within a rucksack and is strapped to the man's back. In this case the antenna, being a source of electromagnetic field, is mounted near the operator head. It turned down that the remaining part of the radio station, e.g., the part of device containing the electronics equipment, is also a source of radiation. From this point of view radio stations should be investigated due to concern of possible health risk from electromagnetic fields emitted from these devices.

RF safety standards should guarantee the operator's protection against electromagnetic fields. Safety standards are established by national laws and they are based on possible biomedical effects of interaction of electromagnetic fields with living organisms or taking into consideration proposals like directive 2004/40/EU of the European Parliament or STANAG NATO. The safety standards provide permissive exposure levels (PEL) in terms of electric (E) and magnetic (H) field strength. According to these standards values of E or H can not exceed PEL in the place of workers. In great majority of cases such measurements like E and H are sufficient to provide the safety work conditions because the electromagnetic fields are spatially homogeneous enough. However, the field distribution around the manpack radio station is not spatially homogeneous. Only the head or trunk of operator are exposed to electromagnetic field while the remaining parts of the body are not exposed. In case of spatially not homogeneous field it is possible to average values of E or H from radio station over the area of head or trunk. This gives the opportunity to locally exceed PEL. It is also possible to determine the induced currents in the operator body. This electrical parameter is suitable to characterize the level of exposure, especially in the case of manpack because in the vicinity of radio station the electromagnetic field has a nature of "near-field", so called also as a "reactive-field". Nevertheless, the only Specific Absorption Rate (SAR) provides the correct value of electromagnetic energy absorbed by the body although the numerical program for this calculation is very complex.

In the work the investigation of field distribution of radio stations situated on the operator's back has been presented and assessing of health risk of operator exposed to electromagnetic field emitted from these radio stations has been discussed.

Free-space Optical Data Link Using Quantum Cascade Laser

Z. Bielecki[1], **W. Kolosowski**[2], **and J. Mikolajczyk**[1]

[1]Military University of Technology, 2 Kaliskiego Str., 00-908 Warsaw, Poland
[2]Telecommunications Research Institute, 20 Poligonowa Str., 04-051 Warsaw, Poland

Abstract— Free Space Optics is the perspective stage of telecommunication development. Special FSO technologies offer mobile connection, non spectrum limits, high level of safety and high speed of data transmission, low value of basic error rate, reduced influence of snow and rain, and high resistivity to magnetic field influence. Progress in construction of FSO systems is connected with development of new radiation sources, optical systems, and photoreceivers. Nowadays, special attenuation was paid to the possibility of using systems operated at three spectral bands, i.e., 780–850 nm, 1 520–1 600 nm, and 10 000 nm. The bands are characterized by minimal atmospheric attenuation of the radiation ("transmission windows"). A lot of telecommunication firms in the USA, Japan, and Europe devote huge financial means to elaboration of cheap, eye-safe, and resistant to weather conditions, systems. The possibility of quick communication has been of special meaning under the conditions of terrorist attacks threat. The September's events in the USA showed a lack of emergency system for the exchange of information between particular civilian and military services in the face of damages of urban infrastructure. Thus, free space optical communication system can be an efficient tool in crisis situations.

The communication systems, operating at the bands of 780–850 nm and 1 520–1 600 nm, have been already designed. At present, intensive investigations of the FSO systems using radiation of the wavelength range of 10 µm is observed in the world. These systems are called "second generation FSO". The preliminary analysis showed that the "2nd generation FSO" systems are competitive for the remaining bands because of lower attenuation caused by fogs of small particles of aerosols and the higher safety for eyesight. A main difficulty for design of 2nd generation FSO systems is a lack of adequate radiation source. The only available CO_2 laser, operating in this range of wavelengths, did not show practical meaning for construction of simple and reliable broadband systems for data transmission. Elaboration of new quantum cascade lasers and hetero-system detectors provided designing the systems operating in the range of 10 µm.

At the Institute of Optoelectronics MUT, Warsaw initial investigation of the free space optical data link using quantum cascade laser is made. The analysis showed that the best parameters of a mobile optical system are obtained with the use of quantum cascade lasers produced by Alpes Lasers SA firm. For the construction of the transmitter optics a radiometric lens of OPHIR 65119 model was applied. The lens provides high transmission and high speed. The system receiver consists of reflectance mirror, detector, and signal processing circuit. The mirror shape is based on off-axis parabolic construction. Such construction ensures to make full use of mirror surface for the assemble radiation. For the designed FSO system, the Polish detector produced by Vigo firm was used. High sensitivity was obtained due to multilayer $Hg_{1-x}Cd_xTe$ heterostructure with immersion lens which was optimised for radiation detection at the wavelength of 10 µm. The transfer band of these photoreceiver is 200–1000 MHz. Basing on the parameters of the system elements, the system virtues (connection range and BER) were determined. The calculation took into consideration a speed of data transmission, divergence angle and atmosphere attenuation. The preliminary laboratory investigations of the system confirmed that due to application of QCL laser and highly sensitive detector it will be possible to construct a second-generation FSO. The system is characterized by larger detection range (about 6 km ar BER= 10^{-9}), in adverse atmospheric conditions, than detection range offered by currently applied optical systems.

Multi-band Antenna with Minimalization of Radiation towards Head

M. Wnuk[1] and R. Kubacki[2]

[1]Military University of Technology, Poland
[2]Military Institute of Hygiene and Epidemiology, Poland

Abstract— Intensive development of cellular personal communications system has been observed lately. Thus, protection of a man, and especially protection of his head against non-ionizing electromagnetic radiation generated by cellular telephones is becoming one of the most important problems. Substantial contributions to this growth have been made in Europe, where three such systems have been developed: Global System for Mobile Communication (GSM), operating in the 900 MHz band, Digital Personal Communication System (DCS-1800), using the 1800 MHz band. The antennas of above systems emit microwave energy in the direction of user's head. This is why it is important to determine possible health effects of using such devices. To minimise the energy deposited in the head, a number of small antennas, differing in shapes and arrays, have been designed for use in mobile communication systems. New antennas have to be cheap to manufacture and have to meet the following operational requirements:

- A radiation pattern ensuring reliable communication regardless of the antenna's orientation;
- A wide operational frequency band, so that the spectrum of transmitted information should not be distorted;
- A minimum impact on the biological tissue of the user, to avoid health risks;
- Little sensibility of the antenna parameters to the user's proximity; and
- Small size to facilitate mounting the antenna and using the telephone

Some of the requirements are mutually exclusive, so a compromise has to be worked out in the designing process.

Presently, there are no formal requirements in force or widely accepted industry standards concerning the recommended radiation pattern. The problem is further compounded by the fact that the user's head is in the so-called near zone of the antenna. There is concern about possible health effects of the field generated by the cellular phone, placed so close to the user's head. These are not groundless fears, as it is known that electromagnetic energy, regardless of its amount, interacts with the tissue of the human body. Its impact is harmless as long as it remains within the adaptation, compensation and regeneration capabilities of man, but may be harmful when it exceeds the limits of tolerance. The point is to make sure that signals emitted by a base station are correctly received from all directions while the user's head (especially bones, the brain and skin, which have a high level of thermal conductivity — 14.6, 8.05, 4.42 $\mathrm{mW/cm^2\,^\circ C}$ respectively) is exposed to as little radiation power as possible. A considerable part (up to 45%) of energy emitted by cellular phones now in use is absorbed by the user's head, which may create a health risk. That is why it is important to protect users against radiation from cellular phones, which can be achieved in two ways:

- by reducing the power of electromagnetic field emission towards the head to the necessary minimum; and
- by limiting the time of exposure to such fields

The second condition is related to the duration of the call and mostly depends on the user himself.

The former condition, i.e., cutting down the amount of radiation power absorbed the user's head, can be met — among other things — by modifying the radiation pattern of the antennas used in cellular phones.

A compromise has to be reached between the requirements regarding the availability of signals received by the antenna from all directions and the protection of the user's head against radiation. Nowadays there are some devices available, which should reduce radiation towards the head. Authors have tested some of those devices and they will show results of these tests. At the same time they have worked out a new type of antenna, which reduces the influence of the cellular phone on human body. One of the ways of achieving this result is to replace stub antennas with an omnidirectional radiation pattern by antennas with a radiation pattern shaped in such as way as to reduce radiation towards the user's head. Such antennas should be relatively small to be

fit for use with cellular telephones. Microstrip antennas on a multilayer dielectric meet all these requirements.

The proposed new model of antennas, which fulfil mentioned conditions, will be presented and discussed.

Usefulness of the Fresnel Approximation in the Field Distribution Calculations in the Vicinity of Mobile Base Station Antennas

Roman Kubacki[1], **Marian Wnuk**[2], **and Jarosław Kieliszek**[1]

[1]Military Institute of Hygiene and Epidemiology, Poland
[2]Military University of Technology, Poland

Abstract— Base station antennas for mobile communication are very popular in our environment. Often they can be located in vicinity of houses for example on the roofs or on the walls of buildings. The increasing popularity of mobile phones in our live has aroused interest about potential health risk due to exposure to microwave energy. From this point of view there is a need to know the exposure level in the area near antennas. In European Countries before installing antennas operators are obliged to assess the field distribution using calculation techniques. It is obvious that the correctness of calculations should be good enough especially in the area were people live or can enter. The most popular methods of field distribution calculations are based on simple formulas thus they can be used far enough from the antennas e.g., in the "far field". Nevertheless, it must be stressed that assessment for occupational and general public purposes are realized much closer to the antennas than the far field. We are going to prove that in the vicinity of the antenna or in the directions of side-lobes calculation errors, caused by the simple formulas, are too high thus they are unacceptable.

It is possible to assess the electric field distribution in the vicinity of the antenna but complex calculation methods e.g., FDTD should be used. However, these methods because of their complexity are not used in practical engineering calculations of the safety zones around antennas located on the roofs.

In the work formulas for calculations of the electric field strength, based on vector potentials have been revealed. The approximation, called as the "Fresnel approximation" was adopted for the calculations. The final equation for E_θ [V/m] is given bellow:

$$E_\theta = A\frac{jk}{4\pi}\frac{e^{-jkr_o}}{r_o}\iint\limits_{Sa} J_x(\xi)J_x(\eta)e^{jk\left[\eta\cos\theta-\frac{1}{2r_o}\left(\xi^2+\eta^2\sin^2\theta\right)\right]}\,d\xi\,d\eta$$

where:

$J_x(\xi)$, $J_x(\eta)$ are functions of current on the aperture of antenna (ξ, η),
A – coefficient,
Sa – surface of the antenna aperture.

The unknown current functions on the antenna ($J_x(\xi)$, $J_x(\eta)$) were calculated using a technique called as a "synthesis of the antenna pattern". Values of electric field, calculated using the above formulas for Kathrein antennas have been presented. The usefulness of this formula and error of calculation have also been discussed.

The Amplitude Weighting Method of LFM Chirp Signals for Radar Application

Edward Sedek[1], **Andrzej Milewski**[1], **Sylwester Gawor**[2], **and Zbigniew Bielecki**[3]

[1]Telecommunications Research Institute, 30 Poligonowa Str., Warszawa, Poland
[2]School of Buisness Administration and Computer Science, 9 Bobrowiecka Str. Warszawa, Poland
[3]Institute of Optoelectronics MUT, 2 Kaliskiego Str., Warszawa, Poland

Abstract— The amplitude weighting method of LFM chirp signals is presented in this paper. Linear frequency modulated (LFM) chirp signals are widely used in radar systems. To increase the maximum range of radar without degradation of spatial resolution, the pulse compression systems are used. Formerly the chirp signals were generated and compressed using surface acoustic wave dispersive delay lines. At present digital signal generators and compressors are used most commonly.

The shape of frequency response of the signal depends on the TB product. For large TB products (over 100) the frequency response is almost rectangular. To compress the signal matched filter may be used. In this case the compressed signal with narrow mainlobe and -13 dB sidelobes is obtained. These sidelobes may mask small targets or may be mistaken for targets themselves [1]. To reduce the sidelobes some amplitude weighting of the compressor, for instance Hamming weighting may be implemented. It allows to lower the sidelobes level below -42 dB.

In practice, especially for signals with TB product less then 100 it is difficult to obtain such low sidelobes level. It is caused by amplitude ripple of LFM chirp signal. Amplitude ripple of the expander can be decreased by adding frequency extensions to transmitted signal (Fig. 1).

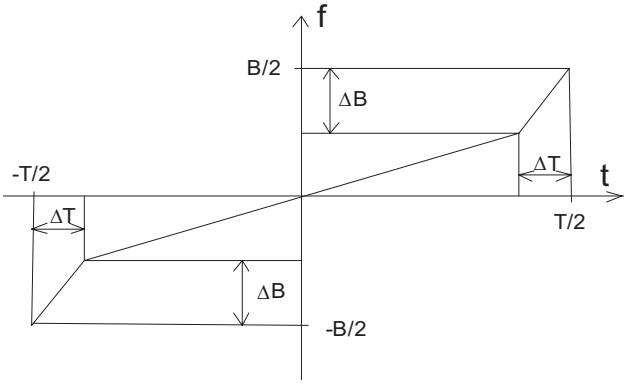

Figure 1: Linear chirp signal with extensions.

The dependence of the sidelobes level on TB product for signals with and without extentions will be presented in the paper. It will be see, if bandwidth is wider, the sidelobes are lower.

Another method of minimizing the sidelobes level is to provide appropriate compensation in the design of the compression weighting function. If the chirp waveform has a spectrum $S(f)$, and desired compressed pulse spectrum is $W(f)$, the compression filter characteristic is given by $H(f) = W(f)/S(f)$. Main disadvantage of the reciprocal ripple design is high sensitivity of output signal sidelobe level to Doppler shift of the transmitted signal. This could be expected since a shift of the transmitted spectrum could cause the ripples in the compensated compression line to add to the ripples in the expanded chirp spectrum rather than cancel them. For Doppler shifts that are so large sidelobes tend to asymptote to the sidelobe levels obtained with two unweighted chirp filters and external weighting filter. Dependence of sidelobes levels on Doppler shift for various values of compression ratio will be presented.

If large values of Doppler shifts are not expected, reciprocal ripple design of the compressor can also be used. The more results of our investigations are presented in full paper.

Electromagnetic Compatibility of the Military Handset with Hidden Authorization Function Based on MIL-STD-461D Results

Z. Piotrowski, **L. Nowosielski**, **L. Zagoździński**, **and P. Gajewski**
Military University of Technology, Poland

Abstract— In this paper we present algorithm and hardware architecture of the new military communication device dedicated for VHF battlefield radio stations. Results of the compatibility tests for this device according to the norm MIL-STD-461D are also presented together with the plots and comments. One of the most important security problems unsolved till this time in the communications links is voice authorization of the telephone or radio subscriber. Problem is more obvious when it is considered both current voice communications over digital and analog channels: VoIP, PSTN, GSM and state-of-the-art real-time, artificial, speech synthesis in the context of potential risk of impersonating, known in information technology as a spoofing. Presented algorithm and hardware architecture are the proposals for increasing security level in unprotected voice calls.

At present, subscriber's authorization in telephone calls is performed in most cases in subjective way using our Human Auditory System. Well known scheme of subjective authorization is based on knowledge of dedicated specific person's voice. New scheme of the authorization is based on watermarking (data hiding) technology. Additional binary signature as a watermark is embedded in host voice in the radio or telephone handset and then transmitted over communications links. At the receiving side, using dedicated hardware based on real-time processing algorithm, watermark is extracted and binary signature is compared with the set of binary signatures storage in handset's memory. Results of the authorization process is displayed on handset's LCD.

Hardware architecture of the handset is based on the fast, floating-point Digital Signal Processor TMS320C6713 and microcontroller ARM7TDMI family. Handset transmits, watermarked, analog voice through the radio station, using standard voice interface in the TRC9200 battlefield VHF PR4G radio station family.

In this paper we described in details, used in our tests, following research procedures according to MIL-STD-461D standard:

1./ RE-102 — radiating perturbations measurement emitted by military devices

2./ CE-102 — conducting perturbations measurement emitted by military devices

In the paper results of those measurements will be shown. Measurements were carried out at the Electromagnetic Compatibility Laboratory, Faculty of Electronics, Military University of Technology. The Laboratory have accreditation given by the Polish Centre for Accreditation for carrying out those military devices measurements. Described results of measurements will be a base for introduction this developed device into the Polish Armed Forces equipment.

Thermal Design and Electromagnetic Capability Design of the Microwave Power Module

Jinling Zhang[1], **Yinghua Lu**[2], **Biao Yang**[2], **Rongrong Li**[1], **and Jinsheng Yang**[3]

[1]School of Electronic Engineering, Beijing University of Posts and Telecommunications
Beijing 100876, China
[2]School of Telecommunication and Networks Technology
Beijing University of Posts and Telecommunications
Beijing 100876, China
[3]Beijing Vacuum Electronics Research Institute, Beijing 100016, China

Abstract— Microwave Power Module (MPM) Microwave Power Module (MPM) is a RF power amplifier providing middle or high RF power, and it has many advantages such as small size, high efficiency, high reliability and making little noise. MPM consists of the solid state amplifier (SSPA) and the vacuum helix miniaturized traveling wave tube (Mini-TWT) as well as the high-voltage switch electronic power conditioner (EPC). MPM is mainly used in military and satellite communications areas. The design of MPM relates to newer technologies of many fields, which is a high technology system project. And the general design is especially important to the whole performance of MPM, as every component in the MPM inside will produce heat. It is very important to transfer this heat for the steady working of the device, so an integrated consider has to be given in the general design. Because there is difference of the highest working condition temperature between vacuum device and solid device, the heat design idea between them should been separated in general design. The other crucial problem in the general design of MPM is the EMC inside and outside. The inside EMC has much influence in its working stability and reliability, while the outside EMC has much influence when many MPM are using in array, and it also has influence to other equipments working near the MPM. Therefore the heat transfer problem and EMC is the questions which have to be considered when we design the MPM. This paper has introduced the thermal design and Electromagnetic Capability (EMC) related to the Reliability of Microwave Power Module (MPM). We have given the primary result of thermal design, and have analyzed the EMC about the dependability of the MPM, and have presented the way of research. So we got the theory of the design about MPM working stability and dependability.

The Method of the Calculating of Frequency Characteristics of Image Gaining and Processing Systems

Konrad Maj and Grzegorz Stępień
Remote Sensing and Geoinformatics Military University of Technology, Poland

Abstract— The basic parameter which describing the quality of the image is its resolution, on which influence:

- conditions in which the image was gain (the conditions of exposure);
- parameters of image gaining system;
- parameters of processing system.

Estimating of a quality of a gaining as well as processing system, required a quantity estimating of this influences. Such an operation is possible on the way of calculating of a modulation transfer function (MTF) of a whole system. The Calculation of that is going across researching of impulse answer system on a model signal. In case of the image, the model signal is a suitably prepared test, which is subject to observation and then to electronic processing to digital form.

The parameters of applied optical arrangement define first of all the resolution of digital image as well as parameters devices of processing such as scanners, converters and recorders. The classic method of researching of influences of parameters of these devices as well as conditions of image gaining, on parameters of image, is gaining of strip tests. In case of remote sensing imageries it requires however the realization of tests about suitably large sizes and covering their with images about definite contrasts. It is expensive procedure and long-lasting, and first of all subjective. The opinion of quality of gain over image is going across optical observation executed by group of people, and then by calculation of average of observation results.

In presented article authors propose hereinto applying to such kind of researching a new method basing on calculating of a modulation transfer function (MTF) of a information gaining and processing system, on the ground of image test about considerably smaller sizes and much more easier to execute. Such an image shows feather edges between areas contains maximum contrast. The principle advantage of method is a objectivity of a measurement, which assures his repeatability.

Improvement of Reverberation Chamber's Simulation: A Stochastic Collocation Approach

F. Diouf[1], **P. Bonnet**[1], **S. Lalléchère**[1], **C. Chauvière**[2], **and F. Paladian**[1]

[1]LaSMEA, Université Blaise Pascal, 24 Avenue des Landais 63177 Aubière, France
[2]Laboratoire de Mathématiques, Université Blaise Pascal
24 Avenue des Landais 63177 Aubière, France

Abstract— Experimental studies of electronic systems immunity are generally performed in Anechoic Chamber. In this case, the equipment is submitted to a plane wave characterized by a well defined polarization and incidence. Nowadays, many different products containing microprocessors may be operating in the same area and different electronic systems may also be operating within metallic enclosures. Thus, the environment may more likely behave as either a Reverberation Chamber (RC). Hence, the actual standards propose the RC as an alternative test facility. Indeed, the equipment is immersed in an electromagnetic environment with random incidence and polarization in a RC. The generation of such statistical environment mainly depends on the number of independent electromagnetic configurations produced inside the structure thanks to the stirrer. Indeed, these configurations depend on the boundaries conditions and, when the number of the stirrer positions is almost infinite, the internal electromagnetic field in the RC is supposed to be homogeneous and isotropic [5]. If one observes suitable comparisons between theory and experimentation, these results nevertheless are obtained at high computing expenses [1, 2].

Thus, compromise between the measurements duration and their representativeness has been the subject of many investigations during last years as well in experimental field as numerical [4].

In this paper, we propose an approach enabling to find the statistical moments of the electromagnetic field (mean, standard deviation) at each point of the RC's working volume thanks to a reduced number (4 or 5) of the stirrer position.

of the stirrer position. In the proposed approach, the rotation angle of the stirrer is supposed to be a random variable which follows a uniform distribution between [0 ; 2π]. The application of a stochastic collocation method [3] and a Gauss-Legendre quadrature allows us getting accurate results with a limited and well chosen number of the stirrer positions named collocation points. The mean value and the variance of the modulus of the total field are obtained, respectively at each point of the working volume, according to:

$$< |E_{\text{tot}}| >= \sum_{i=1}^{n} \omega_i \left|E_{\text{tot}}^i\right| \quad \sigma^2_{|E_{\text{tot}}|} = \sum_{i=1}^{n} \omega_i \left(\left|E_{\text{tot}}^i\right|\right)^2 - \left(\sum_{i=1}^{n} \omega_i \left|E_{\text{tot}}^i\right|\right)^2$$

where ω_i is the weight obtained by the Gauss-Legendre quadrature and E_{tot}^i is the total field obtained at each collocation point "i".

Details related to this method will be given in the full paper. Convergence of the stochastic collocation method will be investigated and comparisons with classical Monte-Carlo method will be discussed.

REFERENCES

1. Bruns, C., "Three-dimensional simulation and experimental verification of a reverberation chamber," PhD Thesis ETH Zurich, 2005.
2. Lalléchère, S., "Modélisations numériques temporelles des CRBM en compatibilité electromagnétique. Contribution aux schémas volumes finis," Thèse de Doctorat, Université Blaise Pascal, 2006.
3. Chauvière, C., J. S. Hesthaven, and L. Wilcox, "Efficient computation of RCS from scatterers of uncertain shapes," *IEEE Trans. Antennas Propagation*, 2006.
4. "Introduction reverberation chamber test methods," *IEC Draft 61000-4-21 Electromagnetic Compatibility (EMC) Part 4: Testing and Measurements Techniques-Section 21*, 2000.
5. Hill, D. A., "Plane wave integral representation for fields in reverberation chamber," *IEEE Trans. on Electromag. Compat.*, Vol. 40, 209–217, August 1998.

Session 2P1
Computer Aided Modeling, Design and Optimization

Comparative Performance of Genetically Initialized Pattern Search Optimization Versus Particle Swarm Optimization Algorithm of Adaptive Beam Forming with the Linear Antenna Array Geometry

Fikret Tokan, Ufuk Özkaya, and Filiz Güneş
Department of Electronics and Communication Engineering
Yıldız Technical University, İstanbul, Turkey

Abstract— Smart antenna systems have been widely considered to provide interference reduction and improve the capacity, data rates, and performance of wireless mobile communication. Smart antenna arrays with adaptive beamforming capability are very effective in the suppression of interference and multipath signals. Many synthesis methods are concerned with suppressing the sidelobe level (SLL) while preserving the gain of the main beam. Other methods deal with the null control to reduce the effects of interference and jamming. The evolutionary algorithms such as genetic algorithms (GA) [1], particle swarm optimization [2], a clonal selection algorithm [3] are still of great interest in synthesizing the antenna arrays. On the other hand, the recent works deals with the most accurate approach to the far field calculations taking into account the indivudual patterns in the real environment where mutual coupling between the antennas exist [4]. In this work, we considered only the linear antenna array factor with all the facilities due to the elements taking place on a line together with the feeding conditions. We followed "the general system approach" and treat each free variable by emphasizing with respect to its technological significance and cost in the antenna engineering. Thus, the free variables to control the far field features are the number of the element N, the inter-element spacing d_i, the excitation amplitude a_i and phase ϕ_i, $i = 1, \ldots, N$. Furthermore all the possible linear configurations are considered under the two groups: (1) The Sum Pattern configurations with the even and odd element numbers; (2) The Difference Pattern configuration. The goal is to maximize the beam of the radiation pattern towards the intended user or Signal of Interest (SOI) and ideally obtain nulls in the directions of interfering signals or Signal not of Interest (SNOI). Thus, the required outputs are the directivities, the (broad) nulls, the sidelobe area(s) to be required for suppression. The new algorithm "Pattern Search (P Search)" is introduced for the optimization of the antenna system, which is initialized with the genetic algorithm(GA). This algorithm is experienced as a fast algorithm for optimization.

The geometry and a typical example for the sum patterns are given in Figs. 1(a), (b) and (c) where the whole sidelobe region is taken for suppression, with the values of the inter-element spacing d_i

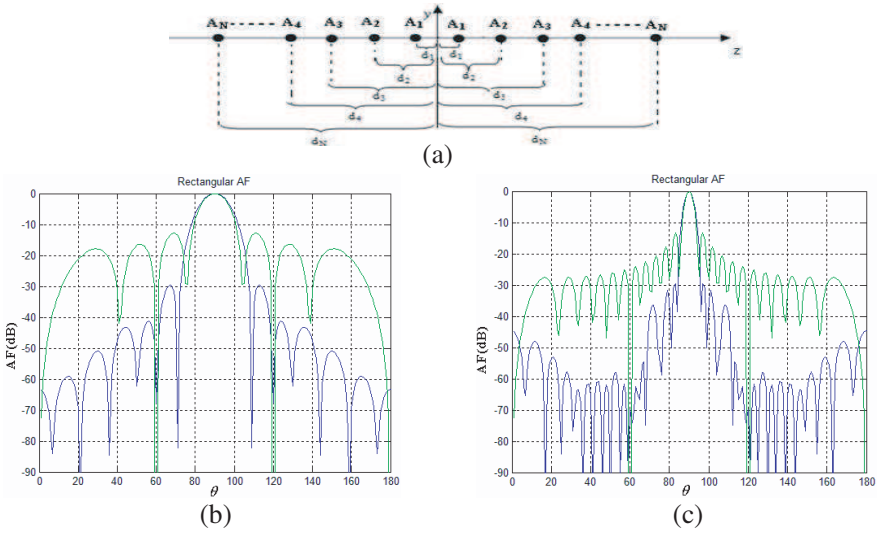

(a) (b) (c)

Figure 1: (a) The linear antenna array geometry for the sum pattern, (b) polar plot for the sum pattern of $N = 4$, (c) polar plot for the sum pattern of $N = 12$, compared with the conventional pattern $\Leftrightarrow d_i = \lambda/2,\ i = 1, \ldots, N$.

and excitation amplitudes a_i. The excitation coefficients and the interelement spacings between the antennas used to obtain Fig. 1(b) and Fig. 1(c) are given in Table 1. This synthesis may be observed to have much greater sidelobe suppression compared to the counterparts in the literature. In conference, many typical examples for the linear array synthesis will be expected to present.

Table 1: The excitation coefficients and the inter-element spacings between the antennas used to obtain Fig. 1(b) and Fig. 1(c).

N = 4	**A**	[1.8758 4 0.597 3.230]
	d	[1.6134 0.320 2.254 0.963]
N = 12	**A**	[5.459 2.061 4.289 1.398 2.346 6.216 1.721 1.175 6.153 0.372 3.664 4.313]
	d	[3.137 5.836 0.387 0.216 4.716 1.453 5.153 6.636 2.282 7.436 0.825 3.978]

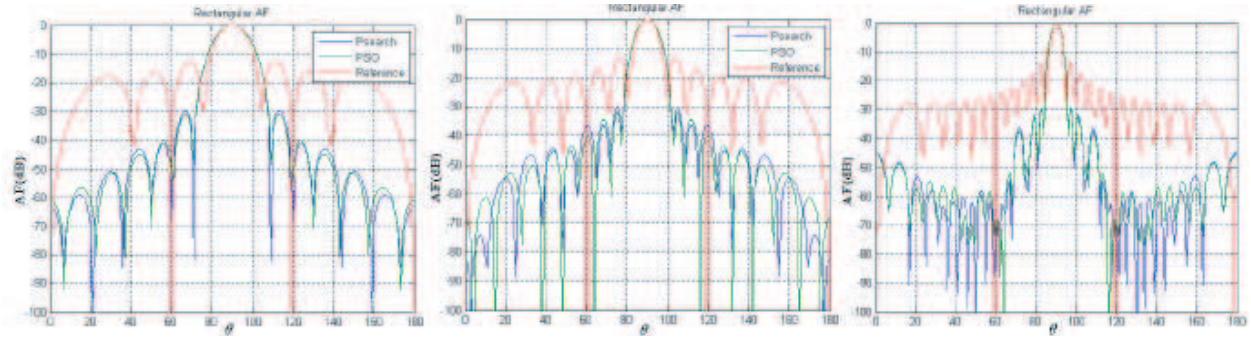

(a) (b) (c)

Figure 2: Comparative polar plot of Psearch versus PSO for the sum pattern of $N = 4$, (b) polar plot of Psearch versus PSO for the sum pattern of $N = 6$, (c) polar plot of Psearch versus PSO for the sum pattern of $N = 12$, compared with the conventional pattern $d_i \Leftrightarrow \lambda/2,\ i = 1, \ldots, N$.

Table 2: The excitation coefficients and the inter-element spacings between the antennas used to obtain Figs. 2(a), (b) and (c).

N = 4	**Psearch**	**A**	[1.875 4 0.597 3.23]
		d	[1.613 0.32 2.254 0.96]
	PSO	**A**	[1.852 4.07 0.582 3.23]
		d	[1.627 0.32 2.272 0.97]
N = 6	**Psearch**	**A**	[3.999 2.41 1.385 0.50 1.44 2.14]
		d	[0.389 1.96 2.724 3.44 1.27 1.11]
	PSO	**A**	[4.073 2.41 1.368 0.48 1.41 2.14]
		d	[0.391 1.97 2.743 3.47 1.27 1.12]
N = 12	**Psearch**	**A**	[5.45 2.06 4.28 1.39 2.34 6.21 1.72 1.17 6.15 0.37 3.66 4.31]
		d	[3.13 5.83 0.38 0.21 4.71 1.45 5.15 6.63 2.28 7.43 0.82 3.97]
	PSO	**A**	[5.45 2.05 4.28 1.38 2.34 6.21 1.71 1.17 6.15 0.36 3.66 4.31]
		d	[3.13 5.83 0.38 0.21 4.71 1.45 5.15 6.63 2.28 7.43 0.82 3.97]

The comparative examples for suppression of whole sidelobe region while obtaining a fairly high gain using the Psearch Algorithm and the PSO Algorithm for $N = 4$, $N = 6$ and $N = 12$ are given in Figs. 2(a), (b) and (c) respectively. The excitation coefficients and the inter-element spacings between the antennas used to obtain Figs. 2(a), (b) and (c) are given in Table 2.

REFERENCES

1. Tonn, D. A. and R. Bansal, "Reduction of sidelobe levels in interrupted phased array antennas by means of a genetic algorithm," *International Journal of RF and Comp. Aided Engineering*, Vol. 17, No. 2, 134–141, March 2007.

2. Khodier, M. M. and C. G. Christodoulou, "Linear array geometry synthesis with minimum sidelobe level and null control using particle swarm optimization," *IEEE Trans. on Antennas and Propagation*, Vol. 53, No. 8, 2674–2679, August 2005.
3. Karaboğa, D., K. Güney, and A. Akdağlı, "Antenna array patern nulling by controlling both amplitude and phase by using modified touring ant colony optimization algorithm," *International Journal of Electronics*, Vol. 91, No. 4, 241–251, April 2004.
4. Mahmoud, K. R., M. I. Eladawy, R. Bansal, S. H. Zainud-Deen, and S. M. M. Ibrahem, "Analysis of uniform circular arrays for adaptive beamforming applications using particle swarm optimization algorithm," *International Journal of RF and Comp. Aided Engineering*, Vol. 18, No. 1, 42–52, Sept. 2007.

Analysis and Synthesis of the Microstrip Lines by Support Vector Regressors

Nurhan Türker Tokan and Filiz Güneş

Electrical and Electronics Engineering Faculty
Department of Electronics and Communication Engineering
Yıldız Technical University, Yıldız, Istanbul, 34349, Turkey

Abstract— Support vector machines and kernel methods, which enable to generalize 'discrete' data into the 'continuous' domain have become one of the most popular learning machines in the last few years. In particular, support vector machines are based on a judicious and rigorous mathematics combining the generalization and optimization theories together and verified to be computationally very efficient (the so-called Vapnik- Chervonenkis theory [1, 2]). This learning machine has found many fruitful applications in science and engineering, especially the typical applications in the signal processing are given in literature.

In this work, the Support Vector Regression is adopted to the analysis and synthesis of microstrip lines on all isotropic/anisotropic dielectric materials, which is a novel technique based on the rigorous mathematical fundamentals and the most competitive technique to the popular artificial neural networks. This adopting process can be described step by step as follows: Firstly, the problem is defined and mathematically formulated; then the support vector regression is adapted and accuracy, computation efficiency and number of support vectors of the support vector regression performance are investigated in details with the ε-parameter of the Vapnik's ε-insensitive loss function. The support vector regressor performance is compared with its artificial neural network competent performance and so it may be concluded that the artificial neural networks can be replaced by the support vector regressors in the regression applications due to its higher approximation capability and much faster convergence rate with the sparse solution technique. Results of the comparison for the accuracy and computation efficiency are given in Tables 1 and 2, respectively.

Table 1: Accuracies of ANN and SVR models for microstrip lines.

% Accuracy	**ANN 1***	**ANN 2****	**SVR**
Z_o	97.64	99.13	99.26
ε_{eff}	98.12	99.55	99.46

*with one hidden layer **with two hidden layers

Table 2: Time analysis of ANN and SVR models for microstrip lines.

	ANN 1	**ANN 2**	**SVR**
Training time(sec)	27.953*	44.156*	1.015
Test time (sec)	0.015	0.017	0.013
Total time (sec)	27.968	44.173	1.028

*trained for 300 epochs

Also, in this work, the black-box defining the problem is utilized bidirectionally by reverse training: Thus mathematically, using this approach it will be possible to obtain reversal of a function with multiple variables provided that one-to-one mapping in both directions. This immediately calls that analysis and synthesis can be achieved by using only analysis black-box. In this work, this is applied to the analysis and synthesis of microstrip lines on all isotropic/anisotropic dielectric materials and can be extended to other types of microwave systems. Furthermore, by using the adaptive step size, a much faster convergence rate is obtained. The performances of the constant and adaptive step sizes are compared for the support vector regressor and artificial neural network in the Table 3 where it can be seen that 20–70 time faster performances can be obtained by the adaptive step sizes.

Table 3: Comparison of the performances with constant and adaptive step sizes.

	constant step size			**adaptive step size**		
	W (mm)	Z_o (Ω)	elapsed time(sec)	W (mm)	Z_o (Ω)	elapsed time(sec)
SVR	3.658	42.93	**11.234**	3.646	43	**0.45**
ANN	3.625	43.13	**36.188**	3.612	43.19	**0.64**

ACKNOWLEDGMENT

This work was supported by the The Scientific and Technological Research Council of Turkey.

REFERENCES

1. Vapnik, V. N., *Statistical Learning Theory*, Wiley, New York, 1998.
2. Cristianini, N. and J. Shawe-Taylor, *An Introduction to Support Vector Machines (and Other Kernel-based Learning Methods)*, Cambridge University Press, 2000.

Support Vector Analysis of the Rectangular Patch Antenna

Nurhan Türker Tokan and Filiz Güneş

Yıldız Technical University, Electrical and Electronics Engineering Faculty
Department of Electronics and Communication Engineering, Yıldız, Istanbul, 34349, Turkey

Abstract— Two kinds of analysis can be used in calculating the resonant frequency, bandwidth, input impedance of the patch antennas. The first group starts from initial physical assumptions, which generally offers simple and analytical formulas, well suited for a physical understanding of phenomena and for future antenna computeraided design (CAD). These methods are known as transmission-line models and cavity models. However, these methods do not consider rigorously the effects of surface waves. The second group is based on an electromagnetic boundary problem, which leads to an expression as an integral equation, using proper Green functions, either in the spectral domain, or directly in the space domain, using moment methods. Without any initial assumption, the choice of test functions and the path integration appear to be more critical during the final, numerical solution. Exact mathematical formulations in the second group rigorous methods involve extensive numerical procedures, resulting in round-off errors, and may also need final experimental adjustments to the theoretical results. They are also time consuming and not easily included in a CAD system. However, the theoretical values obtained by using both these two theoretical methods are also not in very good agreement with the experimental results of both electrically thin and thick rectangular microstrip antennas. For these reasons, in this work an advanced nonlinear learning machine, "Support Vector Machine (SVM)" is employed in analysing the rectangular patch antenna, which enable to generalize 'discrete' data into the 'continuous' domain. In particular, SVMs are based on a judicious and rigorous mathematics combining the generalization and optimization theories together and verified to be computationally very efficient (the so-called Vapnik- Chervonenkis theory [1, 2]). This learning machine has found many fruitful applications in science and engineering, especially the typical applications in the signal processing are given in literature.

In this work, SVMs are employed for regression in the analysis of the rectangular patch antennas, which in these types of applications, may be named as "Support Vector Regressors (SVR)". Given a set of observed discrete data $\{(\boldsymbol{x}_i, y_i), \boldsymbol{x}_i \in \boldsymbol{R}^n, y_i \in \boldsymbol{R}, i = 1, 2, \ldots, N\}$, the support vector machine learning method in its basic form creates an approximation function $f(\boldsymbol{x}) = b + \sum y_j \alpha_j K(\boldsymbol{x}_j, \boldsymbol{x})$ with $y \cong f(\boldsymbol{x})$ for regression and $y = \mathrm{sgn} f(\boldsymbol{x})$ for dichotomous classification for instance. In this work, data ensemble is provided as the two groups: (1) The data resulted from the experiments made in the literature; (2) The data obtained by the EM Simulator. Thus, the three functions characterizing the antenna are approximated in terms of the geometrical parameters which include the electrical thickness, the dimensions of the rectangular patch, the parameter of the feeding position, the electrical properties of the used dielectric material. The outputs of the SVR functions for the patch antennas designed on the widely used dielectrics are compared with the targets and the theoretical counterparts in the literature [3–5]. It is observed that SVR analysis gives faster and more accurate results. We expect to present the results of the SVR analysis of the rectangular patch antenna in the wide input domain in the PIERS 2008.

ACKNOWLEDGMENT

This work was supported by the The Scientific and Technological Research Council of Turkey.

REFERENCES

1. Vapnik, V. N., *Statistical Learning Theory*, Wiley, New York, 1998.
2. Cristianini, N. and J. Shawe-Taylor, *An Introduction to Support Vector Machines (and Other Kernel-based Learning Methods)*, Cambridge University Press, 2000.
3. Sagiroglu, S., K. Guney, and M. Erler, "Calculation of bandwidth for electrically thin and thick rectangular microstrip antennas with the use of multilayered perceptrons," *Int. J. RF Microwave CAE, (Special Issue: Applications of Artificial Neural Networks to RF and Microwave Design)*, Vol. 9, 277–286, 1999.
4. Guney, K., M. Erler, and S. Sagiroglu, "Artificial neural networks for the resonant resistance calculation of electrically thin and thick rectangular microstrip antennas," *Electromagnetics*, Vol. 20, 387–400, 2000.

5. Karaboğa, D., K. Guney, S. Sagiroglu, and M. Erler, "Neural computation of resonant frequency of electrically thin and thick rectangular microstrip antennas," *IEE Proc. Microwaves, Antennas Propagation*, Vol. 146, 155–159, April 1999.

A Novel Approach for Computing Shielding Effectiveness of Conductive Metal Sheets, against AC Magnetic Fields in IF Range in Industrial Environment

F. Dughiero, C. Greggio, and M. Forzan
Department of Electrical Engineering, Universita degli studi di padova
Via Gradenigo, 6/a, Padova 35131, Italy

Abstract— In recent times, a great interest has been devoted by researchers to developing computation procedures that enable to simulate the physical behaviour of metallic bodies in variable electromagnetic fields. One of the aims is to evaluate the shielding effectiveness of shielding structures, against time-varying magnetic fields, particularly in the range of the IF range (from 50 Hz to a few tens of KHz) where, for example, can be found processes employing high current levels (Induction heating applications for example).

The European directive 40/2004/CE imposed to all the E.C. countries to put up national regulations for limiting electromagnetic fields exposure to workers and the public, within the year 2008 (now postpone to 2012); the directive defines the admissible field levels along the electromagnetic spectrum. Among other things, it requires that both at design phase and at installation phase of industrial equipment, those field intensity limits must be respected.

While electric field shielding is a relatively easy task, it is not for shielding time varying magnetic fields. Usual computation practice is used to separate conductive effects from magnetic flux confinement effects of shielding materials, very often leading to separate modelling of the two phenomena.

In present work our aim is to show a novel computational approach for computing shielding effects of conductive metals, shaped in rectangular foils. In fact, industrial applications that require high currents at frequencies up to tens of kHz are becoming more and more common. Generally in such applications the magnetic field sources are solenoids of various sizes, high current bus-bars, high current chokes and transformers. So the easiest way to accomplish a shielding task is to build rectangular boxes containing those sources, by using metallic sheets of various thicknesses.

The model has been developed in such a way to consider that the shielding task is performed by metallic foils, often very close to the high current field source, so the prevalent shielding effect is produced by the induced currents circulating in the shields.

After a description of the mathematical model used for shielding calculation some example of applications will be presented with reference to practical cases of induction crucible furnaces. Some comparison between calculation and measuremnts will be presented in order to evaulte the correcteness and effectiveness of the numerical model proposed.

REFERENCES

1. Bertocco, M., F. Dughiero, C. Greggio, E. Sieni, and A. Sona, "Efficient characterization of magnetic field sources," *IEEE Instrumentation and Measurements Technology Conference*, Sorrento, Aprile 2006.
2. Dughiero, F. and C. Greggio, "Numerical models for the evaluation of shielding effects in induction heating furnaces," *EHE06 International Conference on Electromagnetic Fields, Health and Enviroment*, Isola di Madeira, Portogallo, Aprile 27–29, 2006.
3. Bertocco, M., F. Dughiero, C. Greggio, and E. Sieni, "An efficient model to evaluate the magnetic field in the surrounding of induction heating installations," *EHE06 International Conference on Electromagnetic Fields, Health and Enviroment*, Isola di Madeira, Portogallo, Aprile 27–29, 2006.

Magnetic Anomaly Eigen-detection

A. Sheinker[1], N. Salomonski[2], B. Ginzburg[2]
L. Frumkis[3], and B. Z. Kaplan[3]

[1]R & D Integrated Systems Section
Propulsion Division, Soreq NRC, Yavne 81800, Israel
[2]Nuclear Research Center SOREQ, Yavne 81800, Israel
[3]Department of Electrical and Computer Engineering
Ben-Gurion University of the Negev, Beer-Sheva 84105, Israel

Abstract— A distant ferromagnetic target produces an anomaly in the ambient Earth magnetic field. The anomaly is described as a dipole field. The moving target signal is measured by a static magnetic sensor attempting to detect the presence of the target. We have used a computer simulation to obtain the Eigenvectors of possible target signals. In case of a target moving along a straight line with a constant velocity, the obtained Eigenvectors resemble the orthonormal basis functions produced by analytical decomposition. The computer simulation enables to obtain Eigenvector sets for different target movement patterns and various magnetic sensor types, e.g., a total field sensor, three-axis sensor etc.

The Eigenvectors are used to construct a detector based on matched filtering. Each Eigenvector is used as a matched filter for a component of the input signal. Then the matched filters outputs are squared and summed. Detection occurs whenever the sum arises above a threshold which is determined by considering the magnetic noise level. A priori knowledge about possible target movement patterns can be exploited to obtain the appropriate Eigenvectors, and thereby improve detection. Detection probability may be further increased by using proper weighting of the matched filters outputs.

The proposed method can be similarly adopted to the case of a static target and a moving magnetic sensor. In this case, the movement pattern is known a priori or can be measured instead of being guessed according to certain assumptions.

The method was tested in several scenarios of target movement patterns, showing improvement in detection probability.

A Comparison of Distortion Analyses Based on Volterra Series and Steady State Algorithm

J. Dobeš

Department of Radio Engineering, Czech Technical University in Prague
Technická 2, 16627 Praha 6, Czech Republic

Abstract—

Precise Method Based on Steady State Analysis & FFT: The most accurate method for determining the intermodulation products consists in finding a steady state (SS) [1] followed by FFT. However, this method is time-consuming for many microwave circuits and thus a fast estimation by the Volterra series could be very useful.

Description of the Method Based on Volterra Series: As the resulting formulae which arise by the usage of the Volterra series are very complicated, consider for a simplicity of the explanation that a circuit system is composed of two equations only, i.e.,

$$f_1\left(x_1,\, x_2,\, \dot{x}_1,\, \dot{x}_2,\, t\right) = 0, \quad f_2\left(x_1,\, x_2,\, \dot{x}_1,\, \dot{x}_2,\, t\right) = 0.$$

The 1st step of analysis is finding the operating point, i.e., solving

$$f_1\left(x_{1_0},\, x_{2_0},\, 0,\, 0,\, 0\right) = 0, \quad f_2\left(x_{1_0},\, x_{2_0},\, 0,\, 0,\, 0\right) = 0.$$

The 2nd step is the standard frequency analysis, i.e., solving system

$$F_{1,\,2}(\omega) + \frac{\partial f_{1,\,2}}{\partial x_1}^{(0)} \Delta X_1 + \frac{\partial f_{1,\,2}}{\partial x_2}^{(0)} \Delta X_2 + j\omega \frac{\partial f_{1,\,2}}{\partial \dot{x}_1}^{(0)} \Delta X_1 + j\omega \frac{\partial f_{1,\,2}}{\partial \dot{x}_2}^{(0)} \Delta X_2 = 0, \qquad (1)$$

which must be performed for the frequencies ω_1 and ω_2. In this way, we obtain the first-order products $\Delta X_1(\omega_1)$, $\Delta X_1(\omega_2)$, $\Delta X_2(\omega_1)$, and $\Delta X_2(\omega_2)$. The terms $F_1(\omega)$ and $F_2(\omega)$ represent independent (signal) sources of the circuit.

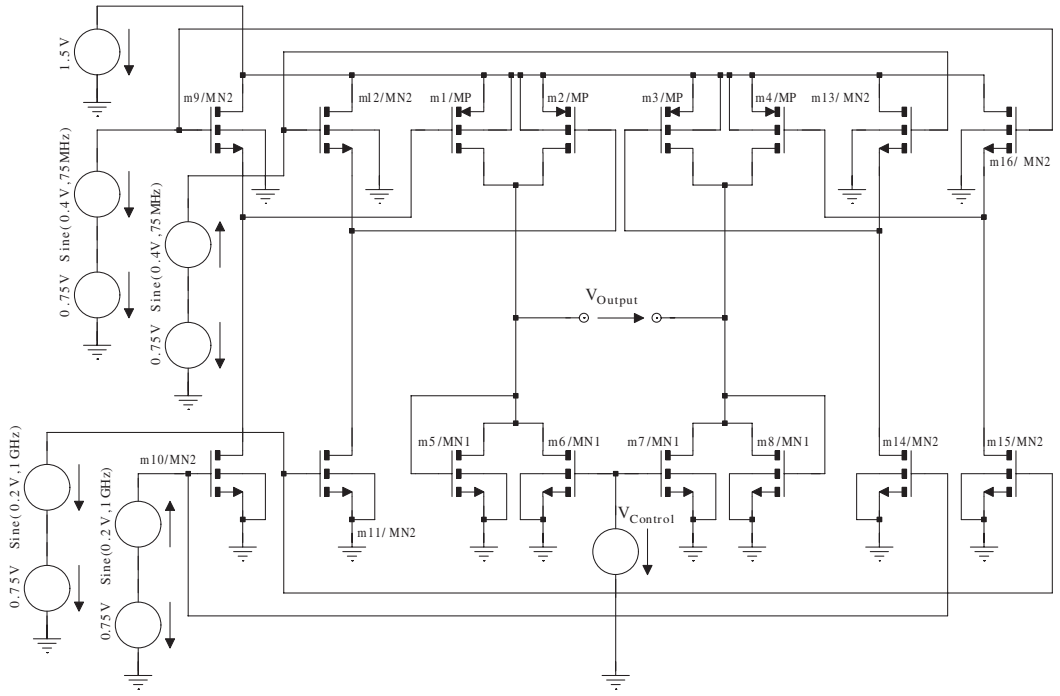

The 3rd step: the second-order intermodulation products can be estimated using the second-order terms in Taylor series as signal sources of circuit (instead of the independent ones), i.e., the system

$$\begin{aligned}
&\frac{\partial f_{1,2}}{\partial x_1}^{(0)}\Delta X_1' + \frac{\partial f_{1,2}}{\partial x_2}^{(0)}\Delta X_2' + j\omega\frac{\partial f_{1,2}}{\partial \dot{x}_1}^{(0)}\Delta X_1' + j\omega\frac{\partial f_{1,2}}{\partial \dot{x}_2}^{(0)}\Delta X_2' + \frac{\partial^2 f_{1,2}}{\partial x_1 \partial x_2}^{(0)}\Delta X_1\Delta X_2 \\
&+ j\omega\frac{\partial^2 f_{1,2}}{\partial x_1 \partial \dot{x}_1}^{(0)}\Delta X_1^2 + j\omega\frac{\partial^2 f_{1,2}}{\partial x_1 \partial \dot{x}_2}^{(0)}\Delta X_1\Delta X_2 + j\omega\frac{\partial^2 f_{1,2}}{\partial x_2 \partial \dot{x}_1}^{(0)}\Delta X_2\Delta X_1 + j\omega\frac{\partial^2 f_{1,2}}{\partial x_2 \partial \dot{x}_2}^{(0)}\Delta X_2^2 \\
&- \omega^2\frac{\partial^2 f_{1,2}}{\partial \dot{x}_1 \partial \dot{x}_2}^{(0)}\Delta X_1\Delta X_2 + \frac{1}{2}\frac{\partial^2 f_{1,2}}{\partial x_1^2}^{(0)}\Delta X_1^2 + \frac{1}{2}\frac{\partial^2 f_{1,2}}{\partial x_2^2}^{(0)}\Delta X_2^2 - \omega^2\frac{1}{2}\frac{\partial^2 f_{1,2}}{\partial \dot{x}_1^2}^{(0)}\Delta X_1^2 \\
&- \omega^2\frac{1}{2}\frac{\partial^2 f_{1,2}}{\partial \dot{x}_2^2}^{(0)}\Delta X_2^2 = 0
\end{aligned}$$

must be solved for the frequencies $\omega_1+\omega_1$, $\omega_2+\omega_2$, $\omega_1+\omega_2$, and $\omega_1-\omega_2$, which gives the second-order harmonic and intermodulation products $\Delta X_1'(\omega_1+\omega_1)$, $\Delta X_1'(\omega_2+\omega_2)$, $\Delta X_2'(\omega_1+\omega_1)$, $\Delta X_2'(\omega_2+\omega_2)$, $\Delta X_1'(\omega_1+\omega_2)$, $\Delta X_1'(\omega_1-\omega_2)$, $\Delta X_2'(\omega_1+\omega_2)$, and $\Delta X_2'(\omega_1-\omega_2)$. The higher-order products can be determined in an analogical way by the higher-order terms.

$\lvert V_{\mathrm{Output}}\rvert_{\max}$	V_{Control}	$V_{\mathrm{Output,\,1.075\,GHz}}$	$V_{\mathrm{Output,\,0.925\,GHz}}$
19.3 mV	1 V	7.02 mV	7.57 mV
22.6 mV	1.1 V	7.59 mV	8.29 mV
26.4 mV	1.2 V	8.38 mV	9.27 mV
33.1 mV	1.3 V	9.47 mV	10.6 mV
41.9 mV	1.4 V	11 mV	12.5 mV
49 mV	1.5 V	13 mV	15 mV

V_{Control}	$V_{\mathrm{Output,\,1.075\,GHz}}$	$V_{\mathrm{Output,\,0.925\,GHz}}$	V_{Control}	$V_{\mathrm{Output,\,3.075\,GHz}}$	$V_{\mathrm{Output,\,2.925\,GHz}}$
1 V	8.97 mV	10.1 mV	1 V	0.217 mV	0.228 mV
1.1 V	10.2 mV	11.5 mV	1.1 V	0.218 mV	0.229 mV
1.2 V	11.9 mV	13.6 mV	1.2 V	0.22 mV	0.232 mV
1.3 V	14.5 mV	16.8 mV	1.3 V	0.227 mV	0.239 mV
1.4 V	18.3 mV	21.2 mV	1.4 V	0.238 mV	0.252 mV
1.5 V	22 mV	25.7 mV	1.5 V	0.273 mV	0.29 mV
V_{Control}	$V_{\mathrm{Output,\,1.225\,GHz}}$	$V_{\mathrm{Output,\,0.775\,GHz}}$	V_{Control}	$V_{\mathrm{Output,\,1.375\,GHz}}$	$V_{\mathrm{Output,\,0.625\,GHz}}$
1 V	0.333 mV	0.377 mV	1 V	49.7 µV	29.9 µV
1.1 V	0.371 mV	0.485 mV	1.1 V	59.6 µV	43.8 µV
1.2 V	0.501 mV	0.712 mV	1.2 V	79 µV	72.3 µV
1.3 V	0.817 mV	1.18 mV	1.3 V	125 µV	145 µV
1.4 V	1.28 mV	1.85 mV	1.4 V	75.9 µV	120 µV
1.5 V	1.22 mV	1.67 mV	1.5 V	387 µV	773 µV

An example: For a microwave four-quadrant multiplier, the intermodulation products have been computed by both Volterra series (left table) and SS & FFT analyses (tables below). As shown, the fast estimations are possible especially for lower values of $V_{\mathrm{Output},\,f_1\pm f_2}$.

REFERENCES

1. Dobeš, J., D. Biolek, and P. Posolda, "An efficient steady-state analysis of microwave circuits," *International Journal of Microwawe and Optical Technology*, Vol. 1, No. 2, 284–289, ISRAMT, Reno, NV, Aug. 2006.

Modeling a Transmission Interconnect by Optimal Number of Lumped Sections

S. R. Nelatury[1], **M. N. O. Sadiku**[2], **and V. K. Devabhaktuni**[3]

[1]School of Engineering, Pennsylvania State University, Erie, PA 16563, USA
[2]College of Engineering, Prairie View A&M University, Prairie View, TX 77446, USA
[3]Department of ECE, Concordia University, Montreal, QC, H3G 1M8, Canada

Abstract— The growing demand for high speed interconnects in VLSI circuits has turned a high impetus for their accurate modeling. The classical uniform transmission line theory based on distributed RLC circuit model has several limitations as far as CAD practices are concerned. Distributed models are being replaced with reduced order lumped models for efficient simulation and design applications. The present literature is replete with numerous reduced order models and macro-models. These models are developed based on an approximating criterion either in time or frequency domain with the aim of reducing computational complexity.

We introduce a technique to find the optimum number of lumped sections for approximating a transmission interconnect of a given length and rise time. This is done by first considering the simple well-known connection between the primary constants of the line and the image parameters of each individual section viewed as a linear two-port network. Next the sensitivity of this relation as a function of frequency is used to develop a formula for the least number of sections needed. This method is further compared with the existing frequency domain based macro-models. Since the final formulas turn out to be simpler, they have excellent use in CAD applications.

REFERENCES

1. Achar, R. and M. Nakhla, "Simulation of high-speed interconnects," *Proc. IEEE*, Vol. 89, No. 5, 693–728, May 2001.
2. Palenius, T. and J. Roos, "Comparison of reduced-order interconnect macromodels for time-domain simulation," *IEEE Trans. Microwave Theory & Tech.*, Vol. 52, No. 9, 2240–2250, Sept. 2004.
3. Gunupudi, P. K., R. Khazaka, M. S. Nakhla, T. Smy, and D. Celo, "Passive parameterized time-domain macromodels for high-speed transmission-line networks," *IEEE Trans. Microwave Theory & Tech.*, Vol. 51, No. 12, 2347–2354, Dec. 2003.
4. Grivet-Talocia, S., S. Acquadro, M. Bandinu, F. G. Canavero, I. Kelander, and M. Rouvala, "A parameterization scheme for lossy transmission line macromodels with application to high speed interconnects in mobile devices," *IEEE Trans. Electromagn. Compat.*, Vol. 49, No. 1, 18–24, Feb. 2007.

Session 2P2
Theory, Modeling and Inversion of Controlled-source Electromagnetic and Magnetotelluric for Geophysical Applications

Rational Krylov Subspace Reduction for Solution of CSEM and MT Problems

Mikhail Zaslavsky[1], **Vladimir Druskin**[1], **and Leonid Knizhnerman**[2]

[1]Schlumberger Doll Research, 1 Hampshire str., Cambridge, MA 02139, USA
[2]Central Geophysical Expedition, 38/3 Narodnogo opolcheniya str., Moscow 123298, Russia

Abstract— Many boundary value problems can be reduced to computation of $u = f(A)\varphi$, where A is an operator in a Hilbert space, u and φ are elements of the same space. In practice A can be large ill-conditioned matrix obtained after discretization of a PDE operator, that is why it is convenient to consider A as an unbounded operator in Hilbert space.

The resolvent and the exponent are the most commonly used functions appeared in the solution of linear evolutionary equations in frequency or time domain respectively. Typically, u should be computed for multiple values of frequencies or times within some range. As important practical application, we consider the magnetic fieldformulation of the frequency-domain Maxwell equations in the infinite 3D domain in low frequency regime (displacement currents are assumed to be negligible) with zero boundary conditions at infinity. Magnetic permeability is assumed to be constant throughout the whole domain.

We solve a frequency domain electromagnetic scattering problem for an interval in the frequency domain using Rational Krylov Subspace (RKS) reduction. The RKS is constructed by spanning on the solutions for certain a priori chosen set of frequencies. We select these frequencies based on Zolotaryov's approximation of resolvent in the spectral domain and show that such a choice is asymptotically optimal. For time domain problems we use also the same RKS but corresponding set of interpolating frequencies was chosen by minimization of error in time domain.

The theory is illustrated by numerical examples for the Maxwell's frequency and time domain equations arising in 3D magneto-telluric geophysical exploration.

Marine CSEM Data for Reservoir Production Monitoring: Feasibility and Initial Identification Results

Shaaban Bakr[1], **Inga Berre**[1,2], **Martha Lien**[1], **and Trond Mannseth**[1,2]

[1]Centre for Integrated Petroleum Research, University of Bergen, Norway
[2]Department of Mathematics, University of Bergen, Norway

Abstract— We present a model study of marine Controlled Source Electromagnetic (CSEM) data, aiming at monitoring of the flooding front during waterflooding of an oil reservoir. An assessment of the feasibility of using marine CSEM data for this purpose is presented, along with some initial estimation results for the electric conductivity, and a suggestion for simplifying the forward model calculations.

Electric conductivity changes of interest for reservoir monitoring typically occur over spatial regions much smaller than the reservoir itself. This application of marine CSEM data therefore requires higher accuracy than exploration. On the other hand, some errors may experience (partial) time-lapse cancellation in the monitoring application.

The feasibility of using marine CSEM data for reservoir monitoring is assessed by computing the response in the data to changes in the electric conductivity that are of interest for monitoring purposes. The strength of the response is then compared to the strength of various errors that can occur in the time-lapse data.

The estimation of the electric conductivity changes is performed using a level set formulation. With this type of formulation, no restrictions are put on the shape of the conductivity changes that can occur. Errors in the data as well as limited resolution properties of the inverse mapping from CSEM data to electric conductivity, however, puts restrictions on the changes that can be identified. Hence, the inverse problem of identifying detailed conductivity changes is illposed and requires some form of regularization to be stable. We regularize the problem by applying a coarse representation of the level set function. We present some initial identification results with this method, and discuss how the forward model calculations can be simplified for typical marine CSEM frequencies.

On the Waveguide Effect in Marine CSEM

L. O. Løseth and L. Amundsen
StatoilHydro ASA, Norway

Abstract— The main goal in marine CSEM for hydrocarbon exploration is to detect and characterize possible thin resistive layers within the conductive surroundings beneath the seabed. How the response from a resistive reservoir varies with characteristic parameters such as layer thickness and conductivity can be investigated using spatial expressions that are derived by analyzing the CSEM field integrals with asymptotic methods.

Background: Marine CSEM hydrocarbon detection exploits that a thin resistive layer transports EM energy with higher velocity and less attenuation than the conductive surroundings. To understand how the EM signals propagate, it has been found useful to analyze the field integrals for stratified media [1] by the method of steepest descents. An asymptotic evaluation of the field integrals in terms of the TE and TM modes shows that, for a stratified three-layer model, the major signal pathway will be via the thin resistive reservoir and that this is a guided TM-polarized mode [2].

Thin Resistive Layer Response: The spatial expression for the inline electric field due to a horizontal electric dipole in a background medium (conductivity σ_1), when a thin resistive layer (conductivity σ_2) is present, can be written as [2]:

$$E_\rho \approx \frac{Il\omega\mu}{4\pi}\frac{\pi}{d_2}\frac{\sigma_2}{\sigma_1}\left[1+\frac{n_1^2}{ik_1d_2\mathcal{Q}}\right]\cos^2\theta_p\left[H_0\left(k_1\rho\sin\theta_p\right)\right.$$
$$\left.-\frac{1}{k_1\rho\sin\theta_p}H_1\left(k_1\rho\sin\theta_p\right)\right]\exp\left(ik_1h\cos\theta_p\right), \qquad (1)$$

where Il is the dipole current moment, ρ is the horizontal offset, H_0 and H_1 are Hankel functions of the zeroth and first order, respectively, and $\mathcal{Q}=[1-n_1^2(1+n_1^2/k_1^2d_2^2)]^{1/2}$. With a low source-signal frequency ω, the wavenumber in the background medium is $k_1 \backsimeq \sqrt{i\omega\mu\sigma_1}$, where μ is the permeability. The conductivity contrast between the reservoir and overburden is $n_1=\sqrt{\sigma_2/\sigma_1}$. It has been assumed that n_1 is small. The parameter h is the vertical propagation distance in the overburden, and d_2 is the thickness of the thin layer. The expressions for the sine and cosine can be approximated as

$$\cos\theta_p \approx \mathcal{Q}-\frac{in_1^2}{k_1d_2} \quad \text{and} \quad \sin\theta_p \approx n_1\sqrt{\frac{2i}{k_1d_2}\mathcal{Q}+1+\frac{2n_1^2}{k_1^2d_2^2}}. \qquad (2)$$

The large parameter that justifies the asymptotic expansion is the horizontal propagation distance, ρ.

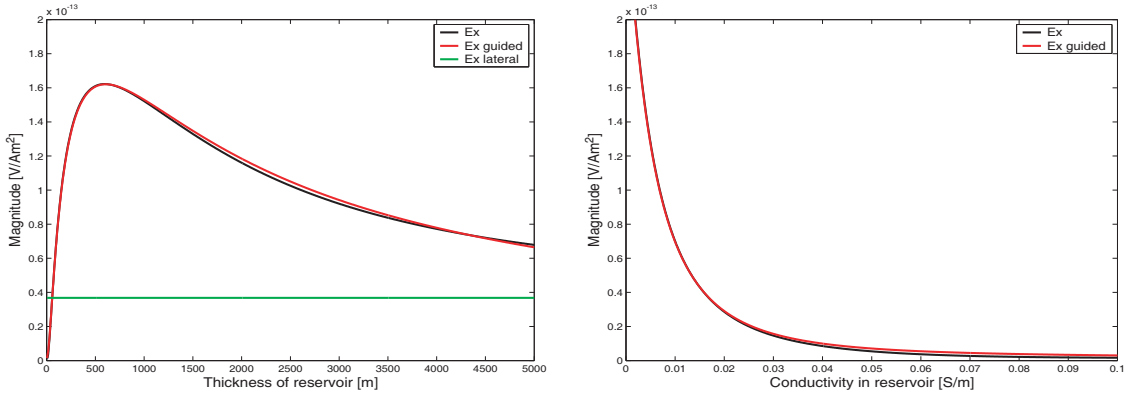

(a) (b)

Figure 1: Electric field magnitude at 8 km offset as function of d_2 to the left and as function of σ_2 to the right.

Results: In Figure 1(a) the electric field response is plotted as a function of layer thickness d_2 for a horizontal offset of 8 km. The response given in Equation (1) is plotted in red, whereas the total field, obtained by numerical simulation, is plotted in black. The model parameters used were $f = 0.25\,\mathrm{Hz}$, $\sigma_1 = 1.0\,\mathrm{S/m}$, $\sigma_2 = 0.01\,\mathrm{S/m}$,, and $h = (1030 + 1000)\,\mathrm{m}$. For reference, the response when $d_2 = \infty$ is shown in green. The plot demonstrates the guiding effect of the thin resistive layer. The maximum response at the offset shown here is for $d_2 \approx 500\,\mathrm{m}$. In Figure 1(b) the response is shown as a function of thin-layer conductivity for $d_2 = 100\,\mathrm{m}$. The reservoir response is enhanced significantly as the conductivity ratio σ_1/σ_2 becomes larger than ~ 20.

REFERENCES

1. Kong, J. A., "Electromagnetic fields due to dipole antennas over stratified anisotropic media," *Geophysics*, Vol. 37, 985–996, 1972.
2. Løseth, L. O., Modelling of Controlled Source Electromagnetic Data, PhD Thesis, NTNU, 2007.

Removal of Sea Surface Related Wavefields from CSEM Data

P. M. van den Berg[1], **A. Abubakar**[2], **and T. M. Habashy**[2]

[1]Delft University of Technology, The Netherlands
[2]Schlumberger-Doll Research, Cambridge, USA

Abstract— For a controlled-source (CSEM) survey in a shallow water environment, the presence of the sea surface hinders the interpretation of the measured data significantly. The electromagnetic (EM) wavefields are partly reflected and partly transmitted by the sea surface. This means that the source signal is contaminated by its so-called source-ghost signal and that the received signals are contaminated by the so-called receiver ghost signal. Further the receiver-ghost signal can be considered as secondary-source signals that are transmitted in the earth. Hence, for shallow water environment, the removal of all these sea-surface ghost signals from the data is an important step in order to robustly interpret the collected data.

We propose a processing method by which the sea-surface related multiples would be removed, while *a priori* knowledge of the EM source wavelet becomes superfluous. The governing equations are obtained from an appropriate application of the EM reciprocity theorem that relates on one side the EM fields in the actual measurement configuration including the sea surface and on the other side the EM fields in a desired source configuration and in the absence of the sea surface, where the water layer is extended to infinity. In general, measurements with two different types of EM sources are needed, such that, in the actual configuration both transversal electric (TE) and transversal magnetic (TM) waves are present. In the desired configuration, the type of EM source can be arbitrarily chosen, with both its spatial layout and its temporal signal. In particular, a preferred choice of the desired configuration will be one with a vertical magnetic dipole source. In this desired configuration mainly TE waves will occur, while TM waves only arise if lateral inhomogeneities of the subsurface are present. Alternatively, a second choice of the desired configuration will be one with a vertical electric dipole source. Then, mainly TM waves will occur, while TE waves only arise if lateral changes of the subsurface are present. This procedure facilitates an enhanced interpretation of the "multiple-free" field data.

Preprocessing of Marine CSEM Data and Model Preparation for Frequency-domain 3D Inversion

J. J. Zach[1], **F. Roth**[1], **and H. Yuan**[2]

[1]EMGS ASA, Stiklestadveien 1, 7041 Trondheim, Norway
[2]EMGS Americas, 16000 Barkers Point Lane, Suite 145, Houston, TX 77079, USA

Abstract— The rapid growth of the marine EM industry during the past decade is driving the evolution of marine CSEM surveys towards the acquisition of 3D grids for detailed resistivity imaging of areas with complex geology or reconnaisance in frontier basins. With algorithms for 3D inversion now being introduced by the industry and research community, the demands to procedures and supporting methods for accurate data preprocessing and quality control (QC) have become more vital for advanced inversion algorithms than was the case in traditional standard processing.

We present a processing sequence starting from time series acquired by electric and magnetic seabed receivers to the generation of frequency domain data and data weights for inversion and other advanced interpretation. Intermediate steps include the short-time Fourier transform to extract the frequency spectrum in the neighborhood of the source modes and the determination of receiver orientations from the data itself. Since noise estimates are required to both QC the data processing itself and generate the data weights for an inversion, it is important to extract the noise for each frequency mode only after proper receiver rotation. The quality of the phase is then assessed and, if necessary, corrections are applied based on data characteristics upon source passage. Effects of different weighting schemes on the input into an inversion are assessed.

On the model preparation side, the first challenge consists in harmonizing navigation data with an existing bathymetry model, which needs to be discretized onto a finite grid. Since in many cases, bathymetry is either not available or coverage is limited, a spline-based algorithm to generate a seafloor from navigation data and accurate water depth measurements along the source towlines is presented. For reasons of numerical complexity, it is desirable to reduce the number of iterations in a full 3D inversion scheme by using a starting model which is, in turn, the result from a numerically less challenging scheme. However, to prevent artifacts at discontinuities of the initial resistivity model inherent to local, particularly gradient-based, inversion approaches, the initial model needs to be sufficiently smooth. We will present a procedure to obtain a smooth starting model to 3D inversion by applying a global, simulated-annealing inversion scheme based on a plane layered subsurface model to selected background receivers.

The benefits of the preprocessing sequence and model preparation for a 3D inversion are explained. Their application extends to processing of coarse grid reconnaissance data, where similar preprocessing and model preparation can be used to create a reference model for anomaly detection.

Regularized and Blocky 3D Controlled Source Electromagnetic Inversion

R.-E. Plessix and P. van der Sman

Shell International E & P, The Netherlands

Abstract— Controlled source electromagnetic (CSEM) surveying allows estimating earth resistivity that are useful for prospecting purposes. The interpretation of CSEM data prove challenging in complex geological settings like for instance those with hydrates, salt or basalt bodies or multiple and stacked resistive bodies. Often a sophisticated imaging strategy is required. In this presentation, we formulated the 3D CSEM anisotropic resistivity imaging problem as an inverse problem and we minimized a least-squares misfit functional. We implemented a local optimization technique since a typical 3D CSEM inversion can contain up to 20 million unknowns. We used a limited BFGS quasi-Newton optimization in order to avoid the computation of the Hessian. Computational and inversion grids are decoupled to simultaneously invert for multiple frequencies without additional computational effort. Furthermore, model and data weights are applied to improve the convergence of the non-linear inversion. To reduce the non-uniqueness of this inverse problem, a-priori information obtained for instance from seismic interpretation may be included. This can be achieved in either a blocky inversion, i.e., where the resistivity cube is parameterized with a small number of parameters or with a regularized inversion. Since earth resistivity contrasts can be high and spatially well defined, the total variation or minimum norm support regularization terms are implemented. In this presentation, we will first describe the inversion and discuss model and data weights in combination with the limited BFGS quasi-Newton algorithm. We will illustrate the relevance of this approach with a few synthetics examples where the number of inversion iterations is divided by at least a factor of two when weights are correctly chosen. Next we will present some results of the blocky and regularized inversion approaches. Although the blocky inversion proves quite powerful, we will show that results can be misleading particularly in complex geological settings. A combination of the blocky and regularized inversions may then provide a more robust approach to interpret CSEM imaging results. We will illustrate this with synthetic examples in deep-water settings and with a real example if permission to publish is granted.

Conductivity Reconstruction from Marine Controlled Source Electromagnetic Data Using a 2.5D Model-based Inversion Algorithm

Maokun Li, **Aria Abubakar**, **and Tarek M. Habashy**
Schlumberger-Doll Research, 1st Hampshire St., Cambridge, MA 02141, USA

Abstract— The marine controlled-source electromagnetic (CSEM) technology has recently gained significant attentions for off-shore oil explorations. In this method, very low frequency electromagnetic sources (0.1 10 Hz), located right above the seabed, are towed by a ship, and multi-component electromagnetic receivers with a wide dynamic range are sent to the seafloor to record data. This method has recently been successful in several field surveys. In physics, the electromagnetic wave couples more to the sea bed due to the large conductivity of the sea water. Moreover, the high contrast in resistivity between saline-filled rocks and hydrocarbons makes this method well suited for detecting thin oil reservoirs.

In the interpretation of CSEM data, nonlinear inversion algorithms are more attractive because of its accuracy for high-contrast regions. A common way in the inversion process is to divide the domain of interest into subgrids with unknown parameters defined on each pixel, and then apply an optimization approach to match the responses between the data observed and the data generated from the estimated model.

In this abstract, we present a model-based inversion scheme for processing the CSEM data, which reconstructs the conductivities and shapes of the regions of interests based on some *a priori information*. The required *a priori* information can come from independent measurements (e.g., seismic) or from the inversion results of the same data using a pixel-based inversion approach. Based on these results, regional geometry models are constructed to describe the geological structures. The parameters that describe the model are optimized according the receiving signal using a Gauss- Newton minimization approach. A multiplicative regularization and a line search algorithm are used to stabilize the inversion process. In the computation of the Jacobian matrix, a chain rule is used with an adjoint approach so that the forward solver is only called once in every iteration of the inversion process. The forward solver used a frequency domain finite difference algorithm to solve the Maxwell equations for electric field. In order to render the forward algorithm more efficient, several techniques have been applied. For example, the regions outside the domain of interest are discretized using optimal grids in both x and z directions. This helps to reduce the number of unknowns while still maintaining a good accuracy. This optimal grid technique is also used to select the spatial frequency components along the invariant y-direction. Moreover, a material averaging formula is used to calculate the effective material properties on both small and large grids. Also, since the matrix generated from the finite-difference method is very sparse, a multi-frontal LU decomposition method is used as the solver, which can be very efficient for solving the electric field equation with multiple right-hand sides. In this model-based inversion algorithm, the shape of the various regions can be reconstructed along with their locations and conductivities. Some initial numerical tests of CSEM models show good reconstructions.

Joint Inversion of Marine CSEM and MT Data for Anisotropic Resistivity

Randall Macki[1] and William Rodi[2]

[1]WesternGeco, 2261 Market St., PMB 643, San Francisco, CA 94114-1600, USA
[2]Massachusetts Institute of Technology, USA

Abstract— Marine controlled source electromagnetic (MCSEM) data are increasingly being used for offshore hydrocarbon exploration because the vertical electric currents generated by electric dipole sources respond dramatically to thin resistive layers associated with hydrocarbon accumulations. Marine magnetotelluric (MMT) data are insensitive to thin resistive layers but because they result from naturally occurring source fields, MMT data are sensitive to the regional conductivity structure to great depths. MCSEM and MMT data therefore provide complementary information and jointly interpreting both datasets can improve resolution and confidence in the interpreted models.

This talk describes a 3D joint inversion algorithm for MCSEM and MMT data that we have implemented on a large parallel cluster for routine application to field data. The forward modeling algorithm is based on 3D finite difference solution of Maxwell's equations using staggered grids. Inversion models solve a regularized least-squares criterion and are computed with a nonlinear conjugate gradients (NLCG) method for optimization. Numerical examples will show that jointly inverting the two complementary datasets can provide increased resolution compared to separate inversions of each individual dataset. However, it is common in the geological settings where these methods are used that the vertical resistivity is different from the horizontal resistivity and therefore it is necessary when interpreting real data to allow for the possibility of anisotropic conductivity structure. We have therefore expanded our inversion algorithm to include diagonal anisotropy, but with the constraint that the anisotropy is only allowed where required to fit the data.

A Joint Inversion Algorithm for the Integration of Controlled-source Electromagnetic and Seismic Measurement Data

W. Hu, **A. Abubakar**, **and T. M. Habashy**

Schlumberger-Doll Research, One Hampshire Street, Cambridge, MA 02139, USA

Abstract— We present a dual-physics frequency-domain two-dimensional data inversion algorithm to improve quantitatively and qualitatively imaging and inversion performance for large scale nonlinear problems in a geophysical setting.

The forward algorithms for seismic and electromagnetic problems employ a finite difference frequency domain (FDFD) method. The optimal grid and PML techniques are used for the controlled-source electromagnetic (CSEM) and the seismic models respectively to minimize artificial reflections from the boundaries due to the truncation of the computational domains. The frequency domain forward model enables us to obtain the fields simultaneously by solving the linear system of equations using an LU decomposition method.

The inverse algorithm that we develop is based on a constrained Gauss-Newton optimization to achieve a quadratic convergence rate. A line-search procedure is used so that the error reduction of the cost function is guaranteed. We employ the so-called multiplicative regularization technique to automatically choose the regularization parameters. The weighted L_2 norm is used to reconstruct structures with sharp boundaries.

In this joint inversion algorithm, the electromagnetic and seismic measurement data are integrated through a cross-gradient regularization function that maximizes the structural similarity between the conductivity image and the P-wave velocity image. Both simultaneous and alternating joint inversion schemes are proposed, tested, and compared. We find the alternating joint inversion has better performance and efficiency than the simultaneous joint inversion scheme. A reliability coefficient is designed to improve the robustness of this algorithm. According to the simulation results, this joint inversion algorithm shows significant improvement over the separate electromagnetic or seismic inversion algorithm. The simulation results also suggest that the multi-frequency data provide better inversion performance. In addition, *a priori* information on the reliability of the measurement data is helpful in further improving the image reconstruction quality.

Integration of Electromagnetic, Seismic and Well Log Data to Characterize Hydrocarbon Reservoirs

Lucy MacGregor, **Peter Harris**, **and David Andreis**
OHM Ltd., UK

Abstract— Improved reservoir management and production optimisation demands require accurate characterisation of reservoir properties and their changes through time. Advances in geophysical data acquisition and interpretation have led to significant improvements in the remote imaging of earth structure and properties. However, when only a single data type is considered, ambiguities in the interpretation can remain. Integration of disparate geophysical data types allows the strengths of each to be exploited. Here we will concentrate on three contrasting methods: surface seismic, marine controlled source electromagnetic (CSEM) and well-log data.

Seismic data are commonly used to provide images of the sub-surface, and develop high resolution geological models of structure and stratigraphy. Amplitude variation with offset (AVO) and inversion for acoustic and elastic impedance may also be used to constrain properties such as elastic moduli and density. However seismic data alone in many situations cannot give a complete picture of the reservoir. For example, AVO anomalies may be caused either by fluid or lithological variations, which cannot be separated on the basis of the seismic data alone.

The CSEM method has gained acceptance in recent years as a technology for hydrocarbon exploration and reservoir characterization. The method uses a high powered electric dipole source to transmit an electromagnetic signal through the seafloor to an array of receivers. Analysis of the resulting data allows remote mapping of the resistivity structure beneath the seafloor. The CSEM technique lacks the fine structural resolution of seismic data, however the method is particularly sensitive to the properties and distribution of fluids within the earth. Whereas traditionally the method has been applied in deepwater exploration areas, recent advances have made surveying in shallow water routine.

Well logs provide a high resolution measurement of the properties of a reservoir and the surrounding strata, however properties can only be determined in a small area local to the well. Often a measurement of reservoir properties across the extent of a field are desirable for reservoir management or production optimization.

It is clear that a careful combination of all three data types can supply information that is not available, or is unreliable from any one data type alone. We will present a case study highlighting the integration of CSEM with other geophysical data to determine reservoir properties.

Session 2P3
Electromagnetics Wave and Media: RF and Microwave Applications including Emerging Technologies for Future Wireless Communication Systems

Anisotropic Turbulance Spectrum: Focus on Some Angular Scattering Properties of a Radiation

R. Talhi[1], **A. Lebrere**[1], **F. Costen**[2], **and J. Watermann**[1]

[1]University of Tours and C.N.R.S — UMR 6115
3A, Avenue de la Recherche Scientifique, 45071 Orleans Cedex 2, France
[2]School of Electrical and Electronic Engineering
University of Manchester, Manchester, M601QD, UK

Abstract— Straddling the border between mathematics (hydrodynamical partial differential equations) and physics (spatial statistics of turbulent flows), turbulence (irregular phenomena related to flows in gases and liquids) although having been studied extensively, remains one of the principal unsolved conceptual problems, with a variety of ramifications from meteorology through astrophysics to wave propagation in the atmosphere and oceans. Difficulties in the theory of turbulence are mainly due to nonlinear interactions between motions on different spatial and temporary scales which generate random flow fields. Furthermore, these turbulent flows may be affected by spatial anisotropy as is the case for example in geophysics (the anisotropic irregularities in the ionosphere aligned with the terrestrial magnetic field) and astrophysics (anisotropic turbulence in the interstellar medium and solar wind due to the presence of strong and quasi-uniform magnetic fields) [1, 2].

In order to accurately predict turbulence effects on angular wave scattering, it is important to best represent turbulence phenomenon by an appropriate spectral model (various forms have been proposed, among them the classical ones: Kolmogorov, Gaussian, or von Karman [3]). The proposed model should be able, in particular if a broad range of spatial scales is to be covered, to precisely describe the whole turbulence spectrum, including the three primary spectral sub-ranges (the energy-containing, the inertial, and the dissipation), in all flows. It is worth noting that only the inertial sub-range has a well-defined spectrum; consequently, in a given propagation problem where large-scale motions are considered, one should know which specific part of the turbulence spectrum contributes significantly to a scattering process.

Among the issues that attracted much interest in recent years, is the role of anisotropic irregularities encountered, as previously indicated, in many scattering problems dealing with various applications (in geophysics, astrophysics, acoustic, etc). Hence, it might be relevant either to use measurement approach [4] for detecting anisotropic spatial statistics of the turbulence (which is not so practical for 3D-structure), or to conduct a theoretical study in order to elucidate some of the scattering salient features of radiation scattered by anisotropic irregularities, regardless of the considered application; the latter solution is the purpose of the present paper. To this end, we assumed a random medium and its anisotropic irregularities (with longitudinal (l_p) and transversal (l_t) scales so that: $l_t \gg l_p > \lambda$) located along the Z-axis, and having a Gaussian correlation function (taking into account its good mathematical "behaviour"). The radio-wave scattering problem is solved by Monte-Carlo approximation, and the 3D-plot of the Angular Scattering Probability Distribution — A.S.P.D — (or angular scattering phase function) is used to characterize scattering properties of this random medium. The ASPD simulation results show that the 3D-plot varies significantly with the direction of incident wave, and that scattering at normal incidence is much more important than at oblique incidence; some ASPD cross-sections will be discussed. These results provide the best agreement with the published ones [5]. Wave intensity and degree of polarization distributions are also investigated at normal and oblique incidence, for weak, moderate and strong average number of collisions (or optical depths). The corresponding results as well as practical limitations of our model will also be discussed.

REFERENCES

1. Ng, C. S., et al., "Anisotropic fluid turbulence in the interstellar medium and solar wind," *Phys. Plasmas*, Vol. 10, No. 5, 2003.
2. Sukoriansky, S., et al., "A new spectral theory of stratified flows," *Non-linear Processes in Geophysics*, Vol. 13, 9–22, 2006.
3. Wilson, D. K., et al., "Acoustic scattering and the spectrum of atmospheric turbulence," *JASA*, Vol. 105, No. 1, January 1999.

4. Havens, T. C., et al., "Measurement and data processing approach for detecting anisotropic spatial statistics of the turbulence-induced index of refraction fluctuations in the upper atmosphere," *Applied Optics*, Vol. 41, 2800–2808, 2002.
5. Gavrilenko, V. G., et al., "Waves in random media," Vol. 10, 435–445, 2000.

Analysis of Complex SAR Raw Data Compression

Navneet Agrawal[1] and K. Venugopalan[2]

[1]Dept. of Electronics & Communication Engineering, College of Technology & Engineering
MPUAT, Udaipur 313 001, Rajasthan, India
[2]Dept. of Computer Science, University College of Science
M.L.S. University, Udaipur 313 001, Rajasthan, India

Abstract— Synthetic Aperture Radar (SAR) is active and coherent microwave radar, which produces high spatial resolution images from a moving platform — an airplane or a satellite. The radar produces 2D (range and azimuth) terrain reflectivity images by emitting a sequence of closely spaced radio frequency pulses and by sampling the echoes scattered from the ground targets. The received echoes are sampled into In-phase (I) and Quadrature (Q) components referred to as raw SAR data. In satellite systems, raw data is directly transmitted to the ground segment via a dedicated transmission link when in view with the ground segment or is stored onboard for later transmission to the ground.

The compression of raw SAR data poses several challenges due to its noise like characteristics. The noise like characteristics arises because signals from several scatters are added incoherently with unknown phase and amplitude. Typically its adjacent samples are uncorrelated in both range and azimuth directions.

For the compression of the satellite SAR raw data, the amplitude and phase are both indispensable for many applications e.g., interferometer. We propose to use two formats of the complex SAR raw data for compression: representation with real and imaginary parts and polar format with magnitude and phase. In both the formats the phase information of the compressed data is preserved to a great extent. A block adaptive Max quantizer is used with 1–5 bit quantization of the components. The quality of the reconstructed data is compared in terms of compression ratio and quality parameters: signal to noise ratio (SNR), standard deviation of the phase (PSD), and mean phase error (MPE). The parameters are calculated for SAR raw data, complex data and 8-bit gray scale image. Finally, original and reconstructed gray scale images are presented.

The reconstructed image for the point was also evaluated in terms of the Peak Side Lobe Ratio (PSLR) and Integrated Side Lobe Ratio (ISLR). The PSLR is defined as the ratio of the peak intensity of the most prominent sidelobe to the peak intensity of the mainlobe. The ISLR is the ratio of the power in the mainlobe to the total power in all the sidelobes. The PSLR and the ISLR of the point targets simulation for 256×256 size complex SAR processed image was generated. There is no degradation in PSLR and the improvement in the ISLR is due to the reduction of the sidelobes power.

THz Rectangular Patch Microstrip Antenna Design Using Photonic Crystal as Substrate

Aditi Sharma, Vivek K. Dwivedi, and G. Singh

Department of Electronics and Communication Engineering
Jaypee University of Information Technology, Solan-173 215, India

Abstract— In this paper, we have simulated the rectangular microstrip patch antenna at THz (0.6–0.8 THz) frequency using photonic crystal substrate. The simulation of this proposed antenna has been performed using CST Microwave Studio, which is a commercially available electromagnetic simulator based on finite difference time domain technique. Photonic crystal has been used as substrate material for highly directional resonant antenna [1–4]. Photonic crystals are a class of periodic dielectric, metallic, or composite structures that when introduced to an electromagnetic signal can exhibit a forbidden band of frequencies, in which the incident signal destructively interferes and thus is unable to propagate. Photonic crystal breaking the periodicity of the crystal results in localization of electromagnetic field within the defected volume. With these properties, photonic crystals are novel structure that can be used to control the behaviours of electromagnetic waves. Microstrip antenna mounted on photonic crystal substrate exhibited high efficiency and directivity compared to conventional antenna on dielectric substrate [4]. It is proposed that such a photonic crystal will reduce surface waves and prohibit the formation of substrate modes, which are commonly known inhibitors of the patch antenna design. By reducing or eliminating the effects of these electromagnetic inhibitors with photonic crystals, a broadband response can be obtained from inherently narrowband antennas. It is also useful to a reduction in pattern side lobes resulting in improvements in the radiation pattern front-to-back ratio and overall antenna efficiency. Agi et al. [2] have experimentally and computationally studied the integration of a microstrip patch antenna with a two-dimensional photonic crystal substrate. This antenna was fabricated on a defect in the two-dimensional photonic crystal lattice that localized the energy under the patch antenna. This work [2] can lead to a new design tool for integrating patch antennas with photonic crystal substrates. Fig. 1 shows the return loss of the proposed rectangular patch microstrip antenna at frequency from 620 GHz to 800 GHz. The 10 dB impedance bandwidth is 16.75%.

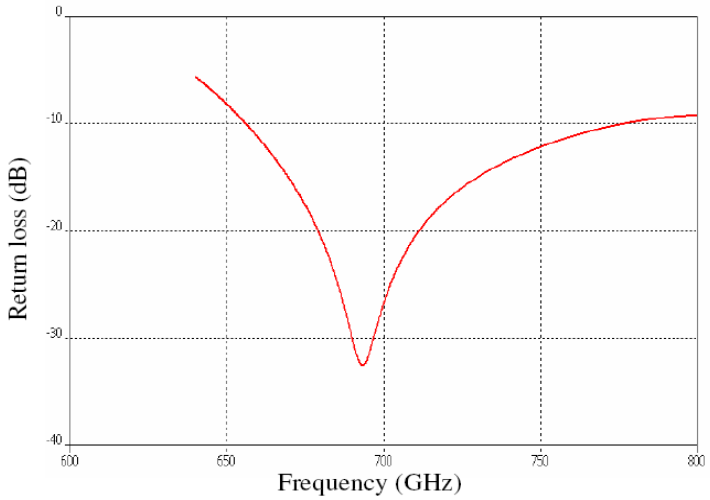

Figure 1: Frequency versus return loss of the proposed rectangular microstrip patch antenna on photonic crystal substrate at THz frequency.

REFERENCES

1. Fernandes, H. C. C. and A. R. B. da Rocha, "Analysis of antennas with PGB substrate," *Int. J. Infrared and Millimeter Waves*, Vol. 24, No. 7, 1171–1176, July 2003.

2. Agi, K., J. Malloy, E. Schamiloglu, and M. Mojahedi, "Integration of a microstrip patch antenna with a two dimensional photonic crystal substrate," *Electromagnetics*, Vol. 19, No. 3, 277–290, May 1999.
3. Radisic, V., Y. Qian, R. Coccioli, and T. Itoh, "Novel 2-D photonic bandgap structure for microstrip lines," *IEEE Microwave and Guided Wave Letters*, Vol. 8, No. 2, 69–71, Feb. 1998.
4. Ozbay, E., B. Temelkuran, and M. Bayindir, "Microwave applications of photonic crystals," *Progress In Electromagnetics Research*, PIER 41, 185–209, 2003.

Novel PSD Function for Multipath Flat Fading Channels

Tao (Stephen) Feng and Timothy Field
McMaster University, Canada

Abstract— Statistical analysis and preperties of wireless channels are essential to wireless communication systems. The traditional *Jakes' spectra* of fading channel is widely accepted in academic and industry, and recommended as a theoretical spectra for channel modeling by international telecommunication union (ITU) for various standards, such as wireless LAN, wireless PAN, etc. Comparing with the real measured spectrum, the Jakes' spectra has some disadvantages, such as 1) the U-shape theoretical spectrum cannot specify the peak value and has a fixed spectral width, i.e., $2f_D$ (f_D is the maximum Doppler frequency shift), whereas the real measured spectrum will reach a peak near the maximum Doppler frequency and then decay to zero. 2) the shape of Jakes' spectra is not adjustable, whereas the real measured spectrum may have variant shapes. In this paper, we extend the traditional Clarke's model incorporating the effect of fluctuations in the component phases, and perform the statistical analysis which results in a closed-form expression of a novel theoretical power spectral density function, which overcomes the above disadvantages of Jake's spectra.

Let the component phases be time-varying, we extend Clarke's model as

$$\varepsilon_t = \sum_{n=1}^{N} a_n \exp\left[j\left(2\pi f_n t + \varphi_t^{(n)}\right)\right], \tag{1}$$

where these component phases $\{\varphi_t^{(n)}\}$ are modeled as a collection of independent Wiener processes with properties

$$d\varphi_t^{(n)} = B^{1/2} dw_t^{(n)}, \tag{2}$$

in which dw_t represents the infinitesimal increments in a Wiener process w_t and $d\varphi_t^{(n)}$ represents the infinitesimal increments in the relative phases $\varphi_t^{(n)}$. Here, B is a positive constant with the dimension of frequency.

Based on (1) and (2), we derive the close form expression for the autocorrelation of the multipath fading channel, i.e., (1), as

$$R_\varepsilon(\tau) = P_0 e^{-B|\tau|/2} J_0(2\pi f_D \tau), \tag{3}$$

where P_0 is average received signal power. The corresponding theoretical power spectrum of the multipath fading channel, i.e., ε_t, is thus the Fourier transform of (3)

$$S_\varepsilon(f) = \int_{-f_D}^{f_D} \frac{B}{\left(\frac{B}{2}\right)^2 + [2\pi(f-\lambda)]^2} \frac{P_0/\pi}{\sqrt{f_D^2 - \lambda^2}} d\lambda. \tag{4}$$

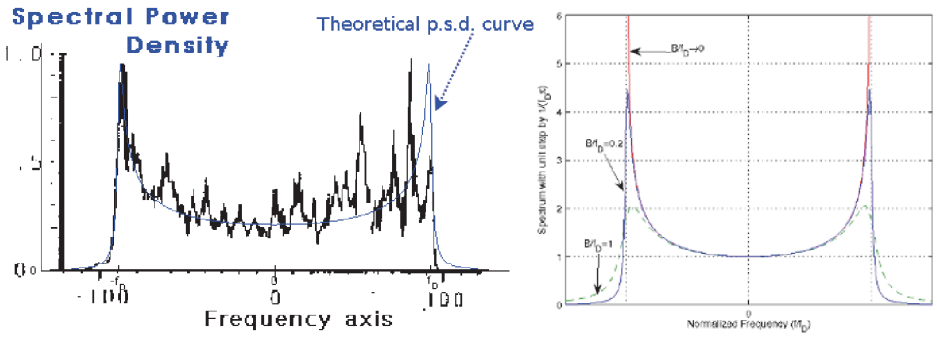

Figure 1: Left: Comparing the novel theoretical power spectrum density with the measured power spectrum density. Theoretical spectrum: $B/f_D = 0.2$, $P_0/f_D = 0.2\pi$. Source of measured spectrum: Research group of Prof. Paul Walter Baier, U. of Kaiserslautern, Germany. Right: The novel theoretical power spectrum vs Jake's spectra (as a special case for $B/f_D \to 0$).

The shape of power spectrum defined in (4) is controlled by the parameter B: Typically, when $B \to 0$, i.e., absence of fluctuations in component phases (cf. (2)), the presented closed-form expression of autocorrelation of the fading (cf. (3)) approaches the autocorrelation for traditional Clarke's model, i.e., $P_0 J_0(2\pi f_{D^\tau})$, whose Fourier transform is the famous *Jakes' spectra*. Thus, the Jakes' spectra is only a special case of the presented novel power spectrum (cf. (4)) when its parameter B approaches to zero.

The peak value and width in the derived power spectrum can be adjusted to fit observed spectra, and we exhibited its shape to conform to the real experimentally measured spectra, in contrast to the situation for the traditional Jakes' spectrum (see Fig. 1). The statistical analysis and results should be essential to effective spectral analysis and channel simulation in real wireless communication systems immersed in time-varying propagation environments, e.g., in the design of a channel simulator based on the proposed multipath channel model for obtaining a desired observed power spectrum.

An Efficient BER Analysis of OFDM Systems with ICI Conjugate Cancellation Method

Vivek K. Dwivedi and G. Singh
Department of Electronics and Communication Engineering
Jaypee University of Information Technology, Solan 173 215, India

Abstract— Orthogonal Frequency Division Multiplexing (OFDM) is broadly considered as an effective approach for the future high speed wireless multimedia communication systems. The basic principle of OFDM is to split the high data stream into number of lower rate data streams which are transmitted simultaneously over a number of subcarriers. High spectral efficiency and multipath immunity are two major features of OFDM technique. However, OFDM system is very sensitive to carrier frequency offset between transmitter and a receiver, which destroys the orthogonality between subcarriers and creates inter carrier interference (ICI). The reduction of the signal amplitude and introduction of the ICI are two destructive effects caused by carrier frequency offset in OFDM systems. So there is a need to reduce ICI. Several methods [1–4] have been developed for bit error rate (BER) analysis of OFDM system. Kang et al. [1] and Zhao and Haggman [2] discuss the self cancellation scheme for OFDM to reduce the effects of frequency offset error. In [3] BER upper bound of OFDM system is analyzed without inter carrier interference (ICI) self cancellation and [4] BER of OFDM system is analyzed using self cancellation but this method is less accurate.

In this paper, we have presented BER analysis of OFDM system with the concept of conjugate cancellation. In the first part of our work an effort has been made to illustrate the mathematical derivation for BER of OFDM system with frequency offset. Later, we have derived a formula for BER analysis of OFDM system with the conjugate cancellation scheme. Fig. 1 shows the compression between BER of ICI self-cancellation method in [4] and proposed conjugate cancellation scheme for frequency offset 0.2. After compensation using ICI self-cancellation method in [4] BER just greater than 10-4 and after compensation using proposed conjugate cancellation method BER approaching 10-5 as shown in Fig. 1. So proposed conjugate cancellation scheme is better than ICI self cancellation in [4] and in proposed scheme upper bound for bit error rate due to frequency offset is tighter than [2]. In this paper, we also discusses carrier to interference ratio and our results are compared with the others reported results.

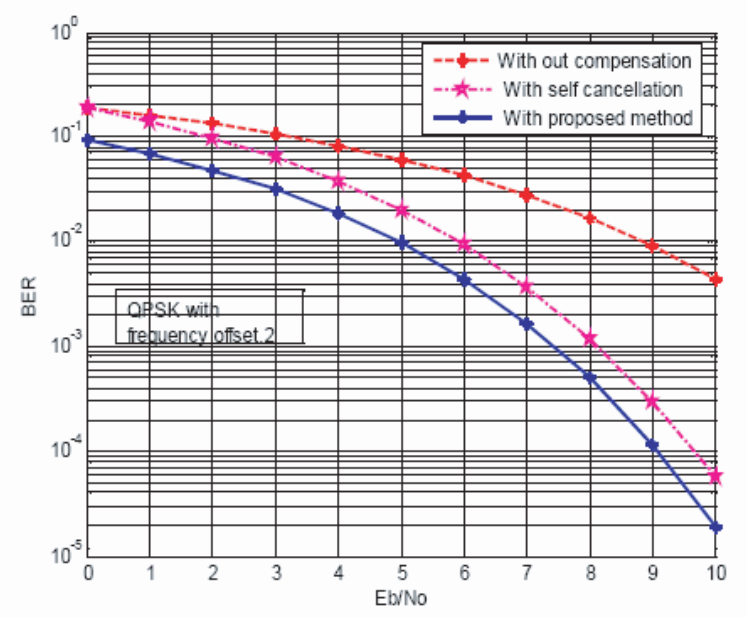

Figure 1: Compression between proposed conjugate ICI cancellation scheme with self cancellation scheme for frequency offset 0.2.

REFERENCES

1. Kang, H., Y. Kim, W. Hwang, and K. Kim, "BER performance of OFDM system with the polynomial self cancellation scheme for OFDM mobile communication systems," *Proc. IEEE APCC/OECC*, Vol. 1, 701–704, Beijing, China, Oct. 1999.
2. Zhao, Y. and S. G. Haggman, "Inter carrier interference self cancellation scheme for OFDM mobile communication systems," *IEEE Trans. Communication*, Vol. 49, No. 7, 1185–91, 2001.
3. Sathananantan, K. and R. M. A. P. Rajatheva, "Analysis of OFDM in presence of frequency offset and method to reduce performance degradation," *Proc. IEEE Globcom.*, Vol. 1, 72–76, San Fransisco, CA, Nov. 2000.
4. Fu, Y. and C. C. Ko, "Theoretical BER analysis of OFDM system with ICI self cancellation," *5th Int. Symposium on Wireless Personal Multimedia Communication*, Vol. 3, 991–994, Oct. 2002.

Empirical Analysis of LCR on a Ku-band Satellite Link

F. Fondjo Fotou[1], **P. F. Tiako**[1], **K. Fujisaki**[2], **and M. Tateiba**[2]

[1]CITR, Department of Computer and Information Sciences
Langston University, USA
[2]Graduate School of Information Science and Electrical Engineering
Kyushu University, Japan

Abstract— Simulation models for fading channels are extremely important for the development, analysis, and test of modern wireless communication systems. The level crossing rate (LCR) analysis of a random process brings out useful information about the underlying process. Combined with the average fade duration (AFD) of the fading channel, it finds diverse applications in the evaluation and design of efficient communication systems. The statistics of fading time intervals is of great importance because it is closely related to the statistics of error bursts, the outage probability and fading rate [1]. It provides useful information for the optimization of the interleaver size as well as for the throughput analysis [2, 3].

The determination of the statistical properties of the fading time intervals is known as the level crossing theory [4]. Only certain aspects in this theory can be solved analytically, e.g., the LCR and the AFD. It is related to the outage probability, fading rate and the average duration of fades. Therefore, the LCR of a random process conveys useful information on the process. Since many analytical aspects of the LCR and AFD have been derived for most random process models with weak or absence of Line of Sight (LOS) component, few experimental tests have been carried out for these models. Moreover, at the level of our knowledge, almost none has been conducted on fixed satellite links.

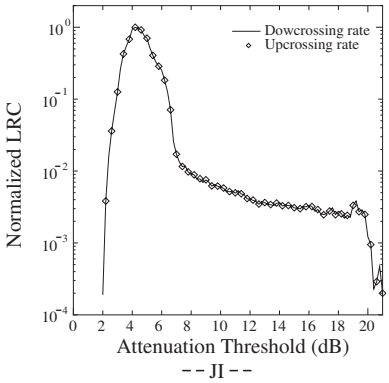

Figure 1: Level crossing conservation law using experimental data.

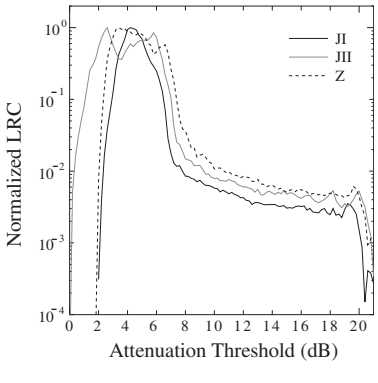

Figure 2: LRC as observed in 3 neighboring experimental stations.

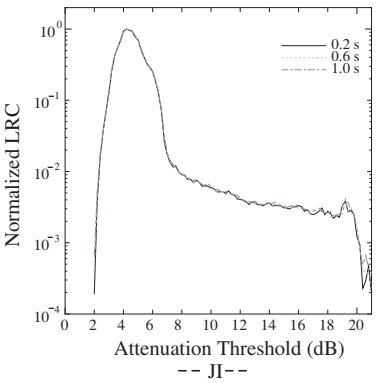

Figure 3: Dependence of the LCR on the data sampling period.

In this article, we briefly analyzed and presented the LCR as it can be observed on satellite links. For a long run, the LCR conservation law (for a given attenuation threshold, the total upcrossing is equal to the total downcrossing) is verified, shown in Figure 1. For 3 neighboring experimental stations, the obtained LCR variation is still conserved (Figure 2). The data sampling period has less effect on LCR for all attenuation threshold as presented in Figure 3. Modeling the LCR on satellite links and comparing the obtained model to theoretical LCR from well known wireless propagation distribution function that takes into account the LOS will be of great importance in satellite communication simulation community.

REFERENCES

1. Ohtani, K. and H. Omori, "Distribution of burst error lengths in Rayliegh fading radio channels," *Electronics Letters*, Vol. 16, No. 23, 889–891, 1981.
2. Tsie, K. Y., P. Fines, and A. H. Aghvami, "Concatenated code and interleaver design for data transmission over fading channels," *Poc. ICDSC-9*, 253–259, Copenhagen, Denmark, May 1992.

3. Patzold, M. and F. Laue, "Level-crossing rate and average duration of fades of deterministic simulation models for rice fading channels," *IEEE Trans. on Veh. Tech.*, Vol. 48, No. 4, July 1999.
4. Brill, P. H., "A brief outline of the level crossing method in stochastic models," *CORS Bulletin*, Vol. 34, No. 4, November 2000.

State-space Model for Multipath Flat Fading Channels

Tao (Stephen) Feng and Timothy Field
McMaster University, Canada

Abstract— This paper develops a novel procedure for a state-space model that represents a Rayleigh flat fading wireless channel. This is achieved by developing the relationship between a continuous-time state-space model and the theory of the rational transfer function. A novel method is presented to obtain a rational even function approximation to the power spectral density of a flat fading channel. Then a state-space approach is applied to the corresponding transfer function (the "root" of the rational even function), obtaining a multi-variable set of stochastic differential equations (SDEs) as the time-dependent dynamical model of the flat fading channel.

We firstly consider a general 'rational even function', which is to approach a general power spectral density function $P(s)$ for a flat fading channel, as

$$R(s) = \frac{a_n s^{2n} + a_{n-1} s^{2n-2} + \ldots + a_1 s^2 + a_0}{s^{2m} + b_{m-1} s^{2m-2} + \ldots + b_1 s^2 + b_0} = \frac{A(s)}{B(s)} \tag{1}$$

where the numerator $A(s)$ and the denominator $B(s)$ are both real even polynomials. Supposing the rational even function $R(s)$ approaches the power spectral density $P(s)$, the polynomial $A(s)$ will approach the product $P(s) \cdot B(s)$. Accordingly we define a square-error function

$$\tilde{Q} = \sum_{i=1}^{L} \left(A\left(s_i\right) - P\left(s_i\right) \cdot B\left(s_i\right) \right)^2, \tag{2}$$

where s_i is defined as $s_i = j2\pi f_i,\ i = 0, 1, \ldots L$, where $f_0, f_1, \ldots, f_L, \in [0, f_{\max}]$ and $0 < f_{\max} < \infty$. If we define a vector $\mathbf{v}$ with components equal to the $n + m + 1$ unknown coefficients in (2) as $\mathbf{v} = (a_0, a_1, \ldots, a_n, b_0, b_1, \ldots, b_{m-1})'$, the square-error $\tilde{Q}$ is a quadratic function of the vector $\mathbf{v}$, i.e., $\tilde{Q}(\mathbf{v})$. To minimize the quadratic function $\tilde{Q}(\mathbf{v})$, we can take partial-derivatives of $\tilde{Q}$ with respect to each individual component of $\mathbf{v}$ and set them to zero, i.e.,

$$\frac{\partial \tilde{Q}}{\partial a_k} = 0, \quad k = 0, \ldots, n \tag{3}$$

$$\frac{\partial \tilde{Q}}{\partial b_k} = 0, \quad k = 0, \ldots, m-1. \tag{4}$$

Expanding (3) and (4), we finally obtain $n + m + 1$ linear equations in the matrix form

$$\mathbf{P} \cdot \mathbf{v} = \mathbf{r}, \tag{5}$$

where $\mathbf{P}$ is a $(n + m + 1) \times (n + m + 1)$ matrix and $\mathbf{r}$ is a $(n + m + 1) \times 1$ vector, both of them from the available values $p(s_i)$ and $s_i,\ i = 1, \ldots, L$. Thus we can obtain the analytical solution for the vector $\mathbf{v}$, i.e., $\mathbf{v} = \mathbf{P}^{-1} \cdot r$.

After obtaining the coefficients, i.e., $\mathbf{v}$, of the rational even function $R(s)$, we can obtain the transfer function $H(s)$ after finding the roots of the polynomials $A(s)$ and $B(s)$ as in (1)

$$H(s) = C \frac{\prod_{l=1}^{n} (s + u_l)}{\prod_{k=1}^{m} (s + v_k)}, \tag{6}$$

where u_l, v_k is the roots of $A(s)$ and $B(s)$ in right half complex plane, i.e., $Re(u_l) > 0$, $Re(v_k) > 0$.

The *Observable Canonical Form* (OCF) realization obtained from (6) is given by

$$\dot{\mathbf{Y}}(t) = \mathbf{C} \cdot \mathbf{Y}(t) + \mathbf{d}x(t) \tag{7}$$

$$z(t) = g \cdot \mathbf{Y}(t) \tag{8}$$

where $x(t)$ and $z(t)$ are the input and output in the time-domain of the given linear system. $\mathbf{Y}(t)$ is a new $m \times 1$ auxilliary state vector introduced to mathematically represent the output $z(t)$ as

$$\mathbf{Y}(t) = \left[y_0(t), y_1(t), \ldots, y_{m-1}(t) \right]'. \tag{9}$$

C and **d** are known from the coefficients of the transfer function 6, g is a constant vector, i.e., $g = [0, 0, \ldots, 0, 1]$.

When the input $x(t)$ is a standard white Gaussian process, the output $z(t)$ will be a Gaussian process with power spectra approaching to the desired spectra $P(s)$. Thus, (7) and (8) are the state-space model representing a flat fading channel with a given spectrum $P(s)$. The presented state-space model is verified by simulations, which show that the model is fast, stable and flexible to the adjustment of parameters, and so has potential for application in various aspects of wireless communications, such as channel estimation/tracking and channel coding, etc.

A Free Access Mat with Ring Patch Resonators for IEEE 802.11 Series

K. S. Eom and H. Arai

Yokohama National University, 79-1 Tokiwadai, Hodogaya, Yokohama 240-8501, Japan

Abstract— A free access mat is sheet-like waveguide for a novel short range wireless access which is free from interference and has small transmission loss characteristics by concentrating the electromagnetic wave into the mat. Recently, the number of wireless devices increases constantly so that restricted wireless coverage area of a device is desirable for many applications in PAN (personal area networks), BAN (body area networks) and indoor wireless sensor networks. Low-power radio, control of protocol, high functional base station antennas for cellular system and waveguide communication system with easy electromagnetic coupling mechanism could be considerable. The free access mat consists of two layers of tightly coupled microstrip resonator array which has a flexible structure applicable to BAN, small transmission loss, strong confinement of electromagnetic wave inside the mat, and easy coupling between mat and external wireless devices in arbitrary place near the mat.

In this paper a free access mat for applications of IEEE 802.11 series is investigated. Designs for the free access mat using resonators on the lower layer connected by microstrip line and ring patch resonators on the lower layer which have small transmission loss at both frequencies of 2.4 GHz and 5 GHz are investigated in Ref. [1]. Small transmission loss characteristics and strong coupling between external antennas and the free access mat are confirmed by measurement. However, the center frequencies did not agree with the designed ones as such the design needed more optimization by consideration of the dielectric permittivity of used substrate in fabrication. In this paper we provide newly optimized design to have small loss at both of 2.4 GHz and 5 GHz.

The outer circumferential length of ring patch resonators is optimized to have a center frequency at 2.4 GHz and the inner one is optimized for 5 GHz. The patch elements on the upper layer and the intervals are optimized to have a small insertion loss. The input/output ports are perfectly matched to the mat and the distance between two ports gives the propagation length L. The electromagnetic wave transmits through the mat by proximate coupling, not through the free space. Small transmission loss characteristics are simulated and the gain which is the difference between the free space transmission loss and the transmission loss through the mat is larger than 18 dB at 2.4 GHz and 19 dB at 5 GHz (where 98 mm$< L <$250 mm), large enough to exclude the effect of multi path caused by the mat. A free access mat for IEEE 802.11 series which has small transmission loss and stability against interference is investigated.

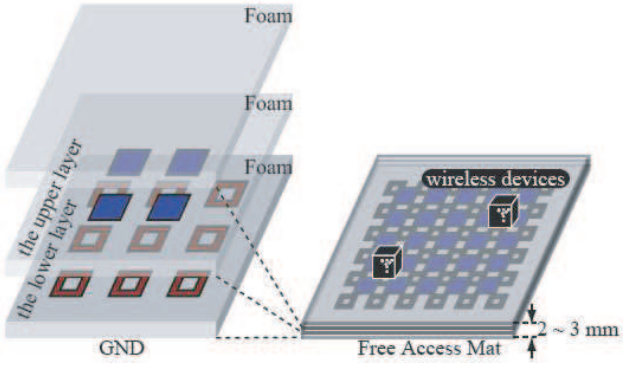

Figure 1: Free access mat with ring patch resonators.

REFERENCES

1. Eom, K. S. and H. Arai, "Dual band free access mat for short range wireless access," *PIMRC'07*, 390, Athens, Greece, September 2007.

A Circularly Polarized Microstrip Ferrite Phase-shifter with Uneven Excitation

Sheikh Sharif I. Mitu and M. M. Dawoud

EE Department, King Fahd University of Petroleum & Minerals, Dhahran, Saudi Arabia

Abstract— Satellite and mobile communications depend on phased array antennas, where ferrite phase shifters are widely used to electronically steer the antenna beams or nulls in the desired direction without physically re-positioning the antenna. However, due to the requirement of large number of phase shifters, the related cost, size and integration process plays an important role in the design of micro/millimeter wave array antennas.

Recently, microstrip ferrite phase shifters received renewed interested due to its low cost, lightweight and compact size. To achieve maximum phase shift per unit length of the device, interaction between the propagating microwave signal and the ferrite substrate needs to be maximized. This can be realized by introducing circularly polarized microwave signal, which interacts strongly or weakly with the biased ferrite substrate depending on the direction of propagation in relation to the externally applied biasing field. Although various techniques are used in the literature [1, 2] to overcome the difficulty of generating circularly polarized waves in a planar structure, they involve complicated geometry and higher insertion loss.

In this paper, three parallel microstrip lines on a ferrite substrate are excited with linearly polarized microwave signals, having uneven magnitude and a progressive phase of 90°, as shown in Figures 1(a) and (b). Note that the propagating signal (*in z axis*) underneath the central microstrip line will be circularly polarized, as shown in 1(c). A novel three way uneven power divider/combiner is used as feed networks to avoid the generation of elliptically polarized signal. The affect of longitudinally and transversely applied biasing field on the insertion phase and insertion loss of the device is observed. The simulated results are compared with that of the equivalent single line microstrip ferrite phase shifter. The resonance region of the ferrite material is carefully excluded to avoid losses.

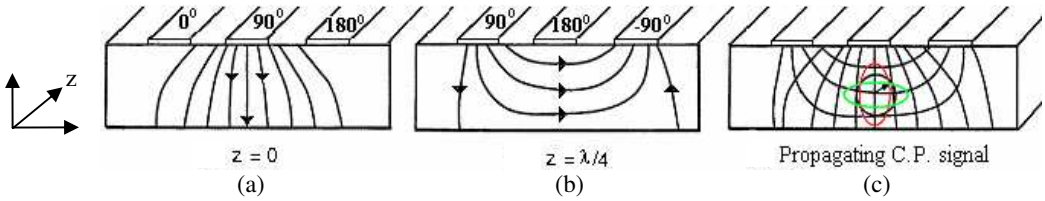

Figure 1: Circularly polarized microwave signal within a ferrite microstrip structure.

REFERENCES

1. Oates, D. E., et al., "Superconductor ferrite phase shifter and circulators," *IEEE Trans. on Applied Superconductivity*, Vol. 7, No. 2, 2347–2350, Jun. 1997.
2. Sorensen, R. K., et al., "Low cost nonplanar microstrip-line ferrite phase shifter utilizing circular polarization," *IEEE MWCL*, Vol. 14, No. 1, 25–27, Jan. 2004.

The Measurement of Angle-of-arrival of Microwave in a Task of Precision Landing of Aircraft

I. B. Shirokov, **A. Ponyatenko**, **and O. Kulish**
Sevastopol National Technical University, Ukraine

Abstract— Methods of positioning of the aircraft with the amplitude methods on large distances are known. This is usual radar task and it is solved and it is implemented almost in all of airports. However accuracy of positioning is not high in this case. It serves for far homing of aircrafts and does not let to make landing.

In present paper the method of automatic overlapping of a longitudinal axis of the aircraft with an axis of a runway is offered. This method is based on the definition of the relative bearing of the aircraft with respect to the axis of runway. So, if the relative bearing is known, there is a possibility to adjust the longitudinal axis of the aircraft with an axis of a runway with the steering gear of the aircraft. The present method is actual, since it allows carrying out this process automatically, with high accuracy.

The method, described in a paper, is based on homodyne method of determining of angle-of-arrival of microwave (A. C. #1718149 (USSR), G01R 29/08; Pat. #58814 (Ukraine), G01R 29/08; "Object positioning based on new approach to microwave angle-of-arrival measurements" *The 10th World Multi-Conf. on Syst., Cyber. and Inf.*, Orlando, Florida, USA, July 16–19, 2006; "The positioning of space objects based on microwave angle-of-arrival measurements," *The 4th ESA Int, Workshop on Tracking, Telemetry and Command Systems for Space Appl.*, Darmstadt, Germany, September 11–14, 2007).

According to the described method several microwave transponders are placed along the axis of the runway. All of transponders consist of antenna, circulator, amplifier and controlled phase shifter. Two (or more pairs) of microwave units are placed on the wings of the aircraft. Each Microwave unit consists of own microwave oscillator, circulator, antenna and mixer. All of microwave oscillators are not synchronized. Microwave units radiate the continuous microwave oscillation. These oscillations are received with the antennas of transponders of a runway. In all of primary received signals with each of transponders are entered monotonously increasing phase shift. In each transponder the speed of changing of phase shift is unique. This shifting of phase results in the appearance of different Doppler shift of frequency by each transponder separately. Then these frequency-transformed oscillations are reradiated in the direction of antennas of the aircraft. These antennas receive the frequency-transformed oscillations. These oscillations are mixed with initial microwave oscillation and combinational low-frequency components with the same pairs of Doppler frequencies are selected in both channels. Thereafter the difference of phases of the selected low-frequency combinational components are measured with the phase detector. The output signals of phase detectors control the steering gear of the aircraft. Here by the operating of the position of the aircraft, the signals on the outputs of all of phase detectors are supported on the zero level, providing with that the automatic overlapping of a longitudinal axis of the aircraft with the axis of the runway.

First aspect of increasing of efficiency from the use of the prospective method is related with the appearance of an opportunity to automate the process of homing of the aircraft at the landing beginning.

Second aspect is related with the opportunity to automate not only the process of homing, but also to automate all process of landing. Here antennas of transponders of a runway can be made not prominent, but for example slot, and can be situated as on all length of a runway as beyond it along its axis. In this case the antennas don't disturb the process of landing itself of the aircraft on a runway; however there is an opportunity to control the position of the aircraft at its movement along the entire runway up to its complete stop.

On Line Wire Diagnosis by Modified Spread Spectrum Time Domain Reflectometry

Adrien Lelong[1], **Marc Olivas Carrion**[1], **Virginie Degardin**[2], **and Martine Lienard**[2]

[1]CEA LIST, 91192 Gif-Sur Yvette, France
[2]IEMN/TELICE, Lille, France

Abstract— A method for "on line" wiring diagnosis is presented. It consists in detecting and locating electric faults in wiring networks while the target system is running. In our case the diagnosis is made by the use of reflectometry. The principle of these systems is to send a wide band test signal down the line, which reflects back at impedance discontinuities such as branches and defects (open or short circuits).

The main problem of "on line" diagnosis is not to disturb the target system and not to be disturbed by it. This results in various contraints on power spectral density of the test signal. Some of these constraints are also related to electromagnetic compatibility (EMC). In the time domain, classical methods used for "on line" diagnosis are Sequence Time Domain Reflectometry (STDR) [3] and Spread Spectrum Time Domain Reflectometry (SSTDR).

The principle of STDR is to send a pseudo noise signal (usually a M Sequence) down the line. The autocorrelation function of such a signal is a single peak, so the reflectometry result is provided by the cross-correlation between the received signal and the probing signal. From a spectral point of view, STDR is equivalent to a standard Time Domain Reflectometry (TDR) [1] which consists in sending a pulse as a test signal. The interest of STDR is to reduce the amplitude of the test signal. STDR is also used to generate orthogonal signals for distributed diagnosis [2].

The aim of SSTDR is to keep low frequency clean, this is achieved by sending a modulated pseudo noise. The modulation is made by mixing the digital signal with a high frequency sinusoidal carrier waveform. The received signal is computed in the same way as for STDR. One of the drawbacks of this method is that it works well only when the carrier frequency is equal to the chip rate of the pseudo noise. Indeed, since the correlation is applied on the modulated signal, peaks of the reflectometry result are also modulated. As a consequence, the final signal is difficult to analyse when the carrier frequency is high. Furthermore, the correlation operation must be implemented by use of analog components.

In some applications it may be necessary to inject higher frequency signals than classical SSTDR. The method proposed in this paper is an evolution of the SSTDR. In a similar way, the test signal is a modulated M Sequence. But before passing through a matched filter, the received signal is demodulated, so the correlation can be computed in baseband and it can be easily implemented using a numeric system such as an FPGA. Only the modulation demodulation part of the system has to be made using analog components.

Thanks to this, the carrier frequency can be adjusted as wished with no in uence on peak's waveform. So it is possible with this method to make a high frequency transposition of the test signal and get a correct reflectometry result. So when a wide band part of the spectrum has to be kept clean for EMC reasons this method is an efficient solution to use reflectometry for "on line" diagnosis. The Modified SSTDR was implemented using Matlab and has been successfully tested on coaxial cables network and twisted pairs via laboratory equipment.

REFERENCES

1. Carrion, M. O., F. Auzanneau, and N. Ravot, "A simple and accurate model for wire diagnosis using reflectometry," *PIERS Proceedings*, 232–236, Prague, Czech Republic, August 27–30, 2007.
2. Ravot, N., F. Auzanneau, Y. Bonhomme, M. O. Olivas, and F. Bouillault, "Distributed reflectometry-based diagnosis for complex wired networks," *EMC: Safety, Reliability and Security of Communication and Transportation Syst.*, EMC Workshop, June 2007.
3. Smith, P., C. Furse, and J. Gunther, "Analysis of spread spectrum time domain reflectometry for wire fault location," *Sensors Journal, IEEE*, Vol. 5, No. 6, 1469–1478, Dec. 2005.

Comparitive Studies on the Effect of Analog and Digital Phase Shifters on Shaped Beam Patterns Generated from Phased Arrays

M. Chakravarthy[1], **G. S. N. Raju**[2], **R. Sreehari Rao**[1], **and R. Ramana Reddy**[2]

[1]Defence Electronics Research Laboratory, DRDO, Govt. of India
Ministry of Defence, Hyderabad 500 005, India
[2]Dept. of Electronics and Communication Engineering
College of Engineering, Andhra University, Visakhapatnam 530 003, India

Abstract— The method of design of the source to produce desired radiation beams is treated extensively in the literature. More concentration is made on the generation of narrow beams from line sources. The well known Chebyshev and Taylor's methods are considered for the above purpose.

In modern radar applications, pattern synthesis is one of the important aspect. It is made conveniently from arrays either with amplitude or with phase control or with both of them. The amplitude control method is useful for non-scan applications and the second method is useful both for scan and non-scan applications. When the array is designed to produce a shaped beam like sector, phase distribution is the main design parameter. It is possible to generate different shaped beam patterns or to convert one shape to the another with optimally designed phase distributions.

The fast scanning and fast conversion of the beams is obtained if the phase distribution is introduced using digital phase shifters. However, it is essential to select appropriate digital phase shifters 2-bit, 3-bit or 4-bit etc.

In the present work, a few sector beams are produced with well designed amplitude and phase distributions. The patterns generated using analog and digital phase shifters are presented. The effect of digital phase shifters on such beams are consolidated. It is found from the results that the 4-bit phase shifters are found to produce the patterns of analog phase shifters. There is considerable deviation between the patterns of analog, 2-bit and 3-bit phase shifters. The resultant patterns are presented in sin domain for different specified sectoral widths.

Admittance Characteristics of Cross-slot Coupled H-plane Tee Junction

R. Ramana Reddy and G. S. N. Raju
Dept. of Electronics and Communication Engineering
College of Engineering, Andhra University, Visakhapatnam 530 003, India

Abstract— The analysis of H-plane Tee junction coupled through a longitudinal slot is reported in the literature. Its admittance characteristics are function of the slot length, width and dimensions of feed and coupled guides, frequency and medium in the waveguides. However, the present work deals with a similar junction but coupled through inclined crossed-slots. The work is aimed to control the admittance with more parameters without disturbing polarization characteristics of H-plane Tee junction coupled through conventional slots.

The electric field distribution in the aperture plane of the each inclined slot is replaced by an equal magnetic current for the purpose of analysis. The electric field distribution is expressed in the form of Fourier series. Its basis functions satisfies the orthogonality conditions and they are Eigen functions for TE and TM modes. The coefficients of the series are obtained using standard method followed for the evaluation of Fourier coefficients. The magnetic field is expressed in terms of modal admittance, modal voltages and modal vector functions.

The admittance characteristics of the proposed junction are obtained using the concepts of self-reaction of the magnetic current and discontinuity in modal current. The effect of energy storage in the primary guide is taken into account for the evaluation of self-reaction. The self-reaction for both the inclined slots are separately evaluated.

Considering the crossed-slots as a single unit, the equivalent network parameter is obtained. It is evident from the literature, the equivalent network parameter is a shunt element. Its variation as a function of frequency is numerically computed for different slot parameters.

In the case of standard X-band feed waveguide, the dimension of the narrow wall cannot accommodate resonant slot at small inclination from broadside. In view of this, some studies are made considering a non-standard feed waveguide which can accommodate resonant slots. The variation of normalized conductance and susceptance with frequency for different slot parameters is presented.

It has been possible in the present work to control the admittance effectively with the proposed waveguide Tee junction.

Session 2P4
Electromagnetic Field in Optical Materials and EM Field Dispersion in Photonic Crystals

Coupling Theory of Asymmetric Photonic-crystal Waveguides

Chih-Hsien Huang[1], **Wen-Feng Hsieh**[1], **and Szu-Cheng Cheng**[2]

[1]Department of Photonics, National Chiao Tung University, Hsinchu, Taiwan
[2]Department of Physics, Chinese Culture University, Taipei, Taiwan

Abstract— The physical properties of asymmetric photonic-crystal directional couplers are studied under the tight-binding theory, which considers the field distribution of photonic-crystal waveguides is localized around periodic defects. From this model, the analytic formulas to describe the dispersion of the coupler and the eigen mode pattern is derived, thus helping to analyze the eigen mode and energy localization of the waveguides. It also helps to explain the novel phenomenon that the mode patterns are exchanged at decoupling point but the dispersion relation curves do not cross at triangular lattice asymmetry photonic-crystal waveguides. By linearly combination of the derived wave vectors and eigen mode, the amplitudes of the electric field can be easily writing down which are consistent with the results gotten by the finite difference time domain method.

Analysis of Homogeneous Optical Fibers with Irregular Boundaries

Serhend Arvas, **Joseph R. Mautz**, **and Ercument Arvas**
Department of Electrical Engineering and Computer Science
Syracuse University, Syracuse, NY 13244, USA

Abstract— A simple numerical technique is developed to analyze optical fibers of arbitrary cross section. The surface equivalence principle is used to replace the fiber by equivalent electric and magnetic surface currents radiating in unbounded media. Each of these equivalent surface currents has both longitudinal and transverse components. Eight coupled integral equations are obtained by applying the conditions on the tangential components of the electric and magnetic fields. They are reduced to four equations by using a combined field approach. These four integral equations are solved using the Method of Moments. The contour describing the fiber cross section is approximated by linear segments. Pulses are used as expansion functions for the longitudinal currents J_Z and M_Z, and triangular functions are used in expanding the lateral components of the currents J_L and M_L. An approximate Galerkin's method of testing is used.

The moment matrix Z is a function of the propagation constant β. The matrix becomes singular when β corresponds to a possible guided mode. These values of propagation constants are determined by monitoring the condition number of the moment matrix as β is varied. No β values corresponding to any spurious modes are detected. For a valid β value corresponding to a particular mode, the eigenvector of Z corresponding to the minimum eigenvalue is found. This eigenvector contains the expansion coefficients for the equivalent surface currents. The tangential components of the electric and magnetic fields over the boundary of the fiber can simply be found once the expansion coefficients are determined. The dispersion relationship and fields inside and outside the fiber can also be computed easily.

The method can be applied to fibers with deformed boundaries, including the elliptical, chipped circle, egg shape or asymmetrical boundary. The computed results for a number of cross sections are in excellent agreement with available exact or numerical data.

Anomalous Microwave Transmission in a Superconducting Periodic Multilayer Structure

Chien-Jang Wu[1] and Tzong-Jer Yang[2]

[1]Institute of Electro-Optical Science and Technology
National Taiwan Normal University, Taipei, Taiwan 106, R.O.C.
[2]Department of Electrical Engineering, Chung Hua University, Hsinchu, Taiwan 300, R.O.C.

Abstract— In this work we theoretically study microwave properties of a superconductor/dielectric periodic layered structure, in which a strongly dispersive superconductor, nearly ferroelectric superconductor (NFE SC), is taken. Microwave transmittance in the dielectric-like response has been calculated based on the transfer matrix method as well as the electrodynamics of NFE SCs. Microwave response is strongly dependent on the number of periods as well as the thickness of superconductor layer. It is found that the first anomalous transmission peak can be created when the number of periods is more than five. In addition, more anomalous peaks are generated by greatly increasing the number of periods. The presence of anomalous sharp peaks can be used to design a nicely frequency-selective filter or sampler using such a multilayer structure.

Electromagnetic Field Energy in a Metamaterial Medium Consisting of Metallic Wires and Split-ring Resonators

Pi-Gang Luan
Department of Optics and Photonics, National Central University, Jhong-Li 32001, Taiwan

Abstract— We derive in this paper the formula of electromagnetic field energy density in a dispersive metamaterial medium with finite loss. The metamaterial consists of arrays of metallic wires and split-ring resonators. Equations of motion for the electric and magnetic dipoles are obtained by analyzing the current and charge responses of the metallic components to the incident fields. Based on the analysis, the relations between currents/charges, dipoles, and fields can be found, and hence the stored energy and energy loss in the medium can be correctly calculated and expressed using either the current/charge or field/dipole variables. We also find that the energy loss in the metamaterial are nothing else than the Joule heat generated by the resistances in the metallic structures. Space averaging the fields and dipoles under the long-wavelength assumption, the macroscopic fields **E**, **B**, **D**, **H**, **P**, **M** can be defined. The equations of motion for the polarization **P** and magnetization **M** are obtained from the corresponding equations for the electric and magnetic dipoles. An effective continuous medium theory for this metamaterial is thus established. We show that the energy density of the fields can be derived from Maxwell's equations of the macroscopic fields (electrodynamics approach), and the result is the same as that obtained from calculating the energy stored in one unit cell (equivalent circuit approach), divided by the cell volume. Our formula gives the same result as that of Boardman's [1] in the lossless limit, but different from theirs when energy loss cannot be neglected. We explain the physically meaning of every term appearing in the energy density formula, and compare the result with those obtained by other authors using electrodynamics [1] or equivalent circuit approach [2]. This comparison reveals that our approach is more satisfactory and physically transparent, and can be easily generalized to establish the effective medium theory of other kinds of metamaterials such as those including of both electric and magnetic resonators in one unit cell.

REFERENCES

1. Boardman, A. D. and K. Marinov, *Phys. Rev. B*, Vol. 73, 165110, 2006.
2. Tretyakov, S. A., *Phys. Lett. A*, Vol. 343, 231, 2005.
3. Ruppin, R., *Phys. Lett. A*, Vol. 299, 309, 2002.
4. Chen, H., L. Ran, J. Huangfu, T. M. Grzegorczyk, and J. A. Kong, *J. Appl. Phys.*, Vol. 100, 024915, 2006.
5. Pendry, J. B., A. J. Holden, D. J. Robbins, and W. J. Stewart, *IEEE Trans. Microwave Theory Tech.*, Vol. 47, 2057, 1999.

The Layered Metamaterial with Parabolic Dispersion

Linfang Shen[1], **Tzong-Jer Yang**[2], **and Jin-Jei Wu**[2]

[1]Department of Information Science and Electronic Engineering, Electromagnetic Academy
Zhejiang University, Hangzhou 310027, China
[2]Department of Electrical Engineering, Chung Hua University, Hsinchu 300, Taiwan, R.O.C.

Abstract— A layered meatmaterial which is predicted by the effective medium theory to have partially permittivity near zero is analyzed. It is shown that such a material has parabolic dispersion relation. This material may be viewed as a homogeneous medium but is spatially dispersive strongly. This material may also have either forward wave or backward wave, depending on the magnitude of the wave vector.

GL EM Modeling for Electromagnetic Wave Propagation in Helix Pipe Crystals and Structures

Ganquan Xie, **Jianhua Li**, **Feng Xie**, **and Lee Xie**
GL Geophysical Laboratory, USA

Abstract— We present a GL EM modeling for electromagnetic (EM) wave propagation in the helical pipe crystal and structure. The helical pipe crystal and structure can be figured as 3D periodic lattice structure. The unit cell is a structure that unit helical is embedded into the cubic crystal. Our GL EM modeling can simulate EM wave propagation in the helical pipe crystal and structure and perform its dispersion engineering. Using GL EM modeling simulation and dispersion engineering, the EM filed wave can be almost focus guiding propagation in the helical pipe crystal and structure. That is useful for making nanometer helical pipe crystal laser, artificial DNA, nanometer material device, sensor and other applications.

Critical Fields in Lithum Niobate Nano Ferroelectrics

A. K. Bandyopadhyay[1], **P. C. Ray**[2], **and V. Gopalan**[3]

[1]Govt. College of Engineering & Ceramic Technology, WBUT, Kolkata-700010, India
[2]Dept. of Mathematics, GCE & LT, WBUT, Salt Lake, Kolkata-700098, India
[3]Dept. of Materials Science and Engineering, Pennsylvania State University, USA

Abstract— An important property like giant polarization with many other properties are commonly observed in ferroelectric materials, which have an wide area of applications. A typical non-linear hysteresis behaviour is observed between polarization (P) and electric field (E). For an uniaxial ferroelectric, such as lithium niobate, we developed a discrete Hamiltonian by taking Landau-Ginzburg functional as potential energy with near-neighbour 'interactions' between the polarization domains. The spatio-temporal behaviour of P is then described by a non-linear Klein-Gordon equation as a governing equation as:

$$\frac{\partial^2 P}{\partial t^2} - \bar{k}\frac{\partial^2 P}{\partial x^2} - \bar{\alpha}_1(P - P^3) - E + \bar{\gamma}\frac{\partial P}{\partial t} = 0$$

where, $\bar{k}$ is an interaction term and $\bar{\gamma}$ is the damping term. Here, all the terms are used as non-dimensional.

The 'analytical solutions' of the above non-linear K-G equation give rise to both slower ($\tan h$) and faster ($\sec h$) solitons in such photonic materials. The stability of these solitons, i.e., up to what field such solitons exist, is worked out in order to find a 'critical field' value, which has not been attempted so far for actual photonic crystals for non-linear device applications.

This particular case of stability analysis is done at $E \neq 0$ and $\bar{\gamma} \neq 0$. Beyond this critical value, the solitons do not exist in our system. If we multiply this non-dimensional E_{crit} value by the coercive field (E_c), we obtain the optimum value of the field (V/nm) to be applied in a given nano device, which has an important relation with impurity content in such inhomogeneous ferroelectrics. This is considered to be due to break-up of Landau potential as we increase the driving force, as shown below.

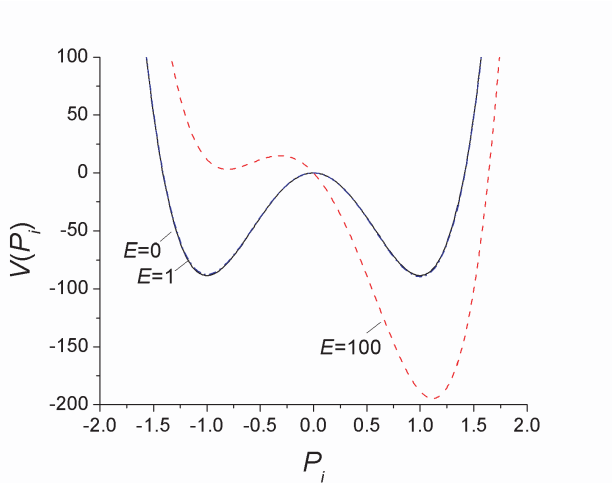

A Potential-based Finite Element Method Based on Wave Scheme for Transient Maxwell's Equations

Tong Kang
School of Sciences, Communication University of China, China

Abstract— In this paper, we investigate the potential-based finite element method (the A-method) based on Wave scheme for transient three-dimensional Maxwell equation system. By appending a penalty function term in the governing equation of magnetic vector potential, we achieve the satisfaction of the Coulomb gauge and guarantee the uniqueness of the vector splitting. As distinguished from the traditional coupled scheme in which an equation system including both vector and scalar potentials is solved at every time-step after time discretization, a decoupled scheme is specially presented here. Because the vector and scalar unknowns are calculated at different equations respectively, it decreases the storage amount of non-zero entries of coefficient matrix and computational costs and achieves the better results under the equal CPU time. Some computer simulation results of the distributions of magnetic flux and electric field are demonstrated to verify the feasibility and efficiency of our algorithm.

REFERENCES

1. Albanese, R. and G. Rubinacci, "Formulation of the eddy-current problem," *IEE Proceedings*, 137, 16–22, 1990.
2. Bossavit, A., *Computational Electromagnetism*, Academic Press, 1997.
3. Jin, J. M., *Finite Element Method in Electromagnetism*, the 2nd Version, Academic Press, 2002.
4. Ren, Z. and A. Razek, "Comparison of some 3D eddy current formulations in dual systems," *IEEE Trans. on Magn.*, Vol. 36, No. 4, 751–755, 2000.
5. Yao, Y., D. Xie, J. Wang, and A. M. Osama, "A Multi-step method for 3-D nonlinear transient eddy current problems," *IEEE Trans. Magn.*, Vol. 37, 3194–3197, 2001.

Session 2P5
Poster Session 2

Design of Low-cost Microstrip Antennas for Glonass Applications

Daniel C. Nascimento, **Ricardo Schildberg**, **and J. C. da S. Lacava**
Laboratório de Antenas e Propagação, Instituto Tecnológico de Aeronáutica, Brazil

Abstract— The design of microstrip antennas as low-cost radiators for mobile communications can be challenging. Additional complexities are introduced in the conventional microstrip design when the FR4 laminate is used as the antenna substrate, due to its high loss tangent and inaccurate relative permittivity. The high losses in the antenna laminate have a direct effect on its radiation efficiency. For a higher efficiency, thicker substrates must be used. In case, for instance, a probe-fed truncated corner square microstrip antenna (frequently used for achieving circular polarization) is designed following the conventional procedure, an extra limitation is posed if the patch is printed on a thick substrate: its inherently inductive input impedance can not be properly matched to a 50-Ω SMA coaxial connector. In addition, the frequency where its axial ratio is best does not coincide with the frequency where its return loss is best.

To overcome these limitations, a new design procedure is proposed here. Instead of the conventional topology (a square patch with two truncated corners), the new procedure utilizes a rectangular patch with four truncated corners. Besides, stubs are added to each corner to compensate for the inaccuracy of the FR4 relative permittivity. This new patch topology gives the antenna designer more flexibility and the ability to properly compensate for the undesirable reactive inductance.

The antenna design and simulations presented here (for GLONASS applications) are performed with the HFSS software; parameters such as radiation patterns, input impedance, axial ratio and return loss are addressed. For the validation of the proposed procedure, a prototype was manufactured (Fig. 1). Comparisons between experimental and simulated results are presented and discussed (Fig. 2), revealing very good agreement.

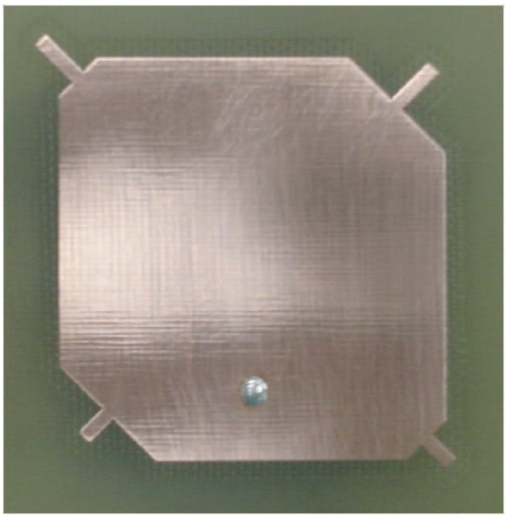

Figure 1: Photo of the antenna prototype.

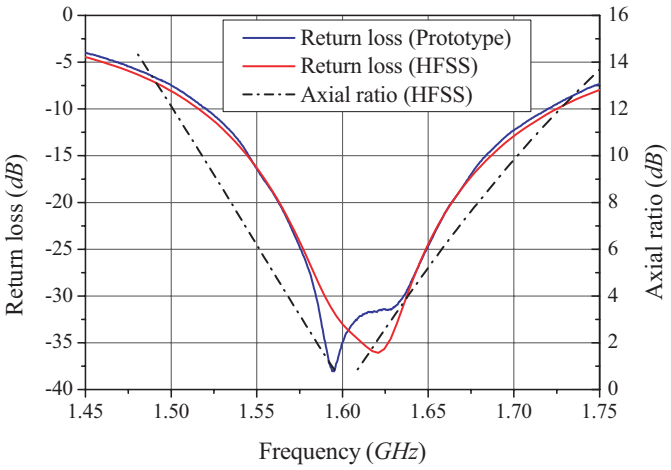

Figure 2: Return loss: experiment and simulation.

Design of a 2.5GHz Differential CMOS LNA

Xuan Chen, **Quanyuan Feng**, **and Shiyu Li**

Institute of Microelectronics, Southwest Jiaotong University, Chengdu 610031, China

Abstract— There are so many merits to use differential architecture, like abiding the noise. Because millimeter wave signal can be easily leaked, so we can use differential signal to eliminate the negative effect of leaking signal. Meanwhile differential LNA can restrain common mode interference, so the noise of source voltage and underlay voltage can also be restrained.

We proposed a 2.5 GHz differential CMOS LNA which fabricated with the 0.18 µm CMOS process. This design used two-input and two-output architecture, adopting L_S as the source inductive degeneration of the C-S amplifier which can enlarge the linear range. In order to reach the input matching, however, the required gate L_g should be very large. In practice, a large-value inductor is difficult to implement on-chip based on a CMOS process, and it will contribute much thermal noise. With the consideration of system integration and reducing the noise figure, we utilize LC parallel network to replace gate inductance. Because a small LC parallel network will generate a larger inductance and replace the large L_g. Meanwhile, through the introduction of L_1C_1 parallel network we know that the R_{p2} is not a fully physical resistor and it will not generate so much thermal noise as a real resistor dose, so the NF might be somehow improved. Furthermore, the low noise figure can also be implemented by reducing the C_{gs} and enhancing the transconductance g_m, and this process can be realized by modulating the width of the transistor and adjusting the bias circuit with restraint of power consumption.

By using the ADS software to make the simulation and we get that when the operating frequency is 2.5 GHz, S_{11} is −50.687 dB, S_{12} is −18.132 dB, S_{21} is 15.053 dB, NF is 1.910 dB and the LNA consumes 5.4 mA bias current at 2V̇ supply voltage. Each index of 2.5 GHz LNA can satisfy our requirement. Considering the circuit application and enhancing the integration, we design this CMOS differential LNAit can be utilized in wireless RF receiver which is operated at 2.5 GHz.

A Novel Anti-collision Algorithm in RFID System

Shiyu Li and Quanyuan Feng
Microelectronic Technology Lab of Southwest Jiaotong University, China

Abstract— Tag anti-collision is a significant issue in RFID system design, which determines the identification speed. Thus a novel anti-collision algorithm based on Balance Incomplete Block Design $(4, 2, 1)$ and Binary Tree Searching Algorithms is proposed to raise the identification speed. In this new algorithm, Tag UID is divided into several sections and each section is only equal to one of the subsets of BIBD $(4, 2, 1)$ (All the subsets of BIBD $(4, 2, 1)$ are the sequences as follows: 0011, 0101, 0110, 1001, 1010, 1100).

A reader can get every UID efficiently by identifying sections form the highest one to the lowest repeatedly. Firstly, a tag sends back its next section after the reader broadcasts 'Request (SNR)' command if its current section is equal to or less than the SNR. Secondly, according to the principle of Manchester coding and the collision of feedback sequence from tags, the reader can tell which subsets are in the next section and then evaluate the minimum value in these subsets to SNR. Thirdly, jump to the first step to identify the following sections. When the reader receives the last section of tags, it can make sure at least one tag and can uses Select, Operation and Unselect commands to operate it or them. Finally, this round of searching finishes and then jumps to the first step. When there is no response to the 'Request (SNR)' of the reader, UID of tags identification has finished.

Mathematics analysis and simulation results show that the algorithm presented improves the identification speed and outperforms the existing ones. The searching speed of this new algorithm is six times that of the Query Tree Protocol. It is especially suitable for the identification conditions which contain lots of tags or tags with long UID.

10 GHz Two-stage Class A RF Power Amplifier in a 0.25 μm CMOS Process

Tanya Vanessa F. Abaya and Marc D. Rosales
University of the Philippines in Diliman, Philippines

Abstract— This report describes the methodology used in designing a CMOS Radio Frequency (RF) power amplifier (PA) operating at 10 GHz. The TSMC 0.25 μm CMOS process is used for design, simulation and testing. While 0.25 μm devices are a relatively old technology, the 0.25 μm CMOS process is cheaper compared to HBTs or shorter channel lengths CMOS and at the same time can be more easily adapted for design in amplifiers operating in the low gigahertz range.

The PA is a two-stage amplifier with both driver and output stages having class-A operation supplied by a singled-ended 2.5 V source. While output power is maximized and linearity is best, the efficiency of class A PA is least among all PA classes. Such design issues and trade-offs, which complicate the design process are discussed together with some optimization techniques learned.

Also, as with any RF circuit, the design and implementation of inductors are problematic. The inductors were modeled and the final components used have a quality factor of 14.

Key specifications and corresponding characteristics are presented. Important design considerations include output power, compression point, power added efficiency and linearity. The amplifier has a 1 dB compression point of 13.18 dBm (output referred) and 1.8 dBm (input referred). For power gain, a 17.2 dB value is achieved. Linearity is quantified by an output referred harmonic IP3 of 26.17 dBm, an intermodulation IP3 of 12.2 dBm and more importantly an IM3 at compression of 31.2 dBc. Lastly, a maximum power added efficiency of 8.1% is realized.

Inductor Modeling Using 3D EM Design Tool for RF CMOS Process

Gian Paolo T. Mayuga and Marc D. Rosales
Microelectronics and Microprocessors Laboratory
Department of Electrical and Electronics Engineering
University of the Philippines Diliman, Quezon City, Philippines

Abstract— This study formulates an RF IC design flow integrating the use of 3D Electro-Magnetic design tool for inductor modeling. The 3D EM tool was used to extract the S-parameters that were subsequently used as RF model for the on-chip spiral-inductors in the simulations. Comparisons were made between the data derived from the prevalent 2D 1/2 tool and the 3D tool. Implementations were done for the 0.25 micron CMOS process.

The physical layers of the CMOS process were modeled into the *ASITIC* 2D 1/2 tool by creating a user defined technology file (.tek), and into the 3D EM design tool by CAD-supported physical geometric construction. *Spiralcalc* was used to calculate the geometric definitions of the inductors. S-parameters, quality factor (Q), and inductance vs. frequency were recorded. Comparisons were made between the 2D and 3D simulation results and also to the results of an actual on-chip fabricated inductor.

On the Absolute Measure of Wavelengths in Telecommunications

S. L. Vesely[1] **and A. A. Vesely**[2]

[1]I. T. B.-C. N. R., Italy
[2]via L. Anelli 13, Milano 20122, Italy

Abstract— In precision mechanics, tiny distances can be proficiently measured by interferometrical methods. Those methods are also employed for forging cavities. However, the requirement to employ optical technologies for high precision mechanics does not conversely provide a metric characterization for radiative *emissions*, because most processes involved in active radiation, e.g., will-o'-the-wisps, have no straightforward geometrical explanations. Accordingly, the usual assumption of electromagnetism, that the radiation frequency ν is bound to the wavelength by $\lambda\nu = c$, where $c = 1/\sqrt{(\varepsilon\mu)}$ is the transmission speed in vacuum, if the space is occupied by a medium has a somewhat weaker physical meaning as ν is just *formally* related to phase velocity.

Nevertheless, mechanics has been used to evaluate wavelengths. While classical electrodynamics relates irradiation with the *dynamics* of charged particles, quantum mechanics carries out an *energetic* balance $h\Delta\nu$ of the interaction between radiation and matter based on gaseous spectra, thereby assigning a physical meaning to the absolute measure of ν, inasmuch as it is related to the energy levels. Absolute length is regained through atomic dynamics, and the progressive filling of electron shells serves to justify the periodic table of the elements. In particular, if an identical spectral pattern appears in different regions, it contributes to the explanation of that periodicity. Even if different emissions may result in different effects on irradiated media, the subject of every linear spectral analysis is the signal. Signals are also studied in telecommunications science: it relates the frequency to the carriers, and allows transmitting the same signal on different channels. Again, telecommunications don't delve into signal's deals but into the information content. Unlike quantum theory, they use to distinguish the received signal from the distortions that can be ascribed to the reception process. For example, by linear analysis a spectral grating certainly has more than one period: the grooves are evenly spaced, but its overall length also results in a period, and can generate aliasing. Forging the grating as a circle arc, as has been done to attribute absolute numerical values to the wave lengths, involves a further frequency modulation due to spacing irregularities [1].

Although at the level of linear analysis dispersion apparently brings a *geometrical* relationship between different colors of light, in a prism it essentially results in detectable angles, which are not directly related to lengths according to Euclidean geometry. Angles have periods of 180° or 360°, depending on the radius definition. Thus, a linear measure turns out to be a multiple of π, an irrational number. The absolute measure of wavelengths by reflection on a Rowland diffraction grating apparently remedies that problem, inasmuch as it is based on the pitch of the grating, which has a straightforward *physical* meaning. However, those grooves don't bear the same geometrical meaning as the lines ruled on the polished surface of the platinum-iridium meter bar in Sèvres. Indeed, a grating is engraved by means of a dividing engine, that is its total length is subdivided as evenly as possible into *exactly* 2^n parts. Now, that silently introduced periodicity is in contrast with the axiom named after Archimedes, that the geometrical measure is based upon.

In conclusion, electromagnetism and telecommunications might evaluate if the absolute measure of wavelength should be replaced with a logarithmic measure similar to the Bel.

REFERENCES

1. Lyman, T., "An Explanation of the false spectra from diffraction gratings," *Phys. Rev.*, Vol. 16, No. 5, 257–266, 1903.

Compact Folded Dipole Antenna for DTV Signal Reception

Ding-Bing Lin[1], **Shiao-Ting Wu**[1], **and Chao-Hsiung Tseng**[2]

[1]Department of Electronic Engineering
Graduate Institute of Computer and Communication Engineering
National Taipei University of Technology, Taipei, Taiwan
[2]Department of Electronic Engineering
National Taiwan University of Science and Technology, Taipei, Taiwan

Abstract— In this paper, a compact simple folded dipole antenna for digital television (DTV) signal reception in the 470–850 MHz band is proposed. The antenna consists of two metal thin lines and narrow rectangular radiating patches. It is feeded by 50 Ω SMA connector and printed on a dielectric substrate FR4. By appropriate tuning geometrical parameters, the final designed antenna has only compact volume with $80 \times 28 \times 0.4\,\text{mm}^3$ .The antenna can be excited to provide a wide bandwidth (−5 dB return loss) of larger than 55%.

Introduction: The DTV reception has thus become very attractive for application in mobile communication devices such as the laptop computers, mobile phones, personal media players [1]. For these perspective trends, it is anticipated that a variety of mobile antenna for DTV signal reception will be increasingly required. The conventional dipole antenna are usually with a center-fed connector structure. It has narrow bandwidth, which is difficult to cover the DTV signal reception. The novel end-fed modified planar dipole antenna has a wide bandwidth more than conventional center-fed planar dipole [2, 3]. In this paper, we present a novel side-fed modified planar dipole antenna having wide bandwidth of larger than 55% which can cover DTV receiver frequency from 470–850 MHz. The proposed antenna also has a planar configuration and is easy to fabricate at low cost by printing on a dielectric substrate.

Antenna Design: Figure 1(a) shows the proposed compact folded dipole antenna. The antenna is printed on a 0.4-mm thick FR4 substrate and look like business card shape (width 28-mm and length 80-mm). It is can generate a fundamental resonant mode centered at about 520 MHz (0.5-wavelength), allowing the antenna to cover the lower-edge frequency (470 MHz) of the DTV band. However, in order to cover the upper-edge frequency (850 MHz) we used inverted U shaped to generate a high-order resonant mode. Fig. 1(b) shows the concept used for impedance matching. The metal thin line take on inductance effect and the patches take on capacitance effect. Fig. 2 shows the measurement Return Loss for proposed antenna effect with and without rectangular patches. It is seen that, for the purpose of adding the rectangular patches, a fundamental resonant mode is can be achieved lower-edge frequency resonant.

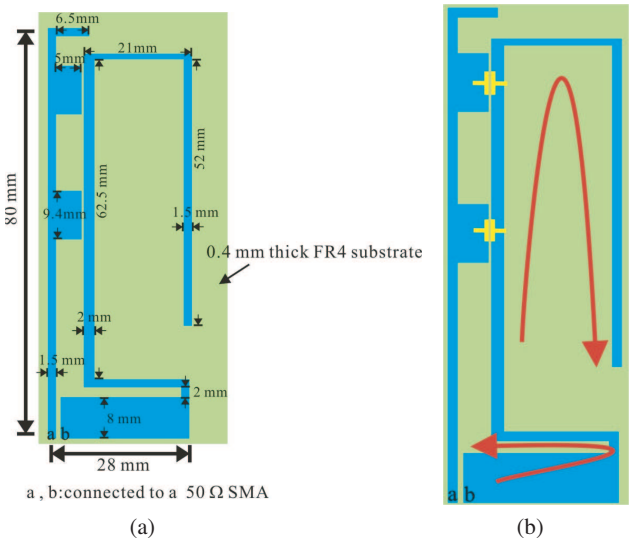

Figure 1: (a) The proposed compact folded dipole antenna. (b) The proposed compact folded dipole antenna a method of the impedance match.

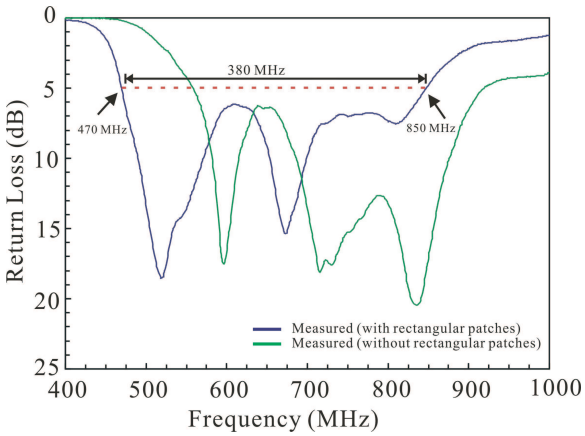

Figure 2: Measurement of Return Loss for proposed antenna with and without rectangular patches.

REFERENCES

1. Digital Television, Major Initiatives of Federal Communications Commission, [Online] Available: http://www.fcc.gov/dtv/.
2. Chi, Y. W., K. L. Wong, and S. W. Su, "Broadband printed dipole antenna with a step-shaped feed gap for DTV signal reception," *IEEE Transactions on Antennas and Propagation*, Vol. 55, 3353–3356, Nov. 2007.
3. Iizuka, H., T. Watanabe, K. Sakakibara, and N. Kikuma, "Stub-Loaded folded dipole antenna for digital terrestrial TV reception," *IEEE Antennas and Wireless Propagation Letters*, Vol. 5, 260–261, Dec. 2006.

Study on Radiation Characteristics of A Conical Conformal Phased Array

Yinsuo Song
Luoyang Optoelectro Technology Development Center, Henan, China

Abstract— This paper provides an effective method for analyzing a cone conformal phased array antenna. Firstly, a fictitious elementary antenna is supposed to be located at the origin of an array coordinate; then, a layout for the antenna to be transformed to a given position and a polarization direction can be obtained, generally by rotation thrice and translation twice.

Based on the above idea, formulas to calculate the radiation pattern of the conformal array on a frustum surface have been deduced, with the elementary number and polarization direction specified. Siminlation software is programed to validate the model. A series of calculations have been conducted on the azimuth and the pitching scan performance of the array composed of 26×95 element slot antennas in order to study the radiation characteristics of frustum conformal phased antenna. The calculations have found that the scan of the beam in the generatrix direction (pitching plane) can be achieved by changing the phase distribution of the elementary antenna along the generatrix, the scan in the circumferential direction (azimuth plane) can be realized by moving the position of the active area, the width of the beam can be adjusted in certain extend by changing the dimension of the active area. The research result shows that at bigger scan angle (axial), the beam becomes obviously wider and worse with severer across polarization. If all the elements participate in the radiation, the axial beam will be greatly improved whereas more back radiations appear. Subsequently, the effects of several typical amplitude distributions (for instance, constant, triangle, taper) and elementary polarization directions (generatrix, circumferential) on the antenna pattern are calculated, and the results indicate that the optimum pattern parameters (for example, side lobe lever) can be obtained through choosing different amplitude distributions and polarization of the elementary antenna.

Application of a SPICE Model for Multiconductor Transmission Lines in Electromagnetic Topology

Haiyan Xie[1], **Jianguo Wang**[1, 2], **Ruyu Fan**[1, 2], **and Yinong Liu**[1]

[1]Department of Engineering Physics, Tsinghua University, China
[2]Northwest Institute of Nuclear Technology, China

Abstract— This paper presents a method in electromagnetic topology, which uses a spice model for multiconductor transmission lines, while the conventional method uses the frequency domain Baum–Liu–Tesche (BLT) equation and inverse fast Fourier transform. This method is used to predict the transient voltage and current induced at the terminators of lossless multiconductor transmission lines (or network) excited by an incident electromagnetic field. The spice model is independent of the terminators and can be implemented as SPICE subcircuit model. The work is done directly in time domain. The proposed method is used to compute three cases, and the transient load voltage of each case is obtained. The three cases are a wire, a transmission line network and a multiconductor transmission lines, all excited by a plane-wave electromagnetic field. The former two cases are above an infinite and perfectly conducting plane. The computed results are compared with transient load voltage obtained using the frequency domain BLT equation and inverse fast Fourier transform, and they are agreed very well. The proposed method can be used to compute the transient voltage response of nonlinear or time-varying load, while the frequency domain BLT equation can only be used to compute the response of linear and time invariant loads. And the time needed by the proposed method is much less than the time used by the frequency domain BLT and inverse fast Fourier transform. Further more, the proposed method is more convenient to use than the time domain BLT equation which calls for the costly temporal convolution.

Pedagogical Considerations in EMC Education

Andrew Nafalski and Özdemir Göl
University of South Australia, Mawson Lakes 5095, Australia

Abstract— The EMC area has been gaining indisputable importance in industry, research and education dictated among others by the increasingly mandatory and thorough legislative framework. Nowadays any product likely to cause electromagnetic interference (EMI) is subject to strict compliance with EMC standards and guidelines. Thus it has become imperative that electrical engineering students are exposed to, understand and be able to apply EMC fundamentals.

It may come as a surprise to the uninvolved observer that EMC constitutes a complex multidisciplinary field of endeavour. It encompasses among others elements of chemistry, physics, astronomy, mechanical engineering, material science and medicine in addition to electrical engineering that is generally perceived to be the core constituent. More specifically, electromagnetic field theory which underpins EMC involves complex mathematical and abstract physical concepts difficult to fathom. Learning challenges are compounded by the nature of phenomena which are largely invisible and difficult to quantify. Thus EMC is difficult to teach and learn.

It is widely recognised that facilitating student learning is critical for effective learning outcomes. Effective learning provides motivation for more insight into the subject thus reinforcing the positive feedback loop of learning. It has been observed that one of the approaches appealing to students is the use of simulation and accompanying visualisation including animation. In order to bridge the gap between often abstract theory and engineering applications, a substantial laboratory component is also needed in EMC education.

The pedagogical issues related to teaching electromagnetic compatibility (EMC) in the Bachelor of Electrical Engineering degrees are discussed in this paper on the basis of reflections on the authors' experiences and also on the practices of others.

Automation of a Clamp Mechanism for EMC Testing

Andrew Nafalski and Özdemir Göl
University of South Australia, Mawson Lakes 5095, Australia

Abstract— This paper reports on the development of an automated mechanism to control the measurement process from outside a screened room where a moving absorbing clamp is used to conduct EMC tests prescribed by relevant standards [1, 2] according to which the measurement of radio frequency disturbance power in the radiation frequency range of 30 MHz–1 GHz is accomplished. The absorbing clamp moves along the track with the mains cable of Equipment Under Test (EUT) running through it as shown in Fig. 1.

Manual operation of the setup is cumbersome and time consuming. Consequently, an automated system to control the absorbing clamp movement has been designed and developed in-house. The system is controlled from outside the screened room and also includes a monitoring camera inside the screened room. The main challenge was to design and construct a system that does not introduce any appreciable EMI levels in the screened room and at the same time meets the functional specifications. An example of the EMC challenges is illustrated in Fig. 2 where radiated emissions as high as 60 dBμV/m from an unscreened camera were observed, exceeding the standard limits.

At the end the design objectives of the system have been achieved by a careful consideration of EMC principles at the design, prototyping and testing stages.

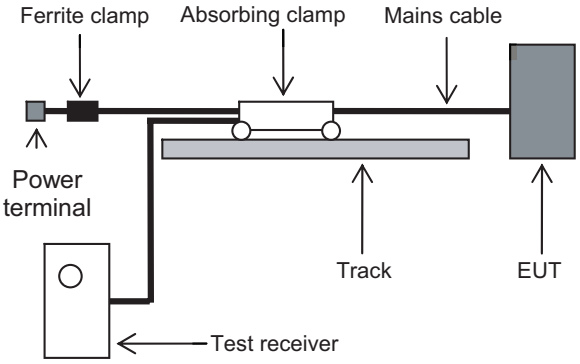

Figure 1: Measurement setup with an absorbing clamp.

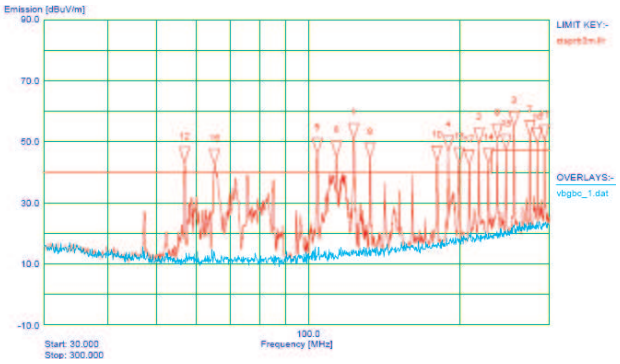

Figure 2: Radiated emissions from unshielded camera measured in the screened room at frequencies from 30 MHz to 300 MHz.

REFERENCES

1. AS/NZS 1052:1992 IEC/CISPR 16:1987, *CISPR Specification for Radio Interference Measuring Apparatus and Measurement Methods*, Australian Standard/New Zealand Standard, 1992.
2. IEC/CISPR 16-1-3-Ed.2.0, *Specification for Radio Disturbance and Immunity Measuring Apparatus and Methods — Part 1-3: Radio Disturbance and Immunity Measuring Apparatus — Ancillary Equipment — Disturbance Power*, 2004.

An Analytical Characterizzation of Metal Foams for Shielding Applications

O. Losito

ITEL Telecommunications Research Laboratory on EM
Via Labriola, 39-70037 Ruvo di Puglia, Italy

Abstract— Since Metal foams was discovery by the scientific world at the beginning of the last decade, they have been subject to investigation for more than 10 years. Characteristic properties like low apparent (or actual) density guarantees, for example, lightweight and high stiffness/specific-load ratios. Moreover, their porous structure and intrinsic non-homogeneity give good acoustic and thermal isolation properties and also strong impact-absorption and vibration damping capabilities.

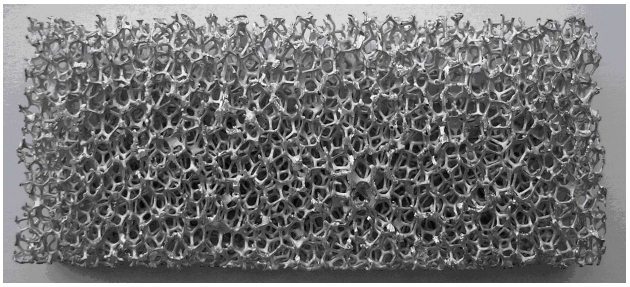

Figure 1: An examples of Duocel® open cell aluminium foam: $9 \times 3 \times 0.5\,\mathrm{cm}^3$ slab (porosity: 10 PPI, apparent density: 8%).

Nevertheless, their employment in EM application is new in literature. Fig. 1 shows an example of an open cell aluminium foam, produced by ERG Aerospace and called Duocel® foam. We can note that its low apparent density, (8%) and its capability to allows both light and air crossing, can be useful in several applications. The analysis of the shielding properties of different kinds of Duocel® aluminium foams slabs obtained by varying porosity and apparent density, has been investigated, performed through experimental measurements, and their shielding properties has been showed and discussed.

Metal foams are complex an random structures which requiring sophisticated analytical models. Moreover, because of its versatility and its capability to deal with heterogeneous media, the Variable-Mesh Finite Difference Time Domain (VM-FDTD) method, is naturally the most appropriate approach [1], though unfortunately, it is computationally onerous. The 2D laminated

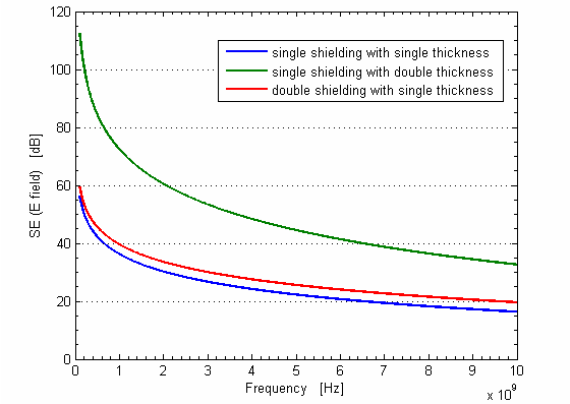

Figure 2: Shielding Effectiveness (E field) for single and double wire-mesh screen with single and double thickness.

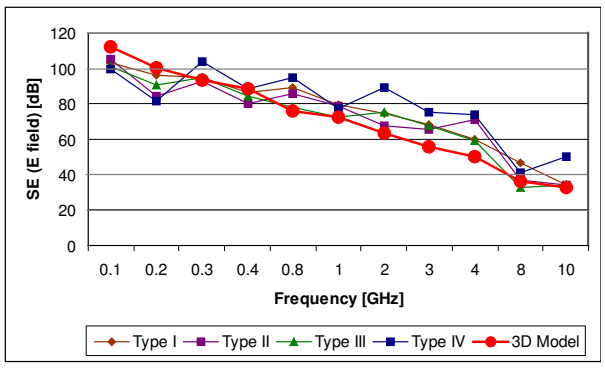

Figure 3: Shielding Effectiveness (E field) for aluminum foam slabs described in Table 1, compared with theoretical values of 3D model.

wire-mesh screen model, developed by Casey [2] and compared with commercial aluminium shield perforated periodically with apertures, was a first step to solve the EM problem of the rigorous evaluation of the metal foam's shielding effectiveness [3]. Encouraged by the results, we have improved the previously 2D model, developing a preliminary analytical 3D models.

Therefore the electromagnetic shielding behavior of a slab of metal foam, has been investigated considering a model with a double wire-screens mesh, separated by an air space. In fact, from the shielding effectiveness analysis of the double wire-mesh, shown in Fig. 2, we can note that the shielding effectiveness of double screen is more than the shielding effectiveness of single screens with double thickness. The single screen, whose meshes are assumed to be square, is described by an equivalent sheet impedance operator as mentioned in [3]. The agreement of both experimental and theoretical data, shown in Fig. 3, is a challenging to optimize this model in 3D.

Table 1: Esaminated foam types.

Duocel® Aluminium foam			
Type I	*Type II*	*Type III*	*Type IV*
10 PPI, 6–8% nominal density, 6.1% actual density. Alloy 6101-F	20 PPI, 6–8% nominal density, 8.5% actual density. Alloy 6101-F	40 PPI, 6–8% nominal density, 7.9% actual density. Alloy 6101-F	40 PPI, 6–8% nominal density, 8.7% actual density. Alloy 6101-F

REFERENCES

1. Catarinucci, L., O. Losito, L. Tarricone, and F. Pagliara, "High added-value EM shielding by using metal-foams: Experimental and numerical characterizzation," *Electromagnetic Compatibility, EMC 2006*, Vol. 2, 285–289, Aug. 2006.
2. Casey, K. F., "Electromagnetic shielding beavior of wire-mesh screens," *IEEE Transactions on Electromagnetic Compatibility*, Vol. 30, 298–306, Aug. 1988.
3. Catarinucci, L., O. Losito, and L. Tarricone, "On the use of metal foams in EM shielding applications," *Proceedings of the Mediterranean Microwave Symposium MMS'2006*, 240–245, Genova, Italy, Sept. 2006.

Estimation and Validation of Soil Moisture Using PALSAR Onboard ALOS over Mongolian Plateau

T. Tadono[1], **M. Shimada**[1], **H. Fujii**[1], **and I. Kaihotsu**[2]

[1]Earth Observation Research Center
Japan Aerospace Exploration Agency (JAXA), Japan
[2]Faculty of Integrated Arts and Sciences, Hiroshima University, Japan

Abstract— Soil moisture is important for fields not only hydrology but also meteorology. It plays important roles in the interactions between the land surface and the atmosphere, as well as in the partitioning of precipitation into runoff and ground water storage. In spite of its importance, soil moisture is not generally used for weather forecasting and water resources management because it is difficult to measure on a routine basis over large areas. The microwave remote sensing has a potential to estimate its important parameter distributions in temporally as well as spatially.

The goal of this study is to develop algorithms to estimate land surface hydrological parameters i.e., soil moisture and snow parameters using new satellite called ALOS, which stands for the Advanced Land Observing Satellite and had been successfully launch on January 24, 2006, and it is operating very well. ALOS has three mission instruments i.e., PALSAR, PRISM and AVNIR-2. PALSAR stands for the Phased Array type L-band Synthetic Aperture Radar, and it can be observed with high spatial resolution. PRISM and AVNIR-2 are optical instruments for cartography and environmental monitoring, disaster management etc.

As first step of this study, we applied existing algorithm to PALSAR data to estimate surface soil moisture. The test sites are located in the Mongolian Plateau, where is spatially homogeneous with basically flat terrain features. We have been installed and are continuously maintaining ground measurement instruments e.g., three Automatic Weather Stations (AWSs) and twelve Automatic Stations for Soil Hydrology (ASSH). The surface soil moisture maps with 100 m spatial resolutions are generated using PALSAR images, and validated seasonal variation using ground truth data. In generally, SAR image has high spatial resolution compared with passive microwave instruments, however revisiting time is longer than that. Therefore, estimated soil moisture values by PALSAR are compared with estimated one by using passive microwave data i.e., AMSR-E onboard AQUA satellite.

Classing and Extracting Information from Radar Images

G. Angiulli[1], **V. Barrile**[1], **G. M. Meduri**[1], **R. Pucinotti**[2], **and S. Tringali**[1]

[1]DIMET, University Mediterranea, Reggio Calabria 89100, Italy
[2]MECMAT, University Mediterranea, Reggio Calabria 89100, Italy

Abstract— GPR techniques had been successfully using for many years to examine structures and materials from inside. They are based on the possibility of sending electromagnetic pulses and registering the echo time and the amplitude of the signals eventually back-scattered by the interface between propagation media of different dielectric constants. The result consists of some radar images (the so-called radargrammes), where incidental targets generate distinctive hyperbolic plots or discontinuities, as an indirect evidence of either changes in the properties, nature and composition of the medium or the presence of internal breaks. The present note aims at expounding some tests and preliminary results drawn by the employment of specific algorithms for automatically interpreting, classing and extracting explicit information from radargrammes, once these have been traced from raw radar data by an ad hoc application designed in the MatLab framework.

Sparse, Active Aperture Imaging

John K. Schindler

AFRL Sensors Directorate (RYHA) and the ARCON Corporation
80 Scott Drive, Hanscom AFB, MA 01731-2909, USA

Abstract— We address the problem of radar imaging of an isolated target using coherent, sparse or highly thinned arrays of transmit/receive elements. The array elements are assumed to be randomly positioned and accurately surveyed after placement. Further, the target is assumed to occupy a limited angular sector and because it is isolated, there is no source of backscatter beyond the sector occupied by the target. The target is assumed to exhibit translational and rotational motion.

It is well known that highly thinned arrays provide enhanced imaging resolution determined by the extended aperture of the array. However, typically the random sidelobes of the sparse array are high and degrade the quality of the image due to leakage of scattering from elements of the target at other angles.

In this work we examine whether the limited complexity of a linear, random, sparse array as expressed by the equivalent number of array elements is sufficient to control the array pattern over the limited angular extent of the target with no requirements for pattern control elsewhere. Conversely, we examine the target angular extent that can be imaged with a given sparse array configuration and suggest radar signal processing techniques that can effectively limit the target angular extent to be imaged.

Our analysis begins by expanding the random scattered field along an arc near the target using orthogonal basis functions. The expansion can be of the form of either (a) a Karhunen-Loève expansion with basis functions determined by the correlation properties of the scattered field on the arc or (b) a sampling expansion with cardinal basis functions and samples of the scattered field on the arc. The latter expansion is especially useful since the errors associated with the use of a limited number of field samples can be quantified using the work of Bucci and Franceschetti [1]. The scattered field samples are estimated using maximum likelihood and maximum à posteriori estimation processes. The data for these estimators are the complex scattered fields measured with receiver noise at the sparse array elements assuming coherent, multiple input/multiple output (MIMO) operation. MIMO operation is important since it yields a substantially greater number of field samples over the random coarray equivalent to the physical transmit/receive array when excited by the complex scattered field from the target. This analysis permits us to compare the sparse array complexity with the number of field samples needed to accurately characterize the target scattering, which in turn are determined by the angular extent occupied by the target.

In a second phase of this work, we suggest and analyze an approach to limit the angular sector of the target scattering to be imaged. When the angle subtended at the target by the sparse array elements is large, only a portion of the target scattering from each range gate is common to all elements of the array and responds to coherent beamforming. Scattering from outside of this common region appears as a kind of non-coherent noise to the beamforming and must be reduced. We describe an inverse synthetic aperture radar (ISAR) approach for each MIMO element pair to limit the observed angular sector of scattering to the common, coherent region. Limiting the ISAR integration time to insure that scatterers remain in a single radar range gate determines the minimum coherent angular region of the target and determines the required sparse array complexity. Basic arguments about the processing and assumptions about the nature of the scattering process indicate that sparse array resolutions that are one to two orders of magnitude smaller than the ISAR resolution are possible with a reasonable number of sparse array, MIMO elements.

REFERENCES

1. Bucci, O. and G. Franceschetti, "On the spatial bandwidth of scattered fields," *IEEE Transactions on Antennas and Propagation*, Vol. 35, No. 12, 1445–1455, December 1987.

Wavelet Based Synthesis of Multifractal Rough Surface

Zhaorui Wang and Shanwei Lv
School of Electronic and Information Engineering, Beihang University, Beijing, China

Abstract— The problem of electromagnetic scattering from rough surface has been extensively studied in a wide variety of scientific and engineering applications, including electromagnetics, microwave remote sensing, integrated optics, underwater acoustics, radar cross section from sea and land surfaces, semiconductor packaging, computer vision and computer graphics, and other many potential applications. For these problems, where the rough surface is either the primary target or the clutter, the understanding of interaction of electromagnetic waves with the rough surface is essential for developing inversion or detection algorithms. So the most definitely necessary thing is to generate needed rough surface profile.

Traditional Gaussian spectrum rough surface is single scale and the roughness is not time varying. During recent years, the fractal geometry is introduced to the study of rough surface. Since the fractal rough surface, as a multi-scale geometry, takes account of surface perturbations in large and small scales, such as the famous band limited Weierstrass-Manderbrot roughness spectrum. It seems better to describe some natural surfaces than traditional model. Whereas the limitation of the fractal model mentioned above is also obvious, its pointwise singularity describing the roughness remains the same all along the sample path. From a physical point of view, this may be too strong an idealization. Since many natural structures are determined by a large number of generating processes operating at different scales and the roughness is dynamic. For modeling these more realistic structures, in this work, a preliminary study is carried out to demonstrate the synthesis of one dimensional multifractal rough surface by means of discrete wavelet transform. The desired local regularity of the multifractal rough surface is obtained by controlling the weights of the wavelet expansion of the Gaussian white noise. The convergence of the synthesized process is controlled by an experimental factor. This algorithm is not only time saving, and also appropriate for generating the multifractal rough surface that is non-Gaussian and autocovariance function unknown in advance. The validity and rationality are verified by numerical experiments.

Numerical Analysis of a Photonic Band Gap by a Multilayered Deep Dielectric Gratings

T. Suyama, Y. Okuno, and A. Matsushima
Kumamoto University, Japan

Abstract— An effective computational method based on a conventional modal-expansion approach is presented for handling a multilayered dielectric grating whose profiles are strongly modulated. The groove depths can be the same as or a little more than the grating period. The materials can be dielectric or metal. In consideration of an application to a photonic crystal, we examine a characteristic of the multilayered dielectric grating. The method is based on Yasuura's modal expansion, which is known as a least-squares boundary residual method or a modified Rayleigh method. In the extended method, each layer is divided into shallow horizontal layers. The Floquet modal functions and approximate solutions are defined in each shallow layer, and the latter are matched with boundary conditions in the least-squares sense. A huge-sized least squares problem that appears in finding the modal coefficients is solved by the QR decomposition accompanied by sequential accumulation. As numerical example, we calculate a diffractive characteristic by a multilayered deep dielectric grating and confirm that a common band gap occurs for both polarizations.

Introduction: A photonic crystal [1–3], which is composed by arraying periodically dielectric material having different permittivity, is receiving much attention nowadays. This type of crystal has a characteristic of what is called photonic band gap, which suppresses propagation in certain wavelength ranges dominated by crystal structure, and has many applications as devices for optical integrated circuits. Recent development of microfabrication technique makes it possible to produce deep gratings whose profile is strongly modulated.

From the viewpoint of numerical analysis, there are few examples which analyze diffraction characteristics of three-dimensional photonic crystals. The three-dimensional photonic crystal which we treat in the present paper is fabricated by laminating deep grating layers. To elucidate a characteristic of such photonic crystal, and to design a crystal having a desired gap, it is necessary to examine an interaction with structure (a laminate of doubly periodic deep gratings) and light (an electromagnetic wave). It is expected that the stop band characteristic is appeared clearly by a multilayered grating, and the polarization dependence is decreased by an introduction of two-dimensional periodicity. We analyze the problem of plane wave diffraction by the multilayered deep grating, and confirm that a characteristic as photonic crystal is provided.

REFERENCES

1. Yablonovitch, E., "Inhibited spontaneous emission in solidstate physics and electronics," *Phys. Rev. Lett.*, Vol. 58, 2059–2062, 1987.
2. Ho, K. M., C. T. Chan, and C. M. Soukoulis, "Existence of a photonic gap in periodic dielectric structures," *Phys. Rev. Lett.*, Vol. 65, 3152–3155, 1990.
3. Villeneuve, P. and M. Piche, "Photonic band gaps in two dimensional square and hexagonal lattices," *Phys. Rev. B*, Vol. 46, 4969–4972, 1992.

A Pseudovariational Technique for the Phase Curve Reconstruction in Reflectarray Design

G. Angiulli and S. Tringali
DIMET, Univ. Mediterranea, Reggio Calabria 89100, Italy

Abstract— Microstrip patch reflectarray is a low profile and light weight antenna that combine some of the best features of printed technology together with those of conventional reflector antenna. It consists of thousands of microstrip elements specifically designed so that the scattered field from each of the elements yields a proper phase delay to achieve a focusing effect and compensate different path length from the element to the feed [1]. At this purpose a design parameter named phase curve must be employed [1–3]. In particular, technical literature provides evidence for two main approaches proposed in order to reconstruct the phase curve, that is to say the infinite array approach and the isolated element one. In both cases a full-wave type analysis of the scattered field is recommended to get the best results. Phase curves reconstructed in this way are in very good agreement with experimental measurements [1–3]. But the reconstruction process based on a full wave technique is very time consuming. In fact, to obtain a carefully characterization of the phase of the total scattered field as a function of the size of the reflectarray element, many numerical simulations are required [2]. Since Pozar's early work on the topic [3], much effort has been devoted for the purpose of overcoming such problem. In this perspective, our work deals with the development and the implementation of a new technique based on the employment of a pseudovariational formula for scattering [4]. As matter of fact, using the reciprocity theorem it is possible to obtain a relationship between induced current and scattered field by a patch in an array environment [5]. Formally, this expression is a pseudofunctional since it is obtained employing a pseudo inner product [4] However it can be usefully employed in a variational procedure in order to evaluate the phase curve. From a practical point of view, this produces as a result the effective speed-up of the phase curve computation process, despite of a meaningless loss of accuracy. Finally, we present some numerical results proving the effectiveness of our approach.

REFERENCES

1. Pozar, D. M., T. S. Targonsky, and H. D. Syrigos, "Design of millimeter wave microstrip reflectarrays," *IEEE Trans. Antennas Propagat.*, Vol. 45, No. 2, 287–295, 1997.
2. Angiulli, G., "Numerical comparison of interpolation techniques for phase curve reconstruction in reflectarray design," *EUROCON 2005*, 856–857, 2005.
3. Pozar, D. M. and T. Metzler, "Analysis of a reflectarray antenna using microstrip patches of variable size," *Electronics Letters*, 657–658, 1993.
4. Ziariani, A. K. and A. Konrad, "Galerkin method and the variational procedure," *IEEE Trans. on Magnetics*, Vol. 38, No. 1, 190–199, 2002.
5. Harrington, R. F., *Time Harmonic Electromagnetic Fields*, IEEE Press Series on Electromagnetic Wave Theory, 2001.

Mixer Methodologies for On-chip RF Test in 0.25 Micron CMOS Process

Gian Paolo T. Mayuga and Marc D. Rosales
University of the Philippines Diliman, Philippines

Abstract— This study pushes to take advantage of the scaling technology of CMOS for Wireless Communications, specifically for Radio Frequency (RF) Mixers. CMOS allows the integration of digital and analog circuits with high level of complexity in the same die, leading to systems with better performance and reliability, but relatively cheaper.

The aim of this study is to present a comprehensive methodology in designing 2.4 GHz RF CMOS mixers that addresses issues regarding key performance parameters. The key parameters include conversion gain; noise figure and third-order intercept point. The mixers are designed for Bluetooth and Wireless LAN standards.

Chosen mixer methodologies were implemented using a 0.25 micron digital CMOS process. Cadence Design System Software is used to aid in the design, simulation and layout phases of the study. This simulator-based design cycle will optimize the key performance parameters during the early stages of the design. Impedance matching, random noise, and linearity were also explored. Pre and Post layout simulation results of the designed mixer are to be presented. Simulation results for the final mixer show conversion gain of 6.5 dB, noise figure of 11.2 dB and 3rd-order intercept point of −10 dBm, at 2.4 GHz input RF frequency and 50 MHz output IF frequency.

The Darlington Amplifier Optimized for Wideband

O. V. Stukach
Tomsk Polytechnic University, 30 Lenin Avenue, Tomsk 634050, Russia

Abstract— A new design and performance for the wideband Darlington amplifier is described. The amplifier configuration consists of a common-emitter transistor pair with low-pass filter. The normalized gain characteristic for the amplifier provides 1.36 multiple extension of frequency band without degradation of the dynamic range, at VSWR and matching of input-output retaining. Expression for the optimum transfer factor was received. On this base the amplifier module for measuring and communication devices is carried out. This paper will discuss the design theory, techniques, and measurements of this newly developed Darlington circuit.

Session 2P6a
Electromagnetic Compatibility 2

Modeling of the Coupling Mechanisms between Lightning and a Complex Telecommunication Network

M. Troubat[1], **Y. Bourgeois**[2], **A. Zeddam**[2], **A. Reineix**[1], **and C. Guiffaut**[1]

[1]XLIM Laboratory, 123 avenue A. Thomas 87060 Limoges, France
[2]France Télécom R&D, 2 avenue Pierre Marzin 22307 Lannion, France

Abstract— In this paper, we propose a new modeling of the coupling mechanisms of the lightning with a complex network of telecommunication. The studied network is composed of a building that can be linked to many sections of buried cables and overhead lines. Moreover a protective earth placed in the ground is added to the study. We also take into account the lightning channel and the mismatching existing at the top of the building in the case of a direct lightning strike.

The modeling is realized in two different parts. On one hand, we show that it is possible to model with a temporal model, the building struck by the lightning channel. The model is an assembly of distributed element by unit length. On the other hand, we have optimized the protection of the buried cables against the lightning direct and indirect effects.

In the first part, the building is studied and linked to a ground rod. The characterization is realized by the free solver OPEN TEMSI-FD using the Finite Difference Time Domain (FDTD) method. The reflection coefficient (S_{11a}) of the building can be obtained, and it permit to know the building's impedance matrix [Z]. Then, the building can be described by an assembly of Pi cells by length unit. So, if some buried cables or overhead lines are connected to the building, it becomes possible to know relatively simply the induced and conducted electromagnetic field over these cables or lines.

In the second part, a theoretical study is set. This study uses a calculation code based on the theory of the Transmission Lines Theory (TLT) associated with a topological approach [1]. Previously in 2006, an artificial release of lightning campaign has been realized at Cachoeira Paulista in Brazil [2]. The test have been realized on a network composed of an overhead line and of a buried cable joined to a protective earth. A comparison is thus realized and the measurement and the simulation results are in quite good agreement. It finally enables to validate our code.

In conclusion, we propose a global modeling of the coupling mechanisms of lightning with a telecommunication network. The proposed tools are very useful because of the implementation simplicity. Furthermore, experimental tests have validated the code based on the TLT. The study realized is a global approach of a network struck by lightning and could be involved by taking into account the presence of non linear element as lightning conductor.

REFERENCES

1. Kerroum, K., F. Paladian, J. Fontaine, M. Vautier, and A. Zeddam, "Approche globale du couplage d'une onde EM avec un système de câbles multifilaires," *CEM94*, 247–252, Toulouse.
2. Barbosa, F., F. E. Nallin, S. Person, and A. Zeddam, "The effect of protection procedures applied to telecommunication lines on the lightning induced surges," *ICPL 2004*, Versailles, 2004.

Study of Electric Field Radiated by Wireless Systems in an Aircraft

E. Perrin[1], **F. Tristant**[2], **C. Guiffaut**[1]
A. Reineix[1], **and J.-P. Moreau**[2]

[1]XLIM-OSA Laboratory, France
[2]Dassault Aviation Company, France

Abstract— In this paper, the electric field radiated by wireless systems in an aircraft is studied. Wireless communications inside an aircraft's cabin, such as laptops using WiFi technology or mobile phones, radiate an electrical field which can disturb equipment. A certification process (in respect with RTCA DO-294 [1]) must be done to guarantee that each critical equipment of the aircraft will not be disturbed by field radiations. The certification of the aircraft is obtained thanks to ground tests. Up to now, no 3D computations has been realized because the frequency band concerned and the aircraft's size were incompatible with computation resources. That is why our study purposes new 3D computations inside a business airplane's cabin until 2.45 GHz. These computations give us preliminary results before real tests, useful during the certification process of the aircraft.

Computations are realized with TEMSI-FD, a 3D simulator based on the finite difference in the time domain method (FDTD) [2]. In our study, the considered aircraft is a Dassault Aviation Falcon which can contain at the most 15 passengers. In order to consider the worst case, we suppose that each passenger uses a portable electronic device (PED) in the cabin. Three different frequency ranges are considered: around 0.9 GHz for the GSM first generation, around 1.8 GHz for the GSM second generation and around 2.45 GHz for the WiFi 802.11b band [1]. In the three cases, the transmitted power of antennas is chosen in respect with the maximum power defined in the norm [1].

The electrical field is computed:

- In several points around each equipment location. From these punctual fields, a statistical field distribution is deduced;
- Over a surface. The spatial distribution of the electrical field is computed on cross surfaces of the cabin: at the table level, at the windows level, under the floor...

The statistical distributions allow to determine the maximum and the average electric field around equipment. These results are compared with the equipment qualification test level and a margin is extracted. The mapping inform us about the global spatial distribution of the electric field in the cabin.

We demonstrate a comfortable margin between the maxima levels computed and the qualification tests' levels. The plan of mapping is useful because it is the only tool through which we can observe the total spatial distribution of the electric field in the cabin. During ground tests, we can punctually measure the electrical field, but it is impossible to know its total spatial distribution. Thanks to these computations, real tests on aircraft are targeted on the particular problems highlighted and are more efficient.

REFERENCES

1. Norm RTCADO-294, "Guidance on allowing transmitting portable electronic devices on aircraft," Oct. 2004.
2. Guiffaut, C., TEMSI-FD, "Solver based on the finite difference in the time domain method," XLIM Laboratory, 2001–2007.

A Simple Numerical Method to Calculate the Q-factor of a Cavity Containing Apertures

Guillaume Andrieu and Alain Reineix
XLIM Laboratory, Limoges, France

Abstract— In electromagnetic compatibility, a current domain of research concerns the electromagnetic (EM) field penetration in an enclosure containing apertures. The EM field penetration is often quantify by the electric (SE) and magnetic (SH) shielding effectiveness corresponding to the ratio of the electric and magnetic fields inside and outside the cavity. Numerous papers have already been published to develop simple methods to calculate the SE and SH for canonic enclosures and apertures [1, 2].

Our paper presents a simple numerical method which permits to calculate the EM field penetration in an enclosure of any geometry containing complex apertures thanks to the calculation of its Q-factor. The Q-factor is obtained with the method used to measure the Q-factor of a mode stirred reverberation chamber (MSRC). Indeed, the Q-factor of a MSRC is calculated thanks to the measurement of the average S-parameters of two antennas located inside the RC for a complete rotation of the mode stirrer.

In an empty cavity, the obtained Q-factor depends of the position of the two antennas. To avoid this, a solution is to calculate the average Q-factor of the cavity for 50 different positions of both antennas. This solution requires 50 modelings of the system. So, our method consists in calculating the average S-parameters of 10 antennas (dipole antennas) located in the enclosure. The results of the 3D modeling using the method of moments formalism is in this case very representative and independent of the position of the antennas. The presence of 10 antennas is considered as negligible on the Q-factor of the cavity because it is mainly dependent of the Q-factor related to the apertures.

To conclude, our method requires only one 3D-modeling to calculate accurately the Q-factor of an enclosure of any geometry containing complex apertures. The knowledge of the Q-factor permits in a second step to calculate the shielding effectiveness of the enclosure, the average electric field inside the enclosure or the coupling on an object located inside.

REFERENCES

1. Robinson, M. P., J. D. Turner, D. W. P. Thomas, J. F. Dawson, M. D. Ganley, A. C. Marvin, S. J. Porter, T. M. Benson, and C. Christopoulos, "Shileding effectiveness of a rectangular enclosure with a rectangular aperture," *Electronic Letters*, Vol. 32, No. 17, August 1996.
2. Belokour, I. and J. LoVetri, "A 2D-transmission line model for the EM fields estimation inside enclosures with apertures," *2002 IEEE International Symposium Proceedings*, 424–429, Minneapolis, August 2002.

Minimum Phase Causal Reconstruction of a Class of Equalizers

Saeed Asgari and Michael Tsuk
Ansoft Corporation, USA

Abstract— To perform signal integrity based simulations in time domain and check for the electrical performance of a communication system, intensive time simulations are needed. The feasibility of such simulations is granted only when accurate and efficient models are available especially those that contribute most to the system performance. Causality check and enforcement is practically important to the performance evaluation of interconnects based on time domain simulation. Most circuit simulators will not be able to perform reliable simulations without ensuring causality.

Minimum phase causal reconstruction of a class of equalizers from only their known amplitude response is discussed. This is performed analytically and in closed form so long as the amplitude response of the equalizer's transfer function belongs to a proposed class of equalizers. As a result reliable causal time domain simulations can be performed on systems utilizing these equalizers thereby enabling eye diagrams and signal constellation plots by post-processing the resulting time simulations.

This paper shows the application of the proposed class of equalizers to the time simulation and compliance testing of the High-definition Multimedia Interference (HDMI) cable. In order to perform reliable time simulation of high-speed interconnects such as the HDMI cable, usually characterized by their tabulated scattering parameters in the frequency domain, one needs to ensure that the related transfer function representation is causal. In the case of the time simulation of the HDMI cable with amplitude equalization where only the amplitude response is known with no available phase information special care must be taken to ensure the causality of the overall transfer function otherwise unreliable non-causal responses as well as eye diagram distortions can occur.

There are different approaches to causality compensation many of which use numerical algorithms with many applications of (fast) Fourier and inverse Fourier transforms. In this paper, we introduce a class of equalizers with only known amplitude response for which analytical expressions for the minimum phase transfer function are derived. Thus, so long as the equalizer with only known amplitude response belongs to the proposed class of equalizers then a closed form expression for the minimum phase transfer function (estimate) is provided that can be used in any transient simulation tool. Application of the proposed class of equalizers in time simulation of other type of communication systems such as to the equalizer block of a partial response channel are also discussed as future extension of this work.

Session 2P6b
Advances in Numerical Methods for Photonics Simulation

Analysis of Dielectric Waveguides with Open Boundaries

H. S. Yoo and A. Gopinath
University of Minnesota, USA

Abstract— To analyze dielectric waveguides, the vector finite-element method is applied to solve the wave equations by using edge-based for the transverse components and the conventional node-based interpolation functions. This method only represents well in the interior region, however, boundary integral equations need to be applied in the homogeneous exterior region. Since the exterior boundary integral equations obtained by the Green's theorem represent boundary conditions, an appropriate procedure is required to solve the problem in the interior and at the boundary. In this paper, an iterative method is used and the robustness of this algorithm is confirmed by the numerical results corresponding the computation of the propagation constant. For the finite-element formulations, the following curl equation which ignores the natural boundary condition is used:

$$\frac{1}{\varepsilon_r}(\nabla \times \mathbf{H}) \cdot (\nabla \times \mathbf{H})^* - k_0^2 \mu_r \mathbf{H} \cdot \mathbf{H}^* = 0 \tag{1}$$

where $\mathbf{H}(x, y, z) = \mathbf{H}(x, y)e^{-j\beta z}$, and β is the propagation constant. The boundary integral equation is derived from the scalar Green's theorem for all three components of fields. This equation takes the form:

$$\mathbf{H}(r)_{\text{external}} = \int \left\{ \mathbf{H}(r_0) \frac{\partial G(r, r_0)}{\partial n} - G(r, r_0) \frac{\partial \mathbf{H}(r_0)}{\partial n} \right\} ds_0 \tag{2}$$

where for the guided mode $G(r, r_0) = K_0(\alpha|r - r_0|)$, $\alpha = \sqrt{\beta^2 - k_0^2}$, K_0 is the modified Bessel function of the second kind. Note that the external field from this equation has the form $\mathbf{H}(r)_{\text{external}} K_0(\alpha|r - r_0|)$. These separate equation [1] and [2] represent the problem in the interior region and at the boundary, respectively. After manipulating it by the matrix form, both equations end up with two generalized eigenvalue formulations like $[A][H] = \beta^2[B][H]$. Therefore, the iterative method is applied to find the solution which satisfies both eigenvalue problems. A new technique will be presented for the analysis of rectangular dielectric waveguides and compared with the published results.

Rigorous Theoretical Study of Local Density of States and Mode Localization in Two-dimensional Aperiodic Photonic Structures

Svetlana V. Boriskina, **Ashwin Gopinath**, **and Luca Dal Negro**
Department of Electrical & Computer Engineering, Boston University
8 Saint Mary's Street, Boston, Massachusetts 02215, USA

Abstract— Aperiodic photonic and plasmonic structures offer new ways of focusing and manipulating optical fields at the nanoscale thus providing exciting opportunities for the design of novel nanophotonics functional elements for light emission and sensing applications [1, 2]. Designing aperiodic photonic structures for specific application tasks is challenging both from a computational and an experimental perspective. In fact, while the fabrication processes impose limitations on the choice of materials and minimum feature sizes, the demands for flexibility, accuracy and robustness of the theoretical analysis are significantly challenged by the lack of global translational symmetries. As a result, the application of conventional theoretical tools developed in the context of periodic photonic crystal structures (e.g., the plane wave expansion method) for the study of aperiodic photonic lattices would require large primitive cells (super-cells), which are computationally intensive.

To address this challenging design task, we make use of highly efficient numerical techniques based on the rigorous spurious-solutions-free two-dimensional (2D) boundary integral equations formulation, which we have previously developed for studying modes of optical microcavities and coupled-resonator optical waveguides [3, 4]. In this work, we modify the methodology and software tools to theoretically investigate optical properties of Fibonacci, Thue-Morse and Rudin-Shapiro two-dimensional arrays. The method is formulated in the complex domain and can be applied to the study of both photonic and plasmonic structures (including the role of material losses and gain). We construct 2D Green's functions of periodic and aperiodic photonic lattices, which enable us to compute the frequency- and position-dependent local density of states (LDOS). LDOS describes how the radiation properties of a radiation source embedded in a photonic crystal are modified by the surrounding aperiodic lattice. In particular, the radiative rate of active materials embedded in a modified photonic environment can be dramatically modified accordingly to the LDOS behaviour. The existence of photonic bangaps in several types of aperiodic structures can now be revealed by directly investigating the LDOS frequency dependence. We also study in detail LDOS scaling with respect to the aperiodic system size and the spectrum of localized optical modes in deterministic aperiodic structures with different degrees of disorder. By studying both orthogonal light polarization states we investigate the effect of spatial correlations and ordering in band-gap formation with respect to resonant properties of a single cylinder. Finally, we explore ways of controllable manipulation of frequency spectra and mode localization by tuning the structural parameters of aperiodic crystals.

REFERENCES

1. Dal Negro, L. and N. Feng, "Spectral gaps and mode localization in Fibonacci chains of metal nanoparticles," *Opt. Express*, Vol. 15, 14396, 2007.
2. Dal Negro, L., N.-N. Feng, and A. Gopinath, "Electromagnetic coupling and plasmon localization in deterministic aperiodic arrays," submitted to *J. of Optics A*.
3. Boriskina, S. V., "Theoretical prediction of a dramatic Q-factor enhancement and degeneracy removal of WG modes in symmetrical photonic molecules," *Opt. Lett.*, Vol. 31, 338–340, 2006.
4. Pishko, S. V., P. Sewell, T. M. Benson, and S. V. Boriskina, "Efficient analysis and design of low-loss WG-mode coupled resonator optical waveguide bends," *IEEE/OSA J. Lightwave Technology*, Vol. 25, 2487–2494, 2007.

Simulation of Non-ideal Pillar-type Cavities Using Finite Element Methods

F. Schmidt and B. Kettner
Konrad-Zuse-Zentrum Berlin, Takustraße 7, D-14195 Berlin, Germany

Abstract— We will discuss the analysis of pillar-type cavities by simulation with the finite element method. This analysis will require solving of scattering problems of light emitted by a point source within an isolated structure in an unbounded domain, solving of eigenvalue problems on unbounded domains as well as solving of scattering problems on axisymmetric structures embedded in unbounded domains.

Summary: Pillar-type cavities that allow for optical coupling of the states of quantum dots via the cavity modes of resonators have recently been examined byM. Hetterich et al. at CFN Karlsruhe. These devices consist of highly reflective bragg-mirrors enclosing a $\frac{\lambda}{2}$-cavity containing quantum dots that may be excited and emit light at a given wavelength. Even though the fabrication and design of these structures is quite elaborate, good numerical simulation for such cavities is a challenging task still requiring further improvement. A first numeric investigation of the effect of two types of imperfections on the quality (Q) factor of these structures was done by Gregersen et al. [1].

Our approach differs since we use the finite element method rather than the finite difference method in our simulation, which allows us to investigate imperfections like sidewall inclination angles without the negative effects of staircasing. For our numerical simulation, we have considered several problem classes: To simulate the emission of the quantum dots in the cavity, we have solved the scattered field resulting from a point source enclosed in an isolated cavity on a 2D cross section through the cavity. This means solving a 2D scattering problem in an unbounded domain for a given frequency ω. For a closer investigation of the resonance modes, a time-harmonic ansatz for the vectorial magnetic field $\mathbf{H}$ leads to the eigenvalue problem

$$\begin{aligned} \nabla \times \frac{1}{\epsilon(\vec{x})} \nabla \times \mathbf{H}(\vec{x}) &= \omega^2 \mu(\vec{x}) \mathbf{H}(\vec{x}), \\ \nabla \cdot \mu(\vec{x}) \mathbf{H}(\vec{x}) &= 0, \ (\vec{x}) \in \Omega \\ + \text{ boundary condition} & \end{aligned}$$

where Ω is the computational domain and ω is an eigenvalue corresponding to a frequency. The boundary condition for this formulation of the problem has to be further specified and is decisive for the quality of the simulation. Transparent boundary conditions are required for realistic modelling.

Since the eigenvalue simulations showed good agreement with the 2D point source scattering and good qualitative agreement with the measurements conducted at CFN Karlsruhe, we extended

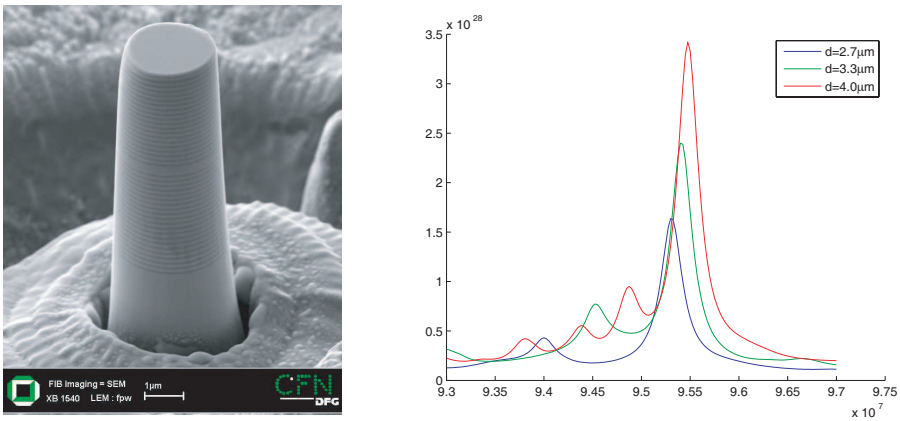

(a) (b)

Figure 1: (a) Pillar cavity with a diameter of 2.7 µm produced by CFN Karlsruhe, (b) Position change of the main resonance for varying pillar radius.

our simulation to a more realistic 3D model consisting of an axisymmetric isolated structure. Here our simulations revealed good quantitative agreement of the simulated resonance peaks with the resonacnce peaks measured by our partners. Thus in the next step, the dependency of the resonances of different parameters were tested and we identified the effects, the radius of the pillar and the number of bragg-mirrors have on the Q-Factor. Further investigations concerning sidewall inclination and other imperfections are still ongoing. In future steps, the simulation will help improve the design of the cavities and help to raise the Q-Factor.

REFERENCES

1. Gregersen, N., T. Nielsen, B. Tromborg, and J. Mork, "Quality factors of nonideal micro pillars," *Appl. Phys. Lett.*, Vol. 91, 011116, 2007.

Modelling Microstructured Optical Fibres

Zheng-Gang Lian[1], **Jim Wykes**[1], **Phillip Sewell**[1], **Ana Vukovic**[1]
Trevor M. Benson[1], **Ella Bekker**[2], **and Leonid Melnikov**[3]

[1]George Green Institute for Electromagnetics Research, University of Nottingham
University Park, Nottingham, NG7 2RD, UK
[2]Photon Design, 34 Leopold St., Oxford, OX4 1TW, UK
[3]Department of Physics, Saratov State University, Saratov 410012, Russia

Abstract— Microstructured optical fibers (MOFs) provide enormous potential for dispersion tailoring, amplification, filtering in optical telecommunications systems, enhanced non-linear interactions for pulse-transformation, ultra-fast optics, new light sources for spectroscopy and optical coherence tomography and specialist sensing applications. In this paper we review the design of both solid and hollow core MOFs where guidance can be the result of 'conventional' total internal reflection, high reflectivity within a photonic bandgap or anti-resonance mechanisms. Our particular interest is in MOFs utilizing tellurite and chalcogenide glasses for the mid-far IR. These glasses tend to have a higher refractive index than that of silica.

Quantitative analysis of the waveguiding properties of MOFs typically requires a rigorous approach. Long-established numerical techniques such as the finite element, finite difference and beam propagation methods provide versatile approaches to simulation. The varied geometries of MOFs lend themselves to the use of unstructured meshes in these numerical methods. Unstructured meshes generally require fewer mesh elements for a given quality of boundary description which typically means that the net computational requirements of unstructured algorithms are far less than those of structured algorithms. Specialist multipole [1] and source model [2] techniques are also widely used. Commercial codes such as Photon Design's Fimmwave, a fully vectorial waveguide solver based on the film mode matching, also prove very effective in the study of MOFs, especially when combined with an optimisation tool, such as Kallistos, to automatically improve existing designs with minimum user intervention.

REFERENCES

1. Kuhlmey, T., T. P. White, G. Renversez, D. Maystre, L. C. Botton, C. M. de Sterke, and R. C. McPhedran, "Multipole method for microstructured optical fibers. II. Implementation and results," *J. Opt. Soc. Am. B*, Vol. 19, 2331–2340, 2002.
2. Hochman, A. and Y. Leviatan, "Analysis of strictly bound modes in photonic crystal fibers by use of a source-model technique," *J. Opt. Soc. Am. A*, Vol. 21, 1073–1081, 2004, The source-model technique package is published on the web http://www.ee.technion.ac.il/leviatan/smtp/index.htm.

Nonlinear Switching Effects in Coupled Micro-photonic Cavities

B. Maes, **K. Huybrechts**, **G. Morthier**, **P. Bienstman**, **and R. Baets**
Photonics Research Group, Ghent University, Belgium

Abstract— Nowadays high-quality micro-cavities are established in several systems, such as photonic crystals, disks or photonic wire rings. Fabrication of multiple coupled cavities has also provided a path towards advanced filters or long delay lines. Here we explore some of the nonlinear effects, which appear when these resonators are coupled to each other.

One of the important issues concerning photonic switching is the lowering of necessary input powers. By judiciously choosing the waveguide distance between two cavities it is possible to establish extremely sharp peaks in the transmission spectrum. Numerical results show that this leads to very low power switching possibilities.

Besides these more traditional interference effects, the coherent feedback provides other opportunities, such as symmetry breaking. One starts with a left-right symmetric structure with equal inputs from left and right. Under certain conditions, it turns out that the symmetric solution destabilizes, if one increases the input power. This leads to asymmetric states, where more output power exits to one side than to the other. Switching between output directions is possible by adding pulses to the correct inputs, which results in optical flip-flop behavior.

Recently we optimized this scheme by using 'blockers' next to the cavities, which lead to Fano resonances, in order to lower the power required for the bifurcation. In addition we extended the scheme towards a circuit of three cavities. This three-cavity structure provides rich dynamics, and functions as a tri-stable integrated memory device.

All these structures are efficiently examined using coupled-mode theory. Conditions for symmetry breaking are derived analytically. These studies are confirmed with rigorous numerical simulations, using finite-difference time-domain and eigenmode expansion methods. Because the concepts are general, they can be implemented in several micro-photonic platforms, such as photonic crystals or photonic wires.

ACKNOWLEDGMENT

This work was supported by the Fund for scientific research — Flanders (FWO Vlaanderen) and the Institute for the Promotion of Innovation through Science and Technology in Flanders (IWT).

Beam Propagation for Tapered Waveguides

G. Ronald Hadley

MS 1085, Sandia National Laboratories, P. O. Box 5800, Albuquerque, NM 87185-5800, USA

Abstract— The beam propagation method (BPM) remains the single most often-used simulation tool for waveguide-based photonics structures, and is known to be accurate and dependable for waveguides with constant cross-section. However, serious issues arise with this technique when the waveguide structure is changing in the direction of propagation and the index contrast is substantial, due to the necessary stair-step approximations employed by most algorithms. Although this deficiency has been remedied for special cases by coordinate transformation approaches [1, 2], only recently has an attempt been reported at deriving BPM equations valid for slanted dielectric interfaces on a general finite-difference grid [3]. A successful derivation of this type is of great utility because it separates the propagation algorithm from the grid, thus allowing the simulation of an extremely wide variety of structures. In addition, other applications have been suggested, including adaptive waveguide modelling [3]. The derivation reported so far has been shown to be both simple and accurate for TE polarization and a single field component, but still problematic for TM polarization. Propagation performed for the latter case is only stable for paraxial propagation. The extension of the method to bi-directional BPM for modelling reflections from tapered waveguides was suggested but not implemented.

The reported derivation employed the use of a power series expansion of the field component around the center of each quadrilateral, with lateral derivatives replaced in terms of derivatives in the direction of propagation by use of the wide-angle propagation equation. Another approach presently being explored involves the integration of the Helmholtz Equation over the same quadrilaterals, together with Green's theorem to replace the area integral with integrals over the perimeter of the normal field derivative. This approach may aid in the derivation of a conservative algorithm since all interface integrals vanish identically. It may also aid in the derivation of a reflective algorithm by incorporating an extra counter-propagating field component.

ACKNOWLEDGMENT

Sandia is a multiprogram laboratory operated by Sandia Corporation, a Lockheed Martin Company, for the United States Department of Energy under contract DE-AC04-94AL85000.

REFERENCES

1. Yamauchi, J., J. Shibayama, and H. Nakano, "Finite-difference beam propagation method using the oblique coordinate system," *Electron. Commun. Jpn.*, Vol. 78, 2, 20–27, 1995.
2. Djurdjevic, D. Z., T. M. Benson, P. Sewell, and A. Vukovic, "Fast and accurate analysis of 3-D curved optical waveguide couplers," *J. Lightw. Technol.*, Vol. 22, No. 10, 2333–2340, 2004.
3. Hadley, G. R., "Slanted-wall beam propagation," *J. Lightw. Technol.*, Vol. 25, No. 9, 2367–2375, 2007.

Analysis of Band-gap Characteristics of Two-dimensional Periodic Structures by Use of a Time-domain Source-model Technique

A. Ludwig and Y. Leviatan
Technion — Israel Institute of Technology, Israel

Abstract— The interest in novel methods for numerical modeling of electromagnetic scattering by periodic structures has increased in recent years due to the fast-growing demand for efficient design tools for photonic-crystal and metamaterial based devices. In this work, we introduce a time-domain source-model technique for analysis of two-dimensional transverse-magnetic plane wave scattering by a photonic crystal slab composed of a finite number of identical layers, each comprising a linear periodic array of dielectric cylinders. The proposed solution technique uses fictitious time-dependent current sources to simulate the time-varying fields in each of the different dielectric regions of which the photonic bandgap crystal is composed. The temporal variation of each current source is expanded in terms of pulse functions of yet-to-be-determined amplitudes. These amplitudes are in turn adjusted to satisfy the continuity conditions for the tangential components of the electric and magnetic fields across the boundaries between the different dielectric regions in some approximate sense. In this work, the continuity conditions are matched over a sequence of time instances at a discrete set of testing points located within the unit cell of the periodic structure. By applying a Fourier transform to the results obtained from a single time-domain run of a solver based on the above technique, the existence of frequency ranges of zero energy transmission is demonstrated for a relatively thick photonic crystal slab. A comparison between these zero energy transmission ranges for different incidence angles and the band-gap regions in the band-structure diagram of the corresponding infinite photonic-crystal reveals a clear correspondence. The time-domain source-model technique based solver is also used to study the effect of the incident pulse bandwidth on the portion of energy that is transmitted through the photonic-crystal slab. It is shown that for a short incident pulse, whose bandwidth exceeds the band-gap region, some energy is transmitted through the slab. Finally, the temporal behavior of the pulse reflected from the slab when it is illuminated by narrow bandwidth pulses of different center frequencies is also studied.

Simulation of Non-radially Symmetric Whispering Gallery Mode Resonators

Michael R. Watts
Sandia National Labs, P. O. Box 5800, MS-1082, Albuquerque, NM 87185, USA

Abstract— Three-dimensional Finite-Difference Time-Domain (FD-TD) simulations have been used to assess the quality factor (Q) and Free-Spectral-Range (FSR) of non-circularly symmetric whispering gallery mode resonators. Non-radially symmetric whispering gallery mode resonators are designed for the purpose of preserving the large FSR and low-loss coupling of a microring-resonator while enabling an internal contact to the resonator for active, and, passive suspended structures.

The ability to make mechanical or electrical contact to a microring-resonator is critical for both sensing and communication applications. Unlike microdisk-resonators which are innately contacted by the disk geometry, microring-resonators lack an internal contact. And, while microdisk-resonators can be made to exhibit a high-Q resonance, the presence of higher-order spatial modes within the microdisk, corrupts the free-spectral-range (FSR) of the resonator thereby limiting the useable bandwidth available to the waveguide bus. Moreover, the presence of higher order modes also causes significant coupling losses to a microdisk. As a result, microdisks represent undesirable resonators for many important applications that require both low-loss and large, useable bandwidths. And, while microring-resonators exhibit both low-loss coupling and large, uncorrupted FSRs, they lack an internal contact. That is, a microring, in its truest form, is surrounded by cladding material, which in many circumstances is not appropriate for electrical or suspended mechanical contact. In order to make electrical contact in silicon microring-resonator modulators, others have used ridge-waveguides. While functional, ridge-waveguides limit the confinement within the resonator which again ultimately limits the resonator FSR and useable bandwidth.

Here, we take an alternate approach that enables low-loss contacts to be made from within the microring while preserving hard outer wall, to enable a tightly confined resonator with a large FSR. The resulting structures are neither pure microring-resonators nor microdisk resonators but represent a new class of whispering gallery mode resonators. Three-dimensional finite-difference time-domain (FD-TD) simulations have been used to verify the designs and demonstrate both low-loss coupling and a large, uncorrupted FSR. Challenges associated with obtaining accurate quality factors and spectral responses in these complex geometries will be presented.

Session 3A1
Electromagnetic Scattering and Absorption

In-SiP Integration of Electromagnetic Shields

O. Alilou, J.-L. Lefebvre, and P. Descamps
NXP Semiconductors and Laboratoire de Microélectronique ENSI Caen-NXP (LAMIPS)
2 rue de la girafe, BP5120, 14079 Caen Cedex 5, France

Abstract— System-in-Package (SiP) is a growing trend of the electronic industry consisting in integrating one or several integrated circuits (ICs) together with discrete components of various technologies in a single package, resulting in one or several electronic systems. SiP allows for higher system miniaturisation, performance and offers higher system integration.

However, new electromagnetic compatibility challenges occur with: on the one hand, the constitutive sub-elements of the SiP within the package are closer than ever to one another. Circuits of heterogeneous technologies originally designed to function in their own packages are now placed together in a same confined environment separated by distances as small as a few tens of microns only. On the other hand, because of their smaller size, complete SiP systems are also closer to one another in the end equipment. Thus, they can suffer from significant noise from the neighbouring sub-systems. Each SiP may therefore need to be protected from external electromagnetic disturbances.

This paper first addresses the need for electromagnetic shielding of sub-systems in a mobile phone. It will be shown that integration of electromagnetic shields within the SiPs against external incident disturbances not only offer more compliance to all types of electromagnetic environments, but also place SiP solutions higher in the system value chain.

Then, the SiP-specific boundary conditions are applied to the Maxwell equations for simplification, and a definition of shielding effectiveness formula applicable to SiP is proposed.

Tri-dimensional electromagnetic simulations of simplified shielding schemes are then presented. In order to assess the shielding effectiveness from thin-film deposited shields in SiP, and its influent variables, simulation results banc shown that a 60 dB isolation from DC until 1.5 GHz, and a 30 dB from 1.5 GHz until 10 GHz can be fitted. Various shielding structures and technologies are then considered and their relative performances and ease of implementation compared.

Last, measurements of shielding effectiveness of a shielded SiP demonstrator are presented and compared to the initial simulations.

On Passive RCS Reduction for Planar Scatterers in a Metal Hull

B. L. G. Jonsson
Electromagnetic Engineering, Royal Institute of Technology, Stockholm, Sweden

Abstract— Thin film absorbers exist with impedance in 10–2300 Ω/square. Such resistive sheets are used to reduce radar cross section (RCS) of antennas integrated into a perfect electric conducting (PEC) surrounding. We consider a large square antenna as scatterer with side 14λ–18λ and a given anisotropic reflectivity. The antenna has one polarization direction which is at 45° with the array edge. We show that the worst-case monostatic RCS for incident waves in [30°, 65°] to be frequency robust and below $-35\,\mathrm{dBm}^2$, with tapering responsible for $-25\,\mathrm{dBm}^2$.

Introduction: RCS reduction in stealth applications is discussed in e.g., [1]. Recent results for sensors in a PEC hull [2] emphasize the directional nonalignment between antenna polarization and array edge. Scattering from large arrays can be approximated with the physical theory of diffraction [3] based on an impedance boundary condition [4].

Problem Description: We consider an array of 36×36 antenna elements, each element is a square, $\lambda/2$ wide at 18 GHz. The 12 outermost rows are tapered. The antenna element has one polarization direction which is aligned at 45° to the array edge and the array is mounted in a PEC sheet. We model the array as a homogeneous anisotropic scatterer with an energy reflectivity of 10% in its polarization direction and PEC in the other direction. This characterization enables us to consider different classes of scatterers with the same reflectivity and hence compare the robustness of the RCS reduction.

A tapering layer is realized as resistive film, one antenna element wide, with resistivity in [10–2300] Ω/square. Such film tapering allows the tapered layer to preserve the angular dependence of the antenna element, and is essential to reduce the monostatic RCS [2].

To simulate this large structure, we associate an impedance to 14 regions based on its two interface reflectivity. It is then used in an approximate boundary condition in a PTD code [3], which has validated performance in the present angular and frequency region.

Results: The anisotropy of the antenna, direct the interest to two main cases: Incident waves in a plane from corner to corner, and incident waves in a plane orthogonal to the side, both with polarization in the direction of the antenna polarization.

We find that the tapering transition between antenna and PEC surrounding should have its free-space reflectivity as samples of $\sin^2 x$. The freedom of scatterer impedance with constant reflectivity shows variations of RCS reduction of about $1\,\mathrm{dBm}^2$. This tapering reduces the worst sidelobe levels with more than −25 dB for incident angles 30°–65°.

The non-aligned polarization and the tapered edges result in an absolute RCS level below $-35\,\mathrm{dBm}^2$ for the frequencies 14, 16 and 18 GHz for incident angles in [15°, 65°] and [30°, 65°] for corner and edge incident wave respectively. The corner RCS decay rapidly with increasing incident angle.

ACKNOWLEDGMENT

The support by VINOVA grant NFFP4/SIGANT #2006-02684, is gratefully acknowledged.

REFERENCES

1. Knott, E. F., et al., *Radar Cross Section*, Artech House, Boston, 1993.
2. Persson, P. and B. Thors, "RCS reduction of antennas integrated in a infinite PEC plane," *Antennas and Propagation Society International Symposium 2005*, Vol. 3A, 74–77, 2005.
3. Thors, B., "A high frequency technique for estimation of the backscattered field from a large array antenna," KTH TRITA-TET report, No. 1, 2005.
4. Syed, H. H. and J. L. Volakis, "An approximate soluion for scattering by an impedance wedge at skew incidence," Radio Science, Vol. 30, No. 3, 505–524, 1995.

A Closed Form for Mie Scattering of an Electromagnetic Generalized Gaussian Beam with Any Angular Extent

Nicole J. Moore and Miguel A. Alonso

The Institute of Optics, University of Rochester, NY 14627, USA

Abstract— The scattering of an incident plane wave from a spherical homogeneous dielectric particle can be described by the Lorenz-Mie theory. For many current practical applications, however, the scattering of focused laser beams is of interest. These applications include optical trapping and manipulation, as well as simultaneous measurements of the size and velocity or chemical composition.

Although one could model such a field as a superposition of plane-waves, the scattering computation for a highly focused field would be computationally intensive. A variety of numerical computation schemes have been proposed in the past.

A focused beam can be modeled by the displacement of an electric or a magnetic dipole to a complex point, the real coordinates of which can be considered the focus of the beam. Such a field varies continuously between the standard dipole field and a paraxial vector Gaussian beam, thus providing a useful model for focalized Gaussian beams. Using this model for generalized Gaussian beams, an analytic solution is found to the problem of scattering of focused beams from spherical particles. The scattered field is found as a superposition of multipole fields, in the usual manner. The coefficients in this superposition take the form of simple combinations of multipole fields evaluated at the complex location of the dipole.

This result will be presented, as will examples calculated using this method, particularly for the cases of incident radially and azimuthally polarized beams, which are of great current interest. The result is valid for any relative position between the focus and the sphere, as well as for a beam of any angular extent.

Numerical Solution for the Problem of Electromagnetic Scattering by a Thin Finite Conducting L-shape Wire

S. Alyones, **M. S. Bawa'aneh**, **and A. M. Alsmadi**
Physics Department, The Hashemite University, Zarqa 13115, Jordan

Abstract— The problem of electromagnetic scattering by a thin L-shape finite conducting fiber has been solved numerically at normal incident to one leg of the fiber (the incident electric field of the wave is parallel to one leg and perpendicular to the other), using the moment method via point matching scheme. The solution represents the first solution for the coupled Pocklington integro- differential equations for the L-shape finite conducting fiber. The solution satisfies the boundary conditions of the problem and the results of this paper show that a current is induced in the perpendicular leg of the fiber. The scattering and absorption cross sections is then calculated and compared to those of the same length straight finite conducing fiber parallel to the incident electric field [1].

REFERENCES

1. Alyones, S., C. W. Bruce, and A. Buin, "Numerical methods for solving the problem of electromagnetic scattering by a finite thin conducting wire," *IEEE. Trans. Antennas and Propag.*, Vol. 55, No. 6, June 2007.

Study of Scattering by Two Conducting Cylinders Using S.W.C.I.P Method

N. Ammar, **T. Bdour**, **and T. Aguili**

Communications Systems Laboratory in Tunis Engineering School, Tunisia

Abstract— In this paper, a new spatial approach of an iterative method based on wave concept (W.C.I.P) is introduced. This method is applied to solve the problems of electromagnetic fields diffraction by arbitrary forms. The WCIP method was firstly used in planar circuit analysis. Its iterative process is based on toggling between spatial and modal domains using Fourier mode transform (FMT) [1]. This integral method is based on the definition of emitted and received waves on the electromagnetic discontinuity. In order to extend such approach to solve scattering problems of arbitrary shaped structures, the diffraction operators are fully expressed in the spatial domain. The scattering surface is always characterized by a spatial operator taking into account the boundary conditions. The external environment is modeled by a diffraction operator defined in free space and used to evaluate coupling between different points of the structure to study [2]. Its expression is deduced from spectral coefficients which are expressed in cylindrical modal bases. In this work, the Spatial Wave Concept Iterative Procedure (S.W.C.I.P) is applied to calculate coupling two conducting cylinders. The current density and the diffracted electric far field are also computed. The numerical results are presented and compared with literature to verify the accuracy of this approach.

REFERENCES

1. Sidina, W., et al., "A new full-wave hybrid differential-integral approach for the investigation of multilayer structures including non uniformly doped diffusions," *IEEE Transactions on Microwave Techniques*, Vol. 53, No. 1, January 2005.
2. Ammar, N., et al., "Study of electromagnetic waves diffraction by rectangular cylinders using the "Wave Concept Iterative Process" W.C.I.P in spatial domain," *Mediterranean Microwave Symposium (MMS'2006)*, 2006.
3. Xiao, F., et al., "Solution of scattering from conducting cylinders using an iterative method," *IEEE Transactions on Magnetics*, Vol. 36, No. 4, July 2000.

Neural Network Modeling of Scattering Parameters from a Conducting Post in Rectangular Waveguide

Manidipa Bhattacharya[1], **B. Gupta**[2], **K. Yasumoto**[3], **and H. Jia**[3]

[1]SAMEER, Plot L2, Block GP, Sector-V, Salt Lake Electronic Complex, Kolkata 700091, India
[2]Department of Electronics and Telecommunication Engineering
Jadavpur University, Kolkata 700032, India
[3]Department of Computer Science and Communication Engineering
Kyushu University, Fukuoka-shi 812-8581, Japan

Abstract— Neural networks are popular as efficient alternatives to conventional computational models like numerical modeling or analytical methods for RF and Microwave modeling and design. Such models reduce both processing time and analytical complexity resulting in simpler computation process. In the present problem generalized reflection and transmission matrices are used to calculate the frequency responses in the reflectance and transmittance of two-dimensional photonic crystals. In this work neural network technique has been used for non-linear modeling of the frequency response of the scattering properties of a long circular conducting cylinder in a three dimensional rectangular waveguide at X band. The scattering properties of the vertical posts are analyzed using finite element method as well as a semi analytical approach based on image theory. The scattered fields are calculated from the lattice sum and the transition matrices. Analysis results have been used to generate S parameter data for the configuration in order to train the proposed network.

For the purpose of neural network modeling of the scattering post embedded in rectangular waveguide, the bipolar sigmoid function is used as activation function. Here an adequate amount of training data is fed as input to the network. The resulting mean-squared error between the network's output and the target value over all the training pairs are minimized. The average error over the entire training data set has been checked repeatedly till the training phase continues. The error has been minimized using gradient descent technique in a multi-layer perceptron model with the help of backpropagation algorithm. After proper training the average error is found to be 0.001 over a set of test data spanning the entire X band of frequencies and different values for the position and radius of the scattering post, which have not been used in the training process.

Preparation and Evaluation of Composite Electromagnetic Wave Absorbers Made of Fine Aluminum Particles Dispersed in Polystyrene Medium

Y. Wada, **N. Asano**, **K. Sakai**, **and S. Yoshikado**
Department of Electronics, Doshisha University, Japan

Abstract— We developed composite electromagnetic wave absorbers made of dispersed aluminum fine particles in polystyrene medium and evaluated those electromagnetic properties to realize single layer electromagnetic wave absorbers with the good absorption property above 10 GHz. According to Snoek limit, electromagnetic wave absorber made of magnetic materials, such as ferrite, shows the upper limit of absorbing frequency. On the other hand, both magnetic dipole and total loss induced from eddy current flowing on the surface of a metal particle, such as aluminum particle, contribute to the absorption of electromagnetic wave. There is no upper limit of the absorbing frequency and it is possible to absorb in the wide frequency range, if appropriate size of aluminum particle is choosen. Because aluminum is para-magnetic substance and the non-dimension magnetic-susceptibility of aluminum is approximately 2.4×10^{-4}, the real part μ_r' of complex relative permeability μ_r^* of aluminum is almost 1. However, the μ_r' becomes less than 1, when the magnetic dipole induced by eddy-current flowing on the surface of a aluminum particle. To examine this phenomenon, qualitative theoretical calculation was estimated. The results of calculation showed the values of $1 - \mu_r'$ and μ_r'' increase propotional to the the volume mixing rate of aluminum particle and the range of $1 - \mu_r'$ was $0 < 1 - \mu_r' \leq 1$. Polystyrene particles with approximately 1 μm diamerer and aluminum fine particles with various sizes from approximately $10 \sim 180$ μm were mixed by mechanical milling to isolate aluminum prticles in polystyrene medium to avoid mutual contacts between aluminum particles which result in the reduce of magnetic loss μ_r'' and the effect of magnetic dipole $1 - \mu_r'$. The values of $1 - \mu_r'$ and the μ_r'' increased proportional to the volume mixing rate of aluminum particle up to 50 vol% and these results agreed with qualitative theoretical prediction, because aluminum particle was isolated with fine polystyrene particles. Thus, the control of μ_r^* is possible by selecting the amount of aluminum particles and the absorption less than −20 dB (the absorption of electromagnetic wave energy of 99%) was expected above 10 GHz.

Composite Electromagnetic Wave Absorber Made of Permalloy or Sendust and Effect of Sendust Particle Size on Absorption Characteristics

K. Sakai, **Y. Wada**, **and S. Yoshikado**
Department of Electronics, Doshisha University, Japan

Abstract— Electromagnetic waves available at frequencies higher than 1 GHz are more widely used with the increasing use of wireless telecommunication systems and their frequencies will shift to high frequency range in the future. Therefore, the development of an electromagnetic wave absorber suitable for these frequency bands is required. The purpose of this study is to prepare practical composite absorbers that operate in the frequency range above 1 GHz using soft magnetic materials such as permalloy (Ni-45%, Fe-55%) or sendust (Al-5%, Si-10%, Fe-85%) and polystyrene resin. Soft magnetic material show high values of permeability in the frequency range above 1 GHz. This characteristic makes it possible to fabricate absorbers that operate in the frequency range above 1 GHz. In addition, sendust is inexpensive because sendust contains no rare metal such as Ni, hence sendust is suited for practical absorber compared with permalloy. In this study, the difference between permalloy and sendust in the absorption characteristics and the grain size dependence of absorption characteristics for sendust were investigated. Grain shape of permalloy and sendust were granular and the grain sizes of sendust particles were 5 μm, 10 μm, and 20 μm. Soft magnetic material is generally conductive. Therefore, if the amounts of sendust particles dispersed in the polystyrene resin increase, magnetic material particles contact directly each other and the average conductivity of composite increases drastically. Finally, the reflection coefficient of electromagnetic wave by the composite increases and absorption characteristics are degraded. To prevent from the increase in conductivity, we attempted to disperse and isolate the soft magnetic material particles by dissolving polystyrene resin in an organic solvent and mixing soft magnetic material particles with dissolved polystyrene. Soft magnetic material particles were isolated in the polystyrene resin and the composite made of permalloy could absorb electromagnetic wave energy above 99% in the frequency range from 1 GHz to 10 GHz. Moreover, the realization of the absorber which can operate above 10 GHz is expected due to the eddy current flowing on magnetic material particles. The frequency dependences of μ_r^* and ε_r^* in the frequency range from 8.2 GHz to 40 GHz were also measured using rectangular waveguide to obtain accurate absorption characteristics.

Stimulated Raman Scattering of Extraordinary Electromagnetic Waves in Weakly Magnetized Plasma

M. S. Bawa'aneh[1], **H. M. EL-Nasser**[2], **Ghada Assayed**[1], **S. Alyones**[1], **A. M. Alsmadi**[1]
S. Al-Awfi[3] **and M. Al-Sughayer**[1]
[1]Physics Department, The Hashemite University, Zarqa 13115, Jordan
[2]Physics Department, AL-al-Bayt University, Mafraq 25113, Jordan
[3]Physics Department, Taybah University, Medina Al-monawara, Saudi Arabia

Abstract— Stimulated Raman backscattering (SRBS) in a homogeneous weakly magnetized plasma has been studied, where a system of coupled equations has been derived and solved for an anlytical formula that describes SRBS instability. The presence of a static magnetic field is found to suppress the SRBS instability and increase the threshold. SRBS suppression increases as the density increases, where the instability growth rate drops to zero near the quarter critical density.

Processing of Metallic Glassy Samples by Using Microwave Radiation

D. V. Louzguine-Luzgin[1], **V. D. Buchelnikov**[2,3], **G. Xie**[2], **S. Li**[2]
A. Inoue[1], **N. Yoshikawa**[4], **K. Mashiko**[4], **S. Taniguchi**[4], **and M. Sato**[5]

[1]WPI Advanced Institute for Materials Research, Tohoku University, Sendai 980-8577, Japan
[2]Institute for Materials Research, Tohoku University, Sendai 980-8577, Japan
[3]Condensed Matter Department, Chelyabinsk State University, Chelyabinsk 454021, Russia
[4]Graduate School of Environmental Studies, Tohoku University, Sendai 980-8579, Japan
[5]National Institute for Fusion Science, 322-6 Oroshi, Toki, Gifu 509-5292, Japan

Abstract— This work represents a relatively modern field related to microwave (MW) radiation-assisted heating and sintering of metallic glassy samples. Metallic glassy alloys can be successfully sintered as they exhibit low viscosity in a temperature range between the glass-transition and the crystallization temperature. Microwave heating has significant advantages over conventional heating in materials processing, such as energy savings, rapid heating rates and process cleanness. In the present study we investigated the stability of the $Fe_{73}Si_7B_{17}Nb_3$, $Fe_{65}Co_{10}Ga_5P_{12}C_4B_4$, $Cu_{50}Zr_{45}Al_5$, $Ni_{52.5}Zr_{15}Nb_{10}Ti_{15}Pt_{7.5}$, $Zr_{55}Cu_{30}Al_{10}Ni_5$ and $Ti_{47.5}Zr_{10}Cu_{30}Pd_{7.5}Sn_5$ metallic glassy powders and the formation of the bulk metallic glassy samples by microwave heating in a single mode cavity with separate electric (E) and magnetic (H) filed maxima in an inert atmosphere.

The metallic glassy alloy powders were produced by a high pressure argon gas atomization method using argon gas. The specimen powders were placed in a position of either E-field or H-field maximum area in the single-mode wave guide applicator and heated by energy absorption of MWs having 2.45 GHz or 915 MHz (for some samples) frequency. The $Fe_{73}Si_7B_{17}Nb_3$ and $Fe_{65}Co_{10}Ga_5P_{12}C_4B_4$, alloys crystallized upon MW heating in both E- and H-field maxima forming a nanostructure. The $Ni_{52.5}Zr_{15}Nb_{10}Ti_{15}Pt_{7.5}$ and $Zr_{55}Cu_{30}Al_{10}Ni_5$ alloys were heated well in H field, and were not heated well enough in E-field. In case of $Cu_{50}Zr_{45}Al_5$ and $Ni_{52.5}Zr_{15}Nb_{10}Ti_{15}Pt_{7.5}$ alloys sintered samples were obtained. Composite $Ni_{52.5}Zr_{15}Nb_{10}Ti_{15}$-$Pt_{7.5}$/Sn and $Cu_{50}Zr_{45}A_{15}$/Fe samples were also produced.

The heating mechanisms of metallic powder samples have also been studied and will be discussed in detail. The heating rate was found to depend upon various factors including electrical conductivity, thickness of the oxide layer, volume fraction of metallic part etc. which will also be discussed.

Theoretical Investigations on Role of Various Elliptical Shapes for Efficient Microwave Processing of Materials

Tanmay Basak

Department of Chemical Engineering, Indian Institute of Technology Madras
Chennai 600036, India

Abstract— A detailed theoretical analysis has been carried out to assess the role of various elliptical shapes/cross sections on microwave heating of 2D cylinders for beef and oil samples. Two types of elliptical cross sections are considered as type A (ellipse with major axis along the horizontal plane) and type B (ellipse with minor axis along the horizontal plane.) A preliminary analysis on microwave heating of samples has been shown via average power within a sample vs sample radius of circular cross section for beef and oil samples. Several regimes (I-III) based on small and large radius for circular cross sections have been selected. The effect of elliptical shapes for type A and B configurations has been studied first via average power vs aspect ratio distributions for various regimes. The contour plots of power absorption have been analyzed further for elliptical cross section with varying aspect ratios for regimes I-III where aspect ratio and types of configuration are shown to influence spatial power absorptions. The detailed temperature profiles have also been shown to illustrate the role of elliptical shapes on uniform heating and thermal runaway. Depending on the material dielectric properties and sample dimension, either type A or B or both configuration has been recommended.

Session 3A2
Scattering by Ordered and Disordered Media: Photonic Applications 1

Manipulating the Transmission and Scattering of EM Waves from Sub-wavelength Microstructures (Ordered and Disordered) by Application of a Strong dc Magnetic Field

Yakov M. Strelniker[1] and David J. Bergman[2]

[1]Department of Physics, Bar-Ilan University, IL-52900 Ramat-Gan, Israel
[2]Raymond and Beverly Sackler School of Physics and Astronomy, Tel Aviv University
IL-69978 Tel Aviv, Israel

Abstract— The extraordinary light transmission (ELT) through a metal film perforated by a periodic array of sub-wavelength holes [1] is widely believed to result from the coupling of light to plasmons on the surface of the patterned metal film. Continuing this idea, we have discussed the effect of an applied static magnetic field on the ELT [2–5] for both ordered and disordered array of holes. It was shown there that the applied static magnetic field shifts the surface plasmon resonance and the ELT to higher frequencies. It was also mentioned there that, in addition to the surface plasmon resonance, there also exists a so-called cyclotron resonance, which can play, in principle, some role in light transmission. We also propose to use the magnetic field for getting a strong polarization effect, which depends on the ratio of the cyclotron to plasmon frequencies, and which can be made arbitrarily large. An interesting film material to consider for this purpose is metallic Bismuth, since the low density of charge carriers can help to make the cyclotron frequency of those carriers equal to or greater than their plasma frequency [6–8]. Another class of interesting materials is semiconductors like GaAs and InAs [6–8]. The exact relations between macroscopic moduli of composite media in three dimensions (3D generalizations of Keller's relations) found recently [9, 10] can be used to obtain connections between different types of physical phenomena. For example, the magneto-optical response of a conducting thin film with an array of sub-wavelength holes, where extraordinary light transmission has been observed, can be related to the magneto-optical response of an array of parallel conducting sticks embedded in a dielectric host, which are being studied and discussed extensively as systems where negative electrical permittivity and negative magnetic permeability are attainable simultaneously. The magneto-optical response of such arrays of parallel conducting sticks is also being studied in connection with other interesting modes of behavior.

REFERENCES

1. Ebbesen, T. W., H. J. Lezec, H. F. Ghaemi, T. Thio, and P. A. Wolff, *Nature*, Vol. 391, 667, London, 1998.
2. Strelniker, Y. M. and D. J. Bergman, *Phys. Rev. B*, Vol. 59, R12763–R12766, 1999.
3. Bergman, D. J. and Y. M. Strelniker, *Phys. Rev. Lett.*, Vol. 80, 857–860, 1998.
4. Strelniker, Y. M., D. Stroud, and A. O. Voznesenskaya, *Eur. Phys. J. B*, Vol. 52, 1–7, 2006.
5. Strelniker, Y. M., *Phys. Rev. B*, Vol. 76, 085409-1–085409-6, 2007.
6. Sherriff, R. E. and R. P. Devaty, *Phys. Rev. B*, Vol. 41, 1340–1346, 1990.
7. Strijkers, G. J., F. Y. Yang, D. H. Reich, C. L. Chien, P. C. Searson, Y. M. Strelniker, and D. J. Bergman, *IEEE Trans. Magn.*, Vol. 37, 2067–2069, 2001.
8. Tornow, M., D. Weiss, K. V. Klitzing, K. Eberl, D. J. Bergman, and Y. M. Strelniker, *Phys. Rev. Lett.*, Vol. 77, 147–150, 1996.
9. Strelniker, Y. M. and D. J. Bergman, *Phys. Rev. B*, Vol. 67, 184416-1–184416-9, 2003.
10. Strelniker, Y. M. and D. J. Bergman, *Phys. Rev. B*, Vol. 61, 6288–6297, 2000.

Electromagnetic Wave Scattering from a Random Layer with Rough Interfaces I: Multiple Scattering Theory

Gerard Berginc[1] and Claude Bourrely[2]

[1]Thales Optronique, 2 Avenue Gay Lussac, 78995 Elancourt Cedex, France
[2]Centre de Physique Théorique, CNRS-Luminy Case 907
13288 Marseille Cedex 9, France

Abstract— Random volume and surface scattering is a topic, which has been studied in many domains such as plasmonics and surface optics. Useful phenomena in the optical range can be produced by these kinds of structures. Designing these disordered slabs with rough surfaces can produce new optical components, which can transmit or scatter optical field with specified angular, spatial or spectral properties.

In this paper, we consider a three-dimensional disordered medium with randomly rough interfaces. We showed in a previous paper [1] how to derive, starting from the Maxwell equations, the radiative transfer equation and its boundary conditions for an inhomogeneous slab with randomly rough interfaces. By applying the Wigner transform to the Bethe-Salpeter integral equation and by considering the ladder approximation, we obtained the integral formulation of the radiative transfer theory. We introduced [1, 2] the randomly rough boundaries in the derivation of the radiative transfer equation and we incorporated the correlations between the scatterers. Finally, we demonstrated that the ladder contribution is identical to the phenomenological radiative transfer theory and satisfies the boundary conditions of the randomly rough interfaces.

With the Maxwell equations, we were also able to give an unambiguous definition of the specific intensity as a function of the incident electric field, and thus we are able to clarify the meaning of this quantity [1]. Finally, we also incorporated the most-crossed contributions in our theory to give the theoretical expression of the enhanced backscattering phenomenon. This contribution also satisfies a radiative transfer equation and boundary conditions, which are slightly modified [1] compared to the usual phenomenological radiative transfer theory.

We gave [1, 2] in an explicit way the theoretical formulas, which describe the wave scattering from a random medium with rough surfaces. The calculation of the intensities scattered by the considered structure for the ladder and most-crossed contributions is given by a Green tensor, which satisfies a Bethe-Salpeter equation. Since we are unable to obtain an exact expression of the Green tensor for practical calculations, we rely on a perturbative method. The Green tensor admits a perturbative expansion. In a previous approach [2], we considered the first-order perturbative expansion. In this paper, we consider and calculate the second-order perturbative expansion of the Green tensor to evaluate numerically its contribution to the diffuse intensity. Most of the study presented in this paper is centered on the formulations of the second-order expansion of the Green tensor to the incoherent cross-section for this disordered slab with randomly rough interfaces. It should be noticed that the first-order Green tensor expansion represents an approximation of a double-scattering theory for the cross-section while the second order corresponds to an approximation of a third-order scattering for the cross-section.

REFERENCES

1. Soubret, A. and G. Berginc, "Electromagnetic wave scattering from a random layer with rough interfaces II: Diffusive intensity," arXiv:physics/0312136, 2003.
2. Berginc, G. and C. Bourrely, "Electromagnetic wave scattering from a random layer with randomly rough interfaces," *Progress In Electromagnetics Research Symposium Abstracts*, 88, Prague, Czech Repulic, August 27–30, 2007.

Electromagnetic Wave Scattering from a Random Layer with Rough Interfaces II: Numerical Experiments

Gerard Berginc[1] and Claude Bourrely[2]

[1]Thales Optronique, 2 Avenue Gay Lussac, 78995 Elancourt Cedex, France
[2]Centre de Physique Théorique, CNRS-Luminy Case 907
13288 Marseille Cedex 9, France

Abstract— Understanding how light interacts with disordered matter is a fundamental issue in optoelectronics and photonics and has huge consequences in communications, imaging and sensing. In this paper, we consider two main objectives. The first one corresponds to the precision improvement of the numerical integration methods. In particular, we propose a mathematical treatment of the different singularities in the cross-section expression. To fulfill the second objective of this paper, we verify numerically the convergence behavior of the perturbative expansion of the considered scattering problem. As we proceeded to a heuristic construction of the perturbative expansion, we address the problem of numerical behavior of the second-order Green tensor. In any case, the perturbative expansion may be considered as a formal mathematical series, from which much information may be extracted.

Calculations of the intensity cross-sections require multi-dimensional integrations on two-dimensional wave vectors. We use an integration method of Gauss-Legendre with N points. But we have to cope with oscillating expressions. To increase the precision of integration, we develop an integration method taking into account suitable domains of integration. Another particularly important point is related to the phase factors associated with various expressions appearing in the intensity cross-section. The values of the cross-section expressions depend strongly on precise calculations of the different phase factors. They involve denominators given by linear combinations of functions whose sum can tend to zero. We have shown that these singularities of the phase factors are artificial, in fact they have a finite limit. It is thus necessary to calculate the limit of the phases for each term, which can cancel out. We were brought to develop these phase factors in Taylor series, which ensures a better continuity of the different functions to be integrated.

In addition, the slab which consists of two randomly rough surfaces and a disordered medium depends on many parameters. Therefore we carry out numerical tests to determine, how light interacts with this structure and which are the pertinent parameters of the slab to understand and explain the contribution of the different orders of the perturbative expansion. We calculate the incoherent cross-sections in the case of metallic scatterers and we also examine the phenomena related to the presence of an imaginary part in the permittivity of the layer and scatterers.

Localization and Propagation of Light in a Disordered Waveguide System

Akira Komiyama
Osaka Electro-Communication University, Hatsu-cho Neyagawa-shi 572-8530, Japan

Abstract— Fifty years ago, Anderson has pointed out that wavefunctions for electrons are localized in a disordered atomic system and no diffusion at all takes place [1]. Amplitudes of localized wavefunctions decrease exponentially away from the center of localization. The strength of localization is indicated by a ratio of the energy band width in a disordered system to the strength of the coupling between electrons. The equation used by Anderson to describe the time-variation of the probability amplitude is equal in form to the coupled mode equation for a multi-waveguide system. This means that mode waves are localized in a waveguide system.

An image fiber composed of a large number of cores and a single cladding is a typical example of waveguide system. In such a fiber the crosstalk between cores takes place. The crosstalk observed can be described as a diffusion phenomenon [2]. The diffusion coefficient (the power coupling coefficient between cores) decreases with increasing the correlation length with respect to geometrical imperfections along the fiber axis. The decrease is caused by the localization of the mode waves.

In this paper, localization properties of mode waves [3] and propagation properties of light [4] in a disordered waveguide system composed of randomly different cores in sizes are presented.

Propagation constants of modes in an ordered waveguide system composed of identical cores of equal space are distributed inside a band region with a width of 4κ where κ is the mode coupling coefficient and the mode density diverges at edges of the band. The modes are extended over the entire system. Modes in a disordered system appear not only inside the band of the ordered system but also outside the band. Amplitudes of the modes decreases exponentially away from the center of localization. The average power distribution of the mode in the cross-section depends only on the ratio of the fluctuation of the propagation constants to the mode coupling coefficient.

In an ordered system light propagates mainly in a certain specific direction. The locus of the light propagation is a straight line given by $n = \pm 2\kappa z$ where n is the core number and z is the distance along the fiber axis. The amplitude of light in a disordered system can be divided into the coherent part and the incoherent part. The coherent part propagates in the same direction as light in an ordered system. The coherent part is transformed into the incoherent part and the amplitude decreases exponentially with increasing distance. The transformation occurs mainly at cores $n = \pm 2\kappa z$ and tails of the power distribution of the incoherent part are formed there. As all the coherent part is transformed into the incoherent part, the power distribution becomes unchanged and only the incoherent part with the distribution propagates. This is the same distribution as the average power of the localized mode.

REFERENCES

1. Anderson, P. W., *Phys. Rev.*, Vol. 109, 1492–1505, 1958.
2. Komiyama, A. and M. Hashimoto, *IEICE Trans.*, Vol. E77-C, 1808–1813, 1994.
3. Komiyama, A., *Opt. Comm.*, Vol. 151, 25–30, 1998.
4. Komiyama, A., *Progress In Electromagnetics Research Symposium*, Tokyo, 2006.

Plasmonic Effects in Dynamic Tunable Metal-dielectric Composites

Y. Y. Feng and M. Willatzen

Mads Clausen Institute for Product Innovation, NanoSyd, University of Southern Denmark, Denmark

Abstract— Sub-wavelength metal-dielectric-metal (MDM) composites support localized electromagnetic modes that are strongly confined in periodic structures. These modes can be controlled by tuning the shape of the composites as we demonstrated in previous works. Moreover, the Localized Surface Plasmon Resonance (LSPR) can be applied in new sensor applications. In this paper, we use the Finite-Difference Time-Domain (FDTD) method to study double-periodic metal-dielectric-metal composites and put emphasis to interactions with the dielectric cover layer. The numerical results demonstrate that variation of the refractive index (RI) of the cover layer as well as the layer thickness affect the LSPR response of the proposed MDM composite. The resonance-curve min/max groove period, the resonance-curve width, and the resonance-curve amplitudes from the MDM sensor output indicate that the proposed composite may find use as an effective sub-wavelength dielectric sensing optical component for photonic applications.

Surface Plasmons and Quasi-periodic Nanohole Arrays

C. Genet, **F. Przybilla**, **and T. W. Ebbesen**
Universite Louis Pasteur, France

Abstract— The phenomenon of enhanced transmission through arrays of sub-wavelength dimensions, perforated through optically thick metal films, is the subject of intense studies. The crucial role played by surface plasmon excitations has often been related to the (long range) periodicity of the array. This however is not necessary, as exemplified by the observation of enhanced transmission through a Penrose metallic hole array. We report some experiments that have focused on the dynamics of surface plasmons excited in a quasi-periodic lattice. When compared to the situation of a periodic array, the measurements show a reduction of the propagation length of the surface modes which lowers the contribution of long-range interactions. Instead, local order is dominating in the transmission spectra.

Permittivity of Nanostructured Silver in Optical Metamagnetics

Alexander V. Kildishev, Vladimir P. Drachev, Uday K. Chettiar, Hsiao-Kuan Yuan Wenshan Cai, and Vladimir M. Shalaev

Birck Nanotechnology Center and School of Electrical and Computer Engineering
Purdue University, West Lafayette, IN 47907, USA

Abstract— Arrays of periodic paired silver strips exhibit the magnetic responses in the visible range forming a novel class of optical metamaterials (metamagnetics) [1, 2]. The dielectric function, $\varepsilon = \varepsilon' + l\varepsilon''$, in a layer of the strips with a moderate width (about 100 nm) and a subwavelength periodicity, differs from bulk and appears to be size-dependent for both polarizations of light. For the samples of various dimensions and surface roughness, ε has been analyzed both experimentally and numerically. Anisotropy in ε'' observed experimentally indicates a significant contribution from the quantum size effect and the chemical interface effect. The classical free-path-effect model implies interactions of the electrons with the particle surface resulting in an additional, size-dependent term in the damping constant $\gamma(R) = \gamma_\infty + AV_F/R$; the A-parameter, the coefficient of the Fermi velocity to particle radius ratio, includes the details of scattering process. As follows from this model, the particle surface roughness should increase the relaxation rate.

Five samples with different nanostrip widths and roughness have been fabricated and examined. Initial test samples with different characteristics of silver surface roughness were fabricated by varying the silver deposition rate from 80 Å/s to 0.5 Å/s. Results for those samples showed that a lower deposition rate provided lower roughness. To further investigate the plasmonic elements with relatively low roughness, four samples were deposited with a rate of about 0.5 Å/s and one with 2 Å/s. There are three samples of similar widths but different roughness values (♯1–3), and three samples of different widths fabricated in the same session (♯3–5).

In parallel with the experimental studies, surface roughness has been also introduced in the finite element modeling of the paired strips [3]. Our analysis indicates that the geometrical effect of roughness is mostly responsible for increased losses at the plasmon resonances of the nanostructure and surface roughness does not affect the Ag dielectric function, although it does increase the loss at the plasmon resonances of the coupled strips. The size effect is significant for both polarizations of light, parallel and perpendicular to the strips with relatively large A-parameter. In addition, the spectra of ε'' for the TE polarization (electric field parallel to the strips) suggest good quality of the Ag crystal structure since the absolute values of ε'' in samples with larger widths are between the known values for bulk Ag [4–6].

REFERENCES

1. Yuan, H.-K., U. K. Chettiar, W. Cai, A. V. Kildishev, A. Boltasseva, V. P. Drachev, and V. M. Shalaev, "A negative permeability material at red light," *Opt. Express*, Vol. 15, 1076, 2007.
2. Cai, W., U. K. Chettiar, H.-K. Yuan, V. C. de Silva, A. V. Kildishev, V. P. Drachev, and V. M. Shalaev, "Metamagnetics with rainbow colors," *Opt. Express*, Vol. 15, 3333, 2007.
3. Drachev, V. P., U. K. Chettiar, H. Yuan, W. Cai, A. V. Kildishev, and V. M. Shalaev, "Size effects in plasmonic metamaterials for the visible range (Invited Paper)," *SPIE 2007*, San-Diego, August 26–29, 2007.
4. Johnson, P. B. and R. W. Christy, "Optical constants of the noble metals," *Phys. Rev. B*, Vol. 6, 4370, 1972.
5. Lynch, D. W. and W. R. Hunter, *Handbook of Optical Constants of Solids*, E. D. Palik, ed., Academic Press, New York, 1985.
6. Weber, M. J., *Handbook of Optical Materials*, CRC, New York, 2003.

Wave Scattering by Multi-valued Random Surfaces

Valerian I. Tatarskii

Radio-Hydro-Physics, LLC, USA

Abstract— The conventional theory of wave scattering by random surfaces is developed for single-valued surfaces that may be described by the equation $z = \zeta(x, y)$. But some environmental and artificial random surfaces have more complicated structure, including multi-valued and self-crossing surfaces. As examples we can mention a water surface covered by foam or porous body. It is known that the scattering cross-section from a single-valued random surface in the first Born approximation is proportional to the surface spatial spectrum. But a priory it is unclear, how to define the spectrum of multi-valued surface. Thus, to analyze a wave scattering by multi-valued surfaces, it is necessary to describe such surfaces by more general manner, using the parametric equations of the type $\mathbf{R} = \mathbf{R}(u_1, u_2)$ where $\mathbf{R} = \{x, y, z\}$.

In this paper, we use the general parametric form of surface equation. Assuming that the random surface may include multi-valued and isolated parts (such as air bubbles in water or water drops in air) we derive some basic equations for describing wave scattering: representation of scattered field in terms of surface sources, surface sources integral equation, and extinction theorem, both for Dirichlet and Neumann boundary conditions.

We considered two approximate methods to solving these problems: Perturbation theory and Tangent Plane (Kirchhoff) approximation. The perturbation theory uses a small parameter, describing deviation of surface from a plane. This parameter is used for expansion both geometric parameters (surface metric tensor) and scattering parameters. The Kirchhoff approximation uses the doubled incident field or doubled normal derivative of the incident field at the surface as source functions. The results depend on the statistical properties of all three random functions $x(u_1, u_2)$, $y(u_1, u_2)$, and $z(u_1, u_2)$, i.e., on their joint probability density function and cross-correlation functions (spectra).

The Design of Random Surfaces That Produce Nonstandard Refraction of Light

T. A. Leskova and A. A. Maradudin

Department of Physics and Astronomy, University of California
Irvine, CA 92697, USA

Abstract— On the basis of the geometrical optics limit of the Kirchhoff approximation we show how to design a one-dimensional randomly rough surface that refracts p- or s-polarized light incident on it through an arbitrary angle. The system we study consists of a dielectric medium characterized by a real positive dielectric constant ϵ_1 in the region $x_3 > \zeta(x_1)$, and a dielectric medium characterized by a real positive dielectric constant ϵ_2 in the region $x_3 < \zeta(x_1)$. We assume that $\epsilon_1 > \epsilon_2$. The surface profile function $\zeta(x_1)$ is assumed to be a single-valued function of x_1 that is differentiable and constitutes a random process, but not necessarily a stationary one. This system is illuminated from the region $x_3 > \zeta(x_1)$ by a p- or s-polarized plane wave of frequency ω, whose plane of incidence is the x_1x_3 plane. The surface profile function $\zeta(x_1)$ is assumed to have the form

$$\zeta(x_1) = a_n x_1 + b_n, \quad nb \leq x_1 \leq (n+1)b, \quad n = 0, \pm 1, \pm 2, \ldots$$

where the $\{a_n\}$ are independent identically distributed random deviates, and b is a characteristic length. The $\{b_n\}$ are determined from the condition that the surface be continuous, and satisfy the recurrence relation $b_{n+1} = b_n - (n+1)(a_{n+1} - a_n)b$, and it is convenient to set $b_0 = 0$. Because the $\{a_n\}$ are independent identically distributed random deviates, the probability density function (pdf) of a_n, $f(\gamma) = \langle(\gamma - a_n)\rangle$, is independent of n. The angle brackets here and in all that follows denote an average over the ensemble of realizations of the surface profile function.

The differential transmission coefficient $(\partial T_\nu/\partial\theta_t)$, where ν is either p or s, is defined in such a way that $(\partial T_\nu/\partial\theta_t)d\theta_t$ is the fraction of the total time-averaged incident flux that is transmitted into the angular interval $(\theta_t, \theta_t + d\theta_t)$, where θ_t is the angle of transmission measured counterclockwise from the $-x_3$ axis. In the geometrical optics limit of the Kirchhoff approximation the differential transmission coefficient averaged over the ensemble of realizations of the surface profile function is related to the pdf $f(\gamma)$ by

$$\left\langle \frac{\partial T_\nu}{\partial \theta_t} \right\rangle (\theta_t, \theta_0) = \frac{\epsilon_2}{\sqrt{\epsilon_1}} \frac{\kappa_\nu}{\mu_\nu} \frac{\cos^2\theta_t}{\cos\theta_0} \frac{|T_\nu^{(0)}(\theta_t|\theta_0)|^2}{|\sqrt{\epsilon_2}\cos\theta_t - \sqrt{\epsilon_1}\cos\theta_0|} f\left(\frac{\sqrt{\epsilon_2}\sin\theta_t - \sqrt{\epsilon_1}\sin\theta_0}{\sqrt{\epsilon_2}\cos\theta_t - \sqrt{\epsilon_1}\cos\theta_0} \right),$$

where $\kappa_p = \epsilon_1$, $\kappa_s = 1$, $\mu_p = \epsilon_2$, $\mu_s = 1$. The function $T_\nu^{(0)}(\theta_t|\theta_0)$ is given by

$$T_\nu^{(0)}(\theta_t|\theta_0) = \mu_\nu\sqrt{\epsilon_1} \frac{\cos\phi - \sqrt{\epsilon_1/\epsilon_2}}{\cos\theta_t(\sqrt{\epsilon_2}\cos\theta_t - \sqrt{\epsilon_1}\cos\theta_0)} \times \frac{s(\sqrt{\epsilon_2/\epsilon_1} - \cos\phi) + |\sqrt{\epsilon_2/\epsilon_1} - \cos\phi|}{\mu_\nu s(\cos\phi - \sqrt{\epsilon_1/\epsilon_2}) + \kappa_\nu|\sqrt{\epsilon_2/\epsilon_1} - \cos\phi|},$$

where $s \equiv sgn(\sqrt{\epsilon_2}\cos\theta_t - \sqrt{\epsilon_1}\cos\theta_0)$, and $\phi = \theta_t - \theta_0$. The change of variable $(\sqrt{\epsilon_2}\sin\theta_t - \sqrt{\epsilon_1}\sin\theta_0)/(\sqrt{\epsilon_2}\cos\theta_t - \sqrt{\epsilon_1}\cos\theta_0) = -\gamma$ enables us to invert this equation to obtain $f(\gamma)$ in terms of $\langle\partial T_\nu/\partial\theta_t\rangle(\theta_t, \theta_0)$ now expressed in terms of γ and θ_0. We assume for the mean differential transmission coefficient the form $A\theta(\theta_t - \theta_1)\theta(\theta_2 - \theta_t)$, where A is a constant and $\theta(x)$ is the unit step function, while $\theta_2 = \theta_1 + \Delta\theta$, with $\Delta\theta$ a small angular interval, of the order of $1 - 2^\circ$, for a specified value of $\theta_0 < \theta_c$, where $\theta_c = \sin^{-1}(\sqrt{\epsilon_2/\epsilon_1})$ is the critical angle for total internal reflection. An ensemble of realizations of the surface profile function can now be generated by the rejection method. The transmission of light through each realization of the interface is calculated by a rigorous computational approach and the mean differential transmission coefficient is determined from the results. The angle θ_1 can be chosen to be negative, for example. The transmitted beam then displays nonstandard refraction.

Session 3A3
Mobile Antennas, RF and Wireless Communication

Investigation of Pear-shaped Monopole Antenna

G. N. Ghvedashvili, D. G. Kakulia, K. N. Tavzarashvili, and T. L. Gogua
3 Chavchavadze Ave., Laboratory of Applied Electrodynamics, Tbilisi State University
Tbilisi 0128, Georgia

Abstract— The objectives of the proposed Paper are: research and development of a new type of PCS antenna with optimal geometric size and shape to provide desirable electric and radiation characteristics; creation of user-friendly program package for simulation of dielectric coated antennas with required parameters, which will allow to manage radiation properties of antenna and for investigation and visualization of antenna's interaction with nearby located objects, particularly with human body. The pear-shaped metallic antenna structure covered with thin dielectric layer with high permittivity is presented in this paper. The geometry of antenna was chosen to be easily matched with feeding cable. The high permittivity dielectric layer reduces the size of antenna and its small thickness helps to decrease antenna Q-factor that leads to larger operating bandwidth [2, 3].

To study the Electromagnetic Compatibility (EMC) and SAR problems, investigation of interaction of the antenna field with the user has performed to meet the claims to EMC, ecological and health safety requirements.

To minimize SAR in User's body and avoid undesirable influence of antenna radiation, the antenna with directed radiation was modeled and simulated. For this purpose, we have placed a spoon-shaped metallic shield partially covering one side of the antenna. Radiation and directional properties of such types of antenna were studied for different geometrical and electro dynamical parameters, also, for different values of covering angle.

The structure was numerically simulated using the Method of Auxiliary Sources (MAS) [2, 3], that provides both computational efficiency and modeling versatility. Based on the MAS we have developed a software package "Pear-Shaped Antenna Designer" with user-friendly interface, which allows a fast parametric optimization of antenna for better performance, investigation of antenna together with the feeding modeling in order to obtain high radiation efficiency and well-matching with open space. Validity of the MAS approach and results of calculations were examined by checking fulfillment of the boundary conditions, energy conservation law and analyzing the physical sense of obtained results, also Experimental data is provided for several PSMA configurations to validate the numerical results.

Some numerical and experimental results demonstrating antenna properties and its interaction with the user are presented.

REFERENCES

1. Zaridze, R., G. Bit-Babik, K. Tavzarashvili, N. Uzunoglu, and D. Economou, "Wave field singularity aspects large-size scatterers and inverse problems," *IEEE Transactions on Antennas and Propagation*, Vol. 50, No. 1, 50–58, January 2002.
2. Ghvedashvili, G. N., G. G. Kajaia, G. S. Saparishvili, and R. S. Zaridze, "Analyze of dielectric coated Personal Communication Systems (PCS) antenna and study of its field interaction with the user," *Proceedings of 17th International Zurich Symposium on Electromagnetic Compatibility*, 517–520, Singapore, February 27–March 3, 2006.
3. Ghvedashvili, G. N., K. N. Tavzarashvili, D. G. Kakulia, and R. S. Zaridze, "Personal Communication Systems (PCS) antenna with managed radiation characteristics and study of its interaction with the user," *Journal of Telecommunications and Radio Engineering*, Vol. 66, No. 14, 1265–1272, 2007.

Numerical and Experimental Investigation of the Characteristics of a High Gain Wi-Fi Antenna

Saeed M. Khan
Kansas State University at Salina, 2310 Centnnial Avenue, Salina, KS 67401, USA

Abstract— This paper concerns itself with the study of a large Wi-Fi antenna designed to enable internet sharing from appreciable distances. The antenna design is based on smaller Wi-Fi antennas commonly referred to as cantennas (gain of about 10 dBi). The smaller version is made with a single can (3–4 inches) in diameter and an appropriately placed feed probe. This version consists of several progressively larger cylindrical sections connected (each 7 inches long) together by 43 degree flared sections (3 inches long). The first cylindrical section has a diameter of 3.5 inches and the last flared section has a diameter of about 36 inches. The overall length of the antenna is about 5 feet long.

During the design phase the antenna was simulated using a commercial 3-D EM solver which predicted a bandwidth of about 300 MHz, highly directional characteristics, and a gain of about 21 dB. The experimental method for gain measurement uses a non-standard technique. The gain was experimentally verified using software called Network Stumbler, and a 2511 PLUS EXT2 Wireless Card possessing antenna ports. The software is capable of measuring signal strengths picked up by antennas attached to the Wireless Card; it can also be used to measure ambient noise levels. The gain of the test antenna was calculated by comparing its signal to noise ratios with that of an antenna of known gain. Apart from discussing the design, the numerical and experimental verification of antenna gain will be described. The results of some field tests concerning the range and other capabilities will also be presented.

Design of Multiband Balanced Folded Dipole Antenna Based on a Dual-arm Structure for Mobile Handsets

D. Zhou, R. A. Abd-Alhameed, C. H. See, and P. S. Excell
Mobile and Satellite Communications Research Centre, University of Bradford
Bradford, West Yorkshire, BD7 1DP, UK

Abstract— Over recent years, balanced antenna systems have become of interest to mobile phone antenna designers due to their stable performance when held adjacent to the human body by mobile phone users [1]. In this type of antenna, balanced currents only flow on the antenna element, thus dramatically reducing the effect of current flow on the ground plane (i.e., phone chassis).

In authors' previous work [2], the characteristics of a built-in wideband balanced folded slotted dipole antenna for mobile handsets are introduced and analysed in order to achieve multiple-band operation (i.e., GSM1800/GSM1900/UMTS). Like most balanced antennas, the planar dipole antenna works best in free space and, on the contrary, performs badly when placed in the vicinity of other conductors (e.g., mobile phone ground plane). Thus, in order to mitigate the effects of the ground plane causing degradation of antenna performance, a technique was applied by inserting a slot in each one of the arms of the planar dipole to reduce the effects of the induced current on the ground plane. Consequently, a ground plane in which current is induced may have less mutual effect on the proposed mobile antenna. In this way, the antenna may be able to be placed close to the ground plane of the handset (e.g., 1 mm away). The slot size and location on the antenna, together with other parameters of the proposed antenna, were optimised to ensure that the design entirely covered the required frequency bands (1710–2170 MHz) (≤ -6 dB return loss).

In this paper, a follow-up study on the basis of this balanced antenna was carried out, in order to achieve a dualband operation, to cover the frequency bands including GSM1800, GSM1900, UMTS, WLAN (2.4 GHz). A new technique was introduced to add additional arms (see Fig. 1) on the reference balanced antenna in [2] to obtain another resonance next to the already existed one, to realise as a dualband operation to cover the intended frequency bands. In the analysis, an electromagnetic simulator based on the finite integration technique (FIT) was applied to calculate return loss and radiation patterns [3]. The performance of optimal antenna structure was validated and the results were compared using commercial simulators (compared results are not shown here). The maximum relative bandwidth for the initial design was covered the designated frequency band in this study, as observed in Fig. 2. This result is encouraging for practical implementation of this antenna for the future work.

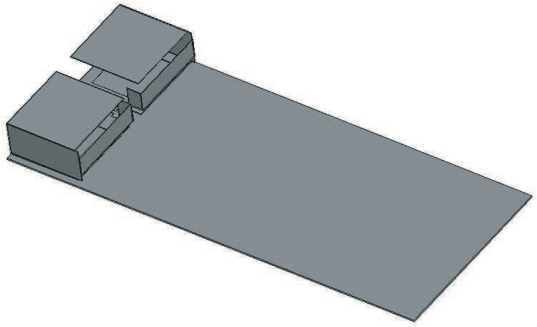

Figure 1: Geometry of the proposed folded balanced antenna with additionally extended arms for handsets.

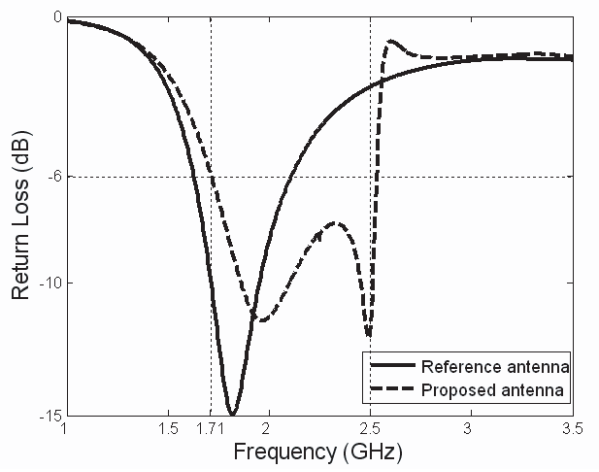

Figure 2: Simulated return loss of the proposed dualband balanced antenna.

REFERENCES

1. Morishita, H., Y. Kim, Y. Koyanagi, and K. Fujimoto, "A folded loop antenna system for handsets," *IEEE AP-S Proc.*, Vol. 3, 440–443, July 2001.
2. Zhou, D., R. A. Abd-Alhameed, and P. S. Excell, "Wideband balanced folded dipole antenna for mobile handsets," *The 2nd European Conference on Antennas and Propagation*, Session MoPA, Paper No. 39, Edinburgh, UK, November 11–16, 2007.
3. Computer Simulation Technology Corporation, CST Microwave Studio, Version 5.0, Germany.

Wideband Loaded Wire Bow-tie Antenna for Near Field Imaging Using Genetic Algorithms

S. W. J. Chung, R. A. Abd-Alhameed, C. H. See, and P. S. Excell
Mobile and Satellite Communications Research Centre, University of Bradford
Bradford, West Yorkshire, BD7 1DP, UK

Abstract— Due to the non-dispersive and ultra-wideband characteristics, the bow tie antenna has been applied on various applications; from Ground Penetrating Radar (GPR) to biomedical imaging tools. The bow-tie antenna play crucial roles in these applications by transmitting and receiving a relatively short transient pulse with minimum distortion and a low level of late time ringing. The lack of adaptive characteristic on the solid bow-tie antenna have motivated [1] to represent it in wire form in order to make it more suitable for GPR application. Drastic improvement is later been made by [2] by representing the typical solid bow tie antenna with a series of wires by means of Genetic Algorithm (GA). The Wire Bow-Tie (WBT) antenna is found more adaptive and advantageous as it is easily loaded with lumped elements to accommodate certain applications need while preserve its characteristics. Further improvement has also been done by the same group by resistively loading the design to minimize late-time ringing. Nevertheless, loading lump elements on wires is somehow impractical and difficult to achieve.

In this paper, a WBT antenna design is reported using GA as the main optimization tool. The antenna is designed based on the fundamental requirement for near field imaging tools such as for microwave breast cancer detector. This can be done by specify certain crucial goals on GA in order to obtain the optimum results. The design will then be analysed in time domain for further inspection using efficient and accurate computational software package where the resistive loading will also be implemented. For the sake of practical measurement, the design will then be transformed to microstrip to realize resistive loading method by using Surface Mount Resistors (SMR). To accommodate short pulses a wideband antenna design is considered taking into the account minimum late time ringing must be achieved.

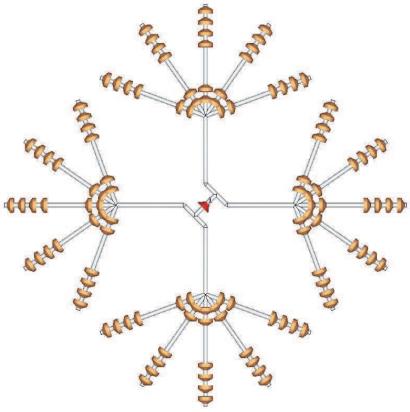

Figure 1: Geometry of the proposed cross polarized WBT antenna in which each arm loaded by six resistors.

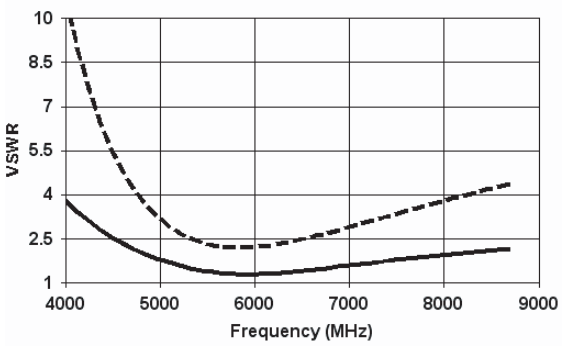

Figure 2: VSWR versus frequency of the proposed WBT, '- - -': unloaded antenna, '——': loaded antenna.

REFERENCES

1. Lestari, A. A., A. G. Yarovoy, and L. P. Ligthart, "Adaptive antenna for ground penetrating radar," *Proceedings of the Tenth International Conference on Ground Penetrating Radar*, Vol. 1, 121–124, 2004.
2. van Coevorden, C. Md. J., A. R. Bretones, M. F. Pantoja, F. J. G. Ruiz, S. G. Garcia, and R. G. Martin, "GA design of a thin-wire bow-tie antenna for GPR applications," *IEEE Trans. Geosci. Remote Sens.*, Vol. 44, No. 4, 1004–1010, April 2006.

A Novel CPW-fed Bow-tie Slot Antenna for 5.8 GHz RFID Tags

Fei Lu, **Quanyuan Feng**, **and Shiyu Li**
Microelectronic Technology Lab of Southwest Jiaotong University, China

Abstract— A Novel Bio-Tie slot antenna with CPW-fed structure is presented. The designed antenna, which is fabricated on a 35×25 mm RF4 substrate can operate at the 5.8 GHz band with 21.7% bandwidth($s_{11} < -10$ dB) and gain 3.9 dBi, respectively. Besides, the radiation patterns are almost omni-directional in H-plane and bidirectional in E-plane. All these properties and the uniplanar structure make the antenna suitable for 5.8 GHz RFID (radio frequency identification) application. The concepts of RFID and RFID tag antennas are introduced at the beginning of the paper. Then, the designed antenna's structure is presented. Different from the common bow-tie antenna, dual bow-tie structure is adopted in this novel antenna. Its simple structure is based on a one-layer FR4 dielectric substrate only, which has 1.6 mm thickness and permittivity of 4.4. This common material can reduce the cost of the RFID tag. A rectangular patch with dual bow-tie slot is printed on the upper-side of the substrate. Based on the pertinent literature, a set of suitable geometric parameters for the antenna is designed, and then checked and adjusted by means of simulation using HFSS v10 software. The figures to perform antenna's radiation pattern and return loss are displayed on the paper. Further, the parameters of bow-tie structure are also discussed and optimized, and the different results are listed in a table. The final antenna's dimension is determined by analyzing the simulation data from the table. It is discussed that why the designed antenna is suitable for 5.8 GHz RFID tags in the end.

A Mode Based Model for Radio Wave Propagation in Storm Drain Pipes

Ivan Howitt, **Safeer Khan**, **and Jumanah Khan**
Department of Electrical and Computer Engineering
The University of North Carolina at Charlotte, Charlotte, NC 28223, USA

Abstract— Wireless communication in confined underground structures, such as circular concrete tunnels, is characterized by their adverse propagation characteristics. The previous research on analyzing RF propagation inside such structures at microwave frequencies was based on using a leaky circular waveguide model [1, 2]. Driven primarily by growing demands of mobile communications, the main focus of historic research was on auto, railroad, subway, mine and sewer tunnels of diameters greater than 1.05 m. There is, however, no published research on analyzing RF propagation inside municipal storm drain pipes (SDPs) which are networked extensively in urban environments.

Analysis of RF propagation inside SDPs is not only relevant because of its tactical usefulness for military operations in urban terrain [3], but also for other civilian applications. The focus of our work has been on understanding RF propagation inside concrete SDPs by using a leaky circular waveguide model. We study the modal content of propagating waves and derive a mode based model (MBM) to predict the received power at distance d from the source inside an SDP. For describing the MBM, we consider the received power as the sum of powers contained in propagating modes. The following mathematical relationship is realized to describe the MBM:

$$P_R(d) = \sum_{n=1}^{N} P_n = \sum_{n=1}^{N} A_{CL_n}^2 \times e^{-2\alpha_n d} \tag{1}$$

In (1), P_n is the power contained in a particular mode n, A_{CL_n} is the antenna coupling coefficient for mode n, α_n is the nth mode attenuation factor in Nepers/m and $P_R(d)$ is the received power at distance d in watts.

To validate the MBM, experimental data was obtained through a measurement campaign at selected sites in Charlotte, North Carolina. The measurement set up is given in Fig. 1. To evaluate the MBM, we compute modal cutoff frequencies and attenuation coefficients for various pipe diameters using the analytical relationships for waveguides. We then estimate the coupling loss parameter $A_{CL_n}^2$ by employing a nonlinear least square curve fitting technique. The values of $P_R(d)$ were predicted using the coefficients obtained for A_{CL_n}, that are plotted along with the measured received powers in Fig. 2.

We also analyze the estimated values of $A_{CL_n}^2$ to understand their contribution in the overall received power solution for 2, 3, 5 and 7 contributing modes. The plot in Fig. 3 highlights the

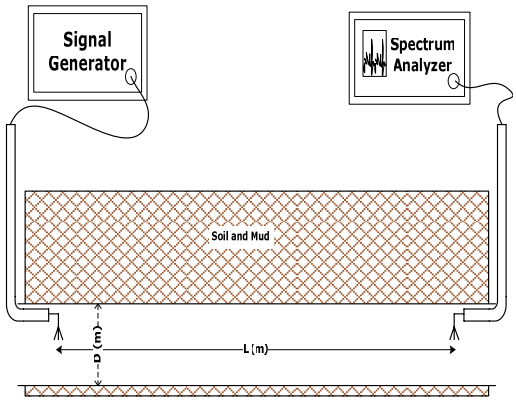

Figure 1: Measurement set up.

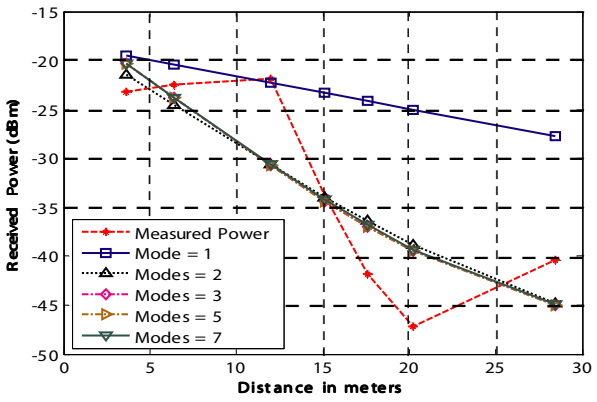

Figure 2: Measured and predicted received power for different number of modes in MBM for 1.07 m diameter SDP.

contribution of $A^2_{CL_n}$ considering first three modes in the MBM for producing the predicted received power. The plot highlights that fitting of predicted received power with the measured power considerably improves by increasing the number of modes in the MBM.

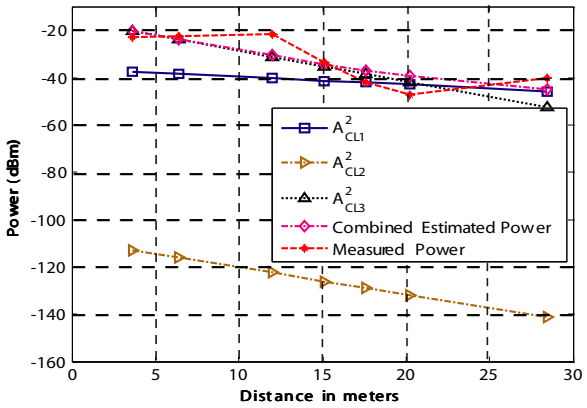

Figure 3: Contribution of antenna coupling coefficients in estimated received power for three modes.

We conclude from our analysis that the MBM not only provides insight into the modal content of the propagating signal but is also a good approximation for estimating $P_R(d)$ in the SDPs. The paper also highlights requirement for further research to improve the fitting of predicted data with the measured received power results.

REFERENCES

1. Dudley, D. G., "Wireless propagation in circular tunnels," *IEEE Trans. Antennas Propag.*, Vol. 53, No. 1, 435–441, Jan. 2005.
2. Holloway, C. L., D. A. Hill, R. A. Dalke, and G. A. Hufford, "Radio wave propagation characteristics in lossy circular waveguides such as tunnels, mine shafts, and boreholes," *IEEE Trans. Antennas Propag.*, Vol. 48, No. 9, 1354–1365, Sep. 2000.
3. Kjeldsen, E. and M. Hopkins, "An experimental look at RF propagation in narrow tunnels," *Proc. IEEE Military Communications Conf. (MILCOM'06)*, Washington D. C., Oct. 23–25, 2006.

Active Quasi-circulator for Wireless Communication

Wai Yin Mung and Wing Shing Chan

Department of Electronic Engineering, City University of Hong Kong
83 Tat Chee Avenue, Kowloon, Hong Kong SAR, China

Abstract— In modern RF/microwave systems, non-reciprocal components such as isolators and circulators play an important role because it provides isolation between ports in both time and frequency. Research using active devices to replace the conventional ferrite circulator has been of interest. Although these active quasi-circulators have limitations, their broad bandwidth offers many possible future applications in front end components such as multiplexers, phase shifters, delay lines, etc. They have numerous advantages as well as disadvantages when compared with conventional ferrite circulators such as small size, light weight, and compatibility with monolithic microwave integrated circuit (MMIC) technology. A simple active quasi-circulator using phase equalization technique is proposed. It is formed by configuring three transistors with a complimenting phase shifter for equalization.

Active quasi-circulators with large bandwidth will have potential applications in the future because it allows signal flow in one direction without interaction between other ports. Each port can transmit and receive signals at the same time and at different frequencies without the need for filters. This work will describe an active and simple quasi-circulator that gives wideband operation, and differs from previous structures that were limited to a narrow frequency range. It is formed by connecting three single stage distributed amplifiers (DAs) together with a T-network phase shifter. Experimental results show that it can operate over the frequency range 0.8–2.2 GHz with sufficient return loss and isolation to make it practical in use. The tremendous growth in the cellular mobile communication with proliferation of different standards is suitable for this wideband quasi-circulator.

Unequally Biased Amplifier with Enhanced Efficiency

Tik Shun Leung and Wing Shing Chan
Department of Electronic Engineering, City University of Hong Kong
83, Tat Chee Avenue, Kowloon, Hong Kong SAR, China

Abstract— Multi-band mobile units have now become common place and may include services such as 2G, 3G, Bluetooth and WiFi. The operating frequency bands of the above services lies mainly between 0.8 GHz to 2.6 GHz. Traditionally multi-band circuits are used rather than wideband circuits. In order to support the above services using a single circuit such as in software defined radios, a wideband topology is needed. Due to the Distributed Amplifiers' (DAs) [1–4] advantage of flat gain and no matching network required, they are ideally suited for addressing these wideband amplification issues. In fact, most of the FET-DAs have operating frequencies that lie between DC to 10 GHz which is subsequently expensive and therefore not cost effective when compared to current solutions based on multiple bands. Moreover, due to the presence of an artificial transmission line at both the input and output, a significant amount of power is wasted in the dummy load. Conventional distributed amplifiers therefore suffer from low power added efficiency which is exasperated at higher operating frequencies.

In the work presented here, a bipolar junction transistor distributed amplifier (BJTDA) is investigated and proposed as a high performance lower cost alternative. The aim of the work is to improve the power added efficiency of the BJTDA and a power amplifier using unequal biasing (UBA). By using the proposed unequal bias method, the power consumed in the dummy load at the output line is eliminated and still exhibits wideband characteristics similar to a conventional BJTDA. A significant improvement in PAE over the operation frequency band from 0.8 GHz to 2.6 GHz is achieved when compared with the conventional BJTDA.

REFERENCES

1. Niclas, K. B., W. T. Wilser, T. R. Kritzer, and R. R. Pereira, "On theory and performance of solid state microwave distributed amplifiers," *IEEE Trans. Microwave Theory Tech.*, Vol. 83, Issue 6, 447–456, 1983.
2. Dixit, R., B. Nelson, W. Jones, and J. Carillo, "A family of 2–20 GHz broadband low noise AlGaAs HEMT MMIC amplifiers," *Proc. IEEE Microwave and Millimeter-Wave Monolithic Circuits Symp. Digest.*, 15–19, 1989.
3. Majidi-Ahy, R., C. K. Nishimoto, M. Riaziat, M. Glenn, S. Silverman, S.-L. Weng, Y.-C. Pao, G. A. Zdasiuk, S. G. Bandy, and Z. C. H. Tan, "5–100 GHz InP coplanar waveguide MMIC distributed amplifier," *IEEE Trans. Microwave Theory Tech.*, Vol. 38, Issue 12, 1986–1993, 1990.
4. Mok, K. T., S. Y. Mok, W. S. Chan, and C. W. Li, "Linearised distributed amplifier with low linearisation loss," *IEE Electronics*, Vol. 40, Issue 1, 4–5, 2004.

Handset Beamforming Synthesis Using PSO for 4G Mobile Communication Systems

K. R. Mahmoud[1,2], **M. El-Adawy**[1], **Sabry M. M. Ibrahem**[1]
R. Bansal[2], **and S. H. Zainud-Deen**[3]

[1]Faculty of Engineering, Helwan University, Cairo, Egypt
[2]Department of Electrical and Computer Engineering, University of Connecticut, CT, USA
[3]Faculty of Electronic Engineering, Menoufiya University, Menoufiya, Egypt

Abstract— In this paper we investigate the integration of monopole-antenna arrays into handheld devices in the 5.0-GHz band and study their capability for beamforming synthesis. Two different antenna array configurations integrated into the handset are considered. The first geometry is a 4-element linear array, but due to its inability to maximize the electric field in a broadside direction and simultaneously minimize in the opposite direction, it has limited applications. The second geometry consists of a 5-element array; four elements located at handset corners and the fifth-element located at the center. The particle swarm optimization (PSO) algorithm is used to optimize the complex excitations of the adaptive arrays elements in a mutual coupling environment for beamforming synthesis. All numerical simulations are performed using the FEKO Suite 5.3 software. To verify the validity of numerical simulations we first perform two validation tests (one-element monopole on a handset) and compare their results with published simulated and measurement results.

A New Call Handoff Technique for Next Generation Systems

P. P. Bhattacharya and Manidipa Bhattacharya

Department of Electronics and Communication Engineering, Dr. B. C. Roy Engineering College
Jemua Road, Fuljhore, Durgapur-713 206, West Bengal, India

Abstract— Now-a-days smaller cell sites or splitted cells or sectorized cells with directional antennas are used to meet the increased demand of channels due to huge traffic density. Hence, there are large number of handoffs in mobile cellular communication networks. Due to large number of subscribers there may be scarcity of free voice channels in mobile cellular communication system. Moreover, there will be both new call attempts and handoff calls which require handoff to other cell site. As a principle priority is given to handoff calls rather than new call attempts. Normally the call is handed over to the approaching target cell from which the MS receives maximum signal strength. MS will also receive signal from neighboring cells. Cases may arise where there may be scarcity of available channel in the target cell. Under this condition there may be call dropping although some of the free channels may be available in the neighboring cells. Thus instead of targeting a particular cell from which the signal strength is maximum, all other surrounding cells may be considered form which the signal strength may be little weaker but there are free available channels and if handoff is executed in one of these cells, call continuity may be maintained. Based on this concept a fuzzy logic based algorithm is proposed which uses signal strengths from surrounding cells, angle between the user movement and base stations and the number of free channels as input parameters. The algorithm is studied and tested where the call may be handed over to any of the surrounding cells depending on the availability of free channels. The proposed algorithm works efficiently and quickly responses to the difference in signal strength between serving base station and possible target base stations, direction of motion of mobile station and available channels. The number of fluctuations in handoff response are low in this case, so the algorithm may be implemented in a small scale fading environment also. Since there are crisis of traffic channels due to high demand by the users, this algorithm may be an effective and useful solution. The software programs for the proposed algorithms are neither complex nor consumes much time to respond. Hence, it can be easily embedded into application programs and can be implemented in real systems. Since the software has controlled complexity and it is thoroughly tested, the codes can be burned-in at the system ROM.

Session 3A4
Electromagnetic Modeling, Inversion and Applications 2

A GLEMFCS Coupled Modeling and Inversion for Icing Disaster on High Voltage Lines

Ganquan Xie, **Jianhua Li**, **and Feng Xie**
GL Geophysical Laboratory, USA

Abstract— We have proposed 3D GL and AGILD Electromagnetic (EM)-Flow-Heat-Stress coupled modeling (GLEMFHS) in PIERS 2007 in Beijing and published the method in PIERS Online. In this paper, we propose a EM-Flow-Cold-Stress (GLEMFCS) coupled modeling and inversion for icing disaster on high voltage lines, in short, we call it GLEMFCS ICINGS modeling and inversion. The GLEMFCS ICINGS modeling imaging can be used to display the EM, flow, temperature, and icing crystal stress field dynamically on the high voltage lines and recover, adjust, monitor, and control the EM, flow, old temperature, icing stress, distance of tie tower supports, and electric network parameters, such that the icing disaster minim. During Chinese Lunar New year, from January 8 to February 8, 2008, there had been serious icing disaster in South of China and North of Nanling mountain that never been happen in recent 100 years. The icing disasters were extremely serious in Hunan, Guizhou, Jiangxi, Hubei, Anhui, Zhejiang, and Jiangsu etc. provinces. The icing on the high voltage wire lines to form very big and length ice cylinders with diameter 350 mm to 400 mm. The big and length ice cylinders flying on the high voltage wire lines produce big tense forces between the tie towers such that the tie towers collapsed and destroyed power network and caused power down in very large areas of the above provinces. The icing disaster may be repeatedly happen in China or other places in the world. Therefore, the GLEMFCS Icing Coupled modeling and inversion for icing disaster on high voltage lines proposed in this paper is necessary and have important and wide applications to investigate and reduce the strange and serious icing disaster. The patent of the GLEMFCS ICINGS modeling and inversion and all rights are reserved by authors in GL Geophysical Laboratory.

REFERENCES

1. Xie, G., J. Li, L. Xie, F. Xie, and J. Li, "The 3D GL EM-Flow-Heat-Stress coupled modeling," *PIERS Online*, Vol. 3, No. 4, 411–417, 2007.
2. Xie, G, J. H. Li, J. Li, and F. Xie, "3D and 2.5D AGLID EMS stirring modeling in the cylindrical coordinate system," *PIERS Online*, Vol. 2, No. 5, 505–509, 2006.
3. Xie, G., J. Li, and J. H. Li, "New AGILD EMS electromagnetic field modeling," *PIERS Online*, Vol. 1, No. 2, 168–172, 2005.
4. Li, J., L. Xie, G. Xie, and J. Li, "A GLEMFHS EMS imaging using the GL EM-Flow-Heat-Stress coupled modeling," *PIERS Proceedings*, Hangzhou, 2008.
5. Xie, G., F. Xie, L. Xie, and J. Li, "New GL method and its advantages for resolving historical diffculties," *Progress In Electromagnetics Research*, PIER 63, 141–152, 2006.
6. Xie, G., J. Li, L. Xie, and F. Xie, "GL metro carlo EM inversion," *Journal of Electromagnetic Waves and Applications*, Vol. 20, No. 14, 1991–2000, 2006.

Validation of 2D FDTD Ground Penetrating Radar Modeling for Bridge Deck Evaluation by 3D FDTD

H. Zhan[1], **K. Belli**[2], **S. Wadia-Fascetti**[1], **and C. Rappaport**[3]

[1]Civil and Environmental Engineering Department, Northeastern University, USA
[2]Mechanical and Industrial Engineering Department, Northeastern University, USA
[3]Electrical and Computer Engineering Department, Northeastern University, USA

Abstract— Ground penetrating radar (GPR) is often used for rapid non-invasive geophysical sensing of concrete structures. In particular, road and bridge pavement diagnostics, including detecting media delaminations and voids, are amenable to GPR probing. The detection and localization of these pavement defects provide knowledge of severity of deterioration of the structure, thus allowing efficient allocation of limited funding for repair and maintenance. GPR modeling indicates signal features characteristic of healthy and deteriorated conditions, and guides in sensor design and placement. Furthermore, accurate and efficient forward modeling forms the basis for model-based inversion for deterioration detection and reconstruction. Two-dimensional models are computationally fast and capable of analyzing large computational regions, but they often suffer from providing an incomplete view of the problem. However, for cases where geometry is invariant in the third dimension and the sensing plane coincides with the incident plane, 2D analysis is often satisfactory. The full 3D models capture all interactions but are limited in computational size, and they can be very computationally intensive. Computation time is a key factor in determining real-time inversion, since the forward model is adjusted to best fit the observed data in the inversion process. This paper quantifies which — and how much — information is left out by the 2D FDTD model, and seeks to answer the question of whether 2D FDTD is sufficiently descriptive for detecting defects in bridge decks.

We are considering sensing with air-coupled GPR, for which the antennas are suspended above the ground surface. Typically the GPR is a longitudinal polarized bistatic transmitter and receiver pair mounted on a vehicle. The bridge deck is usually a two-layer media: 18 cm dry concrete with 2.4 cm asphalt overlay, with horizontal reinforcing steel bars. Air-coupled GPR surveys can be done at highway speeds, avoiding lane closure during assessment. Measured signal responses can be synthesized by determining the model excitation signal which generates the measured response due to reflection from a calibrating metal sheet placed on the ground surface. Since the wave propagated through the geometry is a linear time-invariant response, the desired received response can be obtained by pre-filtering the excitation signal. Due to the geometric spreading of 2D and 3D waves: cylindrical waves propagate with amplitude proportional to the inverse of the square root of distance while spherical waves are proportional to the inverse of the distance, a different filter is used for each case. 2D and 3D FDTD simulations are conducted with a bistatic transmitter and receiver pair moving longitudinally along the bridge, and taking time histories at a fix scanning resolution to form B-Scans. Two modulated Gaussian pulses, one with 1.0 GHz center frequency and bandwidth, and the other at 500 MHz, are used as excitations. The 2D FDTD is a good approximation for modeling bridge deck deterioration. However, the accuracy of the 2D FDTD degrades when there is more variance in the longitudinal direction.

Characterization of a GPR Antenna for Excitation of a 2D Finite-difference Time Domain Model of Reinforced Bridge Decks

K. Belli, C. Rappaport, and S. Wadia-Fascetti
Northeastern University, USA

Abstract— The ability to simulate the ground penetrating radar (GPR) investigation of a bridge deck via a forward computational electromagnetic model provides insight into the response from bridge deck elements and complex interactions between them, as well as changes in the response due to the presence and relative location of anomalies. In a forward problem, the source and model are known, while the field due to the source is estimated. Inversion techniques attempt to use the data recorded by the GPR antenna to approximate the physical geometry and material properties of the bridge deck. Many physics-based inversion techniques iteratively implement a forward model to arrive at a solution. Therefore, forward modeling plays a major role in these approaches to reconstruct the physical geometry and material properties of the bridge deck. The reconstructed structure and/or determined material properties are integral to the condition assessment of the bridge.

The work presented in this paper uses a two-dimensional Finite-difference Time Domain (2D FDTD) model to simulate the GPR investigation of a bridge deck. In order to do this accurately, it is necessary to have an appropriate virtual sensor model to excite the system. Using the reflection from a perfect electrical conducting sheet, a cylindrical wave excitation (a point source in 2D) can be derived that results in simulated layer reflections with a high correlation to real world data. When looking at non-layered objects (such as rebar and voids), accuracy of simulated results compared to field collected results can be greatly improved by considering the antenna's directivity.

To determine an appropriate virtual source for 2D FDTD simulation that captures the characterization of time domain radar, some challenges must be overcome. Time domain radar makes the concepts of gain and impedance matching difficult to implement, and the angle-dependent pulse shape dispersion must be considered. Experiments were performed using a 2 GHz center frequency air-coupled horn antenna. The data collected include amplitude and delay responses from a PEC target placed at various locations under the antenna. The time delay and signal attenuation obtained experimentally include the combined effects from the transmitting and receiving antennas. To determine the excitation signals for the virtual source, the effects from the two antennas are separated and then applied to a pulse shape obtained by reflection from a PEC sheet. With the pulse shape, signal attenuation and time delay at the target positions known, an appropriate virtual source can be modeled. The simulation of a GPR investigation of a reinforced bridge deck is performed using the virtual source, which accounts for the antenna radiation pattern. The simulation is compared to results of the same physical model excited by a cylindrical wave excitation (a point source in 2D) that correlates well to real-world surface reflection. The increase in the accuracy of the virtual source derived from antenna characterization is made evident by comparison to additional laboratory experiments over the best-fit cylindrical wave excitation.

Detecting Tunnels and Monitoring Internal Motion Using Cross-well Radar

Arvin M. Farid, **Karen Cui**, **Edward Vaisman**
Jose Angel Martinez Lorenzo, **and Carey Rappaport**
Northeastern University, USA

Abstract— For thousands of years, prisoners around the world have used underground tunnels to flee prisons.Illegal immigrant and smugglers to avoid security checkpoints also excavate underground tunnels across borders of different countries including the United States. Smugglers have used tunnels for transiting and trafficking weapons, people, drugs, and other materials as well. Furthermore, in the past several years, the threat of international terrorism has become the most important security concern and has made tunnel detection a national priority, both across borders and surrounding highly secured facilities. This threat is no longer a myth; as it has been witnessed in countries like Israel and Yemen.

Currently there are no effective and reliable stand-alone tunnel detection techniques. A non-destructive and versatile tool for tunnel detection is essential. Cross-well radar-based methods have the potential to detect tunnels. The goal of this paper is to evaluate and study real-time monitoring of movement of human bodies within detected tunnels. This problem is computationally modeled and experimentally investigated at the pilot-scale SoilBED facility at Northeastern University. The finite difference frequency domain (FDFD) method is used to predict the scattering response of an air-filled dielectric-lined tunnel, buried in a lossy soil half-space, illuminated by various depths borehole dipole sources. Scale-model experiments were conducted using an automatic network analyzer and custom balun-loaded dipole antennas inserted into PVC-lined boreholes. The results are applied to an inversion technique to reconstruct images of the tunnel.

Using Circular Support Information for Microwave Imaging

Raphaël Lencrerot, **Amélie Litman**, **Hervé Tortel**, **and Jean Michel Geffrin**
Institut Fresnel, Equipe SEMO
Avenue Escadrille Normandie-Niemen, Marseille Cedex 13397, France

Abstract— Institut Fresnel is currently developing a microwave scanner for monitoring moisture content in columns of reconstructed soil. With this setup, the goal is to demonstrate the potentiality of a non-invasive microwave imaging system for water content monitoring, which would provide a complementary non-invasive measurement setup for intermediate scales between remote sensing scales and ground truth measurement scales.

This scanner has the particularity to present a circular configuration, which remains fixed during the experiment. The setup consists of a cylindrical cavity, whose metallic boundaries have been chosen in order to remove external parasitic effects. The emitting and transmitting antennas are all positioned on a ring inside the cavity. Finally, the target which must be monitored is placed at the centre of the setup. As the goal is to monitor monoliths of reconstructed soils, the target consists in a cylindrical column.

It is well known that inverse scattering process suffer from ill-conditioning issues. Any type of a-priori information is more than welcome in order to improve the reconstruction process. Here, we take advantages of the present configuration by imposing the spatial support of the permittivity maps, this support being known before hand. Indeed, this support must be centred and cylindrical and we can measure experimentaly its exact position.

One possible way would be to simply restrict the investigation domain to such area and search for the permittivity of each discretization cell. This has been done in previous work using a finite element mesh with a conformal mapping [1] coupled with a minimization under constraints algorithm [2].

Here, we tackle another approach where we do not define the permittivity in a piecewise way. For this, we introduce a set of basis functions whose support covers exactly the investigation domain. For squared areas, Legendre or Tchebycheff polynomials are well suited. For cylindrical ones, it is more appropriate to deal with Bessel or Zernike polynomials [3]. Due to the good physical interpretation of the Zernike polynomials, we have selected this latter type of representation.

We will show through numerical and experimental results the advantages of such representation. Indeed, we can control the number of parameters to effectively retrieve the permittivity maps, this number being related to the maximum size of the available dataset [4].

REFERENCES

1. Cmielewski, O., H. Tortel, A. Litman, and M. Saillard, "A two-step procedure for characterizing obstacles under a rough surface from bistatic measurements," *IEEE Trans. Geosci. Remote Sens.*, Vol. 45, 2850–2858, 2007.
2. Lencrerot, R., A. Litman, H. Tortel, and J.-M. Geffrin, "A microwave imaging circular setup for soil moisture information," *IGARSS Proc.*, 4394–4397, 2007.
3. Born, M. and E. Wolf, *Principles of Optics*, Pergamon Press, 1959.
4. Bucci, O. M. and T. Isernia, "Electromagnetic inverse scattering: Retrievable information and measurement strategies," *Radio Science*, Vol. 32, 2123–2138, 1997.

Analysis of Electromagnetic Susceptibility Data

Haitao Cai[1] and Jianshu Luo[2]

[1]Eastsouth University, Changsha 410073, China
[2]National University of Defence Technology, Changsha 410073, China

Abstract— Firstly, this paper describes the Logistic regression theory which can be applied to the electromagnetic susceptibility data. Comparing the maximum likelihood estimation method and the weighted least squares method, we learn that the maximum likelihood estimation method is a common approach, and the weighted least squares rule needs to meet certain conditions. And we introduce goodness-of-fit tests of model and give three evaluation methods: deviation test, Pearson test and Hosmer-Lemeshow goodness-of-fit indicators; then introduce the significant tests of the regression model and coefficients and the confidence intervals of the regression coefficients and the event probability. We also introduce the two types of problems which can affect the parameter estimation, and give in-depth discussions of the data structure problems.

Secondly, we introduce the variable selection criteria and model verification methods of the logistic regression model, and these methods are very useful for processing the electromagnetic susceptibility data in the complex electromagnetic environments. Because the factors, which affect the electromagnetic susceptibility of the electronic equipments in the complex electromagnetic environments, are not only the results from the theories, but also some results existing in the surrounding electromagnetic environments, therefore, the variables of the model and model verification before building the model, will help us to establish more effective forecasting model.

Thirdly, this paper analyse electromagnetic susceptibility data of the incident test of single-point source in the hole-infinite flat plate. We mainly study the relationships between R (the distance between point source and the aperture), d (the vertical distance between point source and the infinite flat plate) and the response in the observation point. Then we calculate the corresponding simulation data, and establish the logistic regression model; and using the simulation model test data, we verify the validity of the model. Next, using statistical analysis theory, we estimate the model parameters, and test the goodness-of-fit and the test results show that the model fit the data well. Also, we give the confidence interval of the regression coefficient and the event probability. When the confidence level is 95%, the confidence intervals of regression coefficients are $(-4.5533, -2.3891)$ and $(-2.3891, -0.5060)$ and the confidence interval of the event probability is (0.0455, 0.1318), which show that the model has good credibility. Finally, the interpolation and extrapolation methods can be used to verify the effectivity of the logistic regression forecasts, that is, in which location logistic regression forecast is effective and in which position it needs for further verification. Next, we will use logistic regression to analyse multi-point source, or more complex electromagnetic susceptibility tests.

The Computation of Electromagnetic Field on Torus Knots

Jianshu Luo and Xufeng Zhang
College of Science, National University of Defence Technology, Changsha 410073, China

Abstract— Knot theory is a subfield of topology in mathematics. In the past, the study of knot is primarily in the field of mathematics. However, in recent years, knots have been gaining interest outside the field of mathematics in various fields of science and engineering, for example, plasma physics, molecular biology. Knot theory has been applicated in electromsgnetism, and many research achievements have been achieved. Knot electrodynamics is an new area of research which mainly research the electromagnetic characteristics releated to the knot, such as the electromagnetic radiation and scattering properties of the torus-knot antenna, the calculation of energy of ome special magnetic field structures. In this paper, the electromagnetic nature of a kind of special form of knot — torus knot are discussed, and the main content and innovative results are as follows:

First, in order to analyse the antenna radiation and scattering properties, the surface current distribution of antenna is needed, which requires solution of the electric field or magnetic field integral equation (EFIE or MFIE). In reference, a Electric Field Integral Equation (EFIE)suitable for analysis of toroidally knotted wires has been derived based on the Pocklington Integral Equations for an arbitary curved wire. In this paper, a new EFIE is derived based on another famous Electric Field Integral Equation-Hallen Integral Equations for an arbitary curved wire.

Second, for the torus knot wire, proved its self-inductance also can be calculated by the Neumann formula, and gives the formula.

Analysis of a 1:2 Rectangular Waveguide Power Divider for Phased Array Application Using Multiple Cavity Modeling Technique

Debendra Kumar Panda and Ajay Chakraborty

IEEE, India

Abstract— A method of moment based analysis of a feed network of the waveguide fed two dimensional array antennas has been presented in transmitting mode. Present work was performed for analysis of an H-Plane $1:2$ power divider for a phased array application using Multi Cavity Modeling Technique (MCMT). The technique involves in replacing all the apertures and discontinuities of the waveguide structures, with equivalent magnetic current densities so that the given structure can be analyzed using only Magnetic Field Integral Equation (MFIE). Since only the magnetic currents present in the apertures are considered the methodology involves only solving simple magnetic integral equation rather than the complex integral equation involving both the electric and magnetic current densities. The proposed power divider is unlikely to the family of Tees. The output ports are in the same planes as the input which is an advantage for phased array applications. Finally attempt has been made to improve the frequency response characteristic of the above mentioned waveguide circuit. Codes have been written for analyzing the frequency response characteristic of the structure, mentioned above. The existence of cross polarization components of the field inside the waveguide structures, if exists, have also been considered to obtain an accurate result. The proposed power divider has good agreement with the theoretical, CST microwave studio simulated data and measured data.

Electromagnetic Green's Function in Spherical or Cylindrical System

Jianhua Li, **Ganquan Xie**, **and Lee Xie**
GL Geophysical Laboratory, USA

Abstract— The electromagnetic (EM) wave Green's function tensor plays important role in EM theory and applications. The EM Green's tensor in the rectangle coordinate system is of analytical representation. The EM Green's function tensor in spherical (EM-G-S) or cylindrical (EM-G-C) coordinate system is complicated. In the exist publication, all researchers used TE and TM model approach to derive EM-G-S and EM-G-C. The EM-G-S or EM-G-C by TE and TM model includes Delta function and its derivative. In the integral equation with Green's tensor kernel, the derivative of the Delta function will induce to differential term; the integral equation becomes complicated integral-differential equation. In the differential integral equation with derivative of Green's tensor kernel, the Delta function will induce to differential term; the differential integral equation becomes complicated differential integral-differential equation. For overcoming these difficulties, we propose a new approach to derive EM-G-S and EM-G-C in this paper, which are named GEM-G-S and GEM-G-C. Our GEM-G-S and GEM-G-C does not include Delta function and does not include its derivative. GEM-G-S and GEM-G-C can be used to preserve invariance of the integral and differential integral equation. GL and AGILD EM modeling is constructed by GEM-G-S or GEM-G-C is presented. The method can be extended to construct the Green's function in mechanical and acoustic and all physical mathematical equation system.

Localization of 2D PEC Scatterers by a Multi-bistatic Stepped Frequency Radar

Adriana Brancaccio, **Colomba Di Dio**, **and Giovanni Leone**

Dipartimento di Ingegneria dell'Informazione, Seconda Universita' di Napoli, Italy

Abstract— The problem of localizing objects by measurements of the electromagnetic field scattered under a known incident field is considered. The localization problem is usually addressed in the hypothesis of "small" (with respect to the wavelength) scatterers ([1] and ref. therein). Otherwise, a "shape" reconstruction inverse problem can be formulated ([2] and ref. therein). Here we propose an algorithm for the localization of perfectly electrically conducting (PEC) scatterers, by referring to circular cylinders illuminated by a TM polarized plane wave, under a 2D geometry. Such topic is relevant in applications such as the detection and localization of buried pipes.

We want to find the positions of the centers of N circular cylinders of known radius a embedded into a homogeneous medium of known permittivity ε_r and residing within the investigation domain D. (r_n and θ_n denote the polar coordinates of the nth cylinder). The incident field is assumed to be plane waves with k wavenumber and θ_i incidence angle. The far zone scattered field is collected at the observation angles θ at a distance r from the origin of the reference coordinate system. If the mutual scattering between the cylinders is neglected the relationship between the scattered field measurements and the searched for positions is given by the cylindrical wave expansion as:

$$E_s(k,\,\theta,\,\theta_i,\,r) = -\sqrt{\frac{2i}{\pi kr}}e^{-jkr}\sum_{p=-P}^{+P}\frac{J_P(ka)}{H_P^{(2)}(ka)}e^{jp(\theta-\theta_i)}\sum_{n=1}^{N}e^{-jkr_n[\cos(\theta_n-\theta_i)-\cos(\theta_n-\theta)]} \tag{1}$$

where $P \sim$[ka] and the information about the objects' positions (r_n and θ_n) stand in the exponential phase coefficients. If we introduce as unknown the auxiliary distributional function [4]:

$$\gamma(\underline{r}') = \sum_{n=1}^{N}\delta(\underline{r}' - \underline{r}_n) \tag{2}$$

the problem at hand is recast as the inversion of the linear operator equation:

$$E_s(k,\,\theta,\,\theta_i,\,r) = -\sqrt{\frac{2i}{\pi kr}}e^{-jkr}\left[\sum_{p=-P}^{+P}\frac{J_P(ka)}{H_P^{(2)}(ka)}e^{jp(\theta-\theta_i)}\right]\int_D \gamma(\underline{r}')e^{-jkr'[\cos(\theta'-\theta_i)-\cos(\theta'-\theta)]}d\underline{r}' \tag{3}$$

The model in Eq. (3) is similar to model [1] for the "thin" scatterers, except for a multiplicative factor. So, the same inversion algorithm based on the truncated singular value decomposition and on a proper chosen threshold can be used. The positions of the maxima of the reconstructed function (which is a filtered version of (2)) represent the searched for centers. Numerical results from exact scattered field data show the effectiveness of the approach. In addition an experimental verification has been conducted with scattered field data collected by a portable multibistatic, stepped frequency radar measurement system [3].

REFERENCES

1. Pierri, R., R. Solimene, A. Liseno, and J. Romano, "Linear distribution imaging of thin metallic cylinders under mutual scattering," *IEEE Trans. Ant. Prop.*, Vol. 53, No. 9, 3019–3029, 2005.
2. Soldovieri, F., A. Brancaccio, G. Leone, and R. Pierri, "Shape reconstruction of perfectly conducting objects by multiview experimental data," *IEEE Trans. Geosc. Remote Sens.*, Vol. 43, No. 1, 65–71, 2005.
3. Parrini, F., M. Frattini, M. Pieraccini, C. Atzeni, G. De Pasquale, P. Ruggiero, F. Soldovieri, and A. Brancaccio, "ULTRA: Wideband ground penetrating radar," *Proceeding of the EURAD*, Manchester UK, 2006.

Session 3A5
Poster Session 3

Retrieval of Higher Order Ocean Wave Spectra from Sunglint

G. P. Cureton[1], **S. J. Anderson**[2], **M. J. Lynch**[1], **and B. T. McGann**[1]

[1]Department of Imaging and Applied Physics
Curtin University of Technology, Perth WA, Australia
[2]Defence Science and Technology Organisation, Salisbury SA, Australia

Abstract— A thorough knowledge of the dynamics of the ocean surface, in particular with respect to wind generated waves, is relevant for a range of human activities, including the design and operation of ships, the construction and servicing of marine structures such as offshore oil and gas drilling platforms, the management of coastal environments, and, increasingly, for the design and deployment of wave energy extraction systems. Of particular concern is the effect that higher order dynamical processes, often neglected for the sake of simplicity or computational tractability, have on such things as energy transfer between wave modes, and more importantly, energy transfer to human structures.

One particular approach to the characterization of the wave surface is by interrogation by optical radiation. Light which has been specularly reflected from the wave surface is highly directionally dependent, and hence can provide a precise indication of the wave slope. It is significant that the most celebrated experimental characterization of ocean slope distributions were carried out using sunglint, by [1]. The deviations from gaussianity of the wave slope were able to be determined in this experiment, but none, however, was forthcoming about the spectral distribution of wave power arising from nonlinear interactions, or otherwise.

More recently, [2] has developed a model to retrieve wavenumber spectra from images of sunglint, by determining an invertible relationship between the slope and glint autocorrelations. This technique is highly appealing for its simplicity and ease of implementation. However, this method as implemented relies on the relationship between second order statistical functions of the wave slope and sunglint data, and as such is insensitive to characteristics of the wave surface that would arise from a consideration of higher order terms in the hydrodynamic equations of the wave surface, such as phase coupling between wave components, wave tilting and energy transfer between wave modes.

The work reported in this paper extends the second order technique to account for nonlinear hydrodynamic effects, and shows how additional information about the sea surface geometry and dynamics can be extracted. This was achieved by formulating, and then inverting, a relationship between the wave slope and sunglint triple correlation functions, the fourier transforms of which are the corresponding *bispectra*. The bispectrum $B(k_1, k_2)$ of the wave slope provides an indication of the various wavenumber triads which simultaneously satisfy the relationships $k_1 + k_2 = k_3$ and $\phi_1 + \phi_2 = \phi_3$, for the wavenumber and phase respectively.

It was found that the nonlinear process of clipping the wave slope to model the sunglint introduces broadband phase correlations which manifest themselves in the real part of the sunglint bispectrum, and the imaginary sunglint bispectrum has a small peak corresponding to the phase correlation in the slope bispectrum. As a result of the spurious phase correlations introduced by the clipping process, the sunglint bispectrum, and hence the sunglint triple correlation function, was relatively insensitive to the phase correlations introduced to the slope realisations, reducing the effectiveness of the retrieval of the slope bispectrum. There is scope however for further refinement of the modelled relationship between the slope and sunglint bispectra, which will likely see some improvement in the fidelity of the sunglint bispectrum retrieval.

REFERENCES

1. Cox, C. and W. Munk, "Measurement of the roughness of the sea surface from photographs of the sun's glitter," *J. Opt. Soc. Am.*, Vol. 44, No. 11, 838–850, 1954.
2. Alvarez-Borrego, J., "Wave height spectrum from sunglint patterns: an inverse problem," *J. Geophys. Res.*, Vol. 98, No. C6, 10245–10258, 1993.

Monitoring of Satellite Thermal Pattern of Ocean Front between Coastal and Ocean Water

S. Nakamura
Kyoto University, Japan

Abstract— A satellite thermal pattern of ocean front facing coastal water is introduced which was obtained by a direct receiving of a satellite signal for sea surface thermal pattern in an infrared band at a station in order to demonstrate the ocean front evolution.

Radar Cross Section of Simple and Complex Targets in the C-band: A Comparison between Anechoic Chamber Measurements and Simulations

M. A. Alves[1], **I. M. Martins**[2, 3], **M. A. S. Miacci**[2], **and M. C. Rezende**[1]

[1]Instituto de Aeronáutica e Espaço, Materials Division, Brazil
[2]Instituto Tecnológico de Aeronáutica, Brazil
[3]Universidade de Taubaté, Brazil

Abstract— Detailed measurements of the radar cross section (RCS) of targets in an indoor environment can be a complex task due to factors such as spurious reflections and instrumental errors, which may interfere with the measurements. In order to validate RCS measurements performed in an anechoic chamber, experimental results are compared with simulations made using a commercial electromagnetic software package. The experimental part of this work was performed inside a anechoic chamber, with the radar operating in the C-band (6 GHz) in a quasi-monostatic configuration and horizontal polarization. Two metallic targets, a cylindrical body with four square fins and a section of an actual air-to-air missile, were used for the RCS measurements. In order to improve the accuracy of the experimental data, an active noise suppressing system, based on the principle of phase cancellation, was used [1]. This system performs a sample of the transmitted signals, discriminates signals from spurious reflections and executes the phase translation of the received signals until they are canceled, reducing the interferences to a minimum. The simulation software FEKO [2] was used to calculate the RCS of models of these two targets. FEKO uses the multilevel fast multipole method (MLFMM), which is a fast and efficient algorithm for solving large-scale RCS problems. MLFMM results in significant reduction in CPU and memory usage, allowing the use of use of off-the-shelf computers to solve complex electromagnetic problems. The comparison of simulations and experimental data revealed a good agreement between them, validating the experimental methods used in the collection of RCS data, as well as the results obtained from the simulation software.

REFERENCES

1. Miacci, M. A. S., I. M. Martins, and M. C. Rezende, "Implementation of an active noise suppression system in C-band indoor RCS measurements," *Proceedings of the International Microwaves and Optoelectronics Conference*, 1–4, Salvador, Brazil, November 2007.
2. EM Software and Systems-S. A. (Pty) Ltd, 2007, http://www.feko.co.za.

Angular Radiation of Gold Nanoshells

Ying Hu[1] **and Rebekah Drezek**[1, 2]

[1]Department of Bioengineering, Rice University, USA
[2]Department of Electrical and Computer Engineering, Rice University, USA

Abstract— Nanoshells are popular contrast agents for scattering-based applications, such as Optical Coherence Tomography (OCT), reflectance spectroscopy and microscopy imaging. Conventionally composed of a silica core coated with a thin layer of gold, the extinction peak of nanoshells has been studied as functions of shell thickness, scaled by particle size, and coating materials, surrounding media, as well as for composite multilayer structures. The angular scattering properties, however, have not been systematically investigated. This leaves a gap in understanding the optical enhancement by nanoshells in applications where detection angle and angular acceptance range may inherently differ. The paper addresses this issue by investigating the dynamic radiation pattern of both silica-gold and gold-silica-gold nanoshells as functions of excitation wavelength and geometrical composition.

A computational code based on Mie theory is developed for multilayer concentric spheres. The angular intensity is calculated with water as surrounding medium in the visible-NIR region. While Mie theory describes in general that the degree of radiation symmetry and total radiation power are related to the overall particle size scaled by wavelength, nanoshells bear modulated angular scattering profile due to their highly tunable extinction cross-section. For silica-gold nanoshells with an outer radius of 100 nm, for instance, the wavelength at which radiation pattern becomes isotropic is found directly correlated to the extinction peak wavelength, which is in turn determined by the inner core radius with otherwise fixed configuration. The radiation at shorter wavelengths is mainly forward directed and that at longer wavelengths retains the isotropic shape with slightly backward distortion. For gold-silica-gold nanoshells, addition of an extra gold core further complicates the radiation pattern by introducing multiple extinction peaks and valleys. This complication is also observed to make radiation lobes less tapered for larger particles. For nanoshells smaller than 100 nm in radius, the radiation pattern is found strongly symmetrical in both front and back direction.

Analysis of Two-dimensional Scattering by a Periodic Array of Conducting Cylinders Using the Method of Auxiliary Sources

Naamen Hichem and Taoufik Aguili
Ecole Nationale d'ingénieurs de Tunis
Département Technologie de l'information et de Communications, Tunisia

Abstract— The method of auxiliary sources is a numerical technique used extensively to solve boundary problems [1]. According to the MAS, the EM fields within each domain expressed as a linear combination of analytical solutions of Helmoltz equation. These particular solutions constitute the base of auxiliary sources placed on the auxiliary contour surrounded by the physical one [2].

The MAS applied to model coupling between different, infinitely, and parallel conducting cylinders, illuminated by a monochromatic plane wave. The coupling modelled by the mutual satisfaction of the boundary conditions just on the collocation points of every cylinder.

These boundary conditions lead to a linear system having as solution the amplitude and phase of scattered field [3].

In the general case, every constitutive part of an array interacts with the rest of the array in the purpose to model exact coupling between different parts witch leads to a completely filled matrix entraining a difficult computation.

In the order to decrease the memory cost, we suppose that every cylinder coupled with the adjacent or the two adjacent one. The mathematical calculus shows that the global matrix is fully simplified and the implementation code realized with Mathematica justify the low computational cost achieved by this approximation.

Numerical results (RCS, pattern field) reveal good agreement with references [5, 6].

At the end, we have numerical results justifying the technique and the possibility to extend it to macro arrays (or for the other parts of the physical problems involving many mutual interactions...).

REFERENCES

1. Shubitidze, F., H. T. Anastassiu, and D. I. Kaklamani, "An improved accuracy version of the method of auxiliary sources for computational electromagnetics," *IEEE Transactions on Antennas and Propagation*, Vol. 52, No. 1, January 2004.
2. Anastassiu, H. T., et al., "Electromagnetic scattering analysis of coated conductors with edges using the method of auxiliary sources (MAS) in conjunction with the standard impedance boundary condition (SIBC)," *IEEE Transactions on Antennas and Propagation*, Vol. 50, No. 1, January 2002.
3. Kaklamani, D. I. and H. T. Anastassiu, "Aspects of the method of auxiliary sources (MAS) in computational electromagnetics," *IEEE Transactions on Antennas and Propagation*, Vol. 44, No. 3, June 2002.
4. Harrington, R. F., *Time Harmonic Electromagnetic Fields*, McGraw-Hill, New York, 1961.
5. Henin, B. H., A. Z. Elsherbeni, and M. A. Sharkawy, "Oblique incidence plane wave scattering from an array of dielectric cylinders," *Progress in Electromagnetic Research*, PIER 68, 261–279, 2007.
6. Elsherbeni, A. Z. and M. Hamid, "Scattering by parallel conducting circular cylinders," *IEEE Transactions on Antennas and Propagation*, Vol. AP-35, No. 3, March 1987.

The Study of Electromagnetic Wave's Absorbing in Micro-periodical Structure

Yan Zhou
Baskin School of Engineering, University of California, Santa Cruz, USA

Abstract— The simulation of the micro-periodical structure's absorbing is present in this paper. Based on the research of structural absorb theory, PBG structure character and HIS controlling patch connection method, multilayer micro-periodical structure unit is set up numerically and connect to each other with the active controlling device - varactor. We establish the effective simulation method with software- HFSS for electromagnetic wave's absorbing in one layer, two layer and multilayer micro-periodical structure. The simulation result prove that multilayer micro-periodical structure could decrease the reflection of vertical incident wave more than 10 dB on same frequency band by the controlling of active device effectively. The relative frequency band will be extended in multilayer micro-periodical structure.

Scattering by Lossless Double-negative Metamaterial Slabs

G. Gennarelli and G. Riccio
DIIIE-University of Salerno
Via Ponte Don Melillo, Fisciano, Salerno 84084, Italy

Abstract— In the recent years, metamaterial structures have attracted considerable attention because of their interesting properties and potential applications. They are formed by embedding inclusions and material components in host media to achieve composite media that may be engineered to have qualitatively new physically realizable response functions not easily available in nature [1].

This work deals with the construction of an approximate uniform high-frequency solution for evaluating the field diffracted by the edge of a lossless and isotropic double-negative (DNG) layer illuminated at oblique incidence by a plane wave. The key points to do this are those of considering the radiation integral with a Physical Optics (PO) approximation of the involved current densities, and of attenuating the analytical difficulties by modelling the structure as an infinitesimally thin sheet. The effects of geometric, electric and magnetic characteristics are properly taken into account through boundary conditions. Accordingly, electric and magnetic PO surface currents are here assumed as equivalent sources originated by the discontinuities of the tangential components of the magnetic and electric fields across the slab. Now, by taking into account that the field approaching the slab from the upper side is given by the sum of the incident and reflected fields, whereas the transmitted field furnishes the field approaching the slab from the lower side, these equivalent currents can be easily expressed in terms of the Geometrical Optics (GO) response of the structure. In this framework, the reflection and transmission coefficients of the DNG metamaterial slab are obtained by following the approach reported in [2]. A useful approximation and a uniform asymptotic evaluation of the resulting radiation integral allow one to obtain the three-dimensional diffraction coefficients, which are expressed in terms of the standard transition function of the Uniform Theory of Diffraction (UTD) [3]. The here proposed solution belongs to the set of the Uniform Asymptotic PO (UAPO) solutions developed in recent years to solve many diffraction problems (see [4] as reference for the approach).

Numerical results show that the GO field discontinuities at the reflection and incidence shadow boundaries are perfectly compensated by the UAPO diffracted field contribution. The corresponding solution results to be efficient, easy to handle and simple to implement in a computer code, so that it can be very useful in all applications wherein the truncation effects in DNG metamaterials cannot be neglected. Moreover, at the best authors knowledge, other solutions for the considered problem are not present in literature.

REFERENCES

1. Engheta, N. and R. W. Ziolkowski, "A positive future for double-negative metamaterials," *IEEE Trans. Microw. Theory Tech.*, Vol. 53, No 4, 1535–1556, 2005.
2. Cory, H. and C. Zach, "Wave propagation in metamaterial multi-layered structures," *Microwave Opt. Based Technol. Lett.*, Vol. 40, No. 6, 460–465, 2004.
3. Kouyoumjian, R. G. and P. H. Pathak, "A uniform geometrical theory of diffraction for an edge in a perfectly conducting surface," *Proc. IEEE*, Vol. 62, No. 11, 1448–1461, 1974.
4. Gennarelli, C., G. Pelosi, C. Pochini, and G. Riccio, "Uniform asymptotic PO diffraction coefficients for an anisotropic impedance half-plane," *Journal of Electromagnetic Waves and Applications*, Vol. 13, No. 7, 963–980, 1999.

Mie Resonances in Small Particles with Electric and Magnetic Properties

Braulio García-Cámara[1], **Fernando Moreno**[1], **Francisco González**[1]
José María Saiz[1], **and Gorden Videen**[2]

[1]Grupo de Óptica, Departamento de Física Aplicada, Universidad de Cantabria
Avda de los Castros, s/n 39005 Santander, Spain
[2]Army Research Laboratory, 2800 Powder Mill Road, Adelphi, Maryland 20783, USA

Abstract— The study of light interaction with particles of size much smaller than the incident wavelength has become, in the last years, an important research topic because of its interest in the field of nanotechnology [1]. Resonant behaviours from metallic nanoparticles have especial relevance in this field due to interesting applications in Medicine, Biology or Industry [2, 3].

Many works have studied these resonances from isolated particles, dimers, aggregates or particles above substrates [4, 5 and references there in]. In these cases, particles with electric and non-magnetic response to the incident electromagnetic wave have been considered. Furthermore, the recent interest in the analysis of materials with engineered optical properties (metamaterials) has pushed research in the study of light-matter interaction when the latter presents unconventional optical constants [6]. Bearing this in mind, the purpose of this work it is to perform a detailed study of the light scattering resonances of a spherical isolated particle with a size much smaller than the incident wavelength with electric and magnetic properties (ε, $\mu \neq 0$).

In a previous work, we introduce generalized and approximate expressions of the first four Mie coefficients (a_1, b_1, a_2 and b_2) [7]. From these expressions, in this research we analyze the evolution of the number, position and width (with respect to ε and μ) of the electric and magnetic dipolar and quadrupolar, resonances as a function of the optical properties and size of the particle.

Finally, we also study the evolution of the angular distribution of the scattered intensity by these particles for some interesting resonant cases as a function of particle size.

This research has been supported by project FIS2007-60158 and Braulio García-Cámara wishes to thank to University of Cantabria for his PhD grant.

REFERENCES

1. Prasad, P. N., *Nanophotonics*, Wiley-Interscience, 2004.
2. Kreuzer, M., et al., *Biosensor and Bioelectronics*, Vol. 21, 1345–1349, 2006.
3. Pillai, S., et al., *J. Appl. Phys.*, Vol. 101, 093105, 2007.
4. Jensen, T., et al., *J. Clus. Scien.*, Vol. 10, 295–317, 1999.
5. Moreno, F., F. González, and J. M. Saiz, *Opt. Lett.*, Vol. 31, 1902–1904, 2006.
6. Engheta, N., *Science*, Vol. 317, 1698–1702, 2007.
7. García-Cámara, B., et al., *J. Opt. Soc Am. A*, to be published.

Light Scattering by Interacting Electric and Magnetic Polarizable Particles

O. Merchiers[1], **F. Moreno**[2], **F. González**[2], **and J. M. Saiz**[2]

[1]CETHIL — Centre de Thermique de Lyon, UMR 5008, Villeurbanne 69621, France
[2]Grúpo de Óptica, Departamento de Física Aplicada, Universidad de Cantabria, Santander 39005, Spain

Abstract— The study and development of metamaterials and, more specifically, of the left handed materials (LHM) which are capable of negative refraction is currently a research field of enormous interest. Those metamaterials are built from basic elements (split ring resonators, parallel nanorods, nano fishnets etc...) made from classic materials which have a magnetic permeability $\mu = 1$, but due to their specific design, a magnetic response is obtained, and on a macroscopic scale one has an effective medium with $\mu_{\text{eff}} \neq 1$. The Discrete Dipole Approximation (DDA) has shown to be usefull in order to get insight into optical properties of regular particle arrays [1]. In the case of metamaterials, the elementary building blocks have a magnetic polarizability and the usual DDA formalism has to be extended in order to account for the magnetic dipole moments. This generalization has been done by Lakhtakia [2].

Furthermore, high values of μ_{eff} are usually obtained by placing the subunits in resonance. Knowledge of the building blocks' resonance structure and how it is affected by the presence of neighbouring elements is very important. A powerful tool to perform this analysis is the spectral decomposition of the interaction matrix. This method has been widely studied in case of purely electric interacting dipoles. In a recent publication we describe for the first time this method for interacting electric and magnetic dipoles [3]. Here we present this generalization.

On the other hand, a theoretical study by Kerker et al. [4] showed that small spheres with $\mu \neq 1$ present unusual scattering behaviour like the suppression of either the forward or the backward scattering. The generalization of the eigenvalue decomposition for dipoles with both electric and magnetic polarizabilities we present is thus equally useful to study more hypothetical systems composed of small particles with $\mu \neq 1$. We apply the eigenvalue decomposition for dipoles with both electric and magnetic polarizabilities to the most elementary case of $N = 2$ for which we give a closed mathematical form of the eigenvalues and eigenvectors.

ACKNOWLEDGMENT

The authors wish to thank the Dirección General de Enseñanza Superior for its financial support (project FIS2007-60158).

REFERENCES

1. De Abajo, F. J. G., *Reviews of Modern Physics*, Vol. 79, 1267–24, October 2007.
2. Lakhtakia, A., *Astrophysical Journal*, Vol. 394, 494–499, August 1992.
3. Merchiers, O., F. Moreno, F. González, and J. M. Saiz, *Physical Review A*, Vol. 76, No. 4, 043834, 2007.
4. Kerker, M., D.-S. Wang, and C. L. Giles, *JOSA*, Vol. 73, No. 3, 765–767, 1982.

Fractal Cantor Multilayer in Rectangular Metal Waveguide

F. Chiadini[1], **V. Fiumara**[2], **I. Gallina**[3], **S. T. Johnson**[1], **and A. Scaglione**[1]

[1]Department of Electrical and Information Engineering, University of Salerno, Italy
[2]Department of Environmental Engineering and Physics, University of Basilicata, Italy
[3]Department of Engineering, University of Sannio, Italy

Abstract— The triadic Cantor multilayer is a simple and feasible one-dimensional fractal multilayers. It consists of a stack of alternating media of different type with thicknesses obtained by enforcing the Cantor fractal construction to either geometrical or the optical length of layers [1].

The electromagnetic response of a triadic Cantor multilayer exhibits forbidden frequency bands as well as very narrow transmission peaks thus showing attractive features for devices in the microwave frequency band (frequency selective surfaces, filters, sensors, etc.).

In this work we analyze transmission spectra of triadic fractal Cantor multilayers inserted in a rectangular waveguide for microwave frequency range. Filtering features (bandwidth, quality factor of the transmissivity peaks) of such structures are described and their relationship to the fractal parameters (stage of growth, permittivities of the layers, material losses) are discussed. The field localization phenomenon occurring in the fractal multilayer at the frequencies corresponding to the transmission peaks of its spectral response is also described.

Cantor structures in WR-90 waveguides (8.2–12.4 GHz) have been realized by inserting a stack of plexiglass and styrofoam (permittivity close to the air) layers. Measurements of transmission spectra and comparison with the expected theoretical ones are described.

REFERENCES

1. Chiadini, F., V. Fiumara, and A. Scaglione, "Transmission properties of perturbed optical Cantor multilayers," *J. Appl. Phys.*, Vol. 100, Art. No. 023119, 2006.

Rectangular Junction Ferrite Component in Millimeter Waves

D. Vincent
Saint-Etienne University, France

Abstract— Non reciprocal microwave components in millimetre waves, such as circulators, are based on the gyro-resonance properties of a ferrite material. The integrating of self-biased ferrite devices seems to be possible using thin-film processes [1, 2] or composite materials which can be made from magnetic nano-particles scattered into a host dielectric matrix. The component on study is a "rectangular circulator" made from a stripline structure. There is an inner conductor located between the ferrite slabs and the ground-planes (see Figure 1). The structure can be have three or more ports. The connections do not require bent access lines.

An analytical model can be developed with the same approximations used by Bosma [3] for circular Y-junction circulator. Only the z-axis electric field component, the y-axis and x-axis magnetic field components are considered. A magnetic wall is referred on the ferrite edge.

The Green's function method is used with inhomogeneous boundary conditions to avoid the same location of the source and the observation points.

The non-reciprocal effect is due to the field displacement when a d.c. magnetic field is applied to the ferrite slabs along the z-axis direction.

The analytical model can be compared to numerical simulation results obtained from a 3D software (HFSS). Although some differences which could be due to the access lines, the analytical and numerical methods are in good agreement. The analytical model allows us to determine rapidly the rectangle size, then the design can be improved using the 3D simulation software.

For example, even if the impedance matching is not performed, Figure 2 shows a broadband circulation effect from 40 GHz to 45 GHz. Many parameters which determine the component performances (the ferrite electromagnetic properties and its thickness, dimensions, the access line width, the applied d.c. field intensity) have been studied. The final article will show important results allowing us to design efficient rectangular junction component.

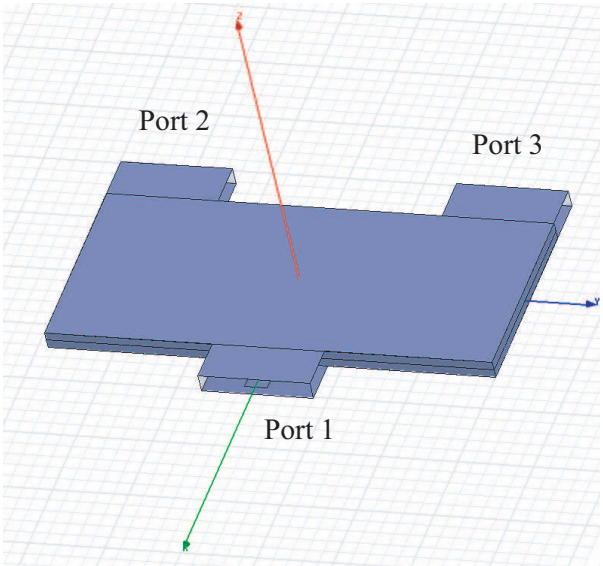

Figure 1: Rectangular junction circulator structure.

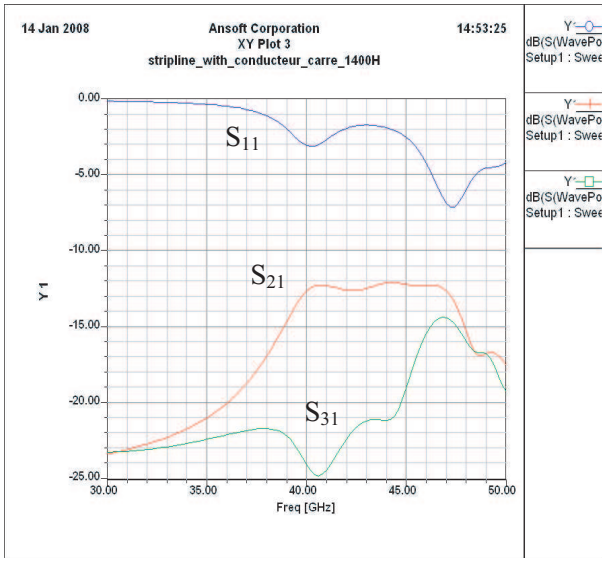

Figure 2: Simulation results S_{11}, S_{21} and S_{31} (dB) obtained from HFSS software.

REFERENCES

1. Olivier, A., P. Shi, and C. Vittoria, *IEEE Trans. Microwave Theory Tech.*, Vol. 49, 385–387, Feb. 2001.
2. Tsankov, M. A. and L. G. Milenova, *J. Appl. Phys.*, Vol. 73, No. 10, 7018–7020, May 1993.
3. Bosma, H., *IEEE Trans. Microwave Theory Tech.*, Vol. 12, 61–72, Jan. 1964.

Modelling SIW Resonators Using Support Vector Regression Machines

G. Angiulli[1], **D. de Carlo**[1], **S. Tringali**[1], **G. Amendola**[2], **and E. Arnieri**[2]

[1]DIMET, Univ. Mediterranea, 89100 Reggio Calabria, Italy
[2]DEIS, Univ. Della Calabria, 87036 Rende (Cs), Italy

Abstract— The Substrate Integrated Waveguide (SIW) technology combines the advantages of the low cost fabrication in printed technology and the low loss characteristics typical of waveguide devices. Using the SIW approach, high factor quality waveguide components and planar circuits can be integrates at low cost using standard printed circuit board processes [1]. A large number of SIW-based devices have been realized in these last years. Many of them, like filters, are based on SIW resonators (see [2, 3] and references within). Very recently, in order to develop fast cad models of microwave components and devices, Support Vector Regression Machines (SVRMs) have been proposed [4]. Support Vector Machines, (SVMs) developed by Vapnik and co-workers [5] are gaining popularity due to many attractive features capable to overcome the limitations connected to Artificial Neural Networks (ANNs). This is due to the Structural Risk Minimisation principle embodied by SVMs, which has been demonstrated to be more effective than the traditional Empirical Risk Minimisation principle employed by ANNs (see [5] and references within). This different philosophy equips SVMs with a greater ability to generalise, if compared with ANNs. At first, SVMs were developed to solve classification problems (see [6] and references within), but subsequently they have been extended to the area of regression problems (see [7] and references within). In this work we investigate the performances of SVRMs to model SIW resonators. Obtained results, compared with published and measured ones [8], are very promising and suggest that SVRMs can be fruitfully employed to obtain an accurate caracterization of the SIW resonators in real time.

REFERENCES

1. Deslandes, D. and K. Wu, "Integrated microstrip and rectangular waveguide in planar form," *IEEE Microwave and Wireless Components Letters*, Vol. 11, No. 2, 1064–1076, 2001.
2. Potelon, B., J. C. Bohorquez, J. F. Favennec, C. Quendo, E. Rius, and C. Person, "Design of Ku-band filter based on substrate integrated circular cavities (SICCs)," *IEEE MTT-S Int. Microw. Symp. Dig.*, 1237–1240, 2006.
3. Tang, H. J. and W. Hong, "Substrate integrated waveguide dual mode filter with circular cavity," *Joint Int. Conf. on Infrared Millimeter Waves and on Terahertz Electronics*, 339, 2006.
4. Angiulli, G., M. Cacciola, and M. Versaci, "Microwave devices and antennas modelling by support vector regression machines," *IEEE Transactions on Magnetics*, Vol. 43, No. 4, 1589–1592, 2007.
5. Cortes, C. and V. Vapnik, "Support vector network," *Machine Learning*, Vol. 20, 273–297, 1997.
6. Angiulli, G., M. Cacciola, and V. Barrile, "SAR imagery classification using multi class support vector machines," *Journal of Electromagnetic Waves and Applications*, Vol. 19, No. 14, 1865–1872, 2005.
7. Gunn, S. R., "Support vector machines for classification and regression," ISIS Technical Report, 1998.
8. Amendola, G., G. Angiulli, E. Arnieri, and L. Boccia, "Analysis and characterization of circular substrate integrated resonators," *IEEE Microwave and Wireless Components Letters*, accepted for publication.

Microwave Unpolar Organic Reactions Using Microwave Absorber

Chunyan Huo, **Jianhua Chen**, **Haisheng Xu**, **and Dong Shen**

Laboratory of Chemical Physics, East China University of Science and Technology
Shanghai 200237, China

Abstract— Organic reaction with low polarity is excluded by the microwave-assisted reaction because of the poor microwave absorption of the reaction mixture. To solve this problem, some methods such as ionic liquid, polar solvent, or cylinder of sintered silicon carbide were reported to adding to the reaction. Compared with the ionic liquid and polar solvent, cylinder of sintered silicon carbide has the advantages of thermo-stability and chemical inertance. As an inorganic additive, SiC can not be dissolved in the reaction medium, so the transferring of energy is not the most efficient due to the limited interface, however, using cylinder of sintered silicon carbide can enhance the unpolar microwave reactions significantly.

Another inorganic microwave absorber, C, attracted our attention because of its strong microwave absorption, different kinds of C, active carbon, graphite powder, micrometer and nanometer carbon were applied to the reactions with polarity from middle to low in an multimode microwave reactor equipped with condenser and stirrer, the results show all of them can enhance the reactions efficiently, even the middle polar reactions. Graphite powder was the most efficient but has flame when the reaction was not stirred. Nanometer carbon has the similar efficiency with active carbon but is much more expensive, and micrometer carbon was the worst, so active carbon is the best for application. Although there was ever before worried about the possibility of ignition of active carbon because there was great temperature grade between active carbon and reaction mixture, there is never happed in our experiments whatever the reaction was stirred or not, indicates active carbon is stable enough and the energy transferring is efficient. It is surprised that active carbon has the similar efficiency with the nanometer carbon although it has much more large size, maybe it was because of its strong absorption of reagents, its application in synthetic chemistry is expected.

Direct Observation of Higher-order Whispering-gallery Modes in a Defect-free Surface Micro-structure VCSEL

Chih-Yao Chen[1], **Yuan Yao Lin**[1], **Tsin-Dong Lee**[2], **and Ray-Kuang Lee**[1]

[1]Institute of Photonics Technologies, National Tsing-Hua University, Hsinchu 300, Taiwan
[2]Graduate School of Optoelectronics, National Yunlin University of Science and Technology
Yunlin 640, Taiwan

Abstract— Whispering-gallery modes (WGMs) are almost grazing incidence patterns confined by the total internal reflection at the interface. With advantages of small mode volume and strong confinement WGMs have attracted much attention in photonics, quantum electrodynamics, and telecommunications, due to their potential application to enhance spontaneous emission and make threshold-less lasing. With optical output vertically emitted from the surface, vertical cavity surface emitting lasers (VCSELs) is a natural choice for lasers with transverse behavior of a WGM and a vertical emission. Typically, WGMs surrounded in such various types of defect cavities are lowest-order modes due to that the defect geometry is with the same order of magnitude to the lasing wavelength. In this work, a 2D photonic crystal micro-structure is fabricated on a VCSEL surface to investigate the transverse optical pattern formation by directly collecting near-field radiation intensity. Instead of forming a defect cavity, we propose to use the surface structure as a deterioration mechanism for the desired lasing characteristics. As the whole vertical emission window of VCSEL is destroyed by the surface micro-structure, we report the observation of higher-order WGMs confined laterally by the native oxide layer in a GaAs-based VCSEL at room temperature. Through the suppression of lower-order cavity modes, up to the 23rd azimuthal order whispering-gallery mode is observed both in experiments and simulations. Moreover, we show that by increasing the injection current, different vertical emission transverse patterns, corresponding to the superposition of modes at different wavelengths, are identified both by the spectrum in experiments and simulations.

Surface-structure-assisted Unidirectional Lasing from a Deformed VCSEL

Chih-Yao Chen[1], **Yuan Yao Lin**[1], **Tsin-Dong Lee**[2], **and Ray-Kuang Lee**[1]

[1]Institute of Photonics Technologies, National Tsing-Hua University, Hsinchu 300, Taiwan
[2]Graduate School of Optoelectronics, National Yunlin University of Science and Technology
Yunlin 640, Taiwan

Abstract— Microcavities provide a controllable confinement and manipulation of photons in all three spatial dimensions. Intense research studies based on microcavities have been carried out in the last decades, e.g., on ultralow threshold lasing, single-photon emitting, cavity quantum electrodynamics, and mesoscopic quantum optics. For the transverse directions, confined by the total internal reflection at the interface, small mode volume and strong confinement whispering gallery modes (WGMs) have been demonstrated in microdisks, microspheres, and microtori. For the vertical direction, confined by high reflective Bragg mirrors, vertical cavity surface emitting lasers (VCSELs) are a natural choice for lasers with transverse behavior of a WGM and an optical output emitted vertically from the surface. Due to rotational symmetry in the transverse cavity geometry, the in-plane light emission in these microcavities is isotropic. Recently, various directional light emitting could be achieved by smoothly deformed the cylindrical cavities. To break rotational symmetry of a microcavity, various types of deformed microcavities, especially asymmetrical resonant cavities, have been well known in semiconductor microresonators for scar modes and chaotic dynamics. In this work we introduce a new scheme to design optical deformed microcavities in VCSELs. Instead of breaking the symmetry in the transverse shape, a surface ring cavity is fabricated on top of the VCSEL with a slightly mismatch between the surface-structure and the native oxide layer. Experimental observation of whispering-gallery modes supported by the native oxide layer is reported at low injection current. By increasing the injection current, unidirectional lasing at the mismatched boundary is demonstrated.

A Novel Broadband Compact Circular Disk Microstrip Antenna for Wireless Applications

H. A. Osman[1], **E. A. Abdallah**[2], **and A. A. Abdel Rhim**[1]

[1]Arab Academy for Science & Technology and Maritime Transport, Egypt
[2]Electronics Research Institute, Egypt

Abstract— The modern wireless communication networks need compatible antennas for compactness and broad bandwidth. Circular and annular ring microstrip antennas are the best candidate configurations for compactness. But these microstrip antennas suffer from the inherent narrow bandwidth. This paper investigates several approaches for improving the bandwidth of an antenna used in the Wireless Local Area Network (WLAN) operating at 5.2 GHz. The percentage bandwidths of conventional circular disk and annular ring microstrip antenna designed at this frequency are found to be 3.4% and 3.7%, respectively. The dielectric substrate is RT-Duroid 5880 ($\varepsilon_r = 2.2$, $h = 1.575$ mm). A study of circular and annular ring microstrip antenna supported by a layer of air is presented in both the normal and inverted configurations by changing the air thickness. Consequently, the percentage bandwidth for circular disk microstrip antenna in the normal and inverted configuration is found to be 15.5% and 12.36%, respectively and for the annular ring microstrip antenna is 7.23% and 6.22%, respectively at an optimum air thickness of 3 mm. On the other hand, embedding a suitable slot on the surface of the patch leads to increasing the percentage bandwidth as long as the resonance frequencies of the slot and the patch are close to each other [1]. A percentage bandwidth of circular disk with U-slot is found to be more than 24%. A novel shape is proposed having a reduction of the conventional size by 85% (see Fig. 1). Two substrate layers of the same parameter ($\varepsilon_r = 2.2$, $h = 1.575$ mm) are stacked and spaced by an air layer of thickness 3 mm. The feeding layer (coaxial probe) contains a simple conventional circular disk with radius 10.65 mm while the radiating layer contains the proposed novel shape that has slightly reduced radius of 9.65 mm (see Fig. 2). The feed location is about 6 mm from the center with radius of 0.4 mm. The suggested design is optimized by the electromagnetic ready-made software Zeland IE3D. Fortunately, a percentage bandwidth of more than 33% is found (see Fig. 3) covering the frequency range from 4.8 GHz up to 6.1 GHz compared to 11% achieved before at 2.4 GHz [2].

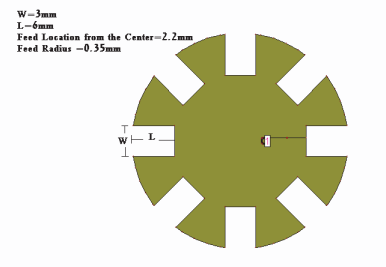

Figure 1: Novel shape.

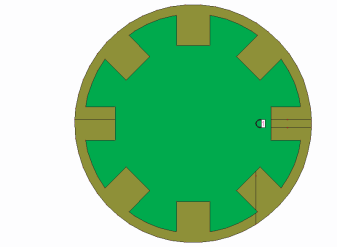

Figure 2: Stacked novel shape.

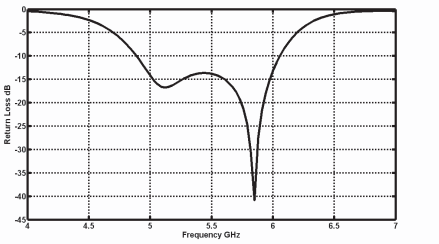

Figure 3: S_{11} vs. Frequency.

REFERENCES

1. Bhalla, R. and L. Shafai, "Resonance behavior of single U-slot microstrip patch antenna," *Microwave and Optical Technology Letters*, Vol. 32, No. 5, 333–335, March 2002.
2. Abdullah, R., D. Yoharaaj, and A. Ismail, "Bandwidth enhancement technique in microstrip antenna for wireless application," *PIERS Online*, Vol. 2, No. 6, 633–639, 2006.

Parametric Amplification of Space Charge Waves in n-GaN Film

Abel García-B.[1] **and V. Grimalsky**[2]

[1]Departamento de Mecatrónica, Universidad Politécnica de Pachuca (UPP)
Km. 20 Carretera Pachuca-Cd. Sahagun, Zempoala, Hidalgo, C.P 43830, Mexico
[2]Facultad de Ciencias, Universidad Autónoma del Estado de Morelos (UAEM)
Cuernavaca, C.P 62210, México

Abstract— The linear interactions of microwaves and their amplification in GaN films have been studied recently. But, the three-wave parametric interactions of space charge waves in GaN films, possessing negative differential conductivity in bias electric field, are of great interest, because of a possibility to realize frequency up-conversion with amplification. The space charge waves in thin semiconductor films can propagate in microwave and millimeter wave range, and possible frequencies are higher than ones of acoustic and spin waves in solids. In the paper, the three-wave parametric interactions with amplification of transversely limited beams of space charge waves in microwave and millimeter wave ranges in semiconductor films (n-GaN) possessing negative differential conductivity are analyzed. Two-dimensional electron gas model is used, and the numerical simulations based on solving a set of nonlinear partial differential equations for non-local carrier transport (quasihydrodynamic equations) and the Poisson's equation for electric field have been carried out. We solve the system of equations, the last two equations are for the electric field, the dc electric field is a bias to the film, to obtain the negative differential conductivity, and the ac electric field is accompanied a propagation of space charge wave beams. The first part of the paper gives the system of equations to simulate a propagation of space charge waves, the second part explains the method used. Finally, the results of spectrum of input and output signals are presented.

Miniaturized Bandpass Filter with Self-biased Magnetic Films

G. M. Yang, **A. Daigle**, **X. Xing**, **J. W. Wang**, **and N. X. Sun**
Center for Microwave Magnetic Materials and Integrated Circuits
Department of Electrical and Computer Engineering
Northeastern University, Boston, MA 02115, USA

Abstract— With the continuous growth of wireless communication technologies, design and manufacturing of miniaturized microwave components are among most critical issues in communication systems. The combined high permeability and permittivity of magnetic film materials provide a great opportunity for achieving miniaturized microwave components, such as antennas [1–3] and filters, etc. In order to be practically feasible in miniature microwave circuit applications, such as handheld wireless communication devices, it is important for the circuit substrates to be comprised of self-biased magnetic materials, in which no external bias field is applied. However, it has been challenging in achieving self-biased magnetic materials for microwave circuit substrate applications in the GHz frequency range. This paper introduces a novel miniaturized bandpass filter operating at 1.575 GHz with low insertion loss and simple planar geometry that makes it compatible with the existing microwave integrated circuit. Miniaturization is achieved by loading a commercially available substrate with self-biased magnetic films. One order Chebyshev hairpin bandpass filter was designed with the central working frequency is 1.575 GHz. Self-biased magnetic film, which the relative permittivity is 13 and relative permeability is 10 with zero loss tangent, was adopted in the simulations. Firstly, the ferrite film with the thickness of the 2 μm was added under the hairpin microstrip, and the simulated results show that the central frequency is 1.50 GHz, that is a frequency shift of 75 MHz. Secondly, the ferrite film was covered over the hairpin microstrip, and the central frequency is 1.505 GHz. Finally, two lays of ferrite films were added in our simulation, one is under the hairpin microstrip and another is just over the hairpin microstrip. The simulated results show that the central frequency is 1.45 GHz that is almost 125 MHz frequency shift, which demonstrated the self-biased magnetic films lead to miniaturized bandpass filter without compromising the bandwidth and the insertion loss.

ACKNOWLEDGMENT

Financial supports from ONR Award N00014-07-1-0761 and from Draper Laboratory are gratefully acknowledged.

REFERENCES

1. Sun, N. X., J. W. Wang, A. Daigle, C. Pettiford, H. Mosallaei, and C. Vittoria, "Electronically tunable magnetic patch antennas with metal magnetic films," *Electronics Letters*, Vol. 43, 434, 2007.
2. Yang, G. M., A. Daigle, J. W. Wang, N. X. Sun, and K. Naishadham, "Tunable miniaturized patch antennas at 2.1 GHz using self-biased magnetic films," *2008 IEEE International Workshop on Antenna Technology: Small Antennas and Novel Metamaterials*, Chiba, Japan, March 4–6, 2008.
3. Yang, G. M., A. Daigle, N. X. Sun, and K. Naishadham, "Circular polarization GPS patch antennas with self-biased magnetic films," *PIERS Online*, Vol. 4, No. 3, 2008.

On the Scattering of Ultra-wideband Signals from Objects behind Opaque Structures

Xiaoyang Huang[1], **Hong-Liang Cui**[1], **and Ke Wang**[2]

[1]Department of Physics & Engineering Physics, Stevens Institute of Technology, Hoboken, NJ 07030, USA
[2]Monterey Bay Aquarium Research Institute, 7700 Sandholdt Road, Moss Landing, CA 95039, USA

Abstract— In this study, scattering of the ultra-wideband (UWB) signals from objects behind opaque obstacles will be carried out using Finite-difference Time-domain (FDTD) with Liao's absorbing boundary condition (ABC). The modeling of scattering of UWB signals from objects behind walls has many potential applications such as through-the-wall imaging, and detection and recognition of targets behind the walls. The understanding of the interaction between UWB signals and objects will help design the state-of-art UWB radar systems. Scattering from two-dimensional (2D) metallic and dielectric cylinders behind walls for TE and TM waves are considered as well as scattering from 3D objects with typical shapes such as sphere. Yee's algorithm is used. An electric-field (**E**) grid offset both spatially and temporally from a magnetic-field (**H**) grid to obtain update equations that yield the present fields throughout the computational domain in terms of the past fields. The update equations are used in a leapfrog scheme to incrementally march the **E** and **H** fields forward in time.

The time variance of the UWB signals propagating through the wall and interacting with targets with different materials have been given. The returned signals are observed broadened, deformed, and attenuated. The delay effects of the walls on the received signal have been investigated. In addition, the returned signals from typical 2D and 3D targets behind the walls are analyzed. In the future, a data set will be set up to include typical target signatures for the purpose of the target reconstruction.

Seawater pH Monitoring Using Long Period Grating Sensors

Ke Wang, **Denis Klimov**, **and Zbigniew Kolber**
Monterey Bay Aquarium Research Institute
7700 Sandholdt Road, Moss Landing, CA 95039, USA

Abstract— A long period grating based fiber-optic sensor is developed to monitor the pH in seawater. The long period grating, fabricated by CO_2 laser with a point-by-point technique, is coated with the pH-sensitive hydrogel. The hydrogel, made through thermal crosslink of poly vinyl alcohol (PVA) and poly acrylic acid (PAA), changes its refractive index according to different pH in the seawater. As a result, the resonant wavelength of the long period grating shifts in response to the different refractive indices of the hydrogel. Thus, pH change in seawater can be measured.

In the experiment, the sensor was tested in a seawater chamber, whose pH can be adjusted by pumping CO_2 gas and air into the chamber with controlled flow rates. The pH was controlled between 6.0 and 8.0. The resonant wavelength is monitored by an optical spectrum analyzer and a pH resolution 0.046/nm has been obtained.

Session 3A6
Photonics, Plasmonic & Nano Scale Electromagnetics

Different Unexpected Squeezing of Light in the Short and Long Chain of Coupled Silver Nanowires

H.-S. Chu, W.-B. Ewe, and E.-P. Li

Advanced Electronics and Electromagnetics, A*STAR Institute of High Performance Computing 117528, Singapore

Abstract— Plasmonic nanostructures by mean of the coupling between metallic nanostructures and light have been exploited for various applications in the nano-optical research community. The understanding of plasmonic properties, namely the near field confinement and the scattering characteristic, of coupled nanowires chains consisting of different lengths are especially important. The reason is as numerous coupled nanowires chain waveguides of vastly different lengths may posses various potential applications such as guiding light beyond the diffraction limit [1], surface-enhanced Raman scattering for ultra-sensitive chemical detection [2], and fluorescence through plasmonic resonant light scattering [3]. Therefore, we will focus on the investigation of plasmonic characteristics for a closely grouped vertically-aligned silver nanowires chain with different finite lengths. The results show that the length of coupled silver nanowires chain becomes an important determining factor on the plasmonic characteristics of the system such as the tunable scattering modes and associated intensity confinement effects in the chain. Particularly, the peak resonance wavelength of scattering parameter, Fig. 1, is monotonically increasing with the number of nanowires in the chain and the near field intensity is strongly dependent on the chain length. For the short chain length such as 10 coupled nanowires, the intensity, shown in Fig. 2(a) is significantly confined and enhanced in the gap of two adjacent nanowires. However when the chain length of coupled nanowires increases to 100 coupled nanowires, the intensity is locally focused at the top and bottom halves of the nanowires perpendicular to the direction of wave propagation as shown in Fig. 2(b).

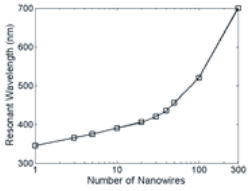

Figure 1: Peak resonance as a function of the number of nanowires in the chain.

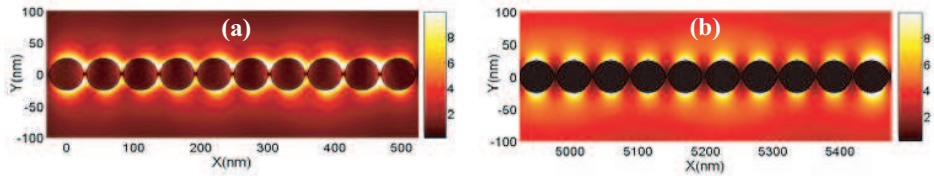

Figure 2: Intensity, observed at plasmonic resonance, as a function of the number of coupled silver nanowires in the chain: (a) 10 nanowires, (b) 100 nanowires.

REFERENCES

1. Brongersma, M. L., R. Zia, and J. Schuler, "Plasmonics — The missing link between nanoelectronics and microphotonics," *PIERS Online*, Vol. 3, No. 3, 360–362, 2007.
2. Felidj, N., J. Aubard, G. Levia, J. R. Krenn, A. Hohenau, G. Schider, A. Leitner, and F. R. Aussenegg, "Optimized surface-enhanced Raman scattering on gold nanoparticle arrays," *Appl. Phys. Lett.*, Vol. 82, No. 18, 3095–3097, 2003.
3. Chen, Y. C., K. Munechika, and D. S. Ginger, "Dependence of fluorescence intensity on the spectral overlap between fluorophores and plasmon resonant single silver nanoparticles," *Nano Lett.*, Vol. 7, No. 3, 690–696, 2007.

Cavity-modulated Resonant Tunneling Effects of Surface Plasmon Polaritons

Yung-Chiang Lan, Chang-Che Jung, and Peng-Hsiao Lee
Institute of Electro-Optical Science and Engineering, National Cheng Kung University
No. 1 University Road, Tainan 701, Taiwan, China

Abstract— Surface plasmons (SPs) are the coherent fluctuations of the electron charges at the metal-dielectric interface. The phenomenon of resonant tunneling through thin metal films with periodic narrow grooves is attributed to excitation of SP via the resonant coupling at the metal surface [1]. The metal cavity, on the other hand, can store the electromagnetic energy and also exhibit the resonant properties. If a cavity is embedded in the metal films with periodic narrow grooves, the frequencies of the SP-induced resonant tunneling would be modified by the cavity.

In this work, the cavity-modulated resonant tunneling of SP in metal film is proposed and studied via computer simulation. The simulated structure is shown in Fig. 1. A p-polarized plane wave is normally incident into a free-standing silver film with periodic grooves on film's both surfaces and embedded periodic cross-type cavities. The finite-difference time-domain (FDTD) method with the Drude dispersion model is utilized in this simulation.

Figures 2 and 3 present the simulated magnetic field contours for the resonant frequencies of 4.92×10^{14} Hz and 5.21×10^{14} Hz, respectively, which have the maximum transmission powers. Our simulation results exhibit that the cross-type cavity has two effects on the resonant tunneling. The first effect is that the cavity modifies the resonant frequencies of the groove structures, which is caused by the SP coupling between the cavity and groove (coupling modes), as shown in Fig. 2. The other effect is that some new tunneling frequencies are introduced by the cavity, due to the resonance of the SP in the arms of the cavity (cavity modes), as shown in Fig. 3. Furthermore, the length and width of the axial part of the cavity will affect the frequencies of the coupling modes, but the length and width of the arms of the cavity will affect the frequencies of the cavity modes. We think these cavity effects will be useful for designing new plasmonics devices.

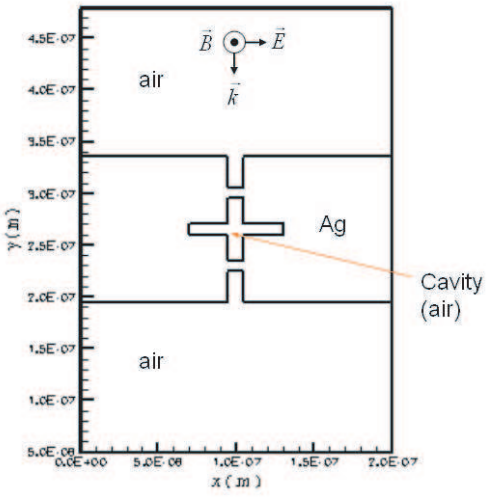

Figure 1: Simulated structure.

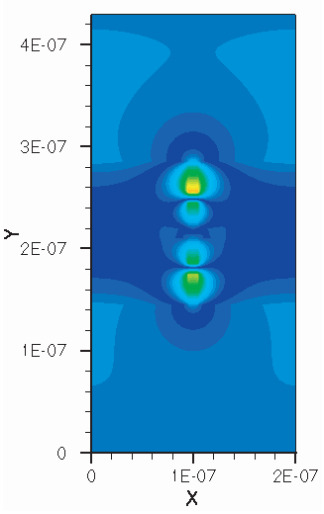

Figure 2: Magnetic field contour for 4.92×10^{14} Hz.

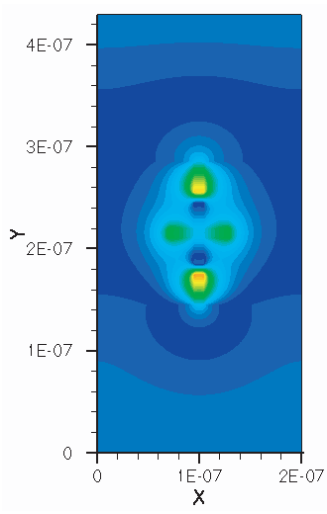

Figure 3: Magnetic field contour for 5.21×10^{14} Hz.

REFERENCES

1. Tan, W. C., T. W. Preist, and J. R. Sambles, *Phys. Rev. B*, Vol. 62, 11134, 2000.

Dispersive Properties and Superluminal Propagation of Surface Plasmon Polaritons in Linear Chains of Metallic Nanoshperoids

Alexander A. Govyadinov[1] **and Vadim A. Markel**[2]

[1]Departments of Bioengineering, University of Pennsylvania, USA
[2]Departments of Radiology and Bioengineering, University of Pennsylvania, USA

Abstract— Periodic linear chains of metallic nanoparticles have recently drawn considerable attention motivated by potential applications in subwavelength wave guiding and nanophotonics. The dispersive properties of surface plasmon polaritons SPPs in such chains composed of Drudean nanospheres has been intensively studied [1–4]. The dispersion curves $\omega(q)$ for the non-radiating SPPs ($q\omega/c$) were previously reported to be very flat, with only a weak dependence of frequency ω on the Bloch wave number q, yielding very slow group velocities v_g and thus, low data rate.

Here we show that this can be dramatically altered by replacing spherical particles with spheroids. In particular the group velocity of the wave packets can be efficiently controlled by varying the aspect ratio of the spheroids. For sufficiently small aspect ratios, a gap appears in the first Brillouin zone of the lattice in which propagating SPPs do not exist. Depending on light polarization this gap extends from a critical value of the wave number, q_c, to either the origin (longitudinal polarization) or to the edge of the first Brillouin zone (transverse). For Bloch wave numbers q close to the critical value $|q - q_c| \ll \pi/h$, with h being the chain period), the dispersion curve acquires a very large positive or negative slope. In both cases wave packets with large magnitudes of group velocity ($v_g \approx c_h$) and possibly superluminal wave packet ($v_g \gg c_h$) are observed, reopening the prospects for fast data transport in linear chains of metallic nanoparticles.

Finally, our theoretical predictions are fully confirmed by frequency domain simulations of pulse dynamics in periodic chains of nanospheroids.

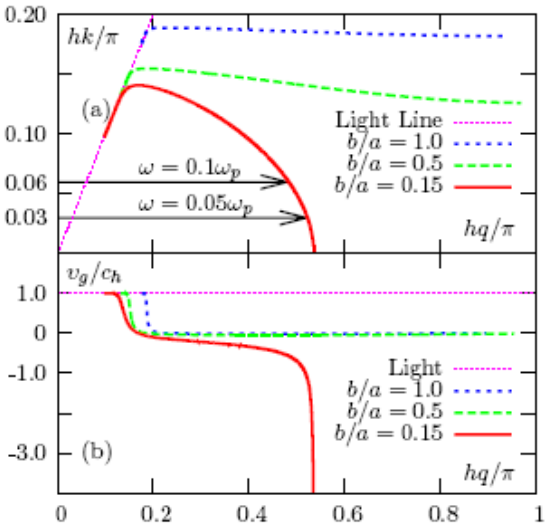

Figure 1: Dispersion curves (a) and group velocities (b) for SPPs with transverse polarizations in linear chains of prolate nano-spheroids.

REFERENCES

1. Weber, W. H. and G. W. Ford, *Phys. Rev. B*, Vol. 70, 125429, 2004.
2. Simovski, C. R., A. J. Viitanen, and S. A. Tretyakov, *Phys. Rev. E*, Vol. 72, 066606, 2005.
3. Koenderink, A. F. and A. Polman, *Phys. Rev. B*, Vol. 74, 033402, 2006.
4. Fung, K. H. and C. T. Chan, *Opt. Lett.*, Vol. 32, 973, 2007.

Artifacts in Near-field Scanning Optical Microscope Spectroscopy and Imaging of Nanoparticles

Shih-Hui Chang and Yun-Chorng Zhang
Institute of Electro-Optical Science and Engineering
National Cheng-Kung University, 1 University Rd., Tainan, Taiwan

Abstract— NSOM spectroscopy and imaging of nanoparticles in both illumination and collection mode were studied. The artifacts of red-shifting in NSOM spectra and polarization dependant dark fringe patterns associated with each scattering resonant peak were explained.

Recent development of near field scanning optical microscopy (NSOM) has lead to unprecedented high resolution and detailed view on the nanoscale optical properties [1, 2]. Under a nanosize aperture, NSOM can optically probe objects with feature size smaller than 50 nm. The interaction between the probe and the object could potentially lead to artifacts in the image obtained. As describe in [3], for NSOM operating in illumination mode, scanning images show dramatic difference at different wavelengths. This is due to the interference effect between the light coming from the NSOM aperture and the scattered light from the nanoparticle. In the NSOM spectroscopy experiment [4], the phase-sensitive spectroscopy of surface plasmons in metal nanoparticles was obtained with a broad-band radiation generated by femtosecond white light continuum in microstructure fiber. Similar interference effect also leads to resonant peak shift in the spectrum.

In this paper, we studied in details the artifacts in the NSOM spectroscopy and imaging of nanoparticles in both the illumination and collection modes with finite-difference time-domain method. A Drude-Lorentz model for the dielectric constant of silver is used. The Ag nanoparticle was modeled as hemisphere shape for the consideration of thermal annealing process in the experiments. The extinction spectrum of a Ag nanoparticle with diameter of 160 nm on glass substrate was calculated. To obtain the near-field scanning image of the Ag nanoparticle, a NSOM tip operated at illumination mode was included in the FDTD grid similar to our earlier report. By positioning the tip at different locations around the Ag nanoparticle, the integrated far field energy flux is collected as the intensity for each pixel. Light sources with three different wavelengths of 632 nm, 532 nm, and 480 nm were used for two-dimensional scanning over area of 0.6 μm by 0.6 μm centered on the Ag nanoparticle. The FDTD results demonstrate a consistent trend that as the probing wavelength moving toward the LSPR peak, the NSOM image of the Ag nanoparticle became brighter. Similar results obtained for Ag nanoparticles of difference sizes are consistent with our experimental observation. Detailed discussion on those images will be discussed. This indicates that onresonant metal nanoparticles will enhance the light extraction from the NSOM tip by a factor of at least several times. Depending on the probing light wavelength relative to the LSPR peak of the nanoparticle, the scanning images show drastically difference contrast. This property is useful for distinguishing nanoparticles of difference size and is potential for differentiating nanoparticles of various materials [5, 6]. We calculated the extinction spectrum, the NSOM illumination and collection mode spectroscopy spectra of the Ag particle with diameter of 160 nm with hemisphere shape. The resonant peak of the NSOM illumination spectrum is red shifted. The shifting effect has the same origin of the interference effect between the NSOM tip source and the phase of LSPR in Ag nanoparticle.

In conclusion, the near field scanning imaging also presented a polarization dependant dark fringe associated with each scattering resonant peak. The NSOM spectroscopy shows a red shift in the illumination mode comparing to the pure extinction spectrum of the Ag nanoparticle.

REFERENCES

1. Wiederrecht, G. P., *Euro. Phys. J. Appl. Phys.*, Vol. 28, 3–18, 2004.
2. Bouhelier, A., *Microscopy Res. Tech.*, Vol. 69, 563–579, 2006.
3. Prikulis, J., H. Xu, L. Gunnarsson, M. Kall, and H. Olin, *J. App. Phys.*, Vol. 92, 6211, 2002.
4. Mikhailovsky, A. A., M. A. Petruska, K. Li, M. I. Stockman, and V. I. Klimov, *Phys. Rev. B*, Vol. 69, 085401, 2004.
5. Cvitkovic, A., N. Ocelic, and R. Hillenbrand, *Nano Lett.*, Vol. 7, 3177, 2007.
6. Pomraenke, R., C. Ropers, J. Renard, C. Lienau, L. Luer, D. Polli, and G. Cerullo, *Nano Lett.*, Vol. 7, 998, 2007.

Observation of Coulomb Noises Assisted Single-electron Tunnel in Nanopillar Transistor

Y. M. Wan[1], **S. Y. Chen**[1], **C. A. Chen**[2], **and H. C. Hsu**[2]

[1]Department of Electronic Engineering, I-Shou Univ., Kaohsiung, Taiwan 84001, R.O.C.
[2]Department of Mechanical Engineering, I-Shou Univ., Kaohsiung, Taiwan 84001, R.O.C.

Abstract— We report observation of giant current noises in nanopillar transistors at room temperature. The noises are due to the elastic property of the multilayer $SiN_x/Si/SiN_x$ structure. When one-electron is charged into each degree of freedom, the noises reach a maximum. At this point, the potential energy stored is also the largest. Subsequent exchange in between electrical and mechanical energy results in vibration and that eventually leads to the tunneling of electrons.

Introduction: Recently, the coupling of single-electron tunnel [1–5] to mechanical vibration in various quantum-dot transistors (SETs) is an interesting topic of much discussion focusing on the issue of how mechanical feedback can influence the current-voltage (I-V) characteristics. It is well known that such transport is featured by a series of isolated peaks in I-Vs and the spacing between them defines the charging energy Ec of one electron, while prior to the process Coulomb blockade (CB) strictly prohibits electrical current to flow. Several recent studies, however, have projected that new features could appear in the CB and quantum shuttling can occur [6, 7] where the central box will vibrate and its amplitude will also reach a stable limit at a large bias. Soon after, it is demonstrated [8–12] that the vibration will create noises. In this paper, we demonstrate these effects by conducting measurements and modeling analysis to show that vibration is generated at low bias and the associated quantum number of electron is also specified. As a consequence, the current (ΔI_{ds}) induced can be precisely described by a coupling model that involves an energy exchange in between electronics and mechanics.

Measurements: Devices were then loaded into a probe station of Thermal Cascade for current-voltage measurements using a three-terminal HP 4156 C with 1 mV and 10 fA resolutions in ambient environment. Because of the small junction size, the typical current measured is very low in the range of sub pico-amp. The high resistance $\sim 10^{12}\,\Omega$ also reflects the excellent insulation of silicon nitrides when electrons have to pass through the double barriers. For all measurements, the bias voltage is always kept low (less than 1 V) in order to fit the need of low power operation.

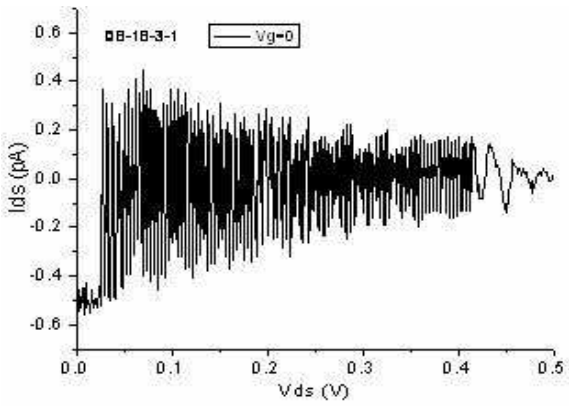

Figure 1.

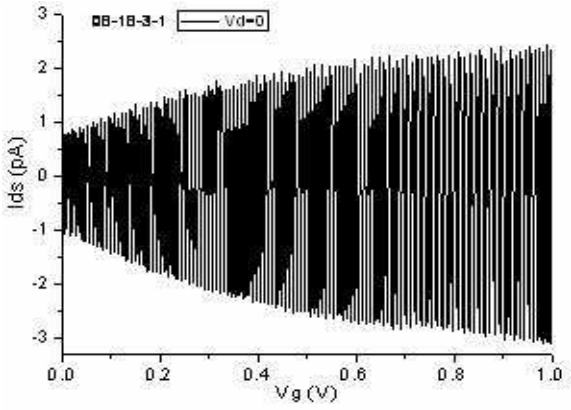

Figure 2.

Discussions: In Fig. 1, the Nanopillar in measurment $Vg = 0$ and Vd is 0 to 0.5 then Id become smaller then smaller, because the damping of nanopillar. In Fig. 2, $Vd = 0$, Vg is 0 to 1, Vd and Id are produce resonance respond are bigger then bigger.

Conclusion: In conclusions, we have fabricated low power $\sim$1 pW nanopillars transistors on cheap dummy silicon wafers for room-temperature operation. Single-electron tunnel and electrical-mechanical induced oscillating currents have also been observed with bias voltage less than 1 V. Realization of such devices is mainly relied on e-beam lithographically defined quantum box as well as the excellent control of a sub-10 nm gate oxide. This breakthrough can help to speed up the fulfillment of vary-large-scale-integration compatible nanoelectronics.

ACKNOWLEDGMENT

The authors are gratefully indebted to the research staff in the National Nano Device Laboratories (NDL) for device fabrication and also to Prof. G. W. Shuy for many stimulating discussions. The work was financially supported by the National Science Council of the Republic of China under Contract No. NSC95-2112-M-214-001-MY2, Contract No. NSC92-2215-E-492-008, and Contract No. NDL-95S-C113.

REFERENCES

1. *Single Charge Tunneling*, edited by H. Grabert and M. H. Devoret, Plenum Press, New York, 1992.
2. Park, H., et al., *Nature*, Vol. 407, 57, London, 2000.
3. Knobel, R. G. and A. N. Cleland, *Nature*, Vol. 424, 291, London, 2003 and references therein.
4. Jarillo-Herrero, P., et al., *Nature*, Vol. 439, 953, London, 2006.
5. Postma, H. W. C., et al., *Science*, Vol. 293, 76, 2001.
6. Fedorets, D., et al., *Phys. Rev. Lett.*, Vol. 92, 166801, 2004.
7. Gorelik, L. Y., et al., *Phys. Rev. Lett.*, Vol. 80, 4526, 1998.
8. Blanter, M., et al., *Phys. Rev. Lett.*, Vol. 93, 136802, 2004.
9. Wan, Y. M., et al., *Appl. Phys. Lett.*, Vol. 87, 123506, 2005.
10. Wan, Y.-M. and H.-T. Lin, quant-ph0707.0524, arXiv.org, 2007.
11. Wan, Y. M., et al., *Appl. Phys. Lett.*, Vol. 89, 053515, 2006.
12. Wan, Y. M., S.-Y. Chen, H.-T. Lin, C.-A. Chen, and H.-C. Hsu, *IEEE-NEMS proceeding*, 82–85, 2008.

Vibrations and Mechanically-induced Electrical Currents in Nanopillars Transistor

Yue-Min Wan, Hein-Tien Lin, Chih-An Chen, and Hsiang-Chen Hsu
Department of Electronic Engineering, I-Shou University, Kaohsiung 84001, Taiwan, R.O.C.

Abstract— We report measurements and numerical modeling of nanopillars transistor in consisting of a multilayer $SiN_x/Si/SiN_x$ structure and an electrical side gate for single-electron tunnel and Coulomb modulation at room temperature. The device has an ultrasmall quantum box of $\sim 10\times10\times10\,nm^3$ and its manufacture is fully VLSI processing compatible. Finite-element analysis shows that the maximum deformation is ~ 3Å and the corresponding elastic energy stored is $\sim 50\,meV$. The vibration frequency calculated is $\sim 10^{12}\,Hz$ in consistent with interference measurement. The current induced ranging from 1 pA to 0.1 pA is also consistent with experimental data, thus confirming that single-electron tunnel indeed can generate mechanical vibrations.

Background: Recently, the coupling of single-electron tunnel [1] to mechanical vibration in various quantum-dot transistors (SETs) [2–4] has attracted much attention targeting at the issue of how mechanical feedback can influence electrical transport. It is well known that electron transport is featured by a series of isolated peaks in the *I-V* characteristics and the spacing between them defines the charging energy Ec, while prior to the charging process Coulomb blockade (CB) strictly prohibits current to flow. Several studies, however, have projected that new features can appear in the CB; Gorelik et al. [5, 6] first pointed out that shuttling can occur, where the central box can oscillate and its amplitude will reach a stable limit at a large bias. Soon after, Blanter et al. [7] demonstrated that this effect can further create noises. In this paper, we execute finite-element calculations to analyze how the central box can vibrate under specific quantum conditions. Fundamental frequencies are obtained and the induced current ΔI_{ds} calculated also show good agreement with data, in confirming that such transistor can be a useful radiation source.

Current Results: In Fig. 1, when the starting voltage is at a sizable value, the ΔI_{ds} oscillation is very stable, indicating a constant charging/discharging of electron [8]. The peak spacing is $\sim 25\pm3\,meV$ and it agrees with the charging energy $Ec = e^2/2C$ very well assuming the parallel plate capacitor with $C = \varepsilon_r\varepsilon_o A/H \sim 3.5\,aF$, $\varepsilon_o = 8.85\times10^{-12}\,C^2/Nm^2$, $A = L\times W = 10^{-16}\,nm^2$, $H = 3\,nm$, and $\varepsilon_r = 11$.

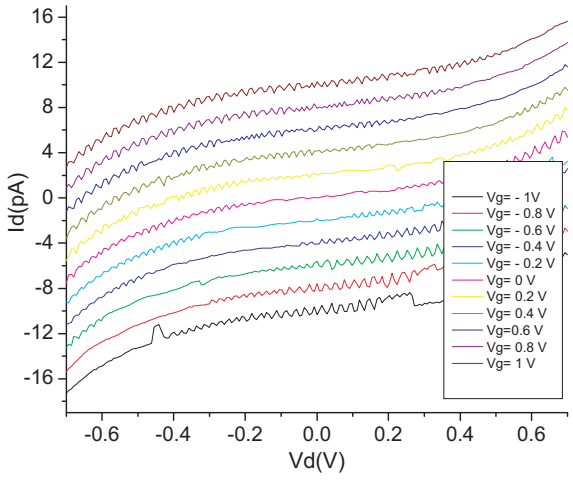

Figure 1: *I-V* curves (offset by 2 pA) starting at −0.7 V.

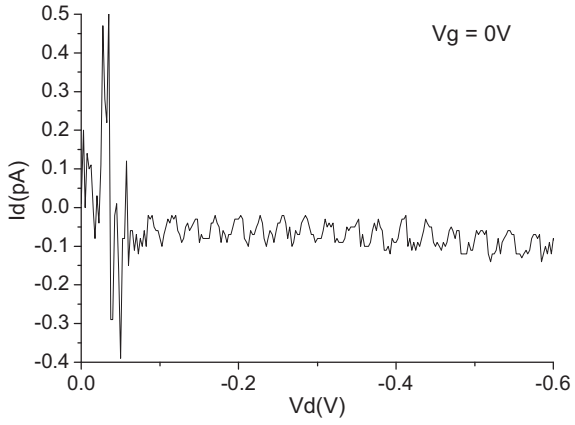

Figure 2: *I-V* for Vg = 0 V starting at 0 V.

In sharp contrast, when the box charging begins at 0 V in Fig. 2, giant noises appears suggesting that the box is unstable and it can vibrate via the coupling of electron and phonons [9]. Obviously, it is important to understand its vibration mode. Here, we use finite-element method to calculate the frequency. The structure used in Fig. 3 is the exact size of the $SiN_x/Si/SiN_x$. The parameters used for Si are: mass density $2.4\,g/cm^3$, Young's modulus $0.16\times10^7\,N/cm^2$ and Poisson ratio 0.23; for nitride, they are $2.9\,g/cm^3$, $0.2\times10^7\,N/cm^2$ and 0.28, respectively.

Figure 3: Modeling the nanopillars transistor of size $9 \times 9 \times 9\,\mathrm{nm}^3$.

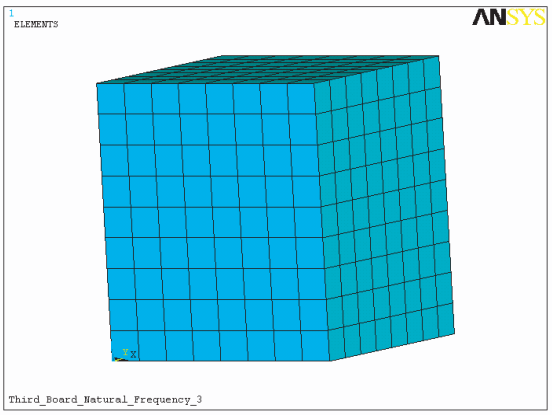

Figure 4: 9^3 meshes in the nanopillars.

For a fixed bottom SiN_x of the state $[1,1,1]$, the initiated vibration is at $\sim 93\omega_0$, where $\omega_0 = (K/M)^{1/2}$ is the basic unit, K is spring constant $\sim 0.16\,N/m$ and $M = \rho V$ is the total mass, with $\rho \sim 2.4 \times 10^3\,Kg/m^3$ and $V \sim 6 \times 10^{-25}\,m^3$. Given these numbers, ω_0 estimated is $\sim 10^8/s$, making a net frequency of $\sim 10^{10}/s$. This value agrees with that derived from the dynamical interference of charge carriers due to the vibration of the central SiN_x barrier between two Si boxes [10].

In Fig. 5, both the top and bottom SiN_x are fixed and the deformation is limited to the horizontal direction and the current induced is normal to the tunneling channel. This is also corresponding to the state of $[1,1,2]$ as marked in Ref. [9]. The maximum deformation ΔX (in between the straight line and the bended) found is $\sim 3\mathring{A}$ (scaling in length), in consistent with the prediction from the elastic model.

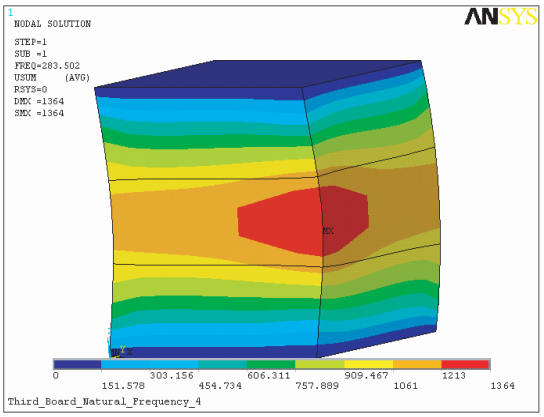

Figure 5: Mode with the top and bottom sides fixed.

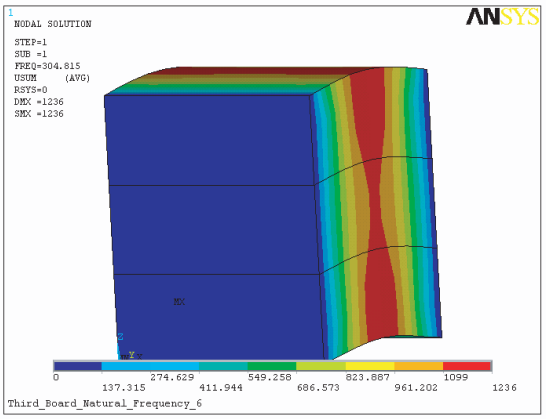

Figure 6: Mode with the front and back sides fixed.

In Fig. 6, the shuttling noise current estimated $\Delta I_{ds} = e\Delta V n_e \Gamma$ with the ΔV affected is $\approx 1\,pA$, where n_e is the charge density in the electrodes $(SiN_x) \propto A\Delta X/3$, A is the tunneling area. Given $A \sim 64\,nm^2$, $e = 1.6 \times 10^{-19}\,C$, $\Gamma = 10^{12}/sec$, $N \sim 10^{16}/cm^3$, and $\Delta X \sim 1\mathring{A}$, in accordance with the data. The single-electron current of the $[2,2,3]$mode measured is much smaller at about $\approx 0.1\,pA$.

REFERENCES

1. Grabert, H. and M. H. Devoret, *Single Charge Tunneling*, Plenum Press, New York, 1992.
2. Park, H., et al., *Nature*, Vol. 407, 57, London, 2000.
3. Knobel, R. G. and A. N. Cleland, *Nature*, Vol. 424, 291, London, 2003.
4. Jarillo-Herrero, P., et al., *Nature*, Vol. 439, 953, London, 2006.

5. Fedorets, D., et al., *Phys. Rev. Lett.*, Vol. 92, 166801, 2004.
6. Gorelik, L. Y., et al., Vol. 80, 4526, 1998.
7. Blanter, M., et al., *Phys. Rev. Lett.*, Vol. 93, 136802, 2004.
8. Wan, Y. M., et al., *Appl. Phys. Lett.*, Vol. 87, 123506, 2005.
9. Wan, Y.-M. and H.-T. Lin, quant-ph0707.0524, lanl.arXiv.org, 2007.
10. Wan, Y. M., et al., *Appl. Phys. Lett.*, Vol. 89, 053515, 2006.

Design of Electrical and Optical Parameters of Photonic Crystal-based Chromatic Dispersion Compensator

C. E. Png, E. P. Li, S. T. Lim, and G. H. Park

Advanced Electromagnetics and Photonics Group, IHPC, A*Star
1 Science Park Rd, ♯01-01, 117528, Singapore

Abstract— We demonstrate 3D simulation of a novel active silicon photonic crystal chromatic dispersion compensator with ultra low power consumption and high efficiency. This is achieved by exploiting a device structure where optical and electrical properties can be individually designed. Due to the unique arrangement of the charge layer, power consumption is reduced by three orders-of-magnitude.

Introduction: Chromatic dispersion plays a significant role in the propagation of short optical pulses, as well as in optical interconnects. Recently, there is increased interest in the research of integrated chromatic dispersion compensators (CDC). This work presents breakthrough results on modeling and power reduction of a CDC with silicon photonic crystals (PhC) patterned on a silicon (Si) substrate. We report the first three-dimensional (3D) simulation of a PhC-based CDC with a power requirement of only 114 nW at a wavelength of 1550 nm. This is three orders-of-magnitude lower compared to one of the lowest reported to date (e.g., [1]). Most simulations of such active devices to-date concentrates on 2D for the obvious reason of it being less computationally expensive [2], however the veracity of such studies proves to be wanting in situations where the device's electrical transport layer consists of photonic crystals. Taken from the front side of the active CDC, the device represents multiple layers of silicon-on-insulators, hence rendering 2D solutions inadmissible as movement of injected carriers will be impeded.

Device Structure and Results: The novel nanostructured electro-optic (EO) waveguide is based on a low-loss Si_3N_4 rectangular core and a 2D Si/SiO_2 PhC layer controlled by voltage bias [3]. The importance of the electrical characteristics is underpinned by the z-direction of the CDC having alternating refractive index (RI) due to the PhC. Due to a thin layer (100 nm) of Si/PhCs for electronic transport and a separate Si_3N_4 core for the bulk of the optical waveguiding, the electrical and optical properties can be individually tailored. This may enable low-cost and highly efficient CDCs. The low-loss Si_3N_4 waveguide is 1 µm wide and 400 nm thick, and the PhC consists of a 2D triangular lattice of 242 nm-diameter SiO_2 pillars embedded in a host Si layer. The lattice pitch is 403 nm. The 100 nm-thick Si layer serves as host medium for the PhC layer, and a 1 µm-thick buried oxide layer provides a lower cladding [3].

Photonic crystal band diagram calculations predict the device to operate as a single mode device and having a transmission loss of approximately 1 dB. For the electrical transport simulation, we assumed the CDC length to be 1.35 µm. The anode and cathode dopant windows are 1 µm wide and doped to a concentration of $10^{20}/\text{cm}^3$ with Boron and Arsenic respectively with an intrinsic spacing of 400 nm in between, creating a *p-i-n* structure. The host Si's RI is controlled by the plasma dispersion effect which then influences the effective guiding RI of Si_3N_4 [4]. A 3D device simulator, which incorporates advanced device physics to account for effects such as field dependent carrier mobility, to model the induced charge density as a function of the drive voltage. We focused on the ON and OFF state of the device which relates to a RI change of $\Delta n \sim 10^{-3}$ and $\Delta n \sim 0$ respectively. Predicted current and voltage required to achieve the ON state are 0.92 V and 114 nA respectively; giving a turn on power of approximately 114 nW, which is a three orders-of-magnitude compared to a 2D Si-based PhC result of 113 µW [1].

Conclusions: Using full 3D simulation, we studied a novel CDC and obtained a power reduction of 3 orders-of-magnitude with minimal optical loss. To the best of our knowledge, this is one of the lowest power efficiency achieved for a CDC.

REFERENCES

1. Jiang, Y., et al., *Appl. Phys. Lett.*, Vol. 87, 221105, 2005.
2. Liu, A., et al., *Nature*, 427, 615–618, 2004.
3. Ogawa, K., et al., *OFC*, OThE4, 2006.
4. Soref, R., et al., *IEEE J. Q. Elect.*, Vol. 23, 123, 1987.

Alternative Routes to Engineer Negative-index Optical Elements for Future Optoelectronics Systems

B. D. F. Casse[1], **R. K. Banyal**[1], **W. Lu**[1], **S. Selvarasah**[2], **Y. J. Huang**[1]
M. Dokmeci[2], **and S. Sridhar**[1]

[1]Department of Physics and Electronic Materials Research Institute, Northeastern University
Boston, MA 02115-5000, USA
[2]Department of Electrical and Computer Engineering, Northeastern University
Boston, MA 02115-5000, USA

Abstract— Optical elements which are currently used in high-resolution imaging systems or micro-optics applications possess a positive index of refraction. In this paper, we reveal new schemes to engineer photonic crystals lenses and binary-staircase optical elements which exhibit an effective negative index of refraction, and thereby expand the range of optical properties theoretically available for future optoelectronic devices. To minimize aberrations in designing flat lenses, we used the theory of flat lens imaging with lens equation $u + v = \sigma d$ ($\sigma = 1$ is the Veselago-Pendry perfect lens). The mechanism for achieving a negative-index binary staircase lens is based on exploiting the periodicity of the surface corrugation, which is easier to fabricate than other proposed designs. The nanoscale optical elements were fabricated in the InP/InGaAsP heterostructure platform using modern lithography techniques. To characterize the optical elements at telecommunications wavelength (1.55 µm), a near-field scanning optical microscope was used to monitor point source imaging and focusing experiments. The beam propagation in the optical elements was studied by 2D and 3D finite difference time domain (FDTD) numerical simulations, and the results were found to be in excellent agreement with the experimental observations.

Experimental Investigation of Transformer Coupled Toroidal Discharges

I. M. Ulanov, **M. V. Isupov**, **and A. Yu. Litvinsev**
Kutateladze Institute of Thermophysics SB RAS
Lavrentiev av. 1, Novosibirsk 630090, Russia

Abstract— As it is known, production of low-temperature plasma by induction (electrodeless) gas discharges is one of the most promising methods to increase the efficiency and service life of the gas-discharge light sources. The urgency of this problem is obvious because of the wide application of gas-discharge lamps in different fields of lighting technology (room and street illumination, biomedical and technical applications, etc.).

There are several types of induction gas discharges, differing both by the construction of inductor and gas-discharge chamber and by the frequency of discharge current, among which the transformer coupled toroidal discharges (TCTD's) should be mentioned specially.

While differing in detail such as the position of excitation coils and chamber materials, all TCTD's (Fig. 1) feature a closed plasma loop in the discharge chamber 1, which acts as a single-turn secondary winding of excitation transformer 2, connected to power supply 3. In contrast to the RF induction discharges, generation of TCTD's can be obtained at relatively low frequencies of $\sim 10 - 100$ kHz (typical frequencies of RF induction discharges is about $\sim 1 - 10$ MHz). Thus, the long lifetime and relatively low frequencies make TCTD promising for creating the new electrodeless discharge devices for the practical application: low temperature plasma generators and light sources.

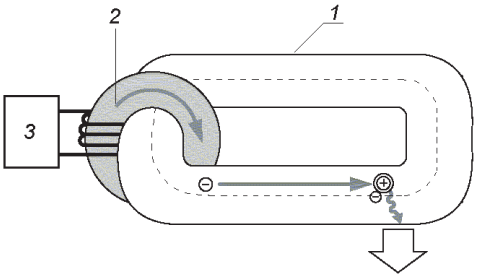

Figure 1: Principle of TCTD generation.

To develop new electrodeless long-life sources of visible and UV radiation, experimental investigations of the TCTD in a mixture of argon and mercury vapor were carried out for a wide range of discharge parameters: mercury vapor pressure (0.1–40 000 Pa), discharge current (1–260 A), diameter of a gas-discharge tube (20–75 mm) and current frequency (10–250 kHz). Also, experimental investigations of the TCTD in pure neon were carried out for neon pressures of 10–600 Pa, discharge currents 1–30 A, tube diameters 20–58 mm and driving frequencies 25–250 kHz.

New experimental data on electric field strength and emission yield to visible and UV-range were obtained as functions of the TCTD parameters. Results obtained were compared with the known characteristics of dc arc discharges in mercury vapor and neon.

It was proved that the dependences of electrical and optical characteristics of TCTD on the discharge current, pressure and tube diameter are close to those of dc arc discharges. In particular, it was shown that for the pressure of mercury vapor above 10 kPa and ratio of discharge gap length L to bulb diameter D $L/D > 15$, the electrical characteristics of TCTD can be approximately calculated by the standard 'channel' model of the dc arc discharges, based on the assumption of LTE presence in the discharge plasma. Besides, the LTE in plasma of the TCTD in mercury vapors at the pressure of ~ 25 kPa was proved by spectral investigations.

The spectral characteristics of TCTD were measured in neon, including the transverse profiles of line brightness, discharge spectra in different ranges of a gas discharge, and line contours. Excited atoms densities, electron and gas temperatures, and electron densities were calculated. Asymmetry of transverse profiles of line brightness, caused non-uniform electric field in a toroidal TCTD, were found.

The optimal conditions of TCTD operation in mercury vapor and neon, corresponding to the maximal emission yield in UV and visible spectral ranges, were determined. Based on the obtained experimental results, we have developed and created the pilot samples of electrodeless lamps: mercury induction middle-pressure lamp with light efficiency of 65 lm/W, and power of 3 kW; germicide UV induction lamps of a low pressure with power of 50, 100, 200 and 500 W and emission yield to the resonant line 253.7 nm at the level of $\sim 30 - 35\%$ of consumed power (Fig. 2); neon induction lamp of a low pressure with power of 500 W and light efficiency of 35 Lm/W (Fig. 3).

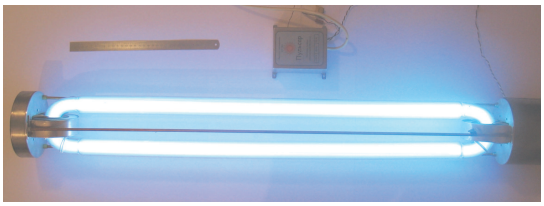

Figure 2: Pilot sample of electrodeless mercury UV lamp with the power of 500 W.

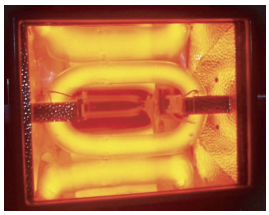

Figure 3: Pilot sample of electrodeless neon lamp.

Lateral Displacements of an Electromagnetic Beam Transmitted and Reflected from a Gyrotropic Slab

Hui Huang[1,2], **Yu Fan**[1], **Bae-Ian Wu**[2], **and Jin Au Kong**[2]

[1]School of Electrical Engineering, Beijing Jiaotong University
Beijing 100044, China
[2]Research Laboratory of Electronics, Massachusetts Institute of Technology
Cambridge, MA 02139, USA

Abstract— It is known that for a gyrotropic medium in the Voigt configuration, waves can be decoupled into TE and TM modes. A detailed study on the lateral displacements of an electromagnetic beam reflected and transmitted from a gyrotropic slab in Voigt configuration is presented, for both TM and TE waves. Using the stationary phase approach, analytic expressions for lateral displacements of the reflected and transmitted waves from a symmetric gyrotropic slab are obtained, and we also give examples for both cases. It is found that the lateral displacements for TM and TE waves have different charateristics. Only the TM mode is affected by the gyrotropy. Due to the external magnetic field, the lateral displacement of a TM wave transmitted from a gyrotropic slab is not the same as the reflected one, even when the configuration is symmetric and the media are lossless. We also discuss the different phenomena when the incident angle is near the Brewster angle.

Ultra-short Photonic Crystal All-optical Switch

Armaghan Eshaghi and S. M. Moghadasi
Department of Electrical Engineering, Ferdowsi University of Mashhad, Iran

Abstract— A new all-optical switching structure using Kerr nonlinearity in a photonic crystal coupled cavity waveguide drop filter is presented. Reducing the group velocity causes the switch length to be as small as $21a$. Switching operation is accomplished by tunning the input wave intensity. Switching behavior is investigated by finite-difference time-domain method.

Introduction: Very small changes in the index of refraction induced by nonlinear optical effects, cause the required length of nonlinear devices, such as all-optical switches, to be too high for large-scale optical integration. Nonlinear effects can be enhanced in systems with slow group velocity as a result of the compression of the local energy density. In this work using slow light which commonly occurs in photonic crystal coupled cavity waveguides, the device length has reduced to $21a$, where a is the lattice constant.

The Switch Structure: Figure 1 shows the schematic view of the proposed structure. The PC is formed by a square lattice of rods with Kerr nonlinearity. The Kerr coefficient is assumed $n_2 = 1.5 \times 10^{-17}\,\mathrm{m}^2/\mathrm{W}$. The radius of the rods is equal to $r = 0.25a$, where a is the lattice constant. The cavities are formed by reducing the radius of rods to $r/3$. In the linear regime, where the input intensity is so low that the nonlinear effects are negligible, the switch output is port 1. By intensifying the input wave, the index of refraction increases due to Kerr effect, hence the resonant frequency of the cavities reduces. This results in transferring the input signal to port 2.

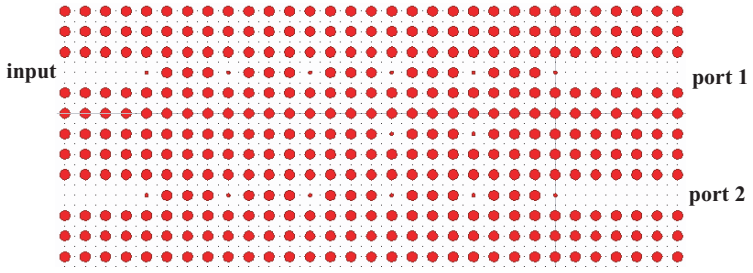

Figure 1: Schematic view of the proposed all-optical switch.

Session 3A7a
Terahertz Theory, Measurements, and Applications

Detection and Classification of Explosives Using Terahertz Synthetic Aperture Spectroscopic Imaging

John F. Federici, **Yew Li Hor**, **Ivan Zorych**
Zhiwei Liu, **Zoi-Heleni Michalopoulou**, **Robert B. Barat**, **and Dale E. Gary**

New Jersey Institute of Technology, Newark, NJ 07102, USA

Abstract— Over the past several years, there has been an increased interest in the potential of terahertz (THz) detection for imaging of concealed explosives. The interest originates from three major factors: (a) THz radiation is readily transmitted through most non-metallic and non-polar mediums, thus enabling THz systems to "see through" concealing barriers (b) explosives have characteristic THz spectra that can be used to identify these concealed materials and (c) Terahertz radiation poses minimal health risk to a suspect being scanned by a THz system. THz detection systems for stand-off detection of explosives have many hardware challenges including the need for high-power illumination sources, detector sensitivity, and fast imaging speed. In addition, the spectroscopic analysis can be challenging due to the requirement of sensing based on small changes in the spectral reflection. In this presentation, our efforts to develop a THz synthetic aperture/interferometric imaging approach to stand-off detection of concealed explosives is detailed. For this application, the imaged object is in the near-field region of the imaging array requiring compensation for near-field distortions. Images at multiple THz frequencies are acquired for spectral analysis. Using spectroscopic analysis in the THz frequency range, it is demonstrated that spectral responses of materials can be used as fingerprints that distinguish explosives such as RDX from other materials, even when measurements at only a limited number of frequencies are available. Details of the hardware system, including recent experimental imaging results, as well as explosive classification analysis will be presented.

Near-field THz Microscopy with Conical Dielectric Probes

Manoja D. Weiss, **Scott Schafer**, **and John Scales**
Colorado School of Mines, Golden, CO, USA

Abstract— We present near-field imaging results at 0.15 THz using a vector network analyzer to measure the field coupling between two conical dielectric probes positioned in the near-field on either side of a sample. Tapered dielectric probes have been used for near-field imaging at millimeter wave frequencies with high sensitivity and sub-wavelength resolution. Compared with near-field scanning using small apertures, the dielectric probe is capable of more directional near-field coupling, making it possible to obtain sharper images with less fringing, thus leading to higher resolution. For example, pyramidal dielectric probes have been reported at 50–75 GHz with a resolution of about 500 µm, and at 80 GHz with an improved resolution of 25 µm due to tiny embedded metallic antennas. However, these probes require precise micro-machining and are fragile due to their fine dimensions. Recently, a simple Teflon cylindrical dielectric probe with a conical tip was reported to give < 3 mm resolution at 93 GHz. This probe is both easy to fabricate and rugged, offering the possibility of being incorporated into low-cost THz imaging systems. One of the authors has recently reported on the use of such a conical Teflon probe to obtain 500 µm resolution at 0.15 THz in a near-field scanner based on a vector network analyzer. In this paper, we present further results of this system, including measurements that demonstrate the versatility of this technique in vector imaging of various samples. We also compare the resolution and sensitivity of probes with different properties: taper angle, probe material, probe-to-horn coupling, and distance from the sample.

Particle-in-cell Simulation of a Novel High Power Terahertz Vacuum Electron Device

Hai Zhang[1], **Jianguo Wang**[1, 2], **and Changjiang Tong**[2]

[1]School of Electronics and Information Engineering, Xi'an Jiaotong University, Xi'an 710049, China
[2]Northwest Institute of Nuclear Technology, Xi'an 710024, China

Abstract— New micromachining techniques now provide us with the technology to fabricate the vacuum electron devices, such as reflex klystron, traveling wave tube, backward wave oscillator, with the dimensions suitable for operation in the terahertz region of the electromagnetic spectrum. For the success of these devices, accurate designs are required since the optimization of certain parameters is critical to obtaining useful amounts of ac power. Classical models for device design have long been in existence, but these are no longer valid at terahertz frequencies. For this reason, a novel computer simulation tool has been developed, specifically aimed at the design of terahertz backward wave oscillator.

This simulation tool is referred to as "UNIPIC", which means a combination of Union, Universal and Particle-in-Cell. It is a user-configurable code that solves Maxwell's equations together with Lorentz particle motion. A variety of 2D, finite-difference electromagnetic algorithms and 3D particle-in-cell algorithms can be combined in problem-specific ways to provide fast, accurate and transient calculations for research and design needs. It is also characterized by many technical improvements. For example, a volume-weighting cloud-in-cell (CIC) model was proposed in this code rather than the area-weighting CIC model in order to enhance the calculation precision in the situations where macro-particles exist near the symmetric axis; another betterment is that a cyclotron and drift correction mechanism was proposed to improve the accuracy of the particle moving algorithms, which could relax the time step limitation and resultantly reduced the total computing time; Other characteristics, such as PML error diffusion method, Monte-Carlo collision consideration as well as main peculiarities expected for devices operation at terahertz frequencies were all taken into account in this new simulation scheme.

For its validation of real design, a 140 GHz MW-Class relativistic backward wave oscillator was simulated with both UNIPIC and KARAT (a traditional, famous PIC code in HPM field) under the same conditions. The effects of device parameters which are critical to the optimization of output power in the prototype 140 GHz micro machined BWO based on an explosive electron emission source were studied, and the contrastive results demonstrated that UNIPIC had the same computation precision as KARAT and owned the more perfect GUI mechanism for data output. Therefore, it is believed that UNIPIC is a reliable, practical and promising 2.5D full electromagnetic PIC code, which must ease the complicated design process of high power terahertz devices in future.

THz Scattering from Random Rough Surfaces

Scott Schecklman[1], **Garth Sundberg**[1], **Lisa M. Zurk**[1]
Antao Chen[2], **and Mohammad Hassan Arbab**[2]

[1]Department of Electrical and Computer Engineering
Portland State University, Portland, Oregon 97207, USA
[2]Applied Physics Laboratory, University of Washington
Seattle, Washington 98195, USA

Abstract— In recent years terahertz (THz) spectroscopy has emerged as a promising technology for sensing and detection of a variety of materials. Many molecules have unique rotational and vibrational resonances at THz frequencies which cause the overall permittivity of the material to vary with frequency in a dramatic but predictable fashion, thus providing a unique spectroscopic signature. Furthermore, many packaging materials are transparent to THz frequencies allowing the wave to penetrate and interact with other materials of interest such as explosives and biological tissue. The opacity of many materials at THz wavelengths suggests that most practical applications of THz spectroscopy will be limited to reflection measurements.

In THz spectroscopy systems the frequency-dependence of a material's permittivity is detected indirectly by measuring the frequency-dependence of the reflected signal's amplitude. Rough surfaces, however, scatter the incident wave energy into different directions, with the amplitude and phase in any given (detection) angle governed by the wavelength of the incident wave relative to the surface dimensions, the permittivity contrast, and the viewing geometry. The scattering creates an additional frequency-dependent variation in the reflected signal amplitude which threatens to distort the THz spectral signature and complicate proper material identification. By applying analytic or numeric surface models it is possible to account for surface scattering and recover the original spectroscopic signature.

In this paper we show the effect of rough surface scattering on THz Time Domain Spectroscopy (TDS) reflection measurements of gold-coated sandpapers with variable surface statistics. These measurements are compared with results generated from analytic models with good agreement in the applicable regime for the approximations. Finally, we use the Lorentz model to incorporate the frequency dependent THz signature into both the analytic models and a dispersive (Finite Difference Time Domain) FDTD formulation to predict the THz response from materials, such as explosives, when the materials contain a rough surface interface.

3D Scattering by Large Inhomogeneous 2D Objects: Validation of a Full-wave 2.5D VIE Solver with Millimeter-wave Gaussian Beam and Microwave Experiments

S. van den Bulcke[1], A. Franchois[1], J. M. Geffrin[2], L. Zhang[3], and J. Stiens[3]

[1]Department of Information Technology, Ghent University, Belgium
[2]Institut Fresnel, Université Paul Cézanne Aix-Marseille, III, France
[3]ETRO-TW, Vrije Universiteit Brussel (VUB), Belgium

Abstract— For the development of active millimeter wave imaging systems, e.g., to detect concealed objects on the human body, it is important to be able to simulate some representative scattering configurations. Typically, Gaussian beams are used in active imaging systems. Since these beams only illuminate a spatially limited region, the human body and various objects can be treated as two-dimensional (2D) (in)homogenous cylinders. However, the incident Gaussian beam has a 3D character. Therefore, a 2.5D full-wave Volume Integral Equation (VIE) forward solver is developed: only the cylinder's cross-section is discretized, reducing the number of unknowns strongly, while the incident fields (e.g., oblique plane waves and 3D Gaussian beams) maintain their full 3D character. In this paper, a vectorial Gaussian beam is constructed by using a dipole source in a complex point. This elegant implementation is valid in the near and far field of the beam. Furthermore, simulation results are compared to measurements to validate the 2.5D numerical scheme. In a first measurement set-up, the scatterer is a long inhomogeneous dielectric cylinder, illuminated by plane waves under different elevation angles at microwave frequencies in the range 1–18 GHz. Simulations agree well with the experimental results for normally incident plane waves and plane waves with a small elevation angle, for all measured frequencies. For larger elevation angles, the finiteness of the cylinder influences the results and decreases the agreement. The second measurement set-up consists of a long teflon cylinder, illuminated by a normally incident Gaussian beam at 94 GHz. The measured incident and total field amplitudes correspond well to the simulated ones. Hence, the 2.5D algorithm is proven to be a valuable simulation tool to study scattering of long inhomogeneous dielectric objects, illuminated by 3D plane waves or 3D Gaussian beams under different elevation angles.

Bow-tie Wideband Antenna Design for CW THz Photonic Transmitters

J. Zbitou[1], **C. Minot**[1,2], **X. Begaud**[1], **and B. Huyart**[1]

[1]Institut TELECOM, TELECOM ParisTech, LTCI CNRS, 46 rue Barrault, Paris 75013, France
[2]CNRS-LPN, Route de Nozay, Marcoussis 91460, France

Abstract— The Terahertz technology attracts more scientists for the fast growing interest in this spectral region. Due to their unique proprieties, THz is attractive for biomedical imaging, national security and packaged goods inspection to remote sensing and spectroscopy [1–5]. In this study we have designed and optimized two structures of a Wideband Bow-tie antenna suitable to be integrated easily in a monolithic THz photonic transmitter using a GaAs substrate. As presented in Fig. 1, we have the top-view of a demonstrated Bow-tie antenna $(370 \times 383)\,\mu m^2$, which we have simulated and designed in a frequency band from 0.4 THz up to 2 THz.

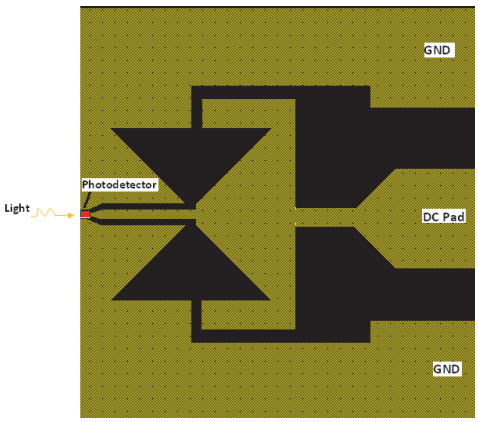

Figure 1: Bow-tie wideband antenna structure.

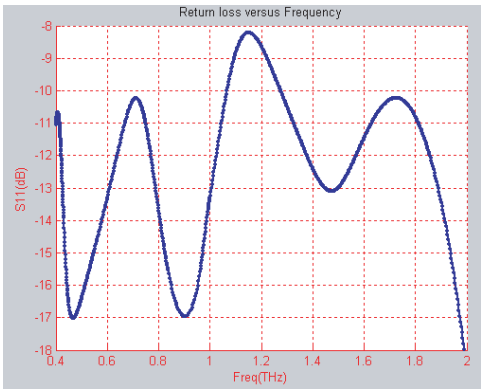

Figure 2: Return losses versus frequency.

To achieve the isolation between the RF and DC signal, we have integrated into the structure of the antenna two slots of 10 µm, which we have optimized using the Electromagnetic ADS Momentum method, as a result of this optimization we obtain return losses under −10 dB as shown in Fig. 2, with a good isolation between the DC and RF signals. After this first study, we were interested in developing a new structure of Bow-tie antenna achieving a good RF and DC isolation; therefore we have inserted a low periodic pass filter [6] behind the bow-tie antenna as presented in Fig. 3 to achieve a photonic transmitter which has dimensions of $(635 \times 383)\,\mu m^2$.

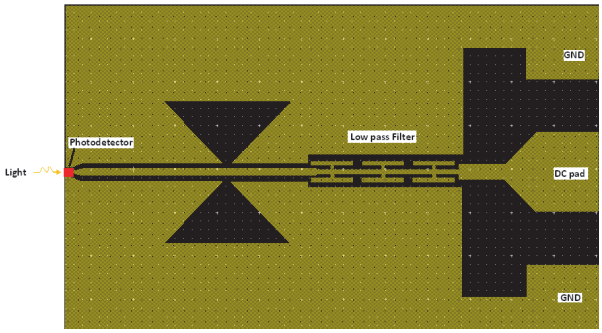

Figure 3: Bow-tie wideband antenna structure.

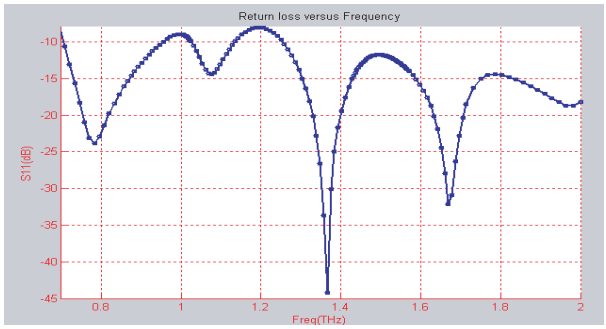

Figure 4: Return losses versus frequency.

In Fig. 4, we have the return losses that are under −10 dB along a wideband frequency up to 2 THz, with a good isolation between RF and DC signal that is due to the good optimization of the low pass periodic filter. By consequent, in this study we have developed and designed two wideband bow-tie antennas structures permitting to achieve a THz photonic transmitter source by using two techniques which were developed and demonstrated.

REFERENCES

1. Wang, Z., "Generation of terahertz radiation via nonlinear optical methods," *IEEE Transactions on Geoscience and Remote Sensing*, Vol. 1, No. 1, 1–5, Nov. 2001.
2. Gregory, I. S. and C. Baker, "Optimization of photomixers and antennas for continuous-wave terahertz emission," *IEEE Journal of Quantum Electronics*, Vol. 41, No. 5, 717–728, May 2005.
3. Li, Y.-T., J.-W. Shi, and C.-L. Pan, "Sub-THz photonic-transmitters based on separated-transport-recombination photodiodes and a micromachined slot antenna," *IEEE Photonics Technology Letters*, Vol. 19, No. 11, 840–842, Jun. 1, 2007.
4. Malcoci, A. and A. Stohr, "Optical submillimeter-wave generation employing antenna integrated ultra-fast travelling-wave 1.55 µm photodetectors," *IEEE MTT-S*, 143–146, 2003.
5. Ito, H. and T. Furuta, "Photonic generation of continuous THz wave using uni-traveling-carrier photodiode," *Journal of Lightwave Technology*, Vol. 23, No. 12, 4016–4020, Dec. 2005.
6. Sor, J. and Y. Qian, "Miniature low-loss CPW periodic structures for filter applications," *IEEE Transactions on Microwave Theory and Techniques*, Vol. 49, No. 12, 2336–2341, Dec. 2001.

Session 3P1
Computational Electromagnetics

Multilevel Green's Function Interpolation Method Using Novel Partitioning Techniques for Modeling Composite Metallic and Dielectric Objects

Yan Shi[1], **Hao Gang Wang**[2], **Long Li**[3], **and Chi Hou Chan**[1]

[1]Department of Electronic Engineering, City University of Hong Kong, Hong Kong SAR, China
[2]EM Academy at Zhejiang University, Hangzhou, China
[3]Xidian University, Xian, China

Abstract— A multilevel Green's function interpolation method (MLGFIM) using novel partitioning schemes has been proposed to analyze electromagnetic scattering from complex objects comprised of both conducting and dielectric objects. The problem is formulated using Poggio-Miller-Chang-Harrington-Wu-Tsai (PMCHWT) approach for multiple homogeneous dielectric objects and electric field integral equation (EFIE) for conducting objects. The integral equations are discretized by the method of moments and the resultant numerical system is then solved by using MLGFIM with $O(N \log N)$ computational complexity and $O(N)$ computer memory complexity.

In order to improve the efficiency of the Green's function interpolation in MLGFIM, two kinds of partitioning schemes, the quasi-2D multilevel scheme and the hybrid quasi-2D/3D multilevel scheme are devised. Compared with the conventional octary-cube-tree multilevel partitioning method, the quasi-2D multilevel scheme adopts the uniform division method in the dimension where the object has the smallest size and the conventional 2D multilevel method in the remaining dimensions. Consequently, the number of interpolation points is greatly reduced, leading to the improvement of the interpolation efficiency. Through detail analyses of the quasi-2D multilevel partitioning scheme, we find that the dimension of each group in the finest level should not be less than half a wavelength. In order to overcome this requirement, the hybrid quasi-2D/3D multilevel scheme is further developed. In the hybrid scheme, the quasi-2D multilevel scheme is easily combined with the conventional 3D multilevel scheme by using a new definition of the group in the quasi-2D scheme. In addition, selection criteria on the number of interpolation points and parameters of interpolating functions are given for yielding good interpolation accuracy and efficiency.

The proposed algorithm is ideal for solutions to problems including objects with small size in some dimension compared with those in other dimensions, such as missile, microstrip antenna arrays, photonic band gap structures, dielectric lens, etc. Numerical examples will be presented to demonstrate the accuracy, efficiency and versatility of the proposed algorithm in dealing with a wide array of scattering problems.

ACKNOWLEDGMENT

The work presented in this paper is supported by the Hong Kong Research Grant Council, Grant CityU 110606.

Accurate Field Distrubution Models for RFID Applications Using Hybrid Computational Electromagnetics Technquies

R. A. Abd-Alhameed[1], **P. S. Excell**[1], **C. H. See**[1], **D. Zhou**[1], **and K. N. Ramli**[1, 2]

[1]Mobile and Satellite Communications Research Centre
Bradford University, Bradford, BD7 1DP, UK
[2]Electrical and Electronic Engineering Faculty
University of Tun Hussein Onn Malaysia (UTHM)
Parit Raja 86400, Batu Pahat Johor, Malaysia

Abstract— The demand for efficient and accurate field modelling tools for electromagnetic (EM) problems is constantly growing. The various numerical methods can be divided into several categories. One possible division can be made, based on the domain in which the procedure is applied: time domain methods and frequency domain methods.

The applications of these two classes of methods mainly depend on the type of problems to be solved and on the form of the required solution, e.g., impulse response or harmonic solution. It is clear that results can be moved from one domain approach to the other by applying a direct or inverse Fourier transform, applying the proper care to avoid aliasing and to ensure causality. However, there are deeper issues of stability which may also influence the decision on which method to use. A second possible classification for numerical methods is based on the type of formulation used: differential formulation and integral formulation.

Differential formulations are local in nature so that the initial and boundary conditions must be imposed as the algorithm proceeds. They tend to require negligible analytical pre-processing. Integral formulations are global in nature so that initial and boundary conditions are included directly in the algorithm that follows. They often require extensive analytical pre-processing.

At the final stage these two approaches typically lead to systems of equations representing a discretised form of the original problem. Differential formulations lead to large, but sparse, matrices as compared to the very dense but small matrices obtained with integral formulations. Each of the methods in these classes can be said to be specific to certain geometries. In this respect, differential formulations are becoming increasingly popular because of the generality of geometries that can be solved. Generality is intrinsic in the procedure as initial and boundary conditions, geometry and media properties, all enter the method after the basic algorithm has been developed.

This paper focuses on one differential method and one integral method, as shown in Fig. 1. The former is the Finite Difference Time Domain (FDTD) method which is a discrete time-domain differential formulation of Maxwell's equations that includes another embedded subgridding FDTD method (SGFDTD) to model small complex structures inside a normal FDTD method. The integral method is the 'Method of Moments' (MoM), most widely used in the frequency domain. The objective of this work is to explore subgridding inside the hybrid combinations between

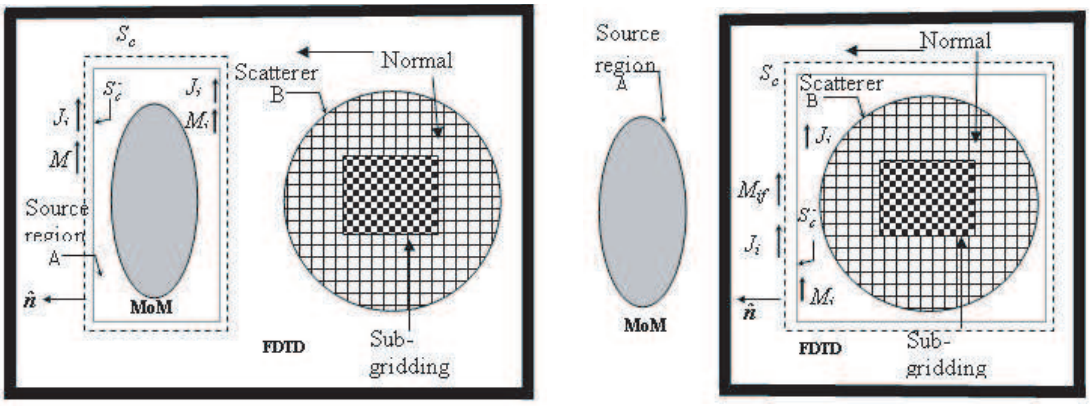

Figure 1: Hybrid MoM/FDTD/SGFDTD configuration for the single source and scatterer geometries; (left) Near field application, (right) Far field application.

these two methods and apply the combined method to different EM scattering applications such as those found in RFID communication systems.

Time Domain Modeling of Invisible Electromagnetic Shells

Cedric Blanchard
Massachusetts Institute of Technology, USA

Abstract— Since the precursor work presented by Pendry et al. [1], cloaking has receive a lot of attention from the scientific community. It is obvious that numerical simulations can provide substantial insight into understanding this phenomenon, which has pushed Cummers et al. [2] to report the first full wave simulations using the commercial software COMSOL Multiphysics based on the finite elements. However, such software does not offer the needed versatility in some situations.

We proposed here the simulation of a cylindrical cloaking with the Transmission Line Modeling (TLM) method [3]. As its name suggest TLM is a time domain method based on the analogy of Maxwell equations and the transmission line theory equations. To do so, TLM uses unitary circuits, termed nodes, which contain the information described in Maxwell equations. TLM is nowadays an efficient and powerful numerical tool for the numerical solution of complex electromagnetic field problems.

The permittivity and permeability tensors of the cloak material are characterized by the presence of off-diagonal elements in Cartesian coordinates. This anisotropic nature makes the modeling more complicated, but Huang et al. [4] have proposed an approach consisting in substituting the anisotropic material by concentric layered structure of alternating homogeneous isotropic materials.

In this work, it is shown that the best results are obtained when the effective permeability of the layers are calculated at the inner boundary of each one and not at the center. Furthermore, a nonlineal transformation permits to improve the effectiveness of the cloak as it has been suggested in [5].

REFERENCES

1. Pendry, J. B., D. Schurig, and D. R. Smith, "Controlling electromagnetic fields," *Science*, Vol. 312, 1780–1782, 2006.
2. Cummer, S. A., B-I. Popa, D. Schurig, D. R. Smith, and J. B. Pendry, "Full-wave simulations of electromagnetic cloaking structures," *Phys. Rev. E*, Vol. 74, 036621, 2006.
3. Johns, P. B., "A symmetrical condensed node for the TLM method," *IEEE Trans. Microw. Theory Tech.*, Vol. 35, 370–377, 1987.
4. Huang, Y., Y. Feng, and T. Jiang, "Electromagnetic cloaking by layered structure of homogeneous isotropic materials," *Opt. Express*, Vol. 15, 11133, 2007.
5. Xi, S., H. Chen, B-I. Wu, B. Zhang, Y. Luo, J. Huangfu, D. Wang, and J. A. Kong, "Effects of different transformations on the performance of a nonideal cylindrical cloak," Submitted.

Variational Integrators for Maxwell's Equations with Sources

A. Stern[1], **Y. Tong**[1,2], **M. Desbrun**[1], **and J. E. Marsden**[1]

[1]California Institute of Technology, USA
[2]Michigan State University, USA

Abstract— In a recent paper, the present authors introduced a framework for computational electromagnetics using variational integrators and discrete differential forms. This approach was developed by considering the electromagnetic Lagrangian (without sources of charge or current) as a discrete 4-form in spacetime, and then applying Hamilton's stationary action principle. The "discrete equations of motion" resulting from this variational principle describe a family of numerical methods for computing approximate solutions to Maxwell's equations.

These methods include Yee's finite-difference time-domain (FDTD) scheme, as well as the more general method of Bossavit and Kettunen, as special cases, but also methods on more general spacetime meshes, including a new integrator featuring asynchronous time stepping. Moreover, this discretization framework was shown to preserve important geometric features of Maxwell's equations, including discrete versions of the correct multisymplectic structure, gauge symmetry, and differential identities (e.g., null space of the curl-curl operator). As a result, these methods can be shown to conserve exactly the zero-divergence constraints on the magnetic flux $\mathbf{B}$ and electric flux $\mathbf{D}$, as well as exhibiting good energy conservation and lack of spurious modes.

In this work, we quickly review this variational approach, and then describe how to extend the previous framework to include free sources of charge and current. This is done, as in the literature on classical field theory, by defining a source 3-form $\mathcal{J}$ on spacetime (often written as a four-vector), which incorporates both the current density $\mathbf{J}$ and charge density ρ. We then add a term $A \wedge \mathcal{J}$ to the Lagrangian density, where A is the electromagnetic potential 1-form. The resulting numerical methods are shown to automatically satisfy a discrete version of the constraint $\mathrm{div}\mathbf{D} = \rho$, as well as the continuity of charge condition $\mathrm{div}\mathbf{J} = -\partial\rho/\partial t$. In addition to developing this theoretical framework, we also show how it applies to the previous algorithms, including our asynchronous integrator, when sources are included. Finally, we show some prototype numerical simulations with these methods, and discuss the observed geometric and numerical behavior.

Efficient Evaluation of 2D Sommerfeld Integrals Encountered in the Dielectric Half-space Problem by Use of Numerically Determined Steepest-descent Paths

Amit Hochman and Yehuda Leviatan
Department of Electrical Engineering
Technion — Israel Institute of Technology, Haifa 32000, Israel

Abstract— The analysis of 2D scattering in the presence of a dielectric half-space by integral equation formulations involves repeated evaluation of Sommerfeld integrals. Deformation of the contour to the steepest-descent path results in a well-behaved integrand that can be readily integrated. The well-known drawback of this method is that an analytic expression for the path is available only for the reflected fields. A simple scheme for numerical determination of the steepest-descent path for the transmitted fields is presented. The computational cost of the numerical determination is virtually the same as that of evaluating the analytic expression for the reflected fields.

When determining the steepest-decent path, attention is given to particular situations which require special treatment. For example, when the source is in the dense medium and the observation point is in the thin medium beyond the critical angle, a contribution from a second saddle-point is taken into account. Similarly, when both source and observation points are in the dense medium, and total internal reflection occurs, a branch-cut integral contribution is taken into account.

Once the steepest-descent path is numerically determined the integration is carried out by use of a Hermite-Gaussian quadrature rule. This procedure yields very accurate results with only a few evaluations of the integrand, provided that the integrand may be approximated by a slowly varying function multiplied by a Gaussian factor. When the source and observation points are close to the interface and to each other this requirement breaks down. Alternative contours and Gaussian quadrature rules are thus presented for this case. Also, the integrands are made to decay more rapidly by subtraction and subsequent addition of appropriate images.

Numerical results for various locations of the source and observation points obtained using the proposed integration method are verified against results obtained via straightforward trapezoidal integration on a path close to the real-line and slightly indented into the first and third quadrants to avoid the branch-points. Also presented are numerical results for some representative problems of scattering by cylinders in the presence of a dielectric half-space carried out by incorporating the proposed integration method into a Source-Model Technique solver. The results obtained from the Source-Model Technique solver are shown to be in good agreement with results available in the literature.

Formulation of the MoM in Space Domain with Two Sets of Basis Functions to Analyze a Microstrip Transmission Lines

M. Bassem Ben Salah, Chaker Essid, and Abdelaziz Samet

URCSE, École Polytechnique de Tunisie, Tunisia

Abstract— The Mixed Potential Integral Equation (MPIE) formulation is combined with complex image technique and solved by the method of moments (MoM) to analyze a printed transmission lines. The two-dimensional space domain Green's functions for the scalar and vector potentials are analytically obtained from the approximation of its spectral domain with complex images in the good sampling path. Thus functions have been efficiency obtained and validated, but the accuracy of this technique, propagation constant for the dispersive modes, don't only depend on the accuracy of the 2-D space domain Green's functions [1], they are strongly dependent on the number and the type of basis functions used in the approximation of the unknown current components. The application of several types of entire and subsectional domain basis functions has been proposed in the literature.

In this paper, we present a comparison between two sets of frequently used basis functions in space domain MoM formulation to analyze the microstrip transmission lines. The entire domain basis functions are presented by first- and second-kind Chebyshev polynomials [1]. The zeroth order modified Bessel function of the second kind [2], in the 2-D space domain Green's functions, presents a logarithmic singularity that might cause problems in the convolution integral. The contribution of these integrals can be handled in closed-form and the rest of the kernel is regular and does not generate integration problems. Due to the type of singularity present in this type of basis functions, Chebyshev quadratures are suitable to carry out the integrations involving the regular part of the Green's functions. The subsectional domain basis functions are presented by the pulse and triangle functions [3, 4], the singularity in Green's function has been also separately treated and its contribution analytically obtained. The remaining regular contribution to the reaction integrals has been evaluated with Gauss quadrature integration. The emphasis in this paper is on the relative accuracy, the convergence and the computational efficiency of both sets of basis functions. Numerical results for the modal currents and dispersion curves, and CPU time consuming are compared for the two types of basis functions.

REFERENCES

1. Bernal, J., F. Medina, R. R. Boix, and M. Horno, "Fast full-wave analysis of multistrip transmission lines based on MPIE and complex image theory," *IEEE Trans. Microwave Theory Tech.*, Vol. 48, 445–452, Mar. 2000.
2. Abramowitz, M. and I. A. Stegun, *Handbook of Mathematical Functions*, Dover, New York, 1972.
3. Soliman, E. A., P. Pieters, E. Beyne, and G. A. E. Vandenbosh, "Numerically efficient method for multislot transmission lines in layered media — Application to multislot lines in MCM-D technology," *IEEE Trans. Microwave Theory Tech.*, Vol. 47, 1782–1787, Sept. 1999.
4. Bernal, J., F. Medina, and R. R. Boix, "Full-wave analysis of nonplanar transmition lines on layered medium by means of MPIE and complex image theory," *IEEE Trans. Microwave Theory Tech.*, Vol. 49, 177–185, Jan. 2001.

Mesh-free Waveguide Mode Computation

Klaus Krohne, **Gi-Ho Park**, **and Er Ping Li**
A*STAR Institute of High Performance Computing, Singapore

Abstract— Mesh-free space discretization methods have gained much attention over the past decades mainly in the fields of mechanical engineering and astrophysics. The application in computational electromagnetics, however, has been rather scarce. Due to the lack of a prescribed mesh that introduces a topological relation between the locations at which the unknown field values are computed, mesh-free methods allow for a much more flexible arrangement of said locations. This can be a tremendous advantage in applications that require such flexibility, such as automatic refinement of the discretization as well as moving boundaries or charges.

One of the most established mesh-free methods is the *smoothed particle hydrodynamics* (SPH) method. It has been intensely studied since its introduction in 1977 and several enhancements and developments have been presented The majority of the research work in computational electromagnetics has been related to static and quasi-static applications. An elementary time-domain implementation for transient fields has been presented in [1]. This is also, where the term (SPEM) has bee introduced. In this work we expand the range of applicability to the frequency domain. As an example we compute the modes in circular hollow metallic waveguide. This motivates the introduction of novel boundary conditions for perfect electric conductors that are conformal with an arbitrary geometry. Furthermore, consistency restoring is implemented to maintain accuracy.

A generalized eigenvalue problem can be solved with direct numerical eigenvalue solvers for moderately sized applications. Figure 1 shows the modes in a waveguide with 1 m radius at 90 MHz that have been computed with SPEM. The field patterns comply with analytically computed patterns.

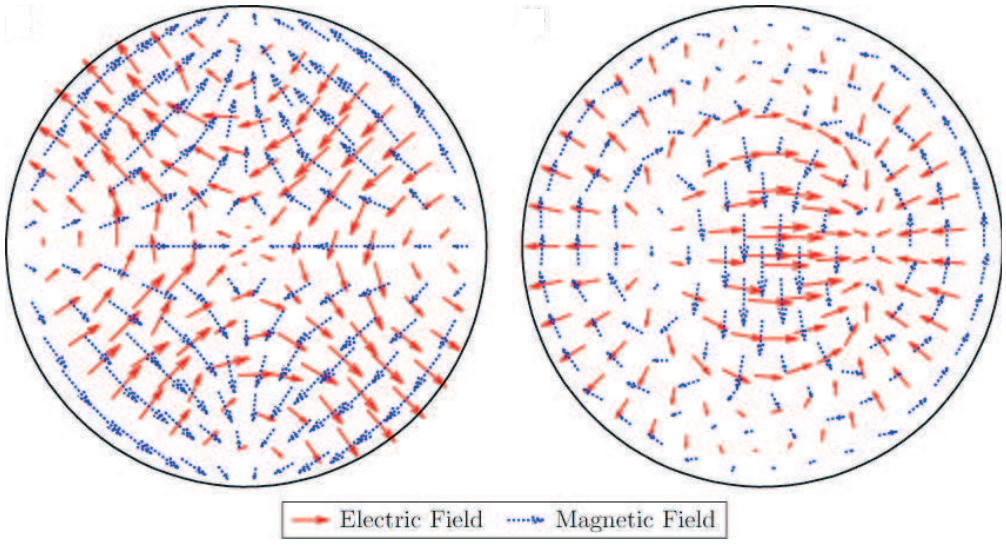

Figure 1: Modes in a circular hollow waveguide, computed with smoothed particle electromagnetics.

Development, Characterization and Simulation of Flexible Single-Layer X-Band Microwave Absorbers Based on Conducting Polyaniline

L. C. Folgueras[1, 2], **M. A. Alves**[1, 3], **M. B. Perotoni**[3], **and M. C. Rezende**[1]

[1]Materials Division, Instituto de Aeronáutica e Espaço, Brazil
[2]Universidade de Taubaté, Brazil
[3]CST, GmbH, Dramstadt, Germany

Abstract— One of the consequences of the ever-growing use of electronic devices operating at microwave frequencies is the increase of spurious electromagnetic radiation, which may interfere with the normal functioning of electric and electronic equipment. To minimize this type of interference, sheets, films and paints that have the ability to absorb some or most of the incident harmful electromagnetic radiation have been developed. In this work, two absorbent materials in the form of single-layer flexible sheets containing the conducting polymer polyaniline (PANI) are produced. In one of the materials, PANI was dispersed in a polymer matrix composed of a mixture of polyurethane (PU) and polyacrylonitrile (PAN) (both PA and PU are transparent to radar in the X-band). The second material consisted of compacted PANI, only. The electromagnetic properties of these materials were analyzed using the waveguide technique in the frequency range of 8 to 12 GHz (X-Band), and the dependence of the electromagnetic radiation absorption, complex permittivity and permeability of these materials as function of frequency were obtained. In order to better understand the absorbent properties of these materials as well as predict their behavior under different sets of conditions, the electromagnetic simulation software package CST Microwave Studio^{TM} was used to simulate the attenuation of the incident electromagnetic wave on the absorbent material. CST software is based on the Finite Integration Technique, which is a numerical method that can be successfully employed to solve various electromagnetic problems. The results show that materials have the potential to be used as narrowband microwave absorbers and the simulations performed with CST agreed well with the experimental data.

Efficient Numerical Strategy for the Coupling of the Fast Multipole Method and a Microlocal Discretization for Maxwell's Equations

E. Darrigrand[1], **L. Gatard**[2], **and K. Mer-Nkonga**[3]

[1]IRMAR, University of Rennes 1, Campus de Beaulieu, 35042 Rennes Cedex, France
[2]University of Bordeaux 1, 351 cours de la Libération, 33405 Talence Cedex, France
[3]CEA, CESTA, 33114 Le Barp Cedex, France

Abstract— An efficient method to solve time harmonic Maxwell's equations in unbounded exterior domain for high frequencies is obtained by using the integral formulation of Després mixed up with a coupling method based on the Microlocal Discretization method and the Fast Multipole Method (FMM) [1]. However, some aspects of this method still remain to study, in order to enhance the accuracy of MD method, and to obtain optimal complexity and high efficiency.

The integral formulation of Després [2], for Léontovitch's type impedance boundary conditions, results in a linear system with good properties which allow us to solve the system with an efficient iterative method. After discretization, we have to solve a dense linear system with a size N proportional to the free wave number $k = \frac{2\pi f}{c}$, where f is the frequency of the incident wave and c the speed of light. By using MLFMA [3], which is based on the reduction of the interactions generated by the Green kernel to interactions between multipole boxes, one can reduce the complexity of the matrix-vector calculation of the iterative solution to $O(N \ln N)$. Another approach consists in reducing the size of the system with the use of microlocal discretization and accelerating the matrix calculation with an adaptation of MLFMA, obtaining the MLFMD method [1].

Recently, improvements of MLFMD have been obtained using curved finite elements of higher order, leading to accurate results for Léontovitch impedance boundary conditions. Furthermore, quasi-linear complexity is obtained with a sparsifying of the translation matrix of MLFMD, using smoothing and thresholding of the transfert function of FMM as in [4]. Concerning the linear system of reduced size, it can be solved either with preconditioned iterative methods or with an efficient parallel direct solver.

These optimizations of MLFMD will be presented, together with results on complex numerical test cases.

REFERENCES

1. Bachelot, A., E. Darrigrand, and K. Mer-Nkonga, "Coupling of a multilevel fast multipole method and a microlocal discretization for the 3-D integral equations of electromagnetism," *C. R. Acad. Sci. Paris*, Vol. 336, Serie I, 505–510, 2003.
2. Collino, F. and B. Després, "Integral equations via saddle point problems for time-harmonic Maxwell's equations," *J. Comput. and Appl. Math.*, Vol. 150, 157–192, 2003.
3. Song, J. M. and W. C. Chew, "Multilevel fast multipole algorithm for solving combined field integral equations of electromagnetic scatte-ring," *Microwave Opt. Tech. Letter*, Vol. 10, No. 1, 14–19, 1995.
4. Cui, T. J., W. C. Chew, G. Chen, and J. Song, "Efficient MLFMA, RPFMA, and FAFFA algorithms for EM scattering by very large structures," *IEEE Trans. on Antennas and Propag.*, Vol. 52, No. 3, 759–770, 2004.

A New Scheme for PML Type Absorbing Boundary Condition Applying Uniaxial-pseudo Propagation Technique for Multi-dimensional Wave Analysis

Kensuke Sasaki and Yukihisa Suzuki
Department of Electrical and Electronic Engineering, Tokyo Metropolitan University, Tokyo, Japan

Abstract— Finite difference time-domain (FDTD) method has commonly used to multi-dimensional electromagnetic wave analysis. The solution with high accuracy will be obtained in the FDTD analysis, if the absorbing boundary conditions (ABCs) have high absorbing ability. Perfectly matched layer (PML) is known as one of ABCs with high absorbing ability for multi-dimensional FDTD analysis. The conventional PML type ABCs, such as Berenger's PML, require for many computational costs. It is meaningful to reduce computational costs from the PML type ABCs by keeping high absorbing ability.

A purpose of this study is to propose a new ABC, which has similar absorbing ability to the PML type ABCs and has lower computational costs than the PML type ABCs. We introduced uniaxial pseudo-propagation (UPP) for multi-dimensional wave propagation. With this concept, multi-dimensional wave propagation was split into one-dimensional wave propagations along x, y, and z directions in Cartesian coordinates. In this study, the new ABC was formulated by applying UPP concept to the wave propagation scheme in PML region. We call this new ABC as UPP-PML.

In this study, absorbing ability and computational costs for UPP-PML were compared with those of the Berenger's PML. As a result, absorbing ability for UPP-PML were almost as same as that of the Berenger's PML. We found that calculation time and required memories in UPP-PML were smaller than those of the Berenger's PML.

A Simple and Efficient Implementation of the Well-conditioned Electric-field Integral Equation

Xin-Qing Sheng and Chu-Qiang Deng

Center for Electromagnetic Simulation, School of Information Science and Technology
Beijing Institute of Technology, China

Abstract— It is well known that the electric-field integral equation (EFIE) is an ill-posed integral equation, whose discretized equation has a large condition number leading to a slow convergence in its iterative solution. Furthermore, if the conventional RWG basis function is used to discretize the EFIE, the numerical solution of the EFIE will suffers from instability at low frequencies, since the condition number of the EFIE has an unbounded increase as the discretization interval tends to zero.

A well-conditioned electric-field integral equation (WEFIE) is presented in Ref. [1]. This WEFIE involves hypersingularity, whose numerical implementation is difficult [2]. Recently, a weak implementation of the WEFIE is proposed and discussed in Ref. [3]. However this implementation is quite complicated, and requires additional memory and CPU time.

A simple and efficient numerical implementation of the WEFIE is presented in this paper. It is proved that the well-conditioned property of the WEFIE can be kept in this numerical implementation. Numerical experiments demonstrate the accuracy, efficiency, and stability of the presented implementation approach, even at low frequencies. The effect of round-off errors to efficiency is analyzed especially at very low frequencies. The numerical performance of the WEFIE for open bodies is also presented at last.

REFERENCES

1. *IEEE Trans. Antennas Propagat.*, Vol. 45, No. 9, 316–328, Sept. 1997.
2. *IEEE Trans. Antennas Propagat.*, Vol. 50, No. 12, 1824–1830, Dec. 2002.
3. *IEEE Trans. Antennas Propagat.*, Vol. 52, No. 9, 2262–2266, Sept. 2004.

Session 3P2a
Scattering by Ordered and Disordered Media: Photonic Applications 2

Full-wave Modeling of Experimental Random Metal Films

Piotr Nyga, Uday K. Chettiar, Mark D. Thoreson, Zhengtong Liu
Vladimir P. Drachev, Alexander V. Kildishev, and Vladimir M. Shalaev

Birck Nanotechnology Center, Purdue University, West Lafayette, IN 47907, USA

Abstract— Random metal-dielectric composites, also known as semicontinuous metal films exhibit unusual optical and electrical properties which can be used for a variety of applications. Due to the enormous complexity of the problem, the numerical studies of semicontinuous films were limited to various approximate methods. In this paper we employ parallelized FDTD (Finite difference time domain) based solver to study the electromagnetic properties of such films without any approximations.

Semicontinuous metal films (SMF) are random metal-dielectric composites with nanometer sized semicontinuous metallic elements. These composites can exhibit unusual optical and electrical properties, especially close to the percolation threshold, that are significantly different from the constituent materials. One of the remarkable properties of such composite films is the localization and enhancement of electromagnetic fields in the visible and infrared spectral ranges. These intense localized fields result in an enhanced nonlinear response, which can be used for a variety of applications ranging from single molecule spectroscopy to optical devices based on nonlinearity.

Due to the complexity resulting from the nontrivial geometry, the numerical studies of SMF were limited to mean field theories, quasi-static approximation or other simplified approaches like lumped circuit model. In order to study the local and effective response of such structures we use the FDTD method which simulates the structures without any approximations except for the discrete nature of the method. We use a parallelized version of our 3D FDTD solver to increase the maximal dimension of samples and to examine an adequate representative set of sample realizations.

SMF were fabricated using E-beam deposition and laser deposition. A wide set of samples was made using different fabrication parameters and metal filling fractions. The samples were characterized by measuring their transmission and reflection spectra, and the experimental spectra qualitatively agree with the effective medium theory.

In order to understand the local field distribution in such films their optical response is simulated using FDTD models. The geometry of the metallic elements was obtained by discretizing the SEM images of actual samples. The simulation was carried out multiple times using SEM images of different regions in the same sample and the results were averaged to obtain the final simulated spectra, which show good correspondence with the experimental data. The local fields exhibit strong enhancement and localization of hot spots in agreement with previously reported observations. Huge local enhancements of up to a four thousand times the incident field intensity are observed in the simulated films.

High-resolution Population Density Imaging of Random Scatterers through Cross-spectral Coherence in Matched Filter Variance

Mark Andrews, **Zheng Gong**, **Daniel Cocuzzo**, **and Purnima Ratilal**
Northeastern University, USA

Abstract— The matched filter enables imaging with high spatial resolution and high signal to noise ratio by coherent correlation with the expected field from what is assumed to be a discrete scatterer. In many imaging systems, however, returns from large numbers of scatterers are received together and the coherent or expected field vanishes. This is the case for various types of imaging systems. In radar systems, the matched filter is used to enhance radar imagery of cloud distributions for weather prediction and migrating bird populations for ecological surveys. In underwater sonar applications, scattered returns are matched filtered to determine the population density of fish and other marine organisms. Here we show that despite the absence of an expected field, cross spectral coherence in the matched filter variance retains a pulse compression property that enables high-resolution imaging of scatterer population density.

A full-field theory is presented for the statistical moments of the matched filtered field simultaneously scattered from a random distribution of scatterers. The moments depend on the characteristic function of the scatterer's spatial distribution, which may extend over multiple range resolution cells of the imaging system. Both analytic and numerical models are demonstrated for active imaging systems. Through illustrative examples representative of physical imaging systems, we show that high-resolution population density imaging of scatterer distributions can be achieved using the matched filtered variance since it is directly proportional to the mean number of scatterers within each resolution footprint. We provide conditions for when the incoherent scattering assumption is valid, and when coherent effects can be neglected depending on the distribution of scatterers. The model is implemented for scenarios where single scattering dominates as well as cases where multiple scattering is important. The models may be applied to imaging in both free space and waveguide environments.

1D Magnetophotonic Crystals Exhibiting Optical Tamm States

Taichi Goto[1], **Alexander V. Baryshev**[1], **Mitsuteru Inoue**[1]
Alexander M. Merzlikin[2], **Alexey P. Vinogradov**[2], **and Alexander B. Granovsky**[3]

[1]Toyohashi University of Technology, Toyohashi, Aichi, Japan
[2]Institute for Theoretical and Applied Electromagnetics, Moscow, Russia
[3]Moscow State University, Moscow, Russia

Abstract— Artificial structures composed of alternating dielectric materials with different refractive indices, known as photonic crystals (PCs), have been shown to affect the propagation of light, providing a new mechanism to control and manipulate the flow of light. Following the concept of photonic band gaps originating in light coupling to the spatially periodic structure and localization of light in the vicinity of defects introduced into the periodic structure [1], various one-, two- and three-dimensional PCs, photonic crystal fibers and waveguides, wave plates have been designed, and new fabrication technologies have been developed within the last two decades [2, 3].

Unique optical and magneto-optical properties are shown to exist when the constitutive materials of PCs are magnetic. For magnetophotonic crystals (MPCs), in which the constitutive elements are magnetic (or even only a defect introduced into the periodic structure is magnetic), there exists an additional degree of freedom to operate the photonic band structure, diffraction patterns, and the state of polarization of light, i.e., these characteristics can be influenced by the external magnetic field [4–6].

In this work we present a new type of MPCs composed of two 1D PCs, namely, magnetic and non-magnetic Bragg mirrors with slightly different photonic properties [6]. Such MPCs exhibit the resonant transmission and are experimentally shown to enhance the magneto-optical response of known materials. The surface state, so-called the Tamm state, is originated by the interface between two 1D PCs, and supports multiple propagation (localization) of light within magnetic layers. When magnetic field is applied, the difference of the wave vectors for left- and right-circular polarized localized Tamm modes, multiple propagation of these modes within the magnetic layer and the nonreciprocal character of the Faraday effect result in an enhancement of the polarization rotation by one order of magnitude. We believe that the Tamm structures are of benefit for localizing light within (or at) any active material introduced at the interface (or built in between two PCs).

REFERENCES

1. Joannopoulos, J. D., R. Meade, and J. Winn, *Photonic Crystals*, Princeton University Press, Princeton, 1995.
2. Lopes, C., "Materials aspects of photonic crystals," *Adv. Mater*, Vol. 15, 1679, 2003.
3. Lourtioz, J.-M., H. Benisty, V. Berger, et al., *Photonic Crystals: Towards Nanoscale Photonic Devices*, Springer, Berlin, 2005.
4. Inoue, M., R. Fujikawa, A. Baryshev, et al., *J. Phys. D: Appl. Phys.*, Vol. 39, R151, 2006.
5. Khanikaev, A. B., A. V. Baryshev, M. Inoue, et al., *Phys. Rev. B*, Vol. 72, 035123/9, 2005.
6. Vinogradov, A. P., A. V. Dorofeenko, S. G. Erokhin, et al., *Phys. Rev. B*, Vol. 74, 045128/8, 2006.
7. Inoue, M., K. I. Arai, T. Fujii, and M. Abe, *J. Appl. Phys.*, Vol. 83, 6768, 1998.
8. Inoue, M., A. A. Fedyanin, A. V. Baryshev, et al., *J. Magn.*, Vol. 11, 195, 2006.

A New Fully Automated Setup for 3D Infrared Wide Band BSDF Measurements and Application to BSDF Models

Thomas Lanternier, **Marie Cerisier**, **Laure Eupherte**, **and Olivier Gilbert**
CEA, Cesta, France

Abstract— We have redesigned our setup for Wide Band BSDF (*Bidirectional Scatter Distribution Function*) measurements [1]. This setup uses a heated ceramic rod as a source instead of a laser, thus allowing Wide Band measurements. Wide Band BSDF measurements pros over laser measurements include the ability to choose any wavelength band inside a given domain whereas laser lines are limited in the infrared. For example, it is possible to reproduce the exact spectral response of an infrared camera. On the negative side are the lower SNR, the lower angular resolution and the difficulty to reach grazing angles.

The redesign of our setup allowed us to make several improvements, in order to limit the negative aspects of Wide Band measurements and make it more versatile. These improvements include:

- A new optical path to increase the SNR;
- A new design to allow a precise control of the angular resolution;
- A new imaging system to control the shape of the spot on the sample, thus allowing grazing angle incidence measurements;
- A new sample mount for 3D (out of plane) measurements;
- A new software including several advanced features (automated alignment, 3D measurements, etc.).

One of the applications of BSDF measurements is the rendering of IR scenes using a ray tracing algorithm. For this purpose, a parameterized model generally has to be derived from the measurements. A number of models have been proposed by different authors. These models may be purely mathematical, or they may have physical roots. Not all models may be used for physical modeling. In particular, some models which don't verify the reciprocity principle or which may result in reflectivity superior to one are not suitable for physical rendering. Therefore, most models are constrained by their authors to guarantee a physical behavior.

Our measurement setup allows us to acquire a complete measured BSDF database for a given material. It is then possible to optimize a model to fit the measured BSDF. If the fit is accurate over the whole set of measurements, then the behavior is physical, even if the model is not constrained to always behave physically. This method can result in more accurate BSDF models. We will present examples of Wide Band BSDF fits based on the Ashikhmin BSDF model [2].

REFERENCES

1. Lanternier, T., S. Mainguy, N. Caillard, T. Donval, M. Henry, and M. Guenet, "Characterization of thermo-optical properties of infrared structures," *Progress in Electromagnetics Research Symposium*, Cambridge, USA.
2. Ashikhmin, M. and P. Shirley, "An anisotropic phong light reflection model," *Journal of Graphics Tools*, 25–32, 2002.

Session 3P2b
3D Electromagnetic Imaging for Geophysical Applications

3D Magnetotelluric Imaging for Geothermal Resource Assessment at Glass Mountain, California

Randall Mackie[1] and William Cumming[2]

[1]WesternGeco, 2261 Market St., PMB 643, San Francisco, CA 94114-1600, USA
[2]Cumming Geoscience, USA

Abstract— A 95 station magnetotelluric (MT) survey acquired in 2005 supplemented over 100 MT stations recorded in the 1980's in order to improve MT resistivity imaging and conceptual interpretation of the geothermal resource at Glass Mountain, California. Although 1D and 2D MT inversions were used for quality assurance, the resistivity interpretation emphasized the results of 3D inversions. The conceptual approach to the 3D MT inversion based on nonlinear conjugate gradients did not change significantly during the project. Adjustment of the regularization and more thorough editing of unrealistic data reduced inversion artifacts, especially at MT station gaps. The most significant advance was motivated by the recognition that smaller model elements were required to resolve important features of the geothermal resource and the discovery that the 3D MT inversion could effectively resolve smooth resistivity variations in this finer model mesh provided that the edited impedances included in the inversion were more closely sampled in frequency.

Optimization of the 3D MT inversion algorithm for parallel processing on larger computer clusters made it feasible to compute more finely sampled models and data. The resulting Glass Mountain 3D resistivity model was correlate with borehole induction log, petrology and temperature data, validating the 3D MT inversion and the conceptual interpretation of resistivity in geothermal settings based on temperature-sensitive clay transitions. The ongoing evolution of parallel computing should further improve 3D MT resistivity imaging, for example, by making it feasible to routinely model MT static distortion related to topography.

The Influence of Electrical Anisotropy in 3D Marine CSEM Surveys

Gregory A. Newman and Micheal Commer

Ernest Orlando Lawrence Berkeley National Laboratory, USA

Abstract— A new geophysical technology recently to emerge, with considerable potential, utilizes low frequency electromagnetic (EM) energy to map variations in the subsurface electrical conductivity or resistivity of offshore oil and gas prospects. With the marine controlled-source electromagnetic (CSEM) measurement technique, a deep-towed electric dipole transmitter is used to excite a low-frequency (∼0.1 to 10 Hz) electromagnetic signal that is measured on the sea floor over electric and magnetic field detectors, where larger transmitter-detector offsets can exceed 15 km. The electric and magnetic fields can be correlated directly to changes in the pore fluid types and the location of oil, given that oil is far more resistive than brine or water. Since the Earth is a lossy medium, the method has to use low frequency EM waves to interrogate the reservoirs; high frequency fields will not propagate very far into the subsurface. Typical depths of investigation range from 2 to 6 km for offshore prospects. This results in a tradeoff; achievement of greater depths of penetration is accompanied by a loss of resolution. Nevertheless, with the incorporation of a priori information, this problem can be mitigated. As an example, seismic methods are very good at delineating the bulk geological structure and that can be used to constrain the interpretation of the EM measurement, allowing one to extract valuable information on fluid properties of the reservoir.

Large-scale 3D CSEM imaging is now receiving considerable attention, (Commer et al. 2008, Commer & Newman, 2008, Carazzone et al. 2005). While one-dimensional (1D) modeling is relatively easy and trial and error 3D forward modeling straight forward (Hoversten et al. 2006; Weiss & Constable 2006), the need for 3D imaging is necessary as the search for hydrocarbons now increasingly occurs in highly complex and subtle offshore geological environments. Moreover it is now recognized that the 3D conductivity imaging of marine controlled-source electromagnetic data in hydrocarbon exploration is strongly influenced by electrical anisotropy of geological media. Failure to incorporate such effects into the imaging processes can produce misleading results. To deal with the problem it is necessary to incorporate anisotropy within the 3D imaging framework. Here we discuss one such approach that considers transverse anisotropy, where finite difference approximations to Maxwell's equations are employed for computing predicted data and cost functional gradients. Solution to the conductivity imaging problem is solved using a non-linear conjugate gradient scheme based upon a regularized least-squares approach. Synthetic and field examples will be discussed.

REFERENCES

1. Carazzone, J. J., K. E. Burtz, K. E. Green, and D. A. Pavlov, "Three-dimensional imaging of marine CSEM data," *SEG Techn. Prg. Abstr.*, Vol. 24, 575–578, 2005.
2. Commer, M. and G. A. Newman, "New advances in three-dimensional controlled-source electromagnetic inversion," *Geophys. J. Int.*, In Press, 2008.
3. Commer, M., G. A. Newman, J. J. Carazzone, T. A. Dickens, K. E. Green, L. A. Wahrmund, D. E. Willen, and J. Shiu, "Massively parallel electrical-conductivity imaging of hydrocarbons using the Blue Gene/L supercomputer," *IBM J. Res. & Dev.*, Vol. 52, No. 1/2, 2008.
4. Hoversten, G. M., G. A. Newman, N. Ceier, and G. Flanagan, "3D modeling of a deepwater EM exploration survey," *Geophysics*, Vol. 71, G239–G248, 2006.
5. Weiss, C. J. and S. Constable, "Mapping thin resistors and hydrocarbons with marine EM methods, Part II — Modeling and analysis in 3D," *Geophysics*, Vol. 71, G321–G332, 2006.

Three-dimensional Combined Inversion of Marine Controlled-source and Magnetotelluric Data

M. Commer and G. A. Newman

Ernest Orlando Lawrence Berkeley National Laboratory, USA

Abstract— Geophysical electromagnetic methods are routinely used to identify subsurface electrical conductivity distributions. The controlledsource electromagnetic (CSEM) method has been used in a marine environment for hydrocarbon resource mapping and subsea exploration. This owes to the fact that the vertical currents generated by the CSEM transmitter respond to thin resistive layers, such as hydrocarbon reservoirs. Magnetotelluric (MT) fields, on the other hand, are plane-wave in nature and horizontally uniform over large distances. The naturally occurring long-wavelength MT fields allow for large exploration depths. Hence, the MT method is suitable for conductivity imaging on a regional scale, such as basin characterization.

We apply the method of nonlinear conjugate gradient minimization to solve the joint three-dimensional (3D) inverse problem for electromagnetic data. A major obstacle in CSEM data imaging is to assess the correct background conductivity distribution in order to identify and reproduce the signals caused by thin embedded targets. Hence, integration of CSEM and MT data offers the potential of greatly enhancing imaging results, because the methods provide complementary information.

A large computational demand arises for the 3D joint inverse problem, since the iterative model update requires a large number of forward modeling solutions for both data types, which are inherently computationally expensive. Several strategies are combined to address this problem. For the forward problem, we employ a fast iterative QMR solver with Jacobi preconditioning on finite-difference (FD) meshes. Moreover, both the forward and inverse problems are solved on different levels of parallelization. At last, we use a grid-optimization strategy for adapting the computational mesh design to each forward problem separately, thus limiting FD mesh sizes. The improved resolution achieved by joint imaging is demonstrated using synthetic data.

Forward and Inverse Models of Electromagnetic Scattering from Layered Media with Slightly Rough Interfaces

A. Tabatabaeenejad and M. Moghaddam

Radiation Laboratory, Department of Electrical Engineering and Computer Science
University of Michigan, Ann Arbor, MI 48109, USA

Abstract— Layered rough surfaces are representative models for many structures such as layered soil, multi-year ice, rivers, and lakes. Researchers have been, and continue, developing different analytical and numerical forward models to calculate the scattering of electromagnetic waves from these structures. Developing these models, however, is not the ultimate goal; what interests us is the knowledge of the structure subsurface properties. Subsurface sensing, whether applied to layered ground, to detect its moisture content, or to smaller scale structures such as human body, for medical imaging purposes, is done via solving inverse problems, which remains an ongoing, challenging research topic.

The success of any inversion depends on the accuracy of the corresponding forward model. However accurate, forward models that are slow to evaluate are usually inappropriate for inversion, because they could be evaluated a large number of times in an inversion algorithm. Therefore, an analytical forward model, as opposed to a numerical one, is often a key to successful inversion. With the development of low-frequency experimental systems such as the Microwave Observatory of Subcanopy and Subsurface (MOSS) tower radar [1], which is designed for estimation of deep soil moisture, the need for an accurate and practical layered-soil scattering model has become evident. To address this need, we have developed an analytical model for scattering of electromagnetic waves from two-layer structures with random, slightly-rough boundaries [2]. The Small Perturbation Method (SPM), which assumes the roughness is small compared to the wavelength, is used up to the first order to calculate the amplitudes of the unknown scattered fields in the frequency domain.

Use of the method of small perturbation raises the question about the region of validity, which in our case, translates into the conditions on each layer roughness, slope, and permittivity for which the first-order SPM is accurate within a specified error bound. To this end, the SPM solution needs to be compared to a solution derived using a method that does not impose roughness restrictions. Analytical solutions are almost always approximate, and therefore, our inquiry should be numerical. We have used a PMCHWT-based integral equation solver [3] to analyze scattering from a large ensemble of two-layer structures. This numerical analysis is not the goal here; rather, a systematic comparison between the analytic and numerical solution needs to be carried out. The method we have proposed is minimization of a cost function through global optimization where the parameters to be optimized are the ones that characterize a rough surface structure. To accelerate the numerical solver, we approximate the off-diagonal blocks in the method of moment interaction matrix in terms of low-rank products using skeleton notions [4]. Simulations are performed for 1D rough surfaces represented by zero-mean stationary random processes, separating homogeneous dielectric layers.

The last part of this work is determining the properties of a rough surface structure from scattering data, using the forward model developed earlier. Despite the practical importance of this problem, it has not been addressed appropriately due to a number of reasons including the complexity of forward models and lack of viable inversion schemes. The method we have applied is known as Simulated Annealing (SA) [5]. This algorithm is able to retrieve the parameters that characterize the layered structure provided a good strategy for escaping from local minima is developed and appropriate values of both the inversion and measurement parameters are selected [6]. In a realistic approach to inverse problems, there are uncertainties that should be taken into account. Part of these uncertainties is due to the fact that noise contaminates the measured data. We have shown that some of the model parameters of a two layer structure, i.e., real part of the first layer dielectric constant and the first layer thickness, are much less sensitive to the measurement noise than other model parameters. We have also showed that by averaging the measurement noise over several data points, the output error can be reduced significantly [6].

REFERENCES

1. Moghaddam, M., Y. Rahmat-Samii, E. Rodriguez, D. Entekhabi, J. Hoffman, D. Moller, L. E. Pierce, S. Saatchi, and M. Thomson, "Microwave observatory of subcanopy and sub-

surface (MOSS): A mission concept for global deep soil moisture observations," *IEEE Trans. Geoscience Remote Sensing*, Vol. 45, No. 8, 2630–2643, Aug. 2007.
2. Tabatabaeenejad, A. and M. Moghaddam, "Bistatic scattering from dielectric structures with two rough boundaries using the small perturbation method," *IEEE Trans. Geoscience Remote Sensing*, Vol. 44, No. 8, 2102–2124, Aug. 2006.
3. Poggio, A. J. and E. K. Miller, "Integral equation solution of three dimensional scattering problems," *Computer Techniques for Electromagnetics*, R. Mittra, Ed., Pergamon Press, 159–264, Elmsford, NY, 1973.
4. Tsang, L., D. Chen, P. Xu, Q. Li, and V. Jandhyala, "Wave scattering with the UV multi-level partitioning method: 1. Two-dimensional problem of perfect electric conductor surface scattering," *Radio Sci.*, Vol. 39, No. 5, Oct. 2004.
5. Kirkpatrick, S., C. D. Gelatt, and M. P. Vecchi, "Optimization by simulated annealing," *Science*, Vol. 220, No. 4598, 671–680, May 1983.
6. Tabatabaeenejad, A. and M. Moghaddam, "Inversion of subsurface properties of layered dielectric structures with random rough interfaces," in review.

Inversion Study of a Large Marine CSEM Survey

J. J. Carazzone[1], T. A. Dickens[1], K. E. Green[1], C. Jing[1], L. A. Wahrmund[1]
D. E. Willen[1], M. Commer[2], and G. A. Newman[2]

[1]ExxonMobil Upstream Research Company, USA
[2]Ernest Orlando Lawrence Berkeley National Laboratory, USA

Abstract— Controlled source electromagnetic (CSEM) surveys can provide important constraints on variations in subsurface resistivity particularly under the favorable circumstances offered by the deep water marine environment. Resistivity cubes created by imaging CSEM surveys collected on an arrangement of transmitter sail lines and sea bottom detectors composing a rectangular grid can assist in answering key questions related to hydrocarbon fluid saturation at depths below seafloor ranging to several kilometers while employing frequencies in the 1/64 to 10 Hertz range. The extremely low electromagnetic noise made possible by the shielding effects of the deep-water marine environment, the strong current damming effects set up by the significant resistivity variations induced by hydrocarbon saturation in clastic rocks, and the power of the finite difference technique in three dimensions combine to allow CSEM measurements to play a useful role in hydrocarbon prospecting. This remains true in spite of the often subtle nature of the hydrocarbon signature in total electric and magnetic field recordings. In the work reported in this study we compare inverted resistivity volumes derived from multiple inversions of data from the same large scale marine survey in order to address questions of non-uniqueness and parameter sensitivity in the context of a fully three dimensional analysis of CSEM data within a general VTI resistivity model. Key inversion strategies appropriate to CSEM data include:

1. Isotropic resistivity inversion of the electric field in-line component resulting only from overflight transmitter sail lines,
2. Isotropic resistivity inversion of electric field in-line and cross-line components resulting from both overflight and broadside transmitter sail lines,
3. Anisotropic (VTI) resistivity inversion of electric field in-line and cross-line components from both overflight and broadside transmitter sail lines.

In CSEM marine surveys the transmitter is a horizontal bipole of up to ∼300 m in length towed continuously at a depth of approximately 50 m above the seafloor. The electromagnetic fields are recorded at stationary detectors sitting on the sea bottom. Recordings can include all three components of the electric and magnetic fields. Due to sea motion and the shorter antenna used in making vertical recordings, the vertical electric field tends to exhibit greater noise contamination as compared to the horizontal electric filed components. The in-line direction refers to the horizontal direction along the average towed sail line direction. The cross-line direction is the horizontal direction perpendicular to the in-line or sail direction. Because of hydrodynamic effects, the in-line direction is approximately the same as the towed transmitter bipole direction except in the case of strong cross-line sea water currents. Overflight sail lines are transmitter sail lines which pass directly over a specified subsea detector location. In-line electric field recordings made from overflight transmitter locations are known to be dependent primarily upon the vertical resistivity to a close order of approximation, even in a general VTI model, thus justifying the procedure of inversion strategy 1 where only vertical resistivity is the inversion objective. Broadside transmitter locations are transmitter locations on sail lines which pass significantly to one side or the other of a specific subsea detector at closest approach. Both electric field in-line and cross-line components from broadside transmitter locations are known to be influenced by both vertical and horizontal resistivity in a general VTI model. The procedure of inversion strategy 2 is used to highlight these effects. Inversion strategy 3 illustrates the extent to which a survey of this kind determines a complete VTI model.

Numerical Reconstruction of Permeability Material Using 3-D T-Ω Formulation of Finite Element Method

F. Yassine[1], **E. Chaker**[1], **K. Ahmed**[2], **K. B. Ammar**[3], **and S. Abdelaziz**[1]

[1]URCSE, École Polytechnique de Tunisie(EPT), Tunisia
[2]Electromagneticworks, Canada
[3]LACIME, École de Technologie Supérieure (ETS), Montréal, Canada

Abstract— Three-Dimensional electromagnetic numerical modelling is used in inversion problems, commonly for determining the distribution of electrical parameters like conductivity or permeability. This topic is up-to-date and it requires a great deal of intention to be paid both at the basic research level and at the level of techniques to be applied and results to be achieved as well. Many non-destructive techniques are used in medical, industrial and geophysical imaging [1–3]. Take the example of Magnetic Induction Tomography (MIT) or Electrical Induction Tomography (EIT). This type of problems is a non-linear and ill-conditioned problem needs two phase resolutions: the forward and the inverse phase. Finite Difference, Finite element and integral equation approaches are the most applied techniques in forward resolution [3–6].

This paper describes a numerical approach to image the electrical permeability distribution within a given object from a non-destructive evaluation signal. Based on the techniques of induced currents (Eddy-Current Techniques), this technique falls within the framework of tomography based on Magnetic Induction Tomography (MIT) and consists in determining the electric parameter of the object of interest ˍ the distribution of permeability is a case in point. Here we shall follow the measures of impedances within a pair of coils (between an emitter and one for detection). Starting from the measurement of tension in the reception coil, we can determine the electromagnetic field which had already scanned the object of interest. By using a method of an electromagnetic analysis, we can determine the magnetic field that contains information about the distribution of the parameter previously aimed at.

One variation of Finite Element Method in 3-D (FEM-3D) is the T-Ω formulation which consists in expressing the magnetic field H according to the potential current vectors and the potential magnetic scalar Φ. Accordingly, we model the potential vector running T by Edge Basis Functions and the potential magnetic scalar Φ by nodal basis functions. The use of two types of basic functions (Edge and Nodal), simultaneously, in only one hybrid formulation makes it possible to solve this type of problems.

In this paper, we have solved the forward solution using a three-Dimensional T-Ω formulation of Finite Element Method in order to determine the magnetic field and a classical Gauss-Newton algorithm with regularization to solve and stabilize the solution of the optimisation problem. The permeability of the object is assumed to be linear and isotropic. Results for the permeability imaging have been reconstructed using synthetically generated data.

REFERENCES

1. Soleimani, M., W. R. B. Lionheart, A. J. Peyton, X. Ma, and S. R. Higson, "A three-dimentional inverse finite-element method applied to experimental eddy-current imaging data," *IEEE Transactions on Magnetics*, Vol. 42, No. 5, May 2006.
2. Hollaus, K., C. Gerstenberger, C. Magele, and H. Hutten, "Accurate reconstruction algorithm of the complex conductivity distribution in three dimensions," *IEEE Transactions on Magnetics*, Vol. 40, No. 2, March 2004.
3. Avdeev, D. B., "Three-dimensional electromagnetic modeling and inversion from theory to application," *Surveys in Geophysics*, Vol. 26, 767–799, 2005.
4. Soleimani, M and K. Jersy-Willuhn, "Image reconstruction for magnetic induction tomography," *Proceedings of the 26th Annual International Conference of the IEEE EMBS*, San Francisco, CA, USA, September 1–5, 2004.
5. İder, Y. Z. and Ö. Birgül, "Use of the magnetic field generated by the internal distribution of injected currents for electrical impedance tomography (MR-EIT)," ELECTRİK, Vol. 6, No. 3, © TÜBİTAK, 1998.
6. Babaeizadeh, S., D. H. Brooks, and D. Issaacson, "3-D electrical impedance tomography for peacewise constant domains with known internal boundaries," *IEEE Transactions on Biomedical Engineering*, Vol. 54, No. 1, January 2007.

Session 3P3
Antenna Theory and Microstrip Antennas

Symbolic Derivation of Spectral Green's Functions for Anisotropic Multilayer Structures

I. Bianchi and J. C. da S. Lacava
Laboratório de Antenas e Propagação, Instituto Tecnológico de Aeronáutica, Brazil

Abstract— Electromagnetic fields created by sources embedded in stratified media are currently used in the analysis of phenomena in optoelectronics, microwave circuits, military surveillance and antenna theory. For accurate results, the analysis requires numerical methods such as the Method of Moments (MoM), Finite Elements or Finite Differences.

It is presently widely accepted that MoM-based algorithms are suitable for a rigorous numerical analysis of printed structures of small to medium sizes (in terms of wavelength) stacked up in layers. However, for the application of this method, the corresponding dyadic Green's functions need be derived. Although rigorous and elegant, these calculations are usually tedious and error-prone when done by hand, what is especially true in the analysis of structures with bi-isotropic or anisotropic materials.

To overcome this limitation, this work presents a new procedure for calculating the spectral fields in multilayer structures. Working in the Fourier domain and utilizing the symbolic capability of the *Mathematica*® package, closed-form expressions for the transformed electromagnetic fields are derived in a straightforward, error-free way. Consequently, the spectral Green's functions can be determined in a compact, closed form, with a considerable reduction of the calculation time.

Using this new procedure, the spectral Green's functions for microstrip structures with *biaxial* anisotropy are derived. Based on these functions, a method-of-moments algorithm is implemented in *FORTRAN* for the analysis of a printed dipole fed by electromagnetic coupling. Effects on its input impedance are discussed. For validation purposes, results obtained with the implemented algorithm are compared to those simulated with commercial software such as *HFSS*™, which makes use of the finite elements technique. Good agreement is observed.

Array Synthesis by Using Singular Value Decomposition

José A. Martínez Lorenzo[1], **Carey M. Rappaport**[1], **and Johanna M. LoTempio**[2]

[1]The Gordon CenSSIS, Northeastern University
360 Huntigton Ave, Suite 302 Stearns Center, Boston, MA 02115, USA
[2]MIT Lincoln Laboratory, 244 Wood Street, A-164, Lexington, MA 02420, USA

Abstract— Traditional array synthesis techniques like: Woodward-Lawson; Fourier-Transform; Dolph-Tschebyscheff or Taylor, do not take into account the array pattern degradation derived from mutual coupling between array elements or passive structures used for mounting the antenna. Moreover, all the elements are required to be uniformly distributed across the array plane.

Recently, some new techniques have been proposed to take into account mutual coupling effects during the array synthesis procedure. All of which use a full wave analysis technique, like the Method of Moments (MoM), as a forward model. Inversion is then performed by means of: Neural Networks (NN); Multiple Support Vector Regression (SVR) or MoM-Matrix Decomposition (MoM-MD), schemes. The later techniques have the following problems: NN needs a great number of training patterns; SVR, although not as computational intensive as NN still requires many training patterns, MoM-MD is limited to a mean-square-error criterion and could break-down for situations where the matrix has bad condition number.

The Singular Value Decomposition (SVD) framework is proposed as a suitable technique for array synthesis problems. The method is equivalent to Woodward-Lawson technique but allowing mutual coupling characterization and non uniform array element distribution. An additional feature of applying SVD to Array Synthesis problems is that only one training pattern is required per array element and regularization schemes can be applied for matrices with high condition number.

The SVD factorization decomposes the matrix of the system — derived from allocating the field produced by each element in a different column of the matrix-in orthogonal-mode voltage basis functions with their corresponding orthogonal-mode field basis functions. When the array is driven with a certain voltage mode, the radiated field is equal to that of its associated field mode multiplied by its mode singular value.

The synthesis technique consists of adding the voltage modes weighted by coefficients derived from projecting the desired pattern into their associated field modes. For the case of ill-posed matrices, the coefficients are filtered in order to remove noisy modes (Tikhonov regularization).

SVD-beam-shaping Synthesis Method

Borja González Valdés[1], **José A. Martínez Lorenzo**[2]
Antonio García Pino[1], **and Carey M. Rappaport**[2]

[1]Depto. de Teoría de la Señal y Comunicaciones, Univ. de Vigo
ETS Ingenieros de Telecomunicación, Campus Universitario, Vigo 36310, Spain
[2]The Gordon CenSSIS, Northeastern University
360 Huntigton Ave, Suite 302 Stearns Center, Boston, MA 02115, USA

Abstract— Contoured beams are widely used in satellite telecommunication systems, especially in direct broadcasting systems for television and digital radio. One way to produce a single contoured beam is to modify the surface shape of the reflector to change the induced surface current distribution and thus the beam shape. The main advantage of this option lies in its simplicity and high degree of polarization purity provided by circular corrugated horns.

This work presents a new method to synthesize contoured beams using reflector antenna surface shaping. The algorithm starts by discretizing the entire reflector surface into triangular patches, then by finding a linear relationship between the local surface distortion and the difference of the distorted and undistorted farfield patterns.

A feasible objective field, derived from coverage data specifications, must be provided to be the target of the synthesis. A numerical interpolation based on sinusoidal functions is proposed to obtain a first estimate of the objective field data in a set of observation directions. This estimation is projected onto a set of bases obtained from Singular Value Decomposition of the matrix relating field and distortions, achieving the desired and feasible objective field on the synthesis domain.

Finally, a linear system of equations with discrete distortions as unknowns results from the relationship between distorted surface field and the scattered field in observation points. The system solution is obtained by again using the Singular Value Decomposition combined with Tikhonov regularization. The discrete distortion values obtained from the system solution are translated into a physically realizable continuous surface by projecting them onto a Polynomial-Fourier-Series basis function in a best fit sense. The later scheme is iteratively repeated in order to minimize the residual error, derived from linearizing the problem. Thus, the method determines the required surface distortions to synthesize the desired pattern.

Results have shown that the method can be applied successfully in order to synthesize simple shaped patterns, showing fast and accurate convergence.

Design Optimization of an Inverted V-dipole

Johanna M. LoTempio[1], **Jose A. Martinez-Lorenzo**[2]
Carey M. Rappaport[2], **and Herbert Aumann**[1]

[1]MIT Lincoln Laboratory, Lexington, MA, USA
[2]The Gordon CenSSIS, Northeastern University, Boston, MA, USA

Abstract— Previous research and measurements have shown the existence of nulls or "blind spots" in the pattern of balun-fed straight-arm dipole phased arrays. This "blindness" effect has been associated with the coupling between the dipole balun feedlines. It can be eliminated by tilting the dipole arms by 45° toward the ground plane forming an inverted V-dipole. This variation to a dipole's shape does address the pattern nulls problem. However, it also changes its impedance characteristics, providing a poor match over the frequencies of interest. The purpose of this paper is to optimize the design parameters of V-dipole arrays by investigating the effect of the coupling between the dipole's arms and the balun feedlines, and the coupling between the dipole's arms and the ground plane on the impedance mismatch.

The antenna-modeling tool CST Microwave Studio was used to model the impedance and radiation characteristics of a V-dipole array. The analysis shows that increasing the distance of the dipole's arms from the ground plane, which is typically a quarter-wavelength, reduces the coupling between them and greatly improves the impedance match. The analysis results show an improved impedance match for a maximum arm height ranging from 0.30λ to 0.40λ. This range is dependent on the desired bandwidth. In addition, analysis results show that an adjustment to the balun feedlines length is needed to maintain the impedance match and achieve a large bandwidth. This adjustment can be achieved by making the balun feedlines shorter than the maximum height of the dipole. The analysis results are verified with antenna impedance measurements.

Design of Beam Steering Antenna Array for RFID Reader Using Fully Controlled RF Switches

D. Zhou, **R. A. Abd-Alhameed**, **P. S. Excell**, **C. H. See**
M. M. Abusitta, **Y. F. Hu**, **S. M. R. Jones**, **and N. J. McEwan**
Mobile and Satellite Communications Research Centre
University of Bradford, Bradford, West Yorkshire, BD7 1DP, UK

Abstract— In recent years Radio Frequency Identification (RFID) has become very popular in many commercial applications such as access control, animal tracking, security, and toll collection, because of its ability to track moving objects and its low-cost implementation [1]. A typical RFID system is always made up of two components, including the tags (transponders) and readers (interrogators). The antennas, as a key part of the system, enable the tag or reader to send and receive the signals. A tag comprises an antenna and an application-specific integrated circuit (ASIC, or microchip) that is given a unique electronic product code. Readers are devices that read tags, and they equipped with antennas, a transceiver, and a processor (server with software system).

Operating frequency determines the capability of an RFID system, and several frequency bands have been assigned to RFID applications examples include: low frequency at 125 Hz, high frequency at 13.56 MHz, high frequency at 868–915 MHz, and microwave at 2.45 and 5.8 GHz. The design of RFID antenna becomes more complicated and critical when the operating frequency rises into the microwave region. A tag antenna should be considered low profile and compact size, for reducing the cost and for convenience in use. However, reader antenna should be characterized as compact, directional with high gain, circular polarization, easily to be integrated and low cost. Recently, many kinds of RFID antenna have been proposed for the tags and the readers [2–7].

With the recent developments of the modern supply chain management (SCM), RFID systems have been paid more and more attention, and have a huge potential market. In this paper, problems encountered in practice associated with RFID reading systems in multi-portal implementation were identified. As a consequence, a solution on reader antenna design with enhanced performance was then developed by using beam steering antenna array approach.

REFERENCES

1. Chen, Z. N., *Antenna for Portable Devices*, Chapter 3, Wiley, 2007.
2. Rao, K. V. S., P. V. Nikitin, and S. F. Lam, "Antenna design for UHF RFID tags: A review and a practical application," *IEEE Transactions on Antennas and Propagation*, Vol. 53, 462–469, 2005.
3. Subramanian, V., J. M. J. Frechet, P. C. Chang, D. C. Huang, J. B. Lee, S. E. Molesa, A. R. Murphy, D. R. Redinger, and S. K. Volkman, "Progress toward development of all-printed RFID tags-materials, processes, and devices 2," *Proceedings of the IEEE*, Vol. 93, 1330–1338, 2005.
4. Qing, X. M. and N. Yang, "A folded dipole antenna for RFID," *Proceedings of the IEEE Antennas and Propagation Society International Symposium*, Vol. 1, 97–100, June 2004.
5. Ukkonen, L., M. Schaffrath, J. Kataja, L. Sydänheimo, and M. Kivikoski, "Evolutionary RFID tag antenna design for paper industry applications," *Int. J. Radio Frequency Identification Technology and Applications*, Vol. 1, No. 1, 107–122, 2006.
6. Marrocco, G., "RFID antennas for the UHF remote monitoring of human subjects," *IEEE Transactions on Antennas and Propagation*, Vol. 53, 1862–1870, 2007.
7. Ma, D. and W. X. Zhang, "Broadband CPW-fed RFID antenna at 5.8 GHz," *Electronics Letters*, Vol. 42, No. 22, October 2006.

Performance Analysis of Wearable Microstrip Antennas with Low Conductivity Materials

Erdem Yilmaz and Dayalan Kasilingam
Department of Electrical & Computer Engineering
University of Massachusetts Dartmouth, North Dartmouth, MA 02747, USA

Abstract— With the advent of personal communications technology, wearable antennas have received growing attention, in recent years. In the near future, clothing will have a wide variety of consumer electronics and communication devices built into them. Antennas are an integral part of all hand-held units used in personal communications. Traditionally, antennas are constructed with metallic elements, which can be treated as perfect electric conductors (PEC). In this research, in order to have sufficient flexibility, weight and conformity, carbon nanostructured conductor inks and conducting polymer inks are studied as possible conductors in wearable antennas. Since the conductivity of these inks is not high enough to be treated as perfect conductors, the objective of this study is the design, characterization and development of wearable microstrip antennas with low conductivity. Microstrip antennas with low conductivity materials are analyzed for radio frequency applications.

The antenna performance is analyzed using Microwave Studio — CST^{TM}. The antenna gain, efficiency and impedance are calculated and used as performance metrics in this study. Microstrip antennas, using perfect conductors, are designed to operate in the ISM bands of 2.4 GHz, 800 MHz and 450 MHz. A $\frac{1}{4}$-wave microstrip transmission line, matching circuit is designed to match the microstrip antenna to the 50 Ω feed. The antenna bandwidth is defined in terms of the S_{11} parameter. Simulations are performed to estimate S_{11} across a wide band of frequencies. The normalized 3 dB bandwidth is found to be around 6–8%.

The microstrip antennas with the same dimensions are then used with low conductivity materials to investigate the degradation in gain and efficiency. For the 2.4 GHz antenna, the gain remained flat around 7 dB, down to conductivity levels of approximately 10^5 S/m. When the conductivity level is lower than 10^5 S/m for the microstrip patch and ground plane, the antenna gain dropped off considerably. The antenna efficiency was around 50% for conductivity levels of the order of 10^5 S/m. The gain was approximately 0 dB for conductivity levels around 2×10^3 S/m. Clearly, down at these conductivity levels the conduction losses are significantly more than the power radiated. It is concluded that for the 2.4 GHz microstrip antenna, conductivity levels have to exceed 10^4 S/m, for acceptable antenna performance.

The effects of low conductivity microstrip patches and ground are also investigated for different substrate thicknesses. Increasing the substrate thickness was found to reduce the effects of low conductivity. The gain of the 2.4 GHz microstrip antenna was found to be 10 dB better for a 6 mm substrate compared to the 1.5 mm substrate with a conductivity of 10^4 S/m. This is attributed to the concentration of current at the strip surface when the thickness is small. The increase in current density results in higher conduction losses and lower gains.

Optimization Using Surrogate Models in Materials-based Electromagnetic Design

Orkun Karabasoglu and Gullu Kiziltas

Mechatronics Engineering, Sabanci University, Orhanli, Tuzla, Istanbul 34956, Turkey

Abstract— Metamaterials have gained considerable interest in the Radio Frequency and optics community due to their unusual properties not available in nature. However, despite their proven potential in theory and some of their practical realization, they are restricted to some known structures/compositions such as the SRR structure. This is largely due to the natural limit imposed by intuitive design efforts and or practical realization challenges. A formal efficient framework allowing for the design of non-intuitive novel structures does not exist. However, similar to metamaterials, examples in literature prompts for the possibility of unique combinations of materials leading to desired electromagnetic behavior such as non-reciprocality. To address this issue, in this paper, we present an efficient design optimization framework for electromagnetic applications. The framework is based on integrating hybrid design optimization concepts with various surrogate modeling tools. The goal is to identify the device structure, both material and conductor in three dimensions, in an automated and efficient manner subject to some performance and size constraints. For the synthesis module, gradient-based optimizers such as Sequential Quadratic Programming (SQP) and global optimizers such as Genetic Algorithms are both utilized to complement each other in terms of global search capability and speed. As the analysis module, full wave electromagnetic wave analyzers, such as the HFSS, and a hybrid FE-BI based electromagnetic solver are integrated to the optimizers. The design framework is primarily based on interfacing the analysis tools with various surrogate based models and linking it to the optimization tools.

Large scale design optimization problems such as volumetric material explorations are computationally very expensive and demand high resources. This drawback can be surpassed by introducing surrogate modeling techniques into the platform as demonstrated in literature. To allow for considerable speed-ups of the versatile automated design process proposed here, automated and adaptive Design of Experiment (DOE) scheme is employed over the design domain and various surrogate models are compared within the design framework with respect to their performance. Multiple surrogate modeling techniques are investigated such as Kriging, Polynomial, RBF (Radial Basis Functions), Artificial Neural Networks (ANN), Support Vector Machines (SVM), etc. Specifically, focus is on the volumetric material distribution, matrix material properties and frequency response, which constitute the design variables of the problem. Results show that RBF is most promising with least number of data samples and best convergence rates. As a further speed-up, resulting surrogate models are linked to reduced frequency based models using a modified Burlisch Stoer Algorithm (BST) of the electromagnetic response such as bandwidth. Results show that the hybridized surrogate model based design framework allows for large number of design variables and an effective exploration of the global large scale design space. At the end, the resulting framework will be applied to the design of an ultra-wide bandwidth SATCOM antenna. The determination of the artificial material structure follows a two step procedure: The effective medium of the antenna is found using the surrogate model based hybrid design optimization framework. The ultimate goal is to extend the capabilities of the framework to the design of the microstructure of metamaterials utilizing inverse topology optimization. The freedom to explore all possible design degrees of freedom and the possibility to design for the material itself is expected to open up entirely new possibilities in microwave and optical applications.

The Design and Optimization of Planar LPDAs

A. A. Gheethan and D. E. Anagnostou
ECE Department, South Dakota School of Mines & Technology, Rapid City, SD 57701, USA

Abstract— Log-Periodic Dipole Antennas are considered as frequency independent antennas. There properties such as high gain, high front to back ratio, low cost and high operating band-width were attractive for many communication applications.

This work shows the design of planar LPDAs for high operating frequencies. Two designs for printed LPDAs are shown in this paper. The first design was made for the conventional Euclidean monopoles while the second design was investigated for the rectangular Meander lines. Both designs achieved a very good return loss response over the entire desired frequency range with a flat gain response. The design frequency range was 2–4 GHz. The prototype for each LPDA shown in Figure 1 consists of N flat dipoles fabricated on a substrate with thickness t. The design procedure is described step by step and the gain was optimized by varying the dipoles width and the paired strip width which were used to connect the dipoles and for feeding. Moreover, a comparison between these designs is also presented. The comparison aspects were: a) Gain Response, b) Radiation Pattern, c) Space Size and d) Operating Band-Width.

One of the most important parts of this work is feeding the LPDA. A novel feeding method was developed herein without the need of using a balun, and thus, the complexity of the design and the cost were reduced. At the top of the substrate, the RF part of the dipoles is located and connected together by a line with width w; meanwhile the ground part is located on at the bottom and also connected to each other by similar line for the RF part with the same width w. To ensure the balance, a special type of coaxial cables was used. This coaxial is made of a metallic cylinder, which represents the ground, filled with a dielectric which covers the RF part of the coaxial. The coaxial is then connected to a male or female SMA. This coaxial was used to feed the LPDA by soldering the cylindrical part of it with the ground part of the antenna while the RF part of the coaxial was extended and connected to the RF part of the antenna by making a small via through the substrate. Notice that the LPDA was fed from the smaller radiating element.

The design was carried out by the design of a single element and then adding other elements one by one. The added elements lengths can be calculated depending on the geometry constant factor τ which should be chosen before the design. The needed number of elements has been calculated using the conventional equations for the wire LPDA. Also, the same equations were used to find the apex angle α and the spacing factor σ. The structures were simulated using the available full wave commercial software Zeland IE3D$^{\text{TM}}$ based on the MoM algorithm. The simulated results for the return loss response and the gain response exhibited very good values.

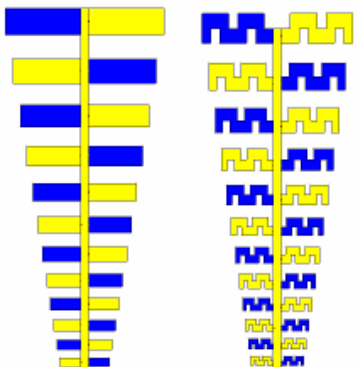

Figure 1: The prototype for the two designs.

Radiation Efficiency of the Metamaterial Zero-order Resonator Antenna

David Vrba and Milan Polívka
Department of Electromagnetic Field, Czech Technical University
Technická 2, Praha 166 27, Czech Republic

Abstract— In this paper a technique for improvement of radiation efficiency of metamaterial zero order antenna based on increasing of vertical antenna height is presented. Comparison of the two microstrip line implementation of the zero order resonator (ZOR) antennas with different height over ground plane is demonstrated. Improved ZOR antenna exhibit 75% efficiency compared to 10% of the reference antenna.

Application of the Neural Network to the Synthesis of Vertical Dipole Antenna over Imperfect Ground

Rached Salem
Department of Physics, Faculty of Sciences of Gafsa
2100, Sidi Ahmed Sarouk, Gasfa, Tunisia

Abstract— In this paper, we propose to study the synthesis of the vertical dipole antenna over imperfect ground.

The synthesis implementation's method for this type of antenna permits to approach the appropriated radiance's diagram. The used approach is based on neural network.

Our main contribution in this paper is the extension of a synthesis model of this vertical dipole antenna over imperfect ground.

Design of Four Iterative Circular Shaped Fractal Antenna for Wireless Applications

Raj Kumar[1], **Yogesh Thakare**[2], **and Mahesh Barari**[3]

[1]Department of Electronics Engineering
Defence Institute of Advanced Technology (Deemed University), Girinagar, Pune-411 025, India
[2]PVG'S College of Engineering and Technology, Pune-411 009, India
[3]Fergussion College, University of Pune, Pune-411 004, India

Abstract— Advances in antenna technology required the antenna of small size, low profile, easily fabricable and low cost. Microstrip antenna is one of them. Rectangular and circular microstrip patch antenna have been studied in open literature [1, 2]. These patches have been excited in a single dominant mode provide for linearly polarized radiation as well circular polarization. Circularly polarized antenna is classified single fed type and dually fed type. The attractive feature is the ability to produce the CP waves easily with single feed. This is achieved by applying some perturbation or modification to the patch. For a nearly square patch and a nearly circular [4, 5], the feed position of antenna is taken at $\pm 45^\circ$ with respect to the symmetrical axis.

This paper presents the four iterative circular fractal antenna and its backscattering RCS with respect to iteration number. First, the solid circular patch antenna has been designed on $\varepsilon_r = 2.2$, $h = 0.787\,\text{mm}$, $a = 40.766\,\text{mm}$ and aspect ratio $b/a = 0.98$ with feed position $-25.346 \times 25.68\,\text{mm}$. The antenna has been simulated using FDTD method. The resonant frequency of this antenna has been observed at 1.42 GHz w shown in Fig. 1. The circular fractal antenna has also been designed on the same substrate with b/a aspect ratio 0.98, $a = 40.766\,\text{mm}$. The fractal geometry has been introduced in this solid patch with four iteration. Solid patch is the zero iteration. In the first iteration, a square patch $56.08 \times 56.08\,\text{mm}$ has been subtracted from nearly circular patch. Then a nearly circular patch $28.32 \times 27.73\,\text{mm}$ with same aspect ratio 0.98 has been made which should touch all four arms of subtracted square. Then the process repeats in the same way upto fourth iteration. The final geometry of antenna is shown in Fig. 2. The antenna is fed at $-25.346 \times 25.68\,\text{mm}$. The antenna has been simulated again by using FDTD technique. As shown in Fig. 3, the first resonant frequency of the fractal antenna shifts to 1.08 GHz i.e., around 340 MHz by applying the fractal geometry in comparison to resonant frequency of solid patch 1.42 GHz. It reveals the size reduction of the antenna. The Fig. 3 also shows the multiple resonances, these are because of fractal properties of antenna. The multiple resonances are observed on 1.08 GHz, 1.66 GHz, 2.91 GHz, and 4.36 GHz. Fig. 4 shows the backscattering RCS of the same fractal antenna shown in Fig. 2 with respect to iterations simulated by MOM. It shows as the iteration increase the backscattering RCS decreases. The fourth iterative structure gives the maximum backscattering RCS reduction. This circular shaped fractal antenna has the privilege of size reduction, multi band and circular polarization and useful for Mobile Communication and military applications where RCS of antenna is an important parameter.

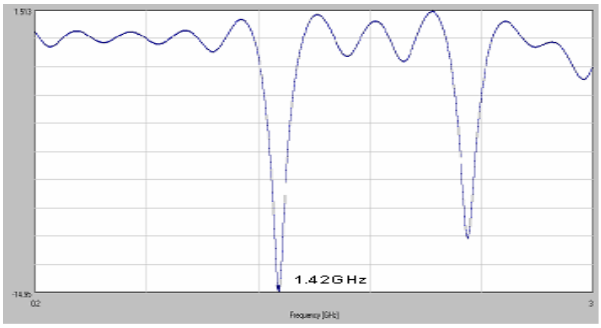

Figure 1: Return loss of circular microstrip patch.

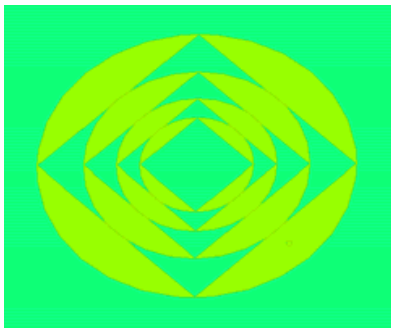

Figure 2: Four iterative circular shaped fractal microstrip antenna.

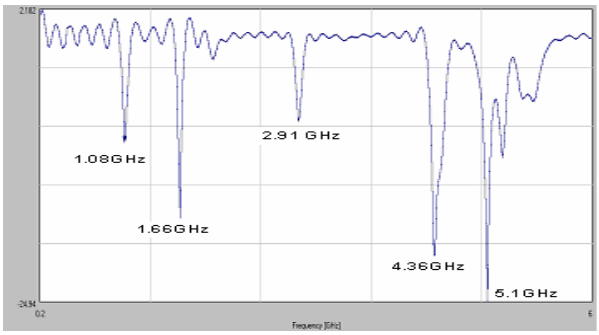

Figure 3: Return loss of circular microstrip patch.

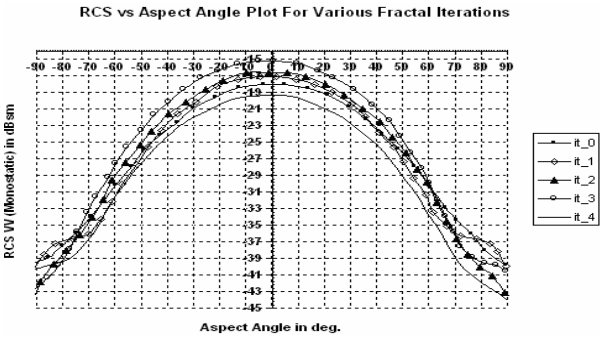

Figure 4: Backscattering RCS of four iterative fractal antenna.

REFERENCES

1. Bahl, J. and P. Bhartia, *Microstrip Antennas*, Artech house, Dedham, Ma, 1981.
2. Garg, R., "Progress in microstrip antennas," *IETE Technical Review*, Vol. 18, No. 2&3, 85–98, March–June 2001.
3. Shen, L. C., "The elliptical microstrip antenna with circular polarization," *IEEE Trans. on Antennas and Propagation*, Vol. 29, 90–94, 1981.
4. Hneishi, M., "Back-feed type circular polarized microstrip disk antenna by one-point feed," *Trans. Inst. Electron.&Comm. Eng. J.*, Vol. J63-B, 6, 559–65, 1980.
5. Puente, C., J. Romus, R. Pous, and P. Cardma, "On behaviour of the Sierpinski multiband fractal antenna," *IEEE Trans. on Antennas and Propagation*, Vol. 46, 517–524, 1998.

Low-sidelobe Microstrip Array with Circular Polarization for RFID Application

Zhu Sun, **Shun-Shi Zhong**, **Xiao-Rong Tang**, **and Kuang-Da Chen**

School of Communication and Information Engineering
Shanghai University, Shanghai 200072, China

Abstract— In recent years, RFID systems have experienced rapid development in some fields such as industrial manufacturing, logistics and retail etc, and held a wide horizon in these areas. Many papers have detailed antennas with circular polarization or dual polarization capability for RFID reader applications, in which, however, low-sidelobe circular polarization (CP) patch arrays are rarely reported. In our application, a UHF RFID system is required to accurately identify a row of adjacent targets at a certain distance. The features such as high gain, narrow beamwidth, low sidelobe level and circular polarization are desired to meet the demands on sensing distance and resolution.

In this paper, a coplanar-fed microstrip array of 4×3 CP elements with narrow beamwidth and low-sidelobe level is proposed for the UHF RFID application. The quasi-square patch is used as the CP element of the array, which is corner-fed to excite two orthogonal modes. By tuning the ratio of the patch length a and width b, good circular polarization performance is achieved at the desired frequency. The microstrip array is designed to have Chebyshev distribution in the horizontal direction and a uniform distribution in the vertical direction.

Each three patches in a vertical column are cascaded-fed and then connected to the horizontal main feeder. The $\lambda_g/2$ microstrip line is used to link two adjacent patches to achieve almost equal and in-phase excitation. For more accurately uniform excitation, the $\lambda_g/2$ microstrip line is split into two $\lambda_g/4$ sections for the impedance transformation to adjust the current distribution. In the horizontal main feeder, four-section $\lambda_g/4$ microstrip lines are used to link the two adjacent vertical columns composed of 3 patches. The characteristic impedance of four sections therein is alternatively changed to tune the current ratio of adjacent columns so as to achieve a Chebyshev distribution.

A test array of 4×3 elements was fabricated on the substrate with relative dielectric constant of 3.5, loss tangent of 0.0005 and thickness of 2 mm. The measured results show that the relative sidelobe level at the center frequency is about -27 dB in the horizontal plane and -13 dB in the vertical plane, the HPBW of main beam is about 25.2° in the horizontal plane and 22.8° in the vertical plane. The antenna's gain is measured to be about 12 dB. The axial ratio in the broadside is about 0.4 dB and keeps less than 3 dB inside the main beam for both horizontal and vertical planes.

Session 3P4
Plasmonics, Metamaterials, and Magneto-Optics

Manipulating the Properties of a Meta-material by Applying a Strong Magnetic Field

Yakov M. Strelniker[1] and David J. Bergman[2]

[1]Department of Physics, Bar-Ilan University, IL-52900 Ramat-Gan, Israel
[2]Raymond and Beverly Sackler School of Physics and Astronomy, Tel Aviv University
IL-69978 Tel Aviv, Israel

Abstract— We studied theoretically and numerically the light transmission through a sub-wavelength perforated metal film (as well as through other types of meta-materials) with Drude *ac* conductivity tensor in the presence of a static magnetic field [1–3]. The film is found to exhibit a magneto-induced light transparency and a decreasing of reflectivity due to cyclotron resonance. We have shown that the applied static magnetic field shifts the surface plasmon resonance and the extraordinary light transmission to higher frequencies. We have also shown that, in addition to the surface plasmon resonance, there also exists a so-called cyclotron resonance, which can play, in principle, some role in light transmission. Therefore, an applied static magnetic field can be used to manipulate the transmission of light through non-magnetic metal films, both with and without an array of sub-wavelength perforations. This could form a basis for a new type of magneto-optical switch and other magneto-optical devices. We also propose to use the magnetic field for getting a strong polarization effect, which depends on the ratio of the cyclotron to plasmon frequencies, and which can be made arbitrarily large [4]. A material which may be suitable for this purpose is Bismuth, where the low free-charge density ($\sim 3\times 10^{17}\,\mathrm{cm}^{-3}$) can make the carrier cyclotron frequency, ω_c, equal to or greater than the plasma frequency, ω_p [5–7]. Another possibility is to use highly doped semiconductors like GaAs and InAs [8]: In that case, it is possible to obtain large values of the Hall mobility μ, and therefore also large values of the dimensionless magnetic field $H = \mu|\boldsymbol{B}_0|$, using lower values of $\boldsymbol{B}_0$ (where $\boldsymbol{B}_0$ is the magnetic field measured in conventional units). Experimental tests of our predictions would be very desirable.

REFERENCES

1. Strelniker, Y. M. and D. J. Bergman, *Phys. Rev. B*, Vol. 59, R12763–R12766, 1999.
2. Bergman, D. J. and Y. M. Strelniker, *Phys. Rev. Lett.*, Vol. 80, 857–860, 1998.
3. Strelniker, Y. M., D. Stroud, and A. O. Voznesenskaya, *Eur. Phys. J. B*, Vol. 52, 1–7, 2006.
4. Strelniker, Y. M., *Phys. Rev. B*, Vol. 76, 085409-1–085409-6, 2007.
5. Sherriff, R. E. and R. P. Devaty, *Phys. Rev. B*, Vol. 41, 1340–1346, 1990.
6. Sherriff, R. E. and R. P. Devaty, *Phys. Rev. B*, Vol. 48, 1525–1536, 1993.
7. Strijkers, G. J., F. Y. Yang, D. H. Reich, C. L. Chien, P. C. Searson, Y. M. Strelniker, and D. J. Bergman, *IEEE Trans. Magn.*, Vol. 37, 2067–2069, 2001.
8. Tornow, M., D. Weiss, K. V. Klitzing, K. Eberl, D. J. Bergman, and Y. M. Strelniker, *Phys. Rev. Lett.*, Vol. 77, 147–150, 1996.

The Magnetic Manipulation of Surface Plasmons — Consideration of Possible Technologies

Dave M. Newman, **M. Lesley Wears**, **and Raphael J. Matelon**
School of Engineering, Computing & Mathematics, University of Exeter, Exeter EX4 4QF, UK

Abstract— Interfaces between dielectric and metallic media possessing negative permittivity (ε) can support electromagnetic waves propagating as longitudinal density oscillations in the free-electron plasma at the metallic surface. Like photons, the quanta of these collective excitations remain bosons and are known as surface plasmons. Moreover, under conditions satisfying the relevant conservation laws, photons and plasmons are mutually transformable. Photons incident on a metallic surface for example may be induced to convert to plasmons that propagate on the surface before their subsequent recovery as photons emitted back into free space. The most exciting confirmation of this behaviour being the work of Altewischer et al. [1] showing that a photon, having followed a path that includes its conversion to a plasmon and back to a photon, retains entanglement with the twin with which it was originally created in a down-conversion process. However, unlike photons, plasmons are subject to influence by applied magnetic fields during propagation as described by the theoretical work of Chiu and Quinn [2] and Nakamura and Paranjape [3] now more that more than 30 years old. Their equations describe a second-order mixing process between the ac plasmon field (E_p) and any applied and appropriately orientated dc magnetic field (H) to produce terms of the form $\chi^{(2)}E_p^2H$ in the plasmon field energy density where $\chi^{(2)}$ is a generalised susceptibility term. At interfaces the breaking of inversion symmetry determines that terms such as $\chi^{(2)}E_p^2$ are always present. The plasmon energy and hence frequency consequently acquire a contribution linear in the applied field H which is real and thus transposable to a photon emission field when the plasmon is intercepted by a grating out-coupler. Our observation of phenomena that can be attributed a direct consequence of magnetically induced shifts in plasmon frequency indicate that the efficiency of the mixing process, as with many process involving plasmons, may be high. In principle we have an as yet unexploited mechanism for the frequency shifting or frequency modulation of optical radiation offering the prospect of new devices and technologies. Theory indicates that frequency shifts of an order relevant to wavelength division multiplexing in optical communications, frequency selection in spectral domain data storage technologies or the novel readout of conventionally recorded magnetic data may all be achievable. Practical realisation of theses concepts is however somewhat constrained by the materials available and the strength of the magnetic fields required. Whilst silver and aluminium are the surfaces of choice for the efficient generation and propagation of plasmons the production of significant frequency shifts in plasmons propagating on the surfaces

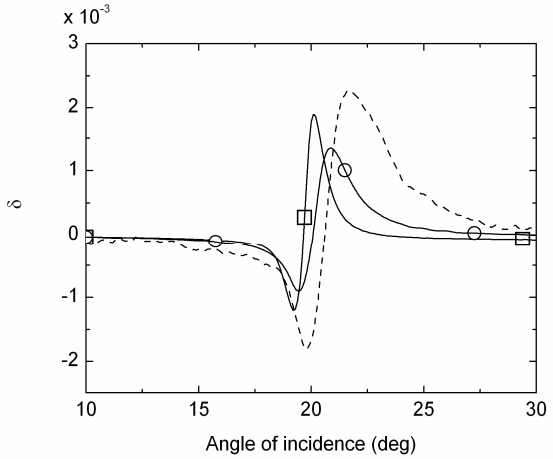

Figure 1: Transverse Kerr effect (δ) measurements *versus* angle of incidence at an optical frequency of 3.66×10^{14} Hz (819 nm) on silver films of different thicknesses (□16 nm and ◯9 nm) supported on a 1200 nm period Ni grating, data for the bare Ni grating is shown for comparison (dotted line).

of these materials is predicted to require the application of rather large localised fields. Much greater frequency shifts are predicted for magnetized ferromagnetic metallic surfaces but at the expense of greatly reduced creation and propagation efficiencies. We have shown that not only do the surfaces of all three of the principle ferromagnetic elements support plasmon creation and propagation but that it is also possible to combine both metallic systems to optimise desired behaviour. Figure 1 for example, shows experimentally that the fields associated with plasmons propagating on thin silver layers deposited on top of a Nickel grating penetrate the Nickel surface to produce enhancement in the magneto-optic behaviour. In this work we explore through the analysis of simple systems the potential to create practical and useful devices based on the magnetic manipulation of propagating plasmons.

REFERENCES

1. Altewischer, E., M. P. van Exter, and J. P. Woerdman, "Plasmon-assisted transmission of entangled photons," *Nature*, Vol. 418, 304–306, 2002.
2. Chiu, K. W. and J. J. Quinn, "Magnetoplasma surface waves in metals," *Phys. Rev. B*, Vol. 5, No. 12, 4707–4709, 1972.
3. Oi Nakamura, Y. and B. V. Paranjape, "Surface plasmon in a parallel magnetic field," *Solid State Commun.*, Vol. 16, 467–470, 1975.

Imaging by a Planar Lens in Quasi-electrostatic and Far Field Regimes

A. L. Efros[1], **N. A. Kuhta**[2], **and V. A. Podolskiy**[2]

[1]Department of Physics, University of Utah, SLC, UT, 84112, USA
[2]Department of Physics, Oregon State University, Corvallis OR, 97331, USA

Abstract— A brief discussion of the imaging by the planar lens is given with a special attention to the absorption inside the lens. The near field regime is considered as the best candidate for the subwavelength imaging. A near field lens with a virtual focus is a subject of a special discussion. It is shown that it does not have some disadvantages of a lens with a real focus. A small absorption is not crucial for such a lens. The theory can be created without taking into account the imaginary part of the dielectric constant ε. The field does not diverge inside the lens at small values of Im ε as it does in the lens with the real focus. Thus, the total absorption in this case may be significantly less. The lens or the sequence of the lenses can be used for three dimensional image transmissions.

In the regime of far field imaging we show [1] that the image has a fundamentally different origin depending on the relationship between losses inside the lens and the wavelength of the light. At small enough wavelength the image is always governed by diffraction theory, and the resolution is independent of the absorption under the conditions Im $\varepsilon \ll 1$ and Im $\mu \ll 1$. For any finite value of the wavelength, however, a critical absorption exists below which the superresolution regime takes place, though this absorption is extremely low and can hardly be achieved. We demonstrate that the transition between diffraction limited and superresolution regimes is governed by the universal parameter combining absorption, wavelength, and lens thickness. Finally, we show that this parameter is related to the resonant excitation of the surface plasma waves.

The Negative Refraction of a Surface Plasmon Polariton

T. A. Leskova and A. A. Maradudin

Department of Physics and Astronomy, University of California
Irvine, CA 92697, USA

Abstract— We study theoretically the negative refraction of a surface plasmon polariton. The physical system we consider consists of vacuum in the region $x_3 > 0$, a metal characterized by a dielectric function $\epsilon_1(\omega)$ in the region $x_3 < 0, x_1 < \zeta(x_2)$, and a metal characterized by a dielectric function $\epsilon_2(\omega)$ in the region $x_3 < 0, x_1 > \zeta(x_2)$. For simplicity we assume that both $\epsilon_1(\omega)$ and $\epsilon_2(\omega)$ are real. The interface profile function $\zeta(x_2)$ is a single-valued function of x_2 that is differentiable. The vacuum-metal interfaces for $x_1 < \zeta(x_2)$ and $x_1 > \zeta(x_2)$ both support a surface plasmon polariton of frequency ω. A surface plasmon polariton of this frequency is incident on the interface $x_1 = \zeta(x_2)$ from the region $x_1 < \zeta(x_2)$. Its angle of incidence is θ_0, measured counterclockwise from the negative x_1 axis. The scattering and transmission of the incident surface plasmon polariton at this interface are studied on the basis of the Leontovich impedance boundary condition on the surface $x_3 = 0$, so that only the electric field in the vacuum region $x_3 > 0$ enters the problem. The integral equation for the amplitude of the transmitted surface plasmon polariton has to be solved numerically. We specialize ths result to the case where the interface profile function $\zeta(x_2)$ is a periodic function of x_2 with a period a. For a suitable choice of the ratio of the period a to the wavelength of the incident surface plasmon polariton, the only nonzero Bragg beams of the refracted surface plasmon polariton in the region $x_1 > \zeta(x_2)$ are the 0-and-1-order beams, for a range of the angle of incidence θ_0. With a suitable choice for the form of $\zeta(x_2)$ the amplitude of the 0-order beam can be made to vanish. In this case the surface plasmon polariton undergoes negative refraction.

Plasmonic Nanostructures and Polarization of Light

A. Drezet, C. Genet, and T. W. Ebbesen
Universite Louis Pasteur, France

Abstract— Metallic nanostructures have revealed this last decade unique and surprising optical properties in the visible. A key point is the coupling of the incident electromagnetic field to surface plasmon polaritons excited at the nanostructured surfaces. It has become possible to tailor these surface excitations by controlling the design of surfaces at the nanometer scale. This allows us to address the intimate relation between structure and polarization of coupled light. We will present some recent results that show the possibility for controlling polarization state of light through surface plasmon manipulations. This confirms some of the interesting perspectives discussed recently in the field of plasmonics.

Application of the General Theory of Exact Relations to Fiber-reinforced Conducting Composites with Hall Effect

Yury Grabovsky
Temple University, USA

Abstract— In this paper we derive all microstructure-independent relations for effective conductivity of fiber-reinforced composites with Hall effect. We also derive all possible links between effective conductivities of two composites that have the same microstructure but are built using different materials. Our results use general theory of exact relations for composite materials and are valid for composites made with an arbitrary number of constituents.

Metamaterials for the Extreme Control of Light

Alexander V. Kildishev, **Evgenii E. Narimanov**, **Wenshan Cai**
Uday Chettiar, **and Vladimir M. Shalaev**

Birck Nanotechnology Center, Purdue University, West Lafayette, IN 47907, USA

Abstract— Increasing attention has been applied to creating an electromagnetic cloak of invisibility based on various schemes, including for example dipolar scattering cancellation [1] and the transformation optics (TO) [2–5]. Yet, practical applications of TO go far beyond just cloaking. The TO theory, built on fundamental variational principles (such as the Fermat principle) allows the control of light in an extreme and ultimate manner by providing a general recipe for obtaining complex spatial distributions of anisotropic permittivity $\overleftrightarrow{\varepsilon}$ and permeability $\overleftrightarrow{\mu}$. Using these distributions, a "curvilinear" optical space is molded, thereby creating the channel for the desired flow of light. The core task here is to approximate the required ideal optical space by manufacturable nanostructured optical metamaterials (MMs), with minimal loss of the required functionality, and move from the TO theories to actual prototypes. A family of new applications are discussed, including for example, *cloaking devices*, which can make objects "invisible" at any given wavelength by completely excluding light from the cloaking area and bending it around the cloak without perturbation [2], a *light concentrator* [6], allowing the "collection" of light from all directions in space and highly localizing that light in nm-scale volumes, and a *hyperlens* [7, 8] transforming evanescent fields into propagating waves and producing magnified far-field images of sub-wavelength structures due to its hyperbolic dispersion. In detail, we discuss improvements of the originally proposed hyperlens suffering from strong light reflection at its inner and outer cylindrical surfaces. With local control of the EM response of MMs we improve the impedance matching at these boundaries [9]. The actual fabrication of the hyperlens is extremely challenging, as in its original concept it requires cylindrical symmetry, which also severely limits applications since placing an object of interest in the hyperlens' inner cylindrical cavity is often impossible. Instead, one would be better served by a planar hyperlens if it were possible. The approach of "engineering optical space" with local control of MM response offers a direct solution to this problem. In a related study of a flat-top hyperlens [6], we show that in order to provide better access to the input cylindrical surface, a part of the lens can be removed.

REFERENCES

1. Alu, A. and N. Engheta, "Achieving transparency with plasmonic and metamaterial coatings," *Phys. Rev. E*, Vol. 72, 016623, 2005.
2. Cai, W., U. K. Chettiar, A. V. Kildishev, and V. M. Shalaev, "Optical cloaking with metamaterials," *Nature Photonics*, Vol. 1, 224, 2007.
3. Leonhardt, U., "Optical conformal mapping," *Science*, Vol. 312, 1777, 2006.
4. Greenleaf, A., M. Lassas, and G. Uhlmann, "Anisotropic conductivities that cannot be detected by EIT," *Physiolog. Measure.*, Vol. 24, 413, 2003.
5. Schurig, D., J. J. Mock, B. J. Justice, S. A. Cummer, J. B. Pendry, A. F. Starr, and D. R. Smith, "Metamaterial electromagnetic cloak at microwave frequencies," *Science*, Vol. 314, 977, 2006.
6. Kildishev, A. V. and V. M. Shalaev, "Engineering space for light via transformation optics," *Optics Letters*, Vol. 1, January, 2008.
7. Jacob, Z., L. V. Alekseyev, and E. Narimanov, "Optical hyperlens: Far-field imaging beyond the diffraction limit," *Opt. Express*, Vol. 14, 8247–8256, 2006.
8. Salandrino, A. and N. Engheta, "Far-field subdiffraction optical microscopy using metamaterials crystals: Theory and simulations," *Phys. Rev. B*, Vol. 74, 075103, 2006.
9. Kildishev, A. V. and E. E. Narimanov, "Impedance-matched hyperlens," *Opt. Lett.*, Vol. 32, 3432–3434, 2007.

Nano-magnetophotonics

Rintaro Fujikawa, **Alexander V. Baryshev**, **and Mitsuteru Inoue**
Toyohashi University of Technology, Toyohashi, Aichi, Japan

Abstract— For magnetophotonic crystals (MPCs), in which the constitutive elements are magnetic (or even only a defect introduced into the periodic structure is magnetic), there exists an additional degree of freedom to operate the photonic band structure, diffraction patterns, and the state of polarization of light, i.e., these characteristics can be influenced by the external magnetic field [1–3]. It is shown that MPCs enhance responses of known magneto-optical (MO) materials.

In this work we present a new type of MPCs composed of two 1D PCs, namely, magnetic and nonmagnetic Bragg mirrors with slightly different photonic properties [3]. Such MPCs exhibit the resonant transmission and are experimentally shown to enhance the magneto-optical response of known materials. The surface state, so-called the Tamm state, is originated by the interface between two 1D PCs, and supports multiple propagation (localization) of light within magnetic layers. When magnetic field is applied, the difference of the wave vectors for left- and right-circular polarized localized Tamm modes, multiple propagation of these modes within the magnetic layers and the nonreciprocal character of the Faraday effect result in an enhancement of the polarization rotation by one order of magnitude. These experimental observations make clear that Tamm structures will be of benefit for localizing light within any active material being used as the constitutive element or introduced at the interface between two PCs.

Studies on electromagnetic scattering from various artificial nanometer-scale media supporting surface plasmon resonances (SPRs) and localized SPRs (LSPRs) are currently attractive due to existence of the novel near-field effects and their contribution to anomalous transmission, surface-enhanced Raman scattering, biosensors, lithography overcoming diffraction limit and, what is of our interest in the present work, magneto-optical (MO) effects. There are theoretical works on the Kerr and Faraday effects for the mentioned magnetic material-noble metal systems, showing that the presence of noble-metal particles (or films) supporting LSPRs (or SPRs) in close proximity to a magnetic material results in enhancement of the MO response [4–6].

Here we report about experimental studies on nano-magnetophotonic structures which are subwavelength-thick artificial MO media (Bi:YIG-Au plasmonic nanostructures) supporting LSPRs. We show that these plasmonic nanostructures exhibit the larger Faraday rotation as compared with the MO response from ordinary Bi:YIG. Two-times enhancement for the Bi:YIG-Au film was demonstrated, suggesting approach to achieve the next level of miniaturization of MO media. It is evident that such attributes as the size and volume fraction of noble-metal nanoparticles, their shape and size deviations, and their arrangement are responsible for MO functionality of plasmonic nanocomposites.

REFERENCES

1. Inoue, M., R. Fujikawa, A. Baryshev, et al., *J. Phys. D: Appl. Phys.*, Vol. 39, R151, 2006.
2. Khanikaev, A. B., A. V. Baryshev, M. Inoue, et al., *Phys. Rev. B*, Vol. 72, 035123/9, 2005.
3. Vinogradov, A. P., A. V. Dorofeenko, S. G. Erokhin, et al., *Phys. Rev. B*, Vol. 74, 045128/8, 2006.
4. Kosobukin, V. A., *Surf. Science*, Vol. 406, 32, 1998.
5. Smith, D. A. and K. L. Stokes, *Opt. Exp.*, Vol. 14, 5746, 2006.
6. Belotelov, V. I., L. L. Doskolovich, and A. K. Zvezdin, *Phys. Rev. Lett.*, Vol. 98, 077401/4, 2007.

Models and Devices Based on Thin-layer Metamaterials

A. N. Lagarkov and V. N. Kisel
Institute for Theoretical and Applied Electromagnetics
Izhorskaya 13, Moscow 125412, Russia

Abstract— In recent years the attention of numerous research groups working in physics and electromagnetics has been focused on studying the artificial substances and structures (metamaterials) which able to support backward waves in their volume together with the entailed surface electromagnetic waves highly localized nearby the interfaces. A lot of important applications were suggested which make use of metamaterials manufactured in the shape of thinlayer structures and even of so-called "metafilms".

This review talk discusses some of the results of the ITAE studies into the theory and applications of the thin-layer metamaterials, including structures that reveal the phenomenon of superresolution. Commonly, metamaterials are described by their permittivity and permeability which can take even negative values. But our investigations show that in many cases the rigorous electromagnetic models which do not imply homogenization theories are more suitable to use. This appears to be of particular importance when considering the fields of filamentary sources located in the vicinity of a thin metamaterial layer with rather big inclusions. In this connection we discuss an interpretation of the emergence of superresolution originating from the selective response of a resonant couple "straight wire + splitted ring" to the different (propagating and evanescent) components of electromagnetic field with rigorous account for all mutual interactions in the composite. The similarity and differences in the performance of realistic composite and hypothetic homogeneous metasubstance are outlined. Electromagnetic simulation and extensive calculations enabled us to make certain conclusions regarding the possibilities to compensate the metamaterial losses by means of incorporating active portions into a metasubstance or switching active devices into inclusions of a realistic composite; as was shown, these possibilities are quite different. A number of interesting microwave applications of metamaterials is considered, including conformal antennas, reflectors, novel open resonators. The discussed theoretical and experimental results show numerous fields to utilize thin-layer metamaterials as low-profile broad-angle absorbers, enhanced frequency-selective and controllable surfaces which may be used to engineer advanced microwave devices, solve the electromagnetic compatibility and security problems.

Theory of the Universal Red Shift in the Optical Response of Gold/DNA Nanocomposites

David G. Stroud
Department of Physics, Ohio State University, USA

Abstract— Aqueous suspensions of DNA-linked gold nanoparticles have very unusual optical properties. At high temperatures, when the gold nanoparticles are unlinked to each other, the suspension exhibits a rather sharp optical absorption peak arising from the plasmon resonances in the gold nanoparticles. At low temperatures, the gold nanoparticles form a connected aggregate, and the optical absorption is always observed to be red-shifted (and usually broadened as well). While various approximate theories often predict this red shift, they do not give insight into its origins. In this presentation, I will demonstrate that this red shift is *universal* — that is, it arises from general properties of the nanocomposite before and after aggregation, and is not due to details of the structure. The proof involves using two sum rules on the imaginary part of the effective composite dielectric function. For a composite having a volume fraction f of Drude metal having dielectric function $\epsilon(\omega) = 1 - \omega_p^2/\omega^2$ and $1-f$ of insulator having dielectric function unity (ω_p is the plasma frequency), the first sum rule states that $\int_0^\infty \omega \mathrm{Im}\epsilon_e(\omega) d\omega = (\pi/2) f \omega_p^2$, while the second states that $\int_0^\infty \omega^3 \mathrm{Im}[\epsilon_e(\omega) - \epsilon_{av}(\omega)] d\omega = (\pi/6) f(1-f)\omega_p^4$, where ϵ_e and ϵ_{av} are, respectively, the effective composite dielectric function and the spatial average of the component dielectric functions. The first sum rule just gives the total spectral weight, while the second sum rule relates the shift in the spectral weight to the spatial inhomogeneity of the dielectric function. I will use these sum rules to derive the magnitude of the red shift when the gold/DNA composite forms an aggregate. The shift will be expressed in terms of the composite properties above and below the aggregation temperature. I will also discuss possible extensions of the sum rules to treat the broadening of the spectral lines.

Phase Behavior of DNA-linked Gold Nanoparticle Assemblies

Ching-Hwa Kiang

Department of Physics and Astronomy, Rice University, Houston, TX 77005, USA

Abstract— I will present our work on the synthesis, properties, and phase behavior of such DNA-linked nanoparticle assemblies. These nanoparticle assemblies have strong optical extinction in the ultraviolet and visible light regions; hence, the technique is used to study the kinetics and phase transitions of the assemblies. The melting transition of DNA-gold nanoparticle assemblies shows unusual trends compared to those of free DNA. The phase transitions are in uenced by many parameters, such as nanoparticle size, DNA linker length, interparticle distance, base pairing defects, and disorders. The physics of the DNA-gold nanoparticle assemblies can be understood in terms of the phase behavior of complex uids, with the colloidal gold interaction potential dominated by DNA hybridization energies [1].

REFERENCES

1. Sun, Y., N. C. Harris, and C.-H. Kiang, *Plasmonics*, Vol. 2, 193, 2007.

Cloaking by Reaction through Plasmonic Resonance

R. C. McPhedran[1], **G. W. Milton**[2], **N. A. Nicorovici**[1], **and L. C. Botten**[1,3]

[1]CUDOS, School of Physics, University of Sydney, Sydney, NSW, Australia
[2]Department of Mathematics, University of Utah, Salt Lake City, Utah,USA
[3]Department of Mathematical Sciences, University of Technology Sydney, Sydney, NSW, Australia

Abstract— There is much current interest in electromagnetic cloaking of objects, by exploiting structured materials. One approach cloaking by refraction, has been pioneered by J. B. Pendry [1] and U. Leonhardt [2], and exploits metamaterials to create electromagnetic guiding around the region to be shielded. A second approach [3, 4], cloaking by reaction, uses electromagnetic resonances in a coated cylinder, designed to have a resonant interaction between its coating and the surrounding material, to quench polarization responses in dipoles within an analytically-determined cloaking region surrounding the cylinder. We have extended the treatment of [4] to include interacting systems of polarizable dipoles or quadrupoles, and present animations illustrating that resonant cloaking still works for complicated assemblies of dipoles, or for higher order multipoles, and that the cloaking region does not depend on the details of the entity to be cloaked. We also give simulation results showing that cloaking is successful for cylinders coated with silver, at a near-ultraviolet wavelength, assuming the quasistatic limit to hold, and using the actual optical constants for silver. We comment on the design parameters necessary for reactive cloaking schemes to work with realistic materials.

REFERENCES

1. Pendry, J. B., D. Schurig, and D. R. Smith, *Science*, Vol. 312, 1780, 2006.
2. Leonhardt, U., *New J. Phys.*, Vol. 8, 118, 2006.
3. Nicorovici, N. A., R. C. McPhedran, and G. W. Milton, *Phys. Rev. B*, Vol. 49, 8479, 1994.
4. Milton, G. W. and N. A. Nicorovici, *Proc. Roy. Soc. A*, Vol. 462, 3027, 2006.

Session 3P5
Poster Session 4

Observations of Cavity Dipole Solitons and Vortex Soliton Clusters in VCSELs with a Surface Photonic Crystal Structure

Yuan Yao Lin[1], **Tsin-Dong Lee**[2], **and Ray-Kuang Lee**[1]

[1]Institute of Photonics Technologies, National Tsing-Hua University, Hsinchu 300, Taiwan
[2]Graduate School of Optoelectronics, National Yunlin University of Science and Technology
Yunlin 640, Taiwan

Abstract— Vertical Cavity Surface Emitting Lasers (VCSELs) are recognized as powerful semiconductor lasers that have played a significant role in high-speed laser printing, optical storage and telecommunications. With optical output vertically emitted from the surface, VCSELs also act as an interesting platform for studying optical pattern formation in mesoscopic system. In this scenario, self-organized linear and nonlinear optical modes have been demonstrated in semiconductor microresonators, such as scar modes and cavity solitons. In recent years, with the advance of new fabrication technologies, it becomes more feasible to actually utilize one- or higher-dimensional photonic bandgap crystals to modify the resonance modes in semiconductor lasers. In this work, a two-dimensional photonic crystal micro-structure is fabricated on a VCSEL surface to investigate the transverse optical pattern formation and its evolution by using near-field scanning optical microscope (NSOM) technology. Various localized optical vortex soliton structures in the output surface are formed and observed. Due to the confinement of the surrounding photonic crystal cavity, experimental evidence of rotating evolutions at different distances above the emitting surface for a fixed driving current are demonstrated directly from the NSOM images. Formation of localized optical cavity patterns, including cavity dipole solitons and vortex soliton clusters, are observed directly at room temperature. Such kind of photonic-crystal-structured VCSELs provide a new platform for the studying of band-gap effects on the dissipative solitons.

Fresnel Rhomb and Other Devices for Handling and Teaching Polarization

B. Ya. Zeldovich, **I. V. Ciapurin**, **and C. Tsai**

University of Central Florida, USA

Abstract— We demonstrate a pair of 90-45-45 prisms from binoculars appropriately attached to serve as Fresnel rhomb, i.e., achromatic quarter-wave plate. One and two Dove prisms with metallic reflection instead of TIR can work as half-wave plate and polarization rotator, respectively; both achromatic.

Fresnel rhomb is an important device to study Total Internal Reflection (TIR), circular polarization and other optical phenomena [1, 2]. It serves as a quarter-wave plate, which allows transformation of linear polarization into circular or elliptical and back. It uses the fact that in the vicinity of 50 degrees of incidence, one TIR between glass ($n \approx 1.5$) and air introduces s/p-phase difference about $\pi/4$, so that two sequential TIRs function as achromatic quarter-wave plate. R. Wood suggests [3], making Fresnel rhomb by cutting at 54° two sides of a thick glass plate, then polishing it to a mediocre quality and attaching thin glass plates with Canada balsam to eliminate roughness of polishing.

We demonstrate here how a pair of 90-45-45 prisms (right-angle prisms) may be attached to function as Fresnel rhomb, see Figure 1. Immersion liquid was added between the prisms to eliminate parasitic reflections. Small adjustment of the incidence angle, about 5 to 10 degrees, allowed to reach quite good performance of the device as transformer of linear polarization into circular one, with the energy fraction of the "wrong" circular polarization less than 0.0015 at $\lambda = 0.6328\,\mu$m.

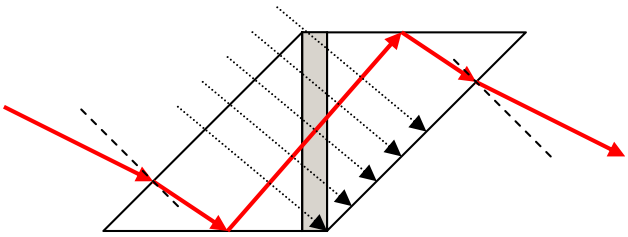

Figure 1: Modified Fresnel rhomb.

The price of a Fresnel rhomb nowadays is typically 5 to 10 times larger than the price of a right-angle prism. Moreover, 4 good right-angle prisms may be extracted from an old and otherwise dysfunctional binocular. It is worth noting that we actually used prisms from a binocular; they had antireflection coatings at the hypotenuse of the prisms and no coatings at short sides. Attempt to introduce light through short sides and use TIRs at hypotenuses yielded 1.41 times wider window, but did not give the desired quarter-wave performance, exactly due to modification of phases by the coatings. The same device can serve as a demo of a very thick flat glass plate (for the rays depicted by dotted arrows).

Dove prisms are conventionally used to rotate image. Most Dove prisms use TIR process for high-quality reflection of light. We suggest here to use metallized reflecting surface, Figure 2. Upper part of the prism is usually cut off. Important property of light reflection from perfect conductor is that the polarization vector is reflected, up to a sign, as an image of a physical object: if $\mathbf{n}$ is the vector of normal to the surface, then

$$\mathbf{E}_{ref} = -\mathbf{E}_{inc} + 2\mathbf{n}(\mathbf{n} \cdot \mathbf{E}_{inc}).$$

One can see that this prism serves as half-wave plate with respect to polarization, and one of the axes coincides with the normal to the mirror plane. Any prism may be used for that purpose, including (but not limited to) right-angle or equilateral.

Small value of the angle α at the top vortex leads, for a given base length, to relatively small window, but makes less of a change of intensity and polarization at the input and output sides

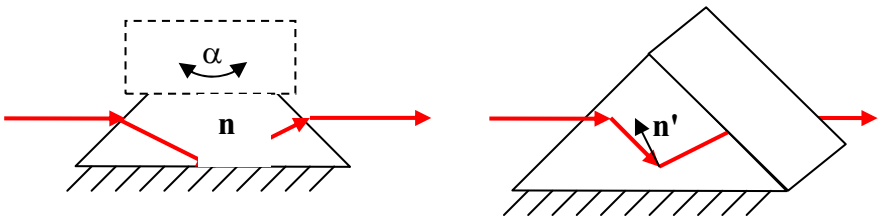

Figure 2: Dove prism modified by metallizing its reflecting surface. Also, a tandem of two such prisms with an angle between the normal vectors $\mathbf{n}$ and $\mathbf{n}'$ to the mirrors.

due to Fresnel reflections. A pair (tandem) of two such prisms with an angle Ψ between the normal vectors $\mathbf{n}$ and $\mathbf{n}'$ to the mirrors yields true rotation of both, the image carried by the beam and the polarization, by the angle 2Ψ, so that change of Ψ allows to continuously rotate the output polarization. It should be emphasized that the action of the above devices in Figure 2 is achromatic, even if the refractive index of the prism's material has arbitrary wavelength dependence. However, high conductivity of the metal and/or highly negative value of its permeability is crucial.

While the process of metal deposition is reasonably inexpensive in the conditions of research laboratory or of industry, even simpler solution exists. One may use existing flat mirror, either with front or with back metallized surface, and attach it to the prism with the immersion liquid in-between.

To conclude, we suggested and demonstrated the performance of 3 inexpensive achromatic devices that function as 1) Fresnel rhomb, 2) thick parallel plate, 3) half-wave plate, and 4) polarization rotator.

REFERENCES

1. Born, M. and E. Wolf, *Principles of Optics*, Sect. 1.5.4, 7-th ed., Cambridge U. Press, 1999.
2. Hecht, E., *Optics*, Sect. 8.7, 3-rd ed., Addison-Wesley, Reading, MA, 1998.
3. Wood, R. W., *Physical Optics*, Chap. IX, 354, 3-rd ed., OSA, Washington DC, 1988.

Simple Way for Introducing the Optical Theorem for Non-spherical Particles

Piero Bruscaglioni

Department of Physics, University of Florence, Via Sansone 1, Sesto Fiorentino 50019, Italy

Abstract— The presence of non-spherical particles have been evidenced in natural media, such as atmosphere (ice particles in high clouds) [1], biological tissues [2, 3], and marine water [4]. In case of non-spherical particles, the optical theorem needs to assume a particular form, with respect to the usual form which can be written as: $C_e = (4\pi/k)\mathrm{Im}(\mathbf{f} \cdot \mathbf{u}^*)$, showing the scalar product of the scattering amplitude $\mathbf{f}$ with the conjugated unit vector defining the incident field polarization.

For non-spherical particles in the place of the scattering amplitude one has to consider the relevant Jones matrix **J**. connecting the scattered field **Es** to the incident field **Ei**. By using transverse axes both for incident and scattered fields the element of the Jones matrix can be written as $\mathbf{f}_{11}$, $\mathbf{f}_{12}$, $\mathbf{f}_{21}$, $\mathbf{f}_{22}$.

$$\mathbf{J} = \frac{\exp(ikr)}{r} \begin{bmatrix} \mathbf{f}_{11} & \mathbf{f}_{12} \\ \mathbf{f}_{21} & \mathbf{f}_{22} \end{bmatrix}$$

and we show that Ce becomes

$$C_e = (4\pi/k)\mathrm{Im}\left\{\mathbf{f}_{11}|a_x|^2 + \mathbf{f}_{12}a_x a_y + \mathbf{f}_{21}a_x a_y^* + \mathbf{f}_{22}|a_y|^2\right\} \tag{1}$$

where $a_x\mathbf{x} + a_y\mathbf{y}$ is the unit polarization vector, and a_x is taken as reference for phase This form can be obtained as follows. Given the field $\mathbf{E^i}$, polarized radiation scattered in the forward direction by a thin layer $\mathrm{d}z$ of the medium is obtained by summing the contributions of the volume elements of the layer and using the stationary phase method. The resulting uniform field component parallel to the x y plane determines an element $\mathrm{d}\mathbf{E^s}$ of plane wave propagating in the z direction. When $\mathbf{E^i}$ is unitary:

$$\mathrm{d}\mathbf{E}^s = \exp\left(ik(\rho^2 + D^2)^{1/2}\right)\left(\rho^2 + D^2\right)^{1/2}\left((ax\mathbf{f}'_{11} + ay\mathbf{f}'_{12})\mathbf{x} + (ax\mathbf{f}'_{21} + ay\mathbf{f}'_{22})\,\mathbf{y}\right) N\mathrm{d}x\mathrm{d}y\mathrm{d}z \tag{2}$$

This can be added to the incident plane wave. As for power W per unit area at the distance D, taking into account the differential, one has (apart from a constant factor $1/(2\ Z)$, with Z medium specific impedance)

$$W = \left|\mathbf{E^i} + \mathrm{d}\mathbf{E^s}\right|^2 = \left|\mathbf{E^i}\right|^2 + 2\mathrm{Re}\left(\mathbf{E^i} \cdot \mathrm{d}\mathbf{E^{s^*}}\right) \tag{3}$$

By considering Eq. (3) one has the increment per unit width of the medium ($\mathrm{d}z = 1$),

$$\begin{aligned} \mathrm{d}W &= (4\pi/k)N\mathrm{Im}\left\{\mathbf{f}^*_{11}|ax|^2 + \mathbf{f}^*_{12}axay^* + \mathbf{f}^*_{21}ax^*ay + \mathbf{f}^*_{22}|ay|^2\right\} \\ &= -(4\pi/k)N\mathrm{Im}\left\{\mathbf{f}_{11}|ax|^2 + \mathbf{f}^*_{12}ax^*ay + \mathbf{f}_{21}axay^* + \mathbf{f}_{22}|ay|^2\right\} \end{aligned} \tag{4}$$

(with $\mathbf{f}_{mn}$ in the forward direction).

If the considered incident power is unitary, one obtains the linear extinction coefficient of the medium. One can verify that the extinction cross section for the particles in the medium of Eq. (1) is in agreement with what is shown by Eq. (4).

One can see that the form of Eq. (1) is equivalent to the form of the extinction matrix for the Stokes vector, which is presented in Ref. 5, Sect. 1. VIII.

REFERENCES

1. Mishchenko, M. I., L. Travis, and A. Macke, "Light scattering by non-spherical paricles in the atmosphere: An overview," *Proceedings International Radiation Symposium 1996*, 801–807, Deepak, Hampton, 1996.
2. Kienle, A. and R. Hibst, "Light guiding in biological tissues due to scattering," *Phys. Rev. Lett.*, Human dentin, Vol. 97, 8104, 2006.
3. Tuchin, V., *Tissue Optics, SPIE Tutorial Texts in Optical Engineering*, Vol. TT38, 2000.
4. Shifrin, K. S., *Physical Optics of Ocean Water*, English translation by Am. Inst of Physics Washington D. C., 1988.
5. Mishchenko, M. I., J. W. Hovenier, L. D. Travis, et al., *Light Scattering by Non Spherical Particles: Theory, Measurements, and Applications*, Academic Press, SanDiego, 2000.

Simultaneous Switching Noise Mitigation in High-speed Circuits Using Ring-type High-impedance Surface Structures

Chin-Sheng Chang[1], **Ding-Bing Lin**[2], **Kuo-Chiang Hung**[2]
I-Tseng Tang[3], **and Mau-Phon Houng**[1]

[1]Institute of Microelectronics, Department of Electrical Engineering
Advanced Optoelectronic Technology Center, National Cheng-Kung University
Tainan 701, Taiwan
[2]Institute of Computer and Communication Engineering
National Taipei University of Technology, Taipei, Taiwan
[3]Department of Environment and Energy, Nation University of Tainan, Tainan, Taiwan

Abstract— In this work, we presents a novel design for ring-type high-impedance surface structures (R-HIS) embedded in printed circuit boards. It is capable of selectively suppressing the simultaneously switching noise (SSN) at several desired frequencies. The suppression range of proposed structures is from dc to 1.56 GHz. The proposed structure is effective to reduce EMI, as well as to ensure signal integrity (SI) issues

Introduction: Isolation moat is a typical method to SSN from dc to several hundred megahertz. A bridge electrically connecting the power planes of the isolated region and the rest area is necessary to eliminate the electromagnetic interference (EMI) problem by supplying the RF return current for signal traces crossing the moat [1]. But the SSN could be transferred to outside of the slits through the connecting bridges. In recent years, high-impedance surface (HIS) structures have been extensively studied in the high-speed circuits. Although the HIS structure provides wide stopband to eliminate the SSN in gigahertz [2]. But limited by low-period design, this structure could not be used in the frequency below 1 GHz. Therefore, this paper proposed the R-HIS which embedded high impedance surface in the substrate. It does not only provide SSN suppression behavior, but also keep the perfect power and ground planes.

Structure Design and SSN Suppression: Figure 1 shows the proposed structure. The power and ground plane are kept continuous and structures for ensuring the good signal integrity. The dimension of three-layer PCB is 100 mm×100 mm. The dielectric constant of the substrate is 4.4 with a thickness of $h_1 = h_2 = 0.8$ mm. The top view of the HIS structure embedded in ground plane, which consists of a rectangular patch with a via post positioned in its center. The corresponding parameters of unit cell are $a = 0.25$ mm, $w = 13$ mm, and $L = 54$ mm. Fig. 2 shows the measurement results of proposed structures. The bandwidth is defined by $|S_{21}|$ lower than -20 dB. The measured results of R-HIS structure is from about 140 MHz to 1.56 GHz.

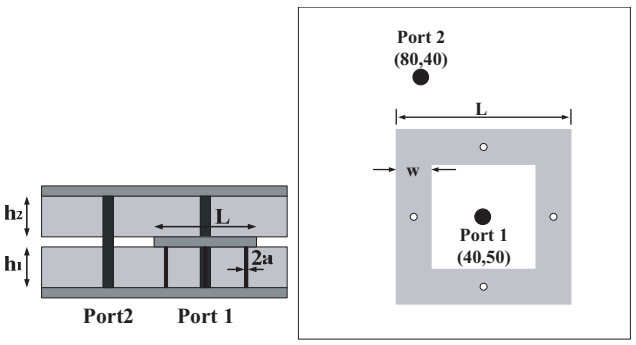

Figure 1: The proposes testing board. (a) side view. (b) top view.

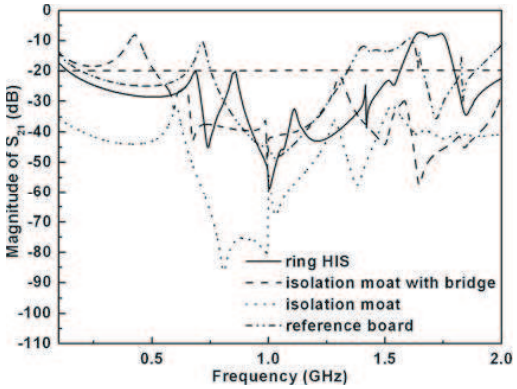

Figure 2: Comparisons of the measured results between reference board, isolation moat, and R-HIS structure.

REFERENCES

1. Hwang, J. N. and T. L. Wu, "The bridging effect of the isolation moat on the EMI caused by ground bounce noise between power/ground planes of PCB," *2001 IEEE EMC Symposium*, Vol. 1, 471–474, Montreal, Canada, Aug. 2001.

2. Sievenpiper, D., L. Zhang, R. F. J. Broas, N. G. Alexopolous, and E. Yablonovitch, "High-impedance electromagnetic surfaces with a forbidden frequency band," *IEEE Trans. Microw. Theory Tech.*, Vol. 47, No. 11, 2059–2074, Nov. 1999.

The Effect of the Microwave Emitted by Mobile Phones on the *in Vitro* and *in Vivo* Neuronal Survival in Rat Central Nervous System

Yongjian Zhu
Department of Neurosurgery, the Second Affiliated Hospital, School of Medicine
Zhejiang University, Hangzhou, Zhejiang 310009, China

Abstract— To investigate the effect of microwave emitted by mobile phones on the survival of the *in vitro* cultured rat cortical neuronal cells and the *in vivo* neuronal cells in rat central nervous system (CNS).

Methods: The *in vitro* cultured neuronal cells and *in vivo* rat brain were exposed to the microwave emitted by a microwave device that mimics the working frequency of mobile phones. After microwave exposure for different time and at different power density, cultured cells were stained with trypan blue to determine their survival state and brain tissues were analyzed with TUNEL method to determine their apoptotic state and stained with immunohistochemistry method to measure the expression level of Bcl-2 and Bax.

Results: Exposure at a power density of $0.05\,\mathrm{mW/cm^2}$ for 12 h or $0.1\,\mathrm{mW/cm^2}$ for 8 h lead to significant *in vitro* culture cell loss and more cell died as the exposure time prolonged. Besides, more brain neuronal cells were stained positive for TUNEL, Bax and Bcl-2 in rat with cranial defect after exposure to microwave than that of the control groups (with intact cranium, or had no microwave exposure) ($P < 0.01$). However, no significant difference was observed in the ratio of Bax/Bcl-2 among the groups studied.

Conclusion: The microwave emitted from mobile phones is detrimental to both *in vitro* cultured rat neuronal cells and *in vivo* brain neuronal cells from rat with cranial defect. The integrity of cranium seems to be important in protecting the CNS against apoptotic injuries inflicted by the microwaves from mobile phones.

Locally Resonant Cavity Cell Model for Three-layer Electromagnetic Band-gap (EBG) Structures

S. Mahdi Moghadasi[1, 2] **and A. Eshaghi**[1]

[1]Electrical Engineering Department, Ferdowsi University of Mashhad, Iran
[2]Communications and Computer Research Center, Mashhad, Iran

Abstract— In recent years, there has been growing interest in artificial electromagnetic materials, such as electromagnetic band-gap (EBG) structures [1, 2]. These structures are typically formed by periodic dielectric and various metallization patterns. They exhibit novel electromagnetic features that have led to a wide range of applications in the antenna and propagation fields. EBG structures have been integrated with microstrip antennas for enhanced performance due to the band-gap of surface wave suppression. They have also been used as new ground planes for low profile antennas due to the special reflection phase feature [3]. This paper focuses on the local resonance behaviors of EBG structures. A simply locally resonant cavity cell model is presented for three-layer mushroom-like EBG structures. This model can be used to gain insight to the physical mechanism of the EBG structures and the interaction of electromagnetic waves with EBG structures. This model proposes two kinds of main resonance modes. One of them is the mode that accurately predicts the position of the surface wave suppression band-gap. Parametric studies including the radius effect of the metal plated vias are effectively presented by using this model. Some numerical simulations of EBG structures are given to illustrate the applications and validation of this model proposed by this paper.

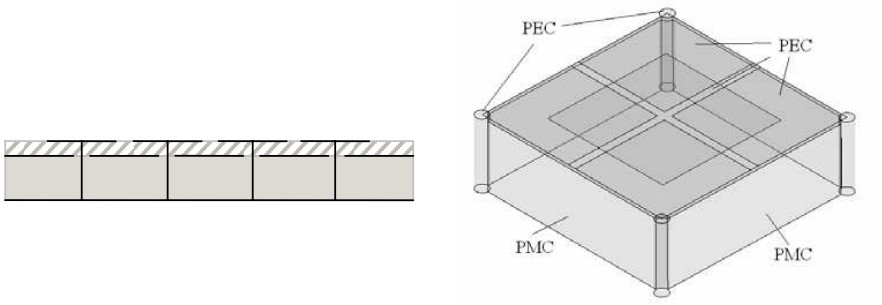

Figure 1: Locally resonant cavity cell model for three-layer EBG structure.

REFERENCES

1. Engheta, N. and R. W. Ziolkowski, *Metamaterials Physics and Engineering Explorations*, Wiley, New York, 2006.
2. Sievenpiper, D., L. Zhang, R. F. J. Broas, N. G. Alexopolus, and E. Yablonovitch, "High-impedance electromagnetic surfaces with a forbidden frequency band," *IEEE Trans. Microwave Theory Tech.*, Vol. 47, 2059–2074, Nov. 1999.
3. Yang, F. and Y. Rahmat-Samii, "Reflection phase characterizations of the EBG ground plane for low profile wire antenna applications," *IEEE Trans. Antennas Propag.*, Vol. 51, 2691–2703, Oct. 2003.

Suspended Electromagnetic Band-gap (EBG) Structures for Wideband Low Frequency Applications

S. Mahdi Moghadasi[1, 2] **and Armaghan Eshaghi**[1]

[1]Electrical Engineering Department, Ferdowsi University of Mashhad, Iran
[2]Communications and Computer Research Center, Mashhad, Iran

Abstract— In recent years, unique properties of electromagnetic band-gap (EBG) structures have made them applicable in many antenna and microwave applications. Two main interesting features associated with EBG structures are suppression of surface waves and in-phase reflection coefficient for plane waves [1–3]. Suppression of surface waves results in higher efficiency, smoother radiation pattern, and less back lobe and side lobe levels in antenna applications [1, 2]. On the other hand, these structures can be used in design of low profile antennas because the radiating current can lie directly adjacent to the ground plane without being shorted [1, 3].

The main reason for proposing suspended EBG surfaces is that lower zero reflection phase frequency can be achieved comparing to conventional EBG structures. The fractional bandwidth of suspended EBG structures do not reduced with reduction of center frequency. This property can be shown by the reflection phase of the structure when a normal incident plane wave is illuminated to the surface. The relation between the reflection phase characteristic of an EBG surface and the input-match frequency band of a wire antenna using the surface as a ground plane is investigated in [3]. It is shown that the frequency region where the EBG surface has a reflection phase between 45° and 135° is very close to the input-match frequency band of the low profile wire antenna using the surface as a ground plane. Therefore, one can use the reflection phase curve to identify the input-match frequency band of the antenna. Reflection phase of a periodic surface can be computed using one unit cell of the structure with periodic boundary condition as described in [4]. In this paper we investigate the effect of suspended structures' parameters on the reflection phase characteristic. By means of these curves, design guidelines for a three-layer circular mushroom-like EBG ground plane are obtained.

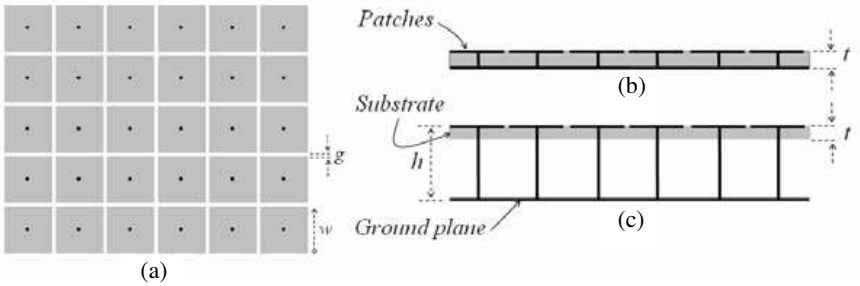

Figure 1: Square patch mushroom-like EBG surface (a) Top view (b) Side view of an ordinary structure (c) Side view of a suspended structure.

REFERENCES

1. Engheta, N. and R. W. Ziolkowski, *Metamaterials Physics and Engineering Explorations*, Wiley, New York, 2006.
2. Sievenpiper, D., L. Zhang, R. F. J. Broas, N. G. Alexopolus, and E. Yablonovitch, "High-impedance electromagnetic surfaces with a forbidden frequency band," *IEEE Trans. Microwave Theory Tech.*, Vol. 47, 2059–2074, Nov. 1999.
3. Yang, F. and Y. Rahmat-Samii, "Reflection phase characterizations of the EBG ground plane for low profile wire antenna applications," *IEEE Trans. Antennas Propag.*, Vol. 51, 2691–2703, Oct. 2003.
4. Remski, R., "Analysis of PBG surfaces using Ansoft HFSS," *Microwave J.*, Vol. 43, No. 9, 190–198, Sept. 2000.

Multiband Mushroom-like Electromagnetic Band-gap (EBG) Structures

S. Mahdi Moghadasi[1, 2] **and Armaghan Eshaghi**[1]

[1]Electrical Engineering Department, Ferdowsi University of Mashhad, Iran
[2]Communications and Computer Research Center, Mashhad, Iran

Abstract— Mushroom-like electromagnetic band-gap (EBG) structures exhibit unique electromagnetic properties that have led to a wide range of electromagnetic device applications [1, 2]. This paper focuses on the reflection phase feature of multiband EBG surfaces. Previously, it is shown that when plane waves normally illuminate an EBG structure, the phase of the reflected field changes continuously from 180 to −180 versus frequency [3]. One important application of this feature is that one can replace a conventional perfect electric conductor (PEC) ground plane with an EBG ground plane for a low profile wire antenna design. In this paper we propose a multiband EBG structure with reduced zero reflection phase frequencies. For the designed EBG surface, the operational frequency bands of an EBG structure is defined as the frequency regions within which a low profile wire antenna radiates efficiently. That means the antenna has a good return loss and radiation patterns. The operational frequency band is the overlap of the input-match frequency band and the surface-wave frequency band-gap. It is revealed that the reflection phase curve can be used to identify the input-match frequency band inside of which a low profile wire antenna exhibits a good return loss. The surface-wave frequency band-gaps of the EBG surface that helps improve radiation patterns is very close to its input-match frequency bands, resulting in an effective operational frequency band. Parametric studies have been performed to obtain design guidelines for multiband EBG ground planes. Reflection phase of a periodic surface can be computed using one unit cell of the structure with periodic boundary condition as described in [4].

REFERENCES

1. Engheta, N. and R. W. Ziolkowski, *Metamaterials Physics and Engineering Explorations*, Wiley, New York, 2006.
2. Sievenpiper, D., L. Zhang, R. F. J. Broas, N. G. Alexopolus, and E. Yablonovitch, "High-impedance electromagnetic surfaces with a forbidden frequency band," *IEEE Trans. Microwave Theory Tech.*, Vol. 47, 2059–2074, Nov. 1999.
3. Yang, F. and Y. Rahmat-Samii, "Reflection phase characterizations of the EBG ground plane for low profile wire antenna applications," *IEEE Trans. Antennas Propag.*, Vol. 51, 2691–2703, Oct. 2003.
4. Remski, R., "Analysis of PBG surfaces using Ansoft HFSS," *Microwave J.*, Vol. 43, No. 9, 190–198, Sep. 2000.

Design of High Performance FPGA Based Face Recognition System

I. Sajid, **M. M. Ahmed**, **I. Taj**, **M. Humayun**, **and F. Hameed**
Department of Electronic Engineering
Mohammad Ali Jinnah University, Islamabad, Pakistan

Abstract— A number of defense, security and commercial applications demand real time face recognition systems, especially when other biometric techniques are not feasible. Eigen values are widely used in engineering problems and particularly in face recognition algorithms. Floating point operations are used in Eigen values algorithms because Eigen values are highly sensitive for precision. Floating point operations are costly and complex in terms of hardware. Whereas fixed point technique with software hardware co-design (SHcoD) methodology reduces machine cycles and provides the flexibility in face recognition systems. It has been demonstrated that SHcoD concept can be used with dynamic partial reconfigurability to improve the conventional face recognition systems. An FPGA based novel design has been developed for efficient face recognition system which provides SHcoD, customization of algorithm and adaptability in the system. It has been shown that the proposed system is reasonably power efficient than floating point architecture and can be employed for portable applications.

High Sensitivity of Phase-based Surface Plasmon Resonance in Nano-cylinder Array

Bing-Hung Chen, **Yih-Chau Wang**, **and Jia-Hung Lin**
Institute of Electronic Engineering, National Dong Hwa University
Hualien 97401, Taiwan, R. O. C.

Abstract— Surface plasmon resonance sensor is used to measure the variation of dielectric constant sample, but its sensitivity is limited to surrounding temperature fluctuation. We present a high sensitivity phase-based surface plasmon resonance sensor made by gold nano-cylinder array. This structure is not only to reduce thermal conduction by the non-continuous gold array, but also to enhance surface plasma by these nano-size surfaces. This device consists of 50 nm diameter, 47 nm height gold cylinders on 3 nm titanium film coated on Corning 1737 glass, and match with BK7 prism by NuSil LS-5252 optical matching liquid. Surface plasma wave was excited by a 632.8 nm HeNe laser irradiating on this prism at a particular angle. The phase variation between the signal light and reference light are collected by a pair of photo-detectors and recorded by a lock-in amplifier (Stanford Research 830). By considering heterodyne interference optical path, the sensitivity of this tool can reach 10^{-8}RIU.

Left-handed Zeroth Order Resonator on Ferrite Substrate

M. A. Abdalla and Z. Hu
MACS Group, School of EEE, University of Manchester
P. O. Box 88, Manchester M60 1QD, UK

Abstract— Recently, there has been a great interest in using left handed materials (LHMs) i.e., both permittivity and permeability are negative, for RF/microwave circuit applications. The LHMs have been realized in different planar configurations. Recently, left-handed (LH) coplanar waveguides (CPW) for RF/microwave applications have been proposed and demonstrated experimentally, where different types of loading series capacitors and parallel inductors have been analyzed.

Ferrite medium substrate has tunable dispersive properties depending on the direction and value of the applied magnetic bias to the ferrite substrate. Therefore, a tunable LH transmission line (TL) is expected on ferrite substrates which has been recently, demonstrated in different planar configurations.

Microwave resonator is one of the desirable devices that can be used in many microwave applications. The resonator condition relating the propagation constant along the guided structure (β) to the physical length of the resonator (l) and the mode order (n) that specifies the resonator order as

$$\beta = \frac{n\pi}{l} \tag{1}$$

In conventional resonators, the propagation constant is always positive, and then the conventional transmission line resonator resonates only at infinite positive order modes.

Microwave resonator has been realized in many configurations as application of LHM either in its volume or planar version. LH transmission line resonator has been introduced as an application of the CRLH TL theory. The principle of its operation is based on cascading a LH transmission line section and a RH one and terminating them by either a short circuit or an open circuit. In balanced CRLH transmission line, the total phase of the two transmission lines can be expressed as the sum of both right and left handed sections. The LH resonator has either positive, negative, or zero values according to the combination of both left and right handed transmission lines sections. A novel zeroth order resonator has been introduced as an application of the LH transmission line resonator. Its resonance condition is based on achieving zero propagation constant due to the phase compensation of the RH and LH TL sections. The resonance frequency can be determined by the values of the loading elements of the transmission line and is independent on the total physical length of the resonator. Therefore, it can achieve zero electric length (infinite guided wavelength) at a certain finite microwave frequency with small size. Thus, this resonator has the advantages of size reduction and its harmonic suppression.

In this paper we present a left handed zeroth order resonator on ferrite substrate. The proposed resonator has been designed using a LH transmission line model in CPW configuration using a shunt inductive load and series capacitive load. An external DC magnetic field is applied horizontally to the ferrite substrate which causes it to be magnetic saturated in the same direction.

The equivalent circuit of the proposed structure is presented. Also, the proposed resonator is analyzed using full wave numerical simulation.

The results show that the proposed resonator has the advantages of its very compact size and its harmonic suppression. Also, the proposed zeroth order resonator has the capability of being tunable due to the effect of the ferrite substrate. Moreover, in comparison with ferrite microstrip configuration, the ferrite CPW one requires lower dc magnetic bias since it has much smaller demagnetization factor.

The Collinear Anisotropic Diffraction of Light by the Standing Wave along X-axis of Lithium Niobate Crystal

Y. A. Zyuryukin and A. N. Yulaev

Saratov State Technical University, Russia

Abstract— At present, the theory of light diffraction by ultrasonic wave is constructed sufficiently completely to change the scientific interest in the field of acousto-optic from general theoretic investigation to the engineer branch, i.e., to design acousto-optic devices in new models. However, the non-reciprocity effects of collinear anisotropic diffraction of light have been described at last time point out that this changing of interests is untimely. The essence of non-reciprocity effects of collinear anisotropic diffraction consists in the change of optimal incident light frequency on value of order acoustic frequency if direction of ultrasonic or light wave propagations has changed from initial direction to opposite ones. In spite of fact that the difference value between optimal frequencies of diffracted light propagating in opposite to each other directions is too little but it leads to diffraction effects principally.

The aim of present works is the description of application of non-reciprocity effects of collinear anisotropic diffraction in the theory of light diffraction by standing acoustic wave for opportunity the creation single-tone amplitude-modulated oscillation of light beam. The acousto-optic interaction of light is represented by the example of light diffraction by longitudinal acoustic wave along x-axis of lithium niobat crystal. The qualitative analysis of acousto-optic interaction of light beam on standing ultrasonic wave composed of two contradirectional waves is presented. Using the method of successive approximations the values of field strengths of interactive waves how function depending on phase mistuning, coordinates and phase shift between acoustic contradirectional waves forming a standing wave are obtained. The all consideration is realized in five-waves assumption.

Bi-frequency Pendulum on a Rotary Platform: Modeling Various Optical Phenomena

M. J. Soileau and B. Ya. Zeldovich

School of Optics/CREOL, University of Central Florid
P. O. Box 16-2700, Orlando, FL 32816-2700, USA

Abstract— The teaching optical phenomena can be enhanced through the use of analogies to the motion of a bi-frequency pendulum. In this talk we target demonstrations to four groups of students and scientists: kindergarten students to high school seniors; high school freshmen to university seniors; university sophomores to 5th year graduate students of Physics, Optics and Engineering; 2nd year graduate students to research scientists. The main difference between the groups is in the level of mathematics required to make the analogy to optical phenomenon. Most of the physical ideas may be understood and appreciated even in middle school and serve as a motivation for deeper study of mathematics and science. Actual device will be placed in the hall before, during and after the talk, and demonstrations will be performed, to the entertainment of the speaker (B. Z.) and, possibly, of the audience.

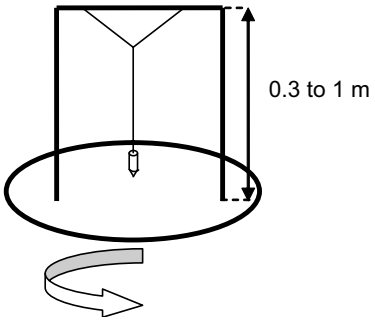

Large part of the material was published by the authors in [1]. The talk will contain about 40 experiments and 40 corresponding optical phenomena, including new experiments, demonstrating modeling of Second Harmonic Generation and Parametric Oscillations.

REFERENCES

1. Soileau, M. J. and B. Y. Zeldovich, "Bi-frequency pendulum on a rotary platform: Modeling various optical phenomena," *Physics Uspekhi* (former *Soviet UFN*), Vol. 47, No. 12, 1239–1255, in English, 2004.

Strength of Electromagnetic Reflection

Sergiy Mokhov and Boris Ya. Zeldovich
College of Optics & Photonics: CREOL & FPCE, University of Central Florida
P. O. Box 162700, Orlando, FL 32816-2700, USA

Abstract— The notion of reflection strength S of a plane wave by an arbitrary non-absorbing layer is introduced, so that intensity of reflection is $R = \tanh^2 S$. We have shown that the total strength of reflection by a sequence of elements has as its possible maximum the sum of strengths of constituents, and as its possible minimum — the difference. We show that the standard Fresnel reflection may be understood in terms of variable S as a sum or difference of two separate contributions, due to impedance-step and due to speed-step.

Consider a reflecting element, where the waves A and B propagate in opposite directions with respect to z-axis, so that power flux $P_z = |A|^2 - |B|^2$, which is conserved in the absence of absorption. Writing the matrix relationship for wave coupling in linear media,

$$A(z) = M_{AA} \cdot A(0) + M_{AB} \cdot B(0), \quad B(z) = M_{BA} \cdot A(0) + M_{BB} \cdot B(0). \tag{1}$$

The most general form of such matrix $\hat{M}$ depends on 4 real parameters: strength S, inessential phase ψ and two phases ζ and η:

$$\hat{M} = e^{i\psi} \begin{pmatrix} e^{i\varsigma} & 0 \\ 0 & e^{-i\varsigma} \end{pmatrix} \begin{pmatrix} \cosh S & \sinh S \\ \sinh S & \cosh S \end{pmatrix} \begin{pmatrix} e^{-i\eta} & 0 \\ 0 & e^{i\eta} \end{pmatrix}, \quad R = |r(B \leftarrow A)|^2 = \tanh^2 S, \tag{2}$$

Physical addition of two sequential elements with the parameters S_1, ψ_1, ζ_1, η_1 and S_2, ψ_2, ζ_2, η_2, yields the element described by the matrix $\hat{M}_3 = \hat{M}_2 \hat{M}_1$, i.e., the matrix (2) with S_3,

$$S_3 = \operatorname{arcsinh} \sqrt{\sinh^2(S_1 + S_2)\cos^2\tau + \sinh^2(S_1 - S_2)\sin^2\tau}, \quad \tau = \varsigma_1 - \eta_2, \tag{3}$$

which can vary due to mutual phase difference between reflective elements.

Consider now reflection of light by the sharp boundary between two media at the incidence angle θ_1, and $n_1 \sin\theta_1 = n_2 \sin\theta_2$, with θ_2 being refraction angle. We denote by ε_1, μ_1, ε_2, μ_2 the values of dielectric permittivity and magnetic permeability in these two media, so that the propagation speed $v_{1,2}$ and impedance $Z_{1,2}$ are

$$v_j = c/n_j, \quad c = 1/\sqrt{\varepsilon_{\rm vac}\mu_{\rm vac}}, \quad n_j = \sqrt{(\varepsilon_j \mu_j)/(\varepsilon_{\rm vac}\mu_{\rm vac})}, \quad Z_j = \sqrt{\mu_j/\varepsilon_j}, \quad j = 1, 2. \tag{4}$$

Amplitudes of reflection for TE and TM-polarization may be easily calculated [1]:

$$\begin{aligned} r_{\rm TE} &= (\cos\theta_1/Z_1 - \cos\theta_2/Z_2)/(\cos\theta_1/Z_1 + \cos\theta_2/Z_2), \\ r_{\rm TM} &= -(Z_1\cos\theta_1 - Z_2\cos\theta_2)/(Z_1\cos\theta_1 + Z_2\cos\theta_2). \end{aligned} \tag{5}$$

Here is truly remarkable relationship, which we found. One can produce the reflection strengths $S_{\rm TE}(\theta_1)$ and $S_{\rm TM}(\theta_1)$ by simple addition (for TE) or subtraction (for TM) of the speed-governed and impedance-governed contributions:

$$S_{\rm TE}(\theta_1) = S_{\Delta Z} + S_{\Delta v}(\theta_1), \quad S_{\rm TM}(\theta_1) = S_{\Delta Z} - S_{\Delta v}(\theta_1), \quad r_{\rm TE,TM} = -\tanh(S_{\rm TE,TM}), \tag{6}$$

$$S_{\Delta Z} = \frac{1}{2}\ln(Z_1/Z_2), \quad S_{\Delta v}(\theta_1) = \frac{1}{2}\ln(\cos\theta_2/\cos\theta_1). \tag{7}$$

One can easily verify that the expressions (6), (7) reproduce standard formulae (5) identically.

We have actually found (6), (7) for ourselves not only empirically, but have derived the result of additivity for reflection strength S directly from Maxwell equations [2].

REFERENCES

1. Staelin, D. H., A. Morgenthaler, and J. A. Kong, *Electromagnetic Waves*, Prentice Hall, 1993.
2. Mokhov, S., L. Glebov, J. Lumeau, V. Smirnov, and B. Zeldovich, "Reflection of light by composite volume holograms: Fresnel corrections and Fabry-Perot spectral filtering," accepted to JOSA A, posted 01/16/2008.

Similarity between Two Targets and Its Application to Polarimetric Target Detection for Sea Area

Wentao An[1, 2], **Weijie Zhang**[1], **Jian Yang**[1], **and Wen Hong**[2]

[1]Dept. of Electronic Eng., Tsinghua University, Beijing 100084, China
[2]National Key Lab of Microwave Imaging Technology
Institute of Electronics, CAS, Beijing 100080, China

Abstract— For target classification and recognition in radar polarimetry, one important problem is how to analyze the similarity between two radar targets. Yang [1] proposed the similarity parameter between two scattering matrices, which is independent of the span of the scattering matrices and the target orientation angle. The similarity parameter is only applied to the case of one-look polarimetric radar. However, nowadays, most data of a polarimetic synthetic aperture radar (SAR) are multi-look and the scattering matrix can not be obtained directly. So the application scope of similarity parameter is restricted. To solve this problem, the similarity parameter is extended in this paper.

Based on matrix theory, the generalized similarity parameter (GSP) between two polarimetric covariance matrices is proposed for describing the similarity of the polarizations of two targets. The GSP can be applied not only to the data case of one-look polarimetric SAR, but also to that of multi-look polarimetric SAR. Six properties of the GSP are presented and demonstrated. Based on the eigenvalue decomposition [2] of a covariance matrix, we demonstrate that the similarity parameter can be considered as the GSP for the case of one-look polarimetric data.

As an application, the GSP is used to target detection for multi-look polarimetric SAR case. According to [3], the Power Maximization Synthesis (PMS) detector doesn't require the prior knowledge of a target and the statistical characteristic of clutter. The GSP is applied to improve the PMS detector. A part of the NASA/JPL AIRSAR 4-look L-band data of San Francisco is used for the experiment of the PMS detector and the improved PMS detectors. By the contrast of the experimental result of different detectors, we find that the numbers of false alarms in sea area has been sharply eliminated by the application of the GSP information. The performance of improved PMS detector is much better than the PMS detector.

According to the analysis and experiment result in this paper, we demonstrate that the generalized similarity parameter can be used to analyze the similarity between the polarizations of two targets and it is helpful to polarimetric target detection.

ACKNOWLEDGMENT

This work was supported in part by the National Natural Science Foundation of China (40571099) and in part by the Research Fund of National Key Lab of Microwave Imaging Technology, Institute of Electronics, Chinese Academy of Sciences.

REFERENCES

1. Yang, J., Y. N. Peng, and S. M. Lin, "Similarity between two scattering matrices," *Electronics Letters*, Vol. 37, No. 3, 193–194, 2001.
2. Cloude, S. R. and E. Pottier, "A review of target decomposition theorems in radar polarimetry," *IEEE Trans. Geosci. Remote Sensing*, Vol. 35, No. 1, 68–78, 1997.
3. Chaney, R. D., M. C. Burl, and L. M. Novak, "On the performance of polarimetric target detection algorithms," *Aerospace and Electronic Systems Magazine, IEEE*, Vol. 5, Issue 11, 10–15, 1990.

Design of Multilayer Frequency Selective Surfaces Using Non-conventional Substrates

Yong Zhou and Fabio Urbani
Department of Engineering, University of Texas at Brownsville
80 Fort Brown, Brownsville, TX 78520, USA

Abstract— In this paper the design of multilayer Frequency Selective Surface (FSS) loaded by non-conventional substrate is presented. To analyze the multilayer unit cell with a symmetric periodicity, the method of lines (MoL) is applied and combined it with Floquet's theorem. The analysis returns the spectral dyadic Greens function of the structure which allows the calculation of the reflection and transmission coefficients per each desired frequency value. The aim of the method is to improve the frequency selectivity of the FSS, which is significant for the application in antenna cover or object stealth etc. The MoL method is adopted to simulate the transmission and reflection characteristics of the proposed FSS in order to show the advantages of low pass-band insertion loss, good frequency selectivity, and insensitivity to the incident angle and wave polarization. Furthermore Genetic Algorithm (GA) is used for the optimization of the unit cell metallization shape. A numerical code has been developed in order to solve the electromagnetic problem for a multilayer FSS and numerical results are presented and discussed.

Features and Mechanism of Satellite Infrared Anomaly before Ocean Earthquakes

Shanjun Liu[1,3], **Lixin Wu**[1,2], **Qunlong Chen**[3], **and Guoliang Li**[3]

[1]Institute for GIS/RS/GPS & Digital Mine Research
Northeastern University, Shenyang 110004, China
[2]Institute for GIS/RS/GPS & Subsidence Engineering Research
China University of Mining and Technology, Beijing 100083, China
[3]College of Resources and Environment, Hebei Polytechnic University, Tangshan 063000, China

Abstract— The phenomenon of satellite thermal Infrared anomaly before earthquake has been reported since the late 1980s. The reported abnormal rise of surface temperatures reaches 2–4°C, occasionally higher. Usually, the anomaly appears one month to several days before the earthquake. Several mechanisms or hypothesis have been put forward to interpret the phenomenon: (i) the uplifted underground fluid leads to the emanation of warm gases; (ii) the uplifted well water and changed moisture contents in the soil leads to surface temperature rise; (iii) the diffuse CO_2 emanation causes a local greenhouse effect; (iv) the near-ground air ionization due to enhanced radon emission leads to the condensation of water vapor from the atmosphere and, hence, to the release of latent heat; (v) the thermo-elastic effect and friction heat due to tectonic stress; and (vi) the recombination of stress-activated positive hole in rock face leads to infrared emission.

There are more than five million earthquakes occur every years, and most of it occur in the ocean region. Taiwan and Japan region are located in the jointed position of Eurasia plate and Pacific Ocean plate. There are many earthquakes occurred every year due to the action of plate movements. The Jiji Ms 7.6 earthquake, which happened in Sept. 21, 1999, caused about 3000 people death and about 10000 people injured. After the terrible event, several violent earthquakes had happened in its adjacent area during the past years. For example, the Hengchun Ms 7.2 earthquake happened in Dec. 26, 2006 is the latest earthquake, which caused 2 people death and about 50 people injured. Besides, the Noto Peninsula Ms 6.9 earthquake happened in March 25, 2007 caused 1 people death and about 170 people injured. The laws and the omens of the ocean earthquake are of great importance.

In this paper, taking Dec. 26/2006 Hengchun Ms 7.2 earthquake and March 25/2007 Noto Peninsula Ms 6.9 earthquake as the cases of ocean earthquakes, the features of active satellite Infrared anomaly before the earthquakes are analyzed. The result shows that the satellite IR anomaly prior to earthquake is intimately linked with the geology tectonics of neighborhood of epicenter. To study the mechanisms of the infrared anomaly before the ocean earthquakes, a group of physical simulation experiments including the infrared radiation imaging detection on rock fracturing and sliding process, and a group of physical test and numerical simulation experiments on the heat transfer measurement of water, are carried out. Furthermore, the laws and the mechanisms of satellite infrared anomaly before the ocean earthquakes are discussed so as to reach valuable omens of ocean earthquake.

Experimental Study on the Role of Water in the TIR Anomaly before Earthquake

Shanjun Liu[1, 2], **Qunlong Chen**[1], **Guoliang Li**[1], **and Lixin Wu**[2]

[1]College of Resources and Environment, Hebei Polytechnic University
Tangshan 063000, China
[2]Institute for GIS/RS/GPS & Digital Mine Research, Northeastern University
Shenyang 110004, China

Abstract— TIR anomaly before tectonic earthquake is becoming a research hotspot for seismology and remote sensing. Past study showed the thermal infrared (TIR) anomaly precursors appear before violent earthquake, and the anomaly appeared mostly in the water area of earth surface. To study the mechanisms of Infrared anomaly some physical simulation experiments of rock fracture were carried out. The experimental results showed that the TIR anomaly precursors appeared before the fracture of rock samples. There were two kinds of TIR anomaly as precursors of rock fracturing and failure: IRR image anomaly and IRR temperature curve anomaly, which are prospectively used as the monitoring index of remote sensing for rock fracturing phenomenon. The results of the simulation experiments indicated that TIR remote sensing will be prospectively applied to monitor the earthquake precursors. However, the IRR feature of hydrous rock was rarely researched in past simulation experiment.

In this paper, a contrastive infrared radiation imaging detection experiment of dry rock and wet rock in uniaxially compressing process is carried out. The types of rock include sandstone, marble and granite diorite. A high-capability infrared thermal imager is used to detect the infrared radiation from rock samples.

The experimental results show that: 1) along with load applying, the IR radiation temperatures of two type of rocks increase. But in the same circumstances, the increment of IR radiation temperature of wet rock increases greater than the dry rock. For example, the infrared radiation temperature of dry sandstone increases averagely about 1 K, meanwhile the that of dry sandstone increases averagely about 0.2 K; 2) AIRT (average infrared radiation temperature)-time curve of the wet rock keeps accordant variation with the load-time curve, whereas dry rock does not, which seems that the relationship of wet rock between stress and IR radiation temperature is closer than that of dry rock. The result indicates that infrared detection technique was better used to monitor the stress change of the wet rock than dry rock.

In the basis of the experimental result analysis the thermomechanical coupling effects for dry rock and wet rock are discussed, and some views are also put forward to explain the experimental phenomenon and the TIR anomaly before earthquake.

Surface Latent Heat Flux (SLHF) Prior to Major Coastal and Terrestrial Earthquakes in China

Jinping Li[1, 2], **Lixin Wu**[1, 3], **Huanping Wu**[4], **Shanjun Liu**[3], **and Jieqing Yu**[1]

[1]Institute for GIS/RS/GPS & Subsidence Research
China University of Mining & Technology, Beijing , China
[2]Department of Surveying and Engineering, Heilongjiang Institute of Technology, Harbin, China
[3]Institute for GIS/RS/GPS & Digital Mine Research, Northeastern University, Shenyang, China
[4]National Meteorological Centre, China Meteorological Administration, Beijing, China

Abstract— Satellite thermal infrared (TIR) imaging data have been proposed to map large linear structure and fault systems in the Earth's crust and to monitor geophysical phenomena associated with major earthquakes. TIR radiation anomaly can provide early warming information for impending earthquakes, and is considered to be a new precursor of shocking. The satellite TIR remote sensing, for the advantages of large observation area and short observation period, is becoming a promising technique for detecting earthquake and for monitoring tectonic activities. Surface Latent Heat Flux (SLHF), as an atmospheric parameter proportional to the evaporation from the Earth's surface, is dependent on meteorological parameters such as surface temperature, relative humidity, wind speed and underlaying surface.

Recently, analysis to SLHF from the epicentral areas of several coastal earthquakes in the world was found be possible to provide meaningful anomaly. The spatial-temporal anomalies of satellite SLHF, observed several months to several weeks before shocking, were suggested to be pre-seismic signals. The results of SLHF anomaly investigations in coastal regions had indicated that: 1) the SLHF anomaly is sensitive to earthquake above Ms 5.0, 2) the SLHF anomaly usually appears from $2 \sim 19$ days before and disappears quickly after the shocking, 3) the anomalous behavior of SLHF is not found for terrestrial earthquakes in India.

In this paper, the SLHF behaviors of the epicentral areas of one coastal earthquake and three terrestrial earthquakes are analyzed. The spatial distribution of the SLHF behavior, from the NCEP-NCAR reanalysis data of the IRI/LDEO Climate Data Library (http://iridl.ldeo.columbia.edu/), prior to each event is studied in a 15° by 15° area with the pixel covering the epicenter. The data set is in resolution of global grid $1.8° \times 1.8°$, and the daily values of a months before and after shocking from 1991 to 2007 are taken for analysis. Since SLHF is affected by the winds, tides and monsoon, it is spatial-temporally changed. To analysis the SLHF anomaly prior to a shocking, the perennial spatial-temporal influences are considered as background trend, and the SLHF data of 16 years (exclude the year shocking) are used to calculate the mean values of SLHF for each pixel as perennial trend. To analyze the SLHF behavior of the epicenter and the adjacent regions of shocking, the procedures are as following:

1) The mean value and the standard deviation (the same month and the same day of 16 years) are calculated so as to get the background trend of each pixel.
2) The daily anomaly index of each pixel can be calculated as:

$$AI = \left(SLHF(r, t) - \overline{SLHF(r)}\right) / \sigma_{SLHF}$$

   $SLHF(r, t)$ is the daily value of SLHF, $\overline{SLHF(r)}$ and σ_{SLHF} are the mean value and standard deviation of each pixel respectively;
3) If $AI > 1.5$, the pixel is considered to be an anomaly pixel;
4) The group of the anomaly pixels is considered to be a potential seismic active region.

The analysis shows that the maximum increase of SLHF was found to be $2 \sim 17$ days before shocking. It was suggested that SLHF together with other meteorological data such as surface temperature, water vapor, cloud liquid water and outgoing long wave radiation can be used for early warning of costal and territorial earthquakes in China.

Surface Signature over Scattering Mechanism of Targets in Imaging Polarimetric Radars

B. Zakeri[1] and A. Ghorbani[2]

[1]Islamic Azad University Garmsar Branch, Garmsar, Iran
[2]Amirkabir University of Technology, Tehran, Iran

Abstract— IN RECENT years, there has been a significant increase in use of Multidimensional Synthetic Aperture Radar (MSAR) imagery as a powerful tool in many arenas such as geological and environmental applications. This in part has to do with characterization of scatterers through electromagnetic scattering Models. In SAR radars, targets dont have deterministic scattering matrix for interpretation. Nowadays, for describing time dependent targets, the coherency matrix as well as the covariance matrix has been scrutinized. In these matrices the elements are linear functions of the ensemble-averaged cross-products. On the other hand, the purpose of target decomposition theory in radar polarimetry is the interpretation of polarimetric scattering data, or more simply the objective for any decomposition is to combine or manipulate the scattering matrix elements in order to obtain more descriptive and discriminative target parameters which are of decisive importance in applications of radar polarimetry. At present, there is an increasing interest in the combination of multidimensional radar imagery along with microwave scattering models with the objective to retrieve quantitative physical information about the earth's surface. For one-dimensional SAR systems, speckle noise has been completely characterized by a multiplicative noise model due to the exponential probability density function of the SAR image intensity. In the case of multidimensional systems and for polarimetric systems in particular, the characterization and reduction of the speckle noise component has been an important area of research since it represents one of the key limitations of this technology. Recently, it has been demonstrated that the speckle noise component for multidimensional SAR data, under a covariance matrix formulation, must be modeled through a combination of multiplicative and additive noise sources. Therefore, it is important to determine in what way the speckle noise affects the retrieval of physical information from multidimensional SAR data. The bridge between radar measurements and the physical parameters of the scatterers under study can be established by the so-called target decomposition theorems. TD theorems based on the eigenvector decomposition of the coherency matrix are the suitable tools to perform data interpretation in the study and characterization of natural scatterers. The extraction of physical information via the eigenvalues and eigenvectors, or the secondary parameters, i.e., the entropy (H), the anisotropy (A) and scattering mechanism (α angle) has been demonstrated by different authors. Consequently, a detailed study of the speckle noise effects over the eigen-decomposition is necessary in order to understand the effects of this noise component on the quantitative estimation of the physical parameters of interest. When dealing with multidimensional SAR data, interest lies in the Hermitian, semidefinite positive coherency or covariance matrices. Recently, several studies have pointed in this direction.

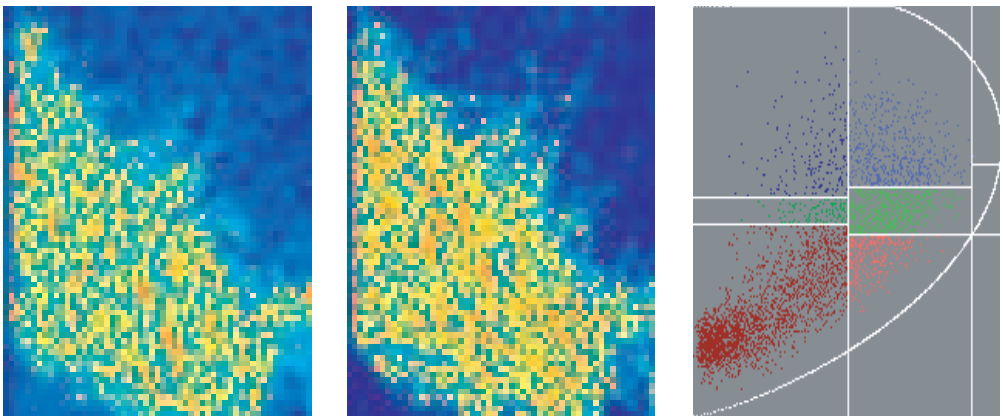

Figure 1: Polarimetric signatures for bridge on San Francisco Bay (CA, US) area. Left: Entropy (H). Middle: Alpha angle (α). Right: H-α plane.

In this paper a new method is applied for assessment of scattering mechanism surface and pure radar targets in remote sensing polarimetry. Coherency matrix eigenvalues is evaluated for analysis and classification of radar images. Also a simulation scheme is developed for calculating entropy and scattering mechanism for discrimination of pure targets within distributed targets. Spheroid targets with random drop size distribution are considered for simulation. As results for compare, radar image data set from European space agency (ESA) is presented.

REFERENCES

1. Cloude, S. R. and E. Pottier, "A review of target decomposition theorems in radar polarimetry," *IEEE Trans. Goesci. Remote Sensing*, Vol. 34, No. 2, 498–518, March 1996.
2. Martinez, C. L., E. Pottier, I. Hajnsek, J. S. Lee, and X. Fabregas, "Polarimetric speckle noise effects in quantitative physical parameters retrieval," *Proc. EUSAR*, Ulm, Germany, May 2004.
3. Galletti, M., M. Chandra, E. Pottier, and A. Ghorbani, "Application of the Cloude/Pottier decomposition to weather radar signatures," *Advances in Radio Science*, Vol. 3, 413–420, Copernicus GmbH, 2005.
4. Zakeri, B., A. Ghorbani, and M. Galletti, "Terrain classification and pure target detection based on Entropy/eigenvector decomposition in imaging radar polarimetry," *PIERS Proceedings*, Beijing, China, March 26–30, 2007.
5. Zakeri, B., A. Ghorbani, and M. Galletti, "Pure target detection based on eigenvector decomposition using H-α method in radar polarimetry," *International RF and Microwave Conference*, Palm Garden Hotel, Putra Jaya, Malaysia, Sept. 12–14, 2006.
6. Martinez, C. L. and E. Pottier, "Speckle noise characterization in correlated measurements," *Education and Science Ministry*, Spanish, 2005.
7. Martinez, C. L. and E. Pottier, "Statistical assessment of eigenvector-based target decomposition theorems in radar polarimetry," *IEEE Trans. on Geos. and Remote Sensing*, 2004.
8. Martinez, C. L. and E. Pottier, "Statistical assessment of eigenvector-based target decomposition theorems in radar polarimetry," *IEEE Trans. on Geos. and Remote Sensing*, Vol. 43, No. 9, Sep. 2005.

Nonintrusive Measurement of Electrical Conductivity for a Eucalyptus Fire

Kgakgamatso Mphale[1] and Mal. Heron[2]

[1]Physics Department, University of Botswana, P/Bag 0022
Gaborone, Botswana
[2]Marine Geophysical Laboratory, James Cook University
Townsville, QLD 4811, Australia

Abstract— Vegetation fires are slightly ionised. The dominant form of particle interaction in the flames is electron-neutral (unionised particles) collisions. Assuming that the electrons are in thermal equilibrium with neutrals, and average electron-neutral collision frequency to be much higher than the plasma frequency, the propagation of microwaves through the flame is predicted to have a considerable attenuation and refractive indices. A controlled fire burner was constructed where various natural vegetation species could be used as fuel. The burner was equipped with thermocouples to measure surface fuel temperature and used as a cavity for microwaves with a laboratory quality 2-port Vector Network Analyser (VNA) to determine electrical conductivity from s-parameters. Electrical conductivity for vegetation material flames is important for numerical prediction in high voltage power transmission faults research. Vegetation fires that burn under high voltage transmission lines reduce flashover voltage (a conductivity dependent parameter) by increasing air electrical conductivity and temperature. Sometimes, the flames may engulf high voltage conductors to provide a current path to the ground. The effect leads to high voltage conductor to ground flashover. The VNA determined fire electrical conductivity ranged from 0.0058 to 0.0079 mho/m for the fire temperatures ranging up to 1240 K for microwave frequencies between 8 to 10 GHz.

Absorption of Microwaves in a Low Intensity Poplar Gum Bark Fire

Kgakgamatso Mphale[1] and Mal. Heron[2]

[1]Physics Department, University of Botswana, P/Bag 0022, Gaborone, Botswana
[2]Marine Geophysical Laboratory, James Cook Univeristy, Townsville, QLD 4811, Australia

Abstract— Omnipresent alkali metal species in plant's organic structure are the main source of thermally produced electrons in vegetation fires. In flames, electron-neutral particle collisions dominate other modes of particle interaction. The collision regime absorbs electromagnetic wave energy when the fire is illuminated with microwaves. The rate of microwave absorption has implications on the safety of fire-fighter safety during fire suppression though the crews use communication devices which operate at lower frequencies (vhf-uhf). The experiment is a propagation test where x-band (7.0–9.5 GHz) microwaves are caused to propagate the combustion zone of a medium intensity poplar gum fire. Attenuation of the microwaves through the fire was measured using a 2-port automatic network analyser (ANA). Data on propagation characteristics of microwave through vegetation fire is scarce and may have very important implications for remote sensing. Microwave attenuations of 0.10–2.34 dB were measured at the frequency range. Using propagation theory, average real electrical conductivities for two poplar gum bark flames sampled were estimated to be in the range; 0.0059–0.0072 mhom^{-1}, and average electron densities for the flames were calculated to range from 6.00–7.16$\times 10^{15}$ m^{-3} when average of experimentally determined electron-neutral collision frequency for flame gases is used.

Session 3P6
Optics and Photonics

Influence of Frequency Allocations and Optical Filters on FDM Optical Fiber Communications

Shinya Kojima and Takahiro Numai

Ritsumeikan University, Japan

Abstract— Transmission characteristics in frequency-division-multiplexing (FDM) lightwave transmission systems with low-dispersion optical fibers such as dispersion-shifted fibers (DSFs) are limited by four-wave mixing (FWM). In recent years, several FWM suppression techniques such as optical multiplexers and demultiplexers with the combination of delay lines, bit-phase arranged return-to-zero (BARZ) signals, hybrid wavelength-division multiplexing/time-division multiplexing (WDM/TDM) technique, polarization-division multiplexing, the hybrid amplitude-shift keying/frequency-shift keying (ASK/FSK) modulation with prechirped pulses, unequally-spaced (US) allocations, repeated unequally-spaced (RUS) allocations, modified RUSs such as equally-spaced RUS (ERUS) and unequally-spaced RUS (URUS) allocations, and offsets from the zero-dispersion frequency have been reported.

In this paper, we focus on the fact that characteristics of FWM are closely related to frequency allocations and a transmission bandwidth of an optical filter. Up to now, US and RUS allocations were proposed and examined to overcome the problems in equally-spaced (ES) allocation. ES has a lot of FWM lights with $f_{\mathrm{FWM}} = f_i$, where f_{FWM} is a frequency of an FWM light and f_i is a frequency of a signal light with a channel index i. As a result, signal-to-noise (S/N) ratios for ES are heavily degraded by FWM. On the other hand, in US it is shown that if the frequency separation of any two channels of a WDM system is different from that of any other pair of channels, no FWM waves will ever be generated at any of the channel frequencies. In US, however, a total bandwidth, which is occupied by all signal lights, expands drastically with an increase in the number of channels N_{C}. Thus, it is difficult to have a lot of channels in US, and it can be said that there is no optimum US, from the viewpoint of the total bandwidth. Especially in lightwave transmission systems using optical fiber amplifiers, it is important to achieve total bandwidths as narrow as possible, because the light frequency range to amplify signal light intensities is limited. To overcome the problems described above, RUS was demonstrated theoretically and experimentally, and it was found that RUS has lower FWM light intensities with $f_{\mathrm{FWM}} = f_i$ than ES and narrower total bandwidths than US.

In this paper, FWM noises are calculated as a function of a transmission bandwidth of an optical filter, and the calculated results for ES, RUS, ERUS, and URUS are compared with each other. In our calculations, it is assumed that the oscillation wavelength for a light source is 1550 nm, the dispersion shifted fiber (DSF) length L is 80 km, the decay rate α is 0.2 dB/km, and the derivative dispersion coefficient $\mathrm{d}D_{\mathrm{c}}/\mathrm{d}\lambda$ is 0.07 ps/km/nm^2.

It is revealed that FWM noises are reduced in URUS more than in ES, RUS, and ERUS with a decrease in a transmission bandwidth of an optical filter. The upper limit of a filter transmission bandwidth to achieve a bit error rate of 10^{-9} is also obtained.

Intermediate Rytov-Berry-Chiao Phase and Rotation Sensors

N. B. Baranova[1], **N. V. Tabirian**[2], **C.-C. Tsai**[3], **and B. Ya. Zeldovich**[3]

[1]Northrop Grumman Laser Systems, 2787 S. Orange Blossom Trail, Apopka, FL 32703, USA
[2]BEAM Corp., 809 South Orlando Ave., Suite I, Winter Park, FL 32789, USA
[3]College of Optics & Photonics/CREOL, University of Central Florida
4000 Ctrl. Florida Blvd., Orlando, FL 32816-2700, USA

Abstract— Light propagation in inhomogeneous medium or in bent and twisted polarizationally neutral fiber is considered theoretically and studied experimentally. Explicit formula is derived for the polarization change, which generalizes Berry's phase for arbitrary ray trajectory.

Evolution of polarization is studied in numerous works [1–7]. We are interested here in the light propagation in an inhomogeneous locally isotropic medium, and also in a single-mode fiber, which is polarizationally neutral, but which is smoothly bent and twisted. Local law of polarization change along the ray's trajectory may be labeled as "Rytov's non-rotation":

$$\mathrm{d}\mathbf{e}/\mathrm{d}l = -\mathbf{t}(\mathbf{e}\cdot\mathrm{d}\mathbf{t}/\mathrm{d}l), \tag{1}$$

Here $\mathbf{e}(l)$ is the polarization vector, $\mathbf{t}(l)$ is (real) unit tangent vector to the trajectory $\mathbf{r}(l)$, and l is the physical path length along the trajectory, so that $\mathbf{t}(l)\cdot\mathbf{t}(l)\equiv 1$, $\mathbf{e}(l)\cdot\mathbf{t}(l)\equiv 0$ and $\mathbf{t}(l)=\mathrm{d}\mathbf{r}/\mathrm{d}l$. Other possible name of the Equation (1) is "pseudo-parallel transport" of polarization.

Propagation direction $\mathbf{t}(l)$ is generally **not** collinear to the initial one, $\mathbf{t}(l_1)$. The purpose of this talk is to produce an explicit formula for $\mathbf{e}(l)$, given the knowledge of $\mathbf{t}(l)$. We give an explicit solution of the Equation (1) of "Rytov's non-rotation", or of "Pseudo-parallel transport". Let us choose an arbitrary real unit vector $\mathbf{a}=(a_x,\,a_y,\,a_z)$. Then for each point of the trajectory l, i.e., for each current value of the unit tangent vector $\mathbf{t}(l)$, we introduce two transverse orthogonal basic unit vectors $\boldsymbol{\alpha}(l)$ and $\boldsymbol{\beta}(l)$, which allow to decompose an arbitrary polarization $\mathbf{e}(l)$:

$$\begin{aligned}\boldsymbol{\alpha}(l) =& N(l)\{\mathbf{a}-\mathbf{t}(l)(\mathbf{a}\cdot\mathbf{t}(l))\},\ N(l)=[1-(\mathbf{a}\cdot\mathbf{t}(l))^2]^{-0.5},\\ \boldsymbol{\beta}(l) =& \boldsymbol{\alpha}(l)\times\mathbf{t}(l),\ \mathbf{e}(l)=f(l)\boldsymbol{\alpha}(l)+g(l)\boldsymbol{\beta}(l).\end{aligned} \tag{2}$$

The main result of this talk is the expression for the "rotation rate" σ [radian per meter], so that

$$f(l) = f(l_1)\cos(\gamma(l)) - g(l_1)\sin(\gamma(l)),\ g(l) = f(l_1)\sin(\gamma(l)) + g(l_1)\cos(\gamma(l)), \tag{3}$$

$$\gamma(l) = \int_{l_1}^{l}\sigma(l')\mathrm{d}l' = -\int_{l_1}^{l}\mathbf{a}\cdot\left(\mathbf{t}(l')\times\frac{\mathrm{d}\mathbf{t}}{\mathrm{d}l'}\right)\frac{\mathbf{a}\cdot\mathbf{t}(l')}{1-(\mathbf{a}\cdot\mathbf{t}(l'))^2}\mathrm{d}l'. \tag{4}$$

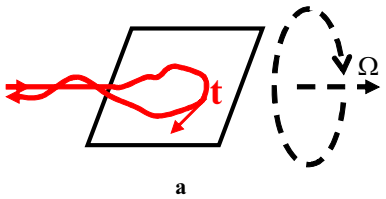

Figure 1: The configuration of a flexible polarizationally-neutral fiber attached to a rigid body, which was subject to various rotations (depicted by a vector of "angular velocity" Ω).

We actually performed the experiments with a rigid body, to which a flexible polarizationally-neutral fiber was attached, Figure 1. The ends of the fiber were fixed in laboratory frame, so that input and output propagation directions were fixed and opposite to each other, while the rigid body was subject to rotation. We observed the change (rotation) of the output polarization corresponding to the rotation of the body. We will also evaluate the possibility of using this configuration as a sensor of angular position of a rigid body.

REFERENCES

1. Rytov, S. M., *Dokl. Akad. Nauk SSSR*, Vol. 18, 2, 1938.
2. Rytov, S. M., *Tr. Fiz. Inst. Akad. Nauk SSSR*, Vol. 2, 1, 1940.
3. Berry, M. V., *Proc. Roy. Soc. A*, Vol. 392, 45, 1984.
4. Berry, M. V., *Nature*, Vol. 326, 277, 1987.
5. Tomita, A. and R. Y. Chiao, "Observation of Berry's phase in optical fiber," *Phys. Rev. Lett.*, Vol. 57, 937–940, 1986.
6. Liberman, V. S. and B. Y. Zeldovich, "Spin-orbit interaction of a photon," *Phys. Rev. A*, Vol. 46, 5199–5207, 1992.
7. Liberman, V. S. and B. Y. Zeldovich, "Spin-orbit interaction of a photon," *Pure Appl. Opt.*, Vol. 2, 367–382, 1993.

Chirped Higher Order Optical Solitons

K. Nakkeeran[1], **K. W. Chow**[2], **K. Senthilnathan**[3], **and P. K. A. Wai**[3]

[1]School of Engineering, Fraser Noble Building, King's College
University of Aberdeen, Aberdeen AB24 3UE, UK
[2]Department of Mechanical Engineering, University of Hong Kong, Pokfulam, Hong Kong, China
[3]Photonics Research Centre and Department of Electronic and Information Engineering
The Hong Kong Polytechnic University, Hung Hom, Kowloon, Hong Kong, China

Abstract— Nonlinear pulse propagation in optical fibers is governed by the famous nonlinear Schrödinger equation (NLSE). NLSE includes the effects of group-velocity dispersion (GVD) and self-phase modulation (SPM). The NLSE is studied extensively in order to understand the influence of linear and nonlinear effects. A particular initial condition of the pulse leads to a particular dynamical process during its propagation in a nonlinear and dispersive optical medium. The more famous of such a process is the conventional soliton which can be observed when the effect of anomalous GVD is exactly balanced by the SPM in optical fibers. Thus formed soliton pulse can then propagate without any deformation of its shape. In simple words one can say that the chirp produced by the linear GVD is balanced by the chirp produced by the SPM to form the soliton which are in general propagates without any chirp. In this work we consider the propagation of chirped optical solitons. An important feature in the considered optical fiber medium is that the dispersion decreases along the propagation direction. The integrability conditions are derived using the Painlev singularity structure analysis. Two dispersion profiles satisfying the integrability criterion are the constant dispersion and exponentially decreasing dispersion profiles. In the latter system, we theoretically discuss the generation of exact chirped higher order solitons using the Hirota bilinear method. As a special case, we find a familiar sech shaped pulse whose amplitude may be doubled, if the pulse is chirped in a proper manner initially, from the general chirped two-soliton solution for certain physical parametric conditions. We also demonstrate the implication for optical communications systems in terms of pulse compression by using these exact chirped higher order solitons. Finally, we analyze the interaction scenarios of the chirped two soliton pulses.

Dispersion-managed Fiber Systems with Zero Hamiltonian

A. B. Moubissi[1], **K. Nakkeeran**[2], **Abdosllam M. Abobaker**[2], **and A. B. Ravi**[3]

[1]Unité de Recherche en Physique, Université des Sciences et Techniques de Masuku
B.P. 943 Franceville, Gabon, France
[2]School of Engineering, Fraser Noble Building, King's College
University of Aberdeen, Aberdeen AB24 3UE, UK
[3]Department of Geology and Petroleum Geology, Kings College
University of Aberdeen, Aberdeen AB24 3UE, UK

Abstract— The dynamics of nonlinear pulse propagation in optical fibers is governed by the famous nonlinear Schrödinger equation (NLSE), in which the group-velocity dispersion (GVD) and self-phase modulation (SPM) form a basic set of optical processes describing a broad range of realistic physical situations. The NLSE is studied extensively in order to understand the influence of combining those effects. A particular initial condition of the pulse leads to a particular dynamical process during its propagation in a nonlinear and dispersive optical medium. The more famous of such a process is the conventional soliton which can be observed when the effect of anomalous GVD is exactly balanced by the SPM in optical fibers. Thus formed soliton pulse can then propagate without any deformation of its shape. Under special cases, the NLSE is completely integrable and the corresponding soliton solutions can be derived using the standard technique called inverse scattering transform. But the family of NLSE equations governing most practical cases like conventional fiber transmission system, dispersion-managed (DM) fiber system are not completely integrable in general. Even though some perturbation methods were reported to investigate the behaviour of physically interesting non-integrable NLSE family, researchers working in nonlinear optics and other fields mostly rely on numerical methods and Lagrangian variational method to study the system dynamics. Variational method is one of the widely used approximation techniques which has been applied to study the dynamics of various pulse parameters with respect to the fiber parameters, to estimate the pulse-to-pulse interaction length and to find the fixed point solutions of the DM fiber systems. In this work, by means of variational formalism for the NLSE, we derive exact analytical expressions for the variational equations corresponding to the amplitude, width and chirp of the pulse in terms of initial pulse parameters, fiber parameters and the distance of propagation of the pulse; under the condition when the Hamiltonian of the system is zero. Then, for Gaussian and hyperbolic secant ansatz, we check the validity of the obtained analytical results to describe pulse propagation in optical fiber in presence of high order effects. As a practical application of our results, we consider the design of the DM fiber systems and we derive an analytical expression for the Gordon-Haus jitter.

Suppression of FWM Noises in FDM Lightwave Transmission Systems by Frequency, Polarization, and Bit-phase Allocations

Takahiro Numai
Ritsumeikan University, Japan

Abstract— Transmission characteristics in frequency-division-multiplexing (FDM) lightwave transmission systems with low-dispersion optical fibers such as dispersion-shifted fibers (DSFs) are limited by four-wave mixing (FWM). In recent years, several FWM suppression techniques such as optical multiplexers and demultiplexers with the combination of delay lines, bit-phase arranged return-to-zero (BARZ) signals, hybrid wavelength-division multiplexing/time-division multiplexing (WDM/TDM) technique, polarization-division multiplexing, the hybrid amplitude-shift keying/frequency-shift keying (ASK/FSK) modulation with prechirped pulses, unequally-spaced (US) allocations, repeated unequally-spaced (RUS) allocations, modified RUSs such as equally-spaced RUS (ERUS) and unequally-spaced RUS (URUS) allocations, and offsets from the zero-dispersion frequency have been reported.

In this paper, we focus on the fact that characteristics of FWM are closely related to frequency allocations, polarization allocations, and modulation formats. From the viewpoint of frequency allocations, it was found that RUS, ERUS, and URUS have lower FWM light intensities with channel frequencies than equally-spaced (ES) allocation and narrower total bandwidths than US. From the viewpoint of modulation formats, non-return-to-zero (NRZ) and return-to-zero (RZ) formats were usually used in optical fiber transmission systems. To reduce FWM noises further, BARZ format is used as a modulation format. From the viewpoint of polarization allocation, it has been shown that FWM noises decrease by allocating the polarization states of the channels. FWM noises are calculated by using several modulation formats with three polarization allocations in ES, RUS, ERUS, and URUS, and the calculated results are compared with each other. In our calculations, it is assumed that an oscillation wavelength for a light source is 1550 nm. A DSF is assumed to have length L of 80 km, the decay rate α of 0.2 dB/km, and the derivative dispersion coefficient $\mathrm{d}D_\mathrm{c}/\mathrm{d}\lambda$ of 0.07 ps/km/nm^2. The base unit and the channel spaces are common in all frequency allocations.

It is revealed that FWM noises are considerably reduced in ES, RUS, ERUS, and URUS by combining BARZ format and polarization allocations. Especially, by optimizing polarization allocations, FWM noises with channel frequencies completely vanish in RUS, ERUS, and URUS.

Suppression of FWM Noises in FDM Lightwave Transmission Systems by Modified Repeated Unequally-spaced Frequency Allocations

Shinya Kojima and Takahiro Numai

Ritsumeikan University, Japan

Abstract— Transmission characteristics in frequency-division-multiplexing (FDM) lightwave transmission systems with low-dispersion optical fibers such as dispersion-shifted fibers (DSFs) are limited by four-wave mixing (FWM). In recent years, several FWM suppression techniques such as optical multiplexers and demultiplexers with the combination of delay lines, bit-phase arranged return-to-zero (BARZ) signals, hybrid wavelength-division multiplexing/time-division multiplexing (WDM/TDM) technique, polarization-division multiplexing, the hybrid amplitude-shift keying/frequency-shift keying (ASK/FSK) modulation with prechirped pulses, unequally-spaced (US) allocations, and repeated unequally-spaced (RUS) allocations have been reported.

In this paper, we focus on the fact that characteristics of FWM are closely related to frequency allocations. Up to now, US and RUS allocations were proposed and examined to overcome the problems in equally-spaced (ES) allocation. ES has a lot of FWM lights with $f_{\mathrm{FWM}} = f_i$, where f_{FWM} is a frequency of an FWM light and f_i is a frequency of a signal light with a channel index i. As a result, signal-to-noise (S/N) ratios for ES are heavily degraded by FWM. On the other hand, in US it is shown that if the frequency separation of any two channels of a WDM system is different from that of any other pair of channels, no FWM waves will ever be generated at any of the channel frequencies. In US, however, a total bandwidth, which is occupied by all signal lights, expands drastically with an increase in the number of channels N_{C}. Thus, it is difficult to have a lot of channels in US, and it can be said that there is no optimum US, from the viewpoint of the total bandwidth. Especially in lightwave transmission systems using optical fiber amplifiers, it is important to achieve total bandwidths as narrow as possible, because the light frequency range to amplify signal light intensities is limited. To overcome the problems described above, RUS was demonstrated theoretically and experimentally, and it was found that RUS has lower FWM light intensities with $f_{\mathrm{FWM}} = f_i$ than ES and narrower total bandwidths than US.

In this paper, equally-spaced RUS (ERUS) and unequally-spaced RUS (URUS) are proposed as modified RUS's and theoretically analyzed by comparing with RUS. It is found that efficiencies of generated FWM lights with $f_{\mathrm{FWM}} = f_i$ for URUS are lower than those for RUS when the number of channels N_{C} is common in both allocations. For example, when the number of channels N_{C} is 22 with the total bandwidth of 2790 GHz, an oscillation wavelength of 1550 nm for a light source, a dispersion shifted fiber length $L = 80$ km, a decay rate $\alpha = 0.2$ dB/km, and a derivative dispersion coefficient $\mathrm{d}D_{\mathrm{c}}/\mathrm{d}\lambda = 0.07\,\mathrm{ps/km/nm^2}$, the efficiencies of generated FWM lights with $f_{\mathrm{FWM}} = f_i$ for URUS are about 1/4 of those for RUS.

Fluctuations in the Zeros of Differentiable Gaussian Processes

K. I. Hopcraft, **E. Jakeman**, **and J. M. Smith**
School of Mathematical Sciences, Applied Mathematics Division
University of Nottingham, NG7 2RD, UK

Abstract— The properties of the zeros and critical points of Gaussian processes and fields are relevant to characterizing topological properties of Gaussian speckle [1] and optical manifestations of phase singularities [2]. Although studied extensively and being the subject of three reviews [3–5], the properties of the zero-crossings of random processes contain many subtleties with an all-encompassing theory remaining elusive. This paper presents results concerning the *distribution* for the number of zeros occurring in an interval as a function of the correlation function of the Gaussian process that generates them, and prefaces two further papers that present results of theoretical and experimental studies of the statistics of caustics generated by phase screens and of scintillation phenomena. We examine the stochastic point-processes formed by the zero-crossings or extremal points of differentiable, stationary Gaussian processes as a function of their autocorrelation function. The properties of these point processes are mapped to the space formed by the parameters appearing in the autocorrelation function, their adopted form being sensitive to the structure of the autocorrelation function principally in the vicinity of the origin. The distribution for the number of zeros occurring in an asymptotically large interval are approximately negative-binomial/binomial depending upon whether the relative variance or Fano factor is greater/less than unity. The correlation properties of the zeros are such that they are repelled from each other or are 'anti-bunched' if the autocorrelation function of the Gaussian process is characterized by a single scale-size, but occur in clusters if more than one characteristic scale-size is present. The intervals between zeros can be interpreted in terms of the autocorrelation function of the zeros themselves. When bunching occurs the interval density becomes bi-modal, indicating the interval sizes within and between the clusters. The inter-event periods are statistically dependent on one another with densities whose asymptotic behavior is governed by that of the autocorrelation function of the Gaussian process at large delay times. Poisson distributed fluctuations of the zeros occur only exceptionally but never form a Poisson process [6].

REFERENCES

1. Kessler, D. A. and I. Freund, "Level-crossing densities in random wave fields," *J. Opt. Soc. Am. A*, Vol. 15, 1608, 1998.
2. Schouten, H. F., et al, "Connection between phase singularities and the radiation of a slit in a metal plate," *Phys. Rev. Lett.*, Vol. 93, 173901, 2004.
3. Leadbetter, M. R., *Stochastic Point Processes*, Ed. P. A. W. Lewis, Wiley Interscience, New York, 1972.
4. Blake, I. F. and W. C. Lindsey, *Trans. IEEE IT*, Vol. 19, 295, 1973.
5. Abrahams J., *Communication and Networks*, Ed. F. Blake and H. V. Poor, Springer-Verlag, New York, 1986.
6. Smith, J. M., K. I. Hopcraft, and E. Jakeman, "Fluctuations in the zeros of differentiable Gaussian processes," *Phys. Rev. E.*, in the Press, 2008.

The Statistics of Caustics

O. E. French[1], **P. C. Chang**[2]
K. I. Hopcraft[1], **E. Jakeman**[1], **and J. G. Walker**[2]

[1]School of Mathematical Sciences
University of Nottingham, Nottingham, NG7 2RD, UK
[2]School of Electronic Engineering
University of Nottingham, Nottingham, NG7 2RD, UK

Abstract— The phase perturbing screen has been used as a canonical model for the study of fluctuations of radiation propagating through both thin and extended turbulent media [1]. The perturbations in the refractive index of the medium are, in the first instance, imparted to the phase of the light. In the Fresnel region, at the screen there are no fluctuations in amplitude but these are generated during propagation and become Gaussian at large distances when many independent elements of the screen contribute to the scattered field, having a scintillation index of unity. In the intermediate 'focusing' region, caustics are generated, being characterized by a highly fluctuating intensity with scintillation index greatly in excess of 1. The caustics are essentially a discrete pulse-like manifestation, and so the phase screen can be interpreted as a system capable of producing behaviours ranging from deterministic through random pulses to a Gaussian process as the propagation distance increases from the screen. This paper reports experimental results for the distribution of the number of caustics that occur in an interval of time — these being quantified by the number of excursions of the intensity above a threshold, and are therefore formed by the level-crossings of a random process. The caustics are generated by a 'phase screen' formed by a fluid whose surface is randomly perturbed by a mechanical piston with prescribed amplitude distribution and spectrum. The distribution for the number of caustics are explored as a function of the properties of the perturbation and the results are compared with recent theoretical work on the zero-crossings and extrema of a Gaussian process [2].

REFERENCES

1. Jakeman, E. and K. D. Ridley, "Modeling fluctuations in scattered waves," Taylor and Francis, New York, 2006.
2. Smith, J. M., K. I. Hopcraft, and E. Jakeman, "Fluctuations in the zeros of differentiable Gaussian processes," *Phys. Rev. E.*, in the Press, 2008.

The Extraction of Higher-order Field Correlations from a First-order Interferometer

Scott Shepard

College of Electrical and Computer Engineering, University of Central Florida
Orlando, FL 32816, USA

Abstract— Quantum interference effects in electromagnetic fields have led to recent applications such as "quantum lithography" (which resolves beyond the classical diffraction limit) and "super-resolving phase measurements" (with accuracies below the standard quantum limit). In essence, N photons of a field at frequency f are utilized to perform with an effective wavelength that would ordinarily be associated with a field at frequency Nf. Thus, standard laser sources and detectors (and most importantly for remote sensing: the propagation properties) all at wavelength λ, could be utilized in a quantum sensor with an effective resolution wavelength of λ/N. It has been thought that these "higher-order fringes" can only be observed in the higher-order correlation functions of the quantum electromagnetic field — hence only observable via coincidence detection schemes of order N. Therein the number of detectors and the splitting of the field (via beam splitters, polarizers, etc.) all scale with N. This severely limits the practicality of such schemes to small values of N (indeed, experimental observations to date are limited to $N = 2$, 3, or 4). Fortunately however, we have found (and present for the first time) a means of extracting this higher-order phase information from a first-order (i.e., standard) interferometer.

The means of extracting the phase also provides exceptional accuracies independent of the actual phase shift to be estimated — thereby eliminating the need to "null" the interferometer. Thus, not only is the apparatus independent of N, so that the scheme is scalable to arbitrary N, but it also is a little bit simpler since it doesn't have to be nulled (mitigating weight and reliability constraints germane to space-based interferometers). An interferometer infers the angle (phase) of a rotated quantum state by projecting it onto the z-component angular momentum eigenkets (difference of photon number at the output beam splitter ports). In contrast, the quantum angle (phase) representation describes the measurement of this angle (phase) directly, i.e., rather than inferring it from the measurement of something else. We compare the accuracies of the extraction of the phase information from the interferometer to those of the estimates of the quantum phase measurement. We also show how the quantum phase representation can be used to calculate the interferometer statistics in a simpler (and conceptually revealing) way. Local performance measures, appropriate for multiple-peaked i.e., "super-resolving" distributions, are defined and the phase representation is used to derive Heisenberg limits for these (binvariance and FWHM) for three classes of quantum states.

2-port Vectorial THz Electro-optic Sampling System

L. Meignien, J. Mangeney, and P. Crozat
Institut d'Electronique Fondamentale, France

Abstract— We present a fiber-based electro-optic sampling system at 1.55 µm wavelength, including an ultrafast $In_{0.53}Ga_{0.47}As$ ion-irradiated photoconductive switch and a freely positionnable prismatic ZnTe ($1^*1^*0.2\,mm^2$) electro-optic probe. The bandwidth is 0.5 THz (the spectrum is extended up to 2 THz) and the dynamic range is larger than 40 dB regardless of the direction of the electromagnetic wave propagating on the waveguide. The symmetrical electro-optic probe enables to sense the propagation direction of the guided picosecond electromagnetic pulses. The photoswitch has been illuminated by a 130 fs 0.3 mW optical pulse and then the transient response guided on a coplanar waveguide was measured by an electro-optic experiment. The rise time measured between 10 and 90% of pulse maximum is 420 fs while the fall time is 2.5 ps. In return, for counter-propagating configuration, the temporal shape is significantly enlarged since the rise time and the fall time are 2.8 ps and 3.3 ps respectively. This distortion of the electro-optic signal is due to the reduction of the interaction length when the optical and electromagnetic wavevectors are opposite. A model has been calculated in both co-propagating and counter-propagating configuration. The only adjustable parameters for the fit are the absolute amplitude, and the electron and hole lifetimes. The only modified parameter between the co- and counter-propagating theoretical waveforms is the amplitude of the electro-optic signal. The excellent fit of the experimental data by the model indicates that the prismatic electro-optic probe allows the determination of the direction of the picosecond electrical transient. These performances are preserved regardless of the direction of electromagnetic signal since the direction of the optical probe pulse can be easily reversed. This feature has a significant practical implication for identification of impedance mismatches and for spectroscopy investigation of opaque media.

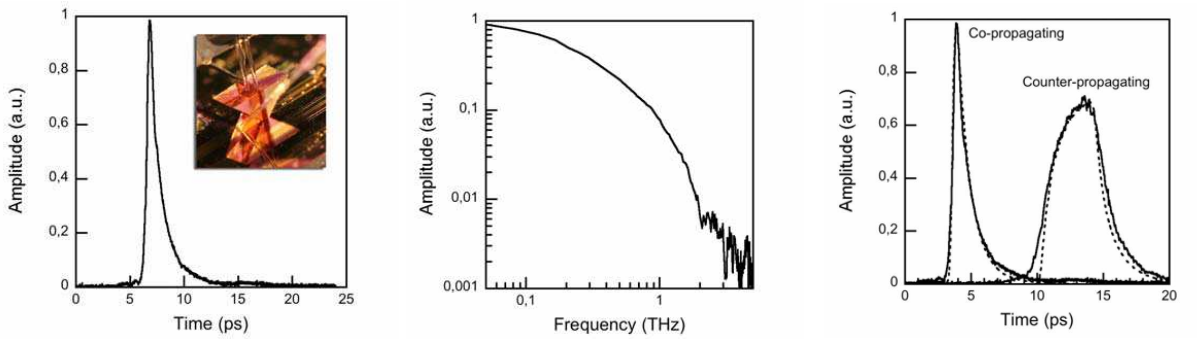

Figure 1.

Ray-optics of Wave Propagation through a Hollow Waveguide

Md. Abdul Matin[1], **Abdul Matin Patwari**[2]
Satya Prasad Majumder[1], **Rummana Matin**[1], **and Saeed M. Khan**[3]

[1]Bangladesh University of Engineering and Technology (BUET), Dhaka, Bangladesh
[2]University of Asia Pacific (UAP), Dhaka, Bangladesh
[3]Kansas State University at Salina, Salina, Kansas, USA

Abstract— In this paper a ray-optical description of propagation of EM-wave through a hollow waveguide is provided to interpret the reason of $\lambda_g > \lambda$, where λ_g is the longitudinal wavelength observed in the waveguide and λ is the wavelength in free-space. It happens due to dispersion in the longitudinal wave number β due to deviation in frequency of the wave. Depending upon the angle of incidence there may be either stimulated emission of radiation (SER) from waveguide walls or straightaway attenuation of fast wave. Ray-optical description of the wave propagation through a hollow waveguide reveals the following facts:

1. The guide wavelength in the longitudinal direction is longer than the wavelength in free space indicating dispersion of wave velocities into group and phase velocities. The group velocity ν_g along with an additional velocity $\nu_g \pm \Delta\nu$ from the scattered ray keeps the resulting speed of the longitudinal wave greater than that of light. This may be attributed to Raman's effect which is different from Compton's effect and Cerenkov's effect.
2. The diffraction mechanism resulting from dispersion in a hollow waveguide is analogous to Bragg diffraction in the lattices of the crystals of solid body. Solid dielectrics of optical fibers may have extinction factor. So metallic shielding of the fiber at successive stages may provide Raman pumping by stimulated emission of radiation (SER). For SER ruby is used in Laser and Maser.
3. Depending on the angle of incidence there may be either (SER) from waveguide walls or extinction of the wave by attenuation.
4. Cerenkov radiation in a plasma filled waveguide is an example of SER. In that case plasma works as a stimulant to SER.

The Effect of Reflectivity Dispersion on Gap Solitons in a Bragg Grating

D. Royston Neill[1], **Javid Atai**[1], **and Boris A. Malomed**[2]

[1]School of Information and Electrical Engineering
University of Sydney, Australia
[2]Department of Interdisciplinary Studies, Faculty of Engineering
Tel Aviv University, Israel

Abstract— Fiber Bragg gratings (FBGs) are produced by a periodic variation of the refractive index along an optical fiber. The resulting coupling between counter-propagating waves results in a strong effective dispersion [1, 2]. When combined with the Kerr nonlinearity, the FBG can give rise to gap solitons (GSs). Standard equations governing the nonlinear pulse propagation in the uniform FBG are found within the framework of the coupled-mode theory (CMT) [2]. A nonuniform modulation of the refractive index gives rise to a FBG subject to *apodization* and spatial chirp. In this paper we make a phenomenological generalization of the standard coupled equations to include the effects of apodization. This adds to the model spatial dispersion of the Bragg reflectivity resulting in the following equations

$$\begin{aligned} iu_t + iu_x + \left(|v|^2 + \frac{1}{2}|u|^2\right) u + v + mv_{xx} &= 0 \\ iv_t - iv_x + \left(|u|^2 + \frac{1}{2}|v|^2\right) v + u + mu_{xx} &= 0 \end{aligned} \tag{1}$$

where u and v are the forward and backward propagating components, while m accounts for the strength of the dispersive reflectivity. In Ref. [3], it was found that quiescent GSs corresponding to Eq. (1) completely fill the bandgap. The dispersive reflectivity was observed to have a stabilizing effect on the quiescent GSs, expanding the stability region previously found in the standard model [4, 5]. However the generalization to moving solitons, which are objects of interest in experiments [6], were beyond the scope of Ref. [3]. The properties of moving solitons in (1) is the subject of this work in which we investigate their properties.

It is found similar to the case of quiescent GSs the presence of a dispersive reflectivity has a stablilising effect on the moving solitons. This stabilising effect is reduced as the velocity increases. Collisions between the solitons result in various outcomes, some found in the standard model and others peculiar to the modified model. Of particular interest is the merger of GS into a standing pulse which is observed in the standard model [7].

REFERENCES

1. Russell, P. St. J., "Bloch wave anaylsis of dispersion and pulse propagation in pure distributed feedback," *J. Mod. Opt.*, Vol. 38, 1599, 1991.
2. De Sterke, C. M. and J. E. Sipe, "Gap solitons," *Prog. Opt.*, Vol. 33, 203, 1994.
3. Atai, J. and B. A. Malomed, "Gap solitons in bragg gratings with dispersive reflectivity," *Phys. Lett. A*, Vol. 342, 404, 2005.
4. Malomed, B. A. and R. S. Tasgal, "Vibration modes of gap soliton in a nonlinear optical medium," *Phys. Rev. E*, Vol. 49, 5787, 1994.
5. Barashenkov, I. V., D. E. Pelinovsky, and E. V. Zemlyanaya, "Vibrations and oscillatory instabilities of gap solitons," *Phys. Rev. Lett.*, Vol. 80, 5117, 1998.
6. Mok, J. T., C. M. de Sterke, I. C. M. Littler, and B. J. Eggleton, "Dispersionless slow light using gap solitons," *Nature Phys.*, Vol. 2, 775, 2006.
7. Mak, W. C. K., B. A. Malomed, and P. L. Chu, "Formation of standing light pulse through collision of gap solitons," *Phys. Rev. E*, Vol. 68, 026609, 2003.

An Adaptive Spectroellipsometric Identifier for Ecological Monitoring of the Aquatic Environment

F. A. Mkrtchyan, **V. F. Krapivin**, **V. I. Kovalev**, **and V. V. Klimov**
Institute of Radioengineering & Electronics RAS
1 Vvedensky Sq., Fryazino, Moscow reg., 141190, Russia

Abstract— The creation of multichannel polarization optical instrumentation and use of spectroellipsometric technology are very important for the real-time ecological control of aquatic environment. It should be mentioned that efficient solution of this multiparametric problem greatly depends on the precision and simplicity of ellipsometric devices.

This report is aimed to describe

- A technology of combined use of spectroellipsometry and algorithms of identification and recognition that allowed the creation of a standard integral complex of instrumental, algorithmic, modular and software tools for the collection and processing of data on the aquatic environment quality with forecasting and decision — making functions
- A compact measuring — information multichannel spectroellipsometric device for monitoring the quality of aquatic environment, that is based on the combined use of spectroellipsometry and training, classification, and identification algorithms

This spectroellipsometric system will differ from modern foreign analogues by the use of a new and very promising method of ellipsometric measurements, an original element base of polarization optics and a complex mathematical approach to estimating the quality of a water object subjected to anthropogenic influence.

Unlike foreign analogues, the system has no rotating polarization elements. This allows one to increase the signal-to-noise ratio and the long-term stability of measurements, to simplify and reduce the price of multichannel spectroellipsometers.

The system will be trainable to the recognition of the pollutants of aquatic environment.

For the first time the combined use of real — time spectroellipsometry measurements and data processing methods has been realized in an **Adaptive Identifier**.

- The algorithmic support of the Adaptive Identifier is based on a complex application of recognition and classification algorithms on the basis of 128 spectra images registered during a fixed period of time.
- A time interval of 1 second is usually established and provides about 30 value of brightness for each of the 128 optical channels.
- The spectra obtained are sources of set of statistical parameters and different characteristics united into vector spaces for their comparison with the standard samples of famous pollutants stored on the computer.
- The technology of this comparison depends on the diversity of identification methods.

The system is trainable to the recognition of the pollutants of aquatic environment.

Session 4A1
Novel Mathematical Methods in Electromagnetics 1

Scattering of Electromagnetic Waves by Inhomogeneous Dielectric Gratings Loaded with Two Adjacent Perfectly Conducting Strips — The Case of TM Waves

Tsuneki Yamasaki, **Ryosuke Ozaki**, **and Takashi Hinata**
Department of Electrical Engineering , College of Science and Technology
Nihon University, Tokyo 101-8308, Japan

Abstract— Recently, many analytical and numerical methods which are applicable to the inhomogeneous dielectric gratings have been proposed such as optical fiber gratings, photonic bandgap crystals, frequency selective devices, and other applications by the development of manufacturing technology of optical devices. However, most theoretical and numerical studies have considered the periodic structures in which the material forming grating was either metallic or dielectric.

In this paper, we proposed a new method for the scattering of electromagnetic waves by inhomogeneous dielectric gratings loaded with two adjacent perfectly conducting strips using the combination of improved Fourier series expansion method and point matching method for TM waves.

n the inhomogeneous dielectric region $S_2(0 < x < D)$, the permittivity profile $\varepsilon_2(x, z)$ is generally not separable with respect to the x and z variables. Main process of our methods are as follows: (1) The inhomogeneous layer is approximated by a stratified layers of modulated index profile with D. (2) Taking each layer as a modulated dielectric grating, the electromagnetic fields are expanded appropriately by a finite Fourier series. (3) In the perfectly conducting strip and gap regions at C_1(or $\overline{C_1}$) and C_2(or $\overline{C_2}$) boundary, the electromagnetic fields are matched using an orthogonality relation which makes the matrix relation on both sides using point matching method. (4) Finally, all stratified layers include the metallic regions are matched using appropriate boundary conditions to get the inhomogeneous dielectric gratings loaded with two adjacent perfectly conducting strips.

Numerical results are given for the transmitted scattered characteristics for the case of incident angle and frequency with δ for TM waves.

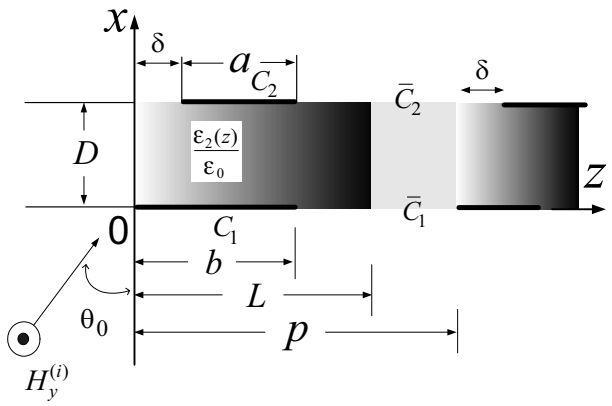

Figure 1: Structure of inhomogeneous dielectric gratings loaded with two adjacent perfectly conducting strips.

Application of a Modified Broyden's Method in the Finite Difference Method for Electromagnetic Field Solutions

Boguslaw Oleksiejuk[1] **and Andrew Nafalski**[1,2]

[1]Lublin University of Technology, Lublin, Poland
[2]University of South Australia, Adelaide, Australia

Abstract— In electromagnetic field modelling, nonlinear and anisotropic media are often used, which increases the complexity of the solution. The fundamental approach to solving nonlinear equation sets is the Newton-Raphson matrix method. It requires time-consuming computations of the Jacobi matrix with evaluations of partial derivative functions. In order to avoid this computational expense, the Broyden's method is used that does not require the evaluation of the Jacobi matrix of partial derivatives. In general the Broyden's method is classified as an extension of the secant method of root finding to higher dimensions.

However, in the case of non-linear and/or anisotropic materials, the basic Broyden's method does not guarantee a successful solution. An alternative method could be the direct application of simple iterative method that in the case of non-linear magnetic circuits also fails to converge.

The method outlined in the paper is a modified Broyden's method that offers an efficient approach to solve the nonlinear equation set obtained as a result of application of the Finite Difference Method and is applicable for an anisotropic and nonlinear electromagnetic environment. As the classical Broyden's method, the new method does not require the determination of the Jacobi matrix elements.

Examples presented in the paper illustrate application of the proposed method to nonlinear magnetic configurations both isotropic and anisotropic described by the Finite Difference Method. A resulting equation system for anisotropic media has specific solutions for singular points present at the border of areas with different material constants (such as magnetic permeability) resulting in the discontinuity of the magnetic vector potential. The solutions using the modified Broyden's method and the Newton-Raphson method are also compared.

Radar Cross Section Analysis of a Finite Parallel-plate Waveguide with Four-layer Material Loading: Part I — The Case of E Polarization

J. P. Zheng and K. Kobayashi
Chuo University, Japan

Abstract— The analysis of electromagnetic scattering by open-ended metallic waveguide cavities has received much attention recently in connection with the prediction and reduction of the radar cross section (RCS) of a target [1]. Various diffraction problems involving two- and three-dimensional cavities have been analyzed thus far based on high-frequency techniques and numerical methods. However, the solutions obtained by these methods may not be uniformly valid for arbitrary cavity dimensions.

In the previous papers [2, 3], we have considered a finite parallel-plate waveguide with three-layer material loading as a geometry that can form cavities, and solved the plane wave diffraction rigorously with the aid of the Wiener-Hopf technique. In this two-part paper, we shall consider a finite parallel-plate waveguide with four-layer material loading shown in Fig. 1 as an important generalization of the waveguide geometry in [2, 3], and analyze the plane wave diffraction using the Wiener-Hopf technique. The case of E polarization is considered in this first part, whereas the analysis for the H-polarized case will be carried out in the second part [4]. This paper is in continuation with our previous two papers [5, 6]. In particular, we shall derive in this paper a new Wiener-Hopf solution with high accuracy based on the results obtained in [5, 6]. Illustrative numerical examples of the monostatic and bistatic RCS are presented for various physical parameters, and the far field scattering characteristics of the waveguide are discussed in detail.

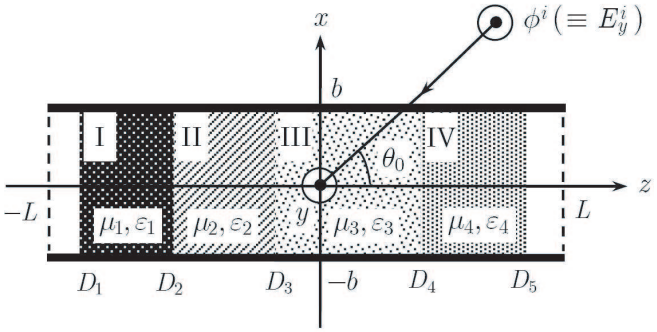

Figure 1: Geometry of the problem.

REFERENCES

1. Stone, W. R., Ed., *Radar Cross Sections of Complex Objects*, IEEE Press, New York, 1990.
2. Okada, S., S. Koshikawa, and K. Kobayashi, "Wiener-Hopf analysis of the plane wave diffraction by a finite parallel-plate waveguide with three-layer material loading: Part I the case of E polarization," *Telecommunications and Radio Engineering*, Vol. 58, No. 1&2, 53–65, 2002.
3. Okada, S., S. Koshikawa, and K. Kobayashi, "Wiener-Hopf analysis of the plane wave diffraction by a finite parallel-plate waveguide with three-layer material loading: Part II the case of H polarization," *Telecommunications and Radio Engineering*, Vol. 58, No. 1&2, 66–75, 2002.
4. Shang, E. H. and K. Kobayashi, "Radar cross section analysis of a finite parallel-plate waveguide with four-layer material loading: Part II — The case of H polarization," *PIERS Proceedings*, Cambridge, MA, USA, submitted July 2–6, 2008.
5. Zheng, J. P. and K. Kobayashi, "Plane wave diffraction by a finite parallel-plate waveguide with four-layer material loading: The case of E polarization," *PIERS Proceedings*, 583, Tokyo, 2006.
6. Shang, E. H. and K. Kobayashi, "Plane wave diffraction by a finite parallel-plate waveguide with four-layer material loading: The case of H polarization," *PIERS Proceedings*, 584, Tokyo, 2006.

Radar Cross Section Analysis of a Finite Parallel-plate Waveguide with Four-layer Material Loading: Part II — The Case of H Polarization

E. H. Shang and K. Kobayashi
Chuo University, Japan

Abstract— Analysis of the scattering from open-ended waveguide cavities is an important subject in the area of the prediction and reduction of the radar cross section (RCS) of a target. A number of cavity diffraction problems have been analyzed thus far by means of high-frequency ray techniques and numerical methods, but it appears that the solutions obtained by these approaches are not uniformly valid for arbitrary cavity dimensions.

This paper is composed of two parts. We shall consider a finite parallel-plate waveguide with four-layer material loading shown in Fig. 1 as a generalization to the geometry in our previous papers [1, 2], and analyze the plane wave diffraction for both E and H polarizations rigorously by means of the Wiener-Hopf technique. In Part I [3] of this two-part paper, we have analyzed the case of E polarization, whereas in this second part, the H-polarized case will be considered. It is shown that a rigorous Wiener-Hopf analysis leads to a solution efficient for numerical computation. Representative numerical examples on the monostatic and bistatic RCS are shown and the far field scattering characteristics of the waveguide are discussed in detail. Some comparisons with the E-polarized case [3] will also be given. Some of the results in this paper are already presented elsewhere [4, 5].

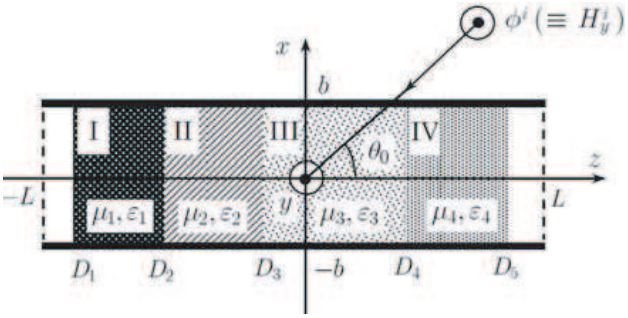

Figure 1: Geometry of the problem.

REFERENCES

1. Okada, S., S. Koshikawa, and K. Kobayashi, "Wiener-Hopf analysis of the plane wave diffraction by a finite parallel-plate waveguide with three-layer material loading: Part I the case of E polarization," *Telecommunications and Radio Engineering*, Vol. 58, No. 1&2, 53–65, 2002.
2. Okada, S., S. Koshikawa, and K. Kobayashi, "Wiener-Hopf analysis of the plane wave diffraction by a finite parallel-plate waveguide with three-layer material loading: Part II the case of H polarization," *Telecommunications and Radio Engineering*, Vol. 58, No. 1&2, 66–75, 2002.
3. Zheng, J. P. and K. Kobayashi, "Radar cross section analysis of a finite parallel-plate waveguide with four-layer material loading: Part I — The case of E polarization," *PIERS Proceedings*, Cambridge, MA, USA, submitted July 2–6, 2008.
4. Zheng, J. P. and K. Kobayashi, "Plane wave diffraction by a finite parallel-plate waveguide with four-layer material loading: The case of E polarization," *PIERS Proceedings*, 583, Tokyo, 2006.
5. Shang, E. H. and K. Kobayashi, "Plane wave diffraction by a finite parallel-plate waveguide with four-layer material loading: The case of H polarization," *PIERS Proceedings*, 584, Tokyo, 2006.

A Reduced Integral Equation for Stationary Currents in Stratified Media

I. R. Ciric
The University of Manitoba, Canada

Abstract— Analysis of direct current distribution for geological explorations, in ground electrode systems or in tomography devices can be performed by applying volume discretization methods or surface integral equations, in the latter case the unknowns to be determined being only associated with the interfaces between different homogeneous regions. A more efficient formulation is presented in this communication, where a reduction procedure is implemented such that the stationary current problem solution for a complex stratified conducting medium is obtained by solving a single reduced integral equation [1–3] relative to only one interface, namely, that between the current region and the outside nonconductive region.

The stationary electric potential in each homogeneous subregion is expressed in terms of single- and double-layer sources over its boundary using a Green function representation. Applying the boundary conditions, these two different kinds of source functions are related, on each interface between the material layers, to a single source function defined over the same interface, for instance a single-layer function, through certain surface integral operators. These operators and single source functions are determined recursively from one interface to the next one, the single function defined over the outer interface being obtained as the solution of a single reduced integral equation relative to this interface in terms of the given excitations on it (i.e., currents injected or electrode potentials). The potential and the current density in the outer layer and, also, anywhere else in the structure considered are determined, respectively, directly or by using simple backward recursions from the solution of this single integral equation.

The computational effort required in the proposed procedure increases only proportionally with the number of layers and is substantially reduced with respect to existing partial differential or surface integral equation methods, especially in the case of multiple tests on the same conductive structure under various given conditions on the outer surface, since the reduction procedure needs to be performed only once.

REFERENCES

1. Ciric, I. R., "New surface integral equations for static and quasistationary fields," *Progress in Electromagnetic Research Symposium*, Honolulu, Hawaii, USA, October 2003.
2. Ciric, I. R. and R. Curiac, "Reduced single integral equation for quasistationary fields in solid conductor systems," *IEEE Trans. Magn.*, Vol. 41, No. 5, 1452–1455, 2005.
3. Ciric, I. R., "Reduced surface integral equations for Laplacian fields in the presence of layered bodies," *Canadian J. Phys.*, Vol. 84, No. 12, 1049–1061, 2006.

The Complex Faraday Tensor for Relativistic Evolution of a Charged Particle in a Constant Field

Y. Friedman and M. M. Danziger
Jerusalem College of Technology, Israel

Abstract— In general, the electromagnetic field tensor $\mathcal{F}$, expressed by a four-by-four matrix is used to describe the electromagnetic field. This tensor provides a convenient expression for the Lorentz force and therefore is often used to describe the evolution of a charged particle. In addition to this representation, the complex Faraday vector $\mathbf{F} = \mathbf{E} + i\mathbf{B}$ has been used widely in the literature to obtain the Lorentz field invariants. Silberstein first combined both concepts in 1907 to define a complex Faraday tensor $\mathcal{F}_\mathcal{C} = \mathcal{F} + i\mathcal{F}^*$.

We use the matrix representation of the complex Faraday tensor defined as $\mathcal{F}_\mathcal{C} = F^k J_k$ where the coefficients F^k are the coefficients of the complex Faraday vector and the matrices J_k are defined as

$$J_1 = \begin{pmatrix} 0 & 1 & 0 & 0 \\ 1 & 0 & 0 & 0 \\ 0 & 0 & 0 & -i \\ 0 & 0 & i & 0 \end{pmatrix}, J_2 = \begin{pmatrix} 0 & 0 & 1 & 0 \\ 0 & 0 & 0 & i \\ 1 & 0 & 0 & 0 \\ 0 & -i & 0 & 0 \end{pmatrix}, J_3 = \begin{pmatrix} 0 & 0 & 0 & 1 \\ 0 & 0 & -i & 0 \\ 0 & i & 0 & 0 \\ 1 & 0 & 0 & 0 \end{pmatrix}.$$

In addition to satisfying the commutation relations of angular momentum, the J_k matrices also satisfy the canonical anti-commutation relations (CAR)

$$\frac{1}{2}(J_k J_l + J_l J_k) = \delta_k^l I.$$

Therefore, $\mathcal{F}_\mathcal{C}$ is a symmetry, ie ${\mathcal{F}_\mathcal{C}}^2 = z^2 I$, implying a simple expression for the exponent of the matrix. The coefficient z^2 is composed of the two Lorentz field invariants.

The 4-velocity $U(\tau)$ in a constant electromagnetic field satisfies the equation

$$\frac{dU}{d\tau} = \frac{q}{2mc}(\mathcal{F}_\mathcal{C} + \bar{\mathcal{F}}_\mathcal{C})U.$$

The solution of such an equation is always an exponent of the matrix applied to the initial 4-velocity. Using the fact that $\mathcal{F}_\mathcal{C}$ and $\bar{\mathcal{F}}_\mathcal{C}$ commute, this exponent is the product of two exponents, each of which has an explicit solution. This gives us the general solution of

$$U(\tau) = \big(\cosh(z\omega\tau)\hat{I} + \frac{\mathcal{F}_\mathcal{C}}{z}\sinh(z\omega\tau)\big)\big(\cosh(\bar{z}\omega\tau)I + \frac{\bar{\mathcal{F}}_\mathcal{C}}{\bar{z}}\sinh(\bar{z}\omega\tau)\big)U_0.$$

This solution is significantly simpler than all of the solutions which appear in the literature. All of the particular cases can easily be derived from it.

By choosing the Newman-Penrose basis in $\mathbb{C}^4$ the J_k matrices come to represent the action of the angular momentum operators on Dirac bispinors. This indicates that $\mathcal{F}_\mathcal{C}$ expresses the action of the electromagnetic field not only upon the charge of an electron but also upon its spin.

Electromagnetic Information Theory for Wireless and Antenna Systems

F. K. Gruber and E. A. Marengo
Department of Electrical and Computer Engineering, Northeastern University
360 Huntington Ave., Boston, MA 02115, USA

Abstract— This research is concerned with the formulation of fundamental wireless communication and antenna engineering problems at the crossroads of the well-established fields of electromagnetic theory and information theory. The interdisciplinary field constituted by such wave- and information-theoretic problems and their solutions can be descriptively termed *electromagnetic information theory* or, within the antenna focus, *antenna information theory*. Specifically, the presentation derives, from the fundamental physical point of view of Maxwell's equations describing electromagnetic fields, the Shannon information capacity [1] of space-time wireless channels formed by electromagnetic sources and receivers in a known background medium, under the assumption of additive Gaussian noise perturbations. Particular attention is given to free space but the results are based on Green functions so that the general procedure and results derived in the presentation can be extended after straightforward substitutions also to more general known media. The theory is developed for the two cases of essentially bandlimited and time-limited systems and of purely bandlimited systems. Among other aspects, the emphasis is on first principles, non-device-specific characterization of these systems. Unlike most past work in this area, and in a spirit analogous to that of recent electromagnetic-oriented wireless communication papers [2–4], the developments take into account the physical radiated power constraint (which is *not* electromagnetically equivalent to the more typical source L^2 norm constraint which has been the focus of past calculations in this area [5–7]). Additionally, we also consider the familiar bounding of the source excitation level as measured by the L^2 norm. Based on such radiated power and/or current L^2 norm constraints we derive the information capacity of canonical antenna systems, for a given additive Gaussian noise level, as well as an associated number of degrees of freedom (NDF) resulting from such capacity calculations which constitute a rigorous, information-theoretic method to define under given Gaussian noise the dimensionality of the field.

ACKNOWLEDGMENT

This research was supported by the United States Air Force Office of Scientific Research (AFOSR) under Grant No. FA9550-06-01-0013.

REFERENCES

1. Shannon, C. E., *A Mathematical Theory of Communication*, CSLI Publications, 1948.
2. Gustafsson, M. and S. Nordebo, "On the spectral efficiency of a sphere," *Progress In Electromagnetics Research*, PIER 67, 275–296, 2007.
3. Wallace, J. W. and M. A. Jensen, "Intrinsic capacity of the MIMO wireless channel," *Proc. IEEE 56th Vehicular Technology Conf. (VTC 2002)*, Vol. 2, 701–705, Vancouver, BC, Canada, September 2002.
4. Sarkar, T. K., S. Burintramart, N. Yilmazer, S. Hwang, Y. Zhang, A. De, and M. Salazar-Palma, "A discussion about some of the principles/practices of wireless communication under a Maxwellian framework," *IEEE Trans. Antenn. Propag.*, Vol. 54, No. 12, 3727–3745, December 2006.
5. Hanlen, L. W. and M. Fu, "Wireless communication systems with spatial diversity: A volumetric model," *IEEE Trans. Wirel. Commun.*, Vol. 5, No. 1, 133–142, January 2006.
6. Hanlen, L. W., A. J. Grant, and R. A. Kennedy, "On capacity for single-frequency spatial channels," *Proc. IEEE Information Theory Workshop*, 446–451, October 2004.
7. Migliore, M. D., "An intuitive electromagnetic approach to MIMO communication systems," *IEEE Trans. Antenn. Propag.*, Vol. 48, No. 3, 128–137, June 2006.

Spatial Filtering Characteristics of Scattered Fields by Inhomogeneous Waveguide Grids for X-ray Image Diagnosis

Yasumitsu Miyazaki
Department of Media Informatics, Aichi University of Technology
50-2 Manori, Nishihazama-cho, Gamagori 443-0047, Japan

Abstract— Medical image diagnosis and computer aided diagnosis using nano-meter electromagnetic waves and X-ray are very important medical techniques. Medical image diagnosis using X-ray is very important technical tool for physiological examination of human body and biological tissues. Image responses of X-ray transmitted wave projection include X-ray absorption effects and also X-ray scattering effects, depending on atomic characteristics of biological tissues and molecules of a few KeV energy levels. Received image signals of receiving plates that contain important information of absorption characteristics in biological interior structures are disturbed by noises of scattered fields due to biological inhomogeneous media. By spatial filtering of scattered fields at output of biological tissues, fine image information containing only absorption characteristics of biological tissues may be obtained.

Spatial filters can be constructed by X-ray inhomogeneous waveguide grids. Each periodic section of grid array is inhomogeneous X-ray waveguide with the graded index distribution. Core region has parabolic index distribution of no absorption characteristics and clad region has parabolic and higher order index distribution of the fourth and sixth of complex absorption characteristics. Electromagnetic fields of X-ray in inhomogeneous waveguide with complex graded index distribution can be expressed by the Hermite or Laguerre functions with complex arguments.

X-ray is incident to biological media and propagates through biological media. After propagation in random biological media, transmitted and scattered X-rays are incident to input of the inhomogeneous graded index type waveguide. On-axial transmitted X-rays are coupled to low modes of inhomogeneous waveguides with low losses. Off-axial scattered X-rays are coupled to higher modes with higher losses. Scattered fields are coupled to higher modes of inhomogeneous waveguides of the grid and filtered in the grid array.

These grid arrays consisting of inhomogeneous X-ray waveguides can operate as spatial filters in X-ray image diagnosis.

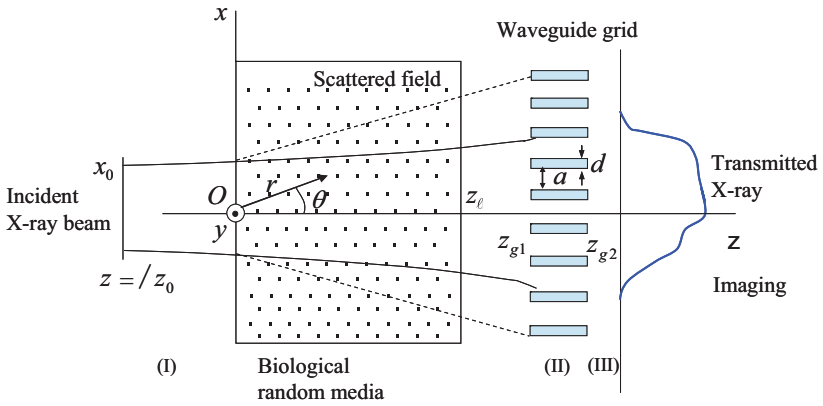

Figure 1: X-ray scattering and X-ray grid.

REFERENCES

1. Miyazaki, Y., "Electromagnetic characteristics of grid structures for scattering fields of nanometer electromagnetic waves and X-rays," *PIERS Proceedings*, 643–647, Tokyo, Japan, August 2–5, 2006.
2. Miyazaki, Y., "Partially coherent optical waves in random gradient fibers," *Optical and Quantum Electronics*, Vol. 9, 153–165, 1977.
3. Miyazaki, Y., "Electromagnetic characteristics of waveguide-type grid filters for scattered nanometer waves in transmitted X-ray diagnostic images," *Proc. of EMTS 2007*, EMTS 128, Ottawa, ON, Canada, July 2007.

Scalar Approximation to Describe Depolarized Light

C.-C. Tsai and B. Ya. Zeldovich

College of Optics & Photonics/CREOL, University of Central Florida
4000 Ctrl. Florida Blvd., Orlando, FL 32816-2700, USA

Abstract— Scalar wave equations are presented, which describe 1) refraction due to change of propagation speed c/n in assumption of constant impedance Z, and 2) reflection due to step of impedance in assumption of constant speed. These Z-Helmholtz and k-Helmholtz equations, taken incoherently, yield surprisingly good description of situations with depolarized light sources and unpolarized detectors.

From theoretical point of view, it is important to understand, which effects in electrodynamics are governed by the gradients of propagation speed $v(\mathbf{r})$ [m/s] and which are controlled by the gradients of impedance $Z(\mathbf{r})$ [Ohm]. Here

$$v(\mathbf{r}) \;=\; \{1/[\varepsilon(\mathbf{r})\mu(\mathbf{r})]\}^{0.5} \equiv c/n(\mathbf{r}),\; n(\mathbf{r}) = \{[\mu(\mathbf{r})\varepsilon(\mathbf{r})]/[\mu_{vac}\varepsilon_{vac}]\}^{0.5}, \tag{1}$$

$$Z(\mathbf{r}) \;=\; [\mu(\mathbf{r})/\varepsilon(\mathbf{r})]^{0.5} \equiv \{[\mu(\mathbf{r})/\mu_{vac}]/[\varepsilon(\mathbf{r})/\varepsilon_{vac}]\}^{0.5} \cdot 377\,\text{Ohm}, \tag{2}$$

and $n(\mathbf{r})$ is the refractive index. Monochromatic [$\exp(-i\omega t)$] Maxwell equations $\text{curl}\mathbf{E} = i\omega\mu(\mathbf{r})\mathbf{H}(\mathbf{r})$, $\text{curl}\mathbf{H} = -i\omega(\mathbf{r})\varepsilon(\mathbf{r})\mathbf{E}(\mathbf{r})$ have well-known symmetry with respect to the transformation $\varepsilon(\mathbf{r}) \to \mu(\mathbf{r})$, $\mu(\mathbf{r}) \to \varepsilon(\mathbf{r})$, $\mathbf{E}(\mathbf{r}) \to \mathbf{H}(\mathbf{r}), \mathbf{H}(\mathbf{r}) \to -\mathbf{E}(\mathbf{r})$. Kinematic parameters — propagation speed and refractive index — are not changed by this transformation, while impedance Z goes into $1/Z$. So it is the impedance, which deals with polarization, while the refractive index is more or less neutral to polarization. This fact was mathematically elucidated in [1], where Maxwell equations in locally isotropic, but spatially inhomogeneous medium were reduced to

$$\begin{gathered}\text{curl}[\mathbf{R}(\mathbf{r})] - k(\mathbf{r})\mathbf{R}(\mathbf{r}) = \mathbf{g}(\mathbf{r}) \times \mathbf{L}(\mathbf{r}),\; \text{curl}[\mathbf{L}(\mathbf{r})] + k(\mathbf{r})\mathbf{L}(\mathbf{r}) = \mathbf{g}(\mathbf{r}) \times \mathbf{R}(\mathbf{r}), \\ k(\mathbf{r}) = (\omega/c)n(\mathbf{r}),\; \mathbf{g}(\mathbf{r}) = -0.5\mathbf{grad}\{ln[Z(\mathbf{r})]\},\end{gathered} \tag{3}$$

$$\mathbf{R}(\mathbf{r}) = \mathbf{E}(\mathbf{r})/[Z(\mathbf{r})]^{0.5} + i\mathbf{H}(\mathbf{r})[Z(\mathbf{r})]^{0.5},\; \mathbf{L}(\mathbf{r}) = \mathbf{E}(\mathbf{r})/[Z(\mathbf{r})]^{0.5} - i\mathbf{H}(\mathbf{r})[Z(\mathbf{r})]^{0.5}, \tag{4}$$

see also [2]. Here $\mathbf{R}(\mathbf{r})$ and $\mathbf{L}(\mathbf{r})$ are the right and left-circularly polarized components of the filed, respectively. Eq. (3) means that coupling between $\mathbf{R}(\mathbf{r})$ and $\mathbf{L}(\mathbf{r})$ is due to the gradient of impedance, and not of the refractive index.

Question: which scalar equation is the next best thing (in comparison with Maxwell equations) to describe depolarized light sources and polarization-insensitive detectors? We know that the case of completely homogeneous isotropic medium is described by the Helmholtz equation $(\nabla \cdot \nabla)u(\mathbf{r}) + k^2 u(\mathbf{r}) = 0$, to which each Cartesian component of all four fields $\mathbf{E}(\mathbf{r}), \mathbf{D}(\mathbf{r})$, $\mathbf{H}(\mathbf{r}), \mathbf{B}(\mathbf{r})$ satisfies. We suggest here two scalar equations:

$$k(\mathbf{r})\nabla\{[1/k(\mathbf{r})]\,\nabla u(\mathbf{r})\} + [k(\mathbf{r})]^2 u(\mathbf{r}) \;=\; 0,\; Z = \text{const}\;(Z - \text{Helmholtz}), \tag{5}$$

$$Z(\mathbf{r})\nabla\{[1/Z(\mathbf{r})]\,\nabla u(\mathbf{r})\} + k^2 u(\mathbf{r}) \;=\; 0,\; k = \text{const}\;(k - \text{Helmholtz}), \tag{6}$$

We call this Z-Helmholtz (ZH) and k-Helmholtz (kH) equations. It can be easily verified that if $k = k(z)$ ("layered medium"), then the reflection coefficients, as follow from ZH and kH, are:

$$r_{\text{ZH}}(\theta_1) = (\cos\theta_1 - \cos\theta_2)/(\cos\theta_1 + \cos\theta_2); \quad r_{\text{kH}}(\theta_1) = (Z_2 - Z_1)/(Z_2 + Z_1) \tag{7}$$

It means that the reflection coefficient is zero for the following case of Z-H problem: wave is incident at a normal to the boundary, and the refractive index $n(z)=k(z)/(\omega/c)$ changes abruptly at this boundary $z = 0$ between two media.

We compared ZH expression with three other functions of the incidence angle θ_i: reflection coefficient for the TE polarization, for the TM polarization, and their arithmetic average; the graphs at the Figure 1(a) are drawn for $n_1 = 1$, $n_2 = 1.5$, like for air/glass boundary. The arithmetic average of R_{TE} and R_{TM} is denoted by $R_D(\theta_i)$ to describe the situation, when incident light is completely depolarized, and detectors are polarization-insensitive. Addition of intensity reflected according to kH (4%) makes the error less than 3.9% in all the range of angles.

We have also calculated the longitudinal shift of the beam's center of gravity in the process of Total Internal Reflection (TIR), i.e., so-called Goose-Hanschen shift. Again, there is a surprising

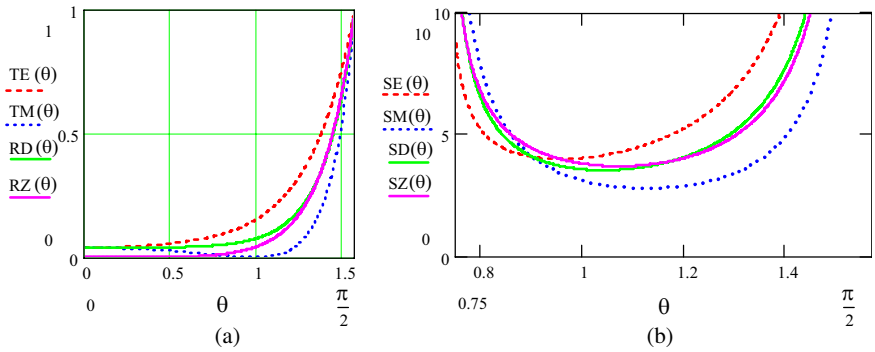

Figure 1: (a) Reflection intensities of TE wave (red dot line), TM wave (blue dot line), and their arithmetic average value $R_D = [R_{\mathrm{TE}} + R_{\mathrm{TM}}]/2$ (green solid line), compared with Z-H reflection intensity (purple solid line), as functions of incidence angle for $n_1 = 1$, $n_2 = 1.5$ (as for air/glass). (b) Goose-Hanschen shift for TE wave (SE, red dot line), TM wave (SM, blue dot line) and their average value SD (green solid line), compared with their shift SZ calculated from ZH equation (purple solid line), as functions of incidence angle for $n_1 = 1.5$, $n = 1$ (as for glass/air).

accuracy, with which ZH equation describes Goose-Hanshen shift for depolarized beams and detectors.

We foresee the use of ZH and kH equations for the discussion of the media with "negative refractive index".

REFERENCES

1. Savchenko, A. Y. and B. Y. Zeldovich, "Birefringence by a smoothly inhomogeneous locally isotropic medium: Three-dimensional case," *Phys. Rev. E*, Vol. 50, 2287–2292, 1994.
2. Savchenko, A. Y. and B. Y. Zeldovich, "Wave propagation in a guiding structure: One step beyond the paraxial approximation," *JOSA B*, Vol. 13, 273–281, 1996.

Volume Singular Integral Equation Method for Determination of Effective Permittivity of Meta- and Nanomaterials

Yu. V. Shestopalov[1], **Yu. G. Smirnov**[2], **and V. V. Yakovlev**[3]

[1]Karlstad University, Karlstad, Sweden
[2]Penza State University, Penza, Russia
[3]Worcester Polytechnic Institute, Worcester, MA, USA

Abstract— This contribution presents the results of further development of solution techniques for the inverse boundary value problems (BVPs) for Maxwell's equations associated with the wave propagation in the waveguides with dielectric inclusions [1, 2]. Such problems arise in determination of complex permittivity of materials in closed cavities [3]. In this work, we extend the analysis to cover a practically valuable emerging technology of reconstruction of effective permittivity of meta- and nanomaterials. We consider the diffraction of an incident electromagnetic wave by a dielectric body in a perfectly conducting single-mode rectangular waveguide. Using characteristics of the scattered field we reduce the inverse problem to nonlinear volume singular integral equations (NVSIE) with respect to the electric field on the body. Effective permittivity of the inclusion is determined with the use of the NVSIE solution. In our approach, the BVPs are formulated in unbounded domains and with the partial radiation conditions at infinity. Our method of solution employs the integral equations constructed using vector 3D Green's function of the domain occupied by the waveguide.

We analyze the NVSIE on the basis of the corresponding BVP using the equivalence of this BVP and the integral equation. This enables us to consider NVSIE in the L_2 space and obtain some results concerning the solutions of BVP. In this method, the resulting NVSIE operator is bounded and the integral equation is solved only inside the body.

A numerical method for solving the NVSIE is also proposed. Its convergence is proved, and some results of numerical experiments are presented.

REFERENCES

1. Smirnov, Y. G. and A. A. Tsupak, "Investigation of electromagnetic diffraction by a dielectric body using the volume singular integral equation," *Computational Mathematics and Mathematical Physics*, Vol. 44. No. 12, 2143–2158, 2004.
2. Shestopalov, Y. V. and V. V. Yakovlev, "Uniqueness of complex permittivity reconstruction in a parallel-plane waveguide," *Radio Sci.*, Vol. 42, No. 10, RS6S20, 2007.
3. Eves, E. E., P. Kopyt, and V. V. Yakovlev, "Determination of complex permittivity with neural networks and FDTD modeling," *Microwave Opt. Tech. Letters*, Vol. 40, No. 3, 183–188, 2004.

Propagation and Scattering Characteristics of Microwaves over Forests in WiMAX Wireless Communications Using FDTD Method

Yasumitsu Miyazaki, **Takuya Takada**, **and Koichi Takahashi**
Department of Media Informatics, Aichi University of Technology
50-2 Manori, Nishihasama-cho, Gamagori 443-0047, Japan

Abstract— WiMAX wireless communication has been rapidly developed for broadband mobile communication. Mobile WiMAX communication system uses microwave carrier of 2.5 GHz frequency band and modulation system is mainly OFDM for transmission of signals. By using OFDM technique, WiMAX provide high speed and reliable communication against the multi pass interference due to the presence of obstacles in communication channels. To design excellent high performance wireless communication systems, accurate evaluation of communication channels are indispensable. By using parallel FDTD, we studied fundamental microwave propagation and scattering characteristics in urban area. In these analyses, building and street effects on high speed signal propagation have been investigated by computer simulation of FDTD method. However, wave propagation and scattering characteristics by presence of forest and trees are not so much studied. The effects of multiple scattering and attenuation of microwave by forest is severe factors of high speed wireless communications. Size of branches and leaves of trees are comparable with microwave wavelength and yield strong interaction phenomena of broadband propagation.

In this paper, propagation and scattering characteristics of microwave over forests in WiMAX wireless communication is numerically analyzed using FDTD method. FDTD method can be applied for signal and noise analysis about several different complex models and inhomogeneous materials such as forests in communication channels. By applying FDTD method for the analysis of communication channels of propagation over trees and forests, numerical simulations of signal and noise propagation for various tree structures at different frequencies and digital signal bit rates are demonstrated. In FDTD simulations, the incident wave is assumed to be a traveling wave from transmission antenna station at a far distance. Numerical results in this paper show and analyze the effects of various structures of forests and frequencies of incident waves. The shape of forest assumed to be constructed by random surface and distribution of branches of trees are inhomogeneous. Forest and trees in radio communication channel is considered to be as random surface and inhomogeneous materials. The effects of multiple scattering and attenuation due to forests are discussed and evaluated using statistical functions, such as average, variance and correlation of conductivities and permittivities for trees. These results may yield important factors for design of high performance and more reliable WiMAX communication systems.

For the analysis of microwave propagation and scattering characteristics over forests, the analysis space including many branches comparable with the wavelength is much larger than the wavelength and a few hundreds meters. Parallel computation of FDTD using grid computer can be proceeded for these analyses. To perform parallel processing using grid computer, the total analysis space is divided into subdomains of $M_z \times M_y$ and each divided subdomain $D_{u,v}$ is assigned to one of PC computers. The electromagnetic fields in $D_{u,v}(1 \leq v \leq M_y)$ are calculated by parallel processing. For the calculation of values on the boundary of subdomains, values in the adjacent subdomain are exchanged and matched for field boundary condition. To proceed the parallel processing, data transfer between adjacent subdomains is carried out using MPI.

REFERENCES

1. Selormey, P. and Y. Miyazaki, "Electromagnetic compativility characteristics of buildings in mobile radio waves propagation channel," *Trans. IEE*, Vol. 119-C, No. 1, 97–104, Japan, 1999.
2. Rodriguez, G., Y. Miyazaki, and N. Goto, "Matrix-based FDTD parallel algorithm for big areas and its applications to high-speed wireless communications," *IEEE Trans. Antennas & Propagat.*, Vol. 54, No. 3, 785–796, 2006.
3. Masuda, T., Y. Miyazaki, and Y. Kashiwagi, "Analysis of electromagnetic wave propagation in out-door active RFID system using FD-TD method," *PIERS Online*, Vol. 3, No. 6, 937–939, 2007.

Session 4A2
Progress on Theory and Numerical Algorithm for Solving the Inverse Scattering Problems

Subspace and Bayesian Compressive Sensing Methods in Imaging

E. A. Marengo
Northeastern University, Boston, USA

Abstract— Compressive sensing is a new field in signal processing and applied mathematics. It allows one to simultaneously sample and compress signals which are known to have a sparse representation in a known basis or dictionary along with the subsequent recovery by linear programming (requiring polynomial (P) time) of the original signals with low or no error [1–3]. Compressive measurements or samples are non-adaptive, possibly random linear projections of the given signal. Most importantly, sparsity arises in many physical signals, hence this approach is of significant importance. The results in this area apply to biomedical imaging, astronomy, single-pixel photography [4, 5], and many other disciplines.

The present work presents new approaches to linear and nonlinear inverse scattering problems that are based on compressive sensing ideas. Particular emphasis is given to the framework termed Bayesian compressive sensing [1]. Past work in compressive sensing has been restricted to linear inverse problems of the form $y = Ax$ where A is a matrix mapping input (object) x to output (data) y. In this linear context, the focus has been to show that despite significant undersampling of the data signal y as projections of the form $y_0 = \Phi y$ where Φ is a measurement matrix obeying a mild incoherency property, one can for a broad class of sparse object signals still carry out perfect inversions or reconstructions with low error to the compressed inverse problem of inverting x from y_0 where $y_0 = \Phi y = \Phi A x$ (refer to [2, 3] for the details). The focus of the present treatment is to show how Bayesian compressive sensing applies to wave inverse scattering, in both the linear regime of the so-called Born approximation for weakly scattering objects as well as in the more general context of strongly scattering objects exhibiting non-negligible multiple scattering interactions. The compressive sensing approach to inverse scattering will be discussed in relation to alternative signal-subspace-based methods for shape reconstruction including sampling and level-set-based approaches [6–8]. The derived developments are motivated mostly by detection and imaging applications requiring computationally non-intensive (P time) signal processing with limited wave data about a given event or target of interest.

ACKNOWLEDGMENT

This research is supported by the US AFOSR under grant FA 9550-06-01-0013.

REFERENCES

1. Ji, S., Y. Xue, and L. Carin, "Bayesian compressive sensing," *IEEE Trans. Signal Proc.*, in press.
2. Candès, E. J., J. Romberg, and T. Tao, "Robust uncertainty principles: Exact signal reconstruction from highly incomplete frequency information," *IEEE Trans. Inform. Theory*, Vol. 52, 489–509, 2006.
3. Donoho, D. L., "Compressed sensing," *IEEE Trans. Inform. Theory*, Vol. 52, 1289–1306, 2006.
4. Wakin, M. B., J. N. Laska, M. F. Duarte, D. Baron, S. Sarvotham, D. Takhar, K. F. Kelly, and R. G. Baraniuk, "An architecture for compressive imaging," *Proc. International Conference on Image Processing (ICIP 2006)*, Atlanta, GA, Oct. 2006.
5. Takhar, D., J. N. Laska, M. B. Wakin, M. F. Duarte, D. Baron, S. Sarvotham, K. F. Kelly, and R. G. Baraniuk, "A new compressive imaging camera architecture using optical-domain compression," *Proc. of Computational Imaging IV at SPIE Electronic Imaging*, San Jose, CA, Jan. 2006.
6. Marengo, E. A., F. K. Gruber, and F. Simonetti, "Time-reversal MUSIC imaging of extended targets," *IEEE Transactions on Image Processing*, Vol. 16, 1967–1984, 2007.
7. Marengo, E. A., "Further theoretical considerations for time-reversal MUSIC imaging of extended scatterers," *IEEE Statistical Signal Processing Workshop 2007*, 304–306, Madison, Wisconsin, August 26–29, 2007 (ISBN:978-1-4244-1198-6).
8. Marengo, E. A., R. D. Hernandez, and H. Lev-Ari, "Intensity-only signal-subspace-based imaging," *J. Opt. Soc. Am. A*, Vol. 24, 3619–3635, 2007.

Parallel Processing of Forward-backward Time-stepping Method for Time Domain Inverse Scattering

T. Moriyama[1], **Y. Yamaguchi**[2], **K. A. Hong Ping**[1], **T. Tanaka**[1], **and T. Takenaka**[1]

[1]Nagasaki University, Japan
[2]Nagasaki Broadcasting Company, Japan

Abstract— Electromagnetic wave inverse scattering problem are investigated in various fields such as medical imaging, geophysical exploration, nondestructive testing, and target identifications. We have proposed a time-domain inverse scattering imaging technique, the forward-backward time-stepping (FBTS) method, to reconstruct the electrical parameter profiles of scattering objects. In our previous works, we have applied the FBTS method to early breast cancer detection, landmine detection, and concrete structure diagnosis. It was clarified that quite good reconstructed results were obtained using the FBTS method in several numerical simulations [1, 2]. We also showed its usefulness in real situations by applying the FBTS method to experimental data [3]. Although the FBTS method is effective to inverse scattering problems, the computation time is quite long to get accurate results. This is a problem in dealing with three-dimensional (3-D) objects. Therefore reconstruction processing time in the FBTS method is required to be greatly reduced.

In this paper, we investigate the reduction of the computation time of the FBTS method by introducing parallel processing of the method. To reconstruct the relative permittivity profile of a 3-D unknown object, a number of antennas are placed in a measurement surface enclosing the object. One of the antennas is used as a transmitting antenna and emits a pulsed wave. The scattered wave by the object is collected by the rest of them. Then, we change the transmitter point to the next antenna point and repeat the same measurement until all the antenna positions are used as a transmitter point. In the FBTS method, it is necessary that the same number of direct scattering problems as that of transmitter points are calculated in order to obtain the gradient vector which is related to the update of the estimation for electrical parameters. In this work, the calculation of direct problems is conducted simultaneously by several computers to reduce the computation time. A cluster of 8 personal computers is constructed and a parallel algorithm for FBTS method is implemented using Message Passing Interface (MPI) library.

REFERENCES

1. Takenaka, T., H. Jia, and T. Tanaka, "Microwave imaging of electrical property distributions by a forward-backward time-stepping method," *Journal of Electromagnetic Waves and Applications*, Vol. 14, No. 12, 1609–1626, 2000.
2. Takenaka, T., H. Zhou, and T. Tanaka, "Inverse-scattering for a three-dimensional object in the time domain," *J. Optical Society of America A*, Vol. 20, 1863–1874, 2003.
3. Johnson, J. E., H. Zhou, and T. Takenaka, "Experimental three-dimensional time-domain reconstruction of dielectric objects for breast cancer detection," *Proc. the VI Mediterranean Microwave Symposium*, 423–426, Genoa, 2006.

On Combining Model Reduction and Gauss-Newton Algorithms for Inverse Frequency Domain Maxwell Equation

Mikhail Zaslavsky and Vladimir Druskin
Schlumberger Doll Research, 1 Hampshire str., Cambridge, MA 02139, USA

Abstract— We propose an approach to acceleration of the solution of the inverse PDE problems using the Gauss-Newton (GN) method. In particularly, we are interested in the large scale problems (e.g., inverse conductivity problems for 3D Maxwell's system), for which the most time consuming part is the solution of the forward problems. We want to minimize the number of these solutions by utilizing information from the previous GN iterations. Additionally, if the forward solver uses an iterative algorithm, we want to generate for it a good initial guess.

In this work we are able to solve inverse problems using rational interpolants of comparably small orders by iteratively adding interpolation points. On each iteration of our inversion algorithm we solve the same forward problems as in the conventional GN algorithm (using the adjoint solutions for the computation of the derivatives). Then we design a Reduced Order Model (ROM) of our measurement data via the pseudo-Galerkin algorithm combining in the same subspace these forward solutions together with the ones obtained on the previous iterations. After that we solve the approximate inverse problem for the obtained ROM and proceed to the next iteration. The only difference compared to the conventional GN is that on every iteration instead of linearization we use the more accurate ROM. Instead of constructing the ROM a priori we update it every iteration. In the case of one parameter inversion the ROM becomes the matrix multipoint Padé approximant matching point values and their first derivatives. In the multivariate case it is a rational approximation matching the data and their Jacobians for all the previous iterations. An important property of our approximants, that at least for positive-definite self-adjoint problems (e.g., Electrical Impedance Tomography) the approximation error decreases monotonically.

Numerical experiments show significant acceleration on examples of 3D Maxwell's equations, however the method can be applied to practically all inverse PDE problems currently employing the Gauss-Newton algorithm or its modifications.

3D Gauss-Newton Quantitative Microwave Imaging Using a Preconditioned LSQR Algorithm and a Constrained Line-search Applied to Breast Imaging

J. De Zaeytijd and A. Franchois
Department of Information Technology, Ghent University, Belgium

Abstract— A three-dimensional (3D) Vectorial Quantitative Microwave Imaging algorithm, based on a Gauss-Newton optimization with line-search of a regularized cost function, which is expressed in the unknown complex permittivities in a voxel grid, was presented in [1]. Accurate quantitative reconstructions were shown for an inhomogeneous lossy cube from multi-view/single-frequency simulated data and for a polyethylene cube from multi-view/multi-frequency far-field experimental data.

In the present contribution, we examine the applicability of this technique to medical imaging, such as breast cancer screening. To this aim, we propose several improvements: (i) A further reduction of the computational effort for the solution of the multi-view forward problem, which we perform in each iteration. A classical volume integral equation formulation is discretized with a Galerkin Method of Moments and solved with an iterative BiCGStab technique. The reduced effort comes from extending the "marching-on-in-source-position" technique with a Distorted Born approximation. (ii) A computationally more efficient and stable solution of the Gauss-Newton permittivity updates — this is required in case of a large number of permittivity optimization variables — by means of a preconditioned LSQR algorithm [2] with a 3D cosine basis. (iii) The possibility to introduce *a priori* information in a flexible way, by allowing the inversion for pre-defined aggregates — of arbitrary shape — of permittivity voxels, instead of for each voxel independently, thus reducing the number of unknowns for the optimization. This is of much importance for biomedical imaging applications and also may be an advantage with respect to the "modified gradient" approach [3], which does not require forward problem solutions, but where the optimization always includes a considerable number of total field unknowns. (iv) The proposal of a new, constrained line-search path in the Gauss-Newton optimization, which incorporates in an elegant manner *a priori* knowledge concerning lower and upper bounds on the breast permittivity.

The data are different components of the scattered field vector in points surrounding the object, resulting from successive dipole illuminations with different polarizations and different source positions at a fixed frequency. The technique is validated with reconstructions from simulated data of biological objects, including malignant breast phantoms without and with a skin layer.

REFERENCES

1. De Zaeytijd, J., A. Franchois, C. Eyraud, and J. M. Geffrin, "Full-wave three-dimensional microwave imaging with a regularized Gauss-Newton method — theory and experiment," *IEEE Trans. Antennas Propagat.*, Vol. 55, No. 11, 3279–3292, 2007.
2. Jacobsen, M., P. C. Hansen, and M. A. Saunders, "Subspace preconditioned LSQR for discrete illposed problems," *BIT Numerical Mathematics*, Vol. 43, No. 5, 975–989, 2003.
3. Abubakar, A., P. M. van den Berg, and J. J. Mallorqui, "Imaging of biomedical data using a multiplicative regularized contrast source inversion method," *IEEE Trans. Microw. Theory Tech.*, Vol. 50, No. 7, 1761–1770, 2002.

Progress of a High-resolution 3-D Microwave Imaging System for Breast Cancer Detection

Qing Huo Liu, **Chun Yu**, **John Stang**, **Mengqing Yuan**, **Rhett T. George**
Gary A. Ybarra, **and William T. Joines**
Department of Electrical and Computer Engineering, Duke University, USA

Abstract— We have developed a prototype 3-D microwave imaging system for breast cancer diagnosis and screening. This presentation will give an overview of the hardware development, forward electromagnetic wave propagation models, nonlinear inverse scattering algorithms for this 3-D microwave imaging system. High-resolution 3-D images that can resolve multiple objects of a few millimeters will be demonstrated by the system.

The microwave data acquisition system consists of 3-D transmitting and receiving array antenna elements mounted on a rectangular tub containing a fluid with matching electrical properties with those of normal breast tissue. The antennas are designed to reduce the mutual coupling while providing the maximum transmission efficiency into the tissue. The measurement is performed in the frequency domain at several discrete frequencies. This array system allows microwaves to penetrate well into the breast tissue without giving rise to large reflections back to the surrounding area.

The collected 3-D data is then processed by a 3-D nonlinear inverse scattering algorithm to unravel the complicated multiple scattering (diffraction) effects. Our nonlinear inverse scattering algorithm is based on the efficient combination of several ingredients: (a) The diagonal tensor approximation (DTA) is used to obtain a fast estimate of the image; (b) the distorted Born iterative method (DBIM) is used to solve the full nonlinear inverse problem with the DTA result as the initial solution; (c) the forward solution based on the stabilized biconjugate-gradient FFT method is used as the computational engine for the data prediction and for gradient information. The product of this processing is a high-resolution 3-D digital image containing the physical properties of the tissue and potential tumors.

In the 3-D microwave imaging system developed, we are able to detect small signals 80 dB below input signals. This high sensitivity enables the 3-D system to collect accurate scattering data from small phantom tumors. We will demonstrate its capability to fully image multiple tumor phantoms as small as 5 mm at 1.74 GHz.

A 3D Level Set Technique for Monitoring Conductive Fluids in Reservoirs

Oliver Dorn[1] and Rossmary Villegas[2]

[1]Universidad Carlos III de Madrid, 28911 Leganes, Madrid, Spain
[2]Institute of Petroleum Engineering, Heriot-Watt University, Edinburgh EH14 4AS, UK

Abstract— Recently low frequency electromagnetic techniques have been discussed for the application of monitoring fluid flow in petroleum reservoirs. The goal is to detect the interfaces between fluids of different conductivity values from data gathered at relatively low frequencies (1 kHz and lower). In the paper we will discuss the application of low frequency electromagnetic induction tomography for monitoring a water flooding process during oil production. Electromagnetic sources are distributed at the surface of the Earth and in some boreholes in the reservoir, and the corresponding electromagnetic data are collected at the surface and in other boreholes. From these data, we aim at reconstructing the interfaces between regions of different conductivity values, typically due to differences in water and hydrocarbon conductivity parameters.

We use the full 3D system of Maxwell's equations for modelling the propagation of the electromagnetic fields in the reservoir. A level set technique in 3D is employed for describing the interfaces between regions of different conductivity values, in our case water and oil. The level set technique is an implicit way of modelling shapes and interfaces where the zero level set of a function defined in the region of interest encodes the interfaces or boundaries of the shapes. The level set technique has the advantage that the topology of the final reconstruction does not need to be known a priori and will be an automatic result of the reconstruction process. An evolution approach for the level set function is employed in order to deform some initial guess for the interfaces and shapes into the final reconstruction. The evolution of the level set function is driven by repeated calculation of descent directions with respect to some cost functional which measures the misfit between true data and estimated data corresponding to the latest best guess. An efficient regularization technique is incorporated in order arrive at regions with well-behaved boudaries.

Numerical experiments are presented which demonstrate the performance of our novel level set technique for synthetic but realistic 3D examples of practical relevance.

Exploiting Support Information and Lamé Curves in 2D Inverse Scattering Problems

M. D'Urso[1], **I. Catapano**[2], **L. Crocco**[2], **T. Isernia**[3], **and A. Litman**[4]

[1]Federico II University of Naples, Naples, Italy
[2]IREA, National Research Council, Naples, Italy
[3]Mediterranea University of Reggio Calabria, Reggio Calabria, Italy
[4]Institut Fresnel, UMR-CNRS 6133, Marseille, France

Abstract— Inverse scattering problems are usually cast as optimization ones, in which the global minimum of a cost functional defines the solution. Such a minimization can be tackled by either adopting global or local methods and many different approaches have been proposed in the literature. However, while applicability of global schemes (see [1] and references therein) is actually limited by the computational cost that grows exponentially fast with the number of unknowns, local schemes (adopted f.i. in [2–4]) may conversely lead to "false solutions", so that their reliability actually depends on the starting guess. Therefore, electrically and geometrically poor images are often obtained from the inversion process, unless a priori information about targets (positivity constraints, lossless nature, etc.) are enforced. Comprehension of the factors affecting the difficulty of the problem may give hints to devise new and more effective imaging strategies. For instance, the analysis of the "degree of non-linearity" of the inverse scattering problem [2] allows to understand how the (approximate) knowledge of position, shape and average permittivity of the unknown targets can strongly improve the effectiveness of the inversion procedures [2]. By exploiting these results, an innovative two-step strategy has been recently proposed and tested on experimental data [5]. In the first step, the Linear Sampling Method (LSM) [6] is adopted to effectively retrieve the geometrical features of the targets. Then, this information is exploited in the second step, devoted to the electromagnetic characterization of targets. This step is based on local optimization scheme and takes decisive advantage from a proper optimization of the Contrast Source - Extended Born (CS-EB) inversion method [3, 5]. Along the same path, in this contribution, we propose a new two-step inversion strategy, wherein, unlike [5], a global optimization method is exploited in the electromagnetic characterization step. As recalled, the crucial point in this case is the "curse of dimensionality", which we effectively tackle by lowering the number of unknown parameters using a representation of the unknown contrast based on Lamé curves. As a matter of fact, these curves allow to map a large class of different shapes by means of a reduced number of parameters, so that they can be of interest in several applications, ranging from biomedical diagnostics to subsurface sensing. A key role in the success of the overall method is also played by the result achieved in the first step using LSM [6]. As a matter of fact, the preliminary, possibly rough, shape estimation allows to fix the number of targets to be retrieved and their (approximate) locations in the test domain, thus providing not only a reliable starting guess for the following step, but also reducing the search-space in the global minimization scheme, thus remarkably reducing the overall computational cost. Numerical examples confirming the effectiveness of the proposed strategy will be presented at the Conference.

REFERENCES

1. Pastorino, M., *IEEE Trans. Antennas Propagat.*, Vol. 55, 538–548, 2007.
2. Bucci, O. M., et al., *J. Opt. Soc. Am. A.*, Vol. 18, 1832–1845, 2001.
3. Isernia, T., et al., *IEEE Geosc. Remote Sens. Letters*, Vol. 1, 331–337, 2004.
4. Van den Berg, P. M., et al., *Inv. Probl.*, Vol. 15, 1325–1344, 1999.
5. Catapano, I., et al., *IEEE Trans. Antennas Propagat.*, Vol. 55, 1895–1899, 2007.
6. Colton, D., et al., *Inv. Probl.*, Vol. 19, S105–S137, 2003.

Retrieval of an Unknown Number of Buried Spheres by Differential Evolution with Multi-resolution Multi-zone Features

A. Breard, G. Perrusson, and D. Lesselier
Département de Recherche en Électromagnétisme, Laboratoire des Signaux et Systèmes
CNRS-SUPÉLEC-Univ. Paris Sud 11, France

Abstract— The work herein focuses onto the characterization of homogeneous 3-D obstacles buried in a subsoil, modeled as a resistive, non magnetic, homogeneous half-space and seen in the induction regime. Fields of application are in the magnetic probing of natural or artificial objects buried in subsoil at some distance from the air/soil interface.

By characterization, it is meant identification of number, locations and main electrical and geometrical features of these obstacles. The latter are assumed to be modeled as penetrable spheres with low contrast of conductivity with respect to the host medium, and they are also supposed somewhat small with respect to the skin depth in this host medium.

The measurements hypothesized are variations of trans-impedance between two electric current loops, one in transmission mode, the other in reception mode. Data are collected along a small set of parallel lines placed above the interface, at one (or few) low frequency (e.g., from 100 Hz to few hundred kHz).

One has first developed an approximate model of diffraction by coupled obstacles buried in subsoil, which is valid for an arbitrary number of obstacles. It is based on the extended Born approximation [1], the assumption of small enough homogeneous obstacles, and is accounting for interaction between obstacles via the application of the Lax-Foldy theory on multiple diffraction [2].

The inversion itself (involving minimization of a least-square cost function) is carried out by means of a hybrid differential evolution algorithm, involving so-called multi-resolution multi-zone features. That is, in a first step, the number and location of different space boxes where there might effectively be buried spheres are retrieved. To that goal, one applies a differential evolution algorithm [3] for a chosen initial number, $NO_{\max\, init}$, of obstacles. Then, after a suitable number of iterations, one reaches the number of spheres among the $NO_{\max\, init}$ reconstructed ones which have a non-negligible influence on the minimization of the cost function. So at this step, one assumes that each sphere may be equivalent in some respect to coupled ones, buried in a box centered at the location of the one just found.

The next step consists in the evaluation of the number of spheres within each such box. This step is an iterative one, denoted as iteration of groups (usually carrying between 1 and 3 iterations, otherwise the computer time calculation might become prohibitive). In each iteration of groups, one applies the differential evolution algorithm during a large enough number of iterations (e.g., 300). First, one assumes that there exist two coupled spheres in each found box; then, one determines whether there is indeed one or two by box. One iterates the procedure each time that one finds two spheres, until a prescribed maximum number of iterations of groups is reached.

With this algorithm, one is able to distinguish distant obstacles in the first step, and in the second step, one is able to separate obstacles (here, spheres) coupled to one another.

In the oral presentation, one will describe the hybrid differential algorithm, follow on by a summary of the approximate model for N spheres, and one will conclude with typical reconstruction results from independently computed synthetic data.

REFERENCES

1. Habashy, T., R. Groom, and B. Spies, "Beyond the Born and the Rytov approximations: A nonlinear approach to electromagnetic scattering," *J. Geophys. Res.*, Vol. 98, 1759–75, 1993.
2. Braunisch, H., "Methods in wave propagation and scattering," PhD Thesis, MIT, 2001.
3. Storn, R., "On the usage of differential evolution for function optimization," *Biennal Conference of the North American Fuzzy Information Processing Society*, 519–23, Berkeley, 1996.

Dort Method as an Imaging Tool for Extended Targets

X. Zhang, H. Tortel, J.-M. Geffrin, A. Litman, and P. Sabouroux
Institut Fresnel, Aix-Marseille Universite, CNRS, Ecole Centrale de Marseille
Campus Universitaire de Saint-Jerome, Case 162, Marseille Cedex 13392, France

Abstract— Probing a medium using waves to detect, localize and characterize objects has many applications.

Generally speaking, quantitative inverse problems (i.e., when one is interested in recovering values of the electromagnetic parameters of an unknown scatterer) are recasted in optimization problems. A starting initial guess representing the unknown object is progressively modified during an iterative process in order to minimize a well-suited quantity.

It is well known that this kind of problem is severely ill-posed and the convergence of the process is extremely linked to many parameters, one of those being the misfit between the initial guess and the true scatterer. It is then very important to determine from the measured scattered field an initial guess which is as close as possible from the object in terms of shape and permittivity allowing a "fast" convergence of the iterative process as well as a reduction of the domain of interest.

We will present here an application of the Decomposition of the Time Reversal Operator (DORT method) to the case of extended targets. The DORT technique has been first applied in the acoustic domain for the detection and localization of point-like scatterers [1]. It had been extended later on to the electromagnetic case and for various geometrical setups [2, 3] (probing antennas completely surrounding the scatterer, probing antennas along a line, buried object...). We will explain how we build images of the extended scatterers from the eigenvectors corresponding the non null eigenvalues of this operator. We will present results of this qualitative and rapid imaging technique obtained from numerical data sets and also true experiments performed in our laboratory with the circular microwave setup which is presently being constructed for soil moisture applications [4]. Comparisons of images obtained with other classical methods such as MUSIC will be displayed in the case of homogeneous targets.

REFERENCES

1. Prada, C. and M. Fink, "Eigenmodes of the time reversal operator: A solution to selective focusing in multiple-target media," *Wave Motion*, Vol. 20, 151–163, 1994.
2. Tortel, H., G. Micolau, and M. Saillard, "Decomposition of the time reversal operator for electromagnetic scattering," *Journal of Electromagnetic Waves and Applications*, Vol. 13, No. 5, 687–719, 1999.
3. Micolau, G. and M. Saillard, "D.O.R.T method as applied to electromagnetic subsurface sensingmethod as applied to electromagnetic subsurface sensing," *Radio Science*, Vol. 38, No. 3, 1038, 2003.
4. Lencrerot, R., A. Litman, H. Tortel, and J. M. Geffrin, "A microwave imaging circular setup for soil moisture information," *IGARSS Proc.*, 4394–4397, Barcelona, 2007.

Session 4A3a
Passive and Active Mircowave Circuits

On the Development of Tunable Microwave Devices for Frequency Agile Applications

Jia-Sheng Hong and Young-Hoon Chun

Department of Electrical, Electronic and Computer Engineering
Heriot Watt University, Edinburgh, EH14 4AS, United Kingdom

Abstract— This paper presents a recent development of electronically tunable microwave devices for frequency agile applications such as emerging cognitive radios and ultra-wide band (UWB) wireless systems. Since the demands for wireless communications increase and become complex, RF front-ends need multi-band or wideband circuits to satisfy several standards of wireless systems, which makes a tunable circuit essential. An adaptive controlled system which can enhance the performances of a wireless system also requires the tunable devices and circuits such as tunable phase shifters. Also, a high performance transmitter with good efficiency or a multi-band transceiver needs a good impedance match between antenna and amplifiers or filters. A wideband antenna, however, does not have an impedance of 50 ohms and neither does a power amplifier, in general. As it may decrease the efficiency of overall system, many authors reported the methods to improve the impedance match and enhance the performances by means of a tunable transformer. In addition, tunable filters are needed in many applications.

These newly developed tunable microwave devices are based on new device structures and tuning elements. For example, a variable capacitor such as varactor diode is the most frequently used device as a tuning element, it has a limitation to meet every requirements. This is mainly caused by the lack of variable inductance devices or circuits. As an alternative way to realize a tunable circuit, we have investigated new tunable device structures comprised of variable characteristic impedance (Z_C) transmission line which can be used as a distributed tuning circuit. Demonstrators for this type of tunable devices have been designed, fabricated and tested. Both simulated and experimental results are presented. Also, we have developed novel tunable dual-mode filters. Unlike a conventional dual-mode resonator, the dual-mode resonator used for our development does not have a coupling between the two degenerate modes. Therefore, a new tunable filter coupling structure is employed, which exhibits some attractive features such as to be able to reconfigure passband selectivity.

In addition to semiconductor tuning elements used, ferroelectric materials are of great interest for the development of electrically tuned microwave components and circuits. Rapid tuning speed, moderate insertion loss at microwave frequencies, high power handling capacity and simple fabrication process make them more attractive. In this paper, as a practical application of ferroelectric materials, we will present some newly developed bandstop filters based on variable capacitors on BST thin film. A tunable bandstop or band reject filter, which is considered as an application of BST varactors in this work, has become more essential for wideband wireless communication systems as it can reduce incoming or emitted unwanted signals effectively. The designs using defected ground structures or electromagnetic bandgap structures will be described.

Usage of RBF Neural Network for the Implementation of a Microwave Waveguide Ten-port Reflectometer

J. Monzó-Cabrera, J. P. Pedreño-Molina
A. Toledo-Moreo, and Alejandro Díaz-Morcillo
Depto. Tecnologías de la Información y las Comunicaciones
Universidad Politécnica de Cartagena, Spain

Abstract— The efficiency of microwave heating systems is one of the key aspects both at laboratory and industry levels. For estimating this efficiency one can measure the reflection coefficient or S_{11} parameter at one-port ovens since a direct relationship can be established:

$$\eta = 1 - |S_{11}|^2 \tag{1}$$

where η is the power efficiency of the oven.

The most extended methods for S_{11} measurement are the so called *six-port reflectometers* [1–3] and the *vector network analyzers (VNA)*. On the one hand, the six-port, designed by Engen in 1977, is an inexpensive solution that avoids the use of network analyzers; on the other hand, it employs simple power detectors (like diodes or thermistors) in opposition to the mixers of the analyzers. It consists in a simple circuit with six ports connected to the source, the unknown load and four power detectors. From the outputs of the detectors, a numerical relationship can be obtained to determine the reflection coefficient in the load. However, several shortcomings were detected for six-port implementation such as: diode non linearities, noise, numerical instabilities during calibration processes, etc.

In this work a low-power scalar waveguide ten-port reflectometer is designed, built, calibrated and tested. Both electromagnetic simulations and experimental tests have been carried out. The calibration process has been based in the usage of conventional RBF neural networks (RBF-NN) which are able to learn the relationship between the actual reflection coefficient and the eight power levels provided by power detectors. Since RBF-NN need many tests to be trained, an automated procedure consisting of moving a dielectric load within a microwave oven has been implemented. In this way hundreds of values were obtained for S_{11} and power detectors. A VNA was used as signal generator and to provide the reference values for S_{11}. Obtained results indicate that this method can be successfully used for S_{11} estimation.

Additionally, it has been proved that the device can be reconfigured in order to work properly even if several power detectors fail. In these situations, the device is still capable to provide accurate results.

REFERENCES

1. Engen, G. F., "The six-port reflectometer: An alternative network analyzer," *IEEE Transactions on Microwave Theory and Techniques*, Vol. 25, No. 12, 1075–1080, 1977.
2. Engen, G. F., "Calibrating the six-port reflectometer by means of sliding terminations," *IEEE Transactions on Microwave Theory and Techniques*, Vol. 26, No. 12, 951–957, 1978.
3. Engen, G., "A least squares solution for use in the six-port measurement technique," *IEEE Transactions on Microwave Theory and Techniques*, Vol. 28, No. 12, 1473–1477, 1980.

A Compact Ultra-wideband Bandpass Filter with Low Insertion Loss Using Stub Circuits with Defected Ground Structure

Wen-Jeng Lin[1], **I-Tseng Tang**[2], **Ding-Bing Lin**[3]
Chi-Min Li[4], **Min-Yuan Chiu**[4], **and Mau-Phon Houng**[1]

[1]Institute of Microelectronics, Department of Electrical Engineering
Advanced Optoelectronic Technology Center, National Cheng-Kung University, Tainan, Taiwan
[2]Department of Environment and Energy, Nation University of Tainan, Tainan, Taiwan
[3]Institute of Computer and Communication Engineering
National Taipei University of Technology, Taipei, Taiwan
[4]Department of Communications and Guidance Engineering
Nation Taiwan Ocean University, Keelung, Taiwan

Abstract— A novel ultra-wideband (UWB) bandpass filter is proposed, designed and implemented. The UWB bandpass filter (BPF) is designed for short-circuited stubs with defected ground structure (DGS). The rectangular slot provides attenuation pole to suppress the spurious in the stopband. The quarter-wave short-circuited stubs are used to realize the lower stopband, and the etching on the ground plane with rectangular slots is employed to attenuate the upper stopband. Both simulated and measured results show that the filter has a good performance, including an ultra-wideband bandpass (3.1–10.6 GHz), a small insertion loss, a group delay variation of less than 0.12 ns.

Introduction: Since the U.S. Federal Communications Commission (FCC) relieved the unlicensed use of the ultra-wideband (UWB) (3.1–10.6 GHz) for indoor and hand-held systems in 2002. Recently the UWB has been developed and applied widely. It usually was used in short distance communication. Generally speaking, traditional parallel-coupled line structure, very strong coupling structure could be achieves a wide bandwidth.

A new concept UWB bandpass filter has been proposed. Etching pattern on the ground plane is called defected ground structure (DGS) [1]. DGS is a novel technique to improve the performance of filter, and it shows that DGS can enhance the attenuation of stopband and eliminate the parasitical passband in stopband.

Design Concept and Improvement: Figure 1 shows the layout of the proposed UWB BPF structure. The UWB BPF has four stubs that via hole in the ground, to design broadband high-pass filter, and attenuation lower than 3 GHz [2]. If the stubs are short circuited, the proposed technique may be used to design high-pass filters with wide bandwidths. Besides a good control of the band-pass characteristics, the filters provide also nearly constant group delay over the passband. Simulation and measurement of the UWB filter with DGS shown in Fig. 2 and the Geometry of the UWB filter is shown in Table 1.

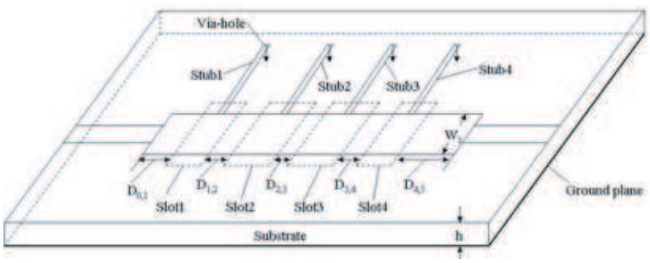

Figure 1: Structure of the novel UWB filter with DGS.

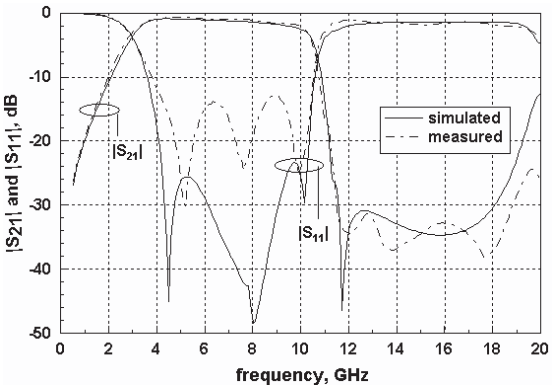

Figure 2: Simulation and measurement of the UWB filter with DGS.

Table 1: Geometry of the UWB filter.

Top layer	Stub1	Stub2	Stub3	Stub4
Length (mm)	6.66	6.59	6.59	6.66
Width (mm)	0.44	0.63	0.63	0.44
Back layer	Slot1	Slot2	Slot3	Slot4
Length (mm)	2.1	2.45	2.45	2.1
Width (mm)	3.8	3.8	3.8	3.8

REFERENCES

1. Kim, C. S., J. S. Lim, S. Nam, K. Y. Kang, and D. Ahn, "Equivalent circuit modeling of spiral defected ground structure for microstrip line," *Electron. Lett.*, Vol. 38, No. 19, 1109–1111, Sep. 2002.
2. Hong, J.-S. and H. Shaman, "An optimum ultra-wideband microstrip filter," *IEEE Microwave Opt. Technol Lett.*, Vol. 47, No. 3, 230–232, 2005.

Measurement of the Dielectric Constant of Liquids Using a Hybrid Cavity-ring Resonator

M. S. Kheir[1], **H. F. Hammad**[1], **and A. S. Omar**[2]

[1]Faculty of Information Engineering and Technology
German University in Cairo, Cairo, Egypt
[2]Microwave and Communication Engineering
University of Magdeburg, Magdeburg, Germany

Abstract— A simple and efficient structure for measuring the dielectric constant of liquids utilizing a microstrip ring resonator and a rectangular waveguide cavity is presented. The waveguide cavity acts as metallic enclosure for the ring circuit. Employing both techniques in a single structure is a double-check procedure rather than comparing the obtained results with any other standard method. The proposed structure has the advantage of being suitable for holding liquid samples without containing air gaps. Avoiding this source of uncertainty enhances the measurement sensitivity. Because of shielding and absence of radiation losses, the structure has a high unloaded quality factor.

The suggested idea is based on exciting both resonators by coaxial-to-microstrip end launchers. The fundamental resonance frequency is detected using a vector network analyzer (VNA). Via observing the peaks of the magnitude and the rapid phase variation of the insertion loss the resonance can be accurately determined. The sample dielectric constant can be then determined using the resonance conditions of both resonators.

The dimensions of the waveguide cavity are designed to operate in the TE101 mode. For the ring resonator the fundamental resonance frequency is considered. Several material types have been investigated to assure measurement accuracy where the relationship between the effective and relative dielectric constant is plotted. The relative dielectric constant of the material under test (MUT) can be extracted by interpolation or alternatively using conformal mapping algorithm.

This technique can be best suitable for characterizing biological liquids such as blood or urine as a promising method for medical diagnostics.

A 802.11a Pulse-swallow Integer-N Frequency Synthesizer

Cheng-Chan Tien[1], **Tsung-Mo Tien**[2], **and Christina F. Jou**[1]

[1]National Chiao-Tung University, Taiwan
[2]National Cheng-Kung University, Taiwan

Abstract— In this paper we will explain thoroughly a 802.11a pulse-swallow integer-N frequency synthesizer using a very conventional architecture to obtain a high phase noise performance. The whole circuit is designed on chip except the loop filter. The reference frequency is set to 10 MHz and a pulse-swallow counter is designed for the purpose of controlling the dual-modulus divider (÷8/9). The frequency tuning range varies from 4.98 GHz to 5.73 GHz, and meanwhile the output power of the voltage-controlled oscillator is −13.5 dBm, and the phase noise measured at 1 MHz is −126 dBc/Hz. The settling time of the closed loop is about 20 µs, the total power dissipation is 26.35 mW with 1.8 V supply voltage. The chip is fabricated under TSMC CMOS 0.18 µm.

Microwave Assisted Processing of $Sm(Zn_{0.5}Ti_{0.5})O_3$ and ZnO-TiO_2 Dielectric Resonators

S. Roopas Kiran, **V. R. K. Murthy**, **and V. Subramanian**
Microwave Laboratory, Department of Physics
IIT Madras, Chennai 600036, India

Abstract— Dielectric resonators are widely used as components of microwave resonant cavities with high dielectric constant, high quality factor and low temperature dependence of resonant frequency. Recent advances in synthesis of materials find several methods of preparation that includes microwave processing. It is possible to use the microwave for the synthesis of materials in two ways. Once the calcination of the required material is performed with conventional furnace, the microwave assisted sintering can be used for more densification. The other way is to directly use the microwave assisted process for obtaining the densified pellets from the stoichiometrically mixed starting reagents. In this paper, we report the synthesis of $Sm(Zn_{0.5}Ti_{0.5})O_3$ and ZnO-TiO_2 using conventional sintering, microwave assisted sintering and microwave assisted synthesis. Phase formation was observed with XRD and surface morphology was observed using AFM. Microwave dielectric properties of all these systems were obtained using Hakki-Coleman method and cavity resonance method. The paper analyzes the variation between the microwave dielectric property and surface morphology of the above two systems synthesized by the three different routes.

Session 4A3b
Microelectronic Packaging 1

Introduction of an ECT Simulator for Microelectronic Packaging

Tian Xiao[1], **Mengqing Yuan**[2], **Joon-Ho Lee**[1], **and Qing Huo Liu**[2]

[1]Wave Computation Technologies, Inc., Durham, NC, USA
[2]Department of Electrical and Computer Engineering, Duke University, Durham, NC, USA

Abstract— Computational electromagnetics for the design simulation of microelectronic packaging problems faces a great challenge because of the complex fine geometrical details in the chip level compounded with the large scale of the package. A time-domain approach such as the finite-difference time-domain method with a uniform grid requires a large number of discretization points to solve such mixed-scale problems. This issue is especially challenging for package-level problems.

We have developed an efficient time-domain simulator for microelectronic packaging and RF applications based on the enlarged cell technique (ECT), an improved version of the conformal finite-difference time-domain method [1, 2]. The ECT eliminates an important limitation, i.e., the reduction in the time step size, in the conformal finite-difference time-domain method, and removes the staircasing error in the FDTD method for curved conductors. We have demonstrated that the ECT is three times as efficient as the conformal finite-difference time-domain method. This technique is further enhanced by a nonuniform grid and by multi-region domain decomposition, and has now been incorporated in a graphic user interface. We will demonstrate the efficacy of this simulator by solving large-scale package level EMI/EMC problems.

REFERENCES

1. Xiao, T. and Q. H. Liu, "Enlarged cells for the conformal FDTD method to avoid the time step reduction," *IEEE Microwave Wireless Compon. Lett.*, Vol. 14, 551–553, 2004.
2. Xiao, T. and Q. H. Liu, "A 3-D Enlarged Cell Technique (ECT) for the conformal FDTD method," *IEEE Trans. Antennas Propagat.*, in press.

Simulation of Multiscale Circuit Problems Using Equivalence Principle Algorithm

Mao-Kun Li[1], **Weng Cho Chew**[2], **and Zhi Guo Qian**[3]

[1]Schlumberger-Doll Research, Cambridge, MA, USA
[2]The University of Hong Kong, Hong Kong, China
[3]University of Illinois at Urbana-Champaign, Urbana, IL, USA

Abstract— As technological devices become smaller, faster, and more complex, computer simulations of physical phenomena become an increasingly important part of the design process. This makes computational electromagnetic (CEM) simulations indispensible. However, many challenges arise when applying CEM solvers to microelectronic structures. Multiscale phenomena are some of them. A single device can be very tiny and dominated by circuit physics, while thousands of devices can extend to several wavelengths in high frequencies that are dominated by wave physics. The existence of both wave and circuit physics introduces large and small eigenvalues simultaneously resulting an ill-conditioned matrix equation. One kind of methods uses multi-resolution basis set to describe different physics. The other approach separates different physics via domain decomposition.

Equivalence principle algorithm (EPA) is essentially a domain decomposition scheme based on equivalence principle and integral equations. By the introduction of virtual equivalence surfaces to enclose the regions with fine features, low frequency physics is isolated from high frequency physics. This results in a better conditioned matrix equation with fewer unknowns. Compared with other integral-equation-based domain decomposition scheme, such as boundary element tearing and interconnecting methods, EPA still allows the interactions between any two basis functions, hence it can catch wave propagation with less dispersion error.

To model continuous current flow in and out of the equivalence surface, a tap basis scheme was introduced. This scheme avoids the computation of current singularities at the cut and can be incorporated with EPA naturally.

In the errors of EPA, a main factor is the high-frequency noise in field projection onto equivalence surfaces. This noise comes from the discretization of the equivalent currents and becomes dominant when objects are very close to the equivalence surfaces. To recover the accuracy, the high-order quadrature point-sampling scheme was used on the equivalence surfaces. This scheme samples the currents directly at points on the equivalence surfaces and integrates using high-order quadrature rules. By using this, EPA is shown to be accurate. The translation procedure in EPA can be accelerated using attached unknown accelerations when equivalence surfaces contact with each other. The current interactions on the touched regions can be computed using local interpolations instead of field integrations. This saves the time in both matrix filling and matrix-vector multiplications. Moreover, the efficiency of EPA can be further improved when accelerated using multi-level fast multipole algorithm. With a proper preconditioning scheme and a careful balancing of the equation, large multiscale problems of over 3 million unknowns can be computed on a personal computer.

A Full-wave Wide-band Surface-integral-equation-based Field Solver

N. Kurt-Karsilayan[1] and K. A. Michalski[2]

[1]Texas A&M University and Mentor Graphics Corporation, USA
[2]Texas A&M University, USA

Abstract— A full-wave, wide-band field solver based on surface integral formulation is introduced. Equivalence principle is used to derive surface integral formulations based on the interior and the exterior electric and magnetic fields and boundary conditions. A general surface integral formulation can be reduced to well-known electric field integral equation (EFIE), magnetic field integral equation (MFIE) or PMCHWT formulations. The method of Moments (MOM) is used to transform continuous surface integrals to a discretized linear matrix system which is then solved by using LU decomposition method. Singularity cancellation and subtraction methods are used to address the numerical integrations of weakly and highly singular terms, respectively. Loop-star basis and testing functions are used along with frequency scaling to address the low frequency problem.

Presented field solver is written in Fortran90 and supports triangular patches in neutral format from any outside mesher. Reference edge current direction for the first encountered edge is assumed to be outward and normal to the edge. The same edge corresponding to a latter element is assigned a negative value which implies that the current direction is inward and normal to the edge. This avoids the computation of current direction based on the surface normal and edge vectors. Each matrix element involves a double integration which is carried out only for element pairs where one and three Gaussian quadrature points are used for the outer and inner integrals, respectively. For roof-top basis and testing functions, each matrix element corresponds to non-boundary testing and source edge pairs and is composed of four contributions due to the interactions between testing and source triangles connected to the edge pairs. For loop-star basis and testing functions, each matrix element corresponds to loop-loop, loop-star, star-loop or star-star pairs. Loop current orientation is counter-clockwise and patch current direction is outward. The same algorithm is used to compute integrals for each element pair and contributions for each edge pair, however each edge-pair contribution is added to sixteen matrix locations with the correct sign. In the case of excitation or right-hand-side vector, contribution from each testing edge is added to four locations with the correct sign.

EFIE and MFIE electric current and system matrices are analyzed and compared for perfect electric conductors (PEC). Electric and magnetic currents and system matrix for PMCHWT formulation are analyzed for a dielectric and a lossy conducting sphere. Accuracy of loop-star basis and testing functions along with frequency scaling are compared to roof-top basis and testing functions with respect to decreasing frequency.

Evolving a 3-D Model for Determining the Impact of Reference Plane Discontinuities

Richard Mellitz and Ted Ballou
Intel Corporation, Columbia, SC, USA

Abstract— Problems of return path management require accurate modeling of reference plane discontinuities when simulating board interconnects. For large structures the preferred transmission line model (w-element) is referenced to ideal ground, and this fact poses a problem for a simulation attempting to capture the effects of multiple reference planes.

Since return path in board interconnects is essentially a 3-D problem, the appropriate model must be derived from a 3D solver such as Ansoft-HFSS^{TM}. While a 3D solver provides robust modeling capability absent in 2D tools, it presents the user with a host of new issues that can make the problem unnecessarily difficult. These are related to accurately sectioning the actual design into a reduced 3D problem that can be solved. In particular, questions of radiation boundaries, port dimensions and meshing effects may derail a straightforward effort into an exercise in discovering the peculiarities of the modeling tool. This is especially problematic for modeling interconnect topologies of the size commonly found in computer and communication boards.

The work describes a study of discontinuous reference plane effects in a DDR3-1600 interconnect, with focus on how to calibrate the target problem vs. the tool details at several steps of model evolution. Emphasis is placed on nourishing an intuitive skepticism of any results that vary significantly with only modest changes in input parameters. The resulting findings show that crosstalk (rather than insertion loss) is by far the most important issue affected by reference plane discontinuity. They further show that, with good reference plane decoupling return paths can be adequately managed for some designs even in the presence of discontinuous reference planes.

Optimization of Vertical Interconnect of a Microprocessor Package Using a Fast Full-wave Electromagnetic Analysis Tool

Arun V. Sathanur[1], **Vikram Jandhyala**[1], **Kemal Aygun**[2]
Henning Braunisch[2], **and Zhichao Zhang**[2]

[1]Department of Electrical Engineering, University of Washington, Seattle, WA, USA
[2]Intel Corporation, Chandler, AZ, USA

Abstract— With the advent of multicore architectures, the need for memory and input/output (I/O) bandwidths of microprocessor packages is growing rapidly. The vertical interconnect part of a microprocessor package is an intricate structure comprising of several features such as traces, pads, vias, and voids. It contributes heavily to the degradation of the channel impedance matching thereby increasing reflections and eventually reducing the bandwidth available and hence the speed of signaling. In the current work, we look to optimize the performance of the vertical interconnect by arriving at the optimum dimensions for the pad, voids, via sizes, and other features in conjunction with a fast full-wave electromagnetic (EM) analysis code. Accelerated Boundary Element Method (BEM) based EM solvers have been recently receiving a lot of interest [1].

Even with the usage of fast solvers, the simulation of complex structures as the package vertical interconnect takes a lot of computing time. This coupled with the high dimensionality of the problem (coming from pads, voids and vias in several layers) makes it a hard problem for a search based optimization or an optimization procedure involving the EM solver in the loop.

To circumvent this difficulty, a sensitivity study is undertaken to identify the most important features affecting the return loss in a single package line. These variables are then sampled at discrete levels and a response surface is fitted to express the return loss in a closed form expression in terms of these feature sizes. A number of global and local optimizers exist, enabling us to easily optimize for the feature sizes using the response surface model. Once an approximate optimum is found, the model around this point can be refined in the design space. Running a local optimizer on the refined model will result in a better approximation for the actual optimum.

A high order response surface is used to reproduce the global variations while a smaller order response surface is used for refinement around the approximate global optimum. Furthermore, an error feedback based mechanism with the solver allows construction of the response surface in an adaptive fashion. Thus, a lesser number of EM simulations can be performed to ensure a specific accuracy of the response surface model. Thus, a multilevel scheme will enable an accurate location of the optimum dimensions of the package vertical interconnect feature sizes while also minimizing the calls to the full-wave EM solver.

REFERENCES

1. Gope, D. and V. Jandhyala, "Efficient solution of EFIE via low-rank compression of multilevel predetermined interactions," *IEEE Transactions on Antennas and Propagation*, Vol. 53, No. 10, 3324–3333, Oct. 2005.

Session 4A4
Photonic Crystals and Metamaterials 1

Transmission Spectra Changes Produced by Decreasing Compactness of Opal like Structures

A. Andueza, R. Echeverría, and J. Sevilla
Departamento Ingeniería Eléctrica y Electrónica, Universidad Pública de Navarra
Campus de Arrosadia, Pamplona 31006, Spain

Abstract— Artificial opal-like structures based on spheres and colloidal particules have been fabricated in a controlled way, presenting optical band-gap properties in the optical frequency range [1]. Non-close packed artificial opals have also been fabricated and studied in optical range using colloidal self-aseembly method [2, 3]. These kinds of structures are very interesting photonic crystals both from the fundamental and applied points of view.

In order to gain a better understanding of these phenomena, we have studied macroscopic models of the compact and the non-close packed (see Fig. 1) three dimensional *fcc* lattices using glass spheres ($\varepsilon = 7$) of several millimetres diameter, and measuring in the microwave region (from 10 to 30 GHz). The scalability of the Maxwell equations governing the physical behaviour of this system assures that the results obtained from our model can be downsized to the optical range, where most promising applications are found.

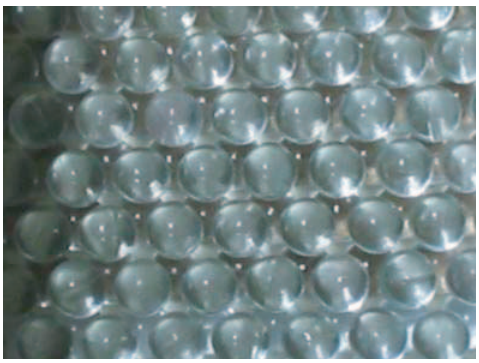

Figure 1.

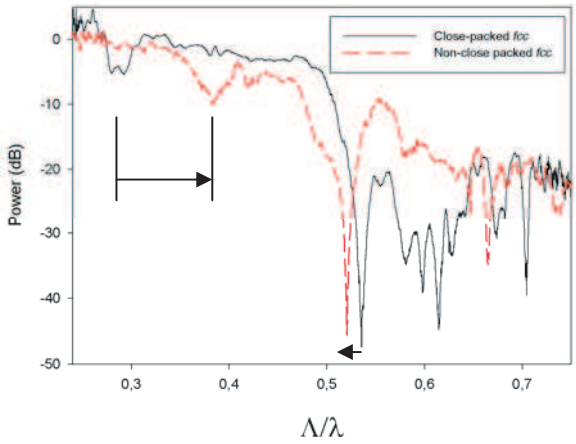

Figure 2.

Figure 2 shows the transmission spectra of both structures in the $< 1, 1, 1 >$ direction. The lower frequency peak (corresponding to the Bragg reflections generated by spheres layers) shifts to higher values in the non compact case. The shift fits with the difference in the separation of the spheres layers in the two structures. A higher order rejection band presents a shift of smaller value and in the opposite direction. As this band is developed over the resonances of a single layer of spheres, this result is consistent with the resonance frequency decrease produced in the single layer by decreasing compactness [4]. In conclusion, we analyze the electromagnetic behaviour of non-close packed *fcc* opal-like, reporting a first gap tuneable with its filling factor, and a strong transmission attenuation at a higher spectral range much less varied by this parameter.

REFERENCES

1. Miguez, H., et al. "Band spectroscopy of colloidal photonic crystal fims," *Appl. Phys. Lett.*, Vol. 84, No. 8, 1239–1241, 2004.
2. Fenollosa, R. and F. Meseguer, "Non-close-packed artificial opals," *Adv. Mater.*, Vol. 15, No. 15, 1282–1285, 2003.
3. Fenollosa, R. and F. Meseguer, "Non-close packed colloidal crystals," *J. of Mater. Chemistry*, Vol. 15, No. 43, 4577–4580, 2005.
4. Andueza, A. and J. Sevilla, "Non compact single layers of dielectric spheres electromagnetic behavior," *Opt. Quant. Electron*, Vol. 39, 311–320, 2007

Clusters of Sub-wavelength Metallic Cylinders as a Convenient Meta-material in the Visible EM Spectrum

David J. Bergman
Raymond and Beverly Sackler School of Physics and Astronomy, Tel Aviv University
IL-69978 Tel Aviv, Israel

Abstract— An isolated finite cylinder, with radius a much less than the wavelength λ and length $L \geq \lambda$, have electromagnetic (EM) eigenstates which are surface plasma waves that bounce back and forth between the cylinder ends. Very good approximations to these states can be written in *closed form*. Moreover, the interactions between two such states of different cylinders can also be written in closed form, using Bessel functions, as long as those cylinders stand in parallel and with their ends at equal heights. This opens the way to calculations of the EM response of finite clusters of such cylinders by expanding the physical EM field in a series of those isolated-cylinder eigenstates. Such an approach can also be used for an infinite periodic array of such cylinders or cylinder-clusters. This works well no matter how densely packed are the cylinders, as long as they do not overlap.

This approach is being used to compute the macroscopic response of such systems. Particularly interesting are the results for such response when the physical parameters (i.e., electric permittivity of the cylinders and that of their host medium, as well as the frequency of the EM field) are such that the entire composite medium is near a sharp EM resonance. In that case, those parameters can be fine-tuned (e.g., by varying the frequency or some details of the microstructure) in order to achieve desired values of the macroscopic electric permittivity and macroscopic magnetic permeability. In particular, a negative value for either one of these moduli, or for both of them simultaneously, can be achieved in this way.

It is important to note that sharp, well separated EM resonances in a dense composite mixture of two constituents will only occur if the microstructure is periodic in space, and if the system is not too far away from the quasistatic regime. For that to occur, the electric permittivity of the cylinders should have a large negative real part and a small imaginary part, while the electric permittivity of the host medium should be real and positive. The magnetic permeability is taken to be 1 in both constituents. This means that the host should be a "conventional" dielectric material, while the cylindrical inclusions should be metallic and the frequency of the EM field should be in the visible or near-infrared range. The conventional metals which best satisfy the necessary requirements are Silver and Gold.

The latest results obtained using this approach will be presented.

Influence of the Number of Layers in the Transmission Properties of Close Packed Structures of Macroscopic Size Dielectric Spheres

A. Andueza, **R. Echeverría**, **and J. Sevilla**
Departamento Ingeniería Eléctrica y Electrónica, Universidad Pública de Navarra
Campus de Arrosadia, Pamplona 31006, Spain

Abstract— Artificial opal-like structures based on spheres and colloidal particules have been fabricated in a controlled way, presenting optical band-gap properties in the optical frequency range [1]. Transmission of opal-like structures in the direction $< 111 >$ present a first gap associated with the stacking of dielectric spheres layers, and a higher order rejection band not so directly related with the morphology of the structure.

In this communication we present the transmission spectra of an opal model built layer by layer in order to clarify the origin of higher order reject band in the three dimensional photonic crystals and how this band is related to physical behaviour of two dimensional array of spheres [2, 3]. A macroscopic model of close packed three dimensional *fcc* lattice was built using glass spheres ($\varepsilon = 7$) of 8 millimetres diameter (see Fig. 1), and was measured in the microwave region, from 10 to 30 GHz.

Figure 1.

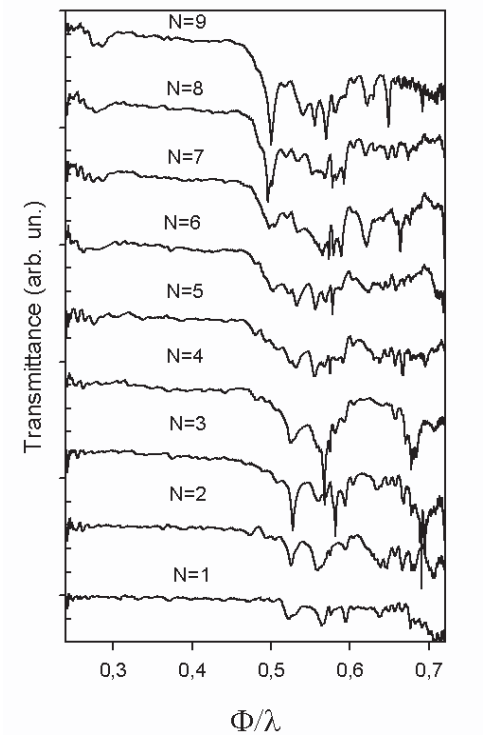

Figure 2.

Normal incidence transmission spectra for lattices with different number of layers (N) are shown in Fig. 2. The appearance of a pseudogap associated with Bragg resonance is observed as more layers are stacked up the structure. It can be slightly appreciated for $N = 5$ and clearly for $N = 9$.

Strong dips are present in low number of layers spectra, as expected from the influence of isolated sphere Mie resonances [2, 3]. The high order rejection band evolves gradually as the number of layers increases, suggesting a direct influence of Mie modes into the opal high order photonic bands. From one spectrum to the next, the main features are conserved but introducing shifts (the three red lines at the right hand side of Fig. 2 are inclined), suggesting a very complex behaviour in the generation of full bands upon the original Mie resonances.

In conclusion, we analyze the electromagnetic behaviour of close packed *fcc* opal-like macroscopic structure, reporting a high influence between a sphere resonances and the high order rejected band associated with transmission spectra of opals when in normal incidence.

REFERENCES

1. Miguez, H., et al., "Band spectroscopy of colloidal photonic crystal fims," *Appl. Phys. Lett.*, Vol. 84, No. 8, 1239–1241, 2004.
2. Andueza, A. and J. Sevilla, "Non compact single-layers of dielectric spheres electromagnetic behaviour," *Opt. Quant. Electr.*, Vol. 39, 311–320, 2007.
3. Kondo, T. and all, "Refractive index dependence of the transmission properties for a photonic crystal array of dielectric spheres," *Phys. Rev. B*, Vol. 70, 235113, 2004.

Theory of Luminescence of One-dimensional Resonant Photonic Crystals

L. I. Deych[1], **M. V. Erementchouk**[2], **A. A. Lisyansky**[1]
E. L. Ivchenko[3], **and M. M. Voronov**[3]

[1]Queens College of the City University of New York, 65-30 Kissena blvd, Flushing, NY 11367, USA
[2]Nano-Science Technology Center, University of Central Florida, Orlando, Fl 32816, USA
[3]Ioffe Physical-Technical Institute, St.-Petersburg, Russian Federation

Abstract— Phenomenological approach to description of luminescence from one-dimensional resonant photonic crystals is introduced and its connection with microscopic quantum description is discussed. Transfermatrix method of calculating emitted intensity is developed and applied to multiple-quantum-well structures.

Resonant photonic crystals (RPC) are systems in which periodically modulated dielectric constant also exhibits resonant frequency dependence. This dependence is usually associated with some internal dipole active excitations (phonons, plasmons, excitons, etc.), which are present in the media constituting the structure. While transmission and reflection spectra of such structures were studied in many papers, the effect of periodicity on their luminescence spectra has only recently become a focus of theoretical research. It should be noted that luminescence of RPCs differs significantly from an apparently similar problem of emission by various sources of radiation embedded in a regular photonic crystal. The difference is due to the fact that in the latter case the emission is affected by a predefined band structure, while in RPCs, the emission of light and emergence of the band structure occur in a selfconsistent manner. Description of luminescence can be developed along two alternative lines. One is a purely quantum approach in which both the radiation field and the material excitations are treated quantum-mechanically. While this approach yields, in principle, a complete theory of radiative properties of such structures, the technical difficulties inherent to the quantum mechanical description obscure some important physical properties, which are classical in nature, and become more transparent in classical treatment of radiation. In this paper we present a quasiclassical phenomenological theory of photoluminescence of one-dimensional resonant photonic crystals and discuss its relation to the quantum approach. Our theory is based on an assumption that initially excited electron-hole pairs first relax to the high energy dark exciton states, which come to the thermal equilibrium with the lattice before scattering to radiative states and recombining with emission of photons. We account for this process by introducing a polarization source term in the Maxwell and material equations, modeled by a random function of time and position; correlation properties of this function are related to the distribution function of the dark excitons. The emission spectrum is obtained by solving Maxwell equations with the help of the transfer matrix technique. This approach allows expressing the spectrum of luminescence in terms of reflection and transmission coefficients of the structure. In particular, we show that in the case of multiple-quantum-well (MQW) structures one can present a field emitted by a quantum well occupying mth place in a structure consisting of N wells in the following form:

$$E_m \propto \frac{t_N}{t_m}\chi(\omega)(v_1 + v_2 r_m) \tag{1}$$

where t_N is the transmission coefficient through the entire N-layer structure, r_m and t_m are the reflection and transmission coefficient for a structure consisting of only m-layers, and $\chi(\omega)$ is the 2-D excitonic susceptibility. Parameters $v_{1,2}$ characterize spatial distribution of the non-coherent polarization. Of particular interest are so called Bragg MQW structures, which are characterized by a strong radiative coupling of quantum wells. This coupling results in opening of a relatively wide photonic stop-band separating two branches of Bragg-MQW excitonpolaritons and manifesting itself as a spectral region with strongly enhanced reflection. Eq. (1) clearly demonstrates how modifications in reflection and transmission spectra manifest themselves in emission spectrum of these structures. One can see, for instance, that decrease in the transmission coefficient results in the respective decrease in the emission. Another important consequence of this expression is the resonant dependence of the emitted field on frequency via the exciton susceptibility. In Bragg multiple-quantum-well structures the exciton frequency lies in the middle of the stop-band, and is separated from the band edges, where the transmission demonstrates maxima corresponding to exciton-polariton modes. This results in significant decrease in luminescence even outside of

the stop-band. Detuning of the structure from the Bragg resonance opens a propagating band around the exciton frequency. As a result, the luminescence for slightly off-Bragg structures is concentrated in a narrow spectral window around the exciton frequency. These conclusions are in a qualitative agreement with recent experiments.

Transmission through Nonlinear Barriers and Junctions

Arthur McGurn
Department of Physics, Western Michigan University, Kalamazoo, USA

Abstract— The transmission characteristics of Kerr nonlinear barriers in a photonic crystal waveguide of linear dielectric media and junctions of Kerr nonlinear media joining multiple photonic crystal waveguides of linear dielectric media are studied theoretically. The photonic crystals and waveguides are all composed of linear dielectric materials and only the barriers or junctions are made from Kerr nonlinear media. The photonic crystal is two dimensional, formed as an array of parallel axis dielectric cylinders arrayed on a square lattice, and waveguides are formed by replacing a row of photonic crystal cylinders. In the barrier problem a finite number of neighboring sites within a waveguide are replaced with Kerr material and the transmission through the barrier of guided modes incident from infinity on the barrier is computed. The transmission maxima of the system are studied as a function of two parameters characterizing the Kerr nonlinearity of the barrier medium and are found to group into various topographical features in the two dimensional space formed by the Kerr parameters. The wave functions of the resonant excitations excited in the barrier are found to be of specific forms associated with the various topographical features of the transmission plot. The excitations within the barrier media can be classified as Fabry-Perot modes, intrinsic localized modes, and dark soliton-like modes. A similar study is made for a junction of three semi-infinite linear media waveguides at a junction of Kerr nonlinear media. A plot of the transmission maxima for a waveguide mode incident in one waveguide and transmitted into the two others can be made in the two dimensional space of parameters characterizing the Kerr nonlinear media. The wave functions of modes excited in the junction can be classified as Fabry-Perot, intrinsic localized modes, etc., similar to the barrier studies. The study presents a method for classifying nonlinear media excitations and understanding them within the context of transmission studies. The interest is from fundamental physics of nonlinear systems as well as from the necessity to understand how small nonlinear barriers and junctions will perform in various applications. Discussions are also presented form other related nonlinear models.

Impedance in Photonic Crystals

L. C. Botten[1], **F. Lawrence**[2], **K. B. Dossou**[1], **and C. M. de Sterke**[2]

[1]1CUDOS and University of Technology, Sydney, Australia
[2]CUDOS and University of Sydney, Australia

Abstract— We show how the concept of impedance can be defined rigorously in terms of Bloch modes for photonic crystal applications and then exploit this to accurately and efficiently design multilayer anti-reflection coatings for photonic crystals.

The ability to define an impedance for photonic crystals (PC) would up significant improvements in key PC applications. Many of these (e.g., superprisms, self-collimation) operate at frequencies outside of, but close to, a bandgap, where the PC's Fresnel-type surface reflection can be very high. This leads to insertion losses and stray light, both of which reduce the device's signal-to-noise ratio. In particular, the use of impedance would facilitate the practical design of anti-reflection coatings for PCs, thus helping to overcome the drawbacks associated with interface reflection.

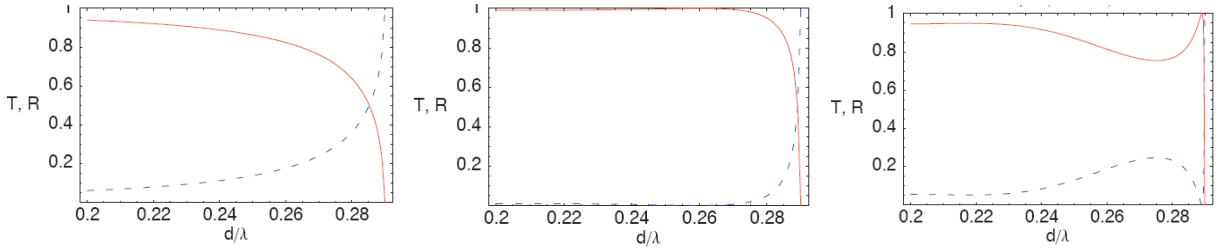

Figure 1: Transmittance (red) and reflectance (blue) curves for (a) the uncoated PC, (b) the 1,1 layer coating for the target frequency $d/\lambda = 0.26$, and (c) the 2,2 layer coating for the target frequency $d/\lambda = 0.289$.

The design of multi-layer anti-reflection coatings requires that the reflectance and relative position of the interfaces be tailored to minimize the reflection at one or more wavelengths. In thin film optics, the computations are handled efficiently as the optical properties of each layer are encapsulated in a single quantity — the impedance. Was this not the case, interface reflection coefficients would have to be recalculated *ab initio*, for a change in any layer. Accordingly, if the design of antireflection coatings for PCs is to be at all practicable, it is vital to define rigorously the concept of impedance for PC layers. To date, two approaches for defining PC impedances have emerged: the first generalizes the field ratio to E/H account for spatial variation, while the second infers an impedance from a Fresnel reflection coefficient. However, both are empirical and insufficiently rigorous to have confidence in their predictive ability. In this paper, we report on the rigorous definition of impedance based on PC Bloch modes, and demonstrate the utility and accuracy of the approach by designing two layer antireflection coatings — a computationally impractical task without an impedance implementation.

We commence with plane wave representations of the electric (E) and magnetic (H) components of Bloch modes, computed by a transfer matrix method. Since the transfer matrix is symplectic, orthogonality relationships of the form $\mathbf{E}^T\mathbf{H} = \mathbf{I}$ where $\mathbf{E}$ and $\mathbf{H}$ are matrices whose columns contain plane wave coefficients of the Bloch mode electric/magnetic fields, allow us to compute Fresnel reflection and transmission matrices between two semi-infinite PCs (PC1 and PC2) using least squares:

$$\begin{aligned}\mathbf{R}_{12} &= \left(\mathbf{A}_{12}\mathbf{A}_{12}^T + \mathbf{I}\right)^{-1}\left(\mathbf{A}_{12}\mathbf{A}_{12}^T - \mathbf{I}\right), \ \mathbf{T}_{12} = \mathbf{T}_{21}^T = 2\mathbf{A}_{12}^T\left(\mathbf{A}_{12}\mathbf{A}_{12}^T + \mathbf{I}\right)^{-1},\\ \mathbf{R}_{21} &= \left(\mathbf{I} + \mathbf{A}_{12}^T\mathbf{A}_{12}\right)^{-1}\left(\mathbf{I} - \mathbf{A}_{12}^T\mathbf{A}_{12}\right),\end{aligned}$$

in which $\mathbf{A}_{12} = \mathbf{H}_1^T\mathbf{E}_2$ is a matrix of overlap integrals. Since $\mathbf{A}_{12}\mathbf{A}_{12}^T$ and $\mathbf{A}_{12}\mathbf{A}_{12}^T$ are relative impedances for crossing an interface in the 1→2 and 2→1 directions, it is impossible to define a unique impedance. Instead, there is the more fundamental $\mathbf{A}_{12}$, akin to the "square root" of the impedance. If, we intro-duce a reference medium (PC0), e.g., free space, and ensure that the mode bases in each region have a common dimension, we can deduce the useful approximation

$\mathbf{A}_{12} \approx \mathbf{A}_{01}^{-1}\mathbf{A}_{02}$ (exact at full rank). We thus catalogue $\mathbf{A}_{0j}$ in each region, compute mixed coefficients $\mathbf{A}_{lj}$, and form the Fresnel coefficients.

We apply this technique to design a V (two layer anti-reflection) coating for a square 2D PC in TM polarization. Fig. 1(a) shows the transmittance of an uncoated PC operating, while Fig. 1(b) shows the transmission optimized for a normalized frequency $d/\lambda = 0.26$ using two single layer coatings. Fig. 1(c) tackles the more challenging problem of optimizing transmittance in the slow light region for $d/\lambda = 0.2897$ near the band gap edge using two double layer coatings. Clearly, the approach works very well and the talk outlines both the theory and its application to anti-reflection coating design.

Theory of Negative Refraction in Arrays of High Index Rods

D. Felbacq, K. Vynck, E. Centeno, and A. I. Cabuz
University of Montpellier 2, Nanophotonics group UMR-CNRS 5650, France

Abstract— Recent experiments have demonstrated negative refraction in arrays of high-refractive index dielectric rods. This theoretical work discusses the physical origin of negative permittivity and permeability in these dielectric rods-based structures. The link between the macroscopic properties and the microscopic properties is exhibited. Rigorous numerical results confirm our predictions.

The macroscopic properties of metamaterials originate from the resonances of the microscopic scatterers that they are made on. Metamaterials are very commonly made of thin metallic wires (for the negative effective permittivity) and split-ring resonators (for the negative effective permeability). However, it has recently been shown that this approach could prove to be problematic because of saturation issues in the optical range of wavelength [1]. Two recent studies by Peng et al. [2] and later by Schuller et al. [3] independently demonstrated the possibility to use dielectric cylinders with a high index to design metamaterials. These results open a way to overcome the difficulties encountered by metallic metamaterials.

We give a rigorous theoretical explanation of the origin of the negative refraction observed in [3, 4]. We show that the rods have very close magnetic and electric resonances allowing to obtain simultaneously a negative permittivity and a negative permeability. Our approach is based on a renormalization scheme that we previously applied to prove the existence of a magnetic activity in high index rods [5] as well as on rigorous numerical computations using multiple-scattering, grating theory and transfer matrix techniques.

ACKNOWLEDGMENT

This work is supported in part by the Eu-NoE project N 511616 PhOREMOST "NanoPhotonics to Realise Molecular Scale Technologies" and by the ANR project POEM PNANO 06-0030.

REFERENCES

1. Soukoulis, C. M., T. Koschny, J. F. Zhou, et al., "Magnetic response of split ring resonators at terahertz frequencies," *Phys. Status Solidi B*, Vol. 244, 1181–1187, 2007.
2. Shalaev, V. M., "Optical negative-index metamaterials," *Nature Photonics*, Vol. 1, 41, 2007.
3. Peng, L., L. Ran, H. Chen, H. Zhang, J. A. Kong, and T. M. Grzegorczyk, "Experimental observation of left-handed behavior in an array of standard dielectric resonators," *Phys. Rev. Lett.*, Vol. 98, 157403, 2007.
4. Schuller, J. A., R. Zia, T. Ter, and M. L. Brongersma, "Dielectric metamaterials based on electric and magnetic resonances of silicon carbide particles," *Phys. Rev. Lett.*, Vol. 99, 107401, 2007.
5. Felbacq, D. and G. Bouchitté, "Theory of mesoscopic magnetism in photonic crystals," *Phys. Rev. Lett.*, Vol. 94, 183902, 2005.

Sensitivity of the Resonance Characteristics of SRR and DSRR (Double-Sided SRR) Type Metamaterials to the Changes in Substrate Parameters and the Usefulness of DSRR Structure for Reduced Electrical Size

E. Ekmekci[1,2] and G. Turhan-Sayan[1]

[1]Dept. of Electrical and Electronics Engineering, Middle East Technical University, Ankara, Turkey
[2]Dept. of Electronics and Communication Engineering, Suleyman Demirel University, Isparta, Turkey

Abstract— The original SRR (Split Ring Resonator) is a well known metamaterial structure suggested for obtaining negative effective permeability over certain microwave frequency bands. While the periodical arrays of SRR unit cells are already shown to be very useful in many applications related to the design of antennas and various microwave devices, reducing the electrical sizes of such devices, i.e., miniaturization, is still an important practical concern. In this paper, it is demonstrated that the Double-Sided Split Ring Resonator (DSRR) is an alternative magnetic resonator that can provide a substantially smaller resonance frequency as compared to the original SRR for a given unit cell size. In other words, a DSRR array, which has the same physical cell size as a comparable SRR array, can simulate a negative effective permeability medium at lower frequencies due to the increase in its total distributed capacitance.

In this study, the transmission characteristics of the SRR and DSRR structures (having the same physical cell size and geometry) are simulated using the Ansoft's HFSS software for varying values of substrate parameters, which are the thickness, the real part of relative permittivity, and the dielectric loss tangent of the substrate. These investigations have shown that the resonance patterns of both SRR and DSRR are affected similarly from the changes in real permittivity and loss tangent of the substrate. However, changes in the substrate thickness affect their resonance characteristics quite differently: The resonance frequency, resonance strength (measured by the depth of the transmission minimum), and the half power bandwidth of the resonance curve noticeably decrease for the DSRR structure in response to decreasing substrate thickness. On the other hand, the resonance frequency of the SRR structure increases at a comparatively slower rate with decreasing substrate thickness, without any noticeable change in resonance bandwidth and in resonance strength.

Influence of Evanescent Waves on Beam Propagation in Photonic Crystals

D. Felbacq[1] and B. Guizal[2]

[1]University of Montpellier 2, Nanophotonics Group UMR-CNRS 5650, France
[2]Institut FEMTO-ST, University of Besançon, France

Abstract— The recent interest in the imaging possibilities of photonic crystals (superlensing, superprism, optical mirages etc.) call for a detailed analysis of beam propagation inside a finite periodic structure. Contrarily to common knowledge, it is not always true that the shift of a beam is given by the normal to the dispersion curve. This phenomenon is explained in terms of evanescent waves

It is known that in an infinite (and non-dispersive) periodic medium the group velocity is proportional to the average Poynting vector (of a Bloch mode) [1, 2]. We show that, in finite size structures, the direction of propagation is not always given by the normal to the isofrequency curves. This fact is due to two reasons. First, in finite size structures, there are evanescent waves near the boundaries which can contribute to the propagation of the beam [3]. Therefore the field inside the structure comprises not only Bloch modes but evanescent waves as well [4]. The latter can have a strong influence on the behavior of the beam. Second, due to multiple scattering, the emerging field is a sum of beams that can strongly interfere. If the beams are well separated spatially, on can clearly distinguish where the first beam emerges from the structure. If the beams overlap strongly, the resulting field can be strongly deformed, and it becomes difficult to define an "emerging point". We define a renormalized Bloch diagram taking into account the evanescent waves and allowing to retrieve the correct shift. The theoretical investigations are confirmed by rigorous numerical results obtained by using the Fourier Modal Method. We also point out the strong influence of the number of periods and of the spectral widths of the beams: these parameters can drastically modify the behavior of the beam. We show that many new effects can be expected due to the presence of evanescent waves. These are not a drawback but rather represent new possibilities to imagine new fonctionnalities.

ACKNOWLEDGMENT

This work is supported in part by the Eu-NoE project N 511616 PhOREMOST "NanoPhotonics to Realise Molecular Scale Technologies" and by the ANR project POEM PNANO 06-0030.

REFERENCES

1. Foteinopoulou, S., et al., *Phys. Rev. B*, Vol. 72, 165112, 2005.
2. Luo, et al., *Phys. Rev. B*, Vol. 65, 201104, 2002.
3. Felbacq, D. and R. Smali, *Phys. Rev. Lett.*, Vol. 92, 193902, 2004.
4. Smaâli, R., D. Felbacq, and G. Granet, *Physica E*, Vol. 18, 443, 2003.

Effect of Negative Refraction on Anderson Localisation

A. A. Asatryan[1], L. C. Botten[1], M. A. Byrne[1], V. D. Freilikher[2]
S. A. Gredeskul[3], I. V. Shadrivov[5], R. C. McPhedran[4], and Y. S. Kivshar[5]

[1]Centre for Ultrahigh-bandwidth Devices for Optical Systems (CUDOS)
Department of Mathematical Sciences, University of Technology, Sydney, NSW 2007, Australia
[2]Department of Physics, Bar-Ilan University, Ramat-Gan 52900, Israel
[3]Department of Physics, Ben Gurion University of the Negev, Beer Sheva 84105, Israel
[4]CUDOS and School of Physics, University of Sydney, NSW 2006, Australia
[5]Nonlinear Physics Centre, Australian National University, ACT 0200, Australia

Abstract— We consider localization in 1D mixed (M) stack comprising disordered right-handed (R) and left-handed (L) slabs, which alternate over its length of N (even) layers. The thickness of the jth layer is $d_j = d + \delta d_j$, while the magnetic permeability and dielectric permittivity ε_j of the layer are respectively $\mu_j = \pm 1$ and $\varepsilon_j = \pm(1 + \delta\nu_j)^2$, with the fluctuations δd_j and $\delta\nu_j$ being independent, zero-mean, random variables uniformly distributed in the intervals $[-Q_d, +Q_d]$ and $[-Q_\nu, +Q_\nu]$ respectively. The localisation length l is calculated as $l = \lim_{L\to\infty} \gamma_L^{-1}$, where $\gamma_L = -\ln T(L)/2L$, with $T(L)$ denoting the transmittance of a unit amplitude plane wave (wavelength λ) incident normally on the random sample (mean length $L = Nd$). In our modelling, we regard the structure as a stack of layers, each of which is separated by an infinitesimal gap, and compute the stack reflection ($R_n = r_n + R_{n-1}t_n^2/(1 - R_{n-1}r_n)$) and transmission ($T_n = T_{n-1}t_n/(1 - R_{n-1}r_n)$) coefficients by recursion. Here R_n and T_n denote the amplitude reflection and transmission coefficients of a stack of n layers, each of which have corresponding reflection and transmission coefficients r_j and t_j. The numerical simulations are for disorder in either refractive index $\nu = \pm\sqrt{\mu\varepsilon}$ or thickness, d the strength of which is respectively Q_ν or Q_d.

The localisation features of a sample depend strongly on the type of randomness. In contrast to H-stacks, the electromagnetic properties of M-stacks can differ strongly depending on whether the disorder is in ν, d, or in both. In the case of only thickness disorder, the localisation length diverges as all configurations are transparent, irrespective of the strength of the thickness fluctuations — a consequence of $\mu_j/\varepsilon_j = 1$. In the case when there is disorder in both ν and d, while there is no essential difference between the properties of M-stacks and those of H-stacks of either R- or L- type, the localisation length for the H stack is always shorter than that for the M stack, for a given wavelength. In the short and long wavelength limits, the localisation length is independent of the sample type. For short λ, this is because the localisation properties are determined solely by Fresnel reflection coefficients, and hence by the relative impedance which is independent on the sign of ε and μ.

The situation is quite different in the case of pure refractive index disorder. While the localisation length of M-stacks for $\lambda/d \ll 1$ is comparable to that for H-slabs, the long λ asymptotic of l_L for M-stacks differs dramatically from that of H-samples. For intermediate λ, where $l_L = 1/<\gamma_L>$ has converged, l_L is well approximated by $l_L \propto \lambda^6$, in contrast to the long-established asymptotic for disordered H-stacks, $l_L \propto \lambda^2$. The dramatic difference between the M and H cases is due to the much weaker interference for M-stacks.

The introduction of thickness disorder strengthens the interference and hence the localisation, causing the localisation length at long wavelength to transition from λ^6 dependence to the classical λ^2 dependence. While the λ^6 asymptotic is only weakly apparent for strong thickness disorder, it becomes increasingly evident with decreasing thickness disorder. The accurate characterisation of the localisation length requires only 10^5 layers in the case of strong thickness disorder, but needs 10^7 layers for the weak thickness disorder case. This contrasts with the samples with no thickness disorder, where well converged results are achieved only for comparatively short wavelengths, $\lambda/d \leq 10$, using very long stacks (10^7 layers).

Surface Electromagnetic Waves on Two-dimensional Doubly Periodic Perfectly Conducting Surfaces

Alexei A. Maradudin[1], **Tamara A. Leskova**[1], **and Ingve Simonsen**[2]

[1]Department of Physics and Astronomy, University of California
Irvine, CA 92697, USA
[2]Department of Physics, Norwegian University of Science and Technology
Trondheim, NO-7491, Norway

Abstract— It is well known that the planar surface of a semi-infinite perfect conductor does not support a surface electromagnetic wave. It supports a surface skimming bulk electromagnetic wave that is not bound to the surface. This wave is "unstable," in the sense that even a slight change of the boundary condition on the perfectly conducting surface converts it into a surface wave or into a surface shape resonance, both of which are bound to the surface.

In this paper we first derive a Rayleigh equation satisfied by the electric field in the vacuum region above a two-dimensional rough perfectly conducting surface defined by $x_3 = \zeta(\mathbf{x}_\parallel)$, where $\mathbf{x}_\parallel = (x_1, x_2, 0)$ is an arbitrary position vector in the plane $x_3 = 0$. The region $x_3 > \zeta(\mathbf{x}_\parallel)$ is vacuum, while the region $x_3 < \zeta(\mathbf{x}_\parallel)$ is the perfect conductor. This equation is specialized to the case where $\zeta(\mathbf{x}_\parallel)$ is a doubly periodic function of $\mathbf{x}_\parallel$: $\zeta(\mathbf{x}_\parallel + \mathbf{x}(\ell)) = \zeta(\mathbf{x}_\parallel)$, where $\{\mathbf{x}_\parallel(\ell)\}$ are the translation vectors of an arbitrary two-dimensional Bravais lattice. On the basis of this equation we calculate the dispersion relation of the surface electromagnetic waves propagating on such a doubly periodic surface, for two forms for $\zeta(\mathbf{x}_\parallel)$. The first is given by $\zeta(\mathbf{x}_\parallel) = \sum_\ell s(\mathbf{x}_\parallel - \mathbf{x}_\parallel(\ell))$, where $s(\mathbf{x}) = H\sqrt{R^2 - x_\parallel^2}$ for $|\mathbf{x}_\parallel| < R$ and $s(\mathbf{x}_\parallel) \equiv 0$ for $|\mathbf{x}_\parallel| > R$. The vector $\mathbf{x}_\parallel(\ell)$ in this case is $\mathbf{x}_\parallel(\ell) = \ell_1\mathbf{a}_1 + \ell_2\mathbf{a}_2$, where $\mathbf{a}_1 = a(1, 0, 0)$ and $\mathbf{a}_2 = a(0, 1, 0)$, while ℓ_1 and ℓ_2 are all the positive and negative integers and zero. The second form for $\zeta(\mathbf{x}_\parallel)$ is $\zeta(\mathbf{x}_\parallel) = \zeta_0[\cos(2\pi x_1/a) + \cos(2\pi x_2/a)]$. In the case of a weakly modulated surface defined by either surface profile function the dispersion curve consists of a single branch in the non-radiative region of the frequency and two-dimensional wave vector space. For a sufficiently strong modulation of the surface a second, higher frequency, branch of the dispersion curve enters the non-radiative region, and can give rise to an absolute bandgap between the two branches.

Session 4A5
Advances in Simulation and Design of Photonic Micro- and Nano-structures

Theoretical Analysis of Sharp Resonances and Resonance Shifts in Silicon Microspheres

Shu-Chia Shiu[1], **Cha-Hsin Chao**[1], **Shih-Che Hung**[1], **and Ching-Fuh Lin**[2]

[1]Graduate Institute of Photonics and Optoelectronics
National Taiwan University, Taipei 10617, Taiwan
[2]Graduate Institute of Photonics and Optoelectronics
Graduate Institute of Electronics Engineering and Department of Electrical Engineering
National Taiwan University, Taipei 10617, Taiwan

Abstract— The spherical cavities possess the whispering-gallery modes (WGMs) in which light will travel near the surface by total internal reflection and orbits many times before absorbed or exiting. This effect causes ultra-high quality factor (Q-factor) in the spherical cavities. The high Q-factor has been found useful in ultra-low threshold pump power of lasers, bio-sensing, and so on. In the past, the related investigation was mainly focused on the silica-based spherical resonators, which usually has to be larger than 70 μm in order to have high Q-factors. In comparison, the silicon spherical resonators are less studied. The silicon-based microspheres can be fabricated on silicon wafers using the standard ULSI processing technology, which enables the mass production of such structures and monolithic integration with electronics. However, very few theoretical studies on the silicon microspheres have been reported. In this work, we theoretically analyze the sharp resonances and resonance shifts in very small silicon microspheres.

The theoretical model developed by Mie is adapted for the analysis. First, the quality factor with absorption loss is calculated in a silicon microsphere. Even with the consideration of free-carrier absorption, the Q-factor in a silicon microsphere could be as large as 5×10^{12}. In addition, such a high Q-factor can be achieved in a silicon sphere as small as 1.64 μm in diameter for the wavelength of 1.55 μm. In comparison, the silica sphere has to be several ten micrometers in order to obtain the same high Q-factor. The resonance shift of the silicon microspheres due to the change of the exterior refractive index is also analyzed. Due to the high Q-factor, tiny change of the exterior refractive index, smaller than 10^{-11}, can produce a distinguishable resonance shift from the 1.64-um-diameter silicon sphere according to our analysis. In contrast, the silica sphere has to be as large as several ten micrometers for the same sensitivity.

In conclusion, the theoretical analyses show that the small silicon microspheres have both the ultra-high Q-factor and high sensitivity to the exterior refractive index. In addition, the silicon microspheres of small sizes are compatible with the standard ULSI processing technology, enabling the integration of Si-photonics or bio-sensing capability with the mature silicon electronics.

Spectral Response and Emission Characteristics of Isolated and Clustered Micro-resonators

K. Bhowmick[1], **T. M. Benson**[1], **Svetlana V. Boriskina**[2]
U. Kuhl[3], **and H.-J. Stöckmann**[3]

[1]George Green Institute for Electromagnetics Research
University of Nottingham, Nottingham NG7 2RD, United Kingdom
[2]Department of Electrical and Computer Engineering
Boston University, Boston, MA 02215, USA
[3]Fachbereich Physik der Philipps-Universitaet Marburg
Renthof 5, D-35032 Marburg, Germany

Abstract— Photonic structures with dimensions comparable to the operating wavelength have been studied widely of late, especially the performance of micro-resonators supporting Whispering Gallery modes (WGMs). Coupled assemblies of two or more resonators have also proved of great interest in the optical regime where they have been shown to offer further control over pertinent properties such as Q-factor, modal volume and emission or sensing properties. These coupled resonator structures have been called photonic molecules (PMs) due to the similarity between their mode structure and the electron orbital structure found in the chemical molecules that they resemble in structural geometry.

Microwave scale models of optical micro-resonators, excited at microwave frequencies, demonstrate similar resonant features to the corresponding optical structures and so provide an extremely useful experimental tool with which to explore the properties of photonic molecules [1, 2]. Dielectric materials used to fabricate the microwave models are easily available and comparatively inexpensive. Further, the dimensions being in the larger centimetre-scale, the structures can be conveniently fabricated with high precision. In this presentation we describe the results of such microwave-scale experiments to determine the resonant and directional emission properties of (i) single resonators with various geometries, including notched microdisk resonators [3], and (ii) an assortment of geometrical arrangements of similar and dissimilar (size-mismatched) micro-resonators. Comparisons are made with the predictions of numerical simulations based on an integral equation analysis.

REFERENCES

1. Pance, K., L. Viola, and S. Sridhar, "Tunneling proximity resonances: Interplay between symmetry and dissipation," *Phys. Lett. A268*, 399–405, 2000.
2. Schäfer, R., U. Kuhl, and H.-J. Stöckmann, "Directed emission from a dielectric microwave billiard with quadrupolar shape," *New J. Phys. 8*, 46, doi:10.1088/1367-2630/8/3/046, 2006.
3. Boriskina, S. V., T. M. Benson, P. Sewell, and A. I. Nosich, "Q factor and emission pattern control of the WG modes in notched microdisk resonators," *IEEE J. Select. Topics Quantum Electron.*, Vol. 12, No. 1, 52–58, 2006.

Enhanced Tunability, Switching Functionality and Polarization Splitting in Microdisk Photonic Molecules

Svetlana V. Boriskina
Department of Electrical and Computer Engineering
Boston University, Boston, MA 02215, USA

Abstract— Simple and complex optical structures composed of electromagnetically-coupled microcavity resonators (termed photonic molecules) have recently become the focus of the intense research effort worldwide. Extra design flexibility offered by photonic molecules over isolated microcavities stimulated their use in many diverse basic science and technological areas where optical microcavities have already found applications, including microlasers, optical signal processing, biosensing, cavity quantum electrodynamics, etc. [1].

Many interesting and useful features of the optical spectra of photonic molecules arise from electromagnetic coupling of high-Q optical mode fields otherwise localized in individual cavities comprising a photonic molecule. Coherent coupling of cavity modes can be manipulated by the photonic molecule design or, at the post-fabrication stage, by external impact factors, including optical, electro-optical, and thermo-optical tuning. Optimally-designed photonic molecule structures can demonstrate high sensitivity to changes in the molecule geometry [2] and/or material parameters of individual resonators [3]. This effect yields enhanced tunability of photonic molecule devices, however, calls for using highly accurate and efficient methods for their design and optimization, especially in the case when cavities support high-Q whispering-gallery modes.

To study optical characteristics of coupled-cavity structure and to explore novel photonic molecule designs, we make use of the high-speed robust algorithms based on the Muller Boundary Integral Equation formulation of scattering or eigenvalue problems for Maxwell's equations for clusters of closely-located dielectric or semiconductor microcavities. In the case of arbitrarily-shaped microcavities, the system of integral equations is discretized by using the trigonometric-trigonometric Galerkin technique accompanied by the analytical extraction of the Green's function singularity. If all the microcavities have circular cross-sections, which is often the case in many practical applications, the problem formulation reduces to the generalized Mie series equations, which can be solved numerically with any desired accuracy by truncating the matrix size.

In this talk, several optimally-tuned photonic molecule designs will be discussed that make possible (i) enhanced bandwidth tuning of symmetrical and asymmetrical photonic molecules [1, 2], (ii) selective switching of various parts of a molecule for applications as optical flip-flops, coupled-resonator optical waveguide splitters and routers, and manipulation of coupling between selectively grown quantum dots [3], and (iii) splitting of modes of two orthogonal polarizations in asymmetrical photonics molecules [4].

REFERENCES

1. Boriskina, S. V., T. M. Benson, and P. Sewell, "Photonic molecules made of matched and mismatched micro-cavities: New functionalities of microlasers and optoelectronic components," *Proc. SPIE*, Vol. 6452, 64520X, 2007.
2. Boriskina, S. V., "Theoretical prediction of a dramatic Q-factor enhancement and degeneracy removal of WG modes in symmetrical photonic molecules," *Opt. Lett.*, Vol. 31, 338–340, 2006.
3. Boriskina, S. V., "Spectral engineering of bends and branches in microdisk coupled-resonator optical waveguides," *Opt. Express*, Vol. 15, 17371–17379, 2007.
4. Boriskina, S. V., "Numerical analysis of a compact polarization splitter based on an asymmetric WG-mode microdisk photonic molecule," submitted 2007.

An Efficient Optical Waveguide Mode Solver Based on the Source-model Technique

Amit Hochman and Yehuda Leviatan
Department of Electrical Engineering, Technion-Israel Institute of Technology, Haifa 32000, Israel

Abstract— The talk will focus on a few of the key features of a Source-Model Technique waveguide mode solver. First, the existence of spurious solutions in some integral-equation formulations, and in the Source-Model Technique in particular, will be reviewed. The detrimental effect of the spurious solutions on mode determination will be explained, and this effect will be shown to be nullified by introduction of a Rayleigh-quotient based matrix singularity measure. Once the spurious solutions are eliminated, the true modes may be determined by an adaptive search algorithm. This algorithm attempts to sample the matrix singularity measure as sparsely as possible without missing any modes. One of the attractive features of the algorithm is the ability to distinguish between degenerate and nearly-degenerate modes by use of a certain quasi-orthogonality principle. This effectively limits the sampling resolution required and affords reliable and efficient mode determination.

Although the algorithm searches for modes with a real propagation constant, the search can be extended to the complex plane. For moderately lossy (or leaky) modes, an estimate for the losses is obtained from the samples on the real line, and this estimate is the starting point for a standard local optimization algorithm.

A few numerical examples that demonstrate the efficacy of the method will be shown. These include an almost circular dielectric waveguide, two unequal touching dielectric cylinders, a plasmonic waveguide, and a realistic micro-structured optical fiber.

A freely downloadable version of the solver is available. This version includes a Graphical User Interface and image processing capabilities for extracting fiber geometries from binary images.

The Interplay of Plasmonic and Channel Waveguide Dispersions in the Transmission Spectrum of a Single Metallic Nanoslit

Shih-Hui Chang and Yu-Lun Su
Institute of Electro-Optical Science and Engineering
National Cheng-Kung University, 1 University Rd., Tainan, Taiwan

Abstract— The interplay of plasmonic and channel waveguide dispersions in the transmission spectrum of a single metallic nanoslit was studied using analytical solutions and FDTD method. A profound red-shift in the transmission resonant peak was explained.

Ebbesen's work in enhanced Light transmission through metallic nanohole arrays [1] has stimulated much interest in the renaissance of surface plasmon research. A simple Fano resonance interpretation can explain such enhanced transmission phenomena [2]. Recently detailed reviews can be found in [3]. A good portion of earlier work had focus on the simplified version of studying the transmission behavior through a single nano slit mainly due to easier fabrication and possible analytical solution to the problem. The main difference from the nanohole was that, in the nano slit, the cut-off frequency limit does not exist and the surface plasmon could play a negative role. Recent experiment in W. Fan's group found that the color of the resonant transmitted light changes as the slit width changes. It brought to our attention and asked a basic question of how the slit width and thickness will affect the transmission peak and what the role of surface plasmon is in this case.

We use analytical solutions and finite-difference time-domain method to study transmission spectrum of a single nano slit in a perfect electric conductor (PEC) film and Au metallic film. A wide range of the slit thickness and width varying from 50nm to 1um was studied. A set of Fabry-Perot like resonant peaks was observed, but the peak wavelengths were red shifted even in the PEC case. A simple effective refractive index model was used to explain the shift. We also use the analytical solution [4–6] to verify these results. In real metals, the transmission resonant peaks were further red shifted due to the well-known surface plasmon dispersion relation. In the case of very nano slit width, the red shifted effect in the transmission resonant peak vanished in the PEC film, however, the transmission spectrum in the real metal case is dramatically red shifted. This phenomenon is dominated by the coupling of the surface plasmon polaritons on both side of the slit wall and thus lead to such further red shift. In the limit of wide slit opening, the result in real metal asymptotically approaches the case of PEC.

In conclusion, the transmission resonant peak of a nano slit present a red shifted Fabry-Perot like peaks in both PEC and real metallic case. In the limit of very nano slit width, the red shift becomes zero for PEC case; however the red shift is significant for the real metallic case. A modified dispersion relation of surface plasmon polaritons due to the strong coupling of surface plasmon waves on both side of the slit wall causes this anomalous red shift.

REFERENCES

1. Ebbesen, T. W., H. J. Lezec, H. F. Gaemi, T. Thio, and P. A. Wolf, *Nature*, Vol. 391, 667, 1998.
2. Chang, S.-H., S. K. Gray, and G. C. Schatz, *Optics Express*, Vol. 13, 3150, 2005.
3. de Abajo, F. J. G., *Rev. Mod. Phys*, Vol. 79, 1267, 2007.
4. Betzig, E., A. Harootunian, A. Lewis, and M. Isaacson, *App. Opt.*, Vol. 25, 1890, 1980.
5. Kukhlevsky, G. P. S. V., M. Mechler, L. Csapó, K. Janssens, and O. Samek, *Phys. Rev. B*, Vol. 70, 195428, 2004.
6. Takakura, Y., *Phys. Rev. Lett.*, Vol. 86, 5601, 2001.

Plasmonic Nanoantenna Arrays for the Visible Range

Vladimir M. Shalaev[1], **Zhengtong Liu**[1], **Reuben Bakker**[1], **Vladimir P. Drachev**[1]
Alexander V. Kildishev[1], **Alexandra Boltasseva**[2], **and Rasmus H. Pedersen**[2]

[1]Birck Nanotechnology Center, Purdue University, West Lafayette, IN 47907, USA
[2]Technical University of Denmark, DK-2800 Kgs Lyngby, Denmark

Abstract— Metalic nanoantennas have been of great interest recently due to their ability to support a very efficient, localized surface plasmon resonance and produce significantly enhanced and highly confined electromagnetic fields. The enhanced local fields have many applications, including for example biosensors, near-field scanning optical microscopy (NSOM), quantum optical information processing, and the Raman scattering. A plasmonic nanoantenna mounted on a NSOM tip can achieve sub-diffraction resolution and modify the fluorescent properties of light emitters in the vicinity of the nanoantenna. A nanoantenna embedded on the facet of a diode laser is capable of generating enhanced and spatially confined optical near fields, which can be used in optical storage and NSOM. Nanoantennae are also used in nanometer-scale optical lithography. It has been shown theoretically and experimentally that the optical nanoantennas consisting of paired nanostructured metallic elements (metal strips, nanorods, bow-tie particles, nanodiscs, spheres, and other shapes) can produce strong resonance and large field enhancement.

In this work, we use the finite element method (FEM) to accurately simulate experimentally measured far-field optical transmittance and reflectance spectra of nanoantenna arrays. First, we demonstrate that although the resonance wavelengths for the principal polarization obtained from simulations with the material properties of bulk Au match those from experiments, the shapes of the spectra can be very different, and that adjusting the geometry of the FEM model can not reduce the discrepancies any further. Possible reasons for this mismatch are the size effect and the surface roughness, which could affect the dielectric function of plasmonic elements and their coupling [1–4]. Since both effects may result in a broadening of the absorption band, their combined end result can be approximated by modifying the Au dielectric function [5]. Then, we show that with modified gold properties taken into account, excellent matching can be achieved between experimental and simulated data. The enhanced FEM model is also used to study the resonance-geometry relationship and the optical near-field distribution. The near-field maps obtained by FEM modeling are compared with NSOM measurements elsewhere [6].

REFERENCES

1. Link, S. and M. A. El-Sayed, "Spectral properties and relaxation dynamics of surface plasmon electronic oscillations in gold and silver nanodots and nanorods," *J. Phys. Chem. B*, Vol. 103, 8410–8426, 1999.
2. Zhang, S., W. Fan, N. C. Panoiu, K. J. Malloy, R. M. Osgood, and S. R. J. Brueck, "Experimental demonstration of near-infrared negative-index metamaterials," *Phys. Rev. Lett.*, Vol. 95, 137404, 2005.
3. Dolling, G., M. Wegener, C. M. Soukoulis, and S. Linden, "Negative-index metamaterial at 780 nm wavelength," *Opt. Lett.*, Vol. 32, 53–55, 2007.
4. Yuan, H.-K., U. K. Chettiar, W. Cai, A. V. Kildishev, A. Boltasseva, V. P. Drachev, and V. M. Shalaev, "A negative permeability material at red light," *Opt. Express*, Vol. 15, 1076–1083, 2007.
5. Drachev, V. P., U. K. Chettiar, H. Yuan, W. Cai, A. V. Kildishev, and V. M. Shalaev, "Size effects in plasmonic metamaterials for the visible range," *SPIE Optics Photonics*, 6642–32, San Diego, California, USA, 2007.
6. Bakker, R. M., A. Boltasseva, Z. Liu, R. H. Pedersen, S. Gresillon, A. V. Kildishev, V. P. Drachev, and V. M. Shalaev, "Near-field excitation of nanoantenna resonance," *Opt. Express*, Vol. 15, 13682–13688, 2007.

Coupling between Fundamental Whispering Gallery Modes in Chains of Microspheres

L. I. Deych[1], **C. Schmidt**[2], **A. Chipouline**[2], **T. Pertsch**[2], **and A. Tünnermann**[3]

[1]Physics Department, Queens College of CUNY, Flushing, NY 11366, USA
[2]Institute of Applied Physics, Friedrich Schiller University Jena, Germany
[3]Fraunhofer Institute for Applied Optics and Precision Engineering, Jena, Germany

Abstract— Propagation of a fundamental WGM in a chain of microspheres is studied. We found that modes with various orbital and azimuthal numbers are excited in this process resulting in significant distortion of the field distribution.

The aim of this contribution is to study theoretically optical coupling between so called fundamental whispering galleries modes (WGM) excited in spherical microresonators. These modes have their azimuthal number m equal to orbital number l, and are characterized by the smallest mode volume with their electric field concentrated most tightly in the equatorial plane. For this reason these modes and their coupling in the chain of microspheres are of primary interest for applications. In many works dealing with propagation of optical signals in such systems it is assumed that such propagation can be described in terms of coupling between such fundamentals modes of individual spheres, see, for instance [1]. In this work we demonstrate that such approach is too naïve and does not account properly for the inter-mode mixing which plays an important role in propagation of optical signals in such structures. This mixing was shown to affect significantly properties of normal modes of the system of coupled spheres [2, 3], one, however, should recognize that the problem of propagation of the single-sphere fundamental mode is different from the problem of finding normal modes in the system of coupled spheres.

Indeed, in the simplest case of two or more coupled spheres aligned along a straight line collective modes of the chain are defined in the coordinate system with polar axes directed along this line [2, 3]. The fundamental ($m = l$) mode in this coordinate system is the one, which is perpendicular to the axis of the chain, and has no significant coupling with respective modes in other spheres. The modes, which couple most strongly, are the ones with $m = 1$, but these are not the modes whose propagation is of primary interest for our and other studies. Field distribution of modes with $m = 1$ is characterized by strong oscillations in the equatorial plane; therefore these modes have a poor mode volume factor and are not as useful for applications as fundamental modes. One should realize that the configuration, in which fundamental modes in two or more spheres couple between themselves, is not possible because such field distribution does not correspond to any normal modes of the system of coupled spheres.

The spatial distribution of the field reproducing that of the fundamental mode but being concentrated in the polar plane of the chain can only be obtained as a superposition of normal modes with different azimuthal numbers. In order to find such a superposition one can use transformation properties of vector spherical harmonics upon rotations of the coordinate system. It can be shown that the distribution of the field similar to that of the fundamental mode but concentrated in the polar rather than equatorial plane can be constructed as follows

$$\mathbf{E}_l(r,\,\theta,\,\varphi) = \frac{(-i)^l}{2^l} \sum_{m=-l}^{l} \sqrt{\frac{(2l)!}{(l+m)!(l-m)!}} \mathbf{M}_{lm}(r,\,\theta,\,\varphi) \tag{1}$$

where $\mathbf{M}_{lm}(r,\,\theta,\,\varphi)$ is a vector spherical harmonics of one of the polarizations. In this work we assume that such superposition is created in one of the spheres of the chain. Subsequently we study its spatial evolution along the chain under steady-state conditions. Using tight-binding equations for the chain of spheres derived in Ref. [3], we find the extent of distortion of the original superposition caused by coupling between modes with different angular numbers in adjacent spheres and its effect on radiative decay of the initial excitation. There are several effects that has to be taken into account for proper analysis of the resulting field distribution. First of all, as it was shown in [2, 3] coupling between modes with different orbital numbers may significantly modify optical response of the system. In the situation considered here, we have to take into account that coupling between modes strongly depends on the azimuthal number m. It is clear, therefore, that contributions of different components of the linear superposition (1) into the resulting field will be modified by the inter-sphere coupling resulting in distortion of the original field distribution. We analyze limitations on applications of chains of spheres for waveguides and other photonic devices caused by the discussed effects.

REFERENCES

1. Naweed, A., G. Farca, S. I. Shopova, and A. T. Rosenberger, *Phys. Rev. A*, Vol. 71, 043804, 2005.
2. Miyazaki, H. and J. Jimba, *Phys. Rev. B*, Vol. 62, 7976–7997, 2000.
3. Deych, L. I. and A. Roslyak, *Phys. Rev. E*, Vol. 73, 036606, 2006.

Optical Negative Index Materials: The Plasmonic Approach

Gennady Shvets[1], **Y. Urzhumov**[1], **M. Davanco**[2], **S. Forrest**[2], **and V. Lomakin**[3]

[1]The University of Texas at Austin, USA
[2]University of Michigan at Ann Arbor, USA
[3]UCSD, USA

Abstract— Negative Index Metamaterials (NIMs) hold the promise for developing novel optical devices such as "perfect" lenses, sub-wavelength waveguides and resonators. Despite the impressive progress in microwave NIMs, extending those to the optical part of the spectrum has proven to be challenging. As will be shown in this talk, relying on the same basic building blocks (split ring resonators and wires) for building optical NIMs is impossible for two reasons: (i) fabrication difficulties, and (ii) plasmonic properties of metals at the optical frequencies. Using a split-ring resonators (SRR) as an example, we demonstrate that, for a given SRR geometry, there is a minimum wavelength $\lambda_{\min}$ at which magnetic response of a plasmonic SRR can be achieved. The more complicated is the SRR design (small gaps, thin wire thickness, etc.), the larger is the $\lambda_{\min}$. Several theoretical techniques for obtaining $\lambda_{\min}$, such as the electrostatic Generalized Eigenvalue Differential Equation (GEDE) and the surface integral eigenvalue equations, will be introduced. Therefore, plasmonics prevents miniaturization of the standard unit cell building blocks used in microwave design.

Fortunately, plasmonics enables optical magnetic activity when alternative design paradigms are used. Several such designs will be explored: (a) Plasmonic Wire Array (PWA) [1], Strip Pair Array [2], Strip Pair One Film (SPOF) array [3], and a few others. The main feature of all these designs is that their unit cells are strongly sub-wavelength in all dimensions, thereby satisfying the most basic requirement for metamaterials (as opposed to photonic crystals whose unit cell is of order $\lambda/2n_d$, where n_d is the refractive index of the imbedding dielectric). Several techniques for analyzing the electromagnetic behavior of such structures will be reviewed: direct electromagnetic simulations, band structure calculations [4], quasi-static simulations [1, 2]. The influence of the structure periodicity and band-folding effects on the effective parameters of the structure will be examined. Experimental results demonstrating an optical NIM with a $\lambda/7$ will be presented

REFERENCES

1. Shvets, G. and Y. Urzhumov, *Phys. Rev. Lett.*, Vol. 93, 243902, 2004.
2. Shvets, G. and Y. Urzhumov, *J. Opt. A: Applied and Pure Optics*, Vol. 8, S122, 2006.
3. Lomakin, V., Y. Fainman, Y. Urzhumov, and G. Shvets, *Opt. Exp.*, Vol. 14, 11164, 2006.
4. Davanco, M., Y. Urzhumov, and G. Shvets, *Opt. Exp.*, Vol. 15, 9681, 2007.

Thermal Radiation in Microstructured Photonic Reservoirs

Marian Florescu
Department of Physics, Princeton University, Princeton, NJ 08544, USA

Abstract— The ability of microstructured photonic systems to significantly alter thermal radiation processes has recently received considerable attention [1–3] as it holds a tremendous potential for applications that range from thermophotovoltaic energy conversion devices [1, 4] to tunable infrared emitters [5].

We analyze the origin of thermal radiation enhancement and suppression inside photonic crystals and demonstrate that the central quantity that determines the thermal radiation characteristics such as intensity and emissive power is the area of the iso-frequency surfaces and not the density of states as is generally assumed [1, 2, 6–8]. We show that for frequencies near photonic band-edges and other van Hove singularities, the thermal radiation flux exhibit profound departures from the conventional model of a blackbody in free space.

Our analysis shows that the directional behavior of the thermal radiation intensity is governed by the topology of the dispersion surface and can be expressed in terms of its gradient and curvature At long wavelengths, the departure of the iso-frequency contour from that of a homogeneous medium is minimal, and the directional spectral emissive power exhibits a Lambertian dependence. As the frequency increases, the thermal radiation becomes more and more anisotropic and the directional thermal radiation flux may become divergent along certain directions. In a manner similar to the phonon focusing in ordinary crystals [9], this behavior gives rise to "photonic caustics" and underscores that the spectral and angular redistribution of the photonic states play equally important roles in determining the thermal radiation flux.

We also discuss the fundamental physical mechanisms determining the thermal radiation emitted by microstructured photonic systems and use these insights to outline design principles that alow the maximization of the the radiation flux. We show that the increased isotropy of the effective Brillouin zone characterizing quasiperiodic photonic lattices make these systems ideal candidates for optimal design structures.

REFERENCES

1. Fleming, J. G., et al., *Nature*, Vol. 417, 52, 2002.
2. Luo, C., et al., *Phys. Rev. Lett.*, Vol. 93, 213905, 2004.
3. Florescu, M., K. Busch, and J. Dowling, *Phys. Rev. B*, Vol. 75, 201101 (R), 2007.
4. Florescu, M., et al., *Solar Energy Materials and Solar Cells*, Vol. 91, 1599, 2007.
5. Pralle, M. U., et al., *Appl. Phys. Lett.*, Vol. 81, 4685, 2002.
6. Cornelius, C. M. and J. P. Dowling, *Phys. Rev. A*, Vol. 59, 4736, 1998.
7. Florescu, M., et al., *Phys. Rev. A*, Vol. 72, 033821, 2005.
8. Kee, C. S., et al., *Phys. Rev. B*, Vol. 60, 10573, 1999.
9. Wolfe, J. P., *Imaging Phonons: Acoustic Wave Propagation in Solids*, Cambridge University Press, Cambridge, England, 1998.

Fullwave Simulation of the Interaction between a Molecule and a Photonic Antenna

R. E. Diaz and D. Lim

Department of Electrical Engineering, Ira A. Fulton School of Engineering
Arizona State University, P. O. Box 875706, Tempe, AZ 85287-5706, USA

Abstract— Plasmonic or Photonic Antennas are nanostructures constructed from noble metals that interact very strongly with a photon field at their "Plasmon" resonance frequency. Thousand-fold increase in radiation efficiency has been reported for molecules in the vicinity of such structures. The accepted explanation of this behavior is that it results from a combination of two phenomena: (i) the physical and resonant concentration of electromagnetic energy in the near field of the antennas and (ii) an increase of the radiative transition rate of the molecules induced by the structure. Fullwave electromagnetic simulations of the first phenomenon are found in the literature under many names including, for instance, the study of "anomalous" transmission of electromagnetic energy through sub-wavelength apertures. The second phenomenon has received little attention. Also missing from this literature are true antenna-like structures. Most of the antennas investigated are simply exhibiting the "quasi-static" Surface Plasmon Resonance (SPR) modified by the geometry of the noble metal structure. If the microwave definition of an antenna is to be used, it would be expected that the structure exhibit resonances due its physical size, that is, due to the constructive interference of electromagnetic waves traveling on its surface. Using a semi-classical model of a molecule embedded in a Finite Difference Time Domain computational space it is shown that the Radiative Rate increase, attributed in the physical literature to a modification of the photonic mode density in the presence of the nanostructure, is equivalent to a modification of the molecule's radiation resistance as a result of its coupling to a nearby resonantly tuned antenna. In the time domain this rate increase can be directly measured as a change in the characteristic time required for the molecule to emit its stored energy. Antennas considered include e-beam lithographed microscopic folded dipoles and antennas composed of noble metal nanospheres amenable to DNA self-assembly. The latter exhibits an antenna mode resonance clearly different from SPR. The radiative rate modification, including both increase and decrease (quenching), is demonstrated in the presence of realistic Drde metal antennas and an idealized Perfect Electric Conductor antenna.

Enhanced Light Scattering by a Dipole Placed in a Narrow Gap between Two Metallic Nanobodies

P. I. Geshev
Institute of Thermophysics, Lavrentyev Ave. 1, Novosibirsk 630090, Russia

Abstract— Strongly enhanced EM fields are found in very narrow gaps between two metallic nanoparticles (NPs) or between STM (AFM) tips and metallic nanofilms. These domains are called often as "hot spots". Molecules adsorbed in the hot spots radiate hugely enhanced Raman signals, which is proportional to the fourth power of electric field in the gap. We consider on the basis of Maxwell equations a light scattering of an axially symmetrical systems composed of two metallic nanobodies and dipole in the narrow slit between them. The field enhancement factor (*FEF*), the dipole energy flux (*DEF*) and the Raman enhancement factor ($REF = FEF^2 DEF$), are calculated by the Green function method [1, 2].

In Fig. 1 the dependence of *FEF* vs. g (the gap distance) is demonstrated for the Ag/Ag dimer composed of two equal spheres of diameters 50 (or 100) nm at wavelength 470 (or 600) nm, respectively. At these wavelengths the first dipole-like plasmon resonances in the scattering systems are excited. One can see that in *log-log* coordinates the curves slopes are close to the value $-4/3$. For these values of *FEF* the maximal *REFs* can reach 10^{10}–10^{12} in the visible light region for gaps ~ 1 nm. Calculated values *DEF* are very close to FEF^2 (not shown). It is connected with the "reciprocity theorem" in optics.

Illumination of the second scattering system shown in the upper inset in Fig. 2 by radially polarized Bessel light beam under conditions of attenuated total reflection (ATR) causes a field enhancement A in the vicinity of the film surface (lower inset in Fig. 2). The metallic NP closely placed at the film surface acts as nanoantenna. Plasmons excited in the particle and film convert the incident propagating EM field into non-propagating evanescent near-field. For small gaps the field is strongly enhanced and confined in the particle/film gap [3].

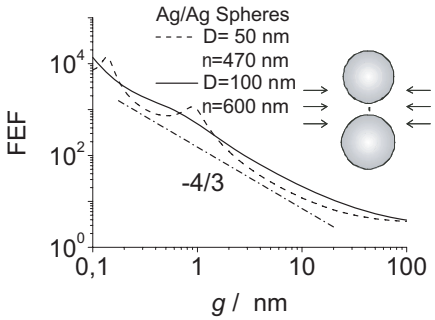

Figure 1: Field enhancement factors.

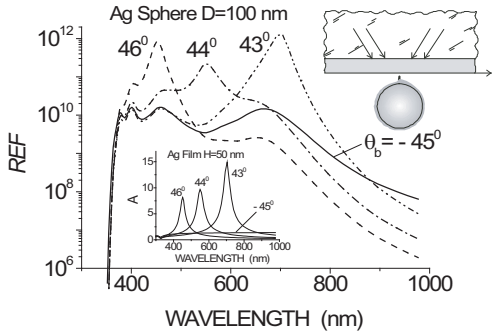

Figure 2: Raman radiation enhancement factor (*REF*) for Ag sphere (100 nm) placed near Ag film (50 nm) with gap $g = 1$ nm.

From our calculations follows that SM-TERS (single molecule tip enhanced Raman scattering) must have the same level of Raman enhancement factor that was found in 1997 in the known SM-SERS experiments, $REF \sim 10^{14}$ (Kneipp et al, and Nie, Emory), provided that the Raman dipole and the electric field at the dipole position are oriented along the symmetry axis and that the NP/film gap is small, $g \sim 1 - -2$ nm.

REFERENCES

1. Geshev, P. I., et al., *Phys. Rev. B*, Vol. 70, 075402, 2004.
2. Geshev, P. I. and K. Dickmann, *J. Opt. A: Pure Appl. Opt.*, Vol. 8, 161, 2006.
3. Geshev, P. I., U. Fischer, and H. Fuchs, *Optics Express*, Vol. 15, 13796, 2007.

Modal Analysis of Straight and Bent Photonic Crystal Fibers Using the Boundary Integral Method for Light Transmission, Sensing and Plasmonic Applications

Elio Pone and Maksim Skorobogatiy

Ecole Polytechnique de Montreal, Canada

Abstract— We develop an accurate and efficient boundary integral method for calculating leaky and guided modes of straight and bent photonic microstructured optical fibers. The method is rapidly converging and can handle a large number of inclusions. Both, solid and hollow core photonic crystal fibers can be treated efficiently. The key advantages of the proposed method are the following; for circular inclusions in a straight fiber, similarly to the multipole method, much of the calculations are done analytically resulting in a highly accurate and rapidly convergent implementation. Additionally, the method can treat inclusions of arbitrary shapes defined by a parametrical curve. The method is able to treat accurately systems that contain a large numbers of inclusions, due to a well behaved nature of matrix elements used in the formulation. Particularly, the method is able to treat efficiently very closely spaced inclusions, which is of particular interest in the case of hollow core air-guiding fibers. Multilayer (coated) inclusions can be easily accommodated. We have established that when spacing between inclusions decreases no convergence problems arise; only the computational cost of some of the matrix elements increases. Finally, symmetries of the fiber geometry can be readily taken into account by the numerical algorithm to speed up modal calculations. We demonstrate versatility of the method by applying it to several challenging problems.

Session 4A7
Electromagnetics in High Field MRI 1

RF Tissue Heating Due to Metallic Implants during MRI

C-K. Chou
Corporate EME Research Laboratory, Motorola Labs, Fort Lauderdale, Florida, USA

Abstract— Exposure to a strong static magnetic field and a pulsed RF field during MRI, five potential adverse effects are anticipated with metallic implants in patients: 1) force on the implant by the strong static magnetic field, 2) current induced in the implants by the RF field, 3) damage of implant electronic circuitry by RF exposure, 4) MRI image distortion caused by the implant, 5) implant and adjacent tissue heating due to absorption of RF energy. Only the last of these, RF tissue heating, will be addressed in this presentation. For safety, the present Food and Drug Administration (FDA) and International Electrotechnical Commission (IEC) recommended limits of RF heating during MRI scanning are 1°C in the brain, 2°C in the torso and 3°C in the extremities [1, 2].

While at the City of Hope National Medical Center in Duarte, California, the author worked on three projects evaluating the safety of three medical implants during MRI. In these studies, temperature rises adjacent to the implants during MRI exposures were measured. Because blood flow was not simulated in the static phantom, the temperature rise in the phantom around the implants would be a worst case scenario. Since RF energy absorption is a function of body size, the implant heating can only be tested in a full-size phantom human model. FDA does not approve tests in small and simple geometry phantoms. Although the RF field is strongest inside the MRI scanner, there is no guaranty that body parts outside the scanner do not affect the energy absorption in the exposed region. Therefore, a whole body model is necessary. Three types of implants, auditory implants, spinal fusion stimulators, and cervical fixation devices were tested on a full size human model. In these studies, temperature rises adjacent to the implants during a 1.5 T MRI exposures were measured with fiberoptic temperature sensors. No heating was found in auditory implants but under certain circumstances, the spinal fusion stimulator can induce unacceptable heating. Severe heating at the head pins of cervical fixation devices was observed under certain conditions. The heating at the metal pins of the cervical fixation devices was caused by the RF induced current in the conductive halos and tongs which flow into tissue through the pins. All observed phenomena are consistent with the RF current flow depending on the resistance of the RF circuit. To solve the RF current flow problem, the insulated titanium/ceramic pins provided insulation to cut off RF current flow, therefore, eliminated heating, regardless of model, halo, or tong. These studies show that RF tissue heating is difficult to predict. A case by case evaluation is necessary.

REFERENCES

1. Food and Drug Administration, "Magnetic resonance diagnostic device: Panel recommendation and report on petitions for MR reclassification," *Federal Register*, Vol. 53, 7575, Mar. 1988.
2. IEC Standard 60601-2-33, "Medical electrical equipment — Part 2-33: Particular requirements for the safety of magnetic resonance equipment for medical diagnosis," *International Electrotechnical Commission*, 28, Geneva, Switzerland, May 2002.

Resistive Tapered Stripline for Deep Brain Stimulation (DBS) Leads at 7 T MRI: Specific Absorption Rate Analysis with High-resolution Head Model

L. M. Angelone[1,2], E. Eskandaar[1], and G. Bonmassar[1]

[1]Massachusetts General Hospital, Harvard Medical School, USA
[2]Biomedical Engineering Department, Tufts University, USA

Abstract—

Introduction: Deep brain stimulation (DBS) is a surgical procedure currently used on over 30,000 patients in US to treat symptoms linked to Parkinson's disease. Patients with intracranial implants may receive numerous clinical benefits from MRI and functional MRI recording [1]. However, potential risks are present due to antenna effect of conductive leads within the radio frequency (RF) field used to elicit the MRI signal [2]. Two cases of serious neurological injury due to RF-induced heating during MRI recording on patients with DBS implants were recently reported [3, 4]. RF-heating is currently evaluated by the international community in terms of specific absorption rate (SAR) [5], namely RF-power absorbed for unit of mass. SAR changes depend on RF source, geometrical and electrical properties of the head, as well as geometrical and physical properties of the implanted leads. A high-resolution numerical model was here used to explore the specific effect on SAR on one of these variables, namely a resistivetapered stripline configuration of lead resistivity [6].

Methods: Numerical simulations based on the FDTD algorithm [7] were performed on an anatomically fine-grained head model [8] with electrical properties selected as in literature [9]. Simulations were conducted using a 16-wires RF source at a frequency of 300 MHz (7 T MRI). Following the standard setup for DBS implant [4], the implant was modeled as an insulated lead (2 mm insulation diameter, $\sigma = 0\,\mathrm{S/m}$, $\varepsilon_r = 1$) extending from the base of the neck (Fig. 1—A) along the subcutaneous fat and anchored to the outer table (Fig. 1—B) with a final section inserted from the outer table (B) into the sub-thalamic nucleus (Fig. 1—C). The total length of the external lead (Fig. 1, points A to B) was 520 mm; the length of section implanted in the brain parenchyma (Fig. 1, points B to C) was 83 mm. Three different lead configurations were tested: a) purely copper-based lead ($\rho_{\mathrm{lead}} = 1.67 \cdot 10^{-8}(\rho_{\mathrm{copper}})$), b) copper leads with mediumresistive section (from B to C, $\rho_{\mathrm{lead}} = 0.0011\,\Omega\mathrm{m}$, $\varepsilon_r = 1$) implanted in the brain; c) copper leads with highly resistive brain-implanted section (from B to C, $\rho_{\mathrm{lead}} = 1\,\Omega\mathrm{m}$, $\varepsilon_r = 1$). Whole-head and 10 g averaged SAR [5] were computed using the XFDTD software (REMCOM Co., USA).

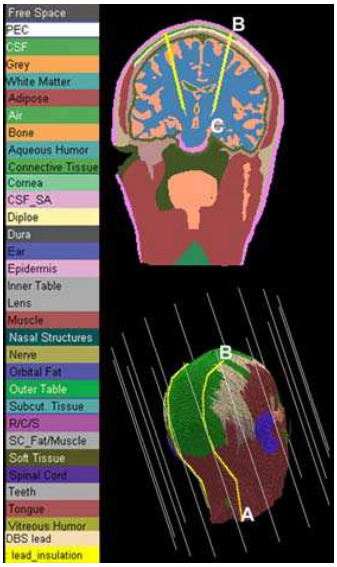

Figure 1.

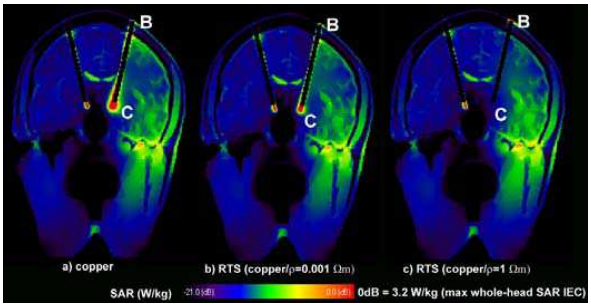

Figure 2.

Results: Whole-head SAR was the same for all configurations (see Table 1, with values normalized to 3.2 W/kg, as for IEC guidelines [5]). The 10 g-averaged SAR evaluated in the point of contact between lead and sub-thalamic nucleus (C) (Fig. 2) was reduced by a factor of 2.4 with configuration b) and 6.7 with configuration c).

Table 1.

	case_a copper	**case_b)**	**case c)**
10 g avg. SAR at tip (C)	19.2	7.0	3.0
Whole-head SAR	3.2	3.2	3.2

Discussion and Conclusions: Theoretical [10], numerical [11], and experimental studies [12], suggest the use of increased lead impedance to reduce electric field enhancement and related potential RF-heating of intracranial implants. On the other hand, increased lead impedance may induce excessive power dissipation at the operational frequencies of the DBS system, reducing the life-time of the DBS system battery [11]. In the configuration showed in this study, the RTS-based approach allowed for a reduced discontinuity profile at the contact (Fig. 1, point C) between lead and subthalamic nucleus, hence reducing potential effect on SAR enhancement in the tissue (see Appendix C [13]). Moreover, the increase in impedance and related power losses were limited to the section implanted in the brain. Considering a lead of 613 m of length and 2 mm^2 cross-section, the overall resistance would be 3.5 Ω for the purely copper-based (case a), 49 kΩ for case b) and 49 MΩ for case c). The flexibility of the RTS design could allow reducing the low-frequency impedance with similar SAR performance [6]. Computational modeling may help to obtain a systematic evaluation of SAR distribution and design optimal RTS leads.

ACKNOWLEDGMENT

Thank to Nikos Makris and the Center for Morphometric Analysis — MGH for the head model segmentation. Work supported by NIH R01 EB002459, P41 RR014075, and the MIND institute.

REFERENCES

1. Arantes, P. R., et al., *Mov. Disord*, Vol. 21, 8, 1154–62, 2006.
2. Rezai, A. R., et al., *Neurosurgery*, Vol. 57, 5, 1056–62, 2005.
3. Spiegel, J., et al., *J. Neurosurg*, Vol. 99, 4, 772–4, 2003.
4. Henderson, J. M., et al., *Neurosurgery*, Vol. 57, 5, E1063, 2005.
5. IEC 601-2-33, 29–31, Geneva.
6. Bonmassar, G., *IEEE Trans on MTT*, Vol. 52, 8, 1992–1998, 2004.
7. Kunz, K. S. and R. J. Luebbers, CRC Press, Boca Raton, 448, 1993.
8. Angelone, L. M., et al., *Proc. ISMRM*, 2005.
9. Gabriel, C., et al., *Phys. Med. Biol.*, Vol. 41, 2231–2249, 1996.
10. Balanis, C. A., John Wiley, 2005.
11. Angelone, L. and G. Bonmassar, *ISMRM-ESMRMB*, 2007.
12. Baker, K. B., et al., *Neurosurgery*, Vol. 57, 4, 392–7, 2005.
13. NCRP, Bethesda, MD, 1981.

Ultimate SAR and Ideal Current Patterns in Parallel Transmission

Riccardo Lattanzi[1, 2], **Aaron K. Grant**[2, 3], **Yudong Zhu**[4], **and Daniel K. Sodickson**[5]

[1]Harvard-MIT Division of Health Sciences and Technology, Cambridge, MA, USA
[2]Department of Radiology, Beth Israel Deaconess Medical Center, Boston, MA, USA
[3]Harvard Medical School, Boston, MA, USA
[4]GE Global Research, Niskayuna, NY, USA
[5]Center for Biomedical Imaging, New York University Medical Center, New York, NY, USA

Abstract—

Introduction: Shortening of the wavelength at high magnetic field strength causes critical interactions between the radiofrequency (RF) transmit fields and the biological tissues, which may result in inhomogeneities of the excitation and local amplifications of the specific absorption rate (SAR). In recent years, parallel transmission techniques have been used to achieve better SAR management and correction of B1 inhomogeneities [1, 2]. There are fundamental constraints on the capabilities of these methods, which have been reported at a recent conference [3]. In this work we calculate ultimate intrinsic SAR using a dielectric sphere as sample and we study the corresponding ideal current patterns on the surface of the object.

Theory and Methods: In the case of an EPI-based trajectory in excitation k-space, the RF power dissipated in the patient over an excitation (ξ) can be related, using Parseval's theorem, to the periodic patterns $\mathbf{f}_n$ that define the excitation profile at each spatial position n [2]: $\xi = 1/P \sum_1^P 1/2 \int_V \sigma(\mathbf{r}) \left|E(\mathbf{r}, p\Delta t)\right|^2 d\mathbf{r} = 1/P \sum_1^P (\mathbf{I}_p^H \mathbf{\Phi} \mathbf{I}_p) \cong 1/N \sum_1^N (\mathbf{f}_n^H \mathbf{\Phi} \mathbf{f}_n)$. In this equation, P is the total number of samples of the current waveforms $\mathbf{I}_p$, σ is the tissue conductivity, E is a linear combination of the electric fields $e_i(\mathbf{r}, t)$ generated by the elements of the transmit array, Φ is a positive definite covariance matrix given by $\Phi_{i,j} = \int_V \sigma(\mathbf{r}) e_j^*(\mathbf{r}, t) \cdot e_i(\mathbf{r}, t) d\mathbf{r}$ and N is the number of voxels. In parallel transmission, the individual coil's current patterns are adjusted at each time point and, among the possible $\mathbf{f}_n$, it is possible to find those that minimize ξ [4]: $\tilde{\mathbf{f}}_n = \mathbf{\Phi}^{-1}\mathbf{C}_n^H(\mathbf{C}_n\mathbf{\Phi}^{-1}\mathbf{C}_n^H)^{-1}\mu_n$, where μ_n is the target profile and $\mathbf{C}_n$ contains the spatial weighting induced by the B_{1+} fields of each coil. In order to calculate ultimate intrinsic SAR, a complete basis set of spherical surface current densities was defined and employed as a hypothetical transmit array. The electromagnetic field of the individual modes was derived with the dyadic Green's function method [5] and used to calculate Φ and the B_{1+} values in $\mathbf{C}_n$. Ideal current patterns on the surface of the sphere were found by weighting the current basis functions with the optimal $\tilde{\mathbf{f}}_n$.

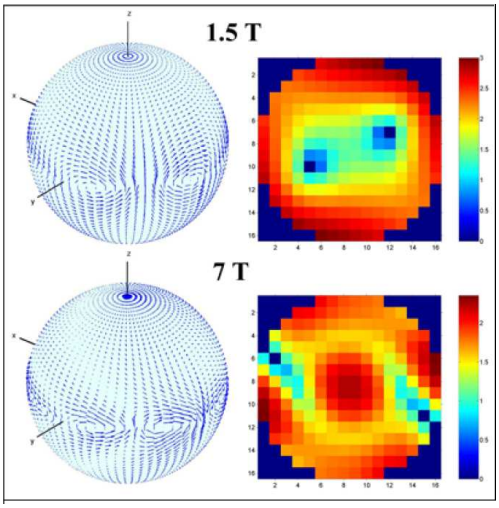

Figure 1: Ideal surface current patterns (left column) resulting in the excitation of a fully homogeneous profile and corresponding normalized distribution (Log scale) of RF power deposition within the FOV. Plots represent temporal snapshots at the center of excitation k-space.

Results and Discussion: Figure 1 shows a temporal snapshot of the ideal net current patterns (obtained summing the optimally-weighted basis currents) and the corresponding RF power deposition, in the case of unaccelerated parallel excitation of a fully homogeneous profile along a plane through the center of the sphere. In order to appreciate the changes in spatial behavior at 1.5 T and at 7 T magnetic field strength, the images are scaled differently. The electrodynamics associated with RF transmission is increasingly complex at higher field strength and knowledge of the ideal current patterns can be used as an important guide for future high-field coil designs.

REFERENCES

1. Katscher, U., et al., *MRM*, Vol. 49, 144–150, 2003.
2. Zhu, Y., *MRM*, Vol. 51, 775–784, 2004.
3. Lattanzi, R., et al., *MRM*, 675, 2007.
4. Zhu, Y., *ISMRM*, 599, 2006.
5. Tai, C. T., *Dyadic Green Functions in Electromagnetic Theory*, 1994.

Correlation between Locally Averaged SAR and Temperature Rise Distributions in a Human Body Exposed to RF Fields

G. Bit-Babik[1], **A. Faraone**[1], **C.-K. Chou**[1], **A. Razmadze**[2], **and R. Zaridze**[2]

[1]Corporate EME Research Laboratory, Motorola Labs, Fort Lauderdale, Florida, USA
[2]Tbilisi State University, Tbilisi, Georgia

Abstract— This paper describes the relationship between the locally averaged specific absorption rate (SAR) computed for different averaging tissue masses and the steady state temperature rise within the human body exposed to RF fields. This work is based on Finite Difference Time Domain (FDTD) simulations of the human body model exposed to plane wave fields in 48 different exposure conditions in the frequency range from 30–1000 MHz. The numerical model used for RF exposure simulations is based on the Visible Human Project data sets [1] which was further segmented by researchers at the Air Force Research Laboratory, Brooks AFB, TX to produce the voxelized model and to indicate the tissue type in each voxel. The model features 39 different tissues with frequency dependent electrical properties defined according to the Cole-Cole dispersion model [2, 3], while the thermal properties including metabolic heat production rates and blood perfusion parameters for each tissue were compiled from different sources [4–7].

In addition to point SAR, eight different SAR quantities were computed based on the IEEE cubic shaped averaging volume containing 0.1–200 g of tissue mass. This work was done to determine the averaging tissue mass that produces the SAR quantity most appropriate to predict and describe the related temperature rise in tissue. The method is based on evaluating the global correlation between the distributions of the described SAR quantities and the corresponding steady state temperature rise in the whole human body and then selecting the SAR metric having the best correlation with temperature. In regards to the robustness of this approach, over 3 million data points were computed from each exposure condition; the large number of data points diminished the possible effect of limited accuracy of FDTD modeling. In addition, by also analyzing the combined pool of data from all exposure conditions at the same frequency, the outcome is further less affected by any single exposure condition.

At each frequency, the results show an inverted U-shaped relation between averaging tissue mass and related SAR correlation with temperature rise. A tissue mass of 5 or 10 g produced the best correlation and thus the most appropriate SAR metric to represent temperature rise in the body exposed to RF energy compared to any other masses including 1 g. This result is consistent for all exposure conditions from 30 MHz to 1 GHz considered in this paper when IEEE SAR averaging procedure is used.

REFERENCES

1. Ackerman, M. J., "The visible human project," *Proc. IEEE*, Vol. 86, 504–511, March 1998.
2. Cole, K. S. and R. H. Cole, "Dispersion and absorption in dielectrics: I. Alternating current characteristics," *Journal of Chemical Physics*, 341–351, April 1941.
3. Gabriel, S., R. W. Lau, and C. Gabriel, "The dielectric properties of biological tissues: III. Parametric models for the frequency spectrum of tissues," *Phys. Med. Biol.*, Vol. 41, 2271–2293, 1996.
4. Bernardi, P., M. Cavagnaro, S. Pisa, and E. Piuzzi, "Specific absorption rate and temperature elevation in a subject exposed in the far-field of radio-frequency sources operating in the 10–900-MHz range," *IEEE Trans. Biomed. Eng.*, Vol. 50, 295–304, March 2003.
5. Flyckt, V., B. Raaymakers, and J. Lagendijk, "Modelling the impact of blood flow on the temperature distribution in the human eye and the orbit: Fixed heat transfer coefficients versus the Pennes bioheat model versus discrete blood vessels," *Phys. Med. Biol.*, Vol. 51, 5007–5021, 2006.
6. Li, Q. and O. Gandhi, "Thermal implications of the new relaxed IEEE RF safety standard for head exposures to cellular telephones at 835 and 1900 MHz," *IEEE Trans. Microw. Theory Tech.*, Vol. 54, 3146–3155, 2006.
7. Hirata, A., "Computational verification of anesthesia effect on temperature variations in rabbit eyes exposed to 2.45 GHz," *Bioelectromagnetics*, Vol. 27, 602–612, 2006.

Progress in Design of Safe, Effective and Relatively Simple RF Pulses for Transmit Arrays in MRI

Sukhoon Oh, Zhangwei Wang, Sylvie Garrett, and Christopher M. Collins
Department of Radiology, College of Medicine, The Pennsylvania State University
Hershey, PA 17033, USA

Abstract—

Introduction: In high-field MR imaging, B_1 homogeneity is degraded by wave behavior and penetration effects. These effects are very significant in human-body imaging due to the large sample size. Recently, several techniques have been proposed to improve the excitation homogeneity in high-field MRI, including RF-shimming [1], transmit SENSE [2], and optimization of composite pulses using transmit coil arrays [3]. However, generally, if the excitation homogeneity is improved then the specific absorption ratio (SAR) may also increase, so homogeneity and SAR should be considered simultaneously during optimization [4]. In this numerical study, a composite RF pulse is designed to simultaneously improve the excitation homogeneity within the human body and reduce the peak SAR. The composite RF pulse can achieve both significantly better excitation homogeneity and significantly lower SAR levels than RF shimming alone.

Method: A 16-element whole-body transmit array coil was modeled at 128 MHz (3.0 T) using xFDTD software (Remcom, USA) with a three-dimensional isometric grid ($5 \times 5 \times 5\,\mathrm{mm}^3$) as shown in Figure 1. The matrix size is $199 \times 199 \times 492$ in x, y, and z direction, respectively. Current sources were placed at each end of each element. The human-body model, containing 36 different tissues, was loaded in the body coil array. A composite pulse comprised of two consecutive RF pulses with individually-optimized field distributions is employed to enhance the excitation homogeneity. Optimization considered 64 variables for composite pulses (magnitude and phase for 16 elements in each of 2 pulses) or 32 variables for RF shimming (magnitude and phase for 16 elements in 1 pulse) with the aim of maximizing the excitation homogeneity and minimize the peak SAR using a home-built optimization routine based on MATLAB (Mathworks, USA). For each iteration step, the mean and standard deviation (STD) of the transverse magnetization vector (M_t) were examined to evaluate the B_1 homogeneity. Theoretically, the mean M_t should be 1 if the B_1 field distribution is perfect (flip angle equal 90° everywhere). Simultaneously, the maximum SAR was also calculated for an entire human-body to reduce the peak SAR. A simple weighting function ($\eta \times \text{inhomogeneity} + (1-\eta) \times \mathrm{SAR}_{\max}$, $\eta : 0 \sim 1$) was employed to consider both excitation homogeneity and the peak SAR, simultaneously [6]. When $\eta = 1$ the optimization of the excitation homogeneity occurs without consideration of SAR, while $\eta = 0$ results in optimization of SAR without consideration of excitation homogeneity. The RF pulse duration of the RF-shimming pulse and the entire composite RF pulses were both 3 ms.

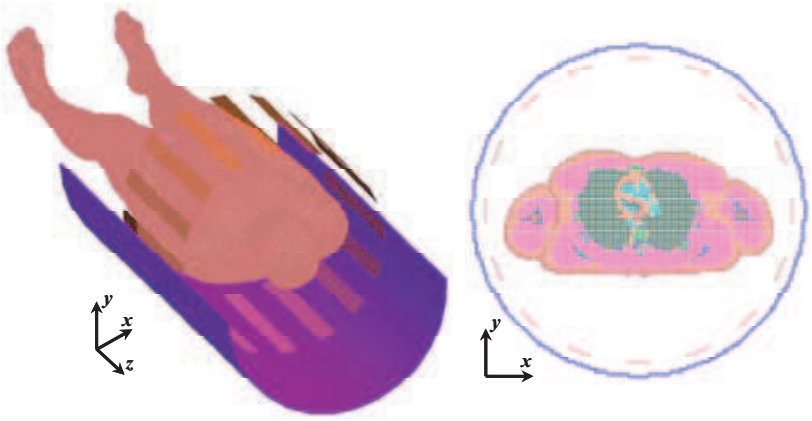

Figure 1: The geometry of the 16-element transmit array coil (left, half of the RF-shield was removed for better view) and one axial plane (right). The diameters of RF-shield and coil are 690 and 630 mm, respectively. The length and width of each element are 500 mm and 50 mm, respectively. The length of RF-shield is 1400 mm.

Table 1: The mean transverse magnetization (M_t), standard deviation of M_t, and SAR (W/kg) are shown. The average and maximum SAR are calculated for the entire human-body model.

	η	RF-Shimming		Composite Pulse	
M_t	1.0	Mean	0.9718	Mean	0.9932
		STD	0.0312	STD	0.0081
	0.6	Mean	0.9392	Mean	0.9745
		STD	0.0515	STD	0.0302
SAR [W/kg]	1.0	Avg.	4.1321	Avg.	4.1385
		Max.	294.28	Max.	205.04
	0.6	Avg.	4.1233	Avg.	4.1154
		Max.	224.27	Max.	112.57

Results and Discussion: Figure 2 shows the M_t and SAR (W/kg) distributions of the RF-shimming and the array-optimized composite pulse for weighting factor η of 1.0 and 0.6. Globally, the array-optimized composite RF pulse shows better excitation homogeneity and SAR than the simple RF-shimming. The mean M_t and SAR values are summarized in Table 1. In the table, the average and maximum SAR values were calculated in the entire human-body model. As expected, lower mean M_t and maximum SAR values were observed when the lower weighting factors were used for both RF-shimming and the array-optimized composite pulse. With no consideration of SAR ($\eta = 1.0$), the mean M_t is close to 1 which means close to 90° flip angle throughout the plane for the array-optimized composite pulse (not shown), whereas RF-shimming shows $M_t = 0.9718$. When the weighting factor is decreased ($\eta = 0.6$), the mean M_t for the optimized composite pulse is still better than the RF-shimming for $\eta = 1.0$. If the homogeneity (STD) is identical between RF-shimming and array-optimized composite pulse (not shown), the array-optimized composite pulse shows a higher mean M_t, slightly lower average SAR, and significantly lower (by about 50%) maximum SAR than RF-shimming. Homogeneous excitation considering SAR with weighting factors is thus potentially very valuable for high-field MRI. While even greater flexibility could be expected for fully-parallel transmit SENSE-type pulses than seen here for a simple 2-pulse composite, slice selection and large flip angles are more readily accomplished for composite pulses.

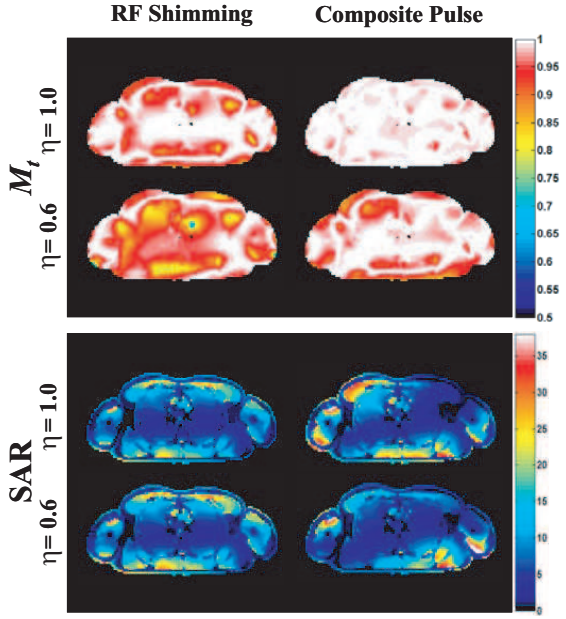

Figure 2: M_t and SAR (W/kg) for RF-shimming (left) and array-optimized composite pulses (right) without consideration of SAR ($\eta = 1.0$) and with consideration of SAR ($\eta = 0.6$) on an axial slice through the heart. When $\eta = 0.6$, both better excitation homogeneity and lower SAR can be observed with the composite pulse.

ACKNOWLEDGMENT

Funding through NIH R01 EB000454.

REFERENCES

1. Hoult, D. I., *J. Magn. Reson. Imag.*, Vol. 12, 46–67, 2000.
2. Katscher, et al., *Magn. Reson. In. Med.*, Vol. 49, 144–150, 2003.
3. Collins, et al., *Magn. Reson. In. Med.*, Vol. 57, 470–474, 2007.
4. Van den Berg, et al., *Magn. Reson. In. Med.*, Vol. 57, 577–586, 2007.
5. Levitt, M. H., et al., *J. Magn. Reson.*, Vol. 33, 474–476, 1979.
6. Wang, et al., *15th ISMRM*, 1022, Berlin, 2007.

Experimental Temperature and Specific Absorption Rate Mapping Using MRI in a Transmit-receive Head Coil at 3.0T

Sukhoon Oh and Christopher M. Collins
Radiology, College of Medicine, The Pennsylvania State University, Hershey, Pennsylvania, United States

Abstract—

Introduction: MRI-based temperature mapping techniques have been applied to detect the temperature changes (ΔT) for a variety of applications, including during the thermoablation of tumors [1], and in verifying minimal temperature increment induced by EEG electrodes and/or its wires during MRI [2]. Although numerical calculations have been used to predict SAR distributions and resulting temperature increase throughout a sample due to excitation with the RF coil [3], experimental measurements with MR thermometry are rarely used for this purpose [4]. In this study, experimentally-acquired temperature maps are used to calculate the SAR distribution from a head-sized transmit-receive birdcage coil in an agar gel phantom at 3.0 T.

Method: Figure 1(a) shows the experimental arrangement of phantoms used in this study. Four reference phantoms of vegetable oil were placed strategically to allow for measurement of temporally and spatially varying phase drift in the case of long duration (30 min$\sim$) RF heating. In this study, however, the reference data was not necessary since heating was accomplished in a short enough duration that phase drift was negligible. A rectangular-shaped conductive agar-gel phantom containing 10 g/L of NaCl, 1 g/L of $CuSO_4$, and 7 g/L of agar, ($w \times h \times d$ $8.5 \times 7 \times 15\,\mathrm{cm}^3$) was used to measure heating and SAR. One fiber optic thermal sensor (OpSens, Canada) was placed at the center of the phantom (where minimum SAR is expected) to assess when thermal conduction effects became significant. Another thermal sensor was placed at a location of expected high SAR to assess when the temperature increases became nonlinear, also indicating significant impact of thermal conduction. Before the experiment began, the phantom was allowed to equilibrate with its surroundings within the magnet for several hours. A baseline phase image was acquired using a general gradient-echo (GRE) sequence (TR 70 ms, TE 20 ms, FOV $175 \times 175\,\mathrm{mm}^2$, matrix size 64×64, slice thickness 10 mm, NEX = 4, FA 30°, scan time about 18 seconds). Then, RF heating pulses were applied to the phantom for 2 minutes. A single quadrature birdcage coil was used for both heating and imaging purposes, in contrast to studies in diathermy and ablation using separate coils at different frequencies [5]. After the RF heating, another phase image was acquired as quickly as possible using the same parameters as the first GRE sequence except NEX = 1 (scan time about 4 seconds). During GRE acquisition, two axial slices were imaged at different locations (coil center, or $z = 0$, and 30 mm offset). The temperature change between the two GRE acquisition periods was assessed by the phase change, as according to the proton resonance frequency shift method of MR thermometry [6]. In a phantom, such as this, with no perfusion and no metabolic effects, and when heating rapidly from equilibrium before thermal conduction has a significant role, the Pennes bioheat equation [7] can be reduced to SAR = $c_{agar}\Delta T/dt$ where c_{agar} is the specific heat capacity of the agar-gel, ΔT is the temperature change, and dt is the duration of RF heating. The specific heat capacity of the agar-gel phantom was 4200 J/kg°C [8].

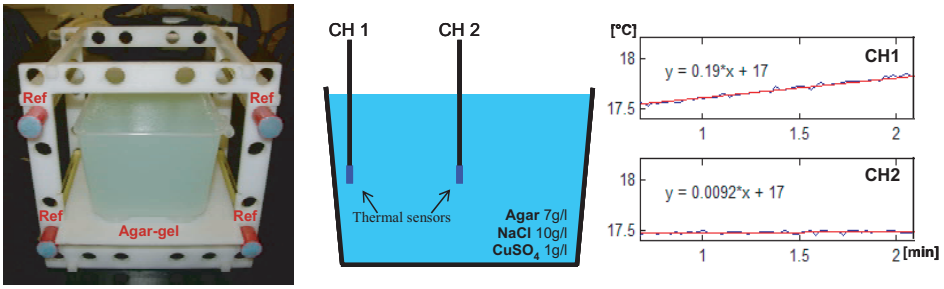

(a) (b) (c)

Figure 1: (a) Conductive agar-gel phantom ($w \times h \times d$ $8.5 \times 7 \times 15\mathrm{cm}^3$) and oil reference phantoms. (b) Setting of optic-fiber thermal sensors. (c) Temperature measurements and linear fitting for fiber optic data. Blue line indicates measurements and red line indicates linear fit.

Results and Discussion: Minimal temperature changes at the center of the phantom (channel 2) were seen at up to 3 minutes of heating, whereas a significant linear increase in temperature was seen near the edge of the phantom (channel 1) over the same time period (Figure 1(c)). The norm of residuals was compared between linear and cubic spline fits for the first 2 minutes of data. The norm of residuals of linear fitting was 0.177 whereas cubic spline was 0.175, indicating that the temperature was changing linearly for at least 2 minutes. In Figure 2(a), ΔT maps and SAR maps are shown on the axial slice passing through the center of the coil and phantom ($z = 0\,\text{mm}$). This result agrees well with expectations from electromagnetic theory, which predict that in the absence of wavelength effects, for a homogeneous B_1 field in an infinite phantom the SAR in the phantom should increase roughly with the square of the radial distance from the center. In Figure 2(b), the ΔT at the center is increased, due to an increased z value (30 mm), also an increase in the radial distance from the center leading to an expected increase in SAR. The maximum SAR near the edge of the phantom is greater at $z = 0$ partly due to the boundary conditions confining currents from other planes to this region on the center plane. The maximum SAR in one image voxel ($2.73 \times 2.73 \times 10\,\text{mm}^3$, or $0.074\,\text{cm}^3$) was found to be around 18 W/kg in Figure 2(a). While this simple demonstration in a phantom with no perfusion appears effective, the addition of perfusion (as well a noise and artifact from motion, etc.) would be expected to significantly hamper efforts to perform a similar experiment successfully *in-vivo* without extraordinary SAR levels. Our future experiments will focus on high-power RF heating in phantoms with transmit-arrays for the purposes of validating predictions from sophisticated numerical calculations.

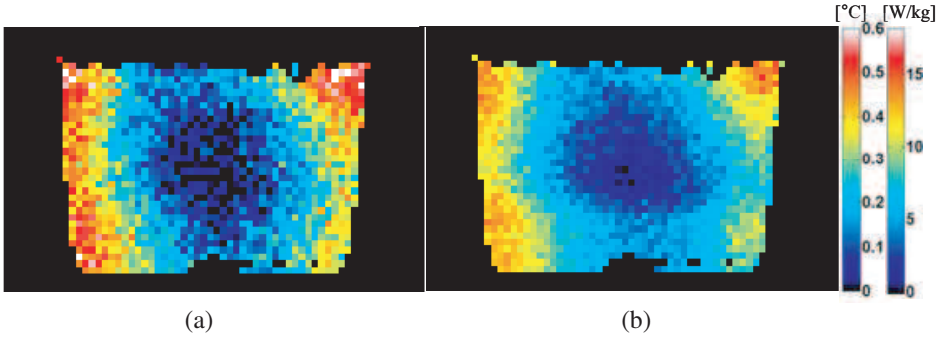

(a) (b)

Figure 2: Temperature change and SAR map at (a) $z = 0\,\text{mm}$ (coil center) and (b) $z = 30\,\text{mm}$. The scale bars on the right indicate temperature (°C) and SAR (W/kg), respectively.

ACKNOWLEDGMENT

Funding through NIH R01 EB000454.

REFERENCES

1. Steiner, et al., *Radiology*, Vol. 206, 803–810, 1998.
2. Angelone, et al., *Magn. Reson. Imag.*, Vol. 24, 801–812, 2006.
3. Collins, et al., *J. Magn. Reson. Imag.*, Vol. 19, 650–659, 2004.
4. Shapiro, et al., *Magn. Reson. In Med.*, Vol. 47, 492–498, 2002.
5. Behnia, et al., *Concepts Magn. Reson.*, Vol. 23B, No. 1, 1–15, 2004.
6. Ishihara, et al., *ISMRM*, 4803, Berlin, 1992.
7. Pennes, et al., *J. Appl. Physiol.*, Vol. 1, 93–122, 1948.
8. Armenean, et al., *Proceedings of the IEEE EMBS*, 501–504, Cancun, 2003.

Ultra Fast Electromagnetic Field Computation for RF Multi Transmit Techniques in High Field MRI

Bob van den Bergen[1], **Chris Stolk**[2], **and Cornelis A. T. van den Berg**[1]

[1]University Medical Center Utrecht, the Netherlands
[2]Department of Applied Mathematics, Faculty of EEMCS
University of Twente, the Netherlands

Abstract—

Introduction: Multi transmit techniques play a key role in the managing of radiofrequency (RF) field challenges of high field MRI. To compensate for the inherent non-uniformity of the transmit field and/or control RF heating, information about the electromagnetic field of each coil element in the patient is essential [1, 2]. Most commonly, the individual B_1^+ fields of the coil elements are obtained by B_1^+ mapping. However, this method is time-consuming and susceptible to noise. More importantly, no information is obtained about the electric field which governs SAR. In this study, we present the Bessel Boundary Matching (BBM) method. This method is capable of calculating the electric and magnetic field inside a multi-layered patient anatomy in a matter of minutes which will bring an online design of a multi transmit excitation scheme within reach.

Methods: The BBM method solves the Helmholtz equation in two dimensions which limits its use to regions where the electromagnetic problem is essentially two-dimensional such as in the pelvic region [3]. Such an electromagnetic field can be completely described by the 2D Helmholtz equation in terms of the magnetic vector potential (A_z). This equation can be solved for each homogeneous region in- and outside the patient (Figure 1). The general solution is described by a base of Bessel functions and has the general form shown below.

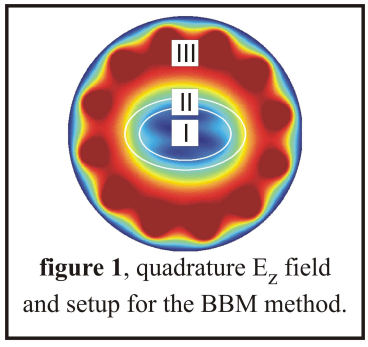

Figure 1: Quadrature E_Z field and setup for the BBM method.

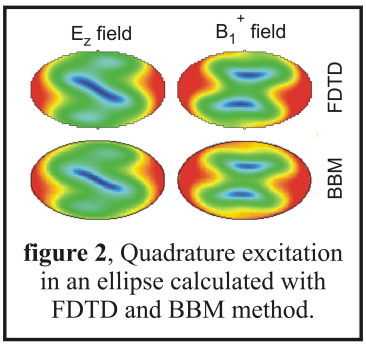

Figure 2: Quadrature excitation in an ellipse calculated with FDTD and BBM method.

$$A_z(r,\theta) = F(r,\theta) + \sum_{l=1}^{N} C_l \left[\sum_{m=-M}^{M} a_m^l J_m(\xi \cdot r) e^{im\theta} + \sum_{n=-M}^{M} b_n^l Y_n(\xi \cdot r) e^{in\theta} \right]$$

F is a fundamental solution which takes the contribution of the antennas into account and is only non-zero in the region where the antennas are located. N is the number of antennas and M is the number of first (J) and second (Y) order Bessel functions that are included. C is the complex amplitude for the antennas ξ is the complex wave number. The coefficients a and b of the Bessel functions are region dependent. The coefficients a and b can be analytically determined from the boundary conditions provided the problem is cylindrically symmetric. Of course this is never the case for a realistic patient geometry. However, by imposing the boundary conditions at the interfaces of the different regions, a least squares solution for the coefficients a and b can be found for a non-circular geometry. In principle, the number of homogeneous regions and their shape can be chosen arbitrarily.

We implemented in MATLAB (the Mathworks, MA, USA) a least squares method to solve the set of boundary equations for each coil element. From the solution for the magnetic vector

potential A_z, the electric and the transverse magnetic field components are computed. The total electromagnetic field was determined by a linear superposition of all the individual fields. The BBM method was applied to calculate the electromagnetic field in a homogenous ellipse and in a human pelvis at 300 MHz (7 T). The pelvis was modelled by an inner region with averaged muscle-bone dielectric properties and an outer layer of fat. The transverse circumference was chosen to follow the real patient outline, which is illustrated in Figures 3 and 5. The results from BBM method were compared with the outcome of three-dimensional FDTD calculations including a full heterogeneous dielectric patient model.

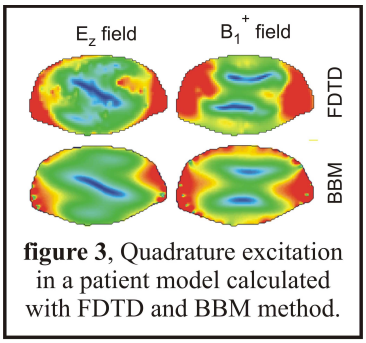

figure 3, Quadrature excitation in a patient model calculated with FDTD and BBM method.

Figure 3: Quadrature excitation in a patient model calculated with FDTD and BBM method.

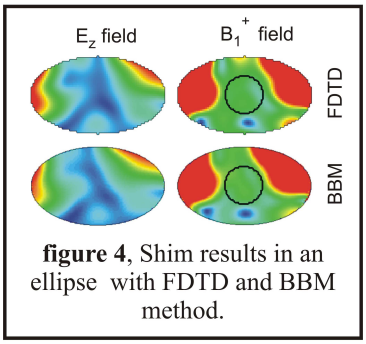

figure 4, Shim results in an ellipse with FDTD and BBM method.

Figure 4: Shim results in an ellipse with FDTD and BBM method.

Results: The presented BBM method is capable of calculating the electric and magnetic field and performing RF shimming in roughly 2 minutes for a coil of 12 coil elements and 4 minutes for a coil of 32 elements. The method can be made even faster by using a low-level programming language instead of MATLAB. Results for two models are shown in Figures 2, 3, 4 and 5 and are compared with standard three-dimensional FDTD results. The results show a very large correspondence for a quadrature excitation both for an ellipse (Figure 2) and for a real anatomy (Figure 3). RF shimming results for the BBM and FDTD are presented in Figures 4 and 5 for an ellipse and an anatomy respectively. The optimal phase-amplitude settings determined with the BBM method were also applied to fields calculated with FDTD simulations.

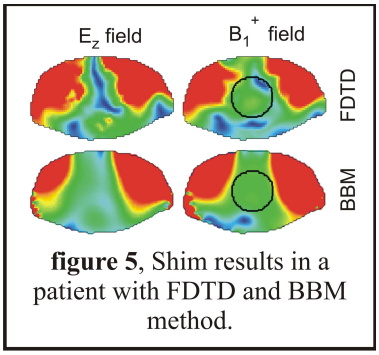

figure 5, Shim results in a patient with FDTD and BBM method.

Figure 5: Shim results in a patient with FDTD and BBM method.

Discussion and Conclusions: The BBM allows a rapid computation of the electric and transverse magnetic field of the individual coil elements. Using FDTD simulations, it was demonstrated that the BBM method correctly calculates the global RF field pattern in the human pelvis at 7 T. This makes the BBM method not only a valuable tool for RF shimming, but also for online RF pulse design in parallel excitation. Its capability to quickly perform patient specific field computations will allow a more balanced trade-off between the desired excitation pattern and SAR constraints.

REFERENCES

1. Katscher, U., et al., *Magn. Reson. Med.*, Vol. 49, 144–150, 2003.
2. Zhu, Y., *Magn. Reson. Med.*, Vol. 51, 775–784, 2004.
3. Van den Bergen, B., et al., *Phys. Med. Biol.*, Vol. 52, 5429–5441, 2007.

Development of a Clinically Relevant 7 T MRI Head Scanner

Piotr Starewicz, **Shahin Pourrahimi**, **William Punchard**, **and John Williams**

Stern Magnetics, LLC., 5 Fortune Drive, Billerica, MA, 01821, USA

Abstract— High field MR provides data that are not available at lower fields. Applications encompass anatomical, metabolic and molecular imaging, functional and diffusion imaging, and spectroscopy. A variety of novel, high-speed and enhanced-contrast techniques have already been developed, while specific highfield clinical applications can be anticipated. Both access to, and dissemination of, high field MR platforms are impeded by their very high cost and demanding siting requirements. The magnet alone can represent over 80% of the total system cost, thereby representing the most important target for cost reduction.

Stern Magnetics LLC is currently conducting a design study for a novel 7T MR magnet that is significantly smaller, lighter and less costly than magnets based on conventional technologies. This neuro-science targeted magnet has an internal diameter of 680 mm and can be installed in a standard clinical MR suite and used for MR studies on humans as well as large animals, such as primates and pigs.

In terms of cost and optimization of performance traditional magnet technologies have reached their limits, so further advances must depend on using novel superconductors, reinforcement technology and the most sophisticated magnet design techniques. Such a technological leap has not yet been taken, partly due to the lack of such novel technologies, but also because of the small number of competitors in the magnet business.

Stern Magnetics, LLC has successfully demonstrated the high performance of internally reinforced superconducting wires with enhanced capability for supporting the high stresses present in high-field large bore magnets. It has also demonstrated highly optimized magnet designs developed to take advantage of the specific characteristics of these novel wires. The cross section of a typical reinforced superconducting wire is shown below.

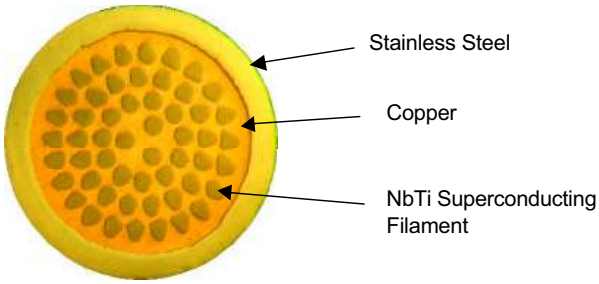

Stainless steel cladding increases the yield strength and elastic modulus of typical NbTi wires and therefore allows high stored energy magnets to be smaller. Another advantage of stainless steel cladding is that it replaces a larger mass of copper commonly used in conventional superconducting wires designed for MRI magnets. In essence our approach allows the use of smaller mass of less expensive superconducting wire in high-field MRI magnets. This technology is patented and proprietary to Stern and, besides lowering costs, allows significantly shorter magnet bores and smaller fringe field footprints.

Our presentation describes: a) the development of a sophisticated magnetics code that takes in magnet performance requirements in term of foot-print, high homogeneity in the bore of the magnet, tight shielding outside of the magnet, and produces the design of an optimized set of coils that achieve the magnet performance requirements with the least number of ampere-turns, b) the advantages of using reinforced superconducting wires in terms of minimizing the mass of superconductor wire needed to form the coils, and c) results of testing of reinforced superconducting wires in model coils.

Optimization of a 7.0 Tesla Receive Coil Array for Brain Imaging by the Surface Integral Equation Method and the Genetic Algorithm

Shumin Wang and Jeff H. Duyn
LFMI, NINDS, National Institutes of Health, Bethesda, USA

Abstract—

Introduction: With the advances of high-field MRI and parallel imaging techniques 1), there is growing interest in the design of RF receive coil arrays for high-field SENSE imaging. Since the array performances depend on the geometric features, an optimized design in terms of geometry is of great importance in practice. In this work, we developed an optimization strategy by using the Genetic Algorithm 2) and the Surface Integral Equation (SIE) method 3). It is applied to 24-channel array for brain imaging at 7.0 Tesla.

Methods: The Genetic Algorithm 2) is based on the evaluation of cost functions and searches for the optimized design in an evolution manner. The cost function is determined by the SNR, which is evaluated via an in-house developed SIE method. The coil profiles as the results of the electromagnetic field distributions are combined into phase-sensitivity SNR maps. Since coil profiles decay rapidly inside phantom, the combined SNR is extracted on a series of sampling lines. The cost on each sampling line is defined as the weighted summation of the average SNR and the signal variation on that line. The cost of a slice is the weighted combination of the cost on each sampling line. Because the SNR of different arrays defers less in deeper region, we assign the highest weight to the shallowest line and the lowest weight to the deepest one. The weight varies linearly in between. If multiple slices are considered, the overall cost is the weighted combination of the cost on each slice.

Results and Discussion: The array consists of 24 small oblong loops that are divided into 8 rows (Fig. 1). The number of coils in each row is fixed and the coil overlap in each vertical row and the inter-row gap size are variables in the optimization. With 2.5 mm increment of the vertical overlap and 5 mm increment of the inter-row gap size, the optimization weights on 14,600,960 designs. Fig. 2 shows the combined SNR map of an oblique slice cutting through the middle of a row of 4 coils. The SNR evaluated on the second shallowest sampling line are also shown. It is observed that large signal variation occurs with the minimum coil overlap (zero overlap) in z-direction. By increasing the coil overlap, the signal variation can be significantly reduced. The optimized coil overlaps for each row of coils with equally weighted average SNR and signal variation are shown in Fig. 1. After optimizing each row of coils, the final optimization is selected from different inter-row gap sizes based on the SNR on 8 axial slices. Fig. 3 shows a combined axial SNR map and the sampling lines defined in the anterior and the posterior sections. The

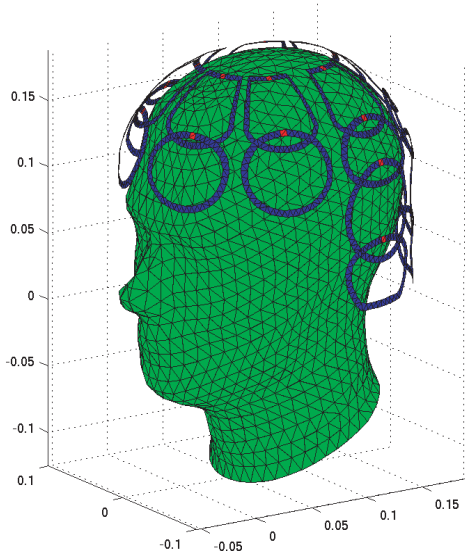

Figure 1: The 24-channel coil array.

final results are shown in Figs. 4 and 5. It is observed that the optimized design depends on the SENSE acceleration rate and whether signal variation is taken into account. In all cases, no inter-row overlap is suggested. Moreover, the higher the SENSE rate is, the wider the inter-row gap size should be.

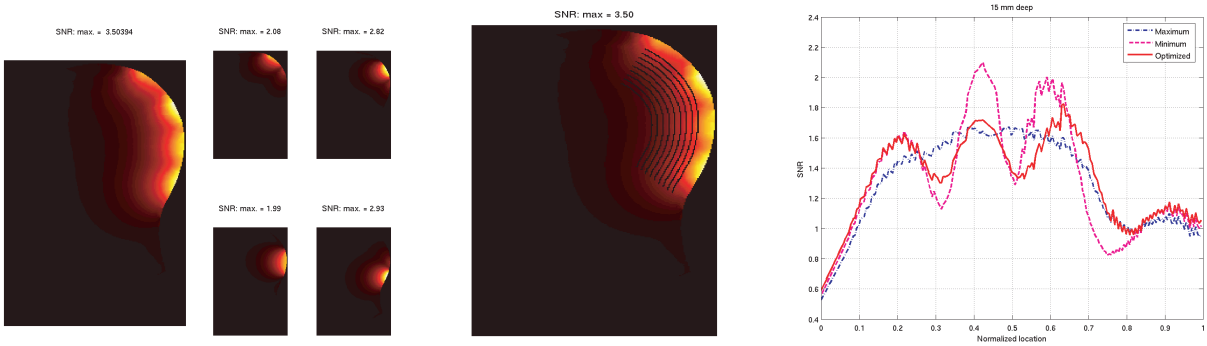

Figure 2: Left: SNR profile of each element in one row. Middle: the phase-sensitive combined SNR map and the sampling lines. Right: the combined SNR on one line.

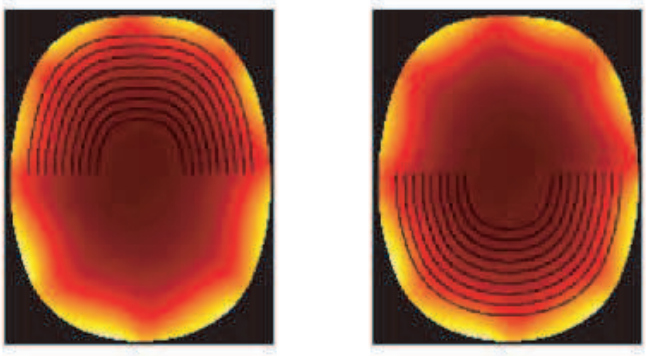

Figure 3: Left: sampling lines in the anterior section. Right: sampling lines in the posterior section.

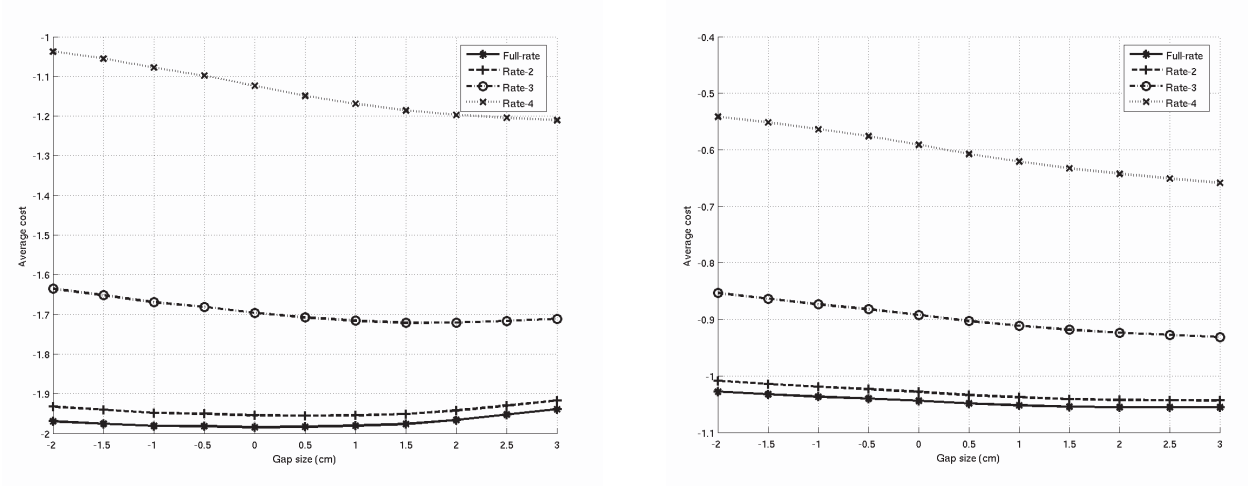

Figure 4: Left: costs of different inter-row gaps evaluated by an equal weight of the average SNR and signal dropout. Right: costs of different inter-row gaps evaluated only by the average SNR. Lower cost means better performance.

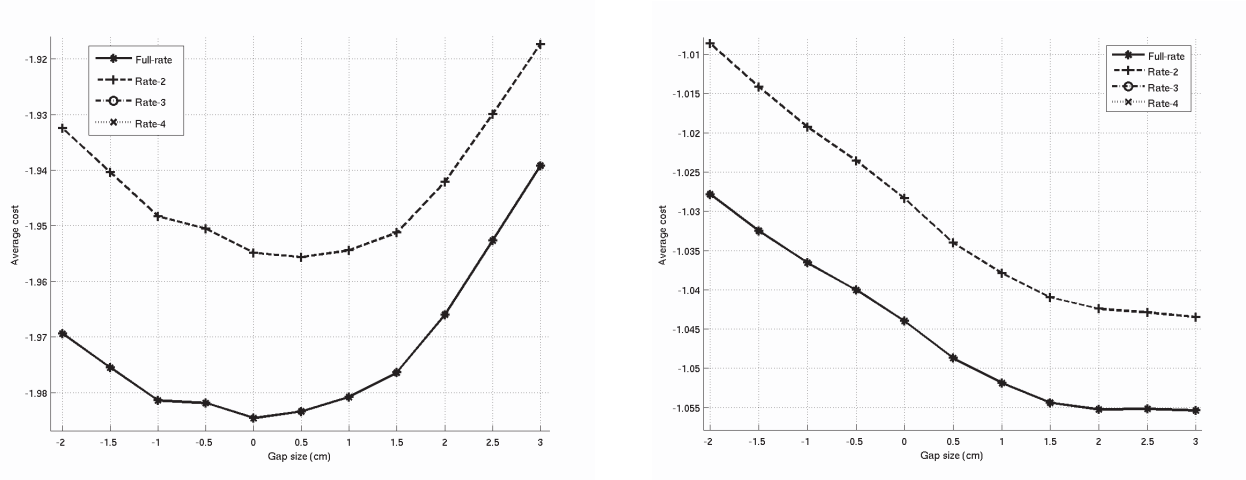

Figure 5: Left: zoomed view of the left of Fig. 4. Right: zoomed view of the right of Fig. 4. Lower cost means better performance.

Conclusion: The results show that the optimized SENSE coil array design depends on the SENSE acceleration rate and how much signal variation is weighted. Coil overlap in z-direction and inter-row gaps are preferred for both better SNR coverage and SENSE performances.

REFERENCES

1. Pruessman, K. P., et al., *MRM*, Vol. 42, 952–962, 1999.
2. Hault, R., et al., *Practical Genetic Algorithms*.
3. Wang, S., et al., *PMB*, Vol. 51, 3211–3229, 2006.

Investigation of High Field Transmit B_1 Inhomogeniety by the Time-Domain Finite-Difference/Finite-Element Hybrid Method

Shumin Wang and Jeff H. Duyn
LFMI, NINDS, National Institutes of Health, Bethesda, USA

Abstract—

Introduction: Full-wave electromagnetic simulations that rigorously solve Maxwell's equations are important in high-field RF coil design. Although the popular FDTD method is good at modeling the inhomogeneous human body, it is inadequate for modeling curved coil structures (1). Methods that accurately model curved coil structures, such as the Finite-Element method (FEM) and the surface integral-equation (SIE) method (2, 3), are computationally expensive. Here we present a stable Time-Domain Finite-Difference/Finite-Element (TD-FD/FE) method that hybridizes the FDTD and the FEM. Since both methods are applied simultaneously in one simulation, the interaction between the human body and RF coils is fully accounted for with well balanced numerical accuracy and computational efficiency.

Methods: The TD-FD/FE hybrid method utilizes unstructured grids in the FEM region while structured Cartesian grids in the FDTD region (Yee's scheme). In the FEM region, the two *curl* equations are combined into the so-called *curl-curl* equation

$$\nabla \times \frac{1}{\mu} \nabla \times \vec{E} + \sigma \frac{\partial \vec{E}}{\partial t} + \epsilon \frac{\partial^2 \vec{E}}{\partial t^2} + \frac{\partial \vec{J}}{\partial t} = 0$$

The electric fields in the *curl-curl* equation are firstly discretized by a set of *curl*-conforming basis functions. Then the Galerkin method is applied to establish a linear system of equations. Finally, the time-domain FEM is obtained by using the Newmark Beta method

$$\frac{1}{\mu}[S]_{ji}\left[\beta e_i^{n+1} + (1-2\beta)e_i^n + \beta e_i^{n-1}\right] + [T]_{ji}\left[\sigma \frac{\left(e_i^{n+1} - e_i^{n-1}\right)}{2\Delta t} + \epsilon \frac{\left(e_i^{n+1} - 2e_i^n + e_i^{n-1}\right)}{\Delta t^2}\right] = 0$$

where $[S]$ and $[T]$ represents stiffness and mass matrix respectively. It has been proven that when $\beta \geq \frac{1}{4}$, the time-domain FEM is unconditionally stable regardless of the size of individual elements. Furthermore, the FDTD method is a special FEM scheme by applying $\beta = 0$ and integral-lumping inside each Cartesian element. In practice, tetrahedral elements are preferred to model arbitrarily shaped geometries in three-dimension. In order to connect them to Cartesian grids, a layer of pyramidal elements can be applied (Fig. 1).

Results and Discussion: AC^{++} program was developed and used to simulated the B_1 and electric field distributions of a 7.0 Tesla 16-rung shielded elliptical high-pass birdcage coil (12-in by 8.9-in axial ratio, 10-in high). The shield is 1-in away from the coil. The results were compared with those of the SIE method (3). In the SIE simulation, the Specific Anthropomorphic Mannequin (SAM) model filled with brain equivalent ($\varepsilon_r = 52$ and $\sigma = 0.552$) was used (Fig. 2). In the TD-FD/FE hybrid simulation, a $3 \times 3 \times 3\,\mathrm{mm}^3$ realistic human model (NLM's Visual Man Project) was used. The *exact* geometry of the birdcage coil was modeled with tetrahedral grids (Fig. 2). The overall number of elements in the unstructured FEM region was about 400,000. The maximum and the minimum dihedral angles of the tetrahedral grids were 147° and 14° respectively. The resulting FEM matrix contained about 1 million unknowns and it was decomposed by an in-house developed sparse Cholesky solver, which took 180 seconds on a 2.6 GHz CPU. Inversion of the FEM matrix during each time step was accomplished by back substitution. A first-order derivative Gaussian pulse was used for 4-port quadrature drive of the coil. Results were obtained after 30,000 time steps. The coil was numerically tuned with thirty-two 5.92-pF capacitors by using the SIE method and exactly the same capacitance was applied in the TD-FD/FE hybrid simulations. The simulated B1 and electric field distributions on corresponding slices are compared in Figs. 3 and 4 respectively. In each individual figure, the field is normalized to its own peak. It is observed that by modeling coil geometry exactly and using the same capacitance, the coil is resonant at 298 MHz in both simulations. The B_1 distributions resemble reasonably well despite the differences between the human models, though the SIE results look more inhomogeneous. However, the electrical field distribution exhibits quite large differences because the SIE method failed to resolve local hot spots due to the lack of

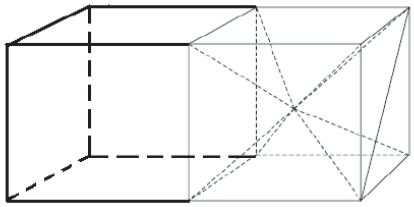

Figure 1: The unstructured/Cartesian grids interface.

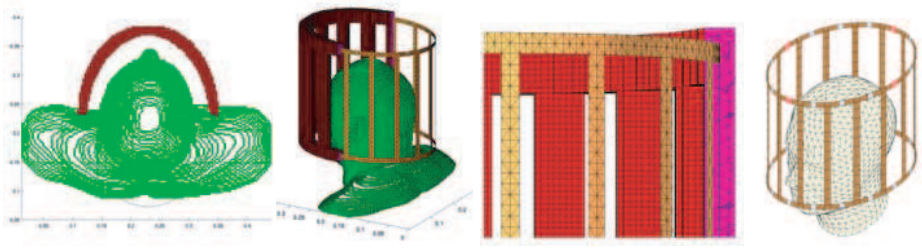

Figure 2: The hybrid grids of the coil and the human body (left-most and mid-left), detailed view of the tetrahedral mesh (mid-right) and the SIE model of the same coil (right-most). Note that the shield is not shown.

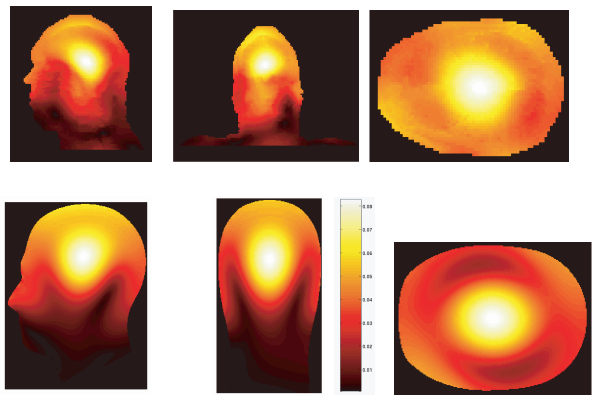

Figure 3: B_1 maps calculated by the TD-FD/FE hybrid method (top row) and the SIE method (bottom row) on corresponding slices.

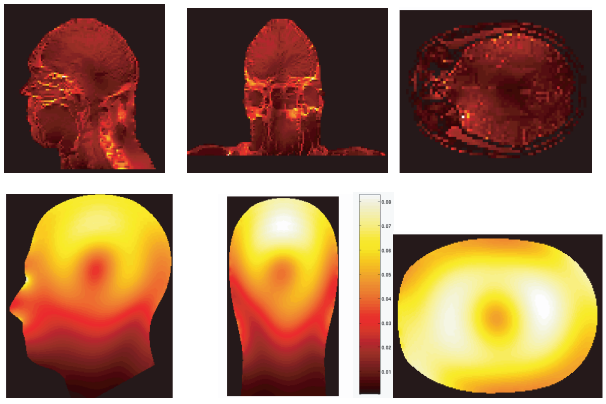

Figure 4: Electric field maps calculated by the TD-FD/FE hybrid method (top row) and the SIE method (bottom row).

anatomical detail. These local electrical field hot spots are critical in evaluating RF safety issues.

Conclusion: We presented a TD-FD/FE hybrid approach that simultaneous applies the FDTD and the FEM methods in a single simulation. This method is accurate and efficient in simulating the interaction between the human body and RF coils at high-field.

REFERENCES

1. Yee, K. S., *IEEE TAP*, Vol. 14, 302–307, 1966.
2. Petropoulos, L. S., et al., *MRM*, Vol. 30, 366–372, 1993.
3. Wang, S., et al., *PMB*, Vol. 51, 3211–3229, 2006.

Session 4P1
Novel Mathematical Methods in Electromagnetics 2

Applications of the Darwin Lagrangian Approach in Electromagnetism

Hanno Essén

Department of Mechanics, Royal Inst. of Technology (KTH), Stockholm, Sweden

Abstract— Darwin (1920) noted that when radiation can be neglected it should be possible to eliminate the radiation degrees-of-freedom from the action of classical electrodynamics and keep the discrete particle degrees-of-freedom only. The electromagnetic field is then completely determined by the positions and velocities of the charged particles.

Darwin derived his well known Lagrangian by series expansion in v/c keeping terms up to order $(v/c)^2$. Since radiation is due to acceleration the assumption of low speed should not be necessary. A Lagrangian, the exact Darwin Lagrangian, is suggested that neglects radiation without assuming low speed. It cures deficiencies of the Darwin Lagrangian in the ultra-relativistic regime and shows that at these velocities the magnetic attraction of parallel currents cancel the Coulomb repulsion.

To get full access to the canonical formalism and thus the use of the Gibbs-Maxwell-Boltzmann statistical mechanics one should go one step further and find the Hamiltonian corresponding to the Darwin Lagrangian. This, however, turns out to be fairly difficult and only various approximate expressions can be written down. Here we discuss some of these and their range of validity, as well as the conclusions that can be drawn from them. Applications to plasmas and to solid state physics are considered. In the latter case the influence of quantum mechanical effects must be discussed.

The classical result of Bohr and van Leeuwen states that classical statistical mechanics cannot explain any equilibrium magnetic response from matter. This theorem is reconsidered in the light of the Darwin expression for the energy of a system of classical charged particles. We also consider the result that matter does not seem to be stable when magnetic interactions between the constituent particles, or self-generated magnetic fields, are included in the Hamiltonian. There are indications that the Hamiltonian based on the exact Darwin Lagrangian solves this problem.

Numerical Calculation of Diffracted Electromagnetic Waves by a Circular Disk of Perfect Conductor Using Multiple Precision Arithmetic

Takashi Kuroki[1], **Teruhiro Kinoshita**[2], **and Toshihiko Shibazaki**[1]

[1]Tokyo Metropolitan College of Industrial Technology, Japan
[2]Tokyo Polytechnic University, Japan

Abstract— In the case of the numerical calculation using the analysis method of Nomura and Katsura [1], good results up to 2.5 or 3.0 wavelengths with the double precision or the quadruple precision are able to be obtained, to electromagnetic diffraction by a circular disk of a perfect conductor [2]. The cause of it can be explained by the fact that the numerical calculation is executed with sufficient precision in the calculation process.

GMP (GNU Multiple Precision Arithmetic Library) [3] is the library that can execute the numerical calculation by multiple precision in C and C++ language. MPFR (Multiple Precision Floating-Point Reliable Library) [4], based on GMP, is the supplementary library equipped with the mathematical library functions, such as trigonometric functions, a gamma function and so on. (As these functions are not equipped in GMP.) GMP++ differs from GMP in terms of the classes. MPFR do not have C++ class interfaces. So, we have to design new interfaces.

The purpose of this study is to investigate the cause of the fault results, and alter them to be good results using GMP, MPFR, GMP++ and the new interfaces while the radius of the disk is over 3 wavelengths.

The flow of the new interfaces between GMP++ classes and MPFR functions is as follows: (1) Convert GMP++ class to MPFR variable. (2) Calculate MPFR function with MPFR variable. (3) Convert MPFR variable to GMP variable (4) Convert GMP variable to GMP++ class. (MPFR variable cannot be directly converted to GMP++.)

In the calculation process of Equations (31) and (32) in [1], the precision gets worse. Fig. 1 shows the digit number in which the two values, $g_1(p,q)$ (are transformed from Equation (31))

$$g_1(p,q) = \sum_{m=q}^{\infty} b_m \equiv \sum_{m=q}^{q+N} b_m, \quad \frac{b_m}{b_{m-1}} = \frac{(2m-1)^2}{(p+m+\frac{1}{2})(p-m+\frac{1}{2})(m+q)(m-q)} \left(\frac{\frac{a}{\lambda}}{2}\right)^2,$$

$$b_q = \frac{(-1)^q 2^2 (\frac{a}{\lambda})^{2q}}{q!} \frac{\{2(p-1)+1-2q\}\{2(p-2)+1-2q\}\ldots\{1-2q\}}{(2p+2q+1)(2p+2q)(2p+2q-1)\ldots(p+q+1)}$$

with the calculation precision 64[bit] and 512[bit] from q to $q+N$, coinside with each other. Where, a is the radius of the disk, λ is the wave length, respectively. (Please refer to [1] for p and q.) In the case of 64[bit], as a/λ grows large, the precision of $g_1(p,q)$ becomes 0 without convergence.

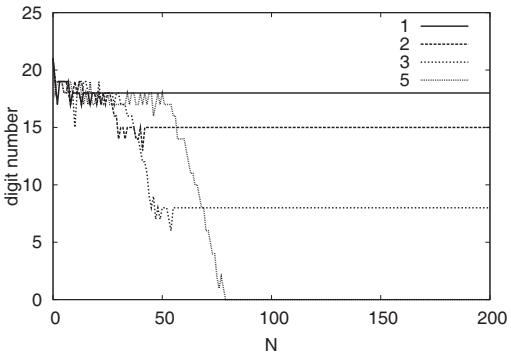

Figure 1: Digit number in which the two values, $g_1(p,q)$ with the calculation precision 64[bit] and 512[bit], coinside with each other ($p = 0$, $q = 0$, $a/\lambda = 1, 2, 3, 5$).

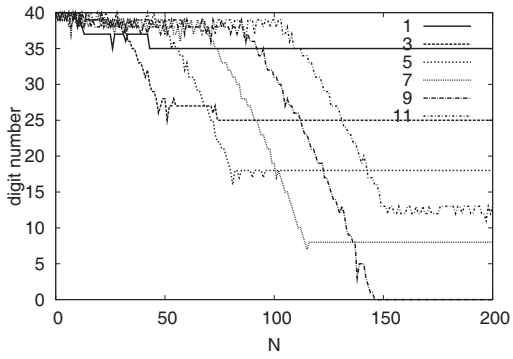

Figure 2: Digit number in which the two values, $g_1(p,q)$ with the calculation precision 128[bit] and 512[bit], coinside with each other ($p = 0$, $q = 0$, $a/\lambda = 1, 3, 5, 7, 9, 11$).

Fig. 2 shows the results with the precision 128[bit] and 512[bit] in different conditions to Fig. 1. As a result, the same digit number can be obtained in $a/\lambda = 3.0$ for the precision 64[bit] and in $a/\lambda = 7$ for the precision 128[bit].

REFERENCES

1. Nomura, Y. and S. Katsura, "Diffraction of electormagnetic waves by circular plate and circular hole," *J. Physical Society of Japan*, Vol. 10, No. 4, 285–304, Apr. 1955.
2. Ando, M., T. Murasaki, and T. Kinoshita, "Elimination of false singularities in GTD equivalent edge currents," *Proc. IEEE*, H-138, No. 4, 289–296, Aug. 1991.
3. "GNU MP—The GNU multiple precision arithmetic library," Edition 4.2.1, May 2006.
4. "MPFR-The multiple precision floating-point reliable library," Edition 2.2.0, Sept. 2005.

Estimating a Statistical Property of a Domain Boundary Geometry from a Set of Noisy Solutions to the Helmholtz Equation

J. Fletcher, **P. Wadhams**, **and M. Spivack**
Department of Applied Mathematics and Theoretical Physics
University of Cambridge, UK

Abstract— In this paper we present a method for tackling the inverse problem of estimating a statistical property of a domain boundary geometry from a set of noisy solutions to the Helmholtz equation within the domain. We utilise recently developed Feynman-Kac type solutions to the Helmholtz equation in order to efficiently compute the solutions corresponding to a large number to particular realisations of a random domain boundary. These are combined with a change of probability measure technique in order to associate a probability with a given statistical property of the domain boundary geometry.

We also comment on the potential application of the technique to problems in remote sensing, in particular the problem of obtaining the freeboard of sea ice from radar altimeter data.

Body Fitted Grid Generation Method with Moving Boundaries and Over Set Grid Generation Method

Hiroshi Iwamatsu, **Ryo Fukumoto**, **Shuichi Masuko**, **and Michiko Kuroda**
School of Computer Science
Tokyo University of Technology, Japan

Abstract— Recently, large scale numerical technique for the analysis of the electromagnetic field equations coupling with vibration is strongly required, especially for the realization of new wireless communications or microwave devices, such as RF-MEMS structures used in phase-shifters, couplers or filters. Here, two kinds of numerical techniques, body fitted grid generation method with moving boundaries and overset grid generation method are discussed to construct the numerical technique for the analysis of moving boundary problems in electromagnetic field. The first one is already proposed for the analysis of the moving boundary problems and applied for the MEMS structures with moving parts [1]. By using transformation technique with time components, it is easy to apply the FDTD method. In the second technique [2], the calculation of the moving object can be done by the overlapped sub-lattice that moves on a stationary main lattice. With this technique, it becomes easily to calculate longer distance of the motion in comparison with the first technique.

In this paper, the received wave at the observation point is calculated when observation point or source points move. It can be shown that the frequency of the received wave are shifted. To verify these methods, some numerical results are compared with the theoretical results and good agreements are obtained. Both results were also compared each other and good agreements are obtained between them. We believe that these numerical techniques will have great promises for the analysis of the moving boundary problems in electromagnetic field.

REFERENCES

1. Kawano, K., S. Shahrani, T. Mori, M. Kuroda, and M. M. Tentzeris, "Numerical modeling of reconfigurable RF MEMS-based structures involving the combination of electrical and mechanical force," *ACES Journal*, Vol. 21, No. 1, 1–8, March 2006.
2. Hanim, N., B. Piao, M. Kuroda, and S. Kuroda, "Novel numerical technique for the analysis of the moving boundary problems by using the overset grid generation," *Proc. of the ACES2006*, Miami, USA, March 2006.

Differential or Integral Equations in Electromagnetics: What's Better

Alexander B. Samokhin
Moscow Institute of Radio Engineering, Electronics and Automatics
78, Vernadsky av., Moscow 117454, Russia

Abstract— The most of actual three-dimensional problems of electromagnetics can be described by differential or integral equations. The main question from the numerical point of view: what kind of equations is better for solving the problem. In this report we consider the following problems: electromagnetic scattering on complicated objects; waveguide propagation; inner tasks.

Number T of arithmetic operations that guarantees the required accuracy of solution and memory volume M required for the implementation of the algorithm are the main efficiency criteria for any numerical method. To solve differential equations (with boundary condition and radiation condition) and integral equations (taking in account discretization method) we estimate input data T and M. Afterwards on the base of estimations obtained we analyze the efficiency of using differential or integral equations for the abovementioned problems.

From Transversality Condition to Vector Symmetry of the Representation of Electromagnetic Beams

Chun-Fang Li[1, 2]

[1]Department of Physics, Shanghai University, Shanghai 200444, China
[2]State Key Laboratory of Transient Optics and Photonics
Xi'an Institute of Optics and Precision Mechanics of CAS, Xi'an 710119, China

Abstract— As we know, the electromagnetic field is a vectorial field. It is therefore necessary to have a concept for characterizing the vector nature. For a plane electromagnetic wave, the established concept is the well-known "state of polarization". The powerful tool of representing the state of polarization is the Jones vector that has only two elements. But for a bound electromagnetic beam, it has been proven [1] that polarization is no longer a global property. Rather, it is a local property so that the direction of the electric field vector associated with a beam changes from point to point. In this paper, we will discuss the representation theory of a bound beam, paying our attention mainly to the vector description of the beam. We will show that apart from the propagation axis of a beam, another symmetry axis is identified to fully characterize the vector nature of an electromagnetic beam. This axis is usually neither parallel nor perpendicular to the propagation axis of the beam.

This work was supported in part by the National Natural Science Foundation of China (Grant 60377025), Science and Technology Commission of Shanghai Municipal (Grant 04JC14036), and the Shanghai Leading Academic Discipline Program (T0104).

REFERENCES

1. Pattanayak, D. N. and G. P. Agrawal, *Phys. Rev. A*, Vol. 22, 1159, 1980.

Electromagnetic Model for the Formation of the Sombrero Rings of Saturn

Vladimir V. Tchernyi (Cherny)
SAIBR, Osennii blvd., 20-2-702, Moscow 121614, Russia

Abstract— Since G. Galileo discovered Saturn's rings in 1610 numerous attempts to explain their origin with the use of notions about gravitation, particles' interaction with solar wind or emergence from dust plasma have not been successful. Moreover, the existing theories of the rings are characteristically heterogeneous and not united by a single physical nature of their origin. But most importantly they cannot explain a multitude of the phenomena observed. A paradoxical situation has taken shape, where, with the exception of a huge database on the properties of the rings, excellent photographs and radar data obtained by means of expensive devices on board the space probes, no full-value physical picture of the rings of Saturn existed till today.

For the first time the role of superconductivity of the space objects within the Solar system located behind a belt of asteroids is considered. Observation of experimental data for the Saturn's rings showing that the rings particles may have superconductivity.

Indeed, the Sun heats the rings weakly, the temperature in area of the rings being only around one hundred degrees above the absolute zero. And high-temperature superconductivity discovered in 1986 can already be observed under such temperatures, and in the same 1986 experimentally demonstrated superconductivity of ice.

Theoretical electromagnetic modelling demonstrates that superconductivity can be the physical reason of the origin of the rings of Saturn from the frozen particles of the protoplanetary cloud. The rings appear during some time after magnetic field of planet appears. It happened as a result of interaction of the superconducting iced particles of the protoplanetary cloud with the nonuniform magnetic field of Saturn. Finally, all the Kepler's orbits of the superconducting particles are localizing as a sombrero disk of rings in the magnetic equator plane, where the energy of particles in the magnetic field of Saturn has a minimum value.

Electromagnetism and superconductivity of the matter of the ring particles allows to explain many experimental data on land-based and space research of Saturn: how the rings came into being, how they were grouped into the disk; why the ring particles do not get mixed; why the microwaves of the circular polarization are reflected from the ring as if from a magnetic mirror; why the magnetic field is pushed out from the rings; why the spokes take shape; why non-polarized electromagnetic radiation ranging from kilohertz to megahertz emerges; where from some kind of an atmosphere appears near the rings; how density waves and bended waves take shape; why earth type planet does not have a rings, and a lot more.

It is also important fact that from electromagnetic modeling follows possibility of collide of the rings particles on the vertical direction within the width of the sombrero. It could be a reason for the formation of the particles of the bigger size due to coalescence, until gravity and centrifugal force will destroy them to the particles of smaller size again.

REFERENCES

1. Tchernyi, V. V. and E. V. Chensky, "Movements of the protoplanetary superconding particles in the magnetic field of Saturn lead to the origin of rings," *IEEE Geoscience and Remote Sensing Letters*, Vol. 2, No. 4, 445–446, 2005.
2. Tchernyi, V. V. and A. Yu. Pospelov, "About hypothesis of the superconducting origin of the Saturn's rings," *Astrophysics and Space Science*, Vol. 307, No. 4, 347–356, Springer, 2007.

Efficient Computional Technique for Size and Shape Effects in Periodic Electromagnetic Bandgap Structures of Magnetic Nanoparticles and Nanowires

Galina S. Makeeva[1], **Oleg A. Golovanov**[2], **and Martha Pardavi-Horvath**[3]

[1]Penza State University, Krasnaya, 40, Penza, 440026, Russia
[2]Penza Military Institute of Artillery, Penza-5, 440005, Russia
[3]Department of Electrical and Computer Engineering, The George Washington University
Washington, D.C. 20052, USA

Abstract— The manufacturing of microwave and photonics nanodevices, based on nanocomposite materials on magnetic nanoparticles, keeping the magnetization high and the losses low, depends on the development of CAD tools, based on the adequacy of mathematical models by solving Maxwell's equations rigorously.

The technique is based on rigorous solving of 3D diffraction boundary problems for Maxwell's equations complemented by the Landau-Lifshitz equation (including the exchange-interaction term) with the condition for the nonasymptotic radiation taking into account electrodynamical boundary conditions and additional boundary conditions, using the decompositional approach on autonomous blocks with Floquet channels (FABs) [1], whose spectra contain TEM-waves.

Accurate modeling of propagating of electromagnetic waves in periodic bandgap structures of nano-sized magnetic particles, embedded in a nonmagnetic matrix, and their interactions with magnetostatic dipole-dipole waves (MSW) and "short" dipole-exchange spin-waves (SW) were made. The dependences of scattering parameters of the multimode multi-channel S matrix from the frequency and the value of biasing magnetic field taken into account MSW and SW spectrum, when the sizes of magnetic particles are reduced to the order of exchange length, were calculated for different shapes (nanospheres and nanowires) and various separations of nanoparticles. The results of computing by FABs method permit to analyze and optimize geometries, sizes of bandgap structures and parameters of magnetic or nonmagnetic materials at microwaves and photonics.

Using this technique the reliable engineering methods applicable in CAD for the numerical computation of electromagnetic properties of magnetic nanocomposite materials, applied in the modern high nanotechnology, and 3D nanodevices may be developed.

ACKNOWLEDGMENT

The work of G. S. Makeeva and O. A. Golovanov was supported by THE RUSSIAN FOUNDATION FOR BASIC RESEARCH, Grant N 05-08-33503-a.

REFERENCES

1. Makeeva, G. S. and O. A. Golovanov, *Physics of Wave Processes and Radiotechnics Systems*, Vol. 8, No. 4, 10, 2005.

Computational Algorithm for Bifurcation Analysis of Threshold Behavior in Three-dimensional Systems of Magnetic Nanoelements

Galina S. Makeeva[1], **Oleg A. Golovanov**[2], **and Martha Pardavi-Horvath**[3]

[1]Penza State University, Krasnaya, 40, Penza, 440026, Russia
[2]Penza Military Institute of Artillery, Penza-5, 440005, Russia
[3]Department of Electrical and Computer Engineering, The George Washington University
Washington, D.C. 20052, USA

Abstract— In the goal to analyze the threshold behavior due to the instability of electromagnetic wave, magnetostatic waves (MSW) and spin-waves (SW) in 3D systems of magnetic nanoelements a special computational algorithm to determine the bifurcation points of the nonlinear Maxwell's operator (including the Landau-Lifshitz's equation with the exchange-interaction term) for the 3D boundary problem was developed.

According to the linearization principle [1], the detection of the bifurcation points of the nonlinear operator is reduced to determining the eigenvalues of the linearized operator. Using numerical methods (e.g., QR-algorithm) to solve the matrix equation eigenvalues and eigenvectors of resulting matrix were determined.

The bifurcation analysis of the parametric excitation of MSW, SW in the array of nonlinear magnetic nanoelements was developed using the bifurcation points of the nonlinear Maxwell's operator (including the Landau-Lifshitz's equation). The qualitative analysis of the stability of the numerical solution was made by using the eigenvalues of resulting matrix, because according to the Lyapunov method [2, 3] in the regions of the solution instability some real parts of complex eigenvalues are positive,

By computing of bifurcation points the threshold magnitudes of pumping wave at which nonlinear processes occur and the parametric excitation of MSW, SW in the array of magnetic nanoelements were determined. The results of the calculation of instability regions for the parametric excitation of MSW, SW depending on the bifurcation parameters, i.e., the magnitude of pumping wave and the value of biasing magnetic field, for the various separations of nanoelements are obtained taking into account constrained geometries.

ACKNOWLEDGMENT

The work of G. S. Makeeva and O. A. Golovanov was supported by THE RUSSIAN FOUNDATION FOR BASIC RESEARCH, Grant N 05-08-33503-a.

REFERENCES

1. Krasnoselskiy, M. A., *Functional Analysis*, Nauka, Moscow, 1964.
2. Lyapunov, M., *The General Problem of the Stability of Motion*, Gostehizdat, Moscow, 1950. (reprint of original thesis, 1892).
3. Lyapunov, M., *Stability of Motion*, Academic Press, New York, 1966.

Using Necessary and Sufficient Conditions for the Existence of Bifurcation Points of the Nonlinear Maxwell's Operator for the Numerical Analysis

Galina S. Makeeva[1], **Oleg A. Golovanov**[2], **and Martha Pardavi-Horvath**[3]

[1]Penza State University, Krasnaya, 40, Penza, 440026, Russia
[2]Penza Military Institute of Artillery, Penza-5, 440005, Russia
[3]Department of Electrical and Computer Engineering, The George Washington University
Washington, D.C. 20052, USA

Abstract— Using the decompositional computational algorithm to solve the nonlinear 3D diffraction boundary problems for the nonlinear Maxwell's equations [1] alone, there is a probability to miss a new second solution, appearing at the bifurcation point. That's why a special computational algorithm to determine and analyze the bifurcation points of nonlinear Maxwell's operator was developed by using the linearization of the operator and the investigation of linearized equations with the use of the characteristic determinant. The bifurcation points exist when the necessary and sufficient conditions for their existence are satisfied [2].

Let us check the necessary and sufficient conditions for the existence of a bifurcation point at the parameter's bifurcation value for an example as the bifurcation analysis of instabilities of electromagnetic waves in the resonator structure loaded with the planar ferrite.

The eigenvalues of the resulting matrix depending on the control-parameter value (the pumping-wave magnitude) were calculated for the several values of coordinate z along the length of the ferrite inclusion. As the control parameter approaches its bifurcation value (both from the left and the right), the eigenvalue determined for three values of z approaches to zero, consequently the necessary conditions are satisfied. The sufficient conditions are fulfilled because the eigenvalues are simple roots of the corresponding characteristic equation.

This algorithm permits to eliminate computational difficulties due to the uncertainty of parameters in the neighborhood of fixed points and to find the solutions of the nonlinear Maxwell's equations complemented by the Landau-Lifshitz's equation in the neighborhood of bifurcation points.

ACKNOWLEDGMENT

The work of G. S. Makeeva and O. A. Golovanov was supported by THE RUSSIAN FOUNDATION FOR BASIC RESEARCH, Grant N 05-08-33503-a.

REFERENCES

1. Makeeva, G. S., O. A. Golovanov, and M. Pardavi-Horvath, "An efficient nonlinear frequency multiplication mechanism in ferrite loaded waveguide structures," *IEEE Trans. Mag.*, Vol. 41, 3559–3561, 2005.
2. Krasnoselskiy, M. A., *Functional Analysis*, Nauka, Moscow, 1964.

Session 4P2a
Transient Effects in Electromagnetic Pulse Propagation

Transitional Characteristics of Optical Precursors between Two Different Parameter Regimes

Heejeong Jeong[1], **Ulf L. Österberg**[1], **and Tobias Hansson**[2]

[1]Thayer School of Engineering, Dartmouth College, Hanover, New Hampshire 03755, USA
[2]Department of Radio and Space Science, Chalmers University of Technology
Göteborg SE-412 96, Sweden

Abstract— Fast modulation of electromagnetic waves is important for the next generation of Tbit/s communications systems. Yet, the transient characteristics are not well understood when the fast modulation of the optical field interacts with a dispersive material. In 1914, Sommerfeld and Brillouin introduced optical precursors, transients associated with a step-modulated pulse propagating through a single Lorentz dielectric. The main purpose of their work was to show that there are no light components moving faster than the speed of light in vacuum, c [1]. Their theory has been further developed by Oughstun [2]. Brillouin and Oughstun were limited to specific parameters:

$$\omega_0 = 4 \times 10^{16}\,\mathrm{sec}^{-1},\ \omega_c = 0.25\omega_0,\ \omega_p = 1.1175\omega_0,\ \delta = 0.07\omega_0,\ z = 10^{-3}\,\mathrm{cm},$$

which has provided the conventional concepts for optical precursors as appeared in textbooks and the literature. The front of the step-modulated pulse propagates at c and is followed by a high and a low transient component before the main signal arrives. The transient parts are Sommerfeld (high-frequency component) and Brillouin precursors (low frequency component). In contrast to Brillouin's results, however, a recent study shows new characteristics of optical precursors in another regime [3]:

$$\omega_0 = 2.45 \times 10^{15}\,\mathrm{sec}^{-1},\ \omega_c = \omega_0,\ \omega_p = 1.22 \times 10^{-8}\omega_0,\ \delta = 1.22 \times 10^{-6}\omega_0,\ z = 0.2\,\mathrm{cm}.$$

In this regime, referred to as the resonant precursor regime, all components arrive almost instantaneously with an instantaneous frequency chirp which produces a 100% transmission peak immediately after the arrival of the front [3]. In this paper, we investigate transitional characteristics of optical precursors between these two different parameter regimes: Brillouin's regime and the resonant precursor regime. The arrival time of each field component and frequency chirp are investigated by changing the following parameters; carrier frequency ω_c, plasma frequencyp ω_p, and medium resonance width δ. To investigate transitional behaviors in a numerically accessible way, we consider the medium resonant frequency in the optical regime rather than in the UV regime. To evaluate the transmitted field and the transient frequency chirp, we use the Fast-Fourier Transform (FFT), Finite-Difference Time-Domain (FDTD), and the asymptotic steepest descent method.

REFERENCES

1. Brillouin, L., *Wave Propagation and Group Velocity*, Academic Press, New York, 1960.
2. Oughstun, K. E. and G. C. Sherman, *Electromagnetic Pulse Propagation in Causal Dielectrics*, Springer-Verlag, Berlin, 1994.
3. Jeong, H., A. M. C. Dawes, and D. J. Gauthier, "Direct observation of optical precursors in a region of anomalous dispersion," *Phys. Rev. Lett.*, Vol. 96, 143901, 2006.

The Effect of Conductivity on the Brillouin Precursor

Natalie A. Cartwright[1] **and Kurt E. Oughstun**[2]

[1]State University of New York at New Paltz, New Paltz, NY 12561, USA
[2]University of Vermont, Burlington, VT 05405, USA

Abstract— Ultrawideband pulses that propagate through dielectric materials have been shown to give rise to a so-called Brillouin precursor whose peak amplitude point only decays algebraically with propagation distance rather than exponentially (N. A. Cartwright and K. E. Oughstun, SIAM Review, 4, 2007). This unusually slow decay rate of the Brillouin precursor is highly desirable in radar applications where the material being interrogated is highly absorptive or in applications that require long interrogation distances. However, many physical applications require propagation of electromagnetic signals through conductive material.

In a dispersive medium, the angular frequency dependence of the electronic response of the material to an applied electromagnetic signal is given by the complex permittivity $\epsilon_c(\omega) = \epsilon(\omega) + i\sigma(\omega)/\omega$, where $\epsilon(\omega)$ and $\sigma(\omega)$ are the temporal frequency spectra of the dielectric permittivity and electric conductivity, respectively. In a purely dielectric material, $\sigma(\omega) \equiv 0$ and $\epsilon_c(\omega) = \epsilon(\omega)$ is analytic at the origin $\omega = 0$, the very point that provides the slow decay rate of the Brillouin precursor. In a conductive material, $\sigma(\omega) \not\equiv 0$ and $\epsilon_c(\omega)$ possesses a pole at the origin. The presence of this pole calls into question the existence and decay rate of the Brillouin precursor. Here, we study the propagation of a step-function modulated sine wave through two types of conductive material: the first is a Debye model with static conductivity; the second is a lossy plasma as described by the Drude model. Our method of analysis is an asymptotic approximation to the integral representation of the propagated field. This analysis provides a closed-form approximation of the Brillouin precursor which we then use to study the decay rate of its peak amplitude point as a function of propagation distance. We find that the peak amplitude point of the Brillouin precursor decays exponentially through the Debye model medium with static conductivity, and that this decay rate increases with increasing levels of conductivity. For Drude model material, we find that the peak amplitude point of the Brillouin precursor decays exponentially for small propagation distances, but algebraically for large propagation distances.

Comparison of Optical Pulse Propagation in Water and Acetonitrile

Marc Currie
Naval Research Laboratory, USA

Abstract— Optical propagation in water has been studied primarily by light sources that have either a constant amplitude in time or have a modulated temporal width greater than a picosecond. Attenuation of light as it propagates through water has been experimentally measured throughout the optical spectrum with these light sources. Quantities such as absorption and scattering have been thoroughly characterized as a function of wavelength of light. Yet with this wealth of measurements, a model that describes the transparency of water in the visible region still does not exist. The reason has been attributed to the complexity in understanding the hydrogen bonding that occurs in water [1].

Recently, an experimental study challenged the well established empirical knowledge of attenuation in water at near-infrared wavelengths. The study examined propagation of ultrafast optical pulses in water and demonstrated increased transmission of ultrafast light pulses as compared to longer pulses or cw light [2]. In these experiments, pulses as short as 60 fs with a center wavelength of 800 nm were propagated through as much as 6 meters of water. To explain their observations, the authors suggested the possibility of light propagation by optical precursors. The question is: How and why were the optical precursors stimulated in the water?

To better understand the propagation of ultrafast pulses of light in water, as demonstrated by Fox and Österberg [2], we will compare measurements in water with those in acetonitrile. Both water and acetonitrile are polar solvents, but water molecules exhibit hydrogen bonding while acetonitrile molecules do not. In addition, this study will compare the differences of the OH bond in water with the CH bond in acetonitrile. Harmonics of these molecular stretching frequencies in the near-infrared region are explored with a femtosecond laser system.

REFERENCES

1. Tokmakoff, A., "Shining light on the rapidly evolving structure of water," *Science*, Vol. 317, 54–55, 2007.
2. Fox, A. E. and U. Österberg, "Observation of sub-exponential absorption of ultra-fast pulses in water," *Optics Express*, Vol. 14, 3688–3693, 2006.

Propagation of 100-fs Laser Pulses on-and-off Water Resonances in the NIR

David Lukofsky, **Heejeong Jeong**, **Jonathan Bessette**, **and Ulf Österberg**
Thayer School of Engineering, Dartmouth College, Hanover, New Hampshire 03755, USA

Abstract— We study the experimental decay of ultrashort pulses in water, in the context of ultimately improving communication/imaging schemes. Wavelength range of incident radiation spanned 730 nm–840 nm, to determine experimentally if water's vibrational overtones introduce coherent quantum effects that produce deviation from Broadband Beer's law. Experimental data suggests that coherent effects are difficult to distinguish for on-and-off resonance 100-fs pulses, and that pulses with width ∼10-fs need to be investigated.

Introduction: Beer law deviations in the linear regime may be observed if (1) The pulse width is smaller, comparable, or even *slightly larger* than the response time of the medium, and (2) The frequency of incident radiation is on resonance with respect to one of the medium's resonances [1]. Thomas and Fournier, using entirely different approaches, concluded that water's response time is on the order of ∼10 fs [2, 3] As well, the overtones of the stretching band of water create resonances in the NIR around 739 nm and 840 nm [3]. This study presents the results of an experiment where 100-fs pulses (SpectraPhysics MaiTai system) were sent through 7 meters of water at wavelengths 730–840 nm in 5 nm increments. This corresponds to on-and-off resonance cases.

Experimental and Simulation Results: Figure 1 shows the absorption curve at the 739 nm resonance — one of the 12 absorption curves gathered during the experiment (12 distinct wavelengths). The solid line represents the absorption function for monochromatic light according to Segelstein's absorption coefficient [4]. The stars are experimentally gathered results.

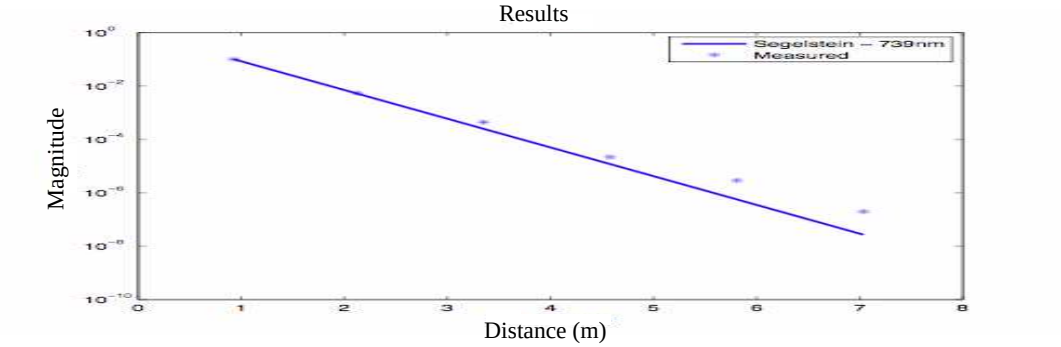

Figure 1: Experimental and theoretical decay of 739 nm, 100-fs pulse.

Discussion: Although deviation from purely exponential decay is observed, the change may not be sufficient to discern coherent interaction effects. This algebraic decay is mainly the result of broadband Beer's law. Current experiments involve using a ∼10 fs pulse to determine if quantum effects can be distinguished from Broadband Beer's law, in which case serious applications to medical imaging and communications can be considered.

ACKNOWLEDGMENT

We acknowledge the financial support of NIST through grant # 60NANB4D1142.

REFERENCES

1. Crisp, M. D., "Propagation of small-area pulses of coherent light through a resonant medium," *Physical Review A*, 1970.
2. Thomas, M. E., "Atmospheric gases and particles, solid-state components, and water," *Optical Propagation in Linear Media*, Oxford University Press, 2006.
3. Fournier, G. R., "Model of the anomalous absorption spectrum of pure water for femtosecond laser pulses," *18th Ocean Optics Conference Proceedings*, Montreal, 2006.
4. Segelstein, D., "The complex refractive index of water," Master's thesis, University of Missouri-Kansas City, 1981.

Ultrawideband Dispersive Pulse Propagation in Double-resonance Lorentz Model Dielectrics

K. E. Oughstun
College of Engineering & Mathematical Sciences, University of Vermont, USA

Abstract— The propagation of an ultrawideband electromagnetic pulse through a linear, dispersive attenuative dielectric medium described by the Lorentz model with two isolated resonance frequencies is presented in the context of the classical [1–3] and modern asymptotic theories [4] as generalized by Shen and Oughstun [5]. This earlier asymptotic description [5] showed that the inclusion of an additional resonance feature in the dispersive medium resulted in the conditional appearance of a new, intermediate frequency precursor field structure in addition to the high-frequency Sommerfeld and low-frequency Brillouin precursor fields described in the classical and modern theories. A sufficient condition for the appearance of this middle precursor was also given there [5] in terms of the energy transport velocity for a time-harmonic wave. These results are extended in this paper through a careful examination of the middle saddle point dynamics and their asymptotic contribution to the middle precursor field. The critical importance of these middle saddle points is fully realized when the input pulse spectrum is centered in the passband between the two resonance frequencies, as typically occurs for optical pulses. In that case these middle saddle points provide the majority of the observed pulse distortion.

ACKNOWLEDGMENT

The research presented in this paper was supported, in part, by the United States Air Force Office of Scientific Research under Grant #9550-04-1-0447.

REFERENCES

1. Sommerfeld, A., "Über die fortpflanzung des lichtes in disperdierenden medien," *Ann. Phys.*, Vol. 44, 177–202, 1914.
2. Brillouin, L., "Über die fortpflanzung des licht in disperdierenden medien," *Ann. Phys.*, Vol. 44, 203–240, 1914.
3. Brillouin, L., *Wave Propagation and Group Velocity*, Academic Press, New York, 1960.
4. Oughstun, K. E. and G. C. Sherman, *Electromagnetic Pulse Propagation in Causal Dielectrics*, Springer-Verlag, Berlin-Heidelberg, 1994.
5. Shen, S. and K. E. Oughstun, "Dispersive pulse propagation in a double-resonance Lorentz medium," *J. Opt. Soc. Am. B*, Vol. 6, No. 5, 948–963, 1989.

Conception and Realization of the Manual and Programmable Command of Stimulating Electric Muscular

S. Bri[1] and L. Zenkouar[2]

[1]Microwave and Materials Group, ESTM, B. P. 3103, Meknès, Maroc
[2]Electronics and Telecommunications Laboratory, EMI, B. P. 765, Rabat, Maroc

Abstract— The objective of this work is to propose a reliable solution allowing restoring deficient functions of the nervous system. This solution passes by an artificial control of certain nervous information in the human body. The objective of the works presented in this paper is to propose a circuit of electric stimulation allowing the contraction of the muscle to restore its function by the generation of an electric signal. Its basic principle rests on the generation of more or less wide impulses and very specific frequency. This solution avoids a habituation of the muscle, an unwanted coetaneous ionization or a polarization of the metal prostheses.

Session 4P2b
Scattering and Rough Surface Problem

Feature Extraction and Classification of Wide Angle Optical Scattering Patterns from Single Aerosol Particles

Giovanni Franco Crosta[1] **and Gustavo Eddino Fernandes**[2]

[1]Dipartimento di Scienze dell'Ambiente & Territorio, Univ. Milan-Bicocca, Milan, Italy
[2]Department of Applied Physics, Yale Univ., New Haven, CT 06520, USA

Abstract— The aim of this investigation is to discriminate between elastic light scattering patterns produced by reference materials, namely clusters of polystyrene (*PSL*) spheres, and by spores of *Bacillus globigii* (*Bg*), a known simulant of anthrax. *TAOS* (two-angle optical scattering) is an experimental technique which records the intensity patterns of laser light scattered by single aerosol particles over an extended range of the scattering angles θ and ϕ [1]. Particles are produced at a controlled rate and illuminated by a Q-switched Nd:YAG laser at $\lambda = 532\,\text{nm}$. The *TAOS* patterns are recorded by an intensified *CCD* camera and stored for off-line processing. Typical patterns from *PSL* aggregates and *BG* spores are shown in Figures 1 and 2, respectively. Since in this context deterministic obstacle inversion is impossible, pattern recognition is a must. The pattern classifier under development consists of four stages. *1)* Pre-processing. *2)* Feature extraction by spectrum-enhancement [2]. *3)* Training, in which principal component (*PC*) analysis is applied to features extracted from a training-set (T) of images and classification is rated

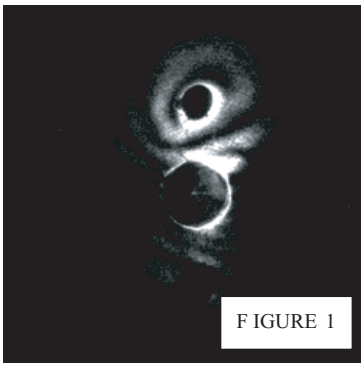

Figure 1: Scattering pattern of a polystyrene (*PS*) sphere aggregate.

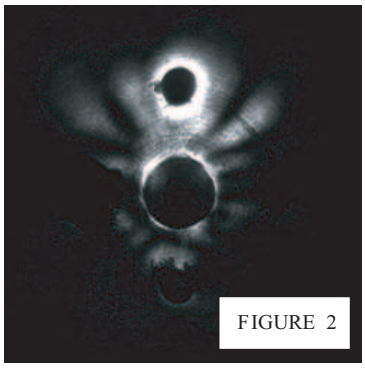

Figure 2: Scattering pattern of *Bacillus globigii* (*Bg*) spores.

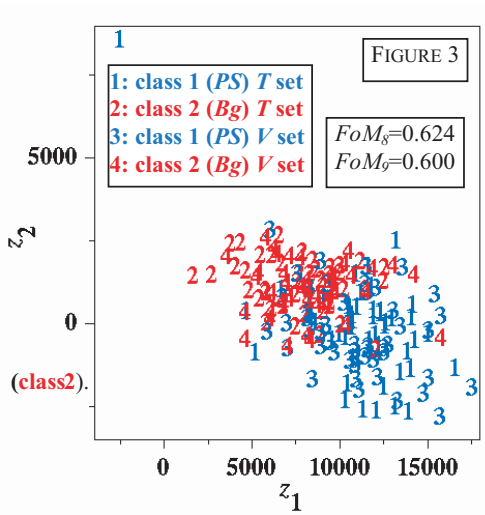

Figure 3: Classifier output: Representation of *TAOS* patterns on the plane of the first two *PCs*, z_1 and z_2.

by the following figure of merit (FoM):

$$FoM_8 = \frac{1}{2} + \frac{1}{2M_T} \sum_{m=1}^{M_T} \sum_{\substack{j=1 \\ j \neq i[m]}}^{2} \frac{d_{m,\,j} - d_{m,\,i}}{d_{j,\,i[m]}}. \tag{1}$$

Here M_T is the number of patterns in the T set, $i[m]$ is the class, 1 or 2, to which pattern m is known to belong and $d_{m,\,j}$ is the distance from pattern m to the class (i or j) centroid. *4)* Validation, rated by FoM_9, a figure of merit where M_V, the number of patterns in the validation (V) set, replaces M_T of FoM_8. A typical classification result, which corresponds to $FoM_8 = 0.624$ and $FoM_9 = 0.600$ is shown in Figure 3. Feature extraction depends on a few parameters. The latter are optimized via the $FoMs$. Sensitivity of results to T and V set composition is assessed by swapping patterns between T and V sets and then repeating classification. The above described classifier can be applied to $TAOS$ patterns in real-time.

REFERENCES

1. Fernandes, G. E., Y.-L. Pan, R. K. Chang, K. Aptowicz, and R. G. Pinnick, "Simultaneous forward- and backward-hemisphere elastic-light-scattering patterns of respirable-size aerosols," *Opt. Lett.*, Vol. 31, 3034–3036, 2006.
2. Crosta, G. F., C. Urani, and L. Fumarola, "Classifying structural alterations of the cytoskeleton by spectrum enhancement & descriptor fusion," *J. Biomed. Optics*, Vol. 11, 2, 024020:1–18, 2006.

Carbothermal Reduction of Magnetite — Carbon Black Composites Using Microwave Heating

K. Ishizaki, **S. Vaucher**, **Y. Y. Pittini**, **M. Stir**, **and R. Nicula**

EMPA — Materials Science and Technology, Feuerwerkerstr. 39, Thun 3602, Switzerland

Abstract— Microwave heating provides an efficient energy saving alternative for the carbothermic reduction of magnetite ore concentrates. Conventional reduction processes proceed at higher temperatures and at comparatively much slower reduction rates. Thus considerable attention is nowadays given to microwave-assisted carbothermic processes related to the treatment of steelmaking slags, e.g., for iron and phosphor recovery and recycling. A detailed analysis is here provided on the structural phase evolution of iron and of its oxides during the thermal reduction of magnetite — carbon black powder mixtures under microwave irradiation. The progress of the reduction was examined by XRD analysis of reaction products at various temperatures. The reduction of magnetite to wustite and in some cases, even directly to iron was observed to occur from at least a measured temperature of 400°C which in conventional heating never happens at such a low temperature. The ex-situ structural and compositional studies are for the first time complemented by time-resolved synchrotron radiation powder diffraction experiments performed *in-situ* during microwave heating. At first, the concurrent process of magnetite oxidation under microwave heating in air was investigated in more detail, in view of its relevance to the overall efficiency of the carbothermal reduction process.

Wave Structure Functions of Multiply Scattered Electromagnetic Waves by Anisotropic Magnetized Turbulent Plasma Layer

G. V. Jandieri[1], A. Ishimaru[2], V. G. Jandieri[3], A. G. Khantadze[1]
I. B. Shirokov[1], Yu. B. Gimpilevich[1], and Zh. M. Diasamidze[1]

[1]Physics Department, Georgian Technical University, Georgia
[2]Department of Electrical Engineering, University of Washington
FT-10 Seattle, Washington 98195, USA
[3]Department of Electrical and Computer Engineering, Kumamoto University, Japan

Abstract— In the last years scintillation has found many applications in Radio-astronomy, Space Weather Program, Space-based radar systems and the observed diverse phenomena have provided a powerful stimulus to theoretical developments. The ionospheric scintillation study comes from its significant impact on satellite radio communications. Power spectral studies of amplitude and phase scintillations is used to obtain information about the power spectrum of ionospheric irregularities, which give rise to a variety of scintillation phenomena, as well as to the irregularity drift speeds transverse to the signal path. Second moments of both amplitude and phase fluctuations of a radio wave signal received on the ground, have proved to be useful for obtaining information about the outer scale of the irregularities or the root mean square deviation of electron density from the background value along the signal path.

Statistical characteristics of the angular power spectrum (APS) (broadening and displacement of its maximum) of multiply scattered electromagnetic waves by plane layer of turbulent anisotropic magnetized collisional plasma are considered. The analysis of these statistical characteristics is related to fluctuations in the radio refractive index in the F-region. The expression for the fluctuating term of the complex phase at the observation point has been obtained in the complex geometrical optic approximation. The transverse correlation function of complex phase fluctuations taking into account the fact that the observation points are spaced apart at a very small distance is considered in complex geometrical optics approximation. The correlation function of the complex field (spatial coherence function) written between the two observation points located on the line normal to the layer and the analytical expression for the APS, which is of great practical importance, are considered for the arbitrary correlation function of electron density fluctuations. The power spectrum and the scintillation level are computed in this section too. The displacement of the spatial power spectrum of the received radiation caused by random irregularities and the widths of this spectrum in the principle and perpendicular planes for anisotropic Gaussian correlation functions of electron density fluctuations, taking into account both factor of anisotropy of irregularities and the angle of inclination of irregularities with respect to the external magnetic field are analyzed. The influence of the distance, both from the emitter to the boundary of the plane layer of the anisotropic turbulent plasma, and from another plasma layer boundary to the receiver, the factor of anisotropy and the angle of inclination of irregularities with respect to geomagnetic field on the statistical characteristics of multiply scattered radiation are studied for F-region of the ionosphere. Variance of the phase fluctuations and the behaviour of scintillation level are numerically calculated. Oscillation minimums of the power spectrum of the intensity fluctuations are in a good agreement with experiment. The action of the Fresnel filter can be used to estimate the height of the irregularities and location of both the transmitter and the receiver relative to the scattered layer. The fact that scintillation is caused by the interference of waves scattered from different portions of the incident wavefront implies that it may also be used to measure the coherence of the incident wave field, which gives information about the angular structure of the radio source. The established patterns can be useful for communication channel modeling and for some remote sensing purposes.

Structural functions of amplitude and phase fluctuations and mutual correlation functions have been calculated for different wave frequencies. Numerical calculations have been carried out for F-region of an ionosphere.

A Circulant Preconditioned Banded Matrix Iterative Method for EM Scattering from Randomly Rough Surfaces

Y. Du[1] and J. A. Kong[2]

[1]The Electromagnetics Academy, Zhejiang University, Hangzhou 310058, China
[2]Department of Electrical Engineering and Computer Science
Massachusetts Institute of Technology, Cambridge, MA 02139, USA

Abstract— In this paper we present a circulant preconditioned banded matrix iterative approach for EM scattering from randomly rough surfaces. It adopts a different matrix splitting, which results in a complex Toeplitz matrix on the left side of the linear system. This proposed method possesses similar convergence properties to BMIA for the outer iteration. However, for the inner iteration, CP-BMIA shows improved performance. Unlike the situation for BMIA where little can be said about either the existence of convergence or the convergence rate of the linear system, CP-BMIA takes advantage of the Toeplitz structure to solve the linear system in $O(\beta \log N + 1)$ steps by alternatively solving the normalized circulant-preconditioned system. Numerical simulations are presented to illustrate the effectiveness of the proposed method.

Electromagnetic Detectability of the Oil Slicks on a Sea Surface in Bistatic Configuration

A. Coatanhay and C. Gervaise
Laboratory E3I2, EA 3876, ENSIETA, 29806 Brest Cedex 9, France

Abstract— The detection of the oil slicks on the sea surface is a very important issue for coastal pollution prevention and for the identification of illegal discharges. The present paper deals with the electromagnetic wave scattered by a polluted (oil) sea surface as a function of weather conditions (wind speed and direction) in bistatic configuration. More precisely, we study the influence of the weather conditions and the physical parameters of the pollutant (dielectric and mechanical properties) upon the detectability of a pollutant spreading film.

Indeed, we introduce a physicochemical-hydrodynamics model [1] to estimate the ripple damping caused by the pollutant. In this study, we assume that the pollutant is insoluble. Knowing the roughness spectrum of a clean sea water (Elfouhaily sea spectrum) for any wind speed and wind direction, we are able to generate realistic polluted sea surfaces (1-D). Then, applying the forward-Backward method, we compute the electromagnetic field scattered by this polluted surface. It is important to note that, in its original formulation [2], the Forward-Backward method only applies to scattering from perfectly conducting surfaces. But, in the present paper, the Forward-Backward method take into account the dielectric properties of the pollutant [3].

Finally, using a Monte carlo approach, we can determine the statistical characteristics of the scattered field for polluted and clean sea surface and for different polarisations (vertical and horizontal). With the nean value and the standard deviation, we can establish a contrast criterion between polluted and unpolluted sea. Based on these results, we can evaluate the detectability of the pollution in various bistatic configuration. This study was done for different weather conditions (wind speed and wind direction), for different sea water salinities and for different pollutants.

REFERENCES

1. Fiscella, B., P. P. Lombardini, and P. Trivero, "Ripple damping on water surface covered by a spreading film: Theory and experiment," *Il Nuovo Cimento*, Vol. 8C, No. 5, 491–500, 1985.
2. Holliday, D., L. L. de Raad, and G. C. St-Cyr, "Forward-backward: A new method for computing low-grazing angle scattering," *IEEE Trans. Antennas Propagat.*, Vol. 44, No. 5, 722–729, 1996.
3. Lastname1, F. M., "Forward-backward method for scattering from dielectric rough surfaces," *IEEE Trans. Antennas Propagat.*, Vol. 50, No. 7, 901–911, 2002.

Surface Integral Scattering Formulation for the EM Wave Scattering from 3D Particles of Arbitrary Shape: Surface Plasmon Resonances in Metallic Nanoantennas

R. Rodríguez-Oliveros, V. Giannini, and J. A. Sánchez-Gil

Instituto de Estructura de la Materia, Consejo Superior de Investigaciones Científicas
Serrano 121, Madrid, Spain

Abstract— We develop theoretically and numerically a rigorous method to investigate the EM wave scattering from 3D objects with arbitrary surfaces and dielectric function. The formulation is based on the surface integral equations for the electric and magnetic fields given by the Stratton-Chu formulas [1]. The integral equations are generalized for a 3D object with its surface in parametric coordinates (recently derived for 2D objects in Ref. [2]). The electric and magnetic fields are expressed in terms of two tangential components to the surface and a normal one, in order to get physical insight into the induced surface currents and charges. In fact, it is shown that the surface integral equations are remarkably simplified if the parametric coordinates are chosen so that an orthonormal basis can be defined on the surface. This simplification is in turn crucial in the numerical implementation of the surface integral scattering equations, converted into matrix equations for the surface EM field components by discretizing the surface through a quadrature scheme. Finally, it should be emphasized that this formalism straightforwardly allows one to deal with an arbitrary number of scatterers and shapes, with the advantage that it scales with the scatterer surface (rather than its volume).

In particular, this method will be exploited to investigate surface plasmon resonances in complex 3D metallic nanoparticles, obtaining scattering cross sections, near-field maps and surface charge distributions as done for 2D nanoparticles (nanowires) in Ref. [2]. If a point dipole source is considered instead of a plane wave, single molecule fluorescence (and/or quantum dot emission) close to metallic nanoantennas can be thoroughly explored by calculating radiative and nonradiative decay rates (and quantum yields), addressing crucial issues as the modification and enhancement (or quenching) of spontaneous emission in (bio)molecular and optoelectronic systems due to the strong impact on the local EM density of states of surface plasmon resonances in dimer nanoantennas [3].

REFERENCES

1. Tran, P. and A. A. Maradudin, *Opt. Commun.*, Vol. 110, 269–273, 1994.
2. Giannini, V. and J. A. Sánchez-Gil, *J. Opt. Soc. Am. A*, Vol. 24, 2822–2830, 2007.
3. Muskens, O. L., V. Giannini, J. A. Sánchez-Gil, and J. Gómez Rivas, *Nano Lett.*, Vol. 7, 2871–2875, 2007.

Electromagnetic Waves Propagation above Rough Surface: Application to Natural Surfaces

O. Benhmammouch, L. Vaitilingom
A. Khenchaf, and N. Caouren

Laboratoire E^3I^2-EA3876 ENSIETA, Ecole Nationale Supérieure des
Ingénieurs des Etudes et Techniques de l'Armement
2 rue Franois Verny 29806, Brest cedex 9, France

Abstract—

Introduction: Because of their independence at meteorological conditions, electromagnetic instruments are often used to study natural surfaces. This paper treats of electromagnetic waves propagation above natural rough surfaces. We divide our study on two sides. First of all, we expose the parabolic equation (PE) method for electromagnetic waves (EMW) propagation and the characterisation of both the medium and the surface. Then, in order to model the influence of rough surfaces in EMW propagation, we introduce a new method based on surface generation using spectrum. Finally we show numerical results and give some perspectives.

Electromagnetic Propagation Methods: Among EMW propagation's models (geometrical optic [1], moments method [2], parabolic equation [3, 4] ...),we will use parabolic equation. This method is easy to solve and to implement unless burdensome conditions in terms of boundary and mesh conditions. We resolve this equation using split step Fourier method (SSF). To take into account wave reflection by surface, we employ the method of image source. To satisfy Sommerfeld radiation conditions (toward infinity), we add, beyond maximum height, an absorption area where the field is multiplied by an attenuation function.

Propagation Medium and Surface Characterisation: The most influent parameter in EMW propagation in the troposphere is refraction index. This parameter depends on temperature, pressure and partial pressure of steam. The surface is characterized by Fresnel coefficients which are function of conductivity and permittivity. For maritime surface, we use Debye model [12] to characterize these parameters knowing temperature, salinity of the surface and frequency of incident wave in X-band. In the case of snowy surface, we use Ozawa & Kuroiwa [5] model which express permittivity in Xband. This parameter is function of the incident wave's frequency, surface's temperature and surface's composition. The complexity of terrestrial surface imposes the use of semi-empirical models. Topp model [7] quantifies permittivity of the ground in function of humidity rate for low frequency (20 MHz–1 GHz) of incident wave. For higher frequencies (1 GHz–17 GHz), we use Dobson-Peplinsky model [6] which depends on incident wave's frequency, surface's temperature and surface's composition.

Rough Surfaces: In aim to observe the influence of terrestrial clutter in EMW propagation, we introduce a new method which consists on generating a ground surface using a Gaussian spectrum [13], or a maritime surface using Elfouhaily [9] spectrum, and a Monte-Carlo simulation [10]. Once the surface created, the EMW is propagated using the method introduced by Mc Arthur and Bebbington [11]. This method allows us to model the effects of surface geometry as well as physical parameters in EMW propagation.

Numerical Results: In this paper, the development of a new approach for the modelling of rough surfaces influence is presented as well as the numerical results computed for different surfaces, source's heights and different atmospheric conditions. To generate the sea surface, we use a Elfouhaily spectrum and for ground and snowy surfaces, we use Gaussian spectrum. The results are used to show the influence of natural surface's geometry in electromagnetic waves propagation.

Conclusion and Perspectives: The main purpose of this paper is to introduce the surface roughness in simulations of electromagnetic waves propagation above natural surfaces. For this we introduced an original method based on generation of surfaces by means of Gaussian spectrum and a Monte-Carlo simulation. An evolution modelling will be the implementation of this method in a tri-dimensional propagation domain in presence of different types of natural surfaces.

REFERENCES

1. Durand, J. C., "Optique géométrique et diagramme de portée Radar en atmosphère satandard," *Revue Technique Thomson*, Vol. 20–21, No. 1, Mars 1989.

2. Fournier, M., "Méthodes d'évaluation de l'effet des conduits d'évaporation à la surface de la mer," *AGARD Meeting, 'Multi Mechanism Propagation Paths'*, Neuilly sur Seine, France, Octobre 1993.
3. Craig, K. H. and M. F. Levy, "Parabolic equation modelling of the effect of multipath and ducting on radar systems," *IEE Proc.*, Vol. 138, No. 2, 153–162, April 1991.
4. Douchin, N., S. Bolioli, F. Christophe, and P. Combes, "Etude théorique de la caractérisation radioélectrique du conduit d'évaporation," *49th Proc. Symposium Int. Agard Remote Sensing of the Propagation Environment*, CESME-Izmir, Turkey, December 1991.
5. Khenchaf, A., "Bistatic scattering and depolarization by randomly rough surfaces: Application to the natural rough surfaces in x-band," *Waves in Random Media*, Vol. 11, 61–89, 2001.
6. Dobson, M. C., F. T. Ulaby, M. T. Hallikainen, and M. A. El-Rayes, "Microwave dielectric behavior of wet soil — Part II — Dielectric mixing models", *IEEE Trans. GRS*, Vol. 23, No. 1, 35–46, 1985.
7. Topp G. C., J. L. Davis, and A. P. Annan, "Electromagnetic determination of soil water content: Measurements in coaxial transmission lines," *Water Ressources Research*, Vol. 16, No. 3, 574–582, 1980.
8. Ozawa, Y. and D. Kuroiwa, "Dielectric properties of ice, snow and supercooled water microwave propagation in snowy districts," *Monograph Ser. Res. Inst. Appl. Electricity*, No. 6, 31–71, ed. Y. Asami, Hokkaido University, Sapporo, 1958.
9. Elfohaily, T., B. Chapron, K. Katsaros, and D. Vansdermark, "A unified directional spectrum for long and short wind-driven waves," *MTS/IEEE Conference Proceedings Oceans'97*, Vol. 102, No. C7, 15781–15796, July 15, 1997.
10. Bein, G. P., "Monte carlo computer techniques for one-dimensional random media," *IEEE Transactions on Antennas and Propagation*, Vol. 21, No. 1, 83–88, January 1973.
11. Mac Arthur, R. J. and D. H. O. Bebbington, "Diffraction over simple terrain obstacles by the method of parabolic equation," *ICAP91, IEE Conf. Pub.*, No. 333, 2824–2827, 1991.
12. Klein, L. and C. Swift, "An improved model for the dielectric constant of sea water at microwave frequencies," *IEEE Journal of Oceanic Engineering*, Vol. 2, No. 1, 104–111, Januaray 1977.
13. Brown, G., "Backscattering from a Gaussian-distributed perfectly conducting rough surface," *IEEE Transactions on Antennas and Propagation*, Vol. 26, No. 3, 472–482, May 1978.

Session 4P3
Microelectronic Packaging 2

An Analytical Method to Calculate via Capacitance

Yaojiang Zhang and Jun Fan

Department of Electrical and Computer Engineering
Missouri University of Science and Technology, Rolla, MO 65401, USA

Abstract— Equivalent circuit model of vias are essential for signal integrity analyses in a multilayer package or printed circuit board (PCB). A physics-based circuit model, as shown in Fig. 1, for a via portion between a pair of plates (or planes) contains via-plate capacitances as well as Zpp, the impedance of the parallel plates. While Zpp has been extensively studied using the cavity model with segmentation method, few efforts have been made for the evaluation of the via-plate capacitances. Previous research often resorts to numerical methods with electrostatic approximations. Although these methods are accurate, they are difficult to be implemented into a circuit simulator.

To address this problem, an efficient analytical formula is derived to calculate the via barrel-plate capacitance. The Green's function inside a bounded coaxial cavity for a concentric magnetic ring source is first derived, by introducing the reflection coefficients for cylindrical waves at the inner and outer cavity walls. These walls can be perfect electric/magnetic conductors (PEC/PMC) or non-reflective perfectly matched layer (PML). By further assuming a magnetic frill current in the via anti-pad aperture, an analytical formula is derived for the via barrel-plate capacitance by summing the higher-order modes in the bounded coaxial cavity. The formula converges very fast with the number of modes as well as with the radius of the outer perfect electric/magnetic conductor (PEC/PMC) walls. The analytical formula is validated by the comparisons with the results obtained using quasi-static numerical methods as well as measurements. Furthermore, the formula allows the investigation of the frequency dependence of the via-plate capacitance, which is not possible with quasi-static methods.

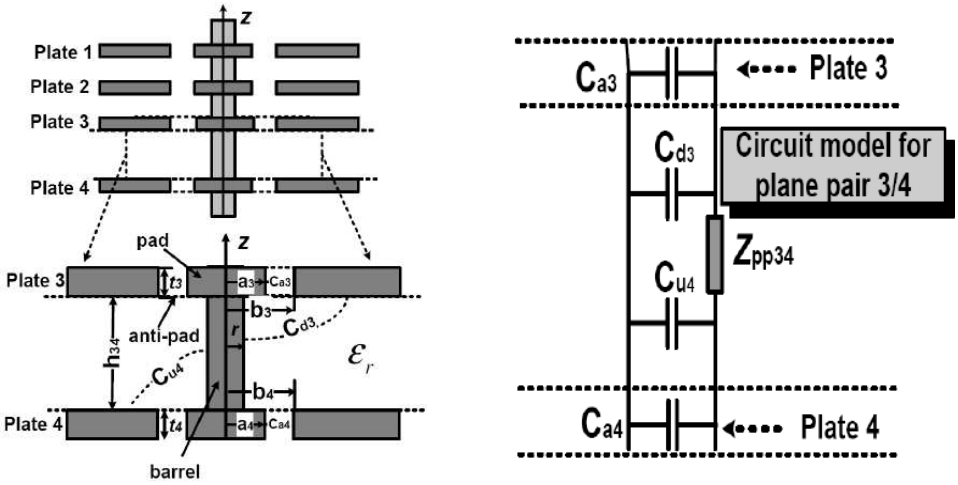

Figure 1: (a) A signal via in a multilayer parallel-plate structure; and, (b) equivalent circuit model for the via portion between Plates 3 and 4.

A Hollow Dielectric Pipe Admittance Tunnel for the Evaluation of Printed Circuit Board Dielectrics

R. E. Diaz, **M. Shen**, **and R. Ormeno**
Ira A. Fulton School of Engineering, Department of Electrical Engineering
Arizona State University, USA

Abstract— Low loss — Low dielectric constant dielectric substrates must be accurately characterized to identify and eliminate as many sources of loss and dispersion as possible in Printed Circuit Board applications. This need extends from the GHz range up to and beyond 50 GHz where traditional dielectrometry approaches become difficult because of the smallness of the wavelength. Since the circuit signals of interest at these frequencies propagate as guided electromagnetic (TEM) waves there are two major contributors to the loss and dispersion: the metal trace itself and the substrate. Therefore when optimizing the substrate, any measurement of the complex dielectric constant (permittivity, ε'-$j\varepsilon''$) must separate the loss due to metal from the loss due to the substrate. The dielectric constant is typically anisotropic, especially when the board is a glass-fiber reinforced composite, with the value normal to the surface of the substrate as the key factor in determining the propagation properties of the substrate. Therefore the challenge is: to measure a thin dielectric substrate (of the order of 1 mm thick) with dielectric loss tangents ($\varepsilon''/\varepsilon'$) in the range of 0.001 in such a way as to obtain the permittivity normal to the surface with a broad band test method scalable to the mm wave range.

After a brief introduction to the various experimental techniques that can be applied to measure these properties (and evaluation of their pros and cons) the features of a new measurement set-up based on a hollow dielectric pipe surface waveguide are discussed. The new set-up functions as an admittance tunnel with two unique features: (i) The wave does not travel in free space but rather is guided as a quasi-TEM mode in the interior of the pipe. The plane wave qualities of this mode result in broad band operation that can be readily scaled up to mm waves. (ii) The material sample is inserted sideways into the pipe so that it is "edge on" to the wave. This orientation almost completely eliminates any scattering from the beginning and end of the sample at the same time that it orients the electric field normal to the surface of the substrate. The weak interaction between the wave and the sample means the sample only perturbs the waveguide and yet since the sample can be long (nominally 4 to 8 inches) it allows this interaction to accumulate over a long enough distance for a vector network analyzer to extract amplitude and phase information well above the noise floor.

Both the results of fullwave simulations and experiments are presented to demonstrate the application of this test device to materials of interest. The real part of the dielectric constant is, of course, the easiest to measure. The loss is more difficult, yet still within the capabilities of present day network analyzers.

Rough Surface Effect on Power Absorption by Signal Traces: Modeling Wave Propagation in a Randomly Rough Parallel Plate Waveguide

Ruihua Ding[1], **Leung Tsang**[1], **and Henning Braunisch**[2]

[1]Department of Electrical Engineering, University of Washington
Box 352500, Seattle, WA 98195, USA
[2]Intel Corporation, Components Research, Chandler, AZ 85226, USA

Abstract— In microelectronic packages, the interface between signal traces and dielectric substrate is often roughened to improve adhesion. However, the rough surface at the interface leads to additional signal distortion due to attenuation when the skin depth on the signal trace is comparable to the rough surface height at multi-gigahertz frequencies.

To study the effects of a random rough surface on the signal, a parallel plate waveguide model excited by a line source is developed and analyzed. The random rough surface is characterized as a statistical stationary random process. Since the variations in the surface roughness are relatively small compared to the wavelength, the second order perturbation method is applied to calculate the power propagation in the waveguide. The propagated power of the coherent wave is expressed in terms of a double Sommerfeld integral. An approximation of the double Sommerfeld integral is used to improve the efficiency of the computation process. Numerical simulation results show that the computational time for the approximated integral is three to four orders of magnitude less than the effort associated with evaluation of the original double Sommerfeld integral with an error of not more than 0.5%.

The enhanced power absorption for the rough signal trace is characterized by an enhancement factor which is defined as the exponential decay constant ratio, or the ratio of the attenuation constant of the rough surface waveguide and that of the corresponding smooth surface waveguide. If the distance between the plates is large as compared to the height of the rough surface, the enhancement factor of the waveguide model is the same as from a previous plane wave model. In other words, the roughness effect on the quasi-TEM mode can be approximated by the roughness effect for a plane wave for appreciable waveguide thicknesses. Compared with the plane wave model, the thickness of the waveguide is a significant factor for the roughness effect. If the thickness of the waveguide is decreased, the interaction of the roughness with the propagating electromagnetic wave will increase, resulting in a larger enhancement factor. The non-TEM characteristics of the lossy waveguide become more pronounced, making the waveguide problem distinctly different from the plane wave model.

Highly Compact Embedded Duplexer Implementation for WiMAX Dual-band Front-end Module with Organic Package Substrate

Kyungo Kim, **Taeeui Kim**, **Donghwan Lee**, **and Sung Yi**
Samsung Electro-Mechanics, Korea

Abstract— In this paper, low cost and high performance band pass filters and duplexers are investigated for Dual-band WiMAX front-end module with multi-layered organic package substrate. This dual band FEM includes a 2.5 GHz power amplifier die with switch and requires tiny PKG form factor. In addition to module size limitation, FEM requires higher gain and stringent attenuation characteristics specification. The embedded BPFs and duplexer were designed on 8 layer organic substrates by using ADS and HFSS for finding out efficient structure and verifying FEM specifications.

The dual-band FEM with embedded passive components incorporates duplexer including 2 GHz, 5 GHz BPFs and balun. BPFs and duplexer have size of $1.65\times1.8\times0.12$ mm, $1.32\times1.45\times0.12$ mm, $2\times2\times0.6$ mm respectively. Integrated dual-band duplexer shows an insertion loss of < -1.8 dB in path band and 22∼40 dB attenuation performance in rejection band. The measured results of BPFs and duplexer show good electrical performance with low insertion loss, high attenuation.

Embedded passive Packaging technology has many advantages such as improving packaging efficiency and better electrical performances for low cost and highly compact RF SOP (System on Package) applications.

Package-embedded Passive Components for High-speed Wired and Wireless Communication Systems

Telesphor Kamgaing[1], **Emile Davies-Venn**[2]
Kemal Aygun[2], **and Kaladhar Radhakrishnan**[2]

[1]Corporate Technology Group, Intel Corporation, Chandler, AZ 85226, USA
[2]Assembly and Test Technology Development, Intel Corporation, Chandler, AZ 85226, USA

Abstract— Package Form Factor for high-speed communication and computing systems is expected to continue to decrease despite the continuous increase in functionality integration. This trend can be seen in devices such as ultramobile personal computers and mobile internet devices, where high level of computing and multiple radio standards have to coexist either at the board or package level. In order to achieve this goal of ever shrinking form factor, it's critical to not only continue to decrease traditional package features such as trace width and trace spacing, via dimensions and dielectric layer thickness. But it's rather important that novel approaches be adopted that can enhance the system performance while simultaneously shrinking the form factor and reducing the costs. One such enhancement of the package is the introduction of embedded passive components, which can be used in place of several discrete passives, hence reducing the component count and simultaneously removing issues such as solder joint reliabilities associated with their discrete counterparts.

In this work we have extended the existing multilayer organic FCBGA packaging substrate technology to include embedded passives, whereby our main focus is on high frequency performance and applications. These passive components, which include inductors, capacitors and resistors, are fabricated as part of the substrate stackup. The resistors are realized by introducing a carbon paste of appropriate resistivity in the stackup. Resistors demonstrated have resistance values ranging from 30 Ohms to several Mega-Ohms and can achieve process tolerance of 5% or better when they are laser-trimmed. The capacitors are obtained by introducing a thin layer of ceramic-filled-polymer that has dielectric constant in the order of 20 and can deliver a capacitance density of about $20\,\mathrm{pF/mm^2}$. The inductors have spiral shape and are made by patterning the different metal layers of the package substrate. For Gigahertz applications, the inductance value is in the order of a few nanohenries with quality factor peaking between 30 and 50. These embedded passive components have been applied to several high-speed communication circuits.

The paper will be organized as followed: First, we present the embedded passive substrate stackup with particular emphasis on the formation of different individual components. Second, we discuss the electrical performance of these individual components. Third we discuss the design flow along with modeling and experimental data for several passive building blocks including filters, baluns and diplexers that have been designed for applications in both WiFi and mobile WiMAX. These structures exhibit very good electrical performance and very small form factors, making them of particular interest for portable wireless communication devices.

On-chip Electro-thermal Analysis Using Electromagnetic Modeling Tools

Lijun Jiang[1], **Seshadri Kolluri**[2], **Barry Rubin**[1], **Howard Smith**[3]
Alina Deutsch[1], **Jason Gill**[4], **Kaushik Chanda**[4], **Evan Colgan**[1], **and Jamil A. Wakil**[5]

[1]IBM T. J. Watson Research Center, IBM, Yorktown Heights, USA
[2]Department of ECE, University of California, Santa Barbara, USA
[3]IBM Server and Technology Group, IBM, Poughkeepsie, USA
[4]IBM Server and Technology Group, IBM, East Fishkill, USA
[5]IBM Server and Technology Group, IBM, Austin, USA

Abstract— Joule heating effects are becoming increasingly important with the scaling of Integrated Circuit (IC) technology because of increasing power densities on chip, inclusion of more metal layers, use of dielectric materials with lower thermal conductivities, and 3D chip stacking. This impacts system reliability, performance, and design optimization of interconnects. In addition to Joule heating in the interconnect layers, devices are also important heat sources on-chip. Analysis of the temperature distribution in interconnects due to different heat sources can provide powerful insight for on-chip thermal optimization. Hence, the accurate and efficient modeling of the temperature rise in interconnects because of Joule heating and other heating boundary condition is critical to current IC designs.

Temperature distribution simulation for IC interconnects involves solving the three-dimensional (3D) or two-dimensional (2D) heat-conduction equation in a multi-level dielectric stack with interconnects, vias and metal fills embedded in it. Most methodologies in use in the industry have been implemented by building tools dedicated to thermal analysis alone. In addition, these approaches are not readily integrated with on-chip CAD tools and design flows. Due to the extremely high integration density on chip, handling the resultant huge simulation structures becomes an intractable problem for most in-house and commercial tools. People are forced to either look at small-sized problems or use approximate analytical models for thermal analysis.

In this paper, we propose a novel methodology of using existing electromagnetic modeling tools for interconnect and packaging structures to simulate and model temperature distribution in interconnects without any major modifications to these tools or the simulated structure. It employs the analogy between electrical and thermal problems to calculate the temperature distribution in the on-chip interconnects that are embedded in a multi-layer dielectric stack, with vias and metal fills. Electrical resistance is used to obtain the thermal resistance by substituting the electrical resistivity with the material thermal conductivity. Any 2D/3D electrical resistance simulation solver that provides resistance solution based on Laplace's equation will be qualified to accomplish this transformation. This methodology can easily be integrated with the chip technology information and electrical circuit simulator into an automatic template based simulation and optimization flow. It is thus possible to readily analyze large, product-level interconnect thermal problems and directly apply the methodology to on-chip interconnect design and optimization with very small additional effort or involvement from the chip designers.

A tool named *ChipJoule* has been developed using IBM electromagnetic modeling tools to verify the proposed idea. It solves both 2D and 3D on-chip interconnect problems based on current multi-layer chip stack technologies. As 2D benchmarks, comparisons with measurement data and simulations from the popular commercial tool *ANSYS* were made. Excellent agreement was obtained when compared to *ANSYS* results. Thereafter, the dummy wire effects and the via effects on power line temperature were studied and verified at a 2D level. Having established the simulation accuracy, a whole 10-layer, 45 nm technology 2D stack has been simulated and a convergent temperature distribution has been obtained with very short calculation time. In the 3D structures, via effects, simulation convergence, port setup and boundary condition effects will be presented to demonstrate the capability of this automatic design and optimization flow.

Effect of Power Supply Noise on Clock Jitter and Data-clock Synchronization in Microprocessors

Isaac Kantorovich and Chris Houghton
Intel, 77 Reed Road, Hudson, MA 01749, USA

Abstract— Power supply noise imposes a major restriction to a microprocessor's performance. High supply noise on-chip together with the demand for the rise in clock frequency and reduction in power supply voltage makes the problem of synchronization of data and clock signals challenging.

This paper presents a new approach to analyze the impact of power supply noise on clock jitter and data-clock synchronization. It can be shown that for a clock signal coming out from the clock generation circuit at time t_0 and propagating in the presence of sinusoidal noise of frequency f_N the clock period T at time of arrival at flops or latches can be expressed by the equation:

$$T = T_o \frac{1 + a^C - \sigma^C \sin c(\pi f_N T) \cos\left[2\pi f_N (t_0 + \tau^C + T/2)\right]}{1 + a^C - \sigma^C \sin c(\pi f_N T_o) \cos\left[2\pi f_N (t_0 + T_o/2)\right]},$$

where T_0 is nominal clock period, τ^C is the clock propagation time, a^C and σ^C are constant values which depend on sensitivity of clock delay to supply noise. It follows from this equation that minimum (worst-case) clock period is achieved when supply voltage goes up with time (i.e., the voltage is on the ascending slope of the voltage droop). Minimum of $T(t_0)$ is the worst-case clock period. The worst-case clock period represented as a function of noise frequency f_N shows resonance behavior. Noise frequency at which clock jitter is largest corresponds to the first resonance pole and is typically within the range 50 to 350 MHz.

Data and clock synchronization in microprocessors can be characterized by the timing margin which is the difference between the clock period seen at latch/flop and the sum of the data path propagation delay and setup time. If the timing margin is negative data transmission fails. Because the timing margin depends on the clock period, its worst-case also shows a resonance pattern but whether the first resonance pole is minimum or maximum depends on sensitivities of data and clock propagation delays to supply noise. When data is more sensitive to noise than clock the first resonance pole is maximum. The maximum of the timing margin indicates that performance is best at the resonance noise frequency. The resonance peak for the worst case timing margin is reached at the same noise frequency as the frequency at which clock jitter is maximum. Therefore, we have come to an interesting conclusion that the best data-clock synchronization is when the clock jitter is worst. As a consequence, increasing clock depth τ^C results in improvement of chip performance, although clock jitter goes up for deeper clock. For strongly interconnect dominated circuits when clock is more sensitive to supply noise than data the picture would be opposite: performance is better for shorter clocks.

Maximum supply noise that can be tolerated by a chip depends on the clock depth, electronic device delay sensitivity to noise and the shape of noise waveform. The proposed noise aware methodology allows one to extract maximum noise for a given clock distribution and sensitivity of propagation delays to supply noise and also find maximum possible power supply noise that can be tolerated by the chip and characteristics of the data and clock distribution required to tolerate this noise. If data is more sensitive to noise than clock the proposed method always predicts larger tolerable noise than conventional static methods.

FDTD/FETD Modeling of Plasmonic Structures for Optical/CMOS Integration

F. L. Teixeira, **K.-Y. Jung**, **B. Donderici**, **and R. M. Reano**
Electro Science Laboratory, The Ohio State University, Columbus, OH 43212, USA

Abstract— We discuss recent developments on time-domain Maxwell's equation solvers for the numerical simulation of subwavelength plasmonic structures towards integration with CMOS microelectronics. Recent developments in both finite-difference time-domain (FDTD) and finite-element time-domain (FETD) are considered [1, 2], including unconditionally stable extensions of these algorithms based upon altenating-direction-implicit (ADI) and locally-one-dimensional (LOD) operator splittings. We also report on recent extensions on both these methods to treat multiple-species Drude and Lorentz-Drude dispersion material models that describe noble metals such as Au and Ag used in plasmonic waveguides at optical, near-IR, and near-UV frequencies [1]. We illustrate these methods in a variety of situations, including zero-index lenses [2], metamaterial refletionless waveguide bends [3], and in the numerical analysis/design of coupled plasmon resonances in linear arrays of nanospheres, nanodisks, and nanorings [4].

REFERENCES

1. Jung, K.-Y. and F. L. Teixeira, "Multi-species ADI-FDTD algorithm for three-dimensional nanoscale photonic metallic structures," *IEEE Photonics Technol. Lett.*, Vol. 19, 586–588, 2007.
2. Donderici, B. and F. Teixeira, "Mixed finite-element time-domain method for transient Maxwell equations in doubly dispersive media," *IEEE Trans. Microw. Theory Tech.*, Vol. 56, No. 1, 2008.
3. Donderici, B. and F. Teixeira, "Metamaterial blueprints for reflectionless waveguide bends," *IEEE Microwave Guded Wave Lett.*, to appear.
4. Jung, K.-Y., F. L. Teixeira, and R. M. Reano, "Au/SiO_2 nanoring plasmon waveguides at optical communication band," *J. Lightwave Technol.*, Vol. 25, 2757–2765, 2007.

Session 4P4
Photonic Crystals and Metamaterials 2

Application of Defect Induced Microwave Band Gap Structure for Non-destructive Evaluation and the Construction of a Frequency Selector Switch

E. D. V. Nagesh, N. Yogesh, and V. Subramanian
Microwave Laboratory, Department of Physics
Indian Institute of Technology Madras, Chennai 600036, India

Abstract— The use of microwave band gap structures for the non-destructive evaluation of material property is being probed in this paper. As a first step, we studied numerically, the appearance of a point defect mode within the band gap of a microwave band gap structure for the use as a tool to evaluate the dielectric constant of the material at the defect site. The simulations were carried out using the FEMLAB software. In a pure 10×10 square lattice constructed with a material of dielectric constant (ε) 5.5 (in the form of a right circular cylinder), a point defect is created by replacing one of the rods with a geometrically similar but with different dielectric constant material. The appearance of the defect mode is governed by the refractive index contrast (defined as the ratio between the refractive index of the material at the defect site (n_d) and the material of the lattice (n_1). In this case, the refractive index contrast (n_d/n_1) was found to be between 0.85 and 1.28. Simulations were also done with the lattice material of dielectric constant 10 and the defect mode appeared for $1.18 < n_d/n_1 < 0.84$. For the contrast less than 1, defect creates the fundamental mode similar to TE_{01} mode whereas for the contrast greater than 1, next higher mode similar to TE_{11} appears. Once a defect mode appears, it moves towards lower frequency as the dielectric constant of the defect site is increased. In this paper, we propose to evaluate the dielectric constant of a material using the above procedure. This paper also proposes the construction of a novel frequency selector switch that has two line defects in a 10×20 square lattice structure constructed with material of dielectric constant 10.

Controllable Microwave Transmission in a Waveguide with a Lateral Variable Periodic Profile

Victor A. Pogrebnyak and James J. Whalen
Department of Electrical Engineering, Faculty of Engineering
State University of New York at Buffalo, 332 Bonner Hall, NY 14260-1920, USA

Abstract— We investigated the microwave transmission spectrum in a rectangular metallic waveguide, having a variable lateral periodic profile. The waveguide was made of lower and upper walls with the identical sinusoidal profile and two smooth side walls. The periodic plates were made movable. Such structure allows to control the transmission in the waveguide at a wide range of frequency due to opening and closing stop bands in the transmission spectrum.

Bragg reflection is a fundamental wave phenomenon arising upon wave propagation in a periodic medium. It results in the opening of the Bragg gap in the transmission spectrum of the signal. The gap arises at $k = q/2$, known as Bragg's law, where $q = 2\pi/a$, a is a period of the structure, k is the wave number.

In this report, we present the results of theoretical and experimental investigation of Bragg and non-Bragg gaps which opens in the transmission spectrum. The non-Bragg gap is caused by the resonant interaction between the transverse modes. The Bragg gaps open only at $k = q/2 \equiv K$, or multiple of K, the values corresponding to the Brillouin zone boundaries. However, the non-Bragg gap can open at any value of k between zero and K. This tuning can be done by shifting one periodic plate with respect to another. Besides controlling the position of the gap in the spectrum, the width of the non-Bragg gap can be also changed between zero and a maximum value (1.2 GHz in our experiment) upon the shift of the plate on the half period of the corrugation $a/2$. It has been found that in a case of the congruent boundaries, all Bragg gaps are closed, and only non-Bragg gaps are present in the transmission spectrum.

We observed the controllable non-Bragg gap at 7.7 GHz in the same periodic waveguide geometry that we used for investigation of the controllable Bragg gap [1]. The conducted experiment showed that a $a/2$ shift of the periodic plate caused the closing of two Bragg gaps at 6 and 10 GHz and opening of a controllable non-Bragg gap at 7.7 GHz. The width of the non-Bragg gap could be changed between zero and 1.2 GHz upon such shift of the plate.

The proposed above structure could be used to control power transmission in different microwave, photonic, integrated optics, and electronic devices.

REFERENCES

1. Pogrebnyak, V. A. and J. J. Whalen, "Controllable microwave transmission in rectangular periodically corrugated waveguide," *Electronics Letters*, Vol. 43, 226–228, 2007.

Towards R-space Bose-Einstein Condensation of Photonic Crystal Exciton Polaritons

D. L. Boiko

Sowoon Technologies S.á.r.l., 1015, Lausanne, Switzerland

Abstract— A search for Bose-Einstein condensation (BEC) in dilute gases was always fascinating the scientific community. A semiconductor microcavity incorporating heterostructure quantum wells (QWs) sandwiched between two distributed Bragg reflectors (DBRs) is often employed as a model system for studies of the two dimensional (2D) BEC in solids, utilizing coupled states of QW excitons and cavity photons as bosonic particles. Due to photonic component, such composite bosonic particles show light effective masses ($\sim 10^{-4}$ of free electron mass) and assume BEC at lower densities and higher temperatures (∼few degrees Kelvin), as compared with the case of atomic gases. Last years reveal several claims on achieving k-space BEC of 2D cavity exciton polaritons. (See, *e.g.*, the most advanced study in Ref. [1].) However, incompleteness of data and short lifetime of the state do not allow the macroscopic coherent quantum state to be testified unambiguously. Thus in [1], the normalized correlation function of the first order $g^{(1)}$ is measured, indicating macroscopic phase correlations. However, such first-order correlations may not be attributed solely to a coherent quantum state since they can be observed in a thermal state as well, an example of which is a quasi-monochromatic light emitted at a particular atomic transition excited in a gas discharge [2]. Therefore, other tests verifying the nature of the observed state are important. In particular, a harmonic oscillator trap with confining potential $U{=}\alpha_{LP} r^2/2$ can provide an additional evidence of BEC by displaying distinct spatial distributions of lower polaritons (LPs) in the condensate and non-condensate fractions. In [3], a claim is made on achieving such r-space BEC by coupling photons in a planar broad-area microcavity with GaAs quantum well excitons (X) in the effective potential $U{=}\alpha_X r^2/2$ introduced via inhomogeneous stress in a semiconductor wafer. However, the observed features of coherent fraction delocalized over a region of 8 μm width differ from the expected point-like localization behaviour of r-space BEC state. Furthermore, the reported force constant in the trap ($\alpha_{LP}{=}480\,\mathrm{eV/cm^2}$) assumes that corresponding potential for excitons is of $\alpha_X{=}1150\,\mathrm{eV/cm^2}$, which exceeds 27 times the value measured for GaAs QW excitons at the same wafer thickness and pin stressor configuration [4]. These allow one to question whether the reported potential trap is suitable for achieving r-space BEC of cavity polaritons. *In this letter*, a 2D harmonic trap for exciton-polaritons is proposed to be implemented by introducing a coupling between the unperturbed QW excitons and photons in effective potential of a photonic crystal heterostructure. The structure considered here is a quasi periodic 2D lattice (of 3 μm pitch) of optically coupled microcavities [5]. The cavities are defined by shallow mesa etching (as in [1]) and share semiconductor QWs in the active region sandwiched between two DBRs of the wafer. The effective potential for photons $U{=}\alpha_P r^2/2$ is defined by parabolically graded lateral size of microcavities. The coupled states of photonic crystal heterostructure photons with quantum well excitons are shown here to exhibit periodic Bloch oscillations in the photonic lattice plane while their envelope functions are tailored by the effective photonic crystal potential. This concept is numerically exemplified for the case of CdTe/CdMgTe structures, yielding a trap of the force $\alpha_P{=}390$ and $\alpha_{LP} = 140\,\mathrm{eV/cm^2}$ for the photons and lower polaritons, respectively. At the temperature $12\,K$, the estimated threshold for r-space BEC is $N_c = 4.4 \times 10^3$ lower polaritons in the trap.

REFERENCES

1. Kasprzak, J., et al., "Bose-Einstein condensation of exciton polaritons," *Nature*, Vol. 443, 409–414, 2006.
2. Hanbury Brown, R. and R. Q. Twiss, "Correlation between photons in two coherent beams of light," *Nature*, Vol. 177, 27–29, 1956.
3. Balili, R., V. Hartwell, D. Snoke, L. Pfeiffer, and K. West, "Bose-Einstein condensation of microcavity polaritons in a trap," *Science*, Vol. 316, 1007–1010, 2007.
4. Vörös, Z., D. W. Snoke, L. Pfeiffer, and K. West, "Trapping excitons in a two-dimensional in-plane harmonic potential: Experimental evidence for equilibration of indirect excitons," *Phys. Rev. Lett.*, Vol. 97, 016803–4, 2006.
5. Boiko, D. L., "Paraxial Hamiltonian for photons in two-dimensional photonic crystal microstructures," *ArXiv* 0710.5287, 1–19, 2007.

Transmission Lines Based on Metamaterial Structures for Si-MMICs

Samir El Rai[1], **Adam Pawlikiewicz**[1], **Ralf Tempel**[2], **and Dieter Jäger**[2]

[1]ATMEL Corp., Colorado Springs, CO 80906, USA
[2]Universität Duisburg-Essen, ZHO, Duisburg 47057, Germany

Abstract— Differential transmission lines (DTLs) are commonly used in Silicon Monolithic Microwave Integrated Circuits (Si-MMICs) for electrical interconnections between devices and components at different positions. In addition, these transmission line structures are of particular interest for devices based upon traveling waves such as resonators or filters where wave propagation phenomena are used. The flexibility of such a design and the high quality of DTLs are considerd as an advantage of this technique. However, in the classical approach, the technical realisation of these DTLs for the a. m. applications requires a large chip area which leads among other things to increasing costs. This is, on the other hand, a clear disadvantage.

In this paper, it is proposed to use DTLs based upon the concepts of photonic bandgap structures and meta materials to reduce by far the required chip area. Correspondingly, the transmission lines are synthesized as a chain of (almost) identical 4-port unit cells and the analysis is based upon equivalent circuits which are discussed in detail. Theoretical as well as experimental results are presented showing a clear reduction in chip area. It is further shown, that tuneable DTLs can be fabricated which lead to new circuit topologies and improved designs. Experimentally, a small-area quarter wavelength transmission line resonator with a quality factor of ca. 10 and a tunability of ca 30% has been achieved which are an excellent results for a Si-MMIC resonator.

Electric and Magnetic Resonances in Double Stacking Split Rings

L. Zhou[1], **Xueqin Huang**[1], **Yi Zhang**[1], **and S. T. Chui**[2]

[1]Surface Physics Laboratory and Physics Department, Fudan University, Shanghai 200433, China
[2]Bartol Research Institute and Department of Physics and Astronomy
University of Delaware, Newark 19716, DE, USA

Abstract— We extended our previous mode-expansion theory [1, 2] to study the complete electric/magnetic resonance spectra of metallic ring systems made by thin wires possessing flat film-like cross sections, and derived simple polynomial equations to determine the entire resonance spectra of split ring structures which can be analytically solved in the limit of narrow wires [3]. Applications of the theory to a single split ring resonator yield essentially the same results with the finite-difference-time-domain (FDTD) simulations on realistic structures, which justify some basic assumptions adopted in the theory. We then employed the theory to study the resonance properties of a double-stacking split ring structure, and showed that such a planar structure could exhibit magnetic responses along all three dimensions in different situations. FDTD simulations on realistic structures were performed to successfully verify the predictions based on the mode-expansion theory.

REFERENCES

1. Zhou, L. and S. T. Chui, "Eigenmodes of metallic ring systems: A rigorous approach," *Phys. Rev. B*, Vol. 74, 039415, 2006.
2. Zhou, L. and S. T. Chui, "Magnetic resonances in metallic double split rings: Lower frequency limit and bi-anisotropy," *Appl. Phys. Lett.*, Vol. 90, 041903, 2007.
3. Huang, X., Y. Zhang, L. Zhou, and S. T. Chui, unpublished.

Abnormal Radiation Pattern of Metamaterial Waveguide

A. N. Lagarkov, V. N. Semenenko, A. A. Basharin, and N. P. Balabukha

Institute for Theoretical and Applied Electromagnetics of Russian Academy of Sciences (ITAE RAS)
Izhorskaya 13, Moscow 125412, Russia

Abstract— Interest to the wave propagation in the metamaterials, particularly in the media with negative refractive index has extremely growth at last time [1].

In this work we demonstrate, in the first time, the idea to inverse the radiation pattern of the microwave antenna due to metamaterial slab. Our experimental investigation deals with the radiation pattern of the open waveguides in S band. The radiation patterns of the metallic waveguide adapter and ones of the magneto dielectric waveguide made from metamaterial slab (see figure) have been compared in H-plane. The isotropic 3D metamaterial is slab loaded by equal mixture of left and right handed nichrome wire helixes with different positions of helix axes in the space (along x, y and z coordinate axes). The frequencies of electric and magnetic resonances in helixes are equal each other. This metamaterial is isotropic prototype of early elaborated anisotropic mateerial [2] demonstrated negative refractive index (both permittivity and permeability) in the vicinity of frequency 3 GHz (the phase of wave transmittance is negative). The used metamaterial possess by refractive index close to zero at the frequency of 3.1 GHz.

The normalized polar radiation patterns of the open metallic waveguide (solid line) and metamaterial waveguide in 10 mm wall thickness (dotted line) are presented in figure at the frequency of 3.1 GHz. The radiation pattern of metamaterial waveguide is inverse to one of metallic waveguide (the ratio between main beam and backside lobe is inverse). The attenuation of main beam is increased sharply with the increasing of wall thickness d of metamaterial waveguide. At the same time the growth of attenuation of backside radiation is negligible and the ratio of backside lobe/main beam is increase.

The electromagnetic simulation of these antenna patterns by moment's methods demonstrates a good agreement modeling antenna patterns with experimental results for values of metamaterial permittivity and permeability obtained from measured S-parameters of slab.

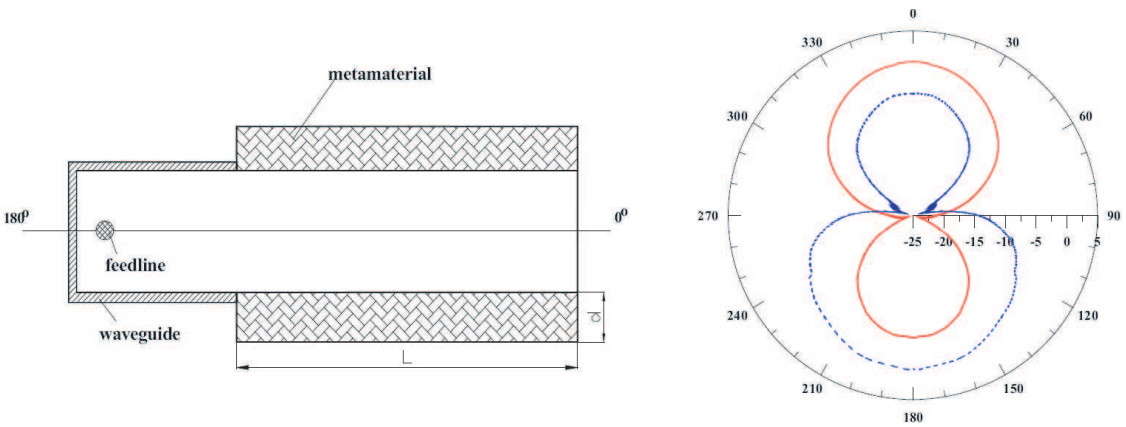

REFERENCES

1. Caloz, C. and T. Itoh, *Electromagnetic Metamaterials: Transmission Line Theory and Microwave Applications*, A John Wiley & Sons, Inc., 2006.
2. Lagarkov, A. N., V. N. Semenenko, V. N. Kisel, and V. A. Chistyaev, "Development and simulation of microwave artificial magnetic composites utilizing nonmagnetic inclusions," *Journal of Magnetism and Magnetic Materials*, Vol. 258–259, 161–166, March 2003.

A Three Output Ports Add-drop Filter Based on Photonic Crystals

F. Monifi, **A. Ghaffari**, **M. Djavid**, **and M. S. Abrishamian**
Department of Electrical Engineering, K. N. Toosi University of Technology, Tehran, Iran

Abstract— We present a Photonic Crystal add-drop filter design based on 3×3 PC ring resonators. This filter consists of an input and three outputs. Our FDTD simulation yields more than 85% efficiency for each output port.

A New Bandstop Filter Based on Photonic Crystals

F. Monifi, **M. Djavid**, **A. Ghaffari**, **and M. S. Abrishamian**
Department of Electrical Engineering, K. N. Toosi University of Technology, Tehran, Iran

Abstract— We present a Photonic Crystal bandstop filter design based on $N \times M$ ring resonators placed beside an ordinary waveguide. Our FDTD simulations show that by choosing proper N and M we can obtain specific filter parameters.

Power Splitter with Adjustable Output Power Levels Based on Photonic Crystal Waveguide Directional Coupler

A. Ghaffari, **M. Djavid**, **F. Monifi**, **and M. S. Abrishamian**
Department of Electrical Engineering, K. N. Toosi University of Technology, Tehran, Iran

Abstract— Here, properties of a wideband photonic crystal power splitter with tunable output power levels based on directional coupling are investigated. Different output power levels are achieved by changing the coupling length and the radius of the coupling rods.

Power Splitters with Different Output Power Levels Based on Directional Coupling

A. Ghaffari, **M. Djavid**, **F. Monifi**, **and M. S. Abrishamian**
Department of Electrical Engineering, K. N. Toosi University of Technology, Tehran, Iran

Abstract— Here, properties of two dimensional photonic crystal power divider based on directional coupling are investigated. Different output power levels are achieved by changing the coupling length and the distance between parallel waveguides. Total transmission up to 96% is achieved in power splitter with two branches.

A New Bi-periodic Photonic Crystal Y-splitter

A. Ghaffari, **F. Monifi**, **M. Djavid**, **and M. S. Abrishamian**

Department of Electrical Engineering, K. N. Toosi University of Technology, Tehran, Iran

Abstract— We investigate the properties of bi-periodic photonic crystal structures. We show that these structures have significantly better performances. A new bi-periodic Y splitter is presented which its normalized transmission is widened and increased in amplitude in comparison with conventional Y splitters.

Session 4P5
Professor Jin Au Kong Memorial Session

Full Wave Analysis for Finlines and Antennas with Metamaterial

Humberto César Chaves Fernandes

Department of Electrical Engineering, Federal University of Rio Grande do Norte
Natal-RN, 59078-970, P. O. Box 1583, Brazil

Abstract— In this paper the bilateral fin line and planar antennas with EBG — Electromagnetic Band Gap — metamaterial (MTM) substrate are analyzed using the full wave TTL — Transverse Transmission Line, method. In order to analyze these structures the effective dielectric constant, the attenuation constant and the pattern fields are determined. A (MTM) is defined as artificial non-homogeneous electromagnetic structure not readily available in nature [1–4]. One characteristic of this material is the negative permittivity, ε, and permeability, μ.

Fin lines are widely used as a millimeter wave components, due to its various advantages such as reducing size, weight, cost and because it interfaces easily with other millimeter wave devices. The metamaterial bilateral fin line is shown in Fig. 1(a). In this analysis the concise full wave TTL method, making possible a significant algebraic simplification of the equations and reducing the computational time [1].

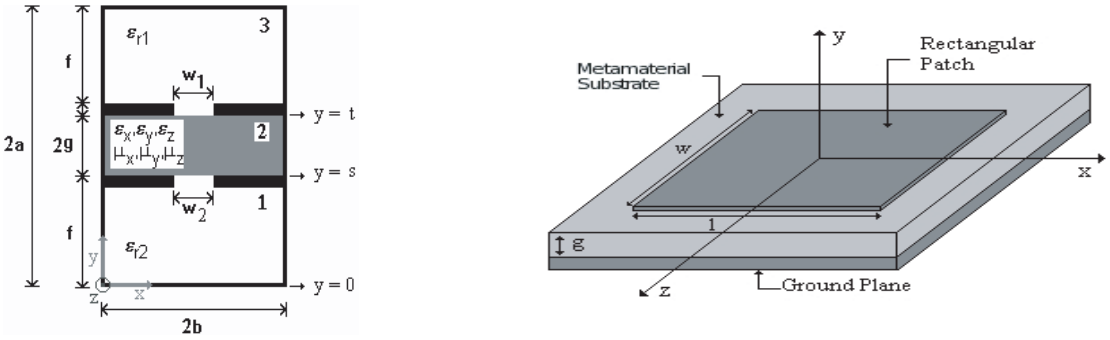

(a) (b)

Figure 1: (a) Transversal cut of a bilateral fin line structure with metamaterial substrate. (b) Microstrip resonator antenna with metamaterial.

The general equations of the fields in the TTL method are obtained after using the Maxwell's equations. The characteristic equation for determining the complex propagation constant Γ, is obtained by setting the determinant of the system matrix equal to zero.

This microstrip antenna is composed of a rectangular patch, metamaterial substrate and a ground plane. The MTM impedes the propagation of electromagnetic waves in some frequency, which can be used to made devices most efficient, and eliminate unwanted frequencies. The analysis is made using the TTL method, with efficient bases function in both x and z direction, as is shown in the Fig. 1(b) [1]. In order to analyze this structure the resonant frequency and pattern fields are obtained.

REFERENCES

1. Fernandes, H. C. C. and G. D. F. Alves, "Meta-material multilayer substrate planar resonators with superconductive patch," *Progress In Electromagnetics Research Symposium Abstracts*, 382, Prague, Czech Republic, Agu. 2007.
2. Smith, D. R., P. Rye, D. C. Vier, A. F. Starr, J. J. Mock, and T. Perram, "Design and measurement of anisotropic metamaterial that exhibit negative refraction," *IEICE Trans. Electron.*, Vol. E87-C, No. 3, Mar. 3, 2004.
3. Caloz, C. and T. Itoh, *Electromagnetic Metamaterials: Transmission Line Theory and Microwave Applications*, John Wiley & Sons, 2006.
4. Fernandes, H. C. C, M. B. L. Aquino, and D. B. Brito, "Rectangular slot resonator with four dielectrics layers," *PIERS Proceedings*, 2121–2126, Beijing, China, Mar. 2007.

Session 4P6a
Electromagnetics in High Field MRI 2

Parallel Transmission: A Comprehensive RF Safety Concept

I. Graesslin
Philips Research Europe, Hamburg, Germany

Abstract— Patient safety in parallel RF transmission systems is more complex due to the extra degree of freedom in the RF pulse design, as existing specific absorption rate (SAR) limits may be violated in case of system failure or miscalibration. This abstract describes a comprehensive safety concept for such a system, part of which is the verification of the SAR limits prior to the scan in combination with RF waveform monitoring during the scan.

For the SAR limit verification before a scan, the electric fields E were pre-calculated using finite-difference time-domain simulations for an ideally decoupled 3T multi-channel body coil (MBC). It was loaded with bio-mesh models, including the "Visible Human Male". The pre-calculated E-fields of the individual coil elements were averaged and stored in a database. This information is used for the pre-scan SAR calculation, which is obtained by superposition of the weighted E-fields with the RF pulses. From the database, a bio-mesh model is selected that best matches the actual patient.

To ensure patient safety during scanning, existing solutions as e.g., the monitoring of the RF with a power-monitoring unit (PMU) are not sufficient. The reason is that only the maximum peak and average power is monitored, so that neither potential phase deviations at the transmit coils elements nor potential channel failures are detected. In addition, in parallel transmission experiments at higher field strength, the local SAR and not the global SAR, which is PMU controlled, is the limiting factor for the allowed maximum duty cycle. The ratio between local and global SAR is not constant and may vary significantly based on the coil/patient interaction as well as on the form of the parallel RF transmission pulses. To ensure patient safety, the current, which is induced by the transmit pulse in each of the RF transmit coil elements, can be monitored during transmission and compared with the demand RF waveform. One individual pick-up coil (PUC) is used per element of the MBC, each integrated into the eight-channel transmit 3T MRI system (Achieva, Philips Medical System, Netherlands). To compensate for coil coupling, the RF pulses are pre-compensated using active decoupling, which is equivalent to a virtual decoupling of the MBC elements. This compensation is necessary to match the RF simulation model to the real coil configuration, so that the SAR calculations are correct for the simulated ideally decoupled MBC.

Two examples for a possible safety margin violation were investigated, namely failure of a receive coil (it remained in tuned state during RF transmission) and patient respiration. The tuned surface coil caused a significant decrease of the transmit amplitude in combination with a transmit phase deviation, which results in an unpredictable behavior in terms of SAR. The malfunctioning of the receive coil is detected in real-time and leads to a scan termination within a few hundred milliseconds. The calculated SAR deviation due to patient respiration was investigated for four subjects and led to a negligible increase of SAR, and also remained small for a worst-case breath-hold situation (with respect to SAR).

Ultra-small-sample Molecular Structure Detection Using Microslot Waveguide Nuclear Spin Resonance

Y. Maguire[1], **I. L. Chuang**[2], **and Neil Gershenfeld**[1]

[1]The Center for Bits and Atoms, Massachusetts Institute of Technology
Cambridge, MA 02139-4307, USA
[2]Electrical Engineering and Computer Science and Physics
Massachusetts Institute of Technology, Cambridge, MA 02139-4307, USA

Abstract— Nuclear Magnetic Resonance is a powerful electromagnetic analytical technique for structure determination of complex biomolecules, but also for monitoring molecular dynamics determination. We here report on the design of a planar microslot waveguide NMR probe with an induction element that can be fabricated at scales from centimeters to nanometers to allow analysis of biomolecules at nano- or pico-mole quantities. This device demonstrates the highest signal-to-noise ratio for a planar detector at publication time, measured using the anomeric proton signal from a 15.6 nanomole sample of sucrose. Analysis of 1.57 nanomoles of ribonuclease-A shows high sensitivity in one- and two-dimensional NMR spectra. In addition to reducing required sample volumes, this integrated geometry can be packed in parallel arrays and combined with microfluidic systems. An overview of this device, its electromagnetic and scaling properties and its use in biomolecular studies will be provided.

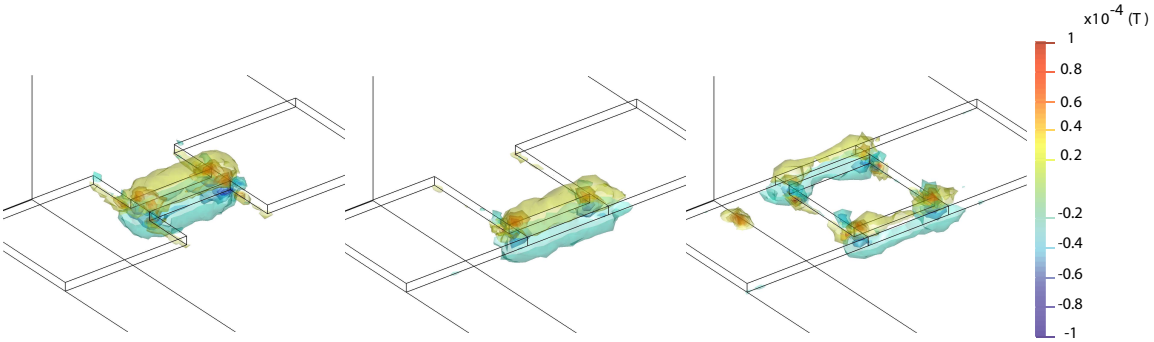

(a) (b) (c)

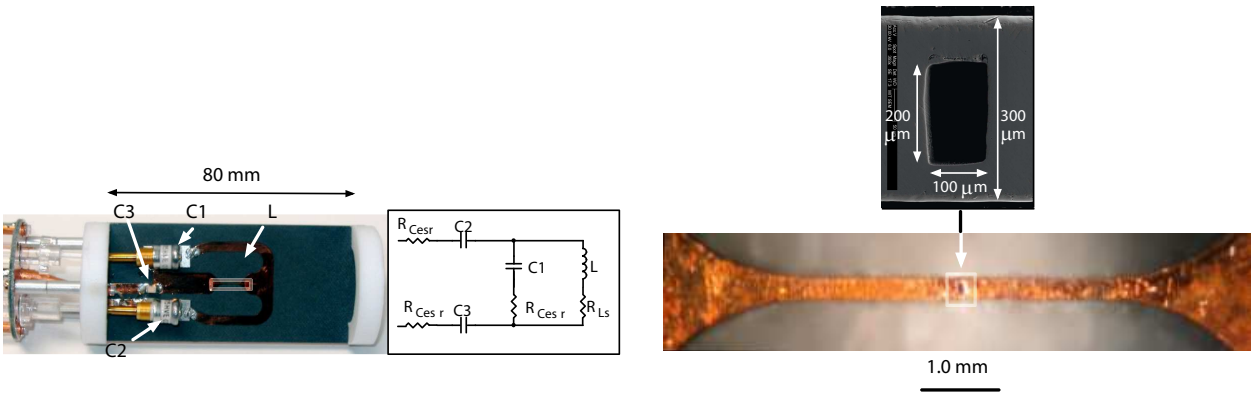

(a) (b)

REFERENCES

1. *Proceedings of the National Academy of Sciences, PNAS.*, Vol. 104, No. 22, 2007.

Basic and Tailored RF Shimming in a Multi-transmit Whole Body MR System

U. Katscher
Philips Research Europe, Hamburg, Germany

Abstract— Wave propagation effects diminish the quality of MR images at main fields of 3T or above. Parallel RF transmission has the potential of compensating for these effects through RF shimming. RF shimming can be performed in two different ways. The basic way of RF shimming is to adjust the glo bal amplitude and phase of the currents in each transmit element, aiming at a constant B1 in the region of interest. For 3D volume imaging, 3D RF shimming is facilitated using multiple frequencies for the different transmit elements. On the other hand, "tailored" RF shimming can be performed via multi-dimensional RF pulses designed to achieve a spatially constant excitation pattern. Using an MR system equipped with parallel RF channels, these multi-dimensional RF pulses can be accelerated via Transmit SENSE.

The potential of both, basic and tailored RF shimming, can be enhanced significantly, if only a constant B1 amplitude is demanded, and an arbitrary spatial distribution of the resulting B1 phase is allowed. This is the case, if only magnitude images are of interest. However, this approach introduces a non-linear problem, requiring corresponding numerical techniques.

Optimal results for basic RF shimming are obtained with transmit arrays owning preferably homogeneous sensitivity distributions of the individual elements. On the other hand, for tailored shimming, the transmit elements require orthogonal sensitivity distributions, which are easier to achieve with inhomogeneous sensitivity distributions. Thus, the transmit coil array cannot be optimized for both, basic and tailored RF shimming simultaneously, and a suitable compromise has to be found.

This study compares the different RF shimming approaches using a whole-body, 8-channel Tx/Rx system at 3T. It shows, that basic RF shimming is able to remove B1 inhomogeneities to a high degree, both in phantoms and in vivo. Tailored RF shimming is able to achieve even higher levels of B1 homogeneity, which, however, might not be necessary for the majority of clinical applications.

SAR in Parallel Transmission

I. Graesslin[1], **D. Glaesel**[1], **S. Biederer**[2], **F. Schweser**[1]
P. Vernickel[1], **P. Börnert**[1], **B. Annighoefer**[1], **H. Stahl**[1]
H. Dingemans[3], **G. Mens**[3], **P. Harvey**[3], **and U. Katscher**[1]

[1]Philips Research Europe, Hamburg, Germany
[2]Institute of Medical Engineering, University of Lübeck, Lübeck, Germany
[3]Philips Healthcare, Best, The Netherlands

Abstract— Parallel transmission bears the potential of compensating B_1 field inhomogeneities induced by wave propagation in (ultra) high field whole body imaging. With increasing field strength, the RF power deposition and the associated local specific absorption rate (SAR) are of high importance with respect to patient safety and as the limiting factor for the allowed RF duty cycle of a scan. In this context, SAR is assessed by simulating a 3T multi-channel body coil with eight ideally decoupled TEM transmit elements using the finite-difference time-domain method ("XFDTD", Remcom, Inc., USA). The coil sensitivities were calculated on a 5 mm grid using perfectly matched layer boundaries (16 layers) and bio-mesh models. The SAR was obtained from the superposition of the averaged pre-calculated E-fields of the individual coil elements weighted with the RF pulses. 2D (accelerated) Transmit SENSE pulses were calculated iteratively in the spatial domain using a conjugate-gradient method as well as directly using a SAR optimized RF pulse design method. Furthermore, the VERSE approach was adopted for parallel transmission. Different local excitation patterns were evaluated using spiral k-space trajectories and reduction factors R of up to eight. Experiments were carried out on an integrated 3T Achieva MRI system with eight RF transmit channels. For the SAR verification experiments, the body coil was loaded with a homogeneous cuboid phantom, and the temperature was measured using a fiber optic probe and an IR-camera.

The SAR depends on the excitation patterns and the reduction factors for whole body Transmit SENSE applications. Moreover, it strongly depends on additional boundary conditions, e.g., the selected k-space trajectory, the regularization parameter, and the coil geometry. For all excitation patterns investigated, the SAR optimized algorithm outperforms the algorithm without SAR optimization. However, the improvement becomes smaller with increasing R, as the degrees of freedom decrease for the SAR reduction. An alternative SAR reduction technique, such as VERSE, represents a method to reduce the SAR for Transmit SENSE pulses by adaptation of the k-space trajectory. In turn, the peak RF amplitudes can be reduced leading to a lower pulse power as well as SAR.

A good correlation was obtained between the measured temperature and the SAR simulations, so that the FDTD method seems to be a useful tool for the a-priory determination of the (local) SAR, the assessment of the patient safety and the coil performance in multi-channel transmission MRI systems.

First Look at 7 Tesla Localized RF Excitation/Reception without B_1 Measurements

Tamer S. Ibrahim[1, 2], **Yik-Kiong Hue**[3], **and Lin Tang**[4]

[1]Departments of Bioengineering and Radiology, University of Pittsburgh
Pittsburgh, Pennsylvania 15213, USA
[2]School of Electrical and Computer Engineering and Bioengineering Center, University of Oklahoma
Norman, Oklahoma 73019, USA
[3]Departments of Bioengineering, University of Pittsburgh
Pittsburgh, Pennsylvania 15213, USA
[4]School of Electrical and Computer Engineering, University of Oklahoma
Norman, Oklahoma 73019, USA

Abstract— Transmit-SENSE and B_1-shimming have accelerated the concepts of variable phase/amplitude (phased array) excitation for hardware (Tx array) development as well as implementation. Such methods however require knowledge of transmit and receive fields produced by the Tx/Rx Array. These fields are typically obtained using time-consuming B_1 measurements. Extracting the receive field is also a challenging experimental problem. In this work using a Tx array exciting a highly coupled-coil, we present an experimental demonstration of a power-controlled, localized, B_1 (both Tx & Rx) shimming and transmit SENSE without B_1 measurements at 7 tesla.

Utilizing Computational electromagnetics (CEM) implements a true coaxial excitation and EM theory, we have developed a 8-element highly-coupled coil model that functions as a transmit array. The array was numerically tuned to 7 tesla operation (298 MHz.) The simulations utilized a 4-port Tx/Rx configuration where every other array element was excited and was used in reception as well. With our modeling approach, the precise electromagnetic coupling between the coil elements while the load is present was considered. Therefore, the excitation and reception on the four Tx/Rx ports can be fully manipulated with direct implementation to the experimental settings.

The simulated coil design was constructed and built to the specifications of the simulations. The preliminary results demonstrate that by properly modeling the load, transmit/receive array, and the excitation/reception scheme, a power-controlled B_1 shimming and transmit SENSE can be 1) guided through simulations with only a minimum of computational time required (seconds) and 2) efficiently implemented without any B_1 measurements. These developments can pave the way for a fully automatic B_1 homogenization/localization scheme for ultrahigh field human MRI.

Hypercapnia-induced Changes in Loss Tangent at Microwave Frequencies

G. Jerome Beers[1,2,3], **Y. Iris Chen**[1,2], **Kenneth K. Kwong**[1,2]
Giorgio Bonmassar[1,2], **Leonardo Angelone**[1,2,4], **and Jerome L. Ackerman**[1,2]

[1]Athinoula A. Martinos Center for Biomedical Imaging, USA
[2]Department of Radiology, Massachusetts General Hospital, USA
[3]Department of Radiology, Brigham and Women's Hospital, USA
[4]Department of Biomedical Engineering, Tufts University, USA

Abstract— Prior authors have used *in situ* probes to demonstrate changes in permittivity-related parameters at microwave frequencies associated with changes in blood flow, ischemia, and death [1–4]. We have previously described changes in reflection coefficient from 100 to 3000 MHz associated with cerebral blood flow (via hypercapnia) and death (via administration of KCl) in a pilot study in which a coaxial probe was directly applied to exposed rat skulls [5]. In order to express the prior data more in terms of the inherent electrical properties of tissue, we now present change in loss tangent ($\tan\delta$) as a response to onset and cessation of hypercapnia.

Session 4P6b
Localized Waves

An Introduction to Localized Waves (Beams or Pulses)

Erasmo Recami[1,2]

[1]Facoltà di Ingegneria, Università Statale di Bergamo, Italy
[2]INFN-Sezione di Milano, Milan, Italy

Abstract— A simple introduction is tentatively presented to the ordinary gaussian and to the Bessel waves, by separating the case of beams from the case of pulses; and an analogous introduction is afterwards presented for the Localized Waves (LW), pulses or beams. One aim of ours is stressing the different characteristics of the gaussian with respect to the Bessel waves, showing the important properties of the latter: Properties that may find application in all fields in which a role is played by a wave-equation (like electromagnetism, optics, acoustics, seismology, geophysics, gravitation, elementary particle physics, etc.).

Some historical information is added.

Moreover, various theoretical approaches are mentioned, which lead to nondiffracting of solutions to the wave equations (in unbounded or bounded media), together with a few applications of these waves. The different case of the Schroedinger equation is also mentioned.

At last, we briefly investigate also the (not less interesting) case of the subluminal Localized Waves, and their connections with the superluminal ones. In particular, we recall the peculiar topic of zero-speed waves: Namely, of the localized fields with a static envelope ("Frozen Waves").

REFERENCES

1. Zamboni-Rached, M. and E. Recami, "Subluminal wave bulletts: Exact localized subluminal solutions to the wave equations," *Phys. Rev. A*, March 2008.
2. Zamboni-Rached, M., E. Recami, and H. E. Hernandez-Figueroa, *Localized Waves*, Chapters 1 and 2, book, ed. by H. E. Hernandez-Figueroa, M. Zamboni-Rached, and E. Recami, J. Wiley, Jan. 2008.
3. Zamboni-Rached, M., E. Recami, and H. E. Hernandez-Figueroa, "Theory of 'frozen waves'," *J. Opt. Soc. Am. A*, Vol. 11, 2465, 2005.
4. Zamboni-Rached, M., "Diffraction-attenuation resistant beams in absorbing media," *Opt. Express*, Vol. 14, 1804, 2006.
5. Zamboni-Rached, M. and E. Recami, "Localized (nondiffracting, nondispersive) solutions to the Schroedinger equation," preprint 2007.
6. Olkhovsky, V. S., E. Recami, and J. Jakiel, "Unified time analysis of photon and nonrelativistic particle tunnelling," *Phys. Reports*, Vol. 398, 133–178, 2004.
7. Olkhovsky, V. S. and E. Recami, "Time as a quantum observable," *Int. J. Mod. Phys. A*, Vol. 22, 5063, 2007.
8. Olkhovsky, V. S., E. Recami, and A. K. Zaichenko, "Resonant and non-resonant tunneling through a double barrier," *Europhys. Lett.*, Vol. 70, 712, 2005.

Programmable Ultrashort-pulse Localized Waves

Ruediger Grunwald[1], **Martin Bock**[1], **Silke Huferath**[2]
Susanta Kumar Das[1], **Stefan Osten**[3], **Peter Staudt**[4], **and Gero Stibenz**[4]

[1]Max-Born-Institute, Germany
[2]Bremen Institute for Applied Beam Technology, Germany
[3]HOLOEYE GmbH, Germany
[4]APE GmbH, Germany

Abstract— From theoretical as well as experimental studies it is well known that the free-space spectral interference of coherent polychromatic conical beams like few-femtosecond laser pulses is capable to generate spatio-temporal Bessel- or Bessel-Gauss-type X-waves. Because of their highly stable propagation over large distances, such pseudo-nondiffracting beams promise to enable for many new applications which can not easily be realized with conventional optical systems, e.g., robust wavefront sensing, two-dimensional autocorrelation of ultrashort pulses, or modified laser-matter interaction schemes. Recently it was shown that small-angle single-maximum Bessel-beams of extraordinarily extended depth of focus ("needle beams") can be formed with ultraflat axicons fabricated by mask-shaded thin-film deposition or lithographical structuring of surfaces. If Bessel-like beams are shaped by transparent or reflective axicons of fixed phase profiles, any variation of the parameters is restricted by the constant angular spectra. To overcome this drawback, static axicons have to be replaced by high-resolution adaptive spatial light modulators (SLM) which are successfully applied to optical tweezers. In the case of extremely short pulse durations, however, chromatic and geometrical dispersion effects have to be carefully minimized. Here we present the most recent experimental results in optimizing the spectral and temporal transfer functions of two novel types of liquid-crystal-on-silicon (LCoS) spatial light modulators [1].

In our experiments, parameter ranges for a high-fidelity pulse transfer were identified. The generation of programmable arrays of localized waves was demonstrated for near-infrared few-cycle pulses of Ti: sapphire laser oscillators and high-power amplified pulses. It is shown that the relevant parameters of parallel-aligned (PAN) as well as vertical-aligned (VAN) LCoS-SLMs like phase, spectrum and amplitude can be modified by a proper choice of gray values and device orientations with respect to the beam polarization. Specific limitations of the electronic control of the liquid crystal properties are discussed as well. The technique enables for a variation of length and shape of nondiffracting zones, an encoding of spatial patterns in the spectral phase

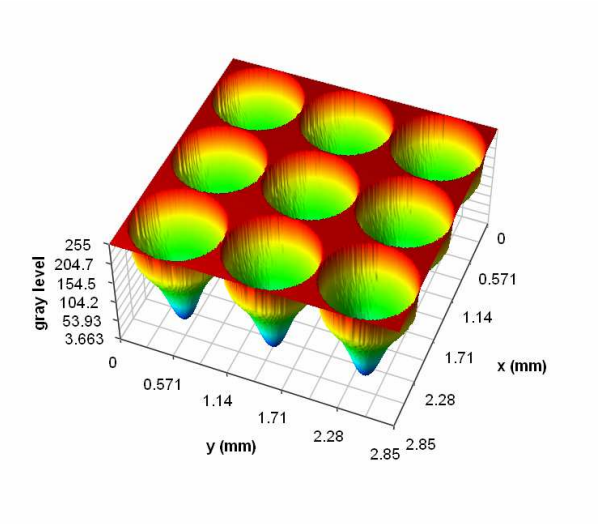

Figure 1: Grayscale pattern programmed in a PAN-type LCoS-SLM representing orthogonally arranged circular axicons of approximately conical shape.

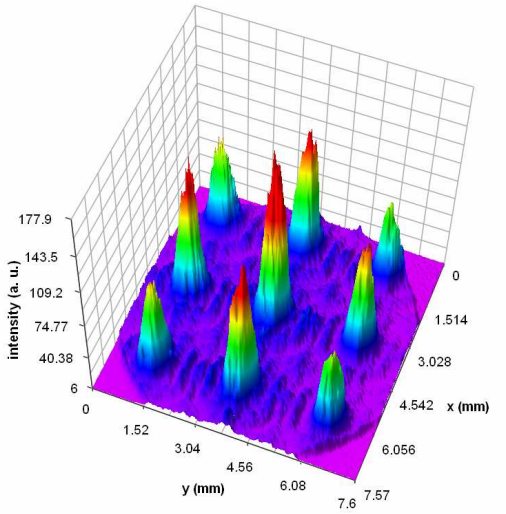

Figure 2: Intensity profiles of arrayed needle-beams generated from a amplified Ti: sapphire laser (pulse duration about 50 fs) detected at a distance of 26.5 cm.

and/or amplitude characteristics, and beam confinement. The pictures show a grayscale pattern representing orthogonally arranged circular axicons (Fig. 1) programmed in a PAN-type LCoS-SLM and the corresponding measured intensity profiles of arrayed needle-beams generated from a amplified Ti: sapphire laser beam (pulse duration about 50 fs) at a distance of 26.5 cm (Fig. 2). The pitch of the axicon array was 880 µm and the effective conical angle (neglecting phase steps) approximately 0.073°. In other experiments, binary amplitude-encoded image information was propagated via nondiffracting subbeams generated by thin-film microaxicon arrays [2].

Currently, the time-dependent phase modulation of such Bessel-like beam arrays for applications in adaptive measuring techniques is investigated. By nonlinear frequency conversion of programmable Bessel-like beams, a confined spatio-temporal manipulation and diagnostics of nondiffracting wavepackets at extremely short pulse durations (sub-10-fs range) is enabled [3]. Furthermore, new classes of localized waves with respect to radial symmetry and propagation (e.g., non-rectilinear focal zones for 3D micromachining of materials) are studied.

REFERENCES

1. Bock, M., S. K. Das, R. Grunwald, S. Osten, P. Staudt, and G. Stibenz, "Femtosecond pulse transfer of liquid-crystal-on-silicon spatial light modulators," *Appl. Phys. Lett.*, submitted, 2008.
2. Grunwald, R., U. Neumann, U. Griebner, G. Steinmeyer, G. Stibenz, M. Bock, and V. Kebbel, "Self-reconstruction of pulsed optical X-waves," *Localized Waves, Theory and Experiments*, 299–313, M. Zamboni-Rached, E. Recami, H. E. Hernández-Figueroa Eds., Wiley & Sons, New York, 2008.
3. Grunwald, R., *Thin-film Microoptics — New Frontiers of Spatio-temporal Beam Shaping*, Elsevier, Amsterdam, 2007.

Spatial and Spatio-temporal Wave Localization in Periodic Media

D. Janner[1], **S. Longhi**[2], **and V. Pruneri**[1,3]

[1]ICFO, Institut de Ciencies Fotoniques
Mediterranean Technology Park, Castelldefels E-08860, Spain
[2]Dipartimento di Fisica and Istituto di Fotonica e Nanotecnologie del CNR
Politecnico di Milano, Milan I-20133, Italy
[3]ICREA, Institució Catalana de Recerca i Estudis Avançats, Barcelona, Spain

Abstract— We present an analysis of spatial three-dimensional wave localization in one- and two-dimensional photonic crystals (PCs) without defects together with an analytical framework, based on the Wannier function technique, to study spatio-temporal wave localization in more general photonic crystals. We present the results of those analyses with a particular emphasis on hyperbolic wave localization. We show that, in one-dimensional photonic bandgaps, wave diffraction due to localization in the translational-invariant directions is deeply affected by the band structure arising from the periodicity of the photonic crystal, leading to different kinds of wave localization. In particular, for a periodic layered structure we show that close to the bandgap edge, diffraction is enhanced with a transition from a parabolic diffraction curve (Gaussian beam propagation) to hyperbolic or elliptic diffraction curves which allow for localization in the form of stationary X-shaped or sinc-shaped waves respectively. In two-dimensional photonic crystals we study out-of-plane propagation and show the existence of two types of X waves at frequencies corresponding to either a top-point of a band, where the in-plane diffraction turns out to be negative, or at band saddle points. In the former case the X-wave is directed along the invariance direction of the PC, whereas in the latter case it lies in the PC plane and is directed along one of the principal direction of the diffraction tensor. Eventually, in order to study spatio-temporal propagation of light in generic PCs (one- to three- dimensional), we use a Wannier function expansion technique which leads to the description of light propagation through an envelope function. In this framework, different kinds of propagating and stationary spatio-temporal localized waves are found and moreover a class of non-diffractive and non-dispersive wave propagation is presented. Analytical predictions of light behaviour were also checked with numerical computation.

Spatiotemporally Localized Luminal and Superluminal Null Electromagnetic Waves

I. M. Besieris[1] and A. M. Shaarawi[2]

[1]The Bradley Department of Electrical and Computer Engineering
VPI&SU, Blacksburg, Virginia 24061, USA
[2]The Physics Department, The American University in Cairo
P. O. Box 2511, Cairo 11511, Egypt

Abstract— Wave packets carrying angular momentum and characterized by vortex structures are of physical importance and are being intensely studied in several areas, e.g., optical vortices, photon entanglement, etc. The systematic exposition in this talk of exact spatiotemporally localized luminal and superluminal null electromagnetic waves is relevant and should prove useful in this direction.

Spatiotemporally localized null electromagnetic waves are characterized by the following salient properties: (1) They are locally transverse electromagnetic (TEM) fields; (2) In free space, the modulus of the local energy transport velocity equals the speed of light in vacuum; (3) The energy is equipartioned between the electric and magnetic fields; (4) Given the null electromagnetic fields $\vec{E}(\vec{r},t)$ and $\vec{H}(\vec{r},t)$, new null fields $\vec{E}(\vec{r},t)\phi[\alpha(\vec{r},t),\beta(\vec{r},t)]$ and $\vec{E}(\vec{r},t)\phi[\alpha(\vec{r},t),\beta(\vec{r},t)]$ can be constructed from scalar solutions $\alpha(\vec{r},t),\beta(\vec{r},t)$ of the nonlinear characteristic equation that, additionally, obey the Bateman constraint. The arbitrary function $\phi(\vec{r},t)$ controls the "singularities" of the electromagnetic fields. If, for example, $\phi(\vec{r},t)$ vanishes, both the electric and magnetic field intensities vanish. The zeros of $\phi(\vec{r},t)$ define vortex lines "riding atop" of null solutions to Maxwell's equations; (5) The spatiotemporally localized null fields have vortex structures on planes transverse to the direction of propagation and, in general, are relatively simple so that explicit calculations can be made of the total energy and the total angular momentum they carry.

The physical importance of one class of luminal null electromagnetic waves due originally to Robinson and Troutman has been brought out in the recent work on electromagnetic vortices by Bialynicki-Birula. The Robinson-Troutman solutions are motivated in this talk by means of the Whittaker-Bateman potential theory and their relationships to well-known scalar luminal localized waves are examined. This allows for the introduction of finite-energy localized null luminal electromagnetic waves with spatiotemporal spectra appropriate for applications in diverse physical areas.

A choice of functions $\alpha(\vec{r},t),\beta(\vec{r},t)$ based on Donkin's theorem, together with the Whittaker-Bateman potential theory and the subluminal Lorentz transformations of Maxwellfs equations allows one to construct a novel wide class of spatiotemporally localized superluminal null electromagnetic waves.

Nonlinear Trapping of Light Pulses by Photonic Potentials

O. V. Farberovich[1], **S. Bar-Ad**[2], **and V. Fleurov**[2]

[1]Department of Physics, Ben-Gurion University, Beer-Sheva 84105, Israel
[2]School of Physics and Astronomy, Beverly and Raymond Sackler Faculty of Exact Sciences
Tel Aviv University, Tel Aviv 69978, Israel

Abstract— We observe, numerically and experimentally, nonlinear trapping of short light pulses that propagate in slabs in which photonic potentials are created by locally changing the refraction index. Such trapping cannot occur in the linear regime, where only reflection and transition of the light are possible, but becomes possible at sufficiently high intensities, due to the Kerr nonlinearity. Trapping may occur into any of the bound states of a multi-mode structure, and the fraction of trapped power is sensitive to the initial conditions (power, incidence angle, beam width, and distance of the coupling position from the structure). Depending on the input power and trapping efficiency, the trapped wave packet may be linear or nonlinear. Furthermore, a pulse propagating in a homogeneous nonlinear Kerr and Raman dispersive medium is unstable in $(2+1)$ dimensions. In that case trapping of the pulse by the photonic potential effectively lowers the dimensionality and stabilizes the pulse, which may now propagate for a long distance within the photonic trap (waveguide). To analyze the trapping dynamics we use the RK4IP algorithm for the $(2+1)$ nonlinear Schrödinger equation including Raman scattering, in the case of a simple rectangular photonic potential, for a Gaussian input wave packet incident at a small angle on the photonic potential. We focus on the influence of the Kerr and Raman nonlinearities on the propagation of the pulse outside and inside the potential, and compare our results to recent experiments on photonic structures embedded in silica and AlGaAs planar waveguides.

Self-organized Propagation of Spatiotemporal Dissipative Solitons in Saturating Nonlinear Media

V. Skarka[1] and N. B. Aleksić[2]

[1]Laboratoire POMA, UMR 6136 CNRS, Université d'Angers
2, Boulevard Lavoisier, Angers 49045, Cedex 1, France
[2]Institute of Physics, Pregrevica 118, Belgrade 11000, Serbia

Abstract— Spatiotemporal soliton is generated whenever the diffraction and dispersion of an optical pulse are compensated by saturating nonlinearity. A soliton completely confined in space and time is called "light bullet". Recent measurements show that the semiconducting conjugated polymer polydiacetylene *para*-toluene sulfonate exhibits cubic-quintic saturating nonlinearity. In atmosphere the focusing of the laser pulse above critical power, due to cubic Kerr nonlinearity of the air, increases field intensity causing multiphoton (or tunneling) ionization of neutral molecules and plasma generation. Plasma acts as a defocusing medium with the negative nonlinearity of twenty-first order that suppress the laser field blow up. A balance between the nonlinear focusing and plasma defocusing may result in a self-guided electromagnetic beam corresponding to the two-dimensional spatial soliton. A laser beam with phase singularity i.e., with vortex structure contributes in general, if not to suppress the breakup of ring into modulation instability induced filaments, at least to distribute filaments symmetrically around the singularity in order to conserve the angular momentum. Hence, a vortex structure prevents chaotic filamentation so often observed in powerful laser beams without the singularity. We demonstrated the possibility of filaments coalescence that seems to be related with the attraction to the equilibrium vortex soliton state.

In a real experiment, soliton cannot propagate without losses. In order to maintain solitonic structure, the linear and nonlinear loss must be compensated by a gain giving self-organized dissipative light bullet. We demonstrated that only cross compensation between saturating nonlinearity excess, loss, and gain maintains such dissipative structure in stable dynamic equilibrium. We developed the dissipative variational method in order to find steady state solutions of complex cubic-quintic Ginzburg-Landau equation that describe well dissipative solitonic structures of one, two, and three dimensions. A stability criterion is established rendering a large domain of dissipative parameters. Analytically obtained symmetric steady state solutions of Ginzburg-Landau equation are stable in this domain. If these approximate solutions are taken as input for numerical simulations of full Ginzburg-Landau equation, their evolution will always lead to stable dissipative solitons in dynamic equilibrium. It is worthwhile to stress that even very asymmetric input pulses, for the same dissipative parameters from our domain, which are far from stable spherically symmetric steady states, always self-organize into solitons. Analytically obtained stable steady states are in the domain of attraction of the exact solution. As a consequence, solitons are very robust resisting to the successive increase of amplitude during evolution. The opportunity to treat analytically and numerically asymmetric input pulses propagating toward necessarily stable and robust dissipative light bullets, opens possibilities for diverse applications in transport and processing of information including experiments.

Subluminal Localized Waves

Michel Zamboni-Rached[1], **Leonardo A. Ambrosio**[2], **and Hugo E. Hernández-Figueroa**[3]

[1]Centro de Ciências Naturais e Humanas
Universidade Federal do ABC, Santo André, SP, Brasil
[2]Centro de Ensino Superior de Educação Tecnológica
Universidade Estadual de Campinas, Campinas, SP, Brasil
[3]Departamento de Microonda e Óptica, Faculdade de Engenharia Elétrica e de Computação
Universidade Estadual de Campinas, Campinas, SP, Brasil

Abstract— A simple method capable to furnish non-diffractive subluminal pulses as exact analytic solutions to the wave equations for either scalar (acoustic and optics) and vectorial (electromagnetic waves) cases will be presented. These new ideal subluminal solutions are herein obtained for arbitrarily chosen frequencies and bandwidths, avoiding in particular any recourse to the non-causal (backwards moving) components that so frequently plague the previously known localized waves. Results of the present kind are valid whenever an essential role is played by a wave-equation (like in electromagnetics, seismology, geophysics, gravitation, elementary particle physics, etc.

Nonlinear Effects in Electromagnetic Field Computations and Related Physical Processes in Nonlinear Media

R. P. Sharma
Centre for Energy Energy Studies, Indian Institute of Technology Delhi, India

Abstract— This work presents the nonlinear dynamical equation of an Electromagnetic wave in a nonlinear media (plasma) by taking into account of appropriate nonlinearty. Then this model equation is recasted into the nonlinear Schrodinger equation (NLS) or modified Nonlinear Schrodinger Equation (MNLS) form. Various invarients are discussed and semianalytical as well as numerical solutions are obtained to study the filamentry (localized structures) in space, transition to chaotic state and self organisation. Relevence of these studies in a variety of situations are discussed.

Session 4P7
Mathematical Models for Light Scattering Applications including Nanooptics and Biophotonics

Light Scattering by Human Erythrocyte: Different Shape Models

Elena Eremina[1] **and Natalia Grishina**[2]

[1]University of Bremen, Badgasteiner Str. 3, Bremen 28359, Germany
[2]Moscow Lomonosov State University, Lenin's Hills, Moscow 119991, Russia

Abstract— Light scattering by blood cells is recently of great interest both in mathematical modeling and in practical applications. In particular, studying of light scattering by erythrocytes is a sutable method for detection of some blood diseases. Between other blood cells, erythrocyte has an advantage for modeling, as it demonstrates no internal structure and can be modeled as homogeneous object with a certain refractive index. In the same time it has some features, which complicate modeling, such as relatively large size and complicated biconcave shape. To simplify erythrocyte modeling often classical shapes of oblate discs and spheroids are used to approximate a real shape.

During the last years different simulation methods have been applied to this problem: Finite Difference Time Domain (FDTD), Discrete Dipole Approximation (DDA), Multipole Multiple Technique (MMP), T-matrix and many others. Some of these methods are not applicable to the real biconcave shape of erythrocyte, others are rather time consuming, and some methods are restricted to small dimensions. Between others the Discrete Sources Method (DSM) looks very attractive, as it allows making use of the axial symmetry of the particle and the polarization of an incident excitation, which sufficiently reduces the time of calculations. Besides, the DSM allows calculation of all the incident angles and polarizations at once [1] unlike volume-based methods, such as DDA and FDTD. In the frame of DSM the scattering problem includes Maxwell equations, infinity conditions and transmission conditions at the interface and boundary conditions at an obstacle surface. An approximate solution of the scattering problem is constructed as a finite linear combination of discrete sources deposited in a domain inside a scatterer with certain amplitudes. The constructed approximate solution satisfies all the terms of the original scattering problem except the boundary conditions at an obstacle surface. At the last stage the amplitudes of the discrete sources are defined from the boundary conditions at the surface of the scatterer following the generalized point-matching technique. Additionally, the DSM gives opportunity to control the accurateness of obtained results by surface residual calculating.

In this work the DSM is applied to investigate the influence of different erythrocyte shape models on light scattering results. For the comparison we chose one of the experimentally based equations, a modified Cassini-based model and a disc-sphere model [2]. Numerical results will be shown in the oral presentation.

ACKNOWLEDGMENT

Author would like to acknowledge financial support of this work by Deutsche Forschungsgemeinschaft (DFG).

REFERENCES

1. Eremin, Y. A., "The method of discrete sources in electromagnetic scattering by axially symmetric structures," *J. Comm. Technology and Electronics*, Vol. 45, No. 2, 269–280, 2000.
2. Eremina, E., J. Hellmers, Y. Eremin, and T. Wriedt, "Different shape models for erythrocyte: Light scattering analysis based on the discrete sources method," *JQSRT*, Vol. 102, 3–10, 2006.

Analysis of Evanescent Waves Scattering by a Single Particle on a Layered Interface for Total Internal Reflection Microscopy (TIRM)

Elena Eremina[1], **Thomas Wriedt**[2], **and Laurent Helden**[3]

[1]University of Bremen, Badgasteiner Str. 3, Bremen 28359, Germany
[2]Institute of Materials Science, University of Bremen, Germany
[3]2nd Institute of Physics, University of Stuttgart, Germany

Abstract— Total Internal Reflection Microscopy (TIRM) is a technique to measure weak interaction forces between spherical colloidal particles and a plane surface. Compared to other methods like the surface force apparatus or atomic force microscopy, TIRM is the more sensitive technique because it utilizes the Brownian fluctuations of a free colloidal particle to deduce the interaction potential. In this way forces in the order of a few femtonewton can be detected. TIRM has proven to be a valuable tool for the precise measurement of weak colloidal interactions as double layer forces, van der Waals forces, magnetic interactions and depletion forces. A review of the state of the TIRM technique can be found in [1].

In TIRM-based experiments typically there is water containing colloidal particles situated near a glass prism. A laser beam propagating in the prism hits the prism-water interface with an angle slightly above the angle of total internal reflection. As a result an evanescent field appears close to the surface. Particles, dispersed in water start to scatter evanescent light and a detector registers its intensity. The scattering intensity contains information about the particle and its distance from the surface. For analysis of the measured signals the TIRM method requires the precise knowledge of the particle-wall distance dependence of the scattering intensity. To simulate this calibration curve Discrete Sources Method (DSM) has been chosen.

The DSM [2] has already been applied to model TIRM experiments. In [2] measurement results have been compared to DSM model for a prism. To enlarge the spectrum of practical applications for TIRM, coated substrates are of interest. In particular, some biological applications use gold (Au) covered substrates. Due to technical reasons an additional layer of titanium (Ti) or chrome (Cr) is required in between glass and the gold film to modify the wetting properties of the Au coating from non-wetting to wetting. In this paper we present a modification of the DSM, which allows taking into account multilayered structure deposited on the prism surface. Numerical results based on DSM will be shown in the presentation. Comparison to experimental results demonstrates a good congruence of theory with measurements.

ACKNOWLEDGMENT

Authors would like to acknowledge financial support of this work by Deutsche Forschungsgemeinschaft (DFG).

REFERENCES

1. Bike, S. G., "Measuring colloidal forces using evanescent wave scattering," *Current Opinion in Colloid & Interface Science*, Vol. 5, 144–150, 2005.
2. Helden, L., E. Eremina, Y. Eremin, N. Riefler, C. Hertlein, C. Bechinger, and T. Wriedt, "Single particle evanescent light scattering simulations for total internal reflection microscopy," *Appl. Optics*, Vol. 45, 7299–7308, 2006.

Application of Microscopic Probes to DNA Sequencing: Thermal Fluctuations and EM Scattering in Near Field

Alex Bijamov[1], **Fridon Shubitidze**[1], **and Dmitri Vezenov**[2]

[1]Thayer School of Engineering, Dartmouth College
8000 Cummings Hall, Hanover, NH 03755, USA
[2]Chemistry Department, Lehigh University, USA

Abstract— The ability to perform full-length genome sequencing fast, accurately, and cost effectively is an essential goal for personal genomics as well as for development of the future personalized medicine. The workhouse of the current genome reading technology, Sanger sequencing, is a costly and time-consuming procedure. Several genome sequencing technologies have been proposed recently and are now under different stages of development. One of such emerging technologies is a massively parallel, single molecule based, label free sequencing technology. It combines concepts of single nucleotide addition (SNA) sequencing, near field optics, single molecule force spectroscopy, and microfluidics. On a sequencing chip, fluorescent magnetic beads are attached to one end of the DNA molecule. During sequencing, DNA molecules are extended using magnetic tweezers to record their mechanical responses. To sense the molecular extension under applied forces, techniques of near field optics are employed in order to detect sub-nanometer-scale changes in bead position when the DNA molecule is shortened upon SNA. One of the major problems of this approach is the noise due to thermal fluctuations, i.e., Brownian motion, of the bead. Our analytical and numerical studies of the thermal fluctuations in this system showed that the bead's Brownian motion indeed causes significant shift in the bead position. In this paper, the effect of the thermal fluctuation on the intensity of the scattered optical signal is investigated. In addition, we carry out statistical signal processing to filter out the noise arising from thermal fluctuations and extract the most valuable information from measured signal for fast and accurate DNA sequencing.

Classical Theory of Optical Nonlinearities Due to Electron Confinement in Conducting Nanoparticles

G. Y. Panasyuk[1], **J. C. Schotland**[1], **and V. A. Markel**[1,2]

[1]Department of Bioengineering, University of Pennsylvania, Philadelphia, PA 19104, USA
[2]Department of Radiology, University of Pennsylvania, Philadelphia, PA 19104, USA

Abstract— We develop a classical theory of electron confinement in conducting nanoparticles. The theory is used to compute the nonlinear optical response of the nanoparticle to a harmonic external field from first principles.

In the case of conducting particles whose linear dimensions are not dramatically larger than the atomic scale (a factor of the order of 10 is typical), finite-size and quantum corrections are of importance [1]. Previously, the above two terms have been used interchangeably and it is accepted that the small-size effects are quantum mechanical in origin. Thus, they can be understood by considering discrete electron states in a nanoparticle [2, 3] or reduction of interband screening and electron spill-over near the nanoparticle surface [4, 5]. In the presented work [6], we demonstrate that there is an additional, purely classical mechanism that leads to finite-size effects and to nonlinearity of the electromagnetic response of conducting nanoparticle. In particular, we derive nonlinear polarizabilities in 1D (slab) and 3D (sphere) geometries. Our theory is non-perturbative and fully accounts for electron-electron interaction within the accuracy of the quasistatic approximation. The predicted effects differ from other optical nonlinearities, most importantly, by the unusual dependence of the nonlinear response on the intensity W of the incident laser beam. In our model, the nonlinear polarizability is proportional to $\sqrt{W}$, while in the models of Refs. [2, 3] it is proportional to W. Therefore, the predicted effect can be distinguished from other optical nonlinearities by investigating the nonlinear response as a function of W.

REFERENCES

1. Kreibig, U. and L. Genzel, *Surf. Sci.*, Vol. 156, 678, 1985.
2. Hache, F., D. Ricard, and C. Flytzanis, *J. Opt. Soc. Am. B*, Vol. 3, 1647, 1986.
3. Rautian, S. G., *J. Exp. Theor. Phys.*, Vol. 85, 451, 1997.
4. Pustovit, V. N. and T. V. Shabazyan, *J. Opt. Soc. Am. A*, Vol. 23, 1369, 2006.
5. Pustovit, V. N. and T. V. Shabazyan, *Phys. Rev. B*, Vol. 74, 085408, 2006.
6. Panasyuk, G. Y., J. C. Schotland, and V. A. Markel, *Phys. Rev. Lett.*, accepted for publication.

Light Transmission through Nanohole in Film in the Evanescent Waves Area Examination via Discrete Sources Method

Yu. Eremin[1], **E. Eremina**[3], **N. Grishina**[1], **and T. Wriedt**[3]

[1]Moscow Lomonosov State University, Moscow, Russia
[2]Universitaet Bremen, Bremen, Germany
[3]Institut für Werkstofftechnik, Bremen, Germany

Abstract— The discovery of enhanced optical transmission through a sub-wavelength hole has attracted considerable interest to this optical phenomena and applications associated with nanoscale apertures in metal films [1]. The ability to localize light in spots much smaller than the volume predicted by diffraction theory offers multiple applications in biophotonics, such as probing a few molecules in a highly concentrated solution or monitoring a cell membrane with a sub-micrometer resolution. Combination of a hole with other surface nanostructures or using nanohole arrays offers a wide variety of potential applications in nanooptics as well. It is generally agreed that surface plasmon resonances play a key role in enhancing of light transmission through apertures in noble metal films [2]. Different groups worldwide have recently examined the transmission properties of sub-wavelength apertures. But the most of them considered normal incidence of a plane wave on the film surface as an external excitation. At the same time, there are multiple practical applications involving an evanescent wave scattering [3, 4]. Using evanescent waves allows to avoid a problem of filtering the scattered light from the refracted one. In this presentation, we consider transmission properties of a single sub-wavelength hole in noble-metal film deposited on a glass prism. The Discrete Sources Method (DSM) [4] is adjusted to model polarized light propagation through cylindric nanohole. The influence of the incident angle, hole's diameter, film material and hole filling on the transmission properties of the nanohole is investigated.

The computer model has been used for the scattering analysis is based on the DSM [4]. This technique constructs the scattered field everywhere outside an axial-symmetric hole as a finite linear combination of the fields resulting from dipoles and multipoles distributed over the axis of symmetry inside the hole or located in the adjacent complex plane area. The Green Tensor of multilayered structure: air-film-glass is employed to account for complete interactions of the hole with a stratified interface analytically [3]. Therefore, the solution for the scattered field satisfies Maxwell's equations, infinity conditions and transmission conditions for the fields at the interfaces. Then the unknown discrete sources amplitudes are determined from transmission conditions enforced at the hole's surface only.

We considered hole diameter 30 nm in Ag (or Au) film of thickness 45 nm. The main result of this research consists in the following: extreme transmission of P-polarized scattered intensity in the evanescent waves area has been detected. This transmission in order exceeds transmission under the normal incidence of a plane wave. The effect of extreme transmission seems to be interesting for different applications in nanooptics and biophotonics, including optical antennas and biosensors.

ACKNOWLEDGMENT

Authors would like to acknowledge support of this work by Russian Foundation for Basic Research.

REFERENCES

1. Ebbesen, T. W., et al., "Extraordinary optical transmission through sub-wavelength hole arrays," *Nature*, Vol. 391, 667–669, 1998.
2. Wannemacher, R., "Plasmon-supported transmission of light through nanometric holes in metallic thin films," *Opt. Comm.*, Vol. 195, 107–118, 2001.
3. Grishina, N. V., Y. A. Eremin, and A. G. Sveshnikov, "Analysis of evanescent waves transformation based on Discrete Sources Method," *J. Commun. Techn. Electron.*, Vol. 49, 117–124, 2004.
4. Eremin, Y. A. and A. G. Sveshnikov, "Mathematical models in nanooptics and biophotonics problems on the base of Discrete Sources Method," *Comput. Maths. Math. Phys.*, Vol. 47, No. 2, 2007.

Spectral Scattering Properties of Nanohole in Film in the Evanescent Waves Area Analysis via Discrete Sources Method

N. Grishina and Yu. Eremin

Moscow Lomonosov State University, Moscow, Russia

Abstract— The discovery of enhanced optical transmission through a sub-wavelength hole has attracted considerable interest to this optical phenomena and applications in nanooptics and biophotonics [1]. Different group of researchers worldwide have recently examined the transmission properties of sub-wavelength apertures. But the most of them considered normal incidence of a plane wave on the film surface as an external excitation. At the same time, there are multiple practical applications involving an evanescent wave scattering [2, 3]. Using evanescent waves allows to avoid a problem of filtering the scattered light from the refracted one. In this presentation, we consider transmission properties of a single sub-wavelength hole in noble-metal film deposited on a glass prism in spectral region. The Discrete Sources Method (DSM) [3] is adjusted to model polarized light transmission through cylindric nanohole. The influence of the incident angle, hole's diameter, film material and hole filling on the transmission properties of the nanohole is investigated.

The realized computer model presented here is based on the DSM [3, 4]. This technique constructs the scattered field everywhere outside an axial-symmetric hole as a finite linear combination of the fields originated by multipoles distributed over the axis of symmetry inside the hole or located in the adjacent complex plane area. The Green Tensor of multilayered structure: air-film-glass is employed to account for complete interactions of the hole with a stratified interface analytically [2]. Therefore, the solution for the scattered field satisfies Maxwell's equations, infinity conditions and transmission conditions at the interfaces. Then the unknown discrete sources amplitudes are determined from transmission conditions enforced at the hole surface.

DSM numerical scheme is based on axial symmetry of the scattering geometry (hole-interface). Exciting plane wave impinging the hole from prism surface is resolve in Fourier series with respect to the azimuth angle. This leads to the reducing surface approximation to a set of one dimensional approximating problems enforced at the hole profile. To fit the transmission conditions we use generalized point-matching technique. Multipoles amplitudes are determined as pseudo-solutions over-determined systems of the linear equations. The DSM scheme enables to consider all incident angles and both polarization P and S at once. The DSM computer model controls convergence and stability of the results by a posterior evaluation of the surface residual at the hole surface.

We considered nanohole of diameter 30 nm in Ag (or Au) film of thickness 45 nm. The main result of this research consists in the following: extreme transmission of P-polarized scattered intensity in the evanescent waves area has been detected. This transmission in order exceeds transmission under the normal incidence of a plane wave. The effect of extreme transmission seems to be important for different kind applications in nanooptics and biophotonics, including optical antennas and biosensors.

ACKNOWLEDGMENT

Authors would like to acknowledge support of this work by Russian Foundation for Basic Research.

REFERENCES

1. Wannemacher, R., "Plasmon-supported transmission of light through nanometric holes in metallic thin films," *Opt. Comm.*, Vol. 195, 107–118, 2001.
2. Grishina, N. V., Y. A. Eremin, and A. G. Sveshnikov, "Analysis of evanescent waves transformation based on Discrete Sources Method," *J. Commun. Techn. Electron.*, Vol. 49, 117–124, 2004.
3. Eremin, Y. A. and A. G. Sveshnikov, "Mathematical models in nanooptics and biophotonics problems on the base of Discrete Sources Method," *Comput. Maths. Math. Phys.*, Vol. 47, No. 2, 2007.
4. Grishina, N. V., Y. A. Eremin, and A. G. Sveshnikov, "Resonance properties of nanorods analysis via Discrete Sources Method," *Moscow University, Physics Bulletin*, Vol. 61, No. 1, 2007.

Far-field Electromagnetic Wave Scattering from Optically Rough Surfaces: Comparison of Measured and Calculated Results

John C. Stover[1] and Vladimir V. Lopushenko[2]

[1]The Scatter Works, Inc., USA
[2]CMC Faculty, Moscow State University, Russia

Abstract— The overall objective of this work is to fabricate a suite of metal samples that can be used to verify or refute a computer model developed on the base of Mean Field Theory (MFT) [1] to predict scatter from optically rough surfaces. The samples are flat metal disks that were measured first to determine their surface roughness statistics and then to determine their optical scatter characteristics under a variety of conditions. There are several samples covering a Root Mean Square (RMS) roughness range of about 0.8λ to 2.8λ in the 0.01 to 1.0 inverse micrometer frequency range.

The process of measuring rough surface statistics is complicated first of all by the need to correct the profilometer measurements at high spatial frequencies [2]. This problem was expected as most profilometers have response problems above spatial frequencies starting about 0.1 to 0.3 inverse micrometers. Another problem arises because profilometers report 1-D Power Spectral Density (PSD) functions [2]. That is, they consider spatial frequencies propagating only in the direction of the scan, but BRDF is related to 2-D PSDs, which contain frequencies propagating on the surface in all directions. This effect is easily seen in the lab as cross diffraction peaks that appear from a surface composed of two perpendicular gratings.

This presentation discusses the issues associated with solving these two problems. The 1-D to 2-D problem is solved by working with isotropic surfaces where a conversion expression can be used. The high frequency cutoff issue is more difficult and requires a correction transfer function for the profilometer. This is developed by measuring a 2-D optically smooth surface and relating the profilometer PSD to that found using the perturbation expression. This is then applied to the measured PSDs of the rougher surfaces. A serious concern is the assumption of linearity (in profilometer response) that may not be true for the rougher surfaces; however, the modeling results seem close enough that this may not be an issue.

We present the comparisons of computer simulations and measurements for the selected metal samples in case both p and s-polarized plane waves at different incident angles. For simplicity, the PSD function is approximated with an ABC model [3] where parameters A, B and C are determined from the corrected profilometer data. The predicted scattering distributions exhibit very good agreement with the measured BRDFs; for a couple of samples one can observe that theoretical and experimental plots are almost identical.

REFERENCES

1. Lopushenko, V. V., "Calculation of scattering from microroughness of filmed wafers," *Proc. of the 4st Conference on Electromagnetic and Light Scattering by Nonspherical Particals: Theory and Applications*, 231–238, Vigo, Spain, September 20–21, 1999.
2. Stover, J. C., "Rough surface characterization and comparison of scatter measurements and models," *SPIE Proc.*, 1215, August 2005.
3. Stover, J. C., "Optical scattering: Measurement and analysis," *SPIE*, 1995.

Far-field Electromagnetic Wave Scattering from Optically Rough Surfaces: Computer Model Based on Mean Field Theory

Vladimir V. Lopushenko
CMC Faculty, Moscow State University, Russia

Abstract— In this paper the Mean Field Theory (MFT) presented recently to model scattering from naturally rough surfaces [1] is extended to calculate incoherent scattering from 2D rough metal flats, which can be categorized as unfinished or everyday surfaces. An important fact to note is that the root-mean square (RMS) height/wavelength ratio is not small parameter for such surfaces. Therefore, MFT is supposed to be applied for the 2D case in scattering from substantially rough surfaces having RMS height comparable with wavelength of the incident radiation.

As it follows from the electric field representation based on the generalized Lippman- Schwinger integral equation, used in the frame of MFT, it is essential to solve accurately the reference problem formulated for the average dielectric permittivity function. Generally speaking, these solutions can be found only numerically. In case of the rough surfaces with the high refractive index like metals more reliable numerical scheme has to be employed to obtain the correct solution. To assure accurate simulations, the approach developed in [2] has been applied and the corresponding Riccati equations have been derived from the reference problems, formulated for the electric field components. Second-order numerical scheme was built then to solve the obtained boundary problem. It was shown that similar technique can be developed to find Green's tensor components. As in [2], it was confirmed, that solutions of the Riccati equations vary slowly, therefore the presented numerical scheme seems to be very accurate.

Another important computational aspect, which affect essentially the accuracy of the predicted results relate to 2D integrations over infinite surface. Previously, such integrals have been computed by means of 2D Fourier transform. In the current model the integration is performed with the improved procedure based on isotropic properties of the considered surfaces, when the required 2D integrals can be converted to 1D Hankel transforms. New Fast Hankel Transform (FHT) procedure similar to well-known FFT has been developed to compute Hankel integrals efficiently. It is essential that the developed FHT does not require computations of the Bessel functions and convolutions.

In the next presentation we consider the experimental verification of the presented approach in case of a number of metal samples having different roughness statistics.

ACKNOWLEDGMENT

Author would like to acknowledge support of this work by Civilian Research & Development Foundation (CRDF), project RC0-1348.

REFERENCES

1. Lopushenko, V. V., "Mean-field theory of light scattering by naturally rough surfaces," *Progress In Electromagnetics Research Symposium Abstracts*, 515, Cambridge, MA, USA, March 26–29, 2006.
2. Dmitriev, V. I., *Fields in the Stratified Media*, Moscow State Univ. ed., Moscow, Russian, 1963.

Session 5A1
EM Methods for ICs or Computational Electromagnetics

Inductance Extraction in ICs using Multilevel Green's Function Interpolation Method with Volume Loop Bases

Hao Gang Wang and Peng Zhao
EM Academy at Zhejiang University, Zhejiang University, China

Abstract— The studying of inductance extractions are very important in designing RFICs, IC packages, and RF MEMs, and so on, because 1) in the deep submicron techniques, inductances effects of interconnects become more and more serious and introduce non-negligible voltage drops; 2) inductances of the lead frame will directly affect the output signals from the chip; 3) in the new package technique, though the bumps are used to reduce the parasitic inductances, this parasitic effects of the bumps become more and more significant, following the further reduction of the chip size; 4) in RF ICs and RF MEMS, mirco spiral inductors are widely used as the passive components of the filters, match networks, resonators, and even RF biasing choke.

In this paper, we will use the recently developed MLGFIM with radial basis function interpolation technique to solve this kind of problems. In discretizing the volume integral equation, we use the volume loop bases. Instead of obtaining the volume loop impedance matrix, we use the method similar to the mesh analysis. However, we adopt the SWG bases instead of the filaments modeling and find the source loop basis functions using the shortest path algorithm. Then, we use this MLGFIM-Volume Loop Algorithm to solve for the inductances encountered in ICs. The numerical results in this paper show its validity and efficiency.

ACKNOWLEDGMENT

This work was supported by national nature science foundation of China No. 60501017 and provincial nature science foundation of Zhejiang, China No. Y105477.

Fabrication and Characterization of Fully On-chip C-band Microwave Resonators with Increased Q-factor and Reduced Chip Size

Rohat Melik[1, 2] **and Hilmi Volkan Demir**[1, 2, 3]

[1]Department of Electrical and Electronics Engineering, Bilkent University, Ankara 06800, Turkey
[2]Nanotechnology Research Center, Bilkent University, Ankara 06800, Turkey
[3]Department of Physics, Bilkent University, Ankara 06800, Turkey

Abstract— We develop and demonstrate fully-integrated microwave resonators working in C-band (4–8 GHz) with high quality-factors (Q-factors) despite their significantly reduced chip size. Here we present our general chip design methodology and modeling, and microfabrication to achieve high Q-factors with small footprint. In particular, we report on a fully on-chip resonator with a chip size of 540 µm × 540 µm that exhibits a Q-factor of 47.10 at 6.97 GHz. In our modeling, we construct a new two-port circuit representation to control the design parameters and minimize losses of our chips to increase their Q-factors. Using this two-port model, our design methodology reduces the effect of skin depth to build high Q-factor resonators even when their metal films are made thinner than the skin depth. In our implementation, unlike the conventional approaches that typically consider the dielectric film capacitance as the parasitic capacitance, we use the film capacitance as the capacitor of our LC tank circuit and thus avoid the need for the use of an external capacitor to tune the resonance frequency. Also, as opposed to the traditional approaches that commonly use a spiral coil only as an inductor, we make use of the coil as the distributed LC resonator to obtain high Q-factor in small footprints. Conventionally, when the chip size is decreased, the resonance frequency is increased and the quality-factor is decreased. However in our implementation, with the reduction of the chip size, we observe that the quality-factor is increased while the resonance frequency is increased. In our experimental characterization, we demonstrate that the results of our analytical modeling and numerical simulations are in good agreement with the experimental data. For the design of our 540 µm × 540 µm chip, we theoretically compute a resonance frequency of 6.70 GHz and experimentally measure a resonance frequency of 6.97 GHz. Furthermore, we numerically compute a Q-factor of 52.40 at 6.70 GHz and experimentally demonstrate a Q-factor of 47.10 at 6.97 GHz. Our proof-of-concept demonstrations show that such compact integrated microwave resonators hold great promise for high-frequency, high-Q resonator applications.

Scale-changing Technique for the Electromagnetic Modeling of Multi-scale Structures

Herve Aubert
INPT-ENSEEIHT and LAAS-CNRS, France

Abstract— Multi-scale structures considered here exhibit multiple metallic patterns whose sizes cover a large range of scales. Examples are given by multi-band frequency-selective surfaces, active or passive reflectarrays, or self-similar (pre-fractal) planar objects. Applying available numerical techniques to such multi-scale structures requires prohibitive execution time and memory resources. In order to overcome these numerical difficulties and to elaborate a fast and accurate design tool, an original monolithic (unique) electromagnetic approach is presented here. This new technique, named the *Scale Changing Technique*, is based on the cascade of multi-modal *Scale Changing Networks*, each network modeling the electromagnetic coupling between two successive scale levels. At a given scale level s the modes that participate to the electromagnetic coupling with the lower scale level s-1 are said *active* and are symbolized by ports in the network representation (see Figure); otherwise the modes are said *passive* and are used for describing the fine-scale variations of the electromagnetic field. Very recently the *Scale Changing Technique* has been applied to the design and electromagnetic simulation of active planar phase-shifters, discrete self-similar scatterers and multi-frequency selective surfaces [1, 2]. In their previous papers the author and his collaborators have not described in detail the theory behind the *Scale Changing Technique*, focusing their attention on the applications of the technique to specific multi-scale structures and on experimental validations.

At the conference, the *Scale-Changing Technique* will be presented in detail and generic bounded and un-bounded electromagnetic scattering problems will be solved via the cascade of *Scale-Changing Networks*. Numerical results will illustrate the key properties of the proposed multi-scale approach.

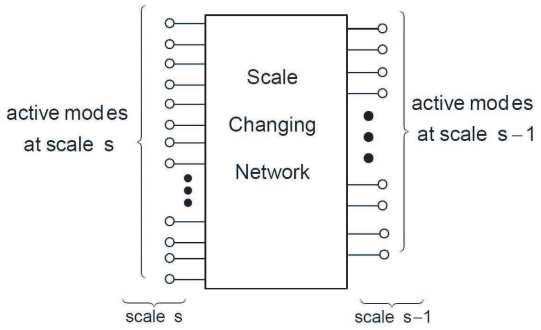

Figure 1: The Scale-changing Network modeling the electromagnetic coupling between the scales s and s-1.

REFERENCES

1. Voyer, D., H. Aubert, and J. David, "Scale-changing technique for the electromagnetic modeling of planar self-similar structures," *IEEE Trans. Antennas Propagat.*, Vol. 54, No. 10, 2783–2789, 2006.
2. Perret, E., H. Aubert, and H. Legay, "Scale-changing technique for the electromagnetic modeling of MEMS-controlled planar phase-shifters," *IEEE Trans. Microwave Theory and Tech.*, Vol. 54, No. 9, 3594–3601, 2006.

An Efficient Space Domain Formulation of the MOM Method for Planar Circuits

Chaker Essid[1], **M. Bassem Ben Salah**[1], **Faleh Yassine**[1]
Abdelaziz Samet[1], **and Ammar B. Kouki**[2]

[1]URCSE, École Polytechnique de Tunisie, Tunisia
[2]LACIME, École de Technologie Superiéure, Montréal, Canada

Abstract— The mixed potential integral equation (MPIE) in conjunction with the spatial-domain MOM is the best suited and most robust approach for planar circuit analysis. This method is based on the closed-form expression of the Green's functions in the space domain using a finite number of discrete complex images (DCIM) that approximate it in the spectral domain and thus avoid the numerical evaluation of Sommerfeld integrals [1, 2]. Using this representation, the matrix elements that arise in the MOM formulation can be evaluated analytically as was proposed in [3, 4] where the closed-form Green's functions expressions were approximated by Taylor series expansions of the exponential terms. The resulting integrals are then evaluated analytically and give rise to mathematical functions with singularities that require special programming precautions [5]. To avoid the singularities problem, an efficient and fast method, which is based on a new Taylor series expansion is proposed in this paper, where the entire integrands are expressed in terms of polynomial functions.

In this paper, we present a new technique for evaluation of spatial-domain method of moment matrix entries, in conjunction with a DCIM two-level approximation [6]. This technique is based on the Taylor series expansion of the complete expression of each complex image, i.e., the term $\frac{e^{-k_0 r}}{r}$ instead of the exponential term only, in terms of well-behaved polynomial functions. The MOM matrix elements are again evaluated analytically in an efficient and fast manner. The proposed technique has been implemented and compared to previous techniques [1–3] for the analysis of microstrip structure. It has been found to yield considerable computational time savings with out compromising the precision.

REFERENCES

1. Chow, Y. L., J. J. Yang, D. G. Fang, and G. E. Howard, "A closed-form spatial Green's function for the thick microstrip substrate," *IEEE Trans. Microwave Theory Tech.*, Vol. 39, 588–592, Mar. 1991.
2. Sarkar, T. K. and O. Pereira, "Using the matrix pencil method to estimate the parameters of a sum of complex exponentials," *IEEE Trans. Antennas and Propagation Magazine*, Vol. 37, 48–55, Feb. 1995.
3. Alatan, L., M. I. Aksun, K. Mahadevan, and M. T. Birand, "Analytical evaluation of the MOM matrix elements," *IEEE Trans. Microwave Theory Tech.*, Vol. 44, No. 4, Apr. 1996.
4. Aksun, M. I., F. Caliskan, and L. Gurel, "An efficient method for electromagnetic characterization of 2-D geometries in stratified media," *IEEE Trans. Microwave Theory Tech.*, Vol. 50, 1264–1274, May 2002.
5. Samet, A. and A. Bouallegue, "Fast and rigorous calculation method for MoM matrix elements in planar microstrip structures," *Electronics Letters*, Vol. 36, No. 9, Apr. 2000.
6. Aksun, M. I., "A robust approach for the derivation of closed-form Green's function for a general microstrip geometry," *IEEE Trans. Microwave Theory Tech.*, Vol. 44, 651–658, May 1996.

Scattering from the Flat Strip Geometries in the Layered Medium by Using the Sinc Based Method of Moments

Fadıl Kuyucuoğlu[1], **Taner Oğuzer**[2], **and İbrahim Avgin**[1]

[1]Electrical and Electronics Eng. Department, EGE University, Bornova, İzmir, Turkey
[2]Electrical and Electronics Eng. Department, Dokuz Eylül University, Buca, İzmir, Turkey

Abstract— The Method of Moments (MOM) is widely used in the electromagnetic scattering problems in 2D and 3D. The integral equation formulation of the MoM depends on the boundary conditions from a given electromagnetic boundary value problem. Then this integral equation is discretized and the solution process in a layered medium, the generalized pencil of function technique (GPOF) is used. This provides us a fast solution of the formulated integral equation of the MoM [1, 2].

However we approached to the solution using the sinc based MoM in the layered medium as a Galerkin procedure and this case only H-polarization is studied. The GPOF technique is used here to find a closed form expression of the Green's function in the solution process. We had already studied the free space case in [4] and our results were compatible with the previous literature. We also worked on the E-polarization case of the strip scattering in the layered medium by using the GPOF technique in [3]. The present study is a solution of the H-polarization of a similar problem in [3]. The properties of the sinc functions consist of an orthogonal set and their convolution is also a sinc function which we frequently used it here. Finally the MoM is reduced to an algebraic matrix equation as in the conventional MoM but the integral elements are computed with the analytical functions except for those close to diagonal elements. Also we observed that the error in the approximation of the main matrix elements reduce to zero as the sinc function bandwidth increases [3]. Therefore we can find fast solutions in a few digits accuracy with an available desktop computer. There are some related studies using sinc basis functions in the recent literature but they are not applied to singular problems and the computation of the main matrix elements are not specified.

The present formulation is applied to strip structures in the layered medium. Upper loaded and down loaded and also multistrips inside the multilayer geometries are tested. The surface current densities are obtained and compared with the previous results given in [1] and [2]. The far field scattering also is obtained and basic concepts of the physics are checked.

REFERENCES

1. Aksun, M. I., F. Çalışkan, and L. Gürel, "An efficient method for electromagnetic characterization of 2-D geometries in stratified media," *IEEE Transactions on MMT*, Vol. 50, No. 5, May 2002.
2. Çalışkan, F., "Efficient methods for electromagnetic characterization of 2-D geometries in stratified media," Msc thesis submitted to Electrical and Electronics Eng. Department of Bilkent University, August 1997.
3. Oğuzer, T., F. Kuyucuoğlu, and İ. Avgin, "Electromagnetic scattering from strip geometry in the layered medium by the method of moments with the sinc type basis functions," *IEEE Transactions on AP*, 2007.
4. Oguzer, T. and F. Kuyucuoglu, "Method of moments solution by using sinc type basis functions for the scattering from a finite number of conducting trip grating," *Turkish Journal of Electrical Engineering and Computer Sciences*, 2007.

A New Monte Carlo Methodology for the Solution of Partial Differential Equations Subject to Neumann and Mixed Boundary Conditions

K. Chatterjee[1], **M. Sandora**[1], **C. W. Yu**[1], **S. Srinivasan**[1], **and J. Poggie**[2]

[1]Department of Electrical Engineering
The Cooper Union for the Advancement of Science and Art
Room 459, 51 Astor Place, New York, NY 10003-7185, USA
[2]Computational Sciences Center, Wright-Patterson Air Force Base, OH 45433-7512, USA

Abstract— We present a new Monte Carlo (random walk) methodology for the numerical solution of partial differential equations subject to Neumann and mixed boundary conditions. In traditional Monte Carlo algorithms, the termination of the random walk becomes a problem for Neumann and mixed boundary condition problems where the solution is not known at all points of the domain boundary. In Monte Carlo literature [1], these boundary conditions are formulated as partially reflecting as the random-walker has a chance of either being absorbed in the problem boundary or being thrown back into the problem domain, resulting in relatively large computational times. In our formulation, we have eliminated the need for reflecting boundaries through the use of novel Green's functions that mimic the boundary conditions of the problem of interest, which leads to the transformation of partially reflecting boundaries into absorbing boundaries. The methodology has been validated by solutions of the one-dimensional Laplace's equation [2] and the modified Helmholtz equation subject to mixed boundary conditions and excellent agreement has been obtained between analytical solutions and Monte Carlo results. The newly developed methodology has been parallelized and a near linear rate of parallelization has been obtained with as many as thirty-two processors. The extension of this methodology to other important equations and to problems in two and three dimensions will form the basis of our future research in this area. The ultimate objective of this research is the application of this methodology to electromagnetic problems, heat transfer problems and plasma flow problems within an aerodynamic context.

ACKNOWLEDGMENT

This research has been supported by the Air Force Office of Scientific Research through a grant (FA9550-06-1-0439) monitored by Dr. F. Fahroo. Additional support has been provided in the form of summer fellowships for Prof. K. Chatterjee and Mr. C. W. Yu at the Air Force Research Laboratory at Wright Patterson Air Force Base (AFRL/WPAFB). We would also like to acknowledge valuable discussions with Dr. D. Gaitonde at AFRL/WPAFB.

REFERENCES

1. Haji-Sheikh, A., Application of Monte Carlo Methods to Thermal Conduction Problems, Doctoral Thesis, University of Minnesota, 106–108, 1965.
2. Chatterjee, K., C. Yu, S. Srinivasan, and J. Poggie, "A new floating random walk methodology for neumann and mixed boundary condition problems without reflections at boundaries: Validation with Laplace's equation in one dimension," *Far East Journal of Mathematical Sciences*, Vol. 26, No. 3, 705–713, September 2007.

A Quasi-Monte Carlo Solver for Partial Inductances in IC Interconnect Structures

I. Dalal, D. Stefan, C. W. Yu, S. Srinivasan
N. Chitrik, M. Sandora, J. Salomon, and K. Chatterjee
Department of Electrical Engineering
The Cooper Union for the Advancement of Science and Art
Room 459, 51 Astor Place, New York, NY 10003-7185, USA

Abstract— With operating frequencies reaching the multi-GHz range, the role of on-chip inductance is becoming increasingly significant. The inclusion of inductance in the interconnect model is particularly necessary in clock distribution networks and also in signal and power lines, which have wide wires and hence low resistance. The principal complexity in the extraction of inductance is that one needs to have the knowledge of the currents in advance. However, the current distribution in today's complicated interconnect structures depends on the device and interconnect resistances, inductances and capacitances. Therefore, the modeling of the current distribution is a difficult proposition. The conventional approaches to inductance extraction involve "loop inductance" models, which make various simplifying assumptions in determining the current distribution. A radically different approach to the modeling of inductance has been suggested in literature, which precludes the need to determine the current distribution in advance. This approach is based on the Partial Element Equivalent Circuit (PEEC) method. In this approach, the interconnect lines are divided into wire segments and self and mutual inductances are extracted for these "partial elements." It has been demonstrated in literature that this PEEC-based approach is more accurate than the loop inductance models.

In a previous work [1], we developed a Monte Carlo algorithm for the stochastic extraction of the mutual inductances of these "partial elements." In this work, the mutual inductance between two "partial elements" was formulated as a six-dimensional integral under the "zero-frequency approximation," and this six-dimensional integral was estimated through Monte Carlo integration. However, this integration was performed with pseudorandom numbers and the statistical sampling error was of the order of $N^{-1/2}$, N being the number of integration samples. In this work, we improve our previously-developed algorithm through the use of quasirandom numbers. We present our work for three quasirandom (Halton, Sobol and Niederreiter) sequences where the statistical error of integration is observed to be of the order of N^{-1}. The increased convergence rate coupled with the almost linear rate of parallelization for the Monte Carlo method makes this algorithm very attractive for the extraction of partial inductances of IC interconnect structures.

ACKNOWLEDGMENT

This research has been funded in part by the Air Force Office of Scientific Research through a grant (FA9550-06-1-0439) monitored by Dr. F. Fahroo. Additional support has been provided in the form of summer fellowships for Prof. K. Chatterjee and Mr. C. W. Yu at the Air Force Research Laboratory at Wright Patterson Air Force Base (AFRL/WPAFB). We would also like to acknowledge valuable discussions with Dr. J. Poggie and D. Gaitonde at AFRL/WPAFB.

REFERENCES

1. Chatterjee, K., "A stochastic algorithm for the extraction of partial inductances in IC interconnect structures," *Applied Computational Electromagnetics Society Journal*, Vol. 21, No. 1, 81–89, March 2006.

Session 5A2a
Inverse and Forward Problems in Radiative Transport

An Efficient Numerical Method for the Radiative Transport Equation: Method of Rotated Reference Frames

M. Machida[1], **G. Panasyuk**[1], **V. A. Markel**[2], **and J. C. Schotland**[1]

[1]Department of Bioengineering, University of Pennsylvania, Philadelphia, PA 19104, USA
[2]Department of Radiology, University of Pennsylvania, Philadelphia, PA 19104, USA

Abstract— The light scattered in random media such as biological tissues is well described by the radiative transport equation (RTE). Various methods including the discrete ordinate method and the P_L approximation have been proposed to solve the RTE. [1–3] However, obtaining the intensity of light from the RTE is still a tough problem. Recently, a new method of solving the RTE for a three-dimensional random medium was proposed [4, 5]. The method is called the Method of Rotated Reference Frames (MRRF). In this talk, we will calculate the specific intensity of the light propagating in a three-dimensional random medium of a slab geometry, and show that the specific intensity is efficiently obtained with the MRRF.

In the RTE, the specific intensity $I(\mathbf{r}, \hat{\mathbf{s}})$ of light flowing in the $\hat{\mathbf{s}}$ direction at position $\mathbf{r}$ obeys the following equation.

$$\hat{\mathbf{s}} \cdot \nabla I(\mathbf{r}, \hat{\mathbf{s}}) + (\mu_{\mathrm{a}} + \mu_{\mathrm{s}}) I(\mathbf{r}, \hat{\mathbf{s}}) = \mu_{\mathrm{s}} \int \mathrm{d}^2 s' \, A(\hat{\mathbf{s}}, \hat{\mathbf{s}}') I(\mathbf{r}, \hat{\mathbf{s}}') + \varepsilon(\mathbf{r}, \hat{\mathbf{s}}), \tag{1}$$

where μ_{a} and μ_{s} are the absorption and scattering coefficients, $A(\hat{\mathbf{s}}, \hat{\mathbf{s}}')$ is the phase function, and $\varepsilon(\mathbf{r}, \hat{\mathbf{s}})$ is the source.

In the MRRF, the specific intensity, which is expressed as a sum over evanescent modes, is expanded in the basis of spherical harmonics *for each mode*. Then, the specific intensity in a medium is calculated as a sum of the evanescent modes. The coefficients in the sum are determined by the boundary conditions.

In the talk, we will first give the formulation of the MRRF and then show numerical results on the specific intensity of light propagating in a slab-shaped random medium.

REFERENCES

1. Thomas, G. E. and K. Stamnes, *Radiative Transfer in the Atmosphere and Ocean*, Cambridge University Press, Cambridge, 1999.
2. Case, K. M. and R. F. Zweifel, *Linear Transport Theory*, Addison-Wesley, Reading, MA, 1967.
3. Ishimaru, A., *Wave Propagation and Scattering in Random Media*, Academic Press, San Diego, 1978.
4. Markel, V. A., "Modified spherical harmonics method for solving the radiative transport equation," *Waves in Random Media*, Vol. 14, No. 1, L13–L19, 2004.
5. Panasyuk, G., J. C. Schotland, and V. A. Markel, "Radiative transport equation in rotated reference fraqmes," *J. Phys. A: Math. Gen.*, Vol. 39, No. 1, 115–137, 2006.

Utilizing the Radiative Transfer Equation in Optical Tomography

T. Tarvainen[1,2], **M. Vauhkonen**[1], **V. Kolehmainen**[1]
J. P. Kaipio[1], **and S. R. Arridge**[2]

[1]Department of Physics, University of Kuopio, P. O. Box 1627, Kuopio 70211, Finland
[2]Department of Computer Science, University College London, Gower Street
London WC1E 6BT, United Kingdom

Abstract— We propose a method which utilizes the radiative transfer equation (RTE) in optical tomography. In this approach, the RTE is used as light propagation model in those regions in which the assumptions of the diffusion theory are not valid and the diffusion approximation (DA) is used elsewhere. Both the RTE and the DA are numerically solved with a finite element method. In the finite element solution of the RTE, both the spatial and angular discretizations are implemented in piecewise linear bases.

The ray effect may disturb the standard finite element techniques when solving the RTE. The ray effect can produce oscillating results or it can visually be seen as "photon rays" radiating from the source into the direction of the discretization angels. To overcome these problems, the streamline diffusion modification is utilized in the finite element solution of the RTE.

We test the method with two-dimensional simulations. We show the finite element solutions of the RTE in medium with different optical properties. Moreover, the RTE is utilized in light transport simulations in realistic two-dimensional head geometry from a newborn baby's head.

Radiance Calculations for Transport Equations with Differential and Integral Scattering Operators

Kevin G. Phillips[1] **and Carlo Lancellotti**[2]

[1]CUNY Graduate Center, USA
[2]The College of Staten Island, USA

Abstract— Using the P_N-method, we present a numerical framework in which to obtain solutions to radiative transport models in the semi-infinite slab with scattering operators of differential or integral type subject to boundary conditions corresponding to plane-wave illumination. The independence of the method from any particular choice of integral or differential scattering operator in the angular variables is demonstrated. Using the radiative transport equation with Henyey-Greenstein phase function, and forward-scattering models such as the Fokker-Planck equation, the modified Leakeas-Larsen equation, and a generalized Fokker-Planck equation involving a pseudo-differential operator due to Pomraning as specific model examples, the backscattered and transmitted radiance at the surfaces of a semi-infinite slab are presented. We comment on the ability of the different forward-scattering approximations to describe photon transport in the limit of unit anisotropy.

Fluorescence Lifetime Imaging Using the Equation of Radiative Transfer and Level Sets

Oliver Dorn

Universidad Carlos III de Madrid, Avda de la Universidad 30, 28911 Leganes, Madrid, Spain

Abstract— We present a novel reconstruction algorithm for fluorescence lifetime imaging which is based on a coupled system of two time-dependent radiative transfer equations and a level set technique. The region of interest is irradiated by a short pulse of incoming laser light of a given frequency ('excitation light') which gives rise to stimulated fluorescence light at a different frequency ('emission light'). The propagation of both the excitation light and the emission light is modelled by radiative transfer equations in 2D which are coupled by the fluorophore concentration, quantum yield and lifetime. Data are gathered both at excitation and emission frequency. The goal is to recover the distribution and lifetime of the fluorophore in the medium from these data simultaneously.

A level set technique is employed for modelling the distribution of the fluorophore in the medium. It is assumed that the fluorophore is concentrated in a well-defined region which might consist of an unknown number of disconnected components. In the level set technique the goal is to determine the boundaries of this region together with some region-internal activity and lifetime profiles from the given data. These boundaries are implicitly encoded as the zero level set of some level set function. For solving the inverse problem, an evolution approach is employed which modifies an initial guess for the level set function in descent directions of some cost functionals until the mismatch between the reference data and the data calculated for the latest best guess is reduced sufficiently according to some criterion. In addition to the internal activity profile of the fluorophore we also aim at estimating the space-dependent lifetime at each location where a fluorophore is detected. Numerical experiments are presented which use a coupled system of two time-dependent radiative transfer equations in 2D for the forward modelling and an adjoint technique for the inversion task. The main application which we have in mind is the monitoring of fluorophore markers in small animals by in-vivo fluorescence tomography.

ACKNOWLEDGMENT

This work is funded by the EU in the Framework Programme 6 Integrated Project with contract number LSHG-CT-2003-503259.

Mesoscale Optical Tomography

Lucia Florescu[1], **John C. Schotland**[1], **and Vadim A. Markel**[1,2]

[1]Department of Bioengineering, University of Pennsylvania, USA
[2]Department of Radiology, University of Pennsylvania, USA

Abstract— We present a novel tomographic imaging modality. The proposed technique utilizes visible or near-infrared light as a tissue probe in the intermediate, or *mesoscopic*, scattering regime when the photon mean free path is of the order of the system size. In this case, the light exhibits sufficiently strong scattering so that the image reconstruction methods of computed tomography are not applicable, yet the detected light is not diffuse and the diffuse tomography can not be employed. The principle idea of this techique that we refer to as the *single scattering optical tomography* (SSOT) is to measure single-scattered light by means of angularly-selective detectors and to use these measurements to reconstruct the tissue optical properties. The light transoport in the disordered medium is described by the fisrt-order scattering approximation to the radiative transport equation. The associated inverse problem of detrmining the extinction coefficient of an inhomogeneous medium from angularly-resolved measurement is similar to the problem of inverting the Radon transform of x-ray tomography, except that the ray integrals are evaluated not along straight lines but along broken rays (which corresponds to the path of a single-scattered photon). As a result, the method does not require rotating the imaging device around the sample and taking multiple projections and, therefore, can be used in backscattering. An algebraic image reconstruction algorithm is numerically implemented. The data is generated by solving the radiative transport equation numerically. An analytic image reconstruction formula analogous to the filtered backprojection formula of x-ray tomography is also derived. We demonstrate that SSOT enables image quality and level of detail that are customary in x-ray tomography but can be hardly expected in optical tomography with multiply scattered light.

Optical Imaging and Spectroscopy in Layered Tissues

Arnold D. Kim and Pedro González-Rodríguez
School of Natural Sciences, University of California
P.O. Box 2039, Merced, CA 95344, USA

Abstract— We study light propagation in layered tissues for applications in reflectance optical tomography and spectrscopy. Layered tissues are important models that take into account the different optical properties of superficial epithelial tissues and those of deep stromal tissues. We present recent theoretical and computational results allowing for parameter estimation or image reconstruction in epithelial tissue layers.

Session 5A2b
Electromagnetics and Photonics: New Applications and Methods 1

Non Perturbing, 3-Axis Electric Field Measurements Using Electro-optic Sensors

Anthony Garzarella and Dong Ho Wu

Naval Research Laboratory, Washington, DC 20375, USA

Abstract— Along with their use in THz generation, optical data storage, and other applications, electro-optic (EO) crystals have gained considerable interest in electric field detection applications. This is due to their compact size (a few mm^3), large intrinsic bandwidth (DC-THz), 3-axis capability, and ability to simultaneously measure both field amplitude and phase. Conventional sensors based on metallic probes perturb the very fields they measure. EO field sensors are all-dielectric, thus minimally perturb the external field. This allows them to be effectively utilized in environments such large magnetic fields and high power microwaves. We have developed both free space and optical fiber-attached EO field sensors using LiNbO3 crystals with minimum field sensitivities as low as several mV/m-$Hz^{1/2}$. In this report, we describe these sensors, their operation, figures of merit and demonstrate their nonperturbative and 3-axis field measurement capability.

New Metamaterial Using Dynamic Analysis at Millimeter Waves

Humberto C. C. Fernandes and Davi B. Brito

Federal University of Rio Grande do Norte, Department of Electrical Engineering, Brazil

Abstract— Electromagnetic metamaterials are broadly used as artificial effectively non-homogeneous electromagnetic structures, recently with desired dielectric and magnetic characteristics. In this paper the bilateral fin line with EBG — Electromagnetic Band Gap — metamaterial substrate is analyzed using the dynamic TTL — Transverse Transmission Line, method. In order to analyze this structure the effective dielectric constant and the attenuation constant are determined. The new results obtained for this application are presented at the first time.

Fin lines are widely used as a millimeter wave component due to its various advantages such as reducing size, weight, and low cost and easily used with other hybrid millimeter wave circuits. This paper presents an application of the EBG metamaterial bilateral finline. The analysis is made using the TTL method and the metamaterial definitions. The objective is to present the effect of the dielectric bi anisotropy bilateral finlines of the structure shown in Fig. 1. The paper discusses the effect of bi anisotropy on the effective dielectric constants and attenuation constant, by applying the anisotropy one by one in all three directions.

For this a non-homogeneous EBG structure medium, the incident wave undergoes a process of multiple scattering. The substrate shown in region 2 of Fig. 1 is modeled by utilizing bianisotropic tensor properties, which are expressed as:

$$\mu = \mu_0 \begin{bmatrix} \mu_{xx} & 0 & 0 \\ 0 & \mu_{yy} & 0 \\ 0 & 0 & \mu_{zz} \end{bmatrix} \tag{1}$$

$$\varepsilon = \varepsilon_0 \begin{bmatrix} \varepsilon_{xx} & 0 & 0 \\ 0 & \varepsilon_{yy} & 0 \\ 0 & 0 & \varepsilon_{zz} \end{bmatrix} \tag{2}$$

To calculate the numerical results it was developed a computational program in Fortran PowerStation language, according to the developed complete theoretical analyses. Compared to other full wave methods the TTL is an efficient and concise method to determine the planar and fin line characteristics, making possible a significant algebraic simplification of the equations involved in the process, and reducing the computational time. The effective dielectric constant and the attenuation constant are determined, and the new results obtained for this application are presented at the first time.

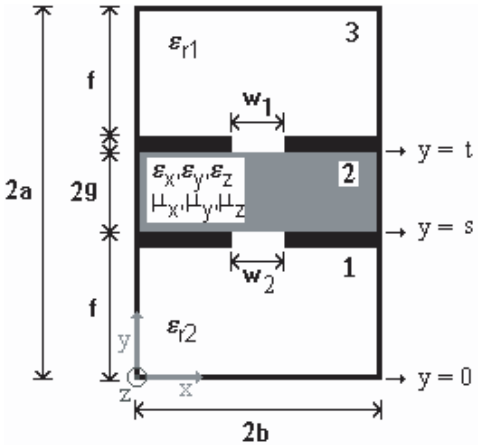

Figure 1: Transversal cut of a bilateral fin line structure with EBG substrate.

A New Application Metamaterial Antenna

Humberto C. C. Fernandes and M. Bonfim L. Aquino
Department of Electrical Engineering, Federal University of Rio Grande do Norte, Brazil

Abstract— Electromagnetic metamaterials are defined as artificial effectively homogeneous electromagnetic structures with peculiars properties not easily found in ubiquitous materials with desired dielectric and magnetic characteristics, so these characteristics can be used in some devices, as: antennas, fin lines, filters, etc. In this paper the EBG — Electromagnetic Band Gap — metamaterial substrate is applied to microstrip resonator. The structure was analyzed using the full wave TTL — Transverse Transmission Line — method. In order to analyze this structure the resonant frequency is obtained. The new results are presented and compared with previous another one of the specialized literature.

The microstrip resonator is widely used as a antenna due to its various advantages such as: reducing size, weight, and cost and in addition because it interfaces easily with other millimeter wave circuits. This device is composed of a rectangular patch, EBG substrate and a ground plane, The EBG material impede the propagation of electromagnetic waves in some frequency, this properties can be used to made devices most efficient, and eliminated unwanted frequencies. The analysis is made using TTL method and the metamaterial theory, together with the moment method and efficient bases function in both direction of the xz plane, as is shown in the Fig. 1.

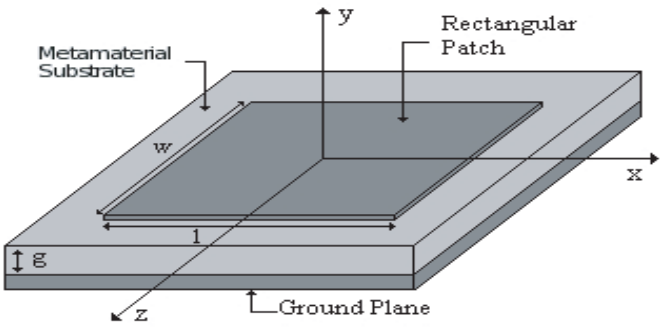

Figure 1: Microstrip resonator with metamaterial.

The metamaterial substrate shown in region 2 of Fig. 1 is modeled by utilizing bianisotropic tensor properties, and wave equations which are expressed as:

$$\mu = \mu_0 \begin{bmatrix} \mu_{xx} & 0 & 0 \\ 0 & \mu_{yy} & 0 \\ 0 & 0 & \mu_{zz} \end{bmatrix} \tag{1}$$

$$\varepsilon = \varepsilon_0 \begin{bmatrix} \varepsilon_{xx} & 0 & 0 \\ 0 & \varepsilon_{yy} & 0 \\ 0 & 0 & \varepsilon_{zz} \end{bmatrix} \tag{2}$$

$$\frac{\partial^2 \tilde{E}y}{\partial y^2} - \gamma^2 \tilde{E}y = 0 \tag{3}$$

$$\frac{\partial^2 \tilde{H}y}{\partial y^2} - \gamma^2 \tilde{H}y = 0 \tag{4}$$

To calculate the numerical results it was developed a computational program in Fortran PowerStation language, according to the previous theoretical analyses. The concise TTL method is easy to determine the microstrip resonator characteristics. The new results are presented and compared with previous another one of the specialized literature.

Spectral Enhancement of the SPOT Imagery Data to Assess Marine Pollution near Port Said, Egypt

M. Kaiser[2], **H. Aboulela**[1], **H. A. El-Serehy**[1], **and H. Ezz Edin**[1]

[1]Marine Science Department, Faculty of Science, Suez Canal University, Egypt
[2]Humanities Department, College of Arts and Sciences, Qatar University, Qatar

Abstract— Remote sensing is a powerful tool providing truly synoptic view of surface water quality. Spectral enhancement of the satellites was improved significantly over recent years. This research aims to utilize satellite image data to detect, monitor and map the different types of pollutants at the five study sites along the El-Gamil beach including; El-Debba, El-Manasra, El-Fardous, El-Gamil inlet and El-Gamil airport. The images are rectified, analyzed and processed by ERDAS IMAGINE 8.7. Image processing techniques were used to analyze the landsat thematic mapper imagery data (30 m resolution) for year 2000 and SPOT image data (10 m resolution) for year 2006. Image enhancement, principal component analysis (PCA), TM band ratios and supervised/unsupervised classifications were applied. Change detection was utilized to monitor water quality degradation due to throwing a high quantity of domestic sewage and virtually total absence of control on toxic components. Surface water samples were collected during summer of year 2006 to verify data extracted from SPOT image. Results of chemical analyses indicate that six heavy metals were detected in water with variable concentrations along the coastal zone; Iron (Fe), Manganese (Mn), Cadmium (Cd), Lead (Pb), Zinc (Zn) and Copper (Cu). Chemical analyses confirm data extracted from the images data indicating that El-Manasra area is the highest polluted site along the coastal zone due to the industrial development, oil exploration, sewage and agricultural drainage and the existence of an electric power. Result accuracy of SPOT data was checked through the field investigation. Water pollution decreases towards the east at El-Gamil inlet; however, significant marine water pollution was noticed from image processing and was confirmed by laboratory analysis at the El-Gamil airport. This due to receiving of the pollutants drifted from Damietta promontory by longshore currents and from the other eastern cities by the reverse seasonal currents. Reasonable management scheme and a suitable sewage treatment planet are suggested to protect beach resorts from water pollution and to mitigate the negative impacts of human activities and development planning.

Modal Propagation Analysis Method for the Design of MMI Coupler Based Microring Resonators

Laurence W. Cahill and Thanh Trung Le
La Trobe University, Melbourne, Victoria 3086, Australia

Abstract— The multimode interference (MMI) coupler based microring resonator is a versatile component for photonic signal processing applications. Based on this basic building block, many functional devices can be fabricated such as optical switches, filters, modulators, add-drop multiplexers, and true time delay devices. In the analysis and design of such structures it is usually assumed that the MMI coupler is described by a 2×2 transfer matrix similar to that of a directional coupler. However, such a simple approximation is inadequate for a detailed design. The purpose of this paper is to present a more appropriate method for the analysis and design of MMI coupler based microring resonators.

In this paper, the modal propagation method is used to determine the fields of the combination of an MMI coupler and a ring resonator. This method has the advantages of good accuracy, and quick computation compared with numerical methods such as FDTD and BPM. It is shown how the structure parameters such as the width and positions of access waveguides, width and length of the MMI coupler, and the waveguide geometry can be optimized to allow the designer to achieve a prescribed performance. This method can be applied to more complicated structures such as the double ring resonator structure, a 3×3 MMI coupler based microring resonator, and microring resonators in series or parallel. The accuracy of the analysis method is checked by comparison with 3D numerical techniques.

Session 5A3
Medical and Industrial Applications of EM Field

Medical Imaging and Diagnostics Based on Microwaves

Jan Vrba[1], **Ladislav Oppl**[1], **R. Zajicek**[1], **L. Visek**[1], **David Vrba**[1], **and Jan Vrba**[2]

[1]Dept. of EM Field, Czech Technical University in Prague, Prague, Czech Republic
[2]RWTH Aachen, Kopernikusstraße 16, Aachen 52074, Germany

Abstract— Future trends in medical applications of microwave technique and technology can be seen in development of new diagnostic and imaging methods based on high frequency EM field. A significant importance for the future can be identified for the following methods: Microwave tomography, Microwave radiometry, Measurement of complex permittivity, Imaging in the Terahertz waves band and Microwave diagnostic radars.

Interactions of EM field with biological systems are utilised in the area of therapy (oncology, physiotherapy, urology atp.) from late seventieth of last century. Wideutilization of microwave thermotherapy can be observed in the countries of EU, USA and Japan. Our activities in microwave thermotherapy in former Czechoslovakia started in the year 1981. Since 1990 we are member of ESHO (European Society for Hyprthermia Oncology), which co-operates with NAHS (North American Hyperthermia Society) and ASHO (Asian Society of Hyperthermia Oncology).

Recent trends in microwave medical applications are to study the possibilities to develop new diagnostics based on EM field resp. on microwace technique. A significant importance for the future can be identified for the next methods:

- Magnetic resonance,
- Microwave tomography,
- Microwave radiometry,
- Measurement of complex permittivity,
- Imaging with terahertz waves,
- Microwave diagnostic radar.

We will not talk here about magnetic resonance, as it is just well known and broadly used application of EM field in medical diagnostics. We will focus here on other above mentioned methods (excluding microwave diagnostics radars).

ACKNOWLEDGMENT

This research is supported by Grant Agency of the Czech Republic, project: "Microwave Imaging for Biomedical Applications" (102/05/0959) and by the research program MSM6840770012 "Transdisciplinary Research in the Area of Biomedical Engineering II" of the CTU in Prague, sponsored by the Ministry of Education, Youth and Sports of the Czech Republic.

REFERENCES

1. Vrba, J., *Medical Applications of Microwaves*, 168, ISBN 80-01-02705-8, 1. ed., Issued by CTU, Prague, 2003.
2. Semenov, S. Y., et al., "Three-dimensional microwave tomography, initial experimental imaging of animals," *IEEE Transactions on BME*, Vol. 49, No. 1, 55–63, Jan. 2002.
3. Gabriel, S., R. W. Lau, and C. Gabriel, "The dielectric properties of biological tissue — II. Measurements in the frequency range 10 Hz to 20 GHz," *Phys. Med. Biol.*, Vol. 41, 2251–2269, 1996.

Medical Diagnostics Using Reflection Method and Waveguide Probes — Feasibility Study

R. Zajíček, **T. Smejkal**, **L. Oppl**, **and J. Vrba**
Department of Electromagnetic Field, Czech Technical University in Prague, Czech Republic

Abstract—

Purpose: Paper deals with the complex permittivity measurement of biological tissues. Application of a waveguide probe for the complex permittivity measurement of biological tissues is shown. Different modifications of the section of metal waveguide are considered including the feasibility study of the waveguide applicator for microwave hyperthermia as a probe.

Materials and Methods: A non-destructive and non-invasive method based on reflection coefficient measurement attaching the material under test (MUT) is used. This method is based on the fact that the reflection coefficient of the probe depends on the dielectric parameters of MUT which is attached to it. New types of the probes are under investigation - the section of waveguide with H cross-section, the section of waveguide with the rectangular cross-section and with shorted walls, the section of waveguide with inserted dielectric wedge and finally the section of waveguide filled by the liquid dielectric. Properties of these prototypes are studied in the frequency range from 300 kHz to 3 GHz. The method of finite difference in time domain is utilized for the numerical modeling and simulation of the reflection coefficient. The condition for the input reflection coefficient of the waveguide probe is the range from (0.7–0.3) in the broad frequency band.

Results and Conclusions: Although the waveguide is a narrowband microwave component, its modifications could have broadband frequency behavior of the reflection coefficient. Results indicate that the most interesting and suitable is the solution with removable dielectric. This liquid dielectric with the low value of permittivity has significant influence on the cut-off frequency of waveguide with dominant mode propagation.

ACKNOWLEDGMENT

This research is supported by Grant Agency of the Czech Republic, project: "Non-standard application of physical fields — analogy, modelling, verification and simulation" (102/08/H081) and by the research program MSM6840770012 "Transdisciplinary Research in the Area of Biomedical Engineering II" of the CTU in Prague, sponsored by the Ministry of Education, Youth and Sports of the Czech Republic.

Intracavitary Applicators for Thermotherapy

J. Vrba, K. Novotna, and M. Pourova
Department of EM Field, Czech Technical University
Technická 2, Prague 16627, Czech Republic

Abstract— Paper deals with new results in the field of intracavitary microwave applicators used for Benign Prostatic Hyperplasia (BPH) treatment.

Costs and risks associated with clasical BPH treatment (TURP and open surgery) have promoted the development of minimally invasive methods. Microwave thermotherapy, varying forms of laser treatment, transurethral needle ablation, etc. have all been developed in the 1990s. The underlying principle behind these methods is to coagulate prostatic adenomatous tissue by means of heat. Of all the available minimal invasive treatment modalities, transurethral microwave is one of the most wide spread at present [1].

We have investigated basic types of microwave intracavitary applicators suitable for BPH treatment, i.e., monopole, dipole and a helical coil structures. These applicators are designed to work at 915 MHz. In the conference contribution we would like to discuss it's effective heating depth, based on the comparison of the theoretical and experimental results. Basic mechanisms and parameters influencing (limiting) heating effective depth are described and explained in Ref. [2–4].

The basic type of intracavitary applicator is a monopole applicator. The construction of this applicator is very simple, but numerically modelled (calculated by software product SEMCAD) and measured "Specific Absorption Rate" ("SAR") distribution along the applicator is more complicated. During measurements of SAR along the applicator we have found, that typically there is not only a one main "SAR" maximum (first from the right side), but also a second and/or higher order maximas can be created, being produced by outside back wave propagating along the coaxial cable. To eliminate this second maximum and optimise the focusing of "SAR" in predetermined area of biological tissue needs to use the helical coil antenna structure. After coil radius and length optimisation we have obtained very good results of "SAR" distribution.

As a novel results of our work we could mention that various microwave applicators for prostate cancer or BPH treatment have been developed and evaluated. Theoretical analysis of effective heating depth of these applicators and its experimental evaluation will be given.

ACKNOWLEDGMENT

This research is supported by the research program MSM6840770012 "Transdisciplinary Research in the Area of Biomedical Engineering II" of the CTU in Prague, sponsored by the Ministry of Education, Youth and Sports of the Czech Republic.

REFERENCES

1. De la Rosette, J., F. D'Ancona, and F. Debruyne, "Current status of thermotherapy of the prostate," *J. Urol.*, Vol. 157, 430–438, 1997.
2. Vrba, J., C. Franconi, and M. Lapes, "Theoretical limits for the penetration depth of the intracavitary applicators," *International Journal of Hyperthermia*, Vol. 12, No. 6, 737–742, 1996.
3. Vrba, J., M. Lapes, and L. Oppl, "Technical aspects of microwave thermotherapy," *Bioelectrochemistry and Bioenergetics*, Vol. 48, 305–309, 1999.
4. Bolmsjö, M., L. Wagrell, A. Hallin, T. Eliasson, B. E. Erlandsson, and A. Mattiasson, "The heat is on — but how? A comparison of TUMT devices," *Br. J. Urol.*, Vol. 78, 564–572, 1996.

Applicators for Treatment of Atherosclerosis

Kateřina Novotná and Jan Vrba
Department of Electromagnetic Field, Czech Technical University in Prague
Technická 2, 166 27 Prague 6, Czech Republic

Abstract—

Introduction: Vascular diseases are the most common cause of death in present time. This project describes the design of two different types of intracavitary applicators for treatment of the atherosclerosis. Basic principle of microwave angioplastic is, that heating gained by microwave energy irradiated into artery by microwave applicator, enables safe clear out of atherosclerotic plates in the wall of vessel.

Problem Formulation: This paper describes the design of special applicators for microwave angioplastic. As the most acceptable structure to create intracavitary applicators, coaxial quarter wave monopole, was chosen. Described applicators were designed for 2.45 GHz and for numerical modelling electromagnetic field distribution the simulating program was used. In our model the type of applicator for treatment of atherosclerosis was inserted in to the vein with blood and surrounded by phantom of muscular tissue.

Original Solution: For design of the intracavitary applicator a coaxial cable RG 178 BU was chosen. The main advantage of use is its flexibility because the wall of vessel is very breakable. First instance goal was to obtain good impedance matching between generator and microwave applicator. Then we studied the distribution of absorbed power (SAR) along the applicator. The distribution of SAR was deciding factor for the future use. The vessel wall is very thin and there is a risk to burn off the wall. We created two different types of applicators:

a) simple monopole applicator in blood,

b) simple monopole applicator with ball-shaped tip in blood.

The ball-shaped tip at the end of the applicator is better for good impedance matching and this type of the tip can change the distribution of SAR along the applicator.

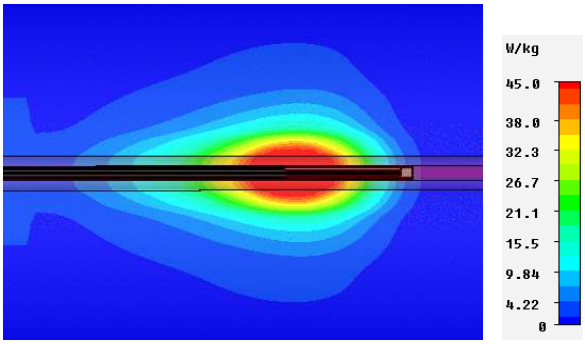

Figure 1: Simple monopole applicator in blood — SAR.

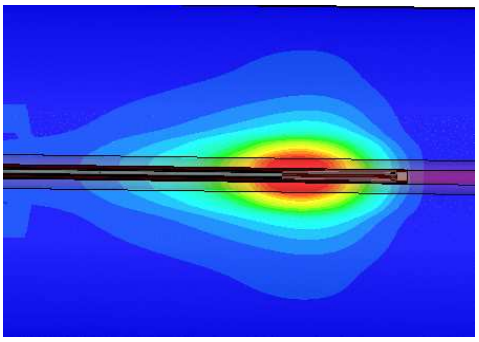

Figure 2: Simple monopole applicator with ball-shaped tip in blood — SAR.

Conclusion: This paper describes two technical solutions to design the intracavitary applicators for treatment of atherosclerosis. In the first case (Fig. 1) the maximum of SAR was at point of termination of outer conductor, but exceeded out of the artery space. This can be dangerous from reason of possible thermal perforation of the wall of the vessel. The second case (Fig. 2) shows from this point of view much better solution. Expected temperature increase is limited to inner part of the vein. This type of applicator is much better for the future use. Final temperature distribution is influenced by blood perfusion too.

The main goal for the future of this project is to determine the optimal temperature distribution and optima distribution of SAR for different stadium of this illness.

ACKNOWLEDGMENT

This research is supported by Grant Agency of the Czech Republic, project: "Non-standard application of physical fields — analogy, modelling, verification and simulation" (102/08/H081) and by the research program MSM6840770012 "Transdisciplinary Research in the Area of Biomedical Engineering II" of the CTU in Prague, sponsored by the Ministry of Education, Youth and Sports of the Czech Republic.

REFERENCES

1. Novotná, K., "Intracavitary applicator for microwave angioplastic (in czech)," Diploma thesis, Prague 2007.
2. Vrba, J., "Medical applications of microwave thermotherapy (in czech)," Publishing by CTU, Prague 2003.
3. Rosen, A., et al., "Percutaneous transluminal microwave catheter angioplasty," United States Patent, number 4643186, Feb. 17, 1987.

Theory of Evanescent Mode Applicators

Jan Vrba[1], **Paolo Togni**[1], **Jan Vrba**[2], **and David Vrba**[1]

[1]Department of EM Field, Czech Technical University in Prague, Czech Republic
[2]Institute of EM Field Theory, RWTH Aachen University, Germany

Abstract— In this contribution we would like to describe our new results dealing with evanescent mode waveguide hyperthermia applicators, typically used for cancer treatment. We have developped theoretical basis of this technology and designed & evaluated different versions of these applicators working below waveguide cut-off frequency.

In our contribution we would like to discuss what happens, when the frequency f of hyperthermia apparatus is either very different (i.e., much higher or lower) from the cut-off frequency f_c or very near (even equal) to the cut-off frequency f_c of the used waveguide applicator. This special case of our interest can happen when either the hyperthermia apparatus is tunable in broader frequency range or the cut-off frequency f_c of the applicator is changed by different dielectric parameters of various types of biological tissues.

There is a substantial difference between the two ways of the waveguide applicator excitation (i.e., above or under the cut-off frequency f_c) and in the propagation and "behaviour" of the EM field inside such applicator also. Basic differences would be explained during the presentation.

For the following discussion we have chosen the case of the rectangular applicator with a flange. But similar results is possible to obtain for other important cases like e.g., rectangular applicators without flange or for the family of circular applicators.

Waveguide flange is in our approach considered as an electric wall, dashed line going into the biological tissue determines the magnetic wall of our model. The distance between these walls determines the cut-off frequency f_c of the applicator aperture. Of course, f_c is influenced by the tissue permittivity also.

The results we would like to describe in our contribution are interesting from theoretical point of view of the knowledges about the general properties of the waveguide applicators. And are very important also for the treatment — our results demonstrate very substantial changes of SAR distribution in the treated biological tissue. If f is going to f_c then so called hot spots complicating the treatment can arise.

ACKNOWLEDGMENT

This research is supported by the research program MSM6840770012 "Transdisciplinary Research in the Area of Biomedical Engineering II" of the CTU in Prague, sponsored by the Ministry of Education, Youth and Sports of the Czech Republic.

Design of an Exposure Chamber for Biological Experiments

L. Visek, J. Vrba, and L. Oppl
Department of Electromagnetic Field, Czech Technical University
Technická 2, 166 27 Prague, Czech Republic

Abstract—

Introduction: In a modern world various sophisticated devices emitting microwave electromagnetic field are ubiquitous. These devices are used in many fields such as industry, medicine and communication. An increasing daily exposure and its possible impact on human health raises a growing concern in our society. Therefore, many researches focus on effects of electromagnetic field and investigate its influence on biological tissues.

Materials and Methods: Our motivation is based on flaws of other researches dealing with electromagnetic field influence on a biological tissue. We are concerned with an exact determination of exposure of mice and elimination of outer influences which can affect results such as stress.

The main aim of our work is to design and to simulate an exposure chamber in order to analyse the impact of electromagnetic field on mice and can simulate mobile phone emission patterns. We need to accomplish these goals for a specific purpose: working frequency 900 MHz, enough space for mice movement to assure non-stressful condition and possibility to measure reflected and transmitted power to achieve an accurate exposure.

In our previous research we found the most suitable type of an exposure chamber. On the basis of comparison of two types of chamber structures we have chosen a waveguide chamber as the most appropriate.

We optimized and verified basic properties such as electromagnetic field distribution and impedance matching of our designed chamber by aid of a 3D electromagnetic field simulator.

Results: As a result of our effort a cylinder waveguide chamber has been designed which satisfies all our requirements mentioned above. In order to even mice exposure we chose cylinder structure where we can excite a circular polarization. The chamber is terminated by matched loads on both lateral sides. The matched loads serve for preventing a possible resonance between sides and mice and therefore we can determine the accurate exposure. The next important issue is to assure a suitable milieu for mice (support air and light). Evanescent waveguides serve for this purpose well.

ACKNOWLEDGMENT

This research is supported by Grant Agency of the Czech Republic, project: "Non-standard application of physical fields — analogy, modelling, verification and simulation" (102/08/H081) and by the research program MSM6840770012 "Transdisciplinary Research in the Area of Biomedical Engineering II" of the CTU in Prague, sponsored by the Ministry of Education, Youth and Sports of the Czech Republic.

Hyperthermia Applicator for Small Superficial Tumor Treatment

P. Togni[1], **J. Vrba**[1], **and L. Vannucci**[2]

[1]Dept. of Electromagnetic Field, Czech Technical University in Prague, Czech Republic
[2]Dept. Immunology, Institute of Microbiology
Academy of Sciences of the Czech Republic, Czech Republic

Abstract— This paper describes a microwave applicator designed to treat small superficial tumour with hyperthermia. Microwave hyperthermia treatment is one of the complex methods to treat cancer diseases. During this kind of treatment the biological tissue is exposed to electromagnetic energy in order to enhance its temperature within the range between 41°C and 45°C. The healing effects are obtained thanks to the higher thermal sensitivity of tumor tissue compared with healthy tissue because of their different perfusion rates. Our target is to treat mice with small melanoma cancer located below the skin. The diameter of these tumors is around 10 to 20 mm with a thickness smaller than 10 mm. For this reasons the applicator has to focus the electromagnetic energy in a small region and the penetration depth of electromagnetic field has to be quite limited in order not to radiate any vital organ which can be in the tumor surround and also not increase too much the body temperature. The applicator is composed by a planar dielectric structure metallized on both sides. The two metallizations are shorted all around the applicator in order to create a cavity resonator. The resonance frequency is in the ISM band 2450 MHz. The dimensions and the permittivity of the resonator material are such to obtain the first resonant mode which, for this squared structure, is TE_{101}. On one metallization is obtained a slot-line ring aperture with the function to radiate the energy to the biological tissue. The feeding is given by a 50 Ω N-type connector located on the other side of the applicator. The optimization of the applicator is given using the 3D electromagnetic field simulator Speag SEMCAD X. By the help of the simulator, the dimensions of applicator were optimized in order to obtain the resonance at the working frequency. Also the shape and dimensions the slot line aperture were optimized in order to obtain the most suitable power absorption distribution inside the biological tissue. The simulator was in fact used to predict the SAR distribution and Temperature distribution inside an agar phantom with electromagnetic characteristics similar to muscles tissue. Both cases, using a bolus containing distilled water or placing the applicator directly on phantom are considered, as well as the influence of the water bolus thickness. The results of simulations are supported by measurement of S_{11} parameter at the applicator input, made using a vector analyzed and with temperature measurements made on agar phantom. These results have shown the possibility to use this applicator for in-vivo experiment on mice with small melanoma tumors.

ACKNOWLEDGMENT

This research is supported by Grant Agency of the Czech Republic, project: "Non-standard application of physical fields — analogy, modeling, verification and simulation" (102/08/H081) and by the research program MSM6840770012 "Transdisciplinary Research in the Area of Biomedical Engineering II" of the CTU in Prague, sponsored by the Ministry of Education, Youth and Sports of the Czech Republic and by the Grant Agency of the Academy of Science Of Czech Republic IAA500200510, Institutional Research Concept No. AV0Z50200510.

Measurement of Yeast Cell Electrical Oscillations around 1 kHz

M. Cifra[1,2], **J. Pokorný**[2], **F. Jelínek**[2], **and J. Hašek**[3]

[1]Department of Electromagnetic Field, Czech Technical University, Czech Republic
[2]Institute of Photonics and Electronics, Academy of Sciences of the Czech Republic, Czech Republic
[3]Institute of Microbiology, Academy of Sciences of the Czech Republic, Czech Republic

Abstract— Mechanical vibrations of yeast cell membrane were detected with AFM (Atomic Force Microscope) and analysed by Fourier analysis by Pelling et al. in the frequency range 0.5–2 kHz and with amplitude of the order of magnitude of 1 nm. They estimate the origin of these nanomechanical vibrations in the action of many proteins working in a concerted and cooperative manner and relate them to the metabolic activity of the cell.

Frőhlich postulated coherent endogenous vibrations of electrically polar structures in living organisms, what implies existence of electrical oscillations in the vincinity of metabolically active cells.

This paper reports on some results from 50 measurements of electromagnetic activity of the yeast cells in the acoustic frequency range.

Synchronous and non-synchronous cold sensitive microtubule mutants of yeast cells were measured. The synchronous cells are measured in the first 40 min period after beginning of the M phase. The non-synchronous pool of cells contains cells in any phase of the cell cycle. Measurement setup consists of a point sensor(~ 50 nm) in a cuvette located with the preamplifiers and batteries in the triple screened (electrically and magnetically) temperature stabilized box connected to the spectrum analyzer Agilent E4448A with semi rigid coaxial cable.

Results clearly and statistically very significantly ($p = 0.001$) show that power in the measured frequency band 0.4–1.6 kHz is higher in the case of synchronous cells than in the case of non-synchronous cells although biological variability is visible. The results coincide with the Pohl et al. findings of higher electromagnetic activity of yeast cells in the M phase. Nevertheless, exhaustion of metabolic sources in the non-synchronous cells may affect the results too.

Comparison of Possibilities Utilization Open — Resonator Type and Meandering Type of Microwave Applicators for Textile Industry

Marika Pourová and Jan Vrba
Faculty of Electrical Engineering, Department of Electromagnetic Field
Czech Technical University, Technická 2, 166 27 Prague 6, Czech Republic

Abstract— In this contribution we would like to describe the possibilities utilization of two different types of microwave applicators. These applicators are designed specially for large thickness sheet of textile materials.

We have designed two types of applicators, which we use for testing. There are intended for the drying at factory production of fabrics. The first applicator is derived from the Fabry-Perrot resonator, which is open type resonator. The second one is waveguide type applicator, which is waveguide with a longitudinal slot in wider side of waveguide and it is created by two branches. The textile material goes through the applicator in the maximum of electric field strength, where it can absorb the maximum of energy. The applicators are designed so that only dominant mode TE_{10} could propagate inside the system.

Both applicators work at frequency 2.45 GHz and use different number of magnetrons. The open-resonator type is made by 17 cells that have every one own magnetron. These 17 cells create the whole drying system. The second one — meandering type is now created with two separated cells also excited with magnetrons. This system is designed for testing of new method for surface treatment of textile materials with microwave energy.

We have created the model of drying system, which solve the distribution of EM waves inside this structure and we reached the resulting expression, which is used for calculation of electric field strength in the plane of drying textile. This quantity depends on electrical characteristics of wet textile such as permittivity and loss factor. We would like to present the results of measurement parameters of wet textile too. Dielectric parameters are changed with decrease moisture content in textile.

The comparison of the simulations of both systems with experimental results has been reported in details. The results of our testing measurements are very good corresponding with simulations and analytical model.

ACKNOWLEDGMENT

This research is supported by Grant Agency of the Czech Republic, project: "Non-standard application of physical fields — analogy, modelling, verification and simulation" (102/08/H081) and by the research program MSM6840770012 "Transdisciplinary Research in the Area of Biomedical Engineering II" of the CTU in Prague, sponsored by the Ministry of Education, Youth and Sports of the Czech Republic.

Session 5A4
Photonic Crystals and Metamaterials 3

Reflection-free Waveguides in a Gyromagnetic Photonic Crystal

Marin Soljacic
Massachusetts Institute of Technology, USA

Abstract— We point out that electromagnetic one-way edge modes analogous to quantum Hall edge states, originally predicted by Raghu and Haldane in 2D gyroelectric photonic crystals possessing Dirac point-derived bandgaps, can appear in more general settings. In particular, we show that the TM modes in a gyromagnetic photonic crystal can be formally mapped to electronic wavefunctions in a periodic electromagnetic field, so that the only requirement for the existence of one-way edge modes is that the Chern number for all bands below a gap is non-zero. In a square-lattice gyromagnetic Yttrium-Iron-Garnet photonic crystal operating at microwave frequencies, which lacks Dirac points, time-reversal breaking is strong enough that the effect should be easily observable. For realistic material parameters, the edge modes occupy a 10% band gap. Numerical simulations of a one-way waveguide incorporating this crystal show 100% transmission across strong defects, such as perfect conductors several lattice constants wide, larger than the width of the waveguide.

Photonic Crystal Concept Applied to Diffractive Optics for Novel Electromagnetic Wave Propagation Control Devices

Ming Li, **Xinhua Hu**, **Zhuo Ye**, **and Kai-Ming Ho**
Ames Laboratory, Iowa State University, Ames IA 50011, USA

Abstract— Photonic crystal structures are proposed to control the phase of propagating electromagnetic waves through their non-linear dispersion relations. By controlling the phase of the propagating electromagnetic wave, novel devices can be designed to meet certain desired functions. One application of this concept is designing diffractive optics elements such as a focal lens with better aberration control and more compact size compared with traditional lenses. Such idea of controlling propagation through phase information can be applied to various frequency ranges of electromagnetic wave from ultraviolet to microwave.

One of the central tasks is to design proper structures to meet the desired functions through numerical simulations. As the size of the photonic crystal structure elements are comparable to the wavelength of propagating wave. The full vector wave properties through Maxwell's Equations must be considered. We modified our planewave based transfer-scattering matrix method to do the numerical simulation. From the simulation, the transmission and reflection spectra as well as the phase information through any photonic crystal structures can be obtained, which in turn can be used to determine the electromagnetic propagation behaviors.

First we confirmed our idea of finding propagation direction through phase difference by the well-known law of refraction at the interface incline between materials with different refractive indices. Then the numerical simulation tool is applied to the compact focal lenses design with better performance. It is also applied to the design of photonic crystal structures to realize electromagnetic wave beam steering with quick response through the slightly mechanical deformation of the structures. Our results show that the idea of controlling the propagation of electromagnetic wave by photonic crystal structures is feasible and it may have many applications in the future.

Line Source Wave Scattering by Line Inhomogeneities inside Left-handed Material Slab: Green Function Approach

Yu. N. Barabanenkov[1], **M. Yu. Barabanenkov**[2], **and S. A. Nikitov**[1]

[1]Institute of Radioengineering and Electronics
Russian Academy of Sciences, Mohovaya 11, Moscow 103907, GSP–3, Russia
[2]Institute of Microelectronics Technology and High Purity Materials
Russian Academy of Sciences, Chernogolovka 142432, Moscow Region, Russia

Abstract— We present an analytical approach to study a problem of getting visible image for Veselago's focus inside left-handed material (LHM) slab [1], provided both the dielectric permittivity and the magnetic permeability are negative and the permittivity has additionally a 2D inhomogeneous perturbation and a line source wave field to be incident on the slab. An integral equation for the Green function of s — polarized electric wave field is derived in a form similar to one in potential scattering, with the volume and a surface potentials, using the extended boundary condition technique [2]. Solution to this integral equation with the surface potential only gives a perfect Veselago's lens Green function, which is obtained also from the empty space Green function by a spatial coordinate transformation [3] for the definite positions of observation and source planes. We rewrite next the derived integral equation in terms of the perfect Veselago's lens Green function and volume scattering potential and solve to the equation asymptotically in the limit of inhomogeneity as linelike (2D pointlike) scatterer. The found asymptotic solution reveals a multiplicative electrostatic singularity of the Green function for inhomogeneous LHM slab if the linelike scatterer is placed near the Veselago's focus inside LHM slab, with respect to positions of the source and the receive points.

REFERENCES

1. Veselago, V. G., *Sov. Phys. Usp.*, Vol. 10, 509, 1968.
2. Tsang, L., J. Kong, and R. Shin, *Theory of Microwave Remote Sensing*, John Wiley, New York, 1985.
3. Leonhardt, U. and T. G. Philbin, *New J. Phys.*, Vol. 8, 247, 2006.

Zero-$\bar{n}$ Bandgap in Photonic Crystal Superlattices at the Near-infrared

S. Kocaman[1], R. Chatterjee[1], N. C. Panoiu[2], M. B. Yu[3]
D. L. Kwong[3], R. M. Osgood[4], and C. W. Wong[1]

[1]Optical Nanostructures Laboratory, Columbia University, New York, NY 10027, USA
[2]Department of Electronic and Electrical Engineering, University College London
Torrington Place, London WC1E 7JE, UK
[3]The Institute of Microelectronics, 11 Science Park Road
Singapore Science Park II, Singapore 117685, Singapore
[4]Department of Applied Physics and Applied Mathematics, Columbia University
New York, NY 10027, USA

Abstract—

Introduction: Left-handed metamaterials (LHMs) are artificial composites having both nergative permittivity and permeability [1], conditions that allow these metamaterials to have negative refraction index. It has been also demonstrated that a periodic superlattice consisting of alternating layers of LHMs and regular dielectric materials with positive permittivity and the permeability (right-handed materials, — RHM) has an omnidirectional bandgap that remains unchanged upon variation of the wave polarization, angle of incidence, or period of the structure [2]. This gap is termed as a zero-$\bar{n}$ gap and emerges when the volume average index is equal to zero. Here we report an experimental verification of zero-n materials in the near-infrared region. As suggested in a previous work [3], for the LHM one can use dielectric-based 2D photonic crystals (PC), which we recently fabricated [4], whose optical losses are much smaller than metal-based LHMs.

Design, FDTD Simulations and Experimental Verification: The photonic superlattice consists of a periodic structure with a period of $\Lambda = d_1 + d_2$ where d_1 and d_2 are the thicknesses of the alternating layers of PC and the RHM. We consider RHM as a regular dielectric slab with a thickness of $t = 320\,\text{nm}$, whereas the PC slab has a hexagonal lattice with air holes etched into a dielectric background (Si), with the period $a = 430\,\text{nm}$, the ratio of the hole radius r and the period, $r/a = 0.279$, and the refractive index of the background $n = 3.46$. We use TM polarized incident plane waves and the orientation of the normal to the input facet has been chosen along the Γ-M symmetry axis (z-axis) of the PC slab. In order to demonstrate the existence of the zero-$\bar{n}$ gap we have designed three different superlattices, with different period Λ, so that their PC thicknesses are $d_1 = 3.5\sqrt{3}a$, $d_1 = 5.5\sqrt{3}a$, and $d_1 = 7.5\sqrt{3}a$. The corresponding RHM slab thicknesses have been designed so as to have a zero-average refractive index, namely $\bar{n} = (n_1 d_1 + n_2 d_2)/\Lambda = 0$ [3], but without changing the ratio between the thickness of the PC and the RHM slabs. In Fig. 1(b), the results of the 3D FDTD simulations for all three superlattices with 3 stacks of PC and RHM layers and the pass band of the PC slab are illustrated. There are several photonic gaps and except for that located near the normalized frequency $\omega = 0.273$, their mid-gap locations are shifted as the period of the superlattice is changed. Varying mid-gap

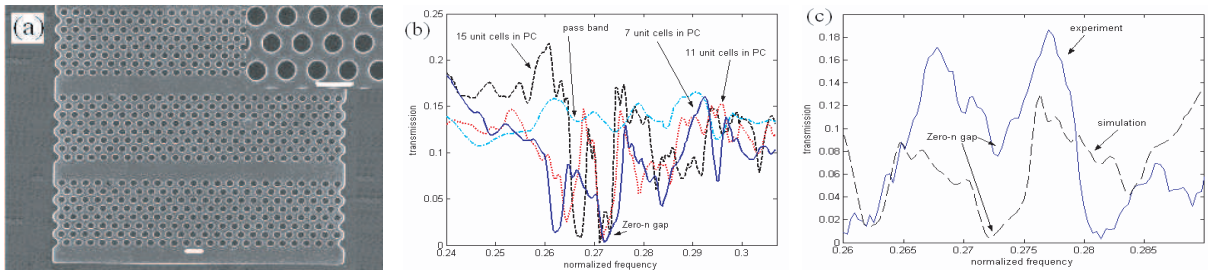

Figure 1: Simulation results for the designed photnic superlattice. (a) SEM of the fabricated samples with 3 Stacks whose PC slabs have a thickness of $d_1 = 3.5\sqrt{3}a$. Inset: SEM of the PC lattice with a higher resolution. Scale bar: 500 nm. (b) FDTD simulation results for the designs with seven, eleven and fifteen unit cells in PC slab and the corresponding thickness of the RHM which satisfies the zero-$\bar{n}$ condition for the normalized frequency $\omega = 0.2737$. (c) Comparison between the simulation and the experimental data in a focused range.

frequency is the expected behavior for the regular Bragg gaps; therefore this bandgap is a zero-$\bar{n}$ gap. In addition, in order to determine the type of each bandgap we have also calculated the $k_0\Lambda/\pi$ [5] and our calculations also showed that the gap which is located at the $\omega = 0.273$ is a zero order gap. Based on the simulation results, we fabricated samples with 3 stacks whose PC slabs have a thickness of $d_1 = 3.5\sqrt{3}a$ using a silicon film, on a SiO_2 insulator substrate which is seen in the Fig. 1(a). The measured frequency corresponding to the zero-$\bar{n}$ mid-gap is slightly higher than the designed frequency. A comparison between the simulations and the experimental data in a narower range of frequencies is seen in the Fig. 1(c).

Conclusion: We demonstrated a zero-n gap, at near-infrared wavelengths with a photonic superlattice consisting of periodic layers of 2D PC's as LHM and regular RHMs. Our experiments show good agreement with our 3D FDTD simulations.

REFERENCES

1. Smith, D. R., W. J. Padilla, D. C. Vier, S. C. Nemat-Nasser, and S. Schultz, *Phys. Rev. Lett.*, Vol. 84, 4184–4187, 2000.
2. Jiang, H., H. Chen, H. Li, Y. Zhang, and S. Zhu, *Appl. Phys. Lett.*, Vol. 83, 5386–5388, 2003.
3. Panoiu, N. C., R. M. Osgood, S. Zhang, and S. R. J. Brueck, *J. Opt. Soc. Am. B*, Vol. 23, 506–513, 2006.
4. Chatterjee, R., K. Liu, N. C. Panoiu, Z. Dios, M. B. Yu, M. T. Doan, L. Kaufman, R. M. Osgood, and C. W. Wong, *CLEO 2006*, Long Beach, CA, 2006.
5. Yuan, Y., L. Ran, J. Huangfu, H. Chen, L. Shen, and J. A. Kong, *Opt. Exp.*, Vol. 14, 2220, 2006.

A Tunable Short-length Photonic Crystal Wavelength Separator

Armaghan Eshaghi and S. M. Moghadasi
Department of Electrical Engineering, Ferdowsi University of Mashhad, Iran

Abstract— In this work, a tunable wavelength separator using nonlinear photonic crystal directional coupler is proposed and analyzed. The structure is modified to have minimum length. Using Kerr nonlinearity in the coupling region, gives the possibility to tune the separated wavelengths. FDTD simulations show the device length reduced to $24a$.

Introduction: Directional couplers can be used to separate light of different wavelengths. Attempts were made to design couplers with shorter coupling lengths. Due to small changes in the index of refraction induced by nonlinear optical effects, in devices which use the benefits of nonlinear effects, the required length is normally too high for large-scale optical integration. Nonlinear effects can be enhanced in systems with slow group velocity as a result of the compression of the local energy density. In this work using slow light which occurs in a modified structure of photonic crystal coupld wavguides, the device length has reduced drastically.

Design of the Device: In a directional coupler consisting of two parallel waveguides, the wave confined to one of the waveguides consists of even and odd supermodes with a phase difference. If the phase difference is equal to an odd product of π, the wave will transfer to the other waveguide. The coupling length depends on the difference, $(k_{even} - k_{odd})$, where k_{even} and k_{odd} are the wavenumbers of even and odd supermodes, respectively. Due to the change in the amount of $(k_{even} - k_{odd})$ in different frequencies, the coupling length varies with respect to operating frequency, so two different frequencies can be separated and go through different output ports.

Using Kerr nonlinearity in the coupling region, gives the possibility to tune the separated wavelengths. The difference between the wavenumbers of even and odd supermodes changes with the change in the input intensity, hence, one can tune the input intensity to separate a desired wavelength.

To reduce the group velocity and hence the device length, the proposed directional coupler which is depicted in Fig. 1, is used in the wavelength separator structure. The radius of the holes in the central row and the position of the holes located beside the parallel waveguides are the design parameters. Schematic view of the structure is shown in Fig. 2.

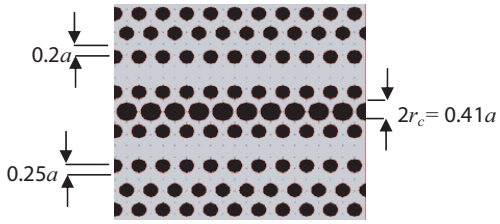

Figure 1: The proposed coupler which reduces the group velocity. (The radius of other holes is equal to $0.3a$).

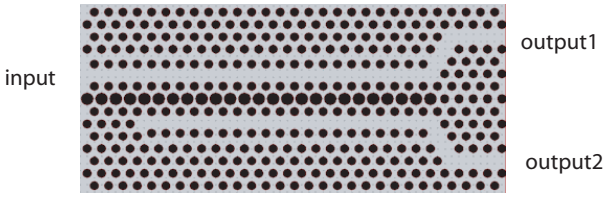

Figure 2: Schematic view of the tunable wavelength separator.

Guiding Waves through Waveguide Bends by Metamaterial Blueprints

B. Donderici and F. L. Teixeira
The Ohio State University, USA

Abstract— In waveguide applications, bends are often employed to conform with the geometrical constraints of the problem. However they are known to produce (i) frequency-dispersion due to differing traveling distances in the bend, and more importantly (ii) reflection and transmission errors due to abrupt transition. In order to alleviate these artifacts in waveguide bends, several methods based on alternative bending shapes or isotropic materials have been proposed [1, 2]. These methods only provide partial improvement and their maximum performance is a function of the problem geometry.

Here, we formulate metamaterial blueprints for reflectionless waveguide-bends [3]. The derivation is based on the metric invariance property of Maxwells equations [4–8] and it allows all waveguide modes to be guided without any reflection (or cross-coupling) through the bend. This is realized by an anisotropic metamaterial filling in the bending region. No other modifications are required in the remaining regions. It is shown by numerical simulations that significant reduction in the reflected fields can be obtained by the metamaterial blueprint. The sensitivity of the results with respect to the perturbations in the metamaterial distribution is also tested with coarse metamaterial distributions and show significant improvement as well.

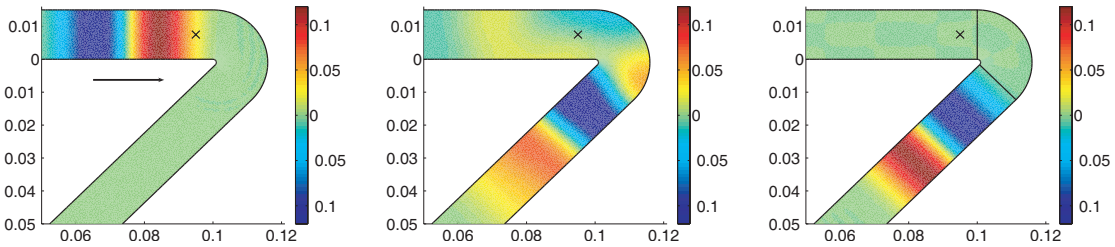

(a) incident wave (b) bend without metamaterial (c) bend with metamaterial

Figure 1: (a) Incident (TM0 mode) wavefield on the waveguide bend. Reflection and distortions due to bending are clearly visible in (b). Metamaterial filling succesfully eliminates these artifacts in (c)..

REFERENCES

1. Lee, C.-T. and M.-L. Wu, "Apexes-linked circle gratings for low-loss waveguide bends," *IEEE Photonics Tech. Lett.*, Vol. 13, No. 6, 597–599, Jun. 2001.
2. Hu, Z. and Y. Y. Lu, "Computing optimal waveguide bend with constant width," *J. Lightwave Tech.*, Vol. 25, No. 10, 3161–3167, Oct. 2007.
3. Donderici, B. and F. L. Teixeira, "Metamaterial blueprints for reflectionless waveguide bends," *IEEE Microw. Wireless Comp. Lett.*, to appear, 2008.
4. Ward, A. J. and J. B. Pendry, "Refraction and geometry in Maxwell's equations," *J. Mod. Opt.*, Vol. 43, 773–793, 1996.
5. Schurig, D., J. J. Mock, B. J. Justice, S. A. Cummer, J. B. Pendry, A. F. Starr, and D. R. Smith, "Metamaterial electromagnetic cloak at microwave frequencies," *Science*, Vol. 314, 977–980, May 2006.
6. Leonhardt, U., "Optical conformal mapping," *Science*, Vol. 312, 1777–1780, Jun. 2006.
7. Teixeira, F. L., "Closed-form metamaterial blueprints for electromagnetic masking of arbitrarily shaped convex PEC objects," *IEEE Antennas Wireless Propagat. Lett.*, Vol. 6, 163–164, 2007.
8. Ozgun, O. and M. Kuzuoglu, "Utilization of anisotropic metamaterial layers in waveguide miniaturization and transitions," *IEEE Microw. Wireless Comp. Lett.*, Vol. 17, No. 11, 754–756, Nov. 2007.

Non-classical Light Generation by a Single-emitter Photonic-crystal Laser

Lucia Florescu[1,2]

[1]NASA Jet Propulsion Laboratory, California Institute of Technology, USA
[2]Department of Bioengineering, University of Pennsylvania, USA

Abstract— We explore the possibility of creating non-classical states of light by a one-atom photonic crystal laser. This study is based on the ability to engineer the photonic structure to produce both abrupt changes in the photonic density of states as a function of frequency and optical micro-cavities characterized by extremely small micro-cavity-mode volumes and very high cavity factors. We consider a coherently pumped two-level emitter (atom or quantum dot) strongly coupled to a high-quality microcavity engineered within a photonic crystal micro-chip characterized by a large discontinuity in the photonic density of states. The cavity field is tuned on resonance with one of the Mollow components of atomic resonance fluorescence. We investigate the emitted light characteristics in terms of the quantum degree of second order coherence. It is shown that the ability to engineer the quantum optical characteristics in coherent light-matter interactions through suitable photonic crystal architectures facilitates light generation characterized by pronounced photon anti-bunching and sub-Poissonian photon statistics, and strongly enhanced relative to that from a one-atom laser in a conventional optical cavity. In order for these characteristics to be attained, a discontinuity in the photonic density of states by a factor of 100 is enough, and a photonic band gap is not necessary, which implies some relaxation regarding the practical implementation of the system. These results suggest the possibility to employ a photonic-crystal one-atom laser as a highly-efficient single-photon source, and the potential of photonic crystals for applications in quantum information technology.

The Dynamical Process and the Causality Limitation of the Dispersive Cloak

Xunya Jiang
Institute of Microsystem and Information Technology, CAS, China

Abstract— For the first time, we simulate the dynamical process of the dispersive cloak (all real cloaking material must be dispersive) by the finite-difference time-domain (FDTD) method with special numerical techniques. The numerical experiments show several important properties of the dispersive-cloak dynamical process: (i) unlike other systems, there is no oscillation in cloaking dynamical process; (ii) an "intensity front", which propagates in group velocity and sweeps through the cloak in the process, can surprisingly construct the "stable-cloaking rays" locally; (iii) the tangent group velocity, which is controlled by the dispersion, is the dominant element, and it determines the time length and total scattered field of dynamical process. Our further study of the dispersive cloak shows the deeper physical picture of the cloaking effect. We find that the causality limitation must be considered in the cloaking process. To avoid the divergence of the group velocity, certain strength of dispersion is required at every radius position. Because of the causality limitation, the group velocity near inner radium of the cloaking must be zero and the absorption is introduced. When the dispersive cloaking structure is near "ideal cloaking design", although the scattering cross-section can be considerably reduced, generally the absorbing cross-section (which is much larger than the scattering cross-section) could be the main obstacle for the "invisibility". Some of our works are published at APL and PRE (R).

The New Nonlinear Phenomena in the Photonic Crystals Around the Self-collimation Frequency

Xunya Jiang
Institute of Microsystem and Information Technology, CAS, Shanghai, China

Abstract— For the first time, we study the new nonlinear mechanism around the self-collimation frequency range. At the self-collimation (SC) frequency, the curvature of equal-frequency surface (EFS) is zero. So that the EFS-curvature sign of the frequency range around SC is very sensitive (such as, with small frequency shift, the sign can be changed from positive to negative). With the nonlinear introduced in, the SC frequency can be tuned. Then the EFS curvature at the working frequency (very near the SC frequency) can be changed by the nonlinearity, and the diffraction (and the refraction) behaviors of the incident beam can be modulated. Many novel nonlinear phenomena are predicted, such as the tunable SC frequency, the tunable micro- lens and coupler. The interaction between the nonlinearity and SC is not one-way, since not only the nonlinearity can tuned the SC frequency, but also the tuned SC frequency can cause the beam focusing (density becomes stronger and the nonlinearity is stronger) or divergent (weaker nonlinearity). The non-trivial interaction can cause more complex nonlinear feedback, then the "SC self-lock" and "nonlinear collapse" can be realized at certain condition. Based on new mechanism, we have also designed several devices based the SC, such as MZ interferometers and sub-ps ultra-fast switches. Some works are published in three Appl. Phys. Lett. papers.

Session 5A5
Nanoscale Materials - Magnetic and Optical Properties

Dual Magnetism in Fe-doped Anatase Nanorods

L. H. Lewis[1], **Y. Ding**[2], **and W.-Q. Han**[3]

[1]Department of Chemical Engineering, Northeastern University, USA
[2]Condensed Matter Physics & Materials Science Department, Brookhaven National Laboratory, USA
[3]Center for Functional Nanomaterials, Brookhaven National Laboratory, USA

Abstract— An enduring scientific challenge is to understand the formation and interaction between magnetic impurities in insulating systems. This challenge has been invigorated by the search for spintronic materials with control of both the electric charge and the magnetic degrees of freedom for novel electronic devices. Dilute magnetic semiconductors (DMS), which are traditional semiconductors doped in the fractions of atomic percentage level with transition metal cations, are an important category of spintronic materials. If, as postulated [1], structural lattice defects lie at the heart of the magnetic properties in such systems it is expected that three-dimensional nanostructured oxide DMS systems will exhibit an enhanced magnetism by virtue of high surface area and defect-rich surface constructions.

With the above motivation, the magnetism of anatase-type TiO_2 nanorods with nominal incorporation of 0.5 at % Fe was studied. The nanorods were synthesized by a hydrothermal route and possess widths of 8–35 nm and are several hundreds nanometers in length. No evidence of pure iron nanoparticles in the sample is detected with TEM or with advanced synchrotron diffraction techniques. The nanorods exhibit ferromagnetism at low magnetic fields that transitions to paramagnetism at higher magnetic fields with a value >100 times that of pure bulk anatase TiO_2. This dual magnetic character is attributed to a variation in Fe content within the nanostructures, with the large measured values of Curie temperature T_C (800 K) and large paramagnetic susceptibility arising from an interaction between Fe cations exchange-coupled by large-orbit hydrogenic electrons originating from oxygen lattice and surface defects.

Research performed under the auspices of the U. S. DOE, Office of Basic Energy Sciences under contract No. DE-AC02-98CH1-886.

REFERENCES

1. Coey, J. M. D., M. Venkatesan, and C. B. Fitzgerald, *Nature Materials 4*, 173, 2005.

Multi-component Nanoparticles by Organic Solution Phase Synthesis

Hao Zeng and Savas Delikanli
Physics, University at Buffalo, SUNY, Buffalo, New York, USA

Abstract— We present a general synthetic strategy for multi-component hybrid nanostructures with paired combinations of plasmonic, semiconductor and magnetic functionalities. A rich combination of materials involving FePt or Fe_3O_4 as the magnetic component, Au or Ag as the metallic component and II-VI (e.g., CdS) or IV-VI (e.g., PbS) as the semiconducting components have been fabricated. These nanostructures are realized by sequential growth of a second and/or third component on pre-synthesized nanoparticle seeds. By rationally tuning the synthetic parameters, such as heating rate, solvents, and ratio of precursors to seeds, a large variety of morphologies have been synthesized including core/shell, peanut-like and dumbbell-like structures. Different components grow on top of each other quasi-epitaxially with common interfaces, which facilitate the charge, spin and energy transfer between them. The optical properties and magnetic properties are appreciably affected by the presence of the conjugate material in the hybrids, as compared to their single component counterparts. These multi-component hybrid nanostructures may have a broad range of potential applications.

Magnetoplasmons and Quasiparticles for Quantum-dots in Graphene

Oleg L. Berman[1] and Godfrey Gumbs[2]

[1]Physics Department, New York City College of Technology, City University of New York, USA
[2]Department of Physics and Astronomy, Hunter College, City University of New York, USA

Abstract— A two-dimensional honeycomb lattice of carbon atoms that form the basic planar structure in graphite (graphene) has recently been produced [1, 2]. The unusual many-body interactions in graphene caused by the facts that the effective electron mass in graphene equals zero, and the electron band structure in graphene is determined by the eigenvalue problem of the Dirac-like Hamiltonian implying the two-component spinor wavefunctions [5]. The influence of the external magnetic field on the many-electron properties of graphene results in unusual quantum Hall effect. The integer quantum Hall effect (IQHE) has been discovered in graphene in recent experiments [6–8]. The quantum Hall ferromagnetism in graphene has been studied theoretically [9]. The spectrum of plasmon excitations in a single graphene layer immersed in a material with effective dielectric constant ε_s without magnetic field ($B = 0$) was calculated in Ref. [10]. We have calculated the spectrum of magnetoplasmon excitations in the two-dimansional (2D) array of the quantum dots formed by the linear confinement potential $U(\mathbf{r}) = \lambda_0|\mathbf{r} - \mathbf{r}_0|$ ($\mathbf{r}_0$ is the center of the confinement). We have mapped the eigenstates of the Dirac equation for electrons in magnetic field in linear confinement onto the problem of electron-hole pairs in an effective magnetic field without confinement. The applied magnetic field and the confinement potential for quantum dots determine this effective magnetic field. The Dirac equation for an electron-hole pair in a magnetic field has been solved in Refs. [11, 12]. The tight-binding model for the array of quantum dots leads to a wavefunction which results in the inter-dot mixing of the quantum numbers associated with an isolated quantum dot analogous to Ref. [13]. The excitation spectrum of the collective modes preserves the periodicity of the lattice, even with the mixing of the quantum numbers.

REFERENCES

1. Novoselov, K. S., et al., *Science*, Vol. 306, 666, 2004.
2. Zhang, Y., et al., *Phys. Rev. Lett.*, Vol. 94, 176803, 2005.
3. DiVincenzo, D. P. and E. J. Mele, *Phys. Rev.*, Vol. B29, 1685, 1984.
4. Kane, C. L. and E. J. Mele, *Phys. Rev. Lett.*, Vol. 78, 1932, 1997.
5. Sarma, S. Das, E. H. Hwang, and W.-K. Tse, *Phys. Rev.*, Vol. B75, 121406(R), 2007.
6. Novoselov, K. S., et al., *Nature*, Vol. 438, 197, London, 2005.
7. Zhang, Y. B., et al., *Nature*, Vol. 438, 201, London, 2005.
8. Zhang, Y., et al., *Phys. Rev. Lett.*, Vol. 96, 136806, 2006.
9. Nomura, K. and A. H. MacDonald, *Phys. Rev. Lett.*, Vol. 96, 256602, 2006.
10. Sarma, S. Das and E. H. Hwang, *Phys. Rev. Lett.*, Vol. 81, 4216, 1998.
11. Iyengar, A., J. Wang, H. A. Fertig, and L. Brey, *Phys. Rev. B*, Vol. 75, 125430, 2007.
12. Berman, O. L., Yu. E. Lozovik, and G. Gumbs, cond-mat/0706.0244.
13. Que, W., G. Kirczenow, and E. Castaño, *Phys. Rev. B*, Vol. 43, 14079, 1991.

Negative Permittivity and Permeability of a Composite Filled with Layered Microspheres

N. Bowler and J. Liu
Department of Materials Science and Engineering, Iowa State University, USA

Abstract— Holloway et al. suggested that simultaneous negative permittivity, ε, and permeability, μ, can be achieved in a material composed of magneto-dielectric spheres dispersed in a matrix [1]. Solving for ε and μ by assuming the particles to be arranged on the nodes of a simple-cubic lattice, it was shown that multiple resonances occurred, at which ε and μ simultaneously become negative over portions of the frequency spectrum, leading to a negative index (NI) of refraction. The ability to engineer this material response is attractive for manipulation of the electromagnetic field in both microwave and optical applications. Present NI materials are highly anisotropic and rely on structured assembly of resonant circuit elements [2]. An NI material created simply by mixing particles in a matrix would be easier to fabricate, isotropic, and potentially applicable at higher frequencies than are presently achieved [2]. On the other hand, no single material is known that exhibits both high relative ε and μ. For this reason, we here investigate the resonances in ε and μ of a material composed of layered microspheres dispersed in a matrix. As in the work of reference [1], a first-order solution in the approach of Mie scattering theory is obtained. Through modeling, the intrinsic dielectric and magnetic parameters of the constituent materials that are needed in order to achieve simultaneous resonance in ε and μ are determined. For example, in Figure 1 the variation in ε is shown for a matrix filled with dielectric microspheres with various values of ε, that are coated with a nanometric layer of conductive material. The results show multiple resonances superimposed on a slower relaxation that is due to interfacial polarization. The role of the material parameters of the three constituent phases in governing the frequency and strength of the resonances will be discussed. Possible combinations of available materials that may exhibit such behavior in practice will also be discussed.

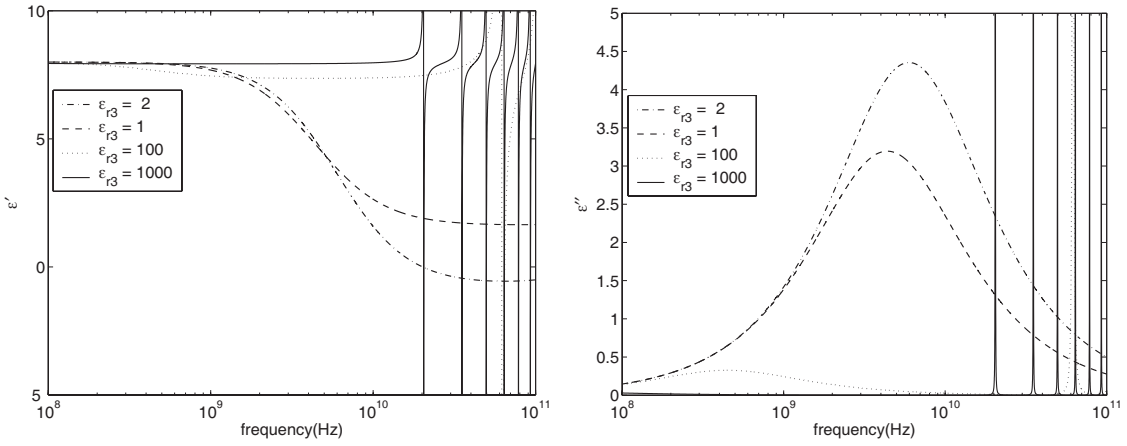

Figure 1: Calculated permittivity for a material composed of coated spheres dispersed in a supporting matrix with $\varepsilon_r = 2.25$. Particle diameter is 500 µm. The conductive layer on the particles is 50 nm thick with conductivity 10^3 S/m. The volume fraction of particles is 0.46. The relative permittivity of the particle core varies as indicated in the legend.

REFERENCES

1. Holloway, C. L., E. F. Kuester, J. Baker-Jarvis, and P. Kabos, "A double negative (DNG) composite medium composed of magnetodielectric spherical particles embedded in a matrix," *IEEE Trans. Antennas Propag.*, Vol. 51, No. 10, 2596–2603, 2003.
2. Soukoulis, C. M., S. Linden, and M. Wegener, "Negative refractive index at optical wavelengths," *Science*, Vol. 315, 47–49, 2007.

Two-photon Absorption Spectra of Cis- and Trans-bifullerene[60]-pentacene Adducts Based on First-principle Simulation

W.-D. Cheng, H. Hu, and J.-Y. Wang
State Key Laboratory of Structural Chemistry
Fujian Institute of Research on the Structure of Matter, Chinese Academy of Sciences
Fuzhou, Fujian 350002, China

Abstract— We employed a combined method of time-dependent density functional theory with sum over states formula to model two-photon absorption spectra of cis- and trans-2[60]-pentacene adducts, in which the two carbon fullerenes 2[60] connects to a pentacene with *syn* (cis) and *anti* (trans) fashions, respectively. The calculated results show that the cis configuration adduct of 2[60]-pentacene exists at lower energy of two-photon absorption peak and has a smaller two-photon absorption cross section. An analysis in term of electronic structural calculations of excitation states, we also identify that the two-photon absorption peaks of cis- and trans-2[60]-pentacene adducts originate from the condensed aromatics to fullerene cages.

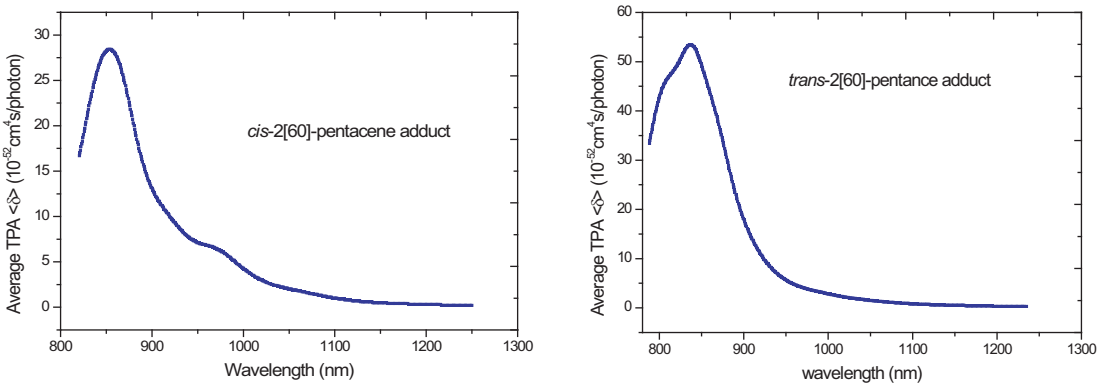

Figure 1.

Self-assembled Magnetic Nanodot Array

Hao Zeng and Chaehyun Kim
University at Buffalo, SUNY, USA

Abstract— Today, nanostructured materials is an important subject in new science and technology because of their unique electronic and magnetic properties that are quite different and not found from the same bulk materials, and must be studied for the future fabrication of new nanodevices. Here, we fabricate ordered magnetic nanodot arrays with extremely high density using physical vapor deposition using porous anodic alumina templates as evaporation mask. We discover a new hystertic behavior, asymmetric hysteresis loops with an additional step of the upper part of the hysteresis loop. We investigate this intriguing behavior to trace out the origin and to find the correlation of this behavior with nanostructure. Also we provide features of magnetic nanodot arrays, such as high anisotropy, large coercivity, and perpendicular easy axis orientation, which are desirable features for the future high density magnetic data storage media.

Poynting Vector, Second Law of Thermodynamics and Negative Refraction

Vadim A. Markel
Departments of Radiology and Bioengineering, University of Pennsylvania, USA

Abstract— I consider the work that the electric field exerts on the total current $\mathbf{J} = \partial\mathbf{P}/\partial t + c\nabla \times \mathbf{M}$ where $\mathbf{P}$ and $\mathbf{M}$ are the polarization and magnetization, respectively, and compute the rate at which the electromagnetic energy is converted to heat. I further subject the result to the restrictions imposed by the second law of thermodynamics. I find that the latter is in a clear contradiction with the phenomenon commonly referred to as the negative refraction. This results holds for active or passive media as well as for anisotropic and nonlocal media. The only essential requirement for applicability of my result is that a running plane wave satisfies the Maxwell's equation in the media. This condition is not satisfied in photonic crystals and similar structures which can support propagating modes in the form of *Blokh waves*. Detailed derivations are given in the reference.

REFERENCES

1. Markel, V. A., "Correct definition of the Poynting vector in electrically and magnetically polarizable medium reveals that negative refraction is impossible," arXiv:0712.0605v1.

Magnetostatic Interactions in Partially Shielded Polyaniline-ferromagnet Composite Nanowire Arrays

Adam L. Friedman

Northeastern University, USA

Abstract— Ferromagnetic nanowires have remarkable magnetic properties including high coercivities and strong magnetic shape anisotropy. These unique properties have been theoretically studied and various models attribute the observed characteristics to inter- and intra-wire magnetostatic interactions, which are a function of the structure of the nanowires and their coupling with the applied magnetic field. In this study, we use porous alumina templates and electrodeposition to fabricate Fe, Ni, and Co nanowires. We also use the same techniques to grow polyaniline nanotubes and then fill them with Fe, Ni, and Co nanowires, creating magnetically shielded ferromagnet structures. We measure the magnetic properties of these structures as a function of their diameter and temperature in order to better understand the magnetic interactions that arise in ferromagnetic nanowire arrays. By partially shielding the wires with PAni, we are able to better discern the effects of these interactions. Results will be presented and compared to theoretical models.

Raman and Photoluminescence Studies on CVD Grown GaN Nanowires

Zhen Wu[1], **Myung Gwan Hahm**[2], **Yung Joon Jung**[2], **and Latika Menon**[1]

[1]Department of Physics, Northeastern University, Boston, MA 02115, USA
[2]Department of Mechanical Engineering, Northeastern University, Boston, MA 02115, USA

Abstract— We describe our results on the growth of single crystal GaN nanowires on Ni-patterned sapphire wafers by means of chemical vapor deposition. We show a strong dependence of morphology and orientation of nanowires on catalyst parameters, such as deposition mode of the catalyst and also the dimensions of the catalyst. For example for very large catalyst dimensions, several nanowires are seen to grow from a single catalyst and the wires grow vertical to the surface of the substrate. On the other hand for very small dimensions of the catalyst, the GaN orientation is seen to demonstrate an epitaxial network-like growth pattern. High resolution scanning electron microscopy, atomic force microscopy, photoluminescence and Raman spectroscopy measurements indicate a marked difference in structural and optical properties as a function of growth pattern. These results may be indicative of reduced defects and strain effects in epitaxially grown nanowires. Such nanowires are expected to have important applications in advanced nanoscale optoelectronic devices.

Ferromagnetic and Magnetic Semiconductor Nanodot Arrays Fabricated Using Porous Alumina Masks

S. Bennett, **L. Menon**, **and D. Heiman**
Department of Physics, Northeastern University, Boston, MA 02115, USA

Abstract— Arrays of magnetic nanodots are fabricated by a novel multi-step process using anodic porous alumina templates. The template is first used as a shadow make to deposit metal nanodots, which are then used to mask the removal of material using a plasma etch process. Magnetic nanodots arrays of ferromagnetic GaMnAs are demonstrated and their nanometer size is confirmed by the observation of superparamagnetism. This fabrication technique is versatile and can be used to prepare uniform and highly ordered nanodot arrays of a wide class of materials, inexpensively, rapidly and over large length scales.

Microwave Characterization of Magnetic Nanoclusters Embedded in Metal-Oxides

Christian Brosseau[1], **Vincent Castel**[1], **and Jamal Ben Youssef**[2]

[1]Laboratoire d'Electronique et Systèmes de Télécommunications, Université de Bretagne Occidentale
CS 93837, 6 avenue Le Gorgeu, 29238 Brest Cedex 3, France
[2]Laboratoire de Magnétisme de Bretagne, Université de Bretagne Occidentale
CS 93837, 6 avenue Le Gorgeu, 29238 Brest Cedex 3, France

Abstract— A comparative study at the ambient temperature of the ferromagnetic resonance (FMR) spectra and static magnetic properties, measured by vibrating sample magnetometry, of Ni/ZnO and Ni/γ-Fe_2O_3 nanocomposites (NCs) is reported. A series of nanogranular composites was fabricated by powder pressing at room temperature from nanosized Ni, ZnO, and γ-Fe_2O_3 particles. A microstrip transmission line technique was used to measure the FMR profiles and linewidths in the 8–24 GHz frequency range. The samples were placed at the center of a microstrip line where the derivative of the absorbed power was measured using a standard ac field modulation technique (10 Oe amplitude) and lock-in detection. We show that the static magnetic response cannot be totally explained by the demagnetization process of noninteracting Ni particles. The analysis of the FMR spectra can be interpreted as arising from aggregates of magnetic nanoparticles, each of which resonates in an effective magnetic field composed of the applied field, the average (magnetostatic) dipolar field, and the randomly oriented magnetic anisotropy field. It is found that frequency and applied magnetic field strongly influence the lineshape of the FMR spectra. Two observations are identified within the FMR spectra. On the one hand, the resonance field increased linearly with frequency as expected from uniform mode theory and yielded a Landé g factor in the range 1.48–2.05. On the other hand, there is no clear correlation between FMR linewidths and frequency. Inhomogeneity based line broadening mechanisms, due to the damping of surface/interface effects and inter-particle interaction, affect the FMR effective linewidth. The importance of the Ni concentration is also discussed in relation to measurements of the spin wave group velocity induced by the samples. Furthermore, the results of a systematic dependence of the room temperature ESR linewidth and resonant field on the Ni content and the corresponding FMR features and effective microwave losses measured in previous works show a remarkable correlation. This correlation indicates that the the dipolar coupling between magnetic nanoparticles is the dominant contribution to the resonant line in these NCs.

Nanophotonic Negative-index Optical Metamaterials: New Concepts in Negative Refraction and Imaging

Srinivas Sridhar
Northeastern University, USA

Abstract— We discuss negative refraction at microwave and optical frequencies in metallo-dielectric and dielectric photonic crystal media. Optical elements, such as photonics crystal prisms and lenses, were nanofabricated in two types of semiconductor materials: the direct bandgap InP/InGaAsP and indirect bandgap SOI (Silicon on Insulator) hetrostructures. The experiments show that materials with tailor-made negative or positive refractive indices over broad spectral ranges can be designed and fabricated at near infrared and microwave frequencies. We have also demonstrated that negative refraction leads to some novel optical elements for imaging, such as flat lenses and focusing by plano concave lenses. A general theory of imaging by a flat lens without optical axis has been developed. These tailor-made negative index materials nanofabricated on monolithic or hybrid platform such as InP/InGaAsP and/or SOI can be used as a basis for designing optical elements for integrated photonic circuits.

ACKNOWLEDGMENT

Work supported by the National Science Foundation and the Air Force Research Laboratories, Hanscom. Collaborators: W. T. Lu, R. Banyal, D. Casse, P. Vodo, Y. Huang,L. Menon, D. Heiman, M. Dokmeci

REFERENCES

1. Lu, W. T. and S. Sridhar, "Superlens imaging theory for anisotropic nanostructured metamaterials with broadband all-angle negative refraction," submitted.
2. Menon, L., W. T. Lu, A. L. Friedman, S. Bennett, D. Heiman, and S. Sridhar, "Negative index metamaterials for superlenses based on metal-dielectric nanocomposites," submitted.
3. Vodo, P., W. T. Lu, Y. Huang, and S. Sridhar, "Negative refraction and plano-concave lens focusing in one-dimensional photonic crystals," *Applied Physics Letters*, Vol. 89, 084104, 2006.
4. Vodo, P., P. V. Parimi, W. T. Lu, and S. Sridhar, "Focusing by plano-concave lens using negative refraction," *Applied Physics Letters*, Vol. 86, 201108, 2005.
5. Parimi, P., W. T. Lu, P. Vodo, and S. Sridhar, "Imaging by flat lens using negative refraction," *Nature*, Vol. 426, 404, 2003.

Session 5A7
Extended/Unconventionl Electromagnetic Theory, EHD (Elecrohydrodynamics)/EMHD (Electromagnetohydrodynamics), Electrobiology

Extending the Theory of Non-quasi-neutral Plasmas

D. K. Callebaut[1] **and H. Kikuchi**[2]
[1]University of Antwerp, Belgium
[2]Institute for Environmental Electromagnetics, Japan

Abstract— Chasmas are a generalization of plasmas, i.e., the condition of quasi-neutrality is dropped. That means that in chasmas the quasi-neutrality may be (strongly) violated over distances many times the Debye length which requires special circumstances (double layers, electric fields, ...).

Here we further analyze some equilibria and some steady state chasmas from various viewpoints (the classical plasma approach and the investigation of an non linear quasi-singular integro-differential equation). Concepts like the chasma frequency and the chasma Debye shielding length are confirmed and refined. The stability is considered and reveals extreme subtleties.

REFERENCES

1. Callebaut, D. K., G. K. Karugila, and A. H. Khater, "Chasma perturbations," *PIERS Online*, Vol. 1, No. 6, 720–723, 2005.
2. Callebaut, D. K. and A. H. Khater, "Chasma including magnetic effects," *PIERS Online*, Vol. 2, No. 4, 403–405, 2006.
3. Callebaut, D. K. and H. Kikuchi, "Debye shielding in chasmas," *PIERS Proceedings*, Prague, August 27–30, 2007.
4. Callebaut, D. K. and H. Kikuchi, "Extending the concept of Debye length for chasmas," *PIERS Proceedings*, Hangzhou, China, March 24–28, 2008.

A Novel Parametrically Amplifying Traveling Fast-wave Antenna (PATA) with a High Gain and Directivity as a Modern Version of the Historical Slow-wave Beverage Antenna Utilizing an Induced Fast Surface Wave by an External Sky Wave: Analogous to Traveling-wave Tube Amplification and Negative Resistivity of Esaki Diodes

Hiroshi Kikuchi[1], **S. Tsuruoka**[2], **and T. Obata**[3]

[1]Institute for Environmental Electromagnetics, 3-8-18, Komagome, Toshima-ku, Tokyo 170, Japan
[2]Takuwa Corporation, 1-4-15, Uchi-Kanda, Chiyoda-ku, Tokyo 101, Japan
[3]Gunma National College of Technology, 580, Toriba-machi, Maebashi 371-0845, Japan

Abstract— Parametrically amplifying fast-wave travelng antennas (PATA) utilizing an induced fast surface wave by an external sky wave have been established theoretically and experimentally as a novel travelling wave antenna with a high gain and directivity as a modern version of the historical sloe-wave Beverage antenna. The principle of this antenna is to make strong resonance or coupling between the induced surface line-wave with the front velocity of the incident sky wave by coinciding the phase velocity of the induced surface wave with the front velocity of the incident sky wave. The function is something similar to traveling-wave amplification and negative resistivity of Esaki diodes. For the Beverage antenna, on the other hand, the coupling between the induced wire wave or wire-array current with ground return is so weak as a coupling distance becomes a half-wavelength or so, since the phase difference between the induced and the sky wave becomes appreciable. In this way, similarities and differences of both antennas are elucidated in detail.

Analysis and Design of Minigenerator

P. Fiala and T. Jirku
Department of Theoretical and Experimental Electrical Engineering
Faculty of Electrotechnical Engineering and Communication, Brno University of Technology
Kolejni 2906/4, Brno 612 00, Czech Republic

Abstract— The paper presents results of the analysis of the vibrational generator. The paper deals with the design of a vibrational generator that is used as a power supply for independent electric circuits. The vibrational generator can be used in the various areas, e.g., traffic, electronics, specialpurpose machines, and robotics. The proposed design employs magnetic damping of the core movement. It was numerically evaluated and it was shown that it was possible to obtain significantly larger output voltage and output power than in experimental settings used previously [1].

Introduction: The development of new devices always requires a bigger emphasis on safety and reliability. One of the areas where safety demands are especially great is civil and military transport. Reduced reliability could lead to the heaviest losses — losses of lives.

One of the ways how to increase the safety of an transport is to possess a sensor net placed at critical points of the aircraft. These sensors monitor important quantities during the run, e.g., temperature or pressure. The data will be compared with those from a previous and all other data available.

This paper presents the results of a vibrational generator (VG) analysis. The VG is intended to provide power to sensors mentioned above. The principle of operation of a VG is based on the utilization of changes in gravity with the aid of Faraday's law [1, 2]. The required output parameters are: output voltage between 3–5 V in ideal case, output power 200–3000 µW. The value of output power depends on the type of sensor used.

The VG body is tightly connected with the source of vibration — the fuselage, and thanks to the oscillation of the system the VG core starts moving with respect to the fuselage. The mechanical part of the VG is designed such that the VG core driven by external vibrations performs non-damped oscillations. The oscillations of the VG core are given by:

$$m\ddot{z} + l_c\dot{z} + kz = F_z \tag{1}$$

where m is the mass of the oscillatory part of generator, l_c is the overall damping, k is the stiffness of the spring, F_z is the input force, z is the displacement in the given direction, $\dot{z}$ stands for dz/dt, and $\ddot{z}$ stands for d^2z/dt^2. The design of the VG allows oscillations of the VG core within the wide spectra of external oscillation frequencies.. The operation of the VG is based on Faraday's law. This fact influences the design of the magnetic circuit and the shape of the windings. There is a drawing of the principle of operation in Fig. 1. The external part of the generator is mechanically coupled to the source of vibration. This part of the VG is mechanically stiff. The VG core of mass m is connected to the mechanical stiff part of the VG by means of an elastic coupling (spring) with given damping l_c. The core is made up of the ferromagnetic material of relative

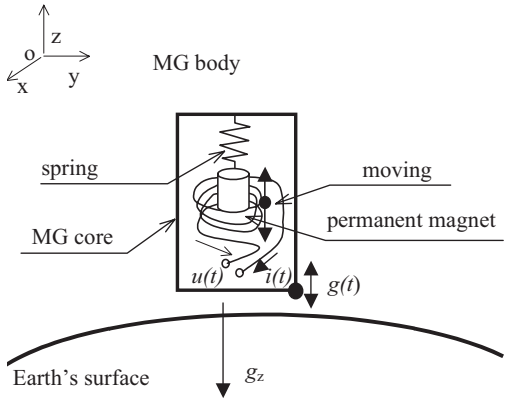

Figure 1: Experimental arrangement for acoustic attenuation measurement 9pt normal italic.

permeability μ_r and permanent magnets with high density of the stored energy, e.g., FeNdB, SmCo. A voltage $u(t)$ is induced in the winding, which is located around the movable parts of the VG.

REFERENCES

1. Li, W. J., Z. Wen, and P. K. Wong, *A Micromachined Vibration Induced Power Generator for Low Power Sensors of Robotic Systems*, World Automation Congress, Maui, Hawai, 2000.
2. Stratton, J. A., *Electromagnetic Field Theory*, SNTL, Prague, 1961.
3. Řičařová, A., "Microgenerator with output power 1 mW," Diploma Thesis, FEKT BUT, Brno, Czech Republic, 2003.
4. Fiala, P., "Conception of vibrational microgenerator," Research Report, DTEEE FEKT BUT, Brno, Czech Republic, 2003.
5. ANSYS, *User's Manual for Revision 5.1–8.0*, Volume I-IV, Swanson Analysis System, Inc., Houston, 1994–2003.
6. Fiala, P., "Modeling of short circuit transformer tests," PhD Thesis, DTEEE FEI BUT, Brno, Czech Republic, 1998.
7. Fiala, P., "Solution of electric field at a bushing support from distribution frame," Research Report No. 1/96, Laboratory of Modeling and Optimization Fields in the Electro-mechanical Systems, FEI BUT and ABB EJF, a.s. BRNO, Brno, 1996.

An Electric Field Test Using the MRI

P. Fiala[1] and K. Bartusek[2]

[1]Department of Theoretical and Experimental Electrical Engineering
University of Technology Brno, Kolejni 4, Brno 612 00, Czech Republic
[2]Institute of Scientific Instruments, Academy of Sciences of the Czech Republic
Královopolská 147, Brno 612 64, Czech Republic

Abstract— The article describes a test of electric field on the water molecules according to present knowledge of references [1–5]. The basic configuration of the test was verified in Institute of Scientific Instruments Academy of Sciences of the Czech Republic experimentally. We prepared the next tests with different mater to find relation between MRI and macroscopic electric field intensity. Actually, it respects classical Electrodynamics Material Wave Theory (MWT). The experiments are aimed to application in health service.

REFERENCES

1. Van Vlaenderen, K. J. and A. Waser, "Electrodynamics with the scalar field," *Physics*, Vol. 2, 1–13, 2001.
2. Kikuchir, H., *Electrohydrodynamics in Dusty and Dirty Plasmas, Gravito-electrodynamics and EHD*, Kluwer Academic Publishers, Dordrecht/Boston/London, 2001.
3. Van Vlaenderen, K. J., "A charge space as the orogin of sources, fields and potentials," *Physics*, arXiv:physics/9910022 v1 16 Oct 1999, 1–13, 1999.
4. Hofer, W. A., "A charge space as the origin of sources, fields and potentials," *Physics*, arXiv: quant-ph/ 9611009 v3 17 Apr 1997, 1–13, 1997.
5. Kolektiv, P. V. A., *Experimentální Metody Biofyziky*, Academia, Praha, 1989.
6. Delong, A., *Verbal Information*, Czech Academy of Science, ISI Brno, 7.2.2006, Brno, 2006.
7. Bartusek, K. and P. Fiala, "A simple numerical simulation of internal structure of particles test," *PIERS Online*, Vol. 2, No. 6, 653–656, 2006.

Numerical Modelling of the Special Light Source with Novel R-FEM Method

P. Fiala, E. Kroutilova, and T. Kriz
Department of Theoretical and Experimental Electrical Engineering
Brno University of Technology, Kolejni 4, Brno 612 00, Czech Republic

Abstract— This paper presents information about verification in the modelling of lighting systems, and an overview of methods for the modelling of lighting systems. The novel R-FEM method is described, which is a combination of the Radiosity method and the Finite Elements Method (FEM). The paper contains modelling results and their verification by experimental measurements.

Introduction: The paper contains information about verification of the design of the special light sources by the numerical simulation of the R-FEM method and verification by experimental measurements.

The R-FEM Method: The R-FEM method is a new direction in the modelling of lighting systems. It utilizes the similarity between physical models. This paragraph demonstrates the usage of analogy between different physical models for the modelling of light problems. The R-FEM method is able to solve tasks that fulfill the condition $\lambda_S \ll \max(D) \wedge \lambda_S < 10 \cdot \max(D)$, where λ_S is the source of light wavelength and D is one of the geometrical dimensions of the modelling task. It can be used for to model more complicated physical problems than the methods mentioned up to now. An example of a more complicated physical problem, which we can solve by the R-FEM method, is the modelling of light intensity distribution in interior or exterior spaces with non-homogeneous environment, where the light has passed through some impure air (e.g., filled with smoke, fog, mist, vapour, dust, etc.).

REFERENCES

1. http://www.lighting-technologies.com/Products/Photopia/Photopia2_pod.htm
2. Kadlecová, E., M. Bernard, and P. Fiala, "Illumination of interiors by the hollow light guides," *14th International Conference Light 2003*, ISBN 80-233-0488-7, Bratislava, 2003.
3. Kadlecová, E. and P. Fiala, "Light guide modeling," *Energy Forum 2004*, 338–341, ISBN 80-986-1619-1, Technical University, Sofia, Bulgaria, 2004.
4. Kadlecová, E., "Automated system of calculation of reflecting surface of light sources," Ph.D. Thesis, VUT v Brně, FEKT, Brno, srpen 2004.

The Measurement of Temperature Characteristics of Cu Bulk Resistivity

Karel Bartušek[1], **Pavel Fiala**[2], **and Premysl Dohnal**[3]

[1]Institute of Scientific Instruments, Academy of Sciences of the Czech Republic
Královopolská 147, Brno 612 00, Czech Republic
[2]Department of Theoretical and Experimental Electrical Engineering
Faculty of Electrical Engineering and Communication, Brno University of Technology
Kolejní 4, Brno 612 00, Czech Republic
[3]Department of Languages, Brno University of Technology
Údolní 53, 602 00 Brno, Czech Republic

Abstract— This contribution contain a presentation of a results of the numerical modeling during design of measurement method for determine of thermal characteristic of specific resistance of Cu bulk. Combine of numerical modeling and experimental verification brings very effective procedure during suggestion and application in cryogenic region. Results of this work are used in research activities of Czech Academy of Science, ISI-Brno.

REFERENCES

1. Kanagawa, T., R. Hobara, I. Matsuda, T. Tanikawa, A. Natori, and S. Hasegawa, "Anisotropy in conductance of a quasi-one-dimensional metallic surface state measured by a square micro-four-point probe method," *Ph. Rev. L.*, Vol. 91, No. 3, 2003.
2. Han, K., A. Ishmaku, and J. D. Embury, "Role of nanotwins and dislocations in high trength and high conductivity bulk Cu," National High Magnetic Field Laboratory Reports, Vol. 11, No. 1, MacMaster Univ., Materials Science and Engineering, Hamilton, Canada, 2004.
3. Webster, J. G., *Electrical Measurement, Signal Processing, and Displays*, CRC Press LLC, ISBN 0-8493-1733-9, London, 2004.
4. Van der Pauw, L. J., "A method of measuring specific resistivity and Hall efect of discs of arbitrary shape," *Philips Res. Rep.*, Vol. 13, 1–9, 1958.

Processing of MR Images in Temporomandibular Joint Examination

K. Bartusek[1], **Z. Smékal**[2], **O. Liberda**[3], **and A. Sprlakova**[4]

[1]Institute of Scientific Instruments, Academy of Sciences of the Czech Republic v.v.i
Kralovopolska 147, Brno 612 00, Czech Republic
[2]Faculty of Electrical Engineering and Communication, Brno University of Technology
Purkynova 118, Brno 612 00, Czech Republic
[3]Faculty of Medicine, Clinic of Oral and Maxillofacial Surgery, Masaryk University
Komenskeho nam. 2, Brno 662 43, Czech Republic
[4]Faculty of Medicine, Department of Radiodiagnostics, Masaryk University
Komenskeho nam. 2, Brno 662 43, Czech Republic

Abstract— The paper deals with the post-processing treatment of MR images in the examination of temporomandibular joints. An increase in contrast corresponding to the relaxation time of cores T_2 in the MR image and enhancement of arthritic areas of diseased temporomandibular joint were obtained by wavelet transform digital filtering and by processing two MR images measured at different echo times. The enhanced area indicates arthritic changes in the temporomandibular joint, which will be compared with the results of arthroscope examination. Experimental verification of the described method of data processing shows the application of wavelet digital filtering to be of advantage. Images weighted by relaxation time T_2 enhance the loosely bonded molecules of water and enable making the area with arthritic changes in temporomandibular visible. The method can also be applied in other MR examinations.

REFERENCES

1. Kimmich, R., *NMR Tomography, Diffusometry, Relaxometry*, Springer-Verlach Berlin Heidelberg, New York, 1997.
2. Mugler, J. P., T. A. Spraggins, and J. R. Brookeman, "T_2-weighted 3-dimensional MR-range MR imaging," *JMRI-Journal of Magnetic Resonance Imaging*, Vol. 1, No. 6, 731–737, 1991.
3. Butts, R. K., F. Farzaneh, S. J. Riederer, et al., "T_2-weighted spin-echo pulse sequence with variable repetition and echo times for reduction of MR image acquisition time," *Radiology*, Vol. 180, No. 2, 551–556, 1991.
4. Watrin-Pinzano, A., J. P. Ruaud, Y. Cheli, et al., "Evaluation of cartilage repair tissue after biomaterial implantation in rat patella by using T_2 mapping," *Magnetic Resonance Materials in Physics Biology and Medicine*, Vol. 17, No. 3–6, 219–228, 2004.
5. Bartusek, K., "Processing of MR images weighted by relaxation time T_2 to increase their contrast resolution," *Measurement Science and Technology*, Vol. 17, No. 4, 1–4, 2006.

Can the Wave Equation Yield a Photon Structure?

Dirk K. Callebaut

Physics Department, Campus Groenenborger, University of Antwerp
B-2020 Antwerp, Belgium

Abstract— Maxwell's equations without charge and without current yield the vector wave equation for the electric and magnetic fields. The usual approximation for electromagnetic waves (light) in free space is a plane wave. However, a photon may be expected to have an extension in all directions. Our attempts to obtain 3-D solutions using cylindrical coordinates all showed the same unsatisfactory feature: to avoid singularities as well at the origin (or axis) as at infinity a kind of arbitrary transition is required. An attempt to avoid this, in order to use Bessel functions (in particular J_0), hit on another arbitrariness. We attempt to give a physical explanation.

Session 5P1
Computational Electromagnetics - Combined Modeling Methods

Mixed Finite-element Time-domain Method for Simulating Doubly Dispersive Media

B. Donderici and F. L. Teixeira
The Ohio State University, USA

Abstract— We introduce here a finite-element time-domain algorithm based on *first-order* coupled Maxwells equations for simulating doubly-dispersive media. In this scheme, an edge-element (Whitney 1-form) expansion for the electric field, $\vec{E}$, and a face-element (Whitney 2-form) expansion for the magnetic flux density, $\vec{B}$ is used [1–3]. This choice satisfies the discrete de Rham diagram [4], and the resulting update equations have similar computational time and memory costs when compared to the finite-element time-domain method based on the second-order wave equation. The other desirable characteristics of this method are: (i) it is free of spurious linear growth, (ii) it produces energy-conserving schemes under appropriate time integration [5], (iii) it can be naturally hybridized with finite-difference time-domain method, (iv) it can be easily extended to complex (frequency-dispersive) media.

So far implementation of frequency-dispersive materials in finite-element method has been based on the second-order wave equation and dispersion is only included in the permittivity [6]. Here we take advantage of the property (iv) above to construct a mixed finite-element time-domain method for doubly-dispersive media where both permittivity and permeability are functions of frequency [7].

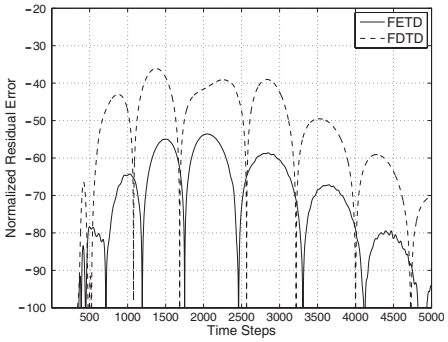

Figure 1: Normalized residual error in the scattered field from a cylinder filled with doubly-dispersive material.

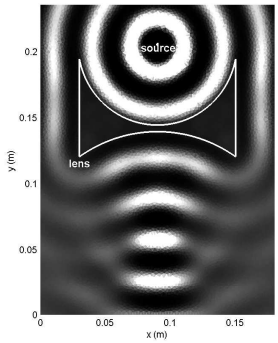

Figure 2: Magnetic field snap-shot for wavefront shaping by a zero-index metamaterial lens.

REFERENCES

1. Wong, M., O. Picon, and V. F. Hanna, "A finite element method based on Whitney forms to solve Maxwell equations in the time domain," *IEEE Tran. Magn.*, Vol. 31, No. 3, 1618–1621, May 1995.
2. Koning, J., R. N. Rieben, and G. H. Rodrigue, "Vector finite-element modeling of the full-wave Maxwell equations to evaluate power loss in bent optical fibers," *IEEE J. Lightwave Technol.*, Vol. 23, No. 12, 4147–4154, Dec. 2005.
3. He, B. and F. L. Teixeira, "Sparse and explicit FETD via approximate inverse Hodge (mass) matrix," *IEEE Microw. Wireless Comp. Lett.*, Vol. 16, No. 6, 348–350, Jun. 2006.
4. Bossavit, A., "Whitney forms: a class of finite elements for three-dimensional computations in electromagnetism," *IEE Proc. A*, Vol. 135, No. 8, 493–500, Nov. 1988.
5. Rieben, R. N., D. A, White, and G. H. Rodrigue, "High-order symplectic integration methods for finite element solutions to time dependent Maxwell equations," *IEEE Tran. Antennas Propagat.*, Vol. 52, No. 8, 2190–2195, Aug. 2004.
6. Jiao, D. and J-M Jin, "Time-domain finite-element modeling of dispersive media," *IEEE Microw. Wireless Comp. Lett.*, Vol. 11, No. 5, 220–222, May 2001.
7. Donderici, B. and F. L. Teixeira, "Mixed finite-element time-domain method for transient Maxwell equations in doubly dispersive media," *IEEE Theory and Tech.*, Vol. 56, No. 1, 113–120, Jan. 2008.

Analytical Linking of Numerical Computational Domains

P. Sewell, **D. W. P. Thomas**, **J. Wykes**
A. Vukovic, **C. Christopoulos**, **and T. M. Benson**
George Green Institute for Electromagnetics Research
University of Nottingham, University Park, Nottingham, NG7 2RD, UK

Abstract— Modern modelling challenges typically encompass both multi-scale and structural complexity issues. Domain decomposition provides significant flexibility in choosing appropriate techniques in each region, typically numerical methods being used to resolve the geometry. The use of analytic coupling between such regions yields a computationally efficient framework for simulation. In this paper we review both the techniques and classes of problems of interest, emphasising the role of unstructured meshes for geometrical definition and present valuable progress in developing the analytical couplings. It is noted that the simplest such configuration is one numerical region embedded in free space and therefore the analytical coupling approach must in effect provide a perfectly matched radiating boundary condition. This work has been pursued in both two and three dimensions. We will show results in both the frequency and time-domains that demonstrate the success of the absorbing boundary condition. Furthermore coupled multiple regions can be simply demonstrated in the frequency domain; the time domain counterpart will be discussed. Unstructured and structured meshing of the computational domains has been explored and the compromises between runtime and accuracy examined. Applications examples will be drawn from the field of photonics including coupled micro-resonators.

Probabilistic Approach of Electromagnetic Interaction Problems Using Quadrature Rules

O. O. Sy[1], **J. A. H. M. Vaessen**[1]
M. C. van Beurden[1], **A. G. Tijhuis**[1], **and B. L. Michielsen**[2]

[1]Eindhoven University of Technology, The Netherlands
[2]ONERA, Toulouse, France

Abstract— A probabilistic approach is presented to perform uncertainty quantification in electromagnetic interaction problems. The aim is to determine the statistical moments of the interaction parameters of interest such as, for example, the voltage induced at the port of a device by an incident field. Several methods to evaluate these moments are analyzed as well as methods to infer or approximate the probability distribution of the interaction parameter from its statistical moments.

Introduction: Probability theory provides a rigorous framework to study uncertain configurations. In this context, several stochastic methods have been developed to characterize electromagnetic interactions between randomly deformed objects and their environment. Brown has proposed a stochastic Fourier integral method to study the field scattered by an infinite rough surface [1]. Rannou et al. have used a Monte-Carlo technique with Transmission-Line theory to analyze the coupling between a deterministic transmission line and a randomly oriented dipole [2]. Michielsen has applied a perturbation method to study the voltage response of a randomly undulating wire structure to a deterministic incident field [3]. However, all these approaches were limited to smoothly varying setups and dedicated analytical formulations. The aim of the present paper is to tackle more general geometries, which correspond to high-dimensional random problems.

Probabilistic Method: In the present approach, a perfectly conducting device of finite size which is illuminated by the incident field E^i is considered. Its boundary surface is denoted $S(\alpha)$, where the vector α contains all the uncertain parameters of the geometry. The electromagnetic interaction parameter can be defined as a reaction integral between E^i and a current distribution j_α induced on $S(\alpha)$ [4]. This current j_α is obtained by solving an Electric Field Integral Equation by a method of moments. The key assumption of this method is that the vector α is a randomly distributed vector in Ω with a *known* probability distribution denoted as p_α. Hence, $V(\alpha)$ becomes a random variable with a, yet, *unknown* probability distribution p_V. Except in some special cases, p_V cannot be directly obtained from p_α. Instead, the statistical moments of V can be defined as a function of p_α in terms of high-dimensional integrals over the domain of the stochastic variable α.

In the presentation, several methods for efficiently computing these integrals will be discussed. These statistical moments, which primarily provide partial information on p_V, are post-processed to extract the key features of the randomness of $V(\alpha)$ and to approximate p_V. These results will be illustrated by the study of a "roughly" undulating thin-wire frame which is illuminated by deterministic or random plane waves or alternatively by a randomly located dipole source. The results obtained for an undulating plate under similar illumination conditions will also be shown.

REFERENCES

1. Brown, G. S., "Simplifications in the stochastic Fourier transform approach to random surface scattering," *IEEE TAP*, Vol. AP-33, No. 1, 48–55, 1985.
2. Rannou, V., et al., "Statistical analysis of the end current of a transmission line illuminated by an elementary current source at random orientation and position," *Proceedings IEEE EMC Symposium*, Vol. 7, No. 5, 1078–83, Montreal, Canada, August 2001.
3. Michielsen, B. L., "Probabilistic modelling of stochastic interactions between electromagnetic fields and systems," *C. R. Physique, Académie des Sciences*, Vol. 7, No. 5, 543–59, 2006.
4. Sy, O. O., et al., "Probabilistic study of the coupling between deterministic electromagnetic fields and a stochastic thin wire over a PEC plane," *Proceedings International Conference on Electromagnetics in Advanced Applications*, No. 10, 543–559, Turin, Italy, September 2007.

Linear and Non-linear Optical Waveguiding in Liquid Crystal Devices

Jeroen Beeckman[1], **Richard James**[2], **F. Anibal Fernandez**[2]
Eero Willman[2], **and Kristiaan Neyts**[1]

[1]Liquid Crystals & Photonics Group, ELIS Dept., Ghent University
Sint-Pietersnieuwstraat 41, 9000 Gent, Belgium
[2]Dept. of Electronics and Electrical Engineering, University College London
Torrington Place, London, WC1E 7JE, UK

Abstract— Liquid crystals are materials with a huge electro-optic response, which is why they are widely used in displays applications. By applying different voltages over the pixels, the liquid crystal molecules reorient, which in turn alters the propagation of polarized light through the device. The electro-optic response can also be used to create optical waveguides inside the material. Different waveguide geometries with liquid crystals have been proposed in numerous publications in the past. One can induce an optical waveguide with a voltage or by using surface effects. Another option is to use a normal solid-state waveguide and use a liquid crystal layer as an overlay. The liquid crystal can then be used to tune the waveguiding properties. In the last decade, a great deal of work has been carried out on non-linear waveguiding in liquid crystals, since the material produces a unique optical non-linear effect: optically induced director reorientation. With this nonlinear effect, it is possible to observe self-confined beams (also referred to as spatial optical solitons) for a few milliwatt of light power. During the last five years, our group has investigated these spatial solitons with experimental and numerical means.

The numerical simulation of light propagation through liquid crystal devices is governed by a complicated set of differential equations. The material is anisotropic, and the optical propagation model should be able to incorporate the full impermeability tensor. In many publications, the system of equations is simplified by making a number of assumptions and approximations. Recently we have developed a tool which incorporates the full description of the material behavior, including a finite-element Q tensor calculation of the liquid crystal orientation and the fully anisotropic optical calculation of guided modes. In this work we present the analysis of optical waveguides with liquid crystals for different configurations, both linear and non-linear.

Computational Modeling of Bound and Radiation Mode Optical Electromagnetic Fields in Multimode Dielectric Waveguides

David R. Selviah and Ioannis Papakonstantinou
UCL, UK

Abstract— The bound modes of optical multimode rectangular buried step index waveguides, in which the core has a uniform refractive index and the cladding has another lower refractive index, are usually calculated using an approximation that the wave equation is separable along two orthogonal axes, so that the modes can be considered to be a combination of modes in two orthogonal slab waveguides. This is useful as multimode waveguides can have many modes so the calculation of modes in a one dimensional slab waveguide is faster to calculate. A more accurate model is now needed to calculate both the bound modes and the radiation modes of multimode waveguides having uniform and non-uniform refractive index profiles within the guide. Non-uniform refractive index profiles are of interest for graded refractive index guides and photonic band gap guides but also because the modes in waveguide bends can be analyzed by performing a conformal transformation to another domain in which the waveguides become straight but in which their refractive index becomes non-uniform, asymmetric and graded. Radiation modes are needed to fully describe wave propagation in waveguides where coupling between modes occurs, for example, in practical waveguides suffering from sidewall roughness. Coupling of bound to radiation modes can be one of the main reasons for propagation loss in such guides. Analytical solutions for radiation modes do not exist for all waveguide geometries of interest and especially for ones in which the wave equation is not separable. For example, radiation modes have not been presented before for multimode rectangular dielectric waveguides.

In this paper, we present for the first time, a semi-analytical method for constructing the radiation modes in buried channel multimode waveguides in the weakly guiding limit. Our method relies on a non-linear transformation, which maps the infinite — xy Cartesian space into an infinite set of periodically arranged sub-spaces. Due to the periodicity of the transformation, fields can be represented by a discrete Fourier series in the new domain. Each radiation mode is next separated into a free-space mode traveling in the cladding and a response or perturbation component, triggered by the particular free-space mode, due to the presence of the waveguide. With this method, the calculation of the radiation mode is simplified to be the solution of a simple system of linear first order equations. In addition, the normalization of the entire radiation mode follows from the normalization of the free-space part.

Radiation modes can include high spatial frequencies and, therefore, the Fourier series may need to contain a large number of terms. This in turn results in an increased number of calculations, which cannot be handled by only one processor for highly multimode waveguides so we used a parallel computing cluster of 16–900 MHz processors. Each radiation mode of a $50\,\mu m \times 50\,\mu m$ waveguide required ~ 17 min to calculate. Although presented for rectangular waveguides our method is applicable to other arbitrary waveguide geometries if they are approximated by a number of thin rectangles and so will find use more widely in graded index optical fibers and photonic band gap fibers.

ACKNOWLEDGMENT

The authors thank Dr. Richard James for aid in parallelizing the computation.

Software Implementation of a New Multi-scale Method for Fractal-shaped Structures' Diffraction Analysis

T. BenSalah and T. Aguili

L. Syscom, ENIT, BP 37 Le Belvedere 1002, Tunis, Tunisia

Abstract— This paper proposes a new software implementation for a new EM Analysis method named MS-MGEC which stands for *Multi Scale Method of Generalized Equivalent Circuit*. With this method, analyzing multi scale antennas with fractal shapes — for example — is made very easy with interesting results.

The proposed method is an extension of the MGEC method (a MoM based method) in which we introduce a new formulation using a Surface Impedance Operator for bypassing conventional 'scalar' surface impedance limitations. Indeed, the study of electromagnetic waves' diffraction by an obstacle with fractal geometry is a difficult problem because of the underlying multi-scale properties of such structures. This difficulty is mainly imposed by multiple length scales (auto-similarity) characteristics of fractal structures that makes their design and analysis using classical methods require huge amount of resources (both memory and execution time). Existing Recursive methods iterate on EM characteristics so that they consider only one length scale per iteration. Usually, the input impedance of iteration is used as surface impedance in the next one. But such surface impedances luck in precision since they handle information only about a single mode (input impedance seen by the fundamental mode). In our work we generalize this approach to divide — automatically — a multi scale structure into smaller domains. Each domain — considered as a mono scale domain — is studied separately maintaining the boundary conditions. Then, it is replaced in the next iteration as a multi modal source which insures a better precision.

As an application we use the new software for studying some fractal structures placed in an infinite waveguide. Particularly, we are interested in Cantor Iris (1D) and Sierpinski Gasket structures (2D).

For what concerns the simulator software it self, it is designed in such a way that new applications can be dealt with by simple addition of pertinent models and functions and may be used for analyzing a wide range of planar structures. It is designed in a modular manner that enables its use either as an extensible stand alone Desktop GUI application or as an embedded library. Besides, as it is implemented in the Java TM language, it benefits of the platform independence of such a language. In fact, the new software aims to become a complete simulation platform for EM analysis.

REFERENCES

1. Aguili, T., "Modélisation des composants SHF planaires par la méthode des circuits equivalents généralisés (MGEC)," Thesis Manuscript, Enit Tunis, 2000.
2. Alatan, L., et al., "Analytical evaluation of MoM matrix elements," *IEEE Transactions on Microwave Theory and Techniques*, Vol. 44, 519–525, No. 4, April 1996.
3. Madelbrot, B., "Fractal objects," Flammarion, 1975.
4. Romeu, J., et al., "Generalized sierpinski fractal multiband antenna," *IEEE Transactions on Antenna and Propagation*, Vol. 49, 1237–1239, August 2001.
5. Elkamchouchi, H. M. and M. N. Abd El-Salam, "Square loop antenna miniaturization using fractal geometry," *Radio Science Conference, NRSC 2003, Proceedings of the Twentieth National*, B4-1–8, March 18–20, 2003.
6. Surre, F., A. S. Saleh, and H. Aubert, "Selective microwave filers based on self similar and lacunar structures," *2002 IEEE Antennas Propagation Symposum, Conference Proceedings*, Vol. 2, 840–843, San Antanio, Texas, June 16–21, 2002.
7. Surre, F., A. S. Saleh, and H. Aubert, "Frequency reponse of self similar planar waveguides," *Microwave and Optical Techology Letters (MWOLT)*, Vol. 27, No. 3, May 5, 2003.
8. Werner, D. H. and S. Ganguly, "An overview of fractal antenna engineering research," *Antennas and Propagation Magazine*, IEEE, Vol. 45, 38–57, Feb. 1, 2003.
9. Werner, D. H., D. Baldacci, and P. L. Werner, "An efficient recursive procedure for evaluating the impedance matrix of linear and planar fractal arrays," *IEEE Transactions on Antennas and Propagation*, Vol. 52, 380–387, Feb. 2, 2004.

10. Berizzi, F. and E. Dalle-Mese, "Scattering from a 2D sea fractal surface: Fractal analysis of the scattered signal," *IEEE Transactions on Antennas and Propagation*, Vol. 50, 912–925, Jul. 7, 2002.
11. Berizzi, F. and E. D. Mese, "Scattering coefficient evaluation from a two-dimensional sea fractal surface," *IEEE Transactions on Antennas and Propagation*, Vol. 50, 426–434, Apr. 4, 2002.
12. Frezza, F., L. Pajewski, and G. Schettini, "Fractal two-dimensional electromagnetic bandgap structures," *IEEE Transactions on Microwave Theory and Techniques*, Vol. 52, 220–227, Jan. 2004.

2D and 3D Finite Element Method Strategies for Computer-aided Design Purposes in the Time-harmonic Maxwell's Equations

Valentín de la Rubia[1], **Jesús Rubio**[2], **and Juan Zapata**[3]

[1]Departamento de Ingeniería Eléctrica, Electrónica, de Computadores y Sistemas
Universidad de Oviedo, Gijón 33203, Spain
[2]Departamento de Informática, Escuela Politécnica de Cáceres
Universidad de Extremadura, Cáceres 10071, Spain
[3]Departamento de Electromagnetismo y Teoría de Circuitos
Universidad Politécnica de Madrid, Madrid 28040, Spain

Abstract— Microwave devices need to satisfy more and more restrictive specifications, requiring computer-aided design (CAD). In the last two decades, a great effort has been made in the development of reliable analysis tools not only for removing the prototyping steps but also for robust microwave circuit and antenna design.

It was not long ago that microwave engineers had no alternative but through circuit models when developing designs. Nevertheless, full-wave simulation advances challenge traditional design to become full-wave optimization processes. In this sense, the use of clever algorithms reducing electromagnetic analyses or their costs is required for efficient optimization design (algorithms that are not always available). However, there are promising achievements in the electromagnetic and mathematic communities that lead us to predict full-wave optimization is only a matter of time.

Some microwave devices are properly analyzed by means of two-dimensional (2D) problem model reduction. Bodies of revolution or H-plane circuits allow for this kind of analysis. Here, a 2D finite element formulation properly handles the problem model reduction, and clearly outperforms three-dimensional (3D) full-wave problem analysis.

Furthermore, when developing a 3D microwave design, it is only a small part of the analysis domain that should be typically modified in order to achieve some required specifications. Here, we take into account a nonconforming domain decomposition method and propose an analysis domain partitioning such that only those parts that evolve in the optimization loop have to be analyzed in each iteration, whereas the other parts are analyzed only once. Thus, our domain decomposition approach draws upon describing each subdomain by means of a matrix-valued transfer function, namely, an admittance-type matrix. Then, tangential field continuity between subdomains is directly enforced by an admittance matrix connection. The nonconforming nature of the approximation is advantageous. For instance, the actual geometrical structure inside a subdomain can be modified without taking into account neighbouring mesh contraints. Thus, not only subdomain resolutions are decoupled but also their mesh generation.

In addition to the methodology proposed, a model-order reduction process is taken into account whithin each partition subdomain to enable a fast frequency sweep for each building admittance-type matrix. Finally, several examples will illustrate the capabilities and versatilities of the proposed methodology.

Electro-hydrodynamics of Liquid Crystals

R. James, E. Willman, F. A. Fernández, and S. E. Day

Department of Electronic & Electrical Engineering, University College London
Torrington Place, London WC1E 7JE, UK

Abstract— The highly anisotropic nature of liquid crystals has long been exploited in optical devices including displays. Due to this property these material lend themselves to a wide range of other applications such as beam steering devices in telecommunication switches and tuneable antennas. In such applications the behaviour of the liquid crystal may be more complex than is seen in a standard display and there becomes a real need for accurate modelling. Modelling is further complicated in these applications by high electric fields or geometrical features, which can give rise to defects; tiny pockets where the liquid crystal favours biaxial ordering. Within these fine scale regions a vector field is inadequate to describe the arrangement of the liquid crystal. Instead an order tensor is required.

The accurate modelling of liquid crystal devices, involves the consideration of the elastic interactions within the material, and between the liquid crystal and the walls of the containing cell, which depending on the surface treatment may be weak or strong [1]. In addition to this a number of other effects must be taken into account. Electric fields, governed by the Poisson equation, reorient the liquid crystal and change the permittivity. Flexoelectric properties, where an elastic distortion induces an electric field and vice-versa, play a role too. Finally reorientation induces flow, governed by the Navier-Stokes equations, which can in turn induce further reorientation. A highly nonlinear system results involving the order tensor, electric potential, pressure and velocity fields [2]. We take a finite element approach in order to solve this coupled system of equations [3]. Full dynamic analysis is performed using an implicit time stepping procedure that provides stability while an adaptive meshing scheme enables fine scale features within the liquid crystal and their associated movements to be resolved.

REFERENCES

1. Willman, E., F. A. Fernández, R. James, and S. E. Day, "Phenomenological anisotropic anchoring energy of nematic liquid crystals for the Landau-de Gennes theory," *IEEE Transactions on Electron Devices*, Vol. 54, No. 10, 2630–2637, 2007.
2. Qian, T. and P. Sheng, "Generalized hydrodynamic equations for nematic liquid crystals," *Physical Review E*, Vol. 58, No. 6, 7475–7485, 1998.
3. James, R., E. Willman, F. A. Fernández, and S. E. Day, "Finite element modelling of liquid crystal hydrodynamics with a variable degree of order," *IEEE Transactions on Electron Devices*, Vol. 53, No. 7, 1575–1582, 2006.

The Shape of Saturn's Moon Titan from Radar Scattering Properties

Howard Zebker[1] and the Cassini RADAR Team

[1]Depts. of Geophysics and Electrical Engineering, Stanford University, USA

Abstract— The detailed shape of Saturn's moon Titan provides much information about its interior and surface geophysical properties. Large-scale deviations from perfect sphericity constrain models of the planetary interior, while small scale elevation changes, or topography, help discriminate among surface evolution and weathering processes. The Cassini spacecraft, a NASA space mission now observing the Saturn system, includes a radar instrument that observes Titan several times per year in great detail. We have operated the radar in imaging SAR, scatterometer, radiometer, and altimeter modes and have recorded radar echoes over much of the moon. The altimetry data in particular provide information about Titan's shape, although we also obtain elevation data from the multibeam imaging antenna using monopulse methods. To be most useful, the altimetry data must be corrected for off-nadir viewing geometries, which introduce an angle dependent bias in the observations. This effect, called electromagnetic bias, is commonly observed and corrected in Earth-orbiting altimeters over the oceans, where the radar scattering is well known. On Titan, the scattering laws are highly variable and poorly understood. We use data from the scatterometer and imaging modes to derive the scattering laws for Titan's surface and volume scatter, and then use these laws to derive corrections for Titan altimetry data. We find that the surface has both a surface specular component that is well-modeled by Hagfors'law, plus a cosine-dependent volume term. After correction, the altimetry data show that Titan is rather smooth but with occasional km-scale mountains, and a systematic departure from sphericity that reduces polar radii. We calculated the 5th order spherical harmonic expansion and are now examining the variation in local radius for the signature of various surface features. We find that we can estimate the mean radius with about 10 times greater precision than occultation-based methods, and also provide unique elevation transects over much of the surface.

Influence of a Logging Tool on Modes of Noncircular Fluid-filled Boreholes in Elastic Formations

E. Simsek and B. K. Sinha

Schlumberger-Doll Research, Cambridge, MA, USA

Abstract— Dispersion curves for propagating modes of a noncircular fluid-filled borehole in homogeneous elastic formations can be calculated with a boundary integral formulation [1]. In this formulation, the displacement and stresses on the borehole wall are expressed as integrals over a surface distribution of effective sources, in the frequency-axial wave number $(\omega - k_z)$ domain. The unknown sources are approximated by sums of finite basis functions, which are then determined by enforcing boundary conditions. The discretized equations form a homogeneous system whose determinant vanishes when $(\omega - k_z)$ correspond to a nontrivial solution for the resonant mode of interest.

A heavy fluid model can be used to account for the effect of a specially designed sonic logging tool in fluid-filled boreholes. In this situation, the influence of a logging tool on borehole propagating modes can be described by placing a concentric heavy fluid column with calibrated mass density and compressional modulus. This fluid column makes the geometry of a three-layer structure and requires additional boundary conditions to be satisfied. In this formulation, we have 6 unknowns and 6 boundary conditions obtained by satisfying the continuity of normal displacement components and normal stresses both at heavy-fluid and borehole-fluid; and borehole-fluid and solid boundaries; and the requirement of vanishing shear stresses in fluid layers. To solve this set of equations numerically, we approximate the unknowns by sums of triangular basis functions, remove the integrable singularities and calculate their contribution analytically. The remaining smooth functions are integrated by third-order Gaussian quadrature. The accuracy of the implementation has been validated by comparing modal dispersions with a Finite-Difference Time-Domain solver. Results will be presented for monopole, dipole, and quadrupole modes of several borehole shapes including elliptical boreholes and boreholes with breakouts, in both fast and slow formations.

REFERENCES

1. Randall, C., *J. Acoust. Soc. Am.*, Vol. 89, 1002–1016, 1991.

Fast Calculation of the Diffraction Operator Kernel Used by the Wave Concept Iterative Process (WCIP) for Problems of Scattering and Radiation by Planar Circuits in Free Space

T. Bdour[1], **N. Ammar**[1], **T. Aguili**[1], **and H. Baudrand**[2]

[1]Communications Systems Laboratory in Tunis Engineering School
Belvedere, BP 37 Tunis, 1002 Tunisia
[2]Electronics Laboratory LEN7, ENSEEIHT, 2 Rue Camichel, Toulouse 31071, France

Abstract— Commonly, the computation of scattering and radiation by planar open circuits can be performed using the method of moments MoM [1]. Nevertheless, such analysis is difficult because of the singular behavior of the Green operator and the poor condition number of the reaction matrix when increasing the discretization fineness [2]. Furthermore; the MoM matrix size is proportional to the meshing cell number. This can severely penalize the CPU run time while performing the MoM matrix fill in and inversion tasks. To overcome these difficulties, an original integral method based on transverse wave formulation WCIP [3–5] has been proposed. The difference between the WCIP method and the previous integral methods is twofold. Firstly; the formulation is not based only on electric fields or magnetic fields equations but on their linear combination which permits us to handle diffraction operators instead of manipulating unbounded impedance or admittance operators. Secondly, as the WCIP distinguishes the topological characteristics of circuits from their embedding environment, a medium representation in the modal domain coexists simultaneously with a surface description in the spatial domain. To each representation is associated an integral matrix equation. These two equations are related by an iterative scheme.

The WCIP algorithm has been firstly designed to treat planar circuits that operate inside a rectangular wall [4]. Therefore, the extension to free space radiation problems is not obvious. However, satisfactory results, involving open structures simulation, have been obtained by an appropriate modeling of the free space environment in the modal domain. The major drawback of such modal approach lies in the fact that the involved spectral expansion double series of the diffraction operator are slowly convergent.

This paper proposes a novel rapid method of calculation of the dyadic diffraction operator kernel for open planar structures. In this method, the spectral expansion double series of the diffraction operator are divided into convergent and divergent parts to be converted separately in next step from modal to spatial domain into integral forms. An analytical form of the diffraction kernel is mathematically determined. As a result, the proposed technique greatly accelerates the calculation of the diffraction operator kernel compared with the spectral summation. The modeling assumptions of this technique are described in detail. Some numerical examples are performed to demonstrate rapidity and accuracy of the proposed method.

REFERENCES

1. Harrington, R. F., *Field Computation by Moment Methods*, Macmillan, New York, 1968.
2. Warnick, K. F. and W. C. Chew, "Error analysis of the moment method," *IEEE Antennas Propag. Mag.*, Vol. 52, 38–53, Dec. 2004.
3. Wane, S., D. Dajon, H. Baudrand, and P. Gamand, "A new full-wave hybrid differential-integral approach for the investigation of multilayer struccture including non uniformly doped diffusion," *IEEE Tansactions on Microwave Theory and Techniques*, Vol. 53, No. 1, 200–214, Jan. 2005.
4. N'Gongo, R. S. and H. Baudrand, "Application of wave concept iterative procedure in planar circuits," *Recent Res. Devel. Microwave Theory and Technique*, Vol. 1, 187–197, 1999.
5. Bdour, T., N. Ammar, T. Aguili, and H. Baudrand, "Modeling of wave penetration through cylindrical aperture using an iterative method based on transverse wave concept," *IEEE Microwave Conference KJMW*, 45–48, Nov. 2007.

Electromagnetic Investigation of Scattering by Arbitrarily Shaped Structures in Free Space Using a Full Wave Transverse Formulation (TWF)

T. Bdour[1], **N. Ammar**[1], **T. Aguili**[1], **and H. Baudrand**[2]

[1]Communications Systems Laboratory in Tunis Engineering School
Belvedere, BP 37 Tunis, 1002 Tunisia
[2]Electronics Laboratory LEN7, ENSEEIHT, 2 Rue Camichel, Toulouse 31071, France

Abstract— In this paper, a new approach of the Wave Concept iterative Process (WCIP) [1–4] method is presented to study the electromagnetic scattering problem by arbitrarily shaped structures in the free space. This iterative integral approach is based on transverse wave formulation TWF. The WCIP principle consists in expressing the boundary and the closing conditions in term of incident and scattered waves related by bounded diffraction operators. A system of equations is deduced from these conditions: The integral relations are described in the spectral domain and the continuity conditions are formulated in the spatial domain. The iterative process is ensured between the two domains in order to compute the unknown electromagnetic fields. The iterations are stopped when a desired precision is reached on the problem value. In the case of embedded circuits, the toggling between the spatial and the spectral domains is accelerated by the fast modal transform FMT. Unlike the MoM method, the WCIP handles bounded and usually convergent integral operator avoiding to treat possible singularities involving the Green operator. It also dissociates its two basic equations which enhances its real-time optimization technique. It has been proven that the iterative process of our full-wave approach is always convergent [3] and a considerable reduction of the computational CPU time can be achieved regarding the MoM simulation time. Despite its performance, the use of WCIP method is limited to closed structures.

The main motivation of this paper is to extend the use of our full-wave approach to the electromagnetic investigation of more general class of open geometries, and in consequence to explore the capability of this method in predicting their scattering features in free space. In this approach, the cylindrical coordinate system is adopted to the formulation of the problem [5]. Diffraction operators describing the coupling between the studied structure and the free space are defined and expanded in an appropriate cylindrical local-domain functions basis. The two basic equations are fully reformulated in the spatial domain. A comparative study of the simulation computational time of the present method and the MoM method is proposed. Numerical results which illustrate the efficiency of our approach are presented for two scattering problems involving structures with sharp edges and wedges (corner reflector [6] and L-shape [7]). The computed currents density and the normalized scattering coefficient present a very good agreement with the literature.

REFERENCES

1. Wane, S., D. Bajon, H. Baudrand, and P. Gamand, "A new full-wave hybrid differential-integral approach for the investigation of multilayer structures including non uniformly doped diffusions," *IEEE Trans. MTT*, Vol. 53, No. 1, 200–214, Jan. 2005.
2. Wane, S., D. Bajon, H. Baudrand, and P. Gamand, "Full wave analysis of isolated pockets to improve isolation performances in silicon based technology," *IEEE MTT-S Int. Microwave Symp. Dig.*, 987–990, Jun. 2002.
3. N'Gongo, R. S. and H. Baudrand, "Application of wave concept iterative procedure in planar circuits," *Recent Res. Devel. Microwave Theory and Technique*, Vol. 1, 187–197, 1999.
4. Raveu, N., T. P. Vuong, I. Terrasse, G.-P. Piau, and H. Baudrand, "Near fields evaluated with the wave concept iterative procedure method for an E-polarisation plane wave scattered by cylindrical strips," *Microwave and Optical Technology Letters*, Vol. 33, No. 1, 57–61, Apr. 2002.
5. Bdour, T., N. Ammar, T. Aguili, and H. Baudrand, "Modeling of wave penetration through cylindrical aperture using an iterative method based on transverse wave concept," *IEEE Microwave Conference KJMW*, 45–48, Nov. 2007.
6. Shijo, T., T. Harino, and M. Ando, "Large-size local-domain basis functions with phase detour and Fresnel zone threshold for sparse reaction matrix in the method of moments," *IECE Trans. Electron.*, Vol. E88-C, 2208–2215, Dec. 2005.

7. Pan, G. W., Y. V. Tretiakov, and B. Gilbert, "Smooth local cosine based Galerkin method for scattering problems," *IEEE Tansactions on Antennas and Propagation*, Vol. 51, No. 6, Jun. 2003.

Inversion 2D in the Measures of the Resistivity of the Ground

Celsa Herminia de Melo Maranhão, Valcir João da Costa Farias and Brígida R. P. Rocha

Universidade Federal do Pará, Brazil

Abstract— The inverse problem is defined in opposition to the direct problem. The present numerical scheme computes the soil layers resistivity by simulating the evolution of the geological scenery and the behavior of the rocks, and the active field of tensions in the modeled area, mainly along the flaws and geological features, in two dimensions. This two-dimensional numerical scheme is a useful tool based on a dipolo-dipolo arrangement, which computes the response of a geological medium by the inversion method.

The minimization of the objective function (or cost function) is made using the Gauss-Newton's iterative method to identify the vertical structures, which characterize the areas of flaws, which influence the measured values of the resistivity.

The adopted geological geometry (model) consists of an area with resistivity of 64 Ωm and 130 Ωm in contact with other two regions of resistivity 270 Ωm and 743 Ωm respectively. The simulation of his geological model permitted to observe that the soil does not behave as a homogeneous medium, due to the existent geological flaws in the underground. For layers with high degree of heterogeneity, limited in the base and in the top for less resistant portions, it is possible to identify the fractured areas by the analysis of displacements or disturbances obtained by the inversion in the resistivity values.

The obtained results permitted to correlate the resistivity values with geological features, more specifically with the geometry of the layers and the contact among different lithologies. It was observed that the structural conditioning, linked to the fractures, influences the resistivity values observed in the model. The use of resistivity data, in conjunction with other geological information permits to identify features that help in the characterization of the typical anomalies of vertical structures, which define the areas of flaws that delimit the structures of the soil.

Forest Effects on Lightning Discharge Signals in the Amazon Region: Preliminary Results

Valcir João da Cunha Farias, **Brígida Ramati P. da Rocha and José Pissolato Filho**
Universidade Federal do Pará, Brazil

Abstract— Several models have been proposed to describe behavior of lightning discharge and predict its effect [1, 5]. According [5] theses models can be classified in four categories: physical models, distributed-circuit models, engineering models and electromagnetic models. The last two are the most used because they can be conveniently tested against observations [1]. The electromagnetic models have received a great deal of attention, in theses models and the Maxwell's equations are solved numerically to obtain the electric field, current distribution and the charge density [1, 3, 4, 6].

The mean standard measurement of current of lightning discharge is normally around 30 kA. This value measured using a network with twelve VAISALA, LPATS-IV model sensors in the eastern Amazonian region of Brazil is much higher showing a mean value of 75 kA, a value almost three times the standard value. A possible explanation to high values is that the measurements are realized inside the rain forest. To study lightning discharge in the amazon region a time-dependent model using the Maxwell's equations was developed. The finite difference time domain (FDTD) method was applied. The mesh of finite difference was refined at the vicinity of the ground to insert in our model a conductive layer to represent the rain forest. The electric field, the current distribution and the charge density are solved within a space defined by a UPML absorbing boundary conditions. The preliminary results shows that the rain forest has large influence on electromagnetic signals produced by the lightning discharge.

REFERENCES

1. Shoory, A., M. Rouzbeh, S. H. H. Sadeghi, and V. A. Rakov, "Analysis of lightning-radiated electromagnetic fields in the vicinity of lossy ground," *IEEE Transactions on Electromagnetic Compatibility*, Vol. 47, No. 1, 131–145, 2005.
2. Almeida, J. F., C. L. da S. S. Sobrinho, and R. O. Santos, "Técnica computacional para implementação de condições de fronteira absorvente UPML por FDTD: Abordagem completa," *IEEE Latino Americana*.
3. Ma, Z., C. L. Croskey, and L. C. Hale, "The electrodynamic responses of the atmosphere and ionosphere to the lightning discharge," *J. Atoms. Terr. Phys*, Vol. 60, 845–861, 1998.
4. Podgorski, A. S. and J. A. Landt, "Three dimensional time domain modelling of lightning," *IEEE Transactions on Power Delivery*, Vol. PWRD-2, No. 3, 931–938, 1987.
5. Rakov, V. A. and M. A. Uman, "Review and evaluation of lightning return stroke models including some aspects of their application," *IEEE Transactions on Electromagnetic Compatibility*, Vol. 40, No. 4, 403–426, 1998.
6. Hu, W. and S. A. Cummer, "An FDTD model for low and high altitude lightning-generated EM fields," *IEEE Transactions on Antennas and Propagation*, Vol. 54, No. 5, 2006.

Session 5P2
Electromagnetics and Photonics: New Applications and Methods

Multilayer Antenna with Metamaterial and Arbitrary Substrate

H. C. C. Fernandes, **R. R. C. França**, **and A. F. Gomes**
Department of Electrical Engineering, Federal University of Rio Grande of Norte, Brazil

Abstract— This paper presents a study and developed of equation consisting of negative refraction index materials, known as metamaterials. The equation developed structure this based in full wave Transverse Transmission Line (TTL method). This method possibilities a significant algebraic simplification of the equations involved in the process. In order to analyze this structure the complex resonant frequency were determined. The results obtained in analyze for this application and the conclusions are presented.

Microstrip antennas are widely used as a microwave component due to its various advantages such as reducing size, weight, and cost and in addition because it interfaces easily with other microwave circuits. This letter demonstrates an application of the metamaterial: an efficient multilayer antenna. The analysis is made using the TTL method and the metamaterial definitions. The objective of this paper is to present the effect of dielectric anisotropy on multilayer antenna shown in Fig. 1. From the Maxwell's rotational equations the electromagnetic fields equations are developed, and the unknown constants are obtained. With this, the general equations of the electromagnetic fields as function of E_{xt} and E_{zt}, which are the tangential components of the electric fields in the slots, are obtained. The initial step to calculate the complex resonant frequency is to isolate, the still unknown, E_{xt} and E_{zt} components using the boundary conditions of magnetic field equations in the patch regions. Substituting the magnetic field equations and isolating the terms in the electric fields, were find the equations that can be written through the admittance functions. Continuing, an matrix inversion is made and the scalar product of the impedance matrix is made using an conjunct of base functions. With this, the electric fields are made zero, and a new matrix equation is obtained. So the system has a non trivial solution, the matrix determinant coefficients must be equal to zero. This determinant is represented by a transcended equation that has as roots the attenuation of the complex resonant frequency. Finally new results can be obtained for this structure.

The metamaterial substrate shown in region 1 of Fig. 1 is modeled by utilizing bianisotropic tensor properties, and constants which are expressed as:

$$\mu = \mu_0 \begin{bmatrix} \mu_{xx} & 0 & 0 \\ 0 & \mu_{yy} & 0 \\ 0 & 0 & \mu_{zz} \end{bmatrix} \tag{1}$$

$$\varepsilon = \varepsilon_0 \begin{bmatrix} \varepsilon_{xx} & 0 & 0 \\ 0 & \varepsilon_{yy} & 0 \\ 0 & 0 & \varepsilon_{zz} \end{bmatrix} \tag{2}$$

$$A_{1h} = \frac{\beta k \tilde{E}_{xy} - \alpha_n \tilde{E}_{zy}}{w\mu_0 \left(\mu_{xx} + \mu_{yy}\right) senh(\gamma y)} \tag{3}$$

$$A_{1e} = \frac{j\left(\alpha \tilde{E}_{xy} + \beta k \tilde{E}_{zy}\right)}{\gamma senh(\gamma y)} \tag{4}$$

To calculate the numerical results it was developed a computational program in Fortran PowerStation language, previous theoretical analyses. Compared to other full wave methods the TTL is an efficient tool to determine the antenna characteristics, making possible a significant algebraic simplification of the equations involved in the process and reducing the computational time.

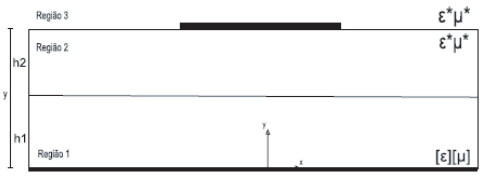

Figure 1: Transversal session of a multilayer antenna structure with metamaterial substrate.

Design and Analysis of Resonant Leaky-mode Broadband Reflectors

M. Shokooh-Saremi and R. Magnusson
Department of Electrical and Computer Engineering, University of Connecticut
371 Fairfield Road, U-2157, Storrs, CT 06269-2157, USA

Abstract— Devices based on the guided-mode resonance (GMR) effect are promising for applications in optics and electromagnetics. They can provide variety of spectral responses founded on periodically patterning a single optical layer on a substrate or as a free-standing membrane. Although the main manifestation of the GMR effect is a sharp resonance in the reflection spectrum, by proper selection of device parameters, attainment of variety of optical signatures such as narrow bandpass/bandstop filters, broadband reflectors, and polarizers is possible. Since in these elements light is coupled into waveguide leaky modes through a subwavelength grating structure, the device works in the second (leaky) stopband. The spectral response is highly dependent on the modal characteristics of the guiding layer. Broadband high reflectors, based on periodically patterned single layers (deposited on a substrate or as membranes), are attractive for use as laser mirrors. In this paper, a single layer, strongly-modulated GMR-based broadband high reflector is designed for the 1.4–2.0 μm band for TE and TM polarizations using the particle swarm optimization (PSO) technique. PSO is a robust, easy to implement evolutionary technique inspired from the behavior of particles in a swarm searching for optimal resources. A silicon-on-insulator (SOI) structure is chosen in which the binary patterned silicon layer acts as both grating and waveguide. The spectral and modal characteristics of these elements are analyzed utilizing rigorous electromagnetic techniques like rigorous coupled-wave analysis and modal techniques. The designed reflectors for TM and TE polarizations provide ∼520 nm and ∼400 nm bandwidth at $> 99\%$ reflectance, respectively. It is shown that these wide flat reflection bands are contributed by three cooperating leaky modes for these example devices. Also, by computing parametric reflection and transmission maps as well as the mode profiles, we investigate the effect of refractive index modulation and layer thickness on the spectral response.

Design of Two-band 150–220 GHz Superconducting Bolometric Detection Structure

D. Rauly[1], **A. Monfardini**[2], **A. Colin**[3], **and P. Febvre**[1]

[1]IMEP-LAHC, UMR 5130 CNRS/INPG/UJF/USAVOIE
MINATEC, Grenoble and Le Bourget du Lac, France
[2]Institut Néel, CNRS/UJF dept MCBT, Grenoble, France
[3]Instituto de Fisica de Cantabria (CSIC-UC), Santander, Spain

Abstract—

Introduction: Nowadays, large number of astrophysical studies, based on Cosmic Microwave Background (CMB) observation require multi-band detecting devices. As examples, combined 150–220 GHz measurements with ground-based equipments are currently used in order to investigate the early Universe, or to detect the presence of remote galaxies clusters, comparing CMB photon flux at 150 and 220 GHz (spectral deformation due to Sunyaev-Zeldovich (SZ) effect).

Moreover the high angular resolution of large aperture telescopes has to be exploited by optimal filling of mm-wave focal plane. It ensues the need for developing array-shape detection structures.

The aim of this paper is to propose the design of one detecting pixel which can meet both twoband and low-size requirements, with filtering characteristics suitable for actual and future astrophysical applications.

Pixel Structure: The studied device includes the following elements (see Figure 1):

* A bow-tie antenna fabricated with superconductive Nb on 30 µm-thick Si substrate, with a reflector back plane located 340 µm below.
* A 150/220 GHz diplexer, composed by coplanar striplines (CPS) and broad side coupled (BCL) transmission lines (superconductive Nb on 30-µm Si). The strips of CPS lines are vertically offseted, by means of a 0.3 µm SiO_2 layer, in order to make easier the transition with BCL lines.
* Palladium resistive loads, located close to NbSi bolometric detection thermometers, on Si_3N_4 membranes with maximal thickness 1 µm.

Computation Results: The design procedure uses two interactive steps of computations.

In the first level, ANSOFT HFSS^{TM} and CST softwares are used in order to model the above-mentioned elements of the studied device (antenna, transmission lines and terminations).

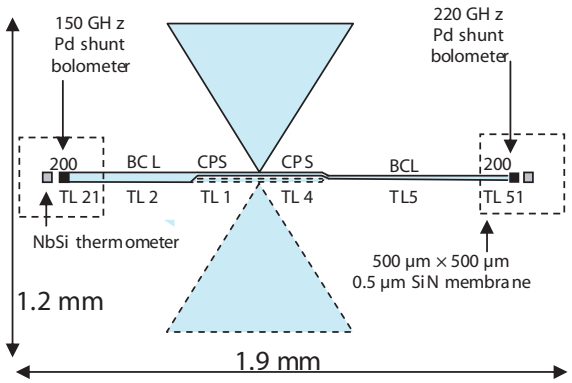

Figure 1: Pixel structure.

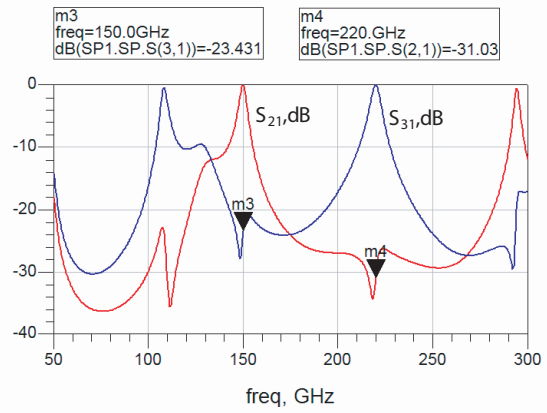

Figure 2: Transmission coefficients.

The second level consists in computing the frequency behaviour of the global structure, by means of previously established models. It uses the Agilent ADS^{TM} software.

Figure 2 shows the computed transmission coefficients between the antenna and loads. It exhibits an expected frequency rejection better than 20 dB. The final paper will present other computation results and conclude on the feasibility of the required detecting pixel.

A Magneto-dielectric Hologram as an Efficient Computational Boundary for Domain Decomposition

R. E. Diaz and A. Panaretos
Ira A. Fulton School of Engineering, Department of Electrical Engineering
Arizona State University, Tempe, AZ 85287-5706, USA

Abstract— A computational boundary is described that mimics the response of an arbitrary complex volume half-space with a single reacting surface: a magneto-dielectric hologram. Its intended application is in the domain decomposition of large computational problems where the bulk of the problem remains invariant while a "small" region varies stochastically. By replacing the "large" part of the scenario, the hologram enables the re-use of that part's solution for a highly efficient rigorous analysis of the smaller region. The approach is particularly well suited for support of Monte Carlo analysis of problems such as the effect on the Radar Cross Section (RCS) signature of a large platform when a "small" portion of that platform is varied or the iterative design of an antenna on a large complex platform.

The equations for the hologram that replaces a complex half-space are derived based on the assumption that the total fields' local transverse impedance can be blamed point-wise on an inhomogeneous magneto-dielectric surface. The 2D canonical case of a Perfect Electrically Conducting (PEC) cylinder illuminated by a line source is used to illustrate the application of the hologram and to compare its fidelity with the traditional interference hologram of optics. As a second example a flat metal plate scatterer with a resonant aperture cut into it, whose position in the plate is only known statistically, is considered. The monostatic RCS statistics are derived using the hologram and by brute force solution of the large scenario 121 times (once for each instance of the position of the aperture). It is shown that the mean RCS of the plate is obtained by running the large scenario only twice. The standard deviation of the 121 brute force runs only takes 7 runs using the holographic boundary. Thus at least an order of magnitude reduction in computational cost can be obtained using this technique.

Nanowire-based Superconducting Single-photon Detectors for Infrared Single-photon Source Characterization

Martin J. Stevens[1], **Burm Baek**[1]
Richard P. Mirin[1], **Sae Woo Nam**[1], **and Robert H. Hadfield**[2]

[1]National Institute of Standards and Technology, 325 Broadway, Boulder, CO 80305, USA
[2]Heriot-Watt University, Edinburgh, EH14 4AS, UK

Abstract— Single-photon sources and detectors enable a wide range of applications, from quantum information technologies to fundamental tests of quantum optics. Semiconductor quantum dots (QDs) have emerged as promising single-photon sources, and recent work has demonstrated their viability at wavelengths longer than 1 μm. Characterization of these sources, however, has been hindered by the poor quality of single-photon detectors in the infrared. Recently, superconducting single-photon detectors (SSPDs) based on nanopatterned NbN have been shown to offer considerable advantages over conventional detectors. Unlike silicon-based devices, SSPDs are sensitive well into the infrared, and have been demonstrated with over 50% detection efficiency at 1550 nm and operation at count rates as high as 1 GHz. Although SSPDs must be operated at temperatures near 4 K, we have minimized the associated difficulty and expense by packaging several fiber-coupled devices in a single cryogen-free refrigerator.

We have demonstrated that SSPDs are well-suited for characterizing infrared single-photon sources by measuring carrier lifetime and second-order coherence. The single-photon source is an InGaAs QD embedded in a micropillar cavity. Short optical pulses ($\sim$ 1 ps duration, 780 nm center wavelength) excite the QD, which then luminesces at 902 nm. We measure the QD's spontaneous emission lifetime using time-correlated single-photon counting. To do this, the photoluminescence (PL) is spectrally filtered, coupled into an optical fiber, and directed to an SSPD inside the cryocooler. A fast photodiode triggered by the laser starts a timer that stops on a signal from the SSPD. High-speed electronics record a histogram of start-stop pairs, yielding a curve that is proportional to the time-resolved PL. The spontaneous emission lifetime of this QD extracted from these data is $\sim$ 400 ps. We have used this SSPD to measure the lifetimes of a variety of semiconductor samples emitting at wavelengths between 0.9 μm and 1.65 μm.

To show that this QD emits only one photon at a time, we measure the second-order coherence, $g^{(2)}(\tau)$, using a standard Hanbury Brown-Twiss configuration. The spectrally filtered PL is incident on a beamsplitter, and each beamsplitter output is coupled into an optical fiber and directed to an SSPD. The timing electronics record a histogram of time delays between a photon detected by one SSPD and a second photon detected by the other SSPD. In the limits used here, this histogram is proportional to $g^{(2)}(\tau)$. We take the area of the peak at zero delay divided by the mean area of all other peaks to find $g^{(2)}(0) = 0.08 \pm 0.04$, which is close to the value of zero expected for an ideal single-photon source. These results show that SSPDs are well-suited to single-photon source characterization, and should prove particularly useful in evaluating single-photon sources that emit at telecommunications wavelengths ($1.3 - 1.5$ μm), as well as in other quantum optics applications in the infrared.

Rigorous Coupled-wave Analysis of Electromagnetic Wave Diffraction by Photo-induced Plasma Gratings

Krzysztof A. Michalski
Department of Electrical and Computer Engineering
Texas A&M University, College Station, TX 77843, USA

Abstract— When a beam of light with sufficient photon energy illuminates a semiconductor, electronhole pairs are generated, resulting in a semiconductor plasma region, whose complex dielectric constant differs from that of the non-illuminated material. By specially patterned illumination, a photo-induced plasma grating (PIPG) can thus be excited in a semiconductor layer. This phenomenon can be used in optical control of electromagnetic waves guided or diffracted by dielectric layers. In this paper, we apply the rigorous coupled-wave analysis (RCWA) method to investigate the microwave and millimeter-wave diffraction by dielectric layered media comprising photo-induced plasma gratings (PIPGs). We assume that the plasma regions are uniform and of rectangular cross-section. Since the grating layer is periodic, the multiple diffraction of the incident wave by the modulated structure gives rise to a series of diffracted plane waves and the scattered field components are given by the Floquet expansion. The RCWA is an analytical technique, which has been widely used in the analysis of diffraction gratings in the visible range. The computation consists of two major steps. First, the Fourier expansion of the dielectric function and the Floquet expansion of the fields inside the grating leads to a system of differential equations. Second, once the eigenvalues and eigenvectors of this system are found, the boundary conditions at the grating interfaces are enforced to compute the electromagnetic field. The fields in the semi-infinite exterior regions and inside any homogeneous finite layers are represented by Rayleigh expansions. We analyze a silicon-layer PIPG deposited on a sapphire slab (which is uniaxially anisotropic) in the general case of an obliquely incident plane wave. Plots of the reflected and transmitted diffraction efficiencies vs. frequency are presented for different plasma densities.

Stability and Interactions of Moving Bragg Grating Solitons in a Semi-dual Core System

Yazhuo Li and Javid Atai

School of Electrical and Information Engineering, The University of Sydney, NSW, 2006, Australia

Abstract— Periodic modulation of the linear dielectric constant in an optical medium results in a photonic band structure. This band structure gives rise to a cross-coupling between counterpropagating waves. As a result, such a medium becomes highly dispersive. An example of an optical medium with these characteristics is a fiber Bragg grating (BG). In this case, the effective dispersion due to the grating is approximately 6 orders of magnitude greater than the underlying chromatic dispersion of the fiber. At sufficiently high intensities the BG-induced dispersion may be counterbalanced by Kerr nonlinearity resulting in a Bragg grating soliton.

BG solitons have been the subject of intense theoretical and experimental research over the past three decades (see for example Refs. [1–4]). It has been shown that BG solitons in a uniform Bragg grating form a two-parameter family of solutions. One of these parameters is related to soliton's velocity, which can range between zero and the speed of light in the medium, and the other is dependent on the detuning frequency, peak power and soliton width. Due to their potential application in optical buffers and storage devices, significant efforts have been directed toward the generation of zero-velocity (quiescent) solitons. To date, moving BG solitons with a velocity in excess of 50% of speed of light have been observed. The existence and stability of solitons have also been investigated in more sophisticated systems. For instance, in Ref. [5] it has been shown that a family of BG solitons exists in a dual core system with nonidentical cores where one core is linear, which may or may not have a Bragg grating, and the other is nonlinear and is equipped with a Bragg grating.

The focus of Ref. [5] was the characterization of quiescent BG solitons in the dual core system. In this paper, we investigate the existence of moving solitons in the model proposed in Ref. [5]. Using the relaxation technique we have been able to obtain moving soliton solutions. The stability of these solitons are investigated numerically. A key finding is that for fixed parameters the stability borders depend on the velocity of solitons. We have also considered the collision of counterpropagating in-phase and π-out-of-phase moving solitons in this model. The outcome of the collisions may be merger of solitons into a single soliton or emergence of two separating solitons.

REFERENCES

1. De Sterke, C. M. and J. E. Sipe, *Prog. Opt.*, Vol. 33, 203, 1994.
2. Aceves, A. B. and S. Wabnitz, *Phys. Lett. A*, Vol. 141, 37, 1989.
3. Eggleton, B. J., C. M. De Sterke, and R. E. Slusher, *J. Opt. Soc. Am. B*, Vol. 14, 2980, 1997.
4. Taverner, D., N. G. R. Broderick, D. T. Richardson, R. I. Laming, and M. Ibsen M, *Opt. Lett.*, Vol. 23, 328, 1998.
5. Atai, J. and B. A. Malomed, *Phys. Rev. E*, Vol. 62, 8713, 2000.

Highly Linear Optical Modulators Based on Gires-Tournois and Double Ring Assisted Mach-Zehnder Interferometers

William dos Santos Fegadolli, José Edimar Barbosa Oliveira and Bráulio Fernando R Sakamoto
Instituto Tecnológico de Aeronáutica, Brazil

Abstract— Optical modulators based on either Gires-Tournois (GT) or ring assisted Mach-Zehnder (RAMZ) interferometers are attracting great interest because they may enable optical modulators having high dynamic range. A modeling which takes into account the front surface mirror reflectance of GT and the ring coupling coefficient of RAMZ modulators is presented. Although relying on a less complex fabrication technology, it is shown that GT's configuration may yield dynamic range as high as that achieved with RAMZ. Illustrative numerical simulations of modulators implemented on Lithium Niobate ($LiNbO_3$) shows that Spur-Free Dynamic Range (SFDR) as high as $112\,\mathrm{dB{\cdot}Hz^{2/3}}$ may be achieved using a push-pull operation on a Y — Cut and Z — propagation $LiNbO_3$ substrate.

Index Terms — Microwave Photonics, Dynamic Range, Electrooptic Modulators, Gires-Tournois Interferometer and Mach-Zehnder modulator.

It is well known that highly linear optical modulators may play a significant role on the subject of microwave photonics signal processing. Therefore, there have been numerous proposals aiming to improve the linearity of integrated optic modulators, such as the Ring-Assisted Mach-Zehnder scheme (RAMZ) and the Gires-Tournois Interferometer (GTI), in which the sublinear characteristics of a Michelson interferoemeter is used to cancel the third order nonlinearity.

The modeling presented in this paper yields a generalized transfer functions which enables an unified analysis of both types of optical modulators, i.e., GTI and RAMZ. The scheme of the proposed GT's modulator, as shown in Fig. 1(a), comprises the standard components of an electrooptic modulators (polarizer, circulator and waveplate) and a GTI made of a $LiNbO_3$ Pockel's cell. Its optical transfer function yields the dependence on the front surface mirror reflectance, Γ, and on the refractive index change, Δn, according to:

$$I_{out} = \frac{E_0^2}{2}\left\{1 - \sin\left\{4\,\mathrm{arctg}\left[\frac{1-\Gamma}{1+\Gamma}\cot\left(\frac{\phi_0}{2} + \frac{2\pi\Delta n}{\lambda}L\right)\right]\right\}\right\} \tag{1}$$

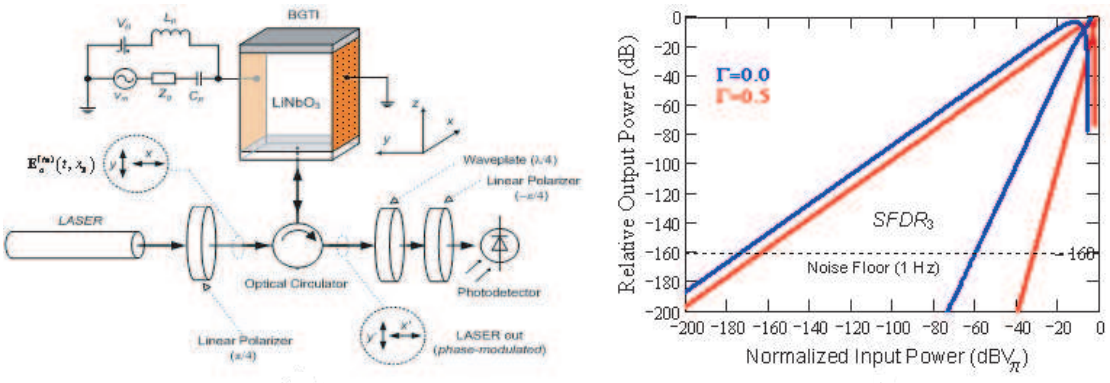

(a) (b)

Figure 1: Part (a) scheme of the proposed modulator and Part (b) signal power and IM power of for BGTI's either having $\Gamma = 0.5$ or $\Gamma = 0.0$.

Bearing in mind the role played by the ring coupling coefficient of a RAMZ, one may readily used Eq. (1) to describe a RAMZ transfer function. Numerical simulation of SFDR was carried out using $LiNbO_3$ material with a noise floor set to be $-160\,\mathrm{dBm}$. Fig. 1(b) shows the signal power and inter modulation (IM) power of for GTI's in two situations, namely: $\Gamma = 0.5$ *e* $\Gamma = 0.0$, as a function of the input signal power. This results reveals que GT modulators can exhibits dynamic range as high as those yielded by the well known RAMZ modulators.

This paper dealt with the analysis of SFDR of BGT RAMZ electrooptic modulators. It worth wile to point out that a BGTI based on a special tailored $LiNbO_3$ substrate may yields a SFDR as high as that issued by a RAMZ structure. It is worthwhile to point out that among the many potential applications of B-GTI, steams out those related to optical sensors of electromagnetic field and optical signal waveform generators.

Plastic Optical Fiber Microbend Sensors

W. S. Fegadolli[1], **J. E. B. Oliveira**[1], **and V. R. Almeida**[2]

[1]Instituto Tecnológico de Aeronáutica — ITA, Brazil
[2]Instituto de Estudos Avançados — IEAv, Brazil

Abstract— It is well know that optical fiber sensors play a major role on the performance of some state of the art measurement devices and systems, namely: gyroscopes, accelerometer, strain sensors and temperature sensors, among many other applications. Nowadays, in order to enable a wider range of application of such type of sensors, researcher activities are guided towards the design an implementation of low-cost sensors, such as those which relays on plastic fiber. This work undertakes both the design and the implementation of a plastic optical fiber microbend sensor, and investigates its potential as low-cost anti-squeeze sensor.

The sensor principle of operation relays on the well known fact that the optical fiber propagation characteristics may be quite sensitive to microbend, mostly because the microbend enables the leakage of optical power from the fiber core towards its cladding. The power leakage depends on the fiber radios of curvature. For instance, for a multimode fiber, the leakage becomes relevant when the radios of curvature is small than the a certain value given by the following equation,

$$R_c \cong \frac{3n_1^2\lambda_0}{4\pi\left(n_1^2 - n_2^2\right)^{3/2}} \tag{1}$$

where n_1 and n_2 are the core and cladding refractive indexes, respectively, and λ_0 is the free space optical wavelength.

When the curvature is slightly smaller than R_c, one may use a low loss approximation to calculate the power loss, and hence the optical power at the exit of the fiber can be written as follow,

$$P_{out} = P_{in}e^{-2\alpha z} \tag{2}$$

where 2α is the low loss attenuation, which depends on curvature radios, the optical fiber V-number and photoelastic coefficient.

The schematic representation of the proposed sensor is shown in Fig. 1(a). It comprises a laser source, a fiber optical strain sensor (plastic optical fiber), optical detection and electronic signal processing devices. Furthermore, the schematics emphasizes that at the block 1 the laser modulation takes place, as a result of the strain generated by applied force, whereas block 2 takes care of the detection of the strain modified laser signal. The electronic processing, which takes place at block 3, is an issue of major concern in this publication. A rather simple, however very suitable electronic detection processing was implemented based on very low-cost components. Further details of the electronic processing will be addressed in the full paper. The photography of the sensor set-up is shown in Fig. 1(b).

The theoretical modeling enabled the design an implementation of a low-price plastic optical fiber with an overall performance suitable for a few practical applications. Such promising results mostly steams from the high performance of the rather simple electronic signal processing scheme. It is believed that such sensor may be used as anti-squeezing alarm and safely tracking the presence of undesirable body at closed environment.

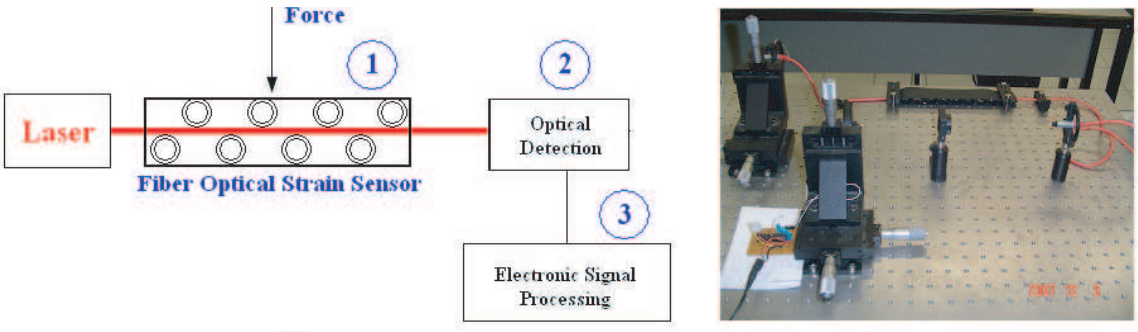

(a) (b)

Figure 1: Proposed sensor part (a) Schematic representation and part (b) Sensor set-up.

Session 5P3
Microwave and Millimeter-wave Devices and Circuits with CAD

Design of a Broadband Filter

Manidipa Bhattacharya

SAMEER, Plot L2, Block GP, Sector-V, Salt Lake Electronic Complex
Kolkata 700091, West Bengal, India

Abstract— Filters are most important passive component used in microwave subsystems & instruments. It can be designed and manufactured with predictable performance. Here the design of a filter having a broad pass band (73.3%) and low insertion loss is realized with broadside-coupled resonator elements in suspended stripline configuration as shown in Fig. 1. Here the inter-element coupling is achieved by fringing fields between resonators. The resulting filter can have a low fabrication cost.

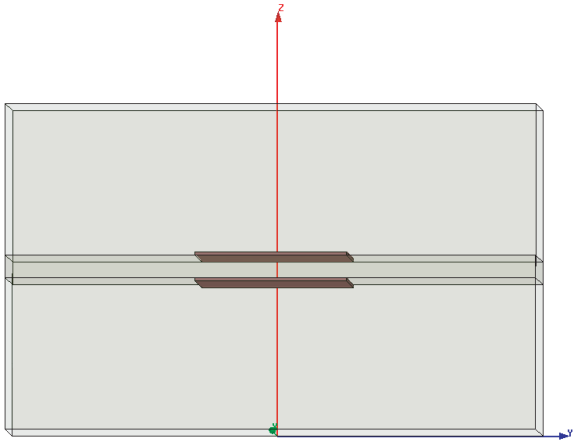

Figure 1: Cross section of broadside-coupled resonator.

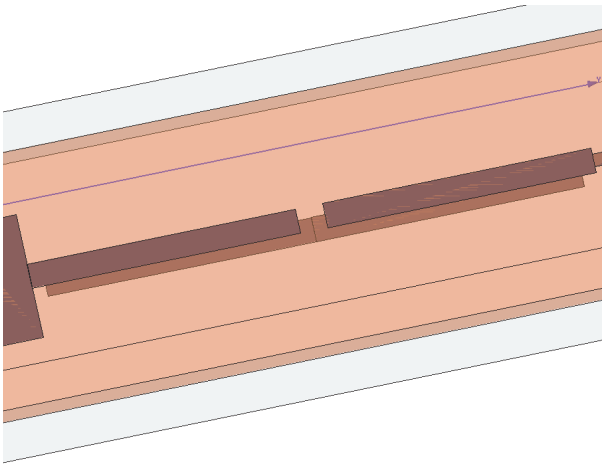

Figure 2: Suspended stripline filter configuration.

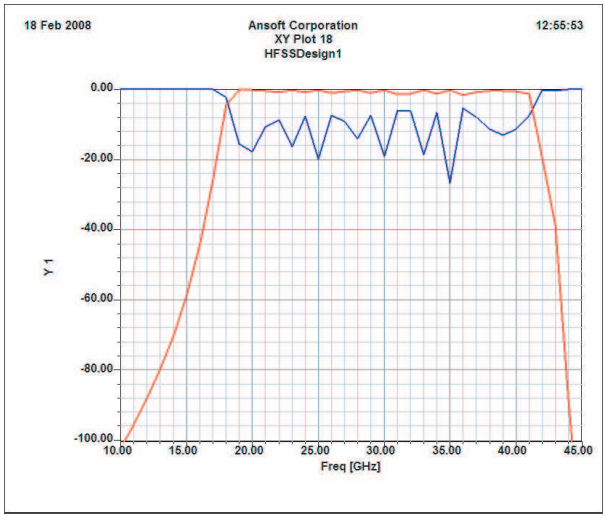

Figure 3: Simulated S_{21} and S_{11} plot.

The physical dimension of the resonators and the spacing can be found from the even and odd mode impedance analysis of the strip elements. This filter has been designed with broadside-coupled resonators in suspended stripline configuration (Fig. 2) for a predetermined channel

dimensions. Here the even and odd mode impedances of a single resonator is used to find the required coupling for the particular filter section. The internal impedance levels are set to have the desired Q of the resonator sections. Here fifteen broadside-coupled sections are used to design the broadband filter at K-Ka band with Chebyshev response. The design data has been used to optimize the filter response where the required gap capacitance is used to couple the filter sections. The filter has been designed and simulated using HFSS and the simulation result shows a 73.3% bandwidth (Fig. 3) with a good insertion loss (1.0 dB).

Smart Use of Non Uniform Transmission Lines to Control Oscillator and Power Amplifier Harmonics

M. Boussalem, **B. Roucariès**, **F. Choubani**, **J. David**, **and R. Crampagne**
6'Tel-SUPCOM, Tunisia, Toulouse université, ENSEEIHT, France

Abstract— The issue of our paper is to expose an original technique to control the harmonic output in a RF power amplifier and RF oscillator. This technique is based on the non uniform transmission lines (LNUT) use.

It is well known for a man of art that non uniform transmission lines have specific frequency behaviour. However to our best knowledge closed from formulae are not available. Therefore the analysis of such structures was given by a numerical program based on the work of Hill, which consists in determining the general solution of the propagation distribution equation of electric and magnetic field. We deduce an accurate model of several profiles including linear, exponential, and hyperbolic shape.

A quite useful property of non uniform transmission lines is that their frequency behaviour strictly depends upon their profiles of non homogeneity adding some degree of freedom compared to uniform counterparts. Whereas uniform transmission structures resonate in a integer multiple of fundamental frequencies, the non uniform lines resonate on frequencies which are different from integer multiples of fundamental.

Indeed, classical active microwave circuits are based on lumped LC elements used as resonator. Usually, these LC elements are converted to a distributed form like a uniform transmission lines. Whereas the lumped LC elements resonate at only one frequency, the distributed counterparts unfortunately introduce spurious frequencies. Our methodology consists of replacing a uniform structure by their equivalent non uniform parts witch have the same fondamental resonance fréquency, in order to ensure the same response at the operating frequency but have non harmonic high order resonant frequencies, in order to dramatically reduce the harmonics response of the circuits.

Our contribution provides an original method using non uniform transmission line in order to control these spurious frequencies. This method was experimentally validated, harmonics were sharply reduced by such use of NUTL. Hence, we have optimised the profiles of different elements of resonator circuits in order to get better frequency response.

REFERENCES

1. Khalaj-Amirhosseini, M., "Analysis of coupled or single nonuniform transmission lines using step-by-step numerical integration," *Progress In Electromagnetics Research*, PIER 58, 187–198, 2006.
2. Khalaj-Amirhosseini, M., "Analysis of coupled or single nonuniform transmission lines using Taylors series expansion," *Progress In Electromagnetics Research*, PIER 60, 107–117, 2006.
3. Hill, G. W., "One the share of motion of the lunar perigee," Cambridge the USA, 1877, reprinted in acta Mathematica, flight 8, 1–36, 1886.
4. Rossetto, B., "Détermination des exposants de Floquet de l'équation de HILL d'ordre n," Professor thesis, Toulon, 1983.

Numerical Characterization of Novel Schemes for Millimeter-wave Signal Generation by Optical Heterodyning

Subal Kar
Institute of Radio Physics and Electronics, University of Calcutta, India

Abstract— In recent times, millimeter-wave signal generation by optical heterodyning has become extremely important to address the need for various emerging communication applications. Broadband wireless access network for mobile communication, soft-ware defined radio, and space-based phased array antenna etc. demand broadly tunable and low phase-noise mm-wave signal source. In this paper we investigate the numerical characterization of two novel schemes which may be useful for such applications.

In one scheme Fig. 1, judicious use of cascaded Mach-Zehnder (MZ) modulator has been made whose output (E_{out}) consists of optical carrier having amplitudes $J_0(x)$ and sideband amplitudes are $J_2(x)$, $J_4(x)$, ..., which are at twice the modulation frequency. This reduces the sideband pulling and pushing effects normally found in conventional injection locked (IL) system thereby increasing the locking capability of the signal. Further the requirement of sub-nano second loop delay of optical phase lock loop (OPLL) is overcome by using additional phase modulator incorporated in the loop. This reduces the effective phase error resulting in better noise rejection capability and also the frequency of cycle slip is considerably reduced making the system very stable. Numerical characterization is done with 520 THz as master laser source frequency, Mach-Zehnder drive signal is 15 GHz to generate a millimeter-wave signal at 60 GHz. The phase noise of the generated signal is -110 dBc/Hz with 10 KHz frequency off-set from the carrier. This signal may be very useful as base station (BS) backbone signal source to feed a large number of pico-cells in pico-celluler mobile communication.

In another scheme Fig. 2, a single laser source is used in conjunction with an external optical modulator (Mach-Zehnder -type). The modulator produces a series of optical side bands from which only two side bands (whose frequency differs by the desired mm-wave frequency) are filtered out by fiber Bragg grating (FBG) notch filter and beated in a photodetector. The generated mm-wave signal will have a good phase-noise performance as the two beating optical signals are originated from the same laser source. The system is cost-effective as optical modulator needs a low frequency microwave drive and the system can realize a broadly tunable mm-wave signal simply by tuning the drive signal. Numerical characterization is done with a laser signal frequency of 400 THz to generate mm-wave signal of 400 GHz which is found to have a clean spectrum and is tunable over 20% with Mach-Zehnder drive signal variation over 2 GHz.This signal generation scheme may be useful in the design of optical beam forming network required in space-based phased array antenna.

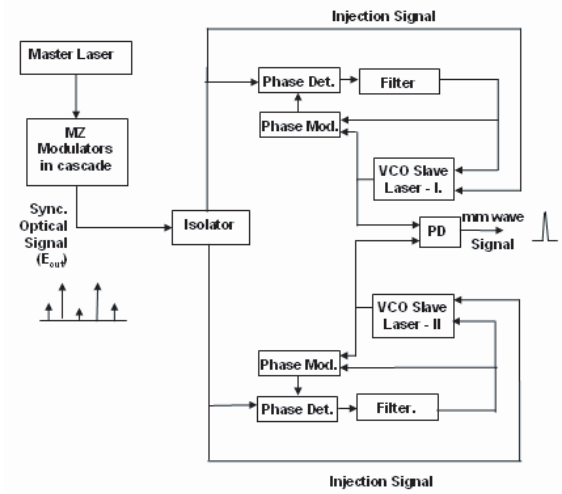

Figure 1: Modified OPLL scheme for optical generation of millimeter-wave signal.

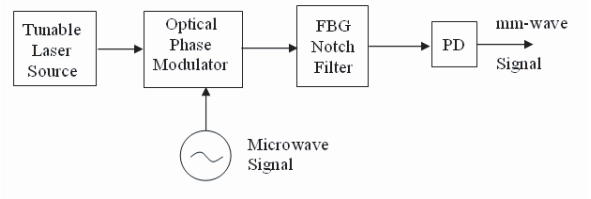

Figure 2: Millimeter-wave signal generation and tuning with external modulation of a laser source.

Left Handed Maxwell (LHM) System: A New Direction for Microwave and Millimeter-wave Research

Subal Kar, **Debashree Banerjee**, **and Tapashree Roy**
Institute of Radio Physics and Electronics, University of Calcutta, India

Abstract— Left-handed Maxwell (LHM) systems behavior is counter-intuitive. They have properties so as to reverse Snell's law, reverse Doppler phenomena, and to reverse various other electromagnetic phenomena. No naturally occurring media is known to behave in this counter-intuitive manner. In these artificially manufactured metamaterials the simultaneous realization of negative permittivity and permeability results in refraction of electromagnetic waves in opposite direction (vide Fig. 1) as a result of counter directance of the group velocity (S_{LH}) and phase velocity (k_{LH}). Focusing of electromagnetic wave is then possible with plane surfaces, unlike the conventional curved surfaces, and also the refocusing of the backscattered signal with significant gain.

Our aim in this paper is to review in details the promising possibilities that lies with the LHM research which started practically with the successful experimental demonstration of negative refraction in 2001. Since then the progress is with leaps and bound both resulting in strong theoretical foundation and experimental efforts to exploit its enormous potential from various application point of view. Though the success with metamterial design and experimentation, as of today, is in the microwave and millimeter-wave frequency region-its possibilities to be realized at terahertz and optical regime is not far from being reality.

The strip-wire (SW) array and split-ring resonators (SRR) are respectively used to realize the negative permittivity and negative permeability by making plasmonic arrays of such structures and the LHM property is realizable using SW-SRR combination at microwave and millimeter-wave frequencies. The periodically loaded transmission line (PLTL) structures are also used for realizing LHM property and are found to provide broadband operation having compact size compared to the SW-SRR structures. In this paper we would also present some analytical and simulation results of both SW-SRR and PLTL structures and would investigate the focusing and imaging capabilities of LHM structures both numerically and experimentally, if possible.

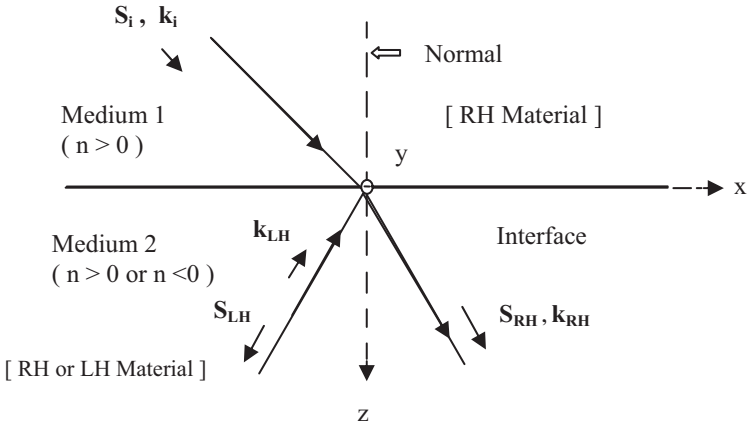

Figure 1: Refraction in RH and LH Materials.

Simulation Studies on Broadband LNA Design: A Distributed Approach

Paramita Biswas[1], **Arijit Majumder**[1], **and Subal Kar**[2]

[1]SAMEER Kolkata Centre, Plot-L2, Block-GP, Sector-V, Salt Lake
Kolkata 700091, West Bengal, India
[2]Institute of Radio Physics & Electronics, University of Calcutta
92 A. P. C. Road, Kolkata 700009, West Bengal, India

Abstract— This paper presents a method of accurate design and realization of a wide band Low Noise Amplifier (LNA) suitable for implementation using GaAs MMIC technology. To realize the wide bandwidth, which can not be implemented using a discrete approach, a broadband distributed configuration has been chosen. The basic active device used is a PHEMT with a transit time of 1.17 ps and a transconductance of 79.2 milli siemens/mm. The device model has been adapted from [2] and the parameters were calculated using the methodology described in [1], which has been applied for a MESFET previously. The design and simulation were carried out in Agilent Advanced Design System and the Method of Moment solver was used to take care of the electromagnetic effect of the interconnects. With the distributed approach a flat gain of 7 ± 0.5 dB and a noise figure of 3.3 dB to 4.7 dB has been achieved over the band of 18–40 GHz. A return loss of better than -12 dB has been achieved over the band which is adequate for a Low Noise design. The simulation results of Noise Figure, Gain, Stability and Return Loss has been depicted in Fig. 1.

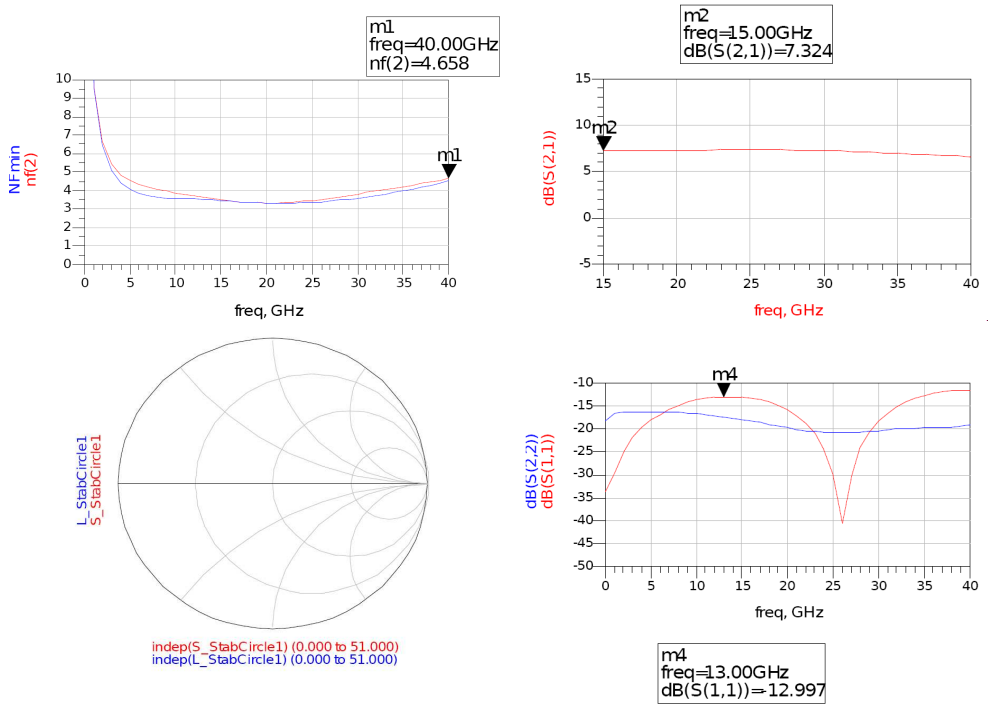

Figure 1: Simulation result of (18 to 40) GHz LNA using distributed amplifier scheme.

REFERENCES

1. Beyer, J. B., S. N. Prasad, R. C. Becker, J. E. Nordman, and G. K. Hohenwarter, "MESFET distributed amplifier design guidelines," *IEEE Trans. Microwave Theory Tech.*, Vol. 32, 268–275, Mar. 1984.
2. Deibele, S. and J. B. Beyer, "Attenuation compensation in distributed amplifier design," *IEEE Trans. Microwave Theory Tech.*, Vol. 37, No. 9, Sept. 1989.

A CAD of Frequency Tripler at Microwave and Millimeter Wave Frequencies

Arun Kumar[1], **Bijit Biswas**[1], **and P. K. Saha**[2]

[1]SAMEER Kolkata Centre, Plot-L2, Block-GP, Sector-V, Salt Lake, Kolkata 700091, India
[2]Institute of Radiophysics and Electronics, University of Calcutta
92, A.P.C Road, Kolkata 700009, India

Abstract— This paper relates to a simple computer aided design technique of 42 GHz frequency tripler. The input frequency is at 14 GHz while the output frequency is 42 GHz. The tripler (shown in Figure 1) is designed with anti-parallel diode pair configuration to achieve good even harmonic rejection. The diodes chosen for the mixer design are GaAs Schottky barrier beam lead diode with low parasitic to achieve good performance. The whole tripler has been realized in microstrip. The minimum conversion loss that has been measured is 17.5 dB in the range of 33 GHz to 42 GHz.

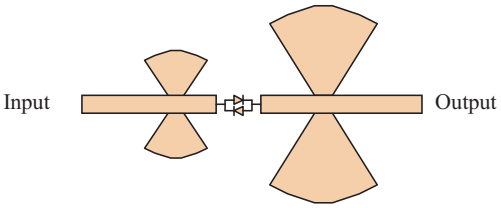

Figure 1: Tripler configuration.

We have carried out 3-D EM and circuit co-simulation with nonlinear analysis. First all the passive circuits have been modeled in 3-D EM simulator with FEM technique. Then those results from the EM simulation are used in circuit simulator. Nonlinear analysis of the tripler has been done with harmonic balance to get conversion loss and output signal harmonic contents. The simulated results have been shown in Figures 2 and 3. Other parameters like power output, frequency spectrum, input and output reflection coefficients as well as the diode current and voltage waveforms can also be found out through simulation. For accurate tripler simulation at microwave and millimeter wave frequencies one should have correct diode model to be incorporated in nonlinear circuit simulation. The accurate diode model can be extracted based on *s*-parameters and DC measurements of the diode mounted in test fixture.

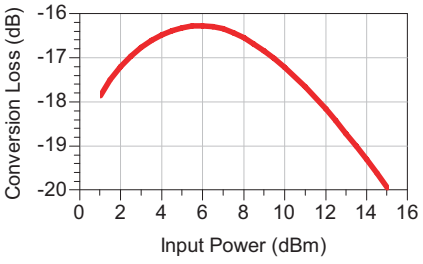

Figure 2: Conversion loss.
(Input frequency = 14 GHz)

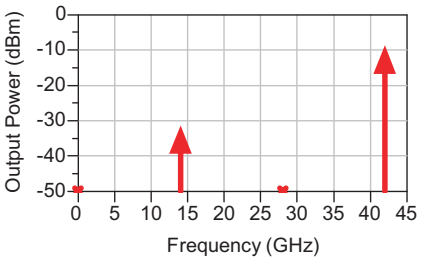

Figure 3: Output signal spectrum.
(Input power = 8 dBm)

CAD of Microstrip Mixer at Microwave and Millimeter Wave Frequencies

Arun Kumar[1], **G. Arun Kumar**[1], **and P. K. Saha**[2]

[1]SAMEER Kolkata Centre, Plot-L2, Block-GP, Sector-V, Salt Lake, Kolkata 700091, India
[2]Institute of Radiophysics and Electronics, University of Calcutta
92, APC Road, Kolkata 700009, India

Abstract— The present paper deals with the design and implementation of a Ka-band single balanced mixer. The RF frequency for mixer is 36 GHz to 36.5 GHz with an LO frequency of 34 GHz. The implementation of the mixer has been done in microstrip. Since the requirement of RF and LO ports are in waveguide, microstrip to waveguide transition is also incorporated in the design. Rat-race hybrid is chosen for the feeding the diodes with RF and LO signals. The diodes used are GaAs Schottky barrier beam lead diode with low parasitic. The circuit layout is as shown in Figure 1. The design of the mixer is simple with minimum matching elements.

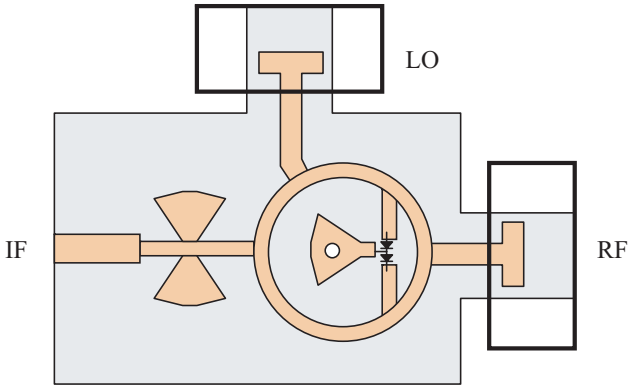

Figure 1: Single balanced mixer circuit.

The passive circuit elements are designed with FEM technique using Ansoft HFSS for optimizing their individual performance. Then harmonic balance analysis of the whole mixer has been carried out to predict conversion loss and port to port isolation. The simulated results have been shown in Figures 2 and 3. The other parameters like RF, LO and IF port VSWR can also be found out through simulation. Diode model used in the simulation has been supplied by manufacturer. For accurate mixer simulation at microwave and millimeter wave frequencies one should have correct diode model to be incorporated in nonlinear circuit simulation.

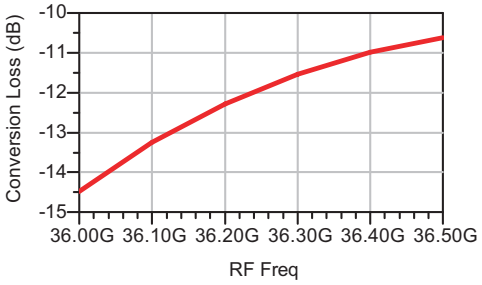

Figure 2: Conversion loss.

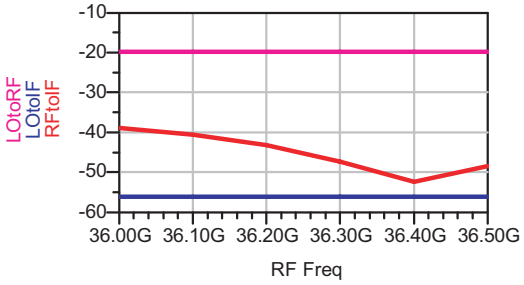

Figure 3: Port to port isolation (dB).

Scale Model Hardware Characterization of an Optical Phase-locked Loop (OPLL) Microwave Photonic Transmitter

Subal Kar, **Somak Bhattacharyya**, **Sujoy Mondal**
Kasturi Mukherjee, **Dibakar Deb**, **and Dipankar de Sarkar**
Institute of Radio Physics and Electronics, University of Calcutta, India

Abstract— The low frequency hardware characterization of an optical phase-locked loop (OPLL) microwave photonic transmitter has been carried out. The hardware realization with circuit fabrication and signal spectrum studies has been presented which shows satisfactory performance characteristics of this master-slave type down conversion signal generation.

In the schematic diagram for OPLL Microwave Photonic Transmitter proposed by Langley in 1999, shown in Fig. 1, the signal from the free-running master laser (ML) is heterodyned with a local oscillator laser (LOL) and the intermediate frequency (IF) signal is amplified. This signal is compared with the signal from a highly stable microwave reference oscillator. The phase detector output is amplified and filtered, which is then fed into the LOL, which is thus forced to track the ML, generating a microwave signal of 40 GHz with a significant reduction of the phase noise of the optically generated microwave signal (which is f_{IF} as indicated in Fig. 1).

Computer-aided analysis of the scheme has been carried out with MATLAB modeling where the ML is at 40 THz and the LOL is initially at 39.9 THz. The reference oscillator is at 40 GHz so the difference frequency of 60 GHz is obtained at the phase detector output which ultimately through locking mechanism drives the P.D. to deliver a stable 40 GHz signal.

In the scale-model hardware characterization of the scheme, the ML and LOL both are generated with IC 8038 with frequencies 77 KHz and 61 KHz respectively. The generated signals are passed through a balanced modulator, LM 1596 and filtered by active Butterworth filter to produce the 16 KHz difference frequency. The reference signal is generated by a Wien-Bridge oscillator operating at 32 KHz. The two signals mentioned above are mixed in another LM 1596 and the resulting 16 KHz signal drives the LOL to track the ML when finally the LOL gets locked to ML as shown in Fig. 2.

The computer-aided analysis of the scheme and the scale-model hardware characterization shows qualitative agreement justifying the novelty of hardware characterization of the scheme.

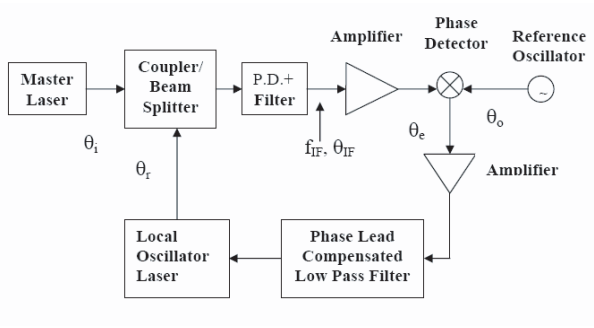

Figure 1: OPLL microwave photonic transmitter.

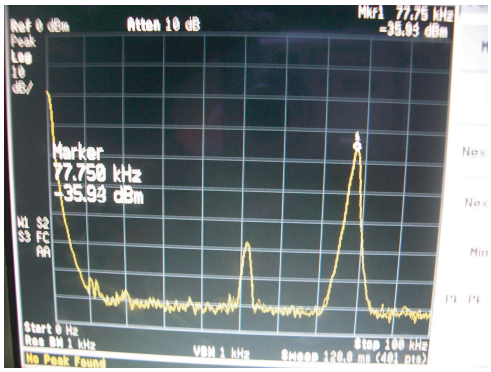

Figure 2: LOL locked with ML.

Computer-aided Analysis of an Optical Heterodyning Scheme for Ultra-stable Microwave Signal Generation and Its Scale-model Hardware Characterization

Subal Kar, **Dipankar de Sarkar**, **Paramita Das**
Sudipta Banerjee, **and Somak Bhattacharyya**
Institute of Radio Physics and Electronics, University of Calcutta, India

Abstract— Computer-aided analysis has been carried out for an optical heterodyning scheme which can generate ultra-stable (i.e., low phase noise) microwave signal. The scheme consists of two slave lasers injection-locked to the selected FM sidebands of a frequency modulated master laser and the injection-locked slave laser signals are finally beated in a HEMT photodetector to obtain the desired microwave signal as the difference of the two beating signals. A scale-model hardware characterization of the scheme has also been done and the injection locking phenomena involved in the process has been understood.

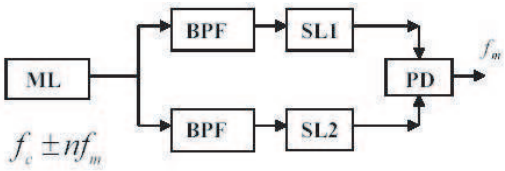

Figure 1: Block diagram of the scheme.

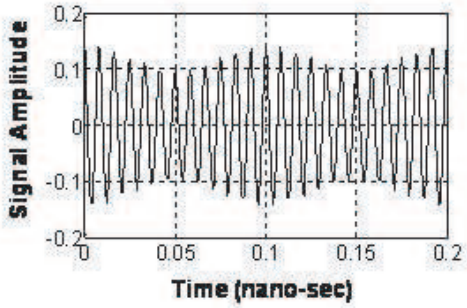

Figure 2: Time domain plot of second sideband with no injection locking of SL1.

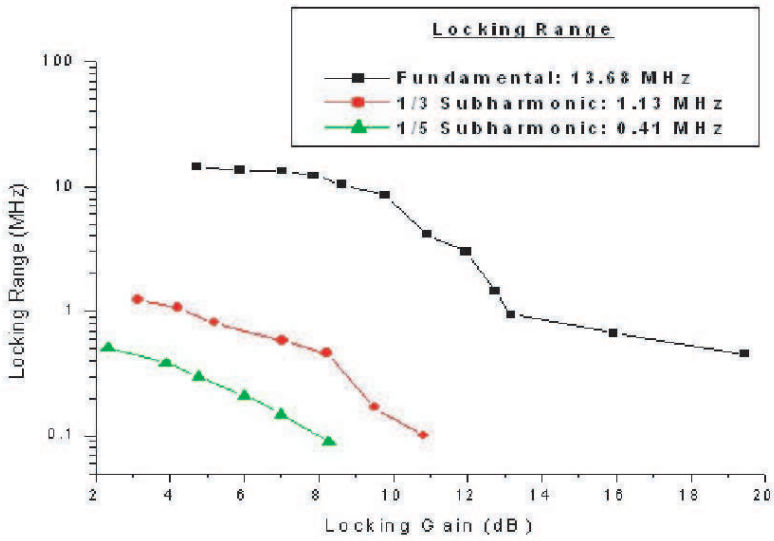

Figure 3: Locking range vs locking gain.
(fundamental and odd harmonics)

The scheme to be analyzed is shown in Fig. 1. Here the free-running slave laser sources (SL1) and (SL2) are injection-locked to the selected FM sidebands of the master laser (ML). The baseband signal (which is the desired microwave signal) is obtained at the output of the photodetector (PD).

Computer-aided analysis of the scheme has been carried out with MATLAB modeling. This is done at optical frequency using $f_c = 400\,\text{THz}$ and $f_m = 4\,\text{THz}$, for THz signal generation.

The second ($2f_m$) and third ($3f_m$) sidebands of the FM spectra of ML is filtered out by the BPFs and the signals of SL1 and SL2 are respectively injection-locked to those sideband frequencies. The effect of injection locking of the SL signals on the phase noise of the signals to be mixed was studied. It was observed that if the SL signals are not injection locked to the FM sidebands of ML (i.e., signals are not coherent) then phase noise is large and its effect is to result in spurious amplitude modulation of SL signal as shown in Fig. 2. However, if SL1 and SL2 are injection locked to the FM sidebands of ML then there is significant improvement of the phase noise of the beat signal. The phase noise improvement with injection locking is calculated to be $-20\,\text{dBc/Hz}$.

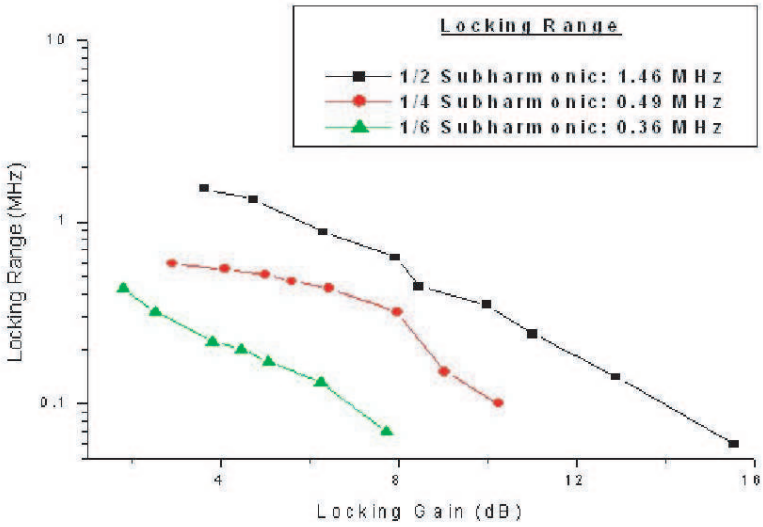

Figure 4: Locking range vs locking gain.
(even harmonics)

For scale-model hardware characterization, fc is taken around 50 MHz. FM signal is being generated with ASM3P2183, ($f_c = 50\,\text{MHz}$ and $f_m = \pm 5\,\text{MHz}$). BPFs are designed with AD827 op-amps and are of 4th order to obtain suitable lower and higher cut-off frequencies to select the 2nd and 3rd FM sidebands of ML. The SLs have been realized in the scale model hardware characterization by synchronous oscillator, the heart of which is a Colpitt oscillator whose free-running frequency can be locked to the injected input signal. The locking characteristics of synchronous oscillator are shown in Fig. 3 and Fig. 4 for odd and even harmonics respectively.

Session 5P4a
Metamaterials

Dynamical Control of Terahertz Metamaterial Resonance Response Using Bimaterial Cantilevers

H. Tao[1], **A. Strikwerda**[2], **C. Bingham**[3]
W. J. Padilla[3], **X. Zhang**[1], **and R. D. Averitt**[2]

[1]Department of Manufacturing Engineering, Boston University, Brookline, MA 02446, USA
[2]Department of Physics, Boston University, Boston, MA 02215, USA
[3]Department of Physics, Boston College, Chestnut Hill, MA 02467, USA

Abstract— Artificially structured electromagnetic (EM) materials have recently become an extremely active research area because of the possibility of creating materials which exhibit novel EM responses not available in natural materials such as negative refractive index [1]. Such EM composites, often called metamaterials (MMs), are especially important for the technologically relevant terahertz ($1\,\mathrm{THz} = 10^{12}\,\mathrm{Hz}$) frequency regime where there is a strong need to create components to realize applications ranging from spectroscopic identification of hazardous materials to noninvasive imaging. For many of these potential applications, it is desirable to create MMs that exhibit a controlled active and/or tunable response [2]. The MM device fabricated in this work is based on planar arrays of split-ring resonators (SRRs) coupled with microfabrication methods to create a bimaterial-cantilever-based THz MM resonance shifter/filter. An individual element consists of two single SRRs put together on the split gap side with a cantilever sitting above. The two rings provide inductances, L, and the split gap provides a capacitance, C. The curvature of bimaterial (Al/SiNx) cantilevers can be precisely changed by controlling the ambient temperature due to the different thermal expansion of Al and SiNx. The effective LC resonance results in a frequency dependent transmission where, on resonance, a strongly enhanced electric field is concentrated in the gap of the SRR, and the resonance will be shifted when the cantilever bends up or down to change the capacitance of the SRR. Simulations indicate that it will be possible to tune the resonance peak by more than 170 GHz which demonstrates the potential of creating THz devices such as switches, dynamic filters, and phase shifters from bimaterial-cantilever-based metamaterials.

REFERENCES

1. Smith, D. R., W. J. Padilla, D. C. Vier, S. C. Nemat-Nasser, and S. Schultz, "Composite medium with simultaneously negative permeability and permittivity," *Phys. Rev. Lett.*, Vol. 84, 4184, 2000.
2. Chen, H. T., W. J. Padilla, J. M. O. Zide, A. C. Gossard, A. J. Taylor, and R. D. Averitt, "Active terahertz metamaterial devices," *Nature*, Vol. 444, 597, 2006.

Controlling the Emission of Electromagnetic Source

Yu Luo[1], **Jingjing Zhang**[1], **Lixin Ran**[1]
Hongsheng Chen[1, 2], **and Jin Au Kong**[1, 2]

[1]The Electromagnetics Academy at Zhejiang University
Zhejiang University, Hangzhou 310058, China
[2]Research Laboratory of Electronics, Massachusetts Institute of Technology
Cambridge, Massachusetts 02139, USA

Abstract— The coordinate transformation on the space that contains electromagnetic sources is studied. We find that, not only the permittivity and permeability tensors of the media, but also the sources inside the media will take another form in order to behave equivalently as the original case. It is demonstrated that, a source in the free space can be replaced by another source of arbitrary shape with an appropriate metamaterial coating around it without being detected by outer observers, because the emission of the source can be controlled at will in this way. As examples, we show how to design conformal antennas and electrically small antennas by covering the sources with transformation media. The method proposed in this letter provides a completely new approach to develop novel active EM devices.

REFERENCES

1. Leonhardt, U., *Science*, Vol. 312, 1777, 2006.
2. Pendry, J. B., D. Schurig, and D. R. Smith, *Science*, Vol. 312, 1780, 2006.

Cylindrical Cloak Created with Multilayered Material

Hongsheng Chen[1], **Sheng Xi**[1], **Baile Zhang**[2], **Bae-Ian Wu**[2], **and Jin Au Kong**[1,2]

[1]The Electromagnetics Academy at Zhejiang University, Zhejiang University, China
[2]Research Laboratory of Electronics, Massachusetts Institute of Technology, Cambridge, MA, USA

Abstract— An ideal cloak is made of anisotropic and inhomogeneous media, while a cloak in application is usually created with multilayered meta-materials. Thus the theoretical predictions of the scattering of a multilayered cloak under the incidence of an electromagnetic wave are very important in designing a cloak. We study the scattering when an electromagnetic wave incident onto a cylindrical cloak created with multilayered materials based on the full wave scattering theory. This scattering model will help further understanding the behavior of a real cloak and will be useful in designing and optimization of a multilayered cloak.

Scattering by a Left-handed Particle on a Left-handed Slab or Surface

O. E. French, **K. I. Hopcraft**, **and E. Jakeman**
University of Nottingham, UK

Abstract— In a recent paper [1] it was shown that the perfect lens proposed by Pendry [2] suffered significant deterioration in resolution as a result of small deviations in the real parts of the material parameters away from the ideal values of $\varepsilon = \mu = -1$. A different perturbation that could be considered is that of a surface imperfection or contaminant on the lens, and a small scatterer would seem a likely candidate for modelling such scenarios. The problem discussed here is how just such a scatterer behaves upon illumination with plane incident radiation.

The relevance of considering the scattering by a small left-handed particle in the presence of bulk media is clear following the result of Engheta et al. [3] in which the standard radiation patterns of electric dipoles are significantly modified by the presence of an adjacent semi-infinite half space: a large proportion of the radiated energy being transmitted across the interface when the refractive index of the half space is large. This would suggest that significant modifications can be made also to the scattering properties of a small left-handed scatterer in the presence of bulk media.

A small left-handed particle situated upon a slab of arbitrary electromagnetic parameter values is modelled as a superposition of electric and magnetic dipoles using an extension of Mie theory. The full-wave solution to the radiation problem is obtained for each of these dipoles using the Hertz potential method of Engheta [3] and Sommerfeld [4], which is extended to account for magnetic effects. The far-field asymptotic forms of the Hertz potentials are used to calculate the far-field scattering characteristics of the system both above and below the slab.

Novel scattering properties are observed in both the right- and left-handed cases, with the scattering patterns displaying enhanced transmission and zero back-scatter along with hitherto unobserved structure and directionality, offering a potential wealth of applications.

REFERENCES

1. French, O. E., K. I. Hopcraft, and E. Jakeman, *New J. Phys.*, Vol. 8, 271, 2006.
2. Pendry, J. B., *Phys. Rev. Letts.*, Vol. 85, 3966–9, 2000.
3. Engheta, N. and C. H. Papas, *Radio Science*, Vol. 17, 1557–66, 1982.
4. Sommerfeld, A., *Partial Differential Equations in Physics*, Academic Press, 1949.

Effect of Losses in a Layered Structure Containing DPS and DNG Media

J. R. Canto, S. A. Matos, C. R. Paiva, and A. M. Barbosa

Instituto de Telecomunicações and Department of Electrical and Computer Engineering
Instituto Superior Técnico, Av. Rovisco Pais 1, 1049-001 Lisboa, Portugal

Abstract— Although the concept of a DNG medium (i.e., a double negative medium with $\varepsilon < 0$ and $\mu < 0$) was first proposed by Veselago as early as 1967 [1, 2], it took many years until experimental evidence for the existence of such a medium was presented [3]. In order to uphold the causality principle the Kramers-Kronig relations show that a dispersive medium should be lossy [4]. In fact, for plane wave propagation of the form $\exp[i(nk_0z - \omega t)]$, the refractive index of the unbounded passive medium is given by $n = \pm\sqrt{\varepsilon\mu}$ and, in order to select the correct sign, losses must be taken into account. Hence, the condition $\mathrm{Im}(n) > 0$ imposes that, for the DPS (double positive) case, we should have $n = \sqrt{\varepsilon\mu}$ whereas, for the DNG case, we should have $n = -\sqrt{\varepsilon\mu}$ instead. Accordingly, in this communication, the Lorentz model is used to describe DNG media:

$$\varepsilon(\omega) = 1 - \frac{\omega_{ep}^2}{\omega^2 - \omega_{eo}^2 + i\gamma_e\omega},\ \mu(\omega) = 1 - \frac{\omega_{mp}^2}{\omega^2 - \omega_{mo}^2 + i\gamma_m\omega}, \tag{1}$$

where $\omega_{e,\,mp}$ are the plasma frequencies, $\omega_{e,\,mo}$ the resonance frequencies and $\gamma_{e,\,m}$ the loss coefficients. In this work we will focus on the reflection and transmission of electromagnetic waves in a periodic multilayered structure containing DPS and DNG layers. The canonical problem of multilayered structures [5] has already been revisited in the literature when DNG layers are included [6–8] although, to the authors' knowledge, a causal model for dispersion has never been taken into account. We show that the inclusion of losses deeply changes the global behavior or the whole structure. Indeed, the reflectance and transmittance are completely different when a causal model is considered. The transmittance, namely, is largely attenuated even for very small losses, thereby limiting the number of periods that can be used. The size of the forbidden bands also dramatically increases when losses are included. The conclusion is that a causal model for dispersion is an essential tool for the study of multilayered structures containing DNG media.

REFERENCES

1. Veselago, V. G., "The electrodynamics of substances with simultaneously negative values of ε and μ," *Sov. Phys.-Usp.*, Vol. 10, No. 4, 509–514, 1968.
2. Veselago, V. G., "The electrodynamics of substances with simultaneously negative values of ε and μ," *Russ. Usp. Fiz. Nauk*, 517–526, Vol. 92, 1967.
3. Smith, D. R., W. J. Padilla, D. C. Vier, S. C. Nemat-Nasser, and S. Schultz, "Composite medium with simultaneously negative permeability and permittivity," *Phys. Rev. Lett.*, Vol. 84, No. 18, 4184–4187, 2000.
4. Peiponen, K.-E., V. Lucarini, E. M. Vartiainen, and J. J. Saarinen, "Kramers-Kronig relations and sum rules of negative refractive index media," *Eur. Phys. J. B*, Vol. 41, 61–65, September 2004.
5. Yeh, P., *Optical Waves in Layered Media*, 1988, 118–134, Wiley, New York, 2005.
6. Tretyakov, S., *Analytical Modeling in Applied Electromagnetics*, 251–353, Artech House, Boston, 2003.
7. Alù, A. and N. Engheta, "Pairing an epsilon-negative slab with a mu-negative slab: Resonance, tunneling and transparency," *IEEE Trans. Antennas Propagat.*, Vol. 51, No. 10, 2258–2571, October 2003.
8. Jiang, H. and H. Chen, "Omnidirectional gap and defect mode of one-dimensional photonic crystals containing negative-index materials," *Appl. Phys. Lett.*, Vol. 83, No. 26, 5386, December 2003.

Complex Aberration Effect in Moving Dispersive DNG Media: A Spacetime Algebra Approach

S. A. Matos, J. R. Canto, C. R. Paiva, and A. M. Barbosa

Instituto de Telecomunicações and Department of Electrical and Computer Engineering
Instituto Superior Técnico, Av. Rovisco Pais 1, 1049-001 Lisboa, Portugal

Abstract— In the electromagnetic theory of moving isotropic media negative refraction [1] and negative phase velocity [2] are now well-known effects. However, as far as the authors are aware, there is no study of moving DNG (double negative) media that takes material dispersion into account. In this work we analyze plane wave propagation in moving dispersive DNG media. Two inertial frames are considered: the DNG medium and its proper co-moving frame (the $\bar{S}$ frame where its index of refraction is $\bar{n}$) are moving with constant velocity $\mathbf{v}$ relative to S (the laboratory frame). Our goal is to characterize this DNG medium from the perspective of the S (or lab) frame where it is seen as a bianisotropic medium. However, to circumvent the cumbersome calculations that such complex constitutive relations (with magnetoelectric coupling) impose we will use the mathematical approach of Clifford's geometric algebra [3–5]. A new derivation of the relation between the refractive indices in both frames is then presented. The Doppler effect is also studied using two different approaches: i) depending on the angle $\bar{\theta}$ between velocity and wave vector (as measured in $\bar{S}$); ii) depending on the angle θ measured in the lab frame. These two different angles are related through aberration. So far the analyses presented in the literature do not take into account the refractive index surfaces (in the lab frame) and the Doppler effect simultaneously. However, both effects interplay and hence they should be simultaneously taken into account. We then present a new graphical method which allows, from the perspective of the lab frame, a simple and clear interpretation of the interaction between the two effects. Since we are considering a fixed frequency in the proper frame (the emitted frequency) one may think that material dispersion can be thought as an independent effect. However, we show how dispersion has a decisive role, namely for $-1 < \bar{n} < 1$. Furthermore, a new complex aberration effect arises: a complex index of refraction is obtained in the lab frame for a real index of refraction in the proper frame. The two aforementioned approaches for the Doppler effect are indeed inconsistent for this particular case: we claim that the only consistent way to analyze this region is by taking losses into account. One should not forget that causality is an important issue in DNG media: dispersion is correlated to losses as the Kramers-Kronig relations show [4].

REFERENCES

1. Grzegorczyk, T. M. and J. A. Kong, "Electrodynamics of moving positive and negative refraction," *Physical Review B*, Vol. 74, 033102, July 2006.
2. Mackay, T. G. and A. Lakhtakia, "Negative phase velocity in a uniformly moving, homogeneous, isotropic, dielectric-magnetic medium," *Journal of Physics A*, Vol. 37, 5697–5711, May 2004.
3. Puska, P., "Covariant isotropic constitutive relations in Cliffords's geometric algebra," *Progress In Electromagnetics Research*, PIER 32, 413–428, 2001.
4. Paiva, C. R. and M. A. Ribeiro, "Doppler shift from a composition of boosts with Thomas rotation: A spacetime algebra approach," *Journal of Electromagnetic Waves and Applications*, Vol. 20, No. 7, 941–953, 2006.
5. Matos, S. A., M. A. Ribeiro, and C. R. Paiva, "Anisotropy without tensors: A novel approach using geometric algebra," *Optics Express*, Vol. 15, 15175–15186, November 2007.
6. Peiponen, K. E., V. Lucarini, E. M. Vartiainen, and J. J. Saarinen, "Kramers-Kronig relations and sum rules of negative refractive index media," *Eur. Phys. J. B*, Vol. 41, 61–65, September 2004.

Rainbow and Blue-shift Effect of a Dispersive Spherical Invisibility Cloak with a Nonmonochromatic Plane Wave Passing through

Baile Zhang[1], **Bae-Ian Wu**[1], **Hongsheng Chen**[1,2], **and J. A. Kong**[1,2]

[1]Research Laboratory of Electronics, Massachusetts Institute of Technology
Cambridge, MA 02139, USA
[2]The Electromagnetics Academy at Zhejiang University
Zhejiang University, Hangzhou 310058, China

Abstract— Invisibility cloaking has recently received much attention in the literature. Based on form-invariant coordinate transformations, cloak of invisibility was proposed which can perfectly conceal arbitrary objects from detection. However, most studies focused on only one single frequency, while any physical wave must have a nonzero bandwidth, and more importantly, metamaterials, based on which cloaking is achieved, must be dispersive. So far, the physics behind the interaction between a dispersive invisibility cloak and electromagnetic waves possessing nonzero bandwidth is still unrevealed. How a physical electromagnetic wave passes the cloak and whether invisibility can be achieved to real detection of nonzero band are still unknown.

In an ideal spherical cloak, the radial constitutive parameters ϵ_r and μ_r are required to vanish at the inner boundary at the single frequency which can be named as the "cloaking frequency". Since any physical wave has nonzero bandwidth, the transition of ϵ_r and μ_r from positive to negative will be formed within the cloak at frequencies entirely below or above the cloaking frequency because of dispersion. Similar positive-to-negative transition of constitutive parameters has been shown to cause some peculiar phenomena such as negative refraction and superlens. Resonances caused by surface polaritons between positive and negative index media has also been shown to produce strong anomalous scattering. Therefore, it is necessary to analyze the influence of this transition of constitutive parameters on the performance of the cloak.

In this paper, a strict and efficient analytic model of a 3D dispersive and lossy spherical invisibility cloak has been established, being able to predict the response of the cloak over an arbitrary bandwidth. Extremely low RCS (radar cross section) can be achieved by narrowing the bandwidth. This result excludes the possibility of existence of some kind of large scattering in the vicinity of the cloaking frequency. Furthermore, there is a singularity of the wave equation for TM (TE) waves inside the cloak, corresponding to the zero value of ϵ_r (μ_r) at some position in the cloak when the frequency is below the cloaking frequency. This singularity will form an impenetrable wall for TM (TE) waves. Based on the peculiar "wall" effct, it is pointed out that a "rainbow" will be formed in the cloak since fields of different frequencies penetrate into different depths inside the cloak. Meanwhile, the concept of group velocity at the inner boundary of the cloak is selectively valid only for those frequencies above the cloaking frequency. Therefore the group velocity at the inner boundary at the cloaking frequency is meaningless. In addition, a plane wave will be reinforced in the forward direction after passing this cloak if the frequency is deviated above while being decreased if the frequency is deviated below. As a result, a quasi-monochromatic wave centered at the cloaking frequency is shown to be blue-shifted toward the high frequency in the forward direction after passing this dispersive cloak. This effect does not depend on the size of the cloak, but the normal dispersion of the cloak. All of these aspects provide us with deep insights into the cloaking phenomena.

Session 5P4b
Modeling and Simulations in Materials Science

Wide Band Gap Semiconductor High-power Coherent THz Source

V. I. Litvinov[1], **H. Morkoc**[2], **and J. Xie**[2]

[1]WaveBand Division, Sierra Nevada Corporartion, 15245 Alton Pkwy, Irvine, CA 92618, USA
[2]Department of Electrical and Computer Engineering, Virginia Commonwealth University
601 West Main Street, Room 338, P. O. Box 843072, Richmond, Virginia 23284, USA

Abstract— Formation of the electrical domains in semiconductor superlattices prevents Bloch oscillations to occur. Despite this, it is practical to explore a microwave source where the domains themselves may provide high-frequency operation. Negative differential dc-conductivity (NDC) in semiconductor superlattices has proven to cause traveling electrical domains oscillations at 147 GHz in InGaAs/GaAs device. High-power operation requires the use of materials capable of withstanding large current/voltage swings. Therefore, the wide band gap semiconductor is a material of choice for the active region of the device. We study III-Nitride material system, a wurtzite (0001)AlGaN/GaN superlattice, where the polarization fields affect the dynamics of miniband electrons. Polarization fields stem from the bulk spontaneous polarization and the lattice-mismatch-induced piezoelectric component. We explore the short-period GaN/AlGaN Stark superlattice as a potential high-power sub-millimeter wave source. We calculate the electron energy, width of the first miniband, and the mobility-field relation. These results create a base for simulation of the source performance using the Atlas-Silvaco package capable of simulating Gunn-type devices. Superlattice source performance (oscillation frequency and power efficiency) depends on the material parameters of its active region and could be of (500–600) GHz with the intrinsic power efficiency of (9–18)%. The frequency of the output signal is tunable by an applied voltage and a series resistance. The GaN superlattices have been grown and characterized. It is shown that the dc-current-voltage characteristics have NDC region that is the prerequisite for the formation of electrical domains.

Morphological Characterization of Two-dimensional Random Media and Patterns by Fractional Differentiation

Giovanni F. Crosta

Inverse Problems & Mathematical Morphology Unit, Department of Environmental Sciences
University of Milan-Bicocca, 1 Piazza della Scienza, Milan 20126, Italy

Abstract— Let $\Omega \subset \mathbf{R}^2$ denote a square of sidelength $\frac{L}{2}$, $\mathbf{x} \equiv \{x_1, x_2\} \in \Omega$ and g denote a scalar function of $\mathbf{x}$ representing a property of the random medium or, more generally, a pattern. Let reflection operators with respect to the coordinate axis (*flip*, *flop*) be applied to Ω and give rise to the square $\mathcal{Q}\Omega$. Denote by $\mathcal{Q}g$ the corresponding function supported in $\mathcal{Q}\Omega$. Let $\mathbf{u} \equiv \{u_1, u_2\}$ be the spatial frequency vector and $|G[\mathbf{u}]|^2$ the (distribution-valued) power spectral density of $\mathcal{Q}g$. The spectrum enhancement (*SE*) algorithm, which has been introduced before [1] consists of suitable transformations carried out on the function $H^{(p)}[\mathbf{u}] = |\mathbf{u}|^{2\beta}\frac{|G[\mathbf{u}]|^2}{|a_{0,\,0}|^2} + \delta[\mathbf{u}]$, where δ is the DIRAC measure, $a_{0,\,0}$ appears in the FOURIER transform at the origin, $\mathcal{F}(\mathcal{Q}g)[\mathbf{0}] = a_{0,\,0}\delta[\mathbf{u}]$ and $\beta \in \mathbf{R}^+$ is the *enhancement order* such that $\beta = 2p$. The intepretation of $H^{(p)}$ when $\beta \in \mathbf{N}$ has already been given [2] and shall not be repeated here. The emphasis herewith is on $\beta \notin \mathbf{N}$. Let $\Phi_0 \subset \mathcal{S}$ denote the LIZORKIN space of functions with vanishing moments $\Phi_0 = \{\omega_1 | \int_{-\infty}^{+\infty} x_1^{k_1}\omega_1[x_1]\mathrm{d}x_1 = 0,\ \forall k_1 = 0, 1, 2, \ldots\}$. Introduce the space of test functions $\Phi = \{\omega | \omega \in \Phi_0 \times \Phi_0\ ;\ \omega[x_1, x_2] = \omega_1[x_1]\omega_2[x_2]\}$ and denote by $\Phi'(\supset \mathcal{S}')$ its dual. By extending to two dimensions the properties stated in Ch. 4 of Ref. [3], a double integral of ω of fractional orders α_1, α_2 is defined by

$$\left(I_{2,+}^{\alpha_2} I_{1,+}^{\alpha_1}\omega\right)[x_1,\, x_2] = \frac{1}{\Gamma[\alpha_1]\Gamma[\alpha_2]}\int_{-\infty}^{x_2}\frac{\omega_2[y_2]}{(x_2 - y_2)^{1-\alpha_2}}\mathrm{d}y_2\int_{-\infty}^{x_1}\frac{\omega_1[y_1]}{(x_1 - y_1)^{1-\alpha_1}}\mathrm{d}y_1.$$

Fractional derivatives $\left(\mathcal{D}_{2,+}^{\alpha_2}\mathcal{D}_{1,+}^{\alpha_1}\omega\right)[x_1,\, x_2]$ are defined in accordance. At this point the main result of the paper can be stated.

THM. Let $\mathcal{Q}g \in \Phi'$, $\beta \in \mathbf{R}^+$, $\beta \notin \mathbf{N}$, $p = 2\beta$, $\gamma = 0, 1, 2, \ldots$. Assume, without loss of generality, $|u_1| > |u_2|$ and let $\frac{\partial^\beta \mathcal{Q}g}{\partial^{(\beta-\gamma)}x_1\partial^\gamma x_2} = \mathcal{D}_{1,+}^{(\beta-\gamma)}\mathcal{D}_{2,+}^{\gamma}\mathcal{Q}g$ if $\beta > \gamma$ or $= I_{1,+}^{(\gamma-\beta)}\mathcal{D}_{2,+}^{\gamma}\mathcal{Q}g$ if $\beta < \gamma$. Then

$$H^{(p)}[\mathbf{u}] = \frac{1}{|a_{0,0}|^2}\sum_{\gamma=0}^{\infty}\binom{\beta}{\gamma}\left|\left(\mathcal{F}\left[\frac{\partial^\beta \mathcal{Q}g}{\partial^{(\beta-\gamma)}x_1\partial^\gamma x_2}\right]\right)[\mathbf{u}]\right|^2 + \delta[\mathbf{u}].$$

In other words *SE* of order p amounts to evaluating derivatives and integrals of fractional order of the pattern $\mathcal{Q}g$, FOURIER-transforming and forming a binomial series. This result contributes to the justification of *SE* as a method for extracting morphological descriptors from 2-dimensional images of random media with the aim of automatic classification and characterization.

REFERENCES

1. Crosta, G. F., C. Urani, and L. Fumarola, *J. Biomed. Optics*, Vol. 11, No. 2, 024020.1–024020.18, 2006.
2. Crosta, G. F., "Feature extraction by differentiation of fractional order," *Progress In Electromagnetics Research Symposium Abstracts*, 425, Cambridge, MA, USA, 2006.
3. Rubin, B., *Fractional Integrals and Potentials*, Longman, Harlow, UK, 1996.

Microwave Characterization of Nickel

Stepan Lucyszyn
Imperial College London, UK

Abstract— Nickel has for many decades been used for realizing ferrites, employed in radio frequency (RF) applications, due to its high magnetic permeability at low frequencies. However, in recent years, electroplated nickel has been used as a structural material in RF microfabricated circuits and even radio frequency microelectromechanical systems (RF MEMS) applications. With the former, at around 30 GHz, weakly magnetized nickel has twice the surface resistance of silver or copper, but is chemically and mechanically more robust. Moreover, it has a relatively small deleterious effect. Also, when used in electrothermal buckle-beam microactuators, since nickel's thermal expansion coefficient is approximately five times greater than that of polysilicon, the same displacements can be obtained at a much lower temperatures. Therefore, its use in RF transmission lines and microactuators permits co-fabrication, having the same lithographic steps.

It is very important for the RF designer to understand and know the frequency characteristics of all the materials to be employed in the development of a future device, circuit of system. Surprisingly, very little has been reported on the magnetic permeability of nickel. This makes the design of nickel structures for microwave applications very difficult indeed. This paper tries to address the issue of characterizing the frequency dispersive nature of magnetic permeability for nickel.

Scientists have been investigating the properties of magnetic materials for a century. In 1951, Bozorth collated all the data that was available during that time for the frequency dispersion characteristics of permeability. It has been found that the frequency behaviour show a low frequency value that drops off at around 1 GHz. However, at any one frequency, the results from different researchers give large discrepancies in their measured values. Surface conditions are thought to be an important factor at microwave frequencies. For example, a thin oxide film, formed on the metal during heat treatment, may cause the apparent permeability to decrease by a factor of 10. Moreover, Arkadiew also noted an increase of high-frequency permeability when magnetic material is annealed.

This inconsistency in measurement data makes the characterization of nickel very difficult. The paper reviews some of the experimental approaches undertaken and highlights key findings. It has been found that RF engineers are currently faced with the problem that there is insufficient data available to undertake simulation designs with a high degree of confidence at microwave frequencies. While some experimental data exists for the real part of the relative initial permeability, there is still considerable uncertainly as to how this relates to the deposition process, material purity and level of oxidation. Moreover, to the best of the authors' knowledge, no measured data exists for the imaginary part of permeability. The well-known Drude model is expected to be able to give an empirical fit to future experimental data. In addition, extraction techniques using 3D electromagnetic modelling software may offer another way forward. Here, both the magnitude and phase angle of the transmission characteristics for impedance-matched transmission lines must be considered, in order to be able to produce frequency-dependent complex values of permeability at microwave frequencies.

Theoretical Study of the High Pressure Phase Transitions in the Calcite Rock

A. Zaoui
L.M.L. (UMR 8107), Polytech'Lille, Université des Sciences et Technologies de Lille
Cité Scientifique, Avenue Paul Langevin, 59655 Villeneuve D'Ascq Cedex, France

Abstract— We present a nanoscale simulation study based on a new force field model [1] to investigate the high pressure phases in the calcite rock. We found that the longitudinal wave velocity increases rapidly; whereas the shear wave velocity increases very slowly up to the transition pressure [2]. In addition we show the presence of a softening mode in the Γ-F direction. The phonon frequencies of the post-aragonite phase show more modes than for the calcite and aragonite phases.

REFERENCES

1. Rohl, A. L., K. Wright, and J. D. Gale, *American Mineralogist*, Vol. 88, 921–925, 2003.
2. Sekkal, W., N. Taleb, A. Zaoui, and I. Shahrour, *American Mineralogist*, in press, 2008.

A Closed Form Analysis on Generalized Scaling for Forecasting Heating Patterns during Microwave Processing

Madhuchhanda Bhattacharya[1] and Tanmay Basak[2]

[1]Indian Institute of Technology
D-29-81, Adyar Avenue, Madras, Chennai 600036, India
[2]Department of Chemical Engineering, Indian Institute of Technology
Madras, Chennai 600036, India

Abstract— A closed form analysis based on Finite Fourier Transformation (FFT) has been carried out to predict the heating characteristics in presence of microwave induced volumetric heat sources. A scaling analysis shows that temperature distributions within a material during microwave heating evolve in two stages, namely small time and large time. The inverse of square of second eigenvalue along with thermal diffusivity determines the threshold time scale between these two regimes. During small time evolution, the spatial temperature distribution follows absorbed power profiles, whereas the temperature distributions are slaved by first eigenfunction and independent of volumetric heat distribution at large time evolution. In all the cases, the variation of temperature within the material is guided by a dimensionless number $N_G = L^2 q_0 / kT_{ref}$, which represents the relative strength of internal heat sources compared to thermal diffusion within the material. For $N_G \ll 1$, almost uniform temperature distributions are attained and a lump parameter model can be used. In contrast, nonuniformity in absorbed power distributions amplifies in temperature distribution for materials with $N_G \gg 1$, where there exists a possibility of local hot spot formation if absorbed power exhibits local maxima. The applicability of this analysis has been illustrated to forecast heating characteristics within various materials.

Dielectric Mixtures, Structure/property Relations and Spectral Density Representation

Enis Tuncer[1] **and Gunnar A. Niklasson**[2]

[1]Oak Ridge National Laboratory, USA
[2]Uppsala University, Sweden

Abstract— The description of optical and electrical properties of composites is a long standing problem. The dielectric properties of these materials are of importance in diagnostics, characterization and design of material systems in various engineering FIelds. There have been numerous mixture expresions proposed, which were based on approximations, to predict electrical properties of mixtures. One way to avoid model based material property analysis or *a-piori* assumptions on the materials properties is to adopt the spectral density representation. In this method the dielectric permittivity of the mixture is expressed as an integral function which contains the depolarization factors of the constituents as a distribution density. A numerical method based on the Monte Carlo integration hypothesis and constrained-least-squares resolves unique distribution densities for material mixtures. In this paper, we will introduce the spectral density formulation and a mixture expression derived from the analogy between the spectral density and distribution of relaxation times representations. Several worked examples will be presented to illustrate the utility of the spectral density representation in structure/property relationships in composites.

Electromagneto-mechanical Coupling Response of Plasto-ferrites

Christian Brosseau and Wilfried NDong

Laboratoire d'Electronique et Systèmes de Télécommunications, Université de Bretagne Occidentale
CS 93837, 6 avenue Le Gorgeu, 29238 Brest Cedex 3, France

Abstract— The impetus of this work was to investigate the electromagnetic and tensile properties of several commercially available plasto-ferrites (PFs) at ambient conditions. The approach involved selection of a set of PFs, and measuring their complex effective permittivity $\varepsilon = \varepsilon' - j\varepsilon''$ and permeability $\mu = \mu' - j\mu''$ under uniaxial stress at microwave frequencies (0.1–4.5 GHz) and room temperature. We analyze the ε and μ spectra for tensilely strained PFs up to 3%. Comparing our experimental ε data against several dielectric relaxational behaviors, we find that the main physics cannot be understood with a single relaxation mechanism. We then go on to consider the magnetic permeability spectra in the microwave range of frequencies and show that an appropriate magnetization mechanism is given by the gyromagnetic spin resonance mechanism. We use a combination of Bruggeman mean field analysis and Landau-Lifshitz-Gilbert modeling to reproduce the experimental bimodal line-shape characteristics of the effective complex magnetic permeability. The vibrating sample magnetometry investigations of the static magnetization are found to be consistent with this modeling. More importantly we show that the ε and μ measurements under stress can be explained in terms of a Gaussian molecular network model in the limit of low stress. The present results have important applications in magnetoactive smart composite materials, e.g., flexible circuit technology in the electronics industry (sensors, actuators and micromechanical systems), functionalized artificial skin and muscles for robotic applications.

Session 5P5
Medical Electromagnetics, RF Biological Effect and Biological Media

Rotation of the Leaky Dielectric Particle in a Rotating Electric Field

Yu. Dolinsky and T. Elperin
The Pearlstone Center for Aeronautical Engineering Studies
Department of Mechanical Engineering, Ben-Gurion University of the Negev
P. O. B. 653, Beer-Sheva 84105, Israel

Abstract— We study rotation of a weakly conducting particle around its axis of symmetry under the action of the external electric field which spins in the plane normal to the axis of symmetry of the particle. The particle is imbedded in a homogeneous stationary medium with finite electric conductivity and permittivity that are different from the corresponding parameters of the particle. We determined the dependence of the particle angular velocity upon the amplitude and angular velocity of the electric field. It is shown that depending upon the ratios of the particle electric conductivity and permittivity to the corresponding parameters of the host medium, the direction of rotation of the particle can be identical or opposite to the direction of rotation of the external electric field. We determined the amplitude dependent critical angular velocity of the external electric field that separates the domains with two possible regimes of rotation of the particle. In the first domain the particle rotates only in one direction while in the second domain the particle may rotate in two directions. We investigated also the stability of different regimes of rotation of the particle.

Developments in Voxel Models and Whole-body Averaged SAR Calculations at the HPA

Peter Dimbylow

Radiation Protection Division, Health Protection Agency, Chilton, Didcot, OX11 0RQ, UK

Abstract— The prevention of excessive heating of the body is the basis for the restriction of electromagnetic field exposures for frequencies greater than $\sim 100\,\mathrm{kHz}$. Restrictions are expressed in terms of the specific energy absorption rate, SAR in a unit of $\mathrm{W{\cdot}kg^{-1}}$. However, SAR is a difficult quantity to measure and calculations must be performed to provide a link between the internal dose quantity SAR and external fields, which can be more readily measured or characterised. This paper describes FDTD calculations of SAR in anatomically realistic models of the body for plane wave RF irradiation and makes comparison between the calculated external electric fields required to produce the ICNIRP basic restriction and the corresponding reference levels. The presentation will focus mostly on the application to child and pregnant female models.

The University of Florida (UF) Series B paediatric phantoms were developed for medical and radiation protection photon dosimetry. The series includes a 9-month male, a 4-year female, an 8-year female, an 11-year male and a 14-year male. They have been adapted to calculate the whole-body averaged SAR in children for plane wave exposure from 50 MHz to 4 GHz. The consideration of children is important in the application of the ICNIRP public exposure reference levels above $\sim 1\,\mathrm{GHz}$. The uniformly scaled adult models of NORMAN and NAOMI suggested that the ICNIRP reference level does not provide a conservative estimate of the whole-body averaged SAR restriction for 5-y and 1-y old models. Mathematical models of the developing foetus at 8-, 13-, 26- and 38-weeks gestation were converted into voxels and combined with the reference adult female model, NAOMI at a resolution of 2 mm. Comparison shows that the ICNIRP public reference level is a conservative predictor of local SAR averaged over 10 g in the foetus.

Theoretical Analysis of Temperature Elevation in a Human Body Exposed to Millimeter Wave

A. Kanezaki[1, 2], **T. Sakai**[2], **S. Watanabe**[2], **A. Hirata**[2, 3], **and H. Shirai**[1]

[1]Chuo University, Japan
[2]National Institute of Information and Communications Technology, Japan
[3]Nagoya Institute of Technology, Japan

Abstract— In recent years, expectations for millimeter wave (MMW: 30–300 GHz) technology has risen due to the growth and need for high data transmission rates. It is important to evaluate safety of the MMW exposure because the chances of human body exposure are expected to increase. Most of MMW power would be absorbed around the human body surface, and lead to temperature elevation. Safety guidelines for MMW exposure are based on warmth sensation [1]. However detailed characteristics of the warmth sensation threshold have not been investigated yet. Therefore, studies on the validity of the guideline value are required.

Temperature elevation in a human body depends on various parameters such as tissue thickness, thermal parameters, physiological parameters, and so on. Therefore detailed investigation is difficult for numerical simulation because huge numbers of calculation are required. In this study, we derived a general solution of temperature elevation at a steady state due to human body exposure to MMW. We considered a bioheat equation [2] for one dimensional three-layer human body model that consists of skin, fat and muscle. With the general solution, we can conduct detailed parametric analysis of the temperature elevation.

Analytical solution for the three-layer tissue model has been derived first to estimate the specific absorption rate (SAR [W/kg]), which is a function of depth z. Then, regarding the derived SAR(z) and the local tissue density as a heat potential, temperature distribution $T(z)$ can be obtained by solving the second order bioheat differential equation with the following boundary conditions: 1) a heat transfer between the skin surface and air, 2) isothermal and continuous heat flux between the different tissues, and 3) a constant temperature at far end. This bioheat equation can be solved analytically using Laplace transform. Temperature distribution $T(z)$ in the human body model and the temperature elevation at the surface are, then compared with those derived from the numerical solution. Good agreement has been found between them, and the validity of our solution has been established.

The derived expression is useful to clarify the effects of various parameters on the basis of the safety guideline in the MMW region, and utilized to discuss parameter dependency on the temperature elevation.

REFERENCES

1. "Guidelines for limiting esposure to time-varying electric, magnetic, and electromagnetic fields (up to 300 GHz)," *Health Phys.*, ICNIRP, Vol. 74, No. 4, 494–522, 1998.
2. Pennes, H. H., "Analysis of tissue and arterial blood temperature in resting forearm," *J. Appl. Phys.*, Vol. 1, 93–122, 1948.
3. Patankar, S. V., *Numerical Heat Transfer and Fluid Flow*, Hemisphere Publishing Corporation, New York, 1980.

A Non-surgical Interrogating Vector Field Brain Activity Recovery Method

D. Cohoon[1], **G. Erdmann**[2], **R. Albanese**[2], **J. Harvey**[3]
R. Medina[3], **and S. Samn**[2]

[1]West Chester University of Pennsylvania, USA
[2]Air Force Research Laboratory, USA
[3]L-3 Communications, USA

Abstract— We have two inverse source solutions for the recovery of the orientation of an activity on each of any number of individual neurons. As a confirmation of the correctness of our computer implementation of our theory, a computer simulation showed numerically that the left and right sides of the equations that the theory said should be satisfied were in agreement to 10 or more significant digits.

We apply the M. T. Hirvonen (Acta Polytechnical Scandinavica Ma39 1983) expansion of the vector potential of a generally oriented and arbitrarily located current carrying dipole in the presence of a spherical interface in terms of the L, M, and N vector spherical harmonics described in Julius Stratton's *Electromagnetic Theory* to a lattice of such dipoles in a multiple tissue region model of the human head. We first predicted the electric and magnetic fields outside the skull bone using a brain-bone-air model using a Cole-Cole dispersion model to describe the permittivity and conductivity of brain tissue and bone as a function of frequency.

Our brain activity recovery solution uses brain-activity independent interrogating vector fields relating surface integrals to a linear combination of inner products of complex amplitudes of activity vectors and neuronal locations with the interrogating vector fields in brain tissue. After using an amplitude-argument representation of spherical Bessel and Hankel functions to overcome overflow in representation of sources close to the head surface, a singular value decomposition was used to predict the neuronal orientation and recover the time profile of brain activity of a Hodgkin-Huxley type representation on each of the model neurons. Several hundred vector spherical harmonics were needed to accurately represent sources just under the skull bone in our model the head.

Resonance as a Tool to Transfer Information to Living Systems: The Effect of 7 Hz Calcium Ion Energy Resonance on Human Epithelial Cells (HaCaT) Differentiation

Antonella Lisi[1], **Alberto Foletti**[2], **Mario Ledda**[1], **Flavia De Carlo**[1]
Livio Giuliani[3], **Enrico D'Emilia**[3], **and Settimio Grimaldi**[1]

[1]Istituto di Neurobiologia e Medicina Molecolare CNR, Rome, Italy
[2]BITITALIA, Milan, Italy
[3]ISPESL, DIPIA, Rome, Italy

Abstract— Electromagnetic therapy is a treatment method in which an electromagnetic or magnetic stimulus is used to achieve physiological changes in the body.

The middle of the eighties was marked with the discovery by Blackman (Blackman et al., 1985) and Liboff (1985) of a surprising phenomenon: a low frequency alternating (AC) magnetic field (MF) changed free calcium concentration in nervous tissue only in the presence of a simultaneously acting static (DC) MF. The most prominent effect was observed at the AC field frequency close to the cyclotron frequency of a calcium ion. The cyclotron frequency is defined (Liboff, 1985) as

$$f_C = \frac{q}{2\pi m} B_o$$

where q and m are the charge and mass of the ion, and B_o is the DC field. These works opened a new line of research in Bioelectromagnetics.

There were three unexpected qualities in this phenomenon: 1) the necessity simultaneous action of DC and AC MFs, 2) the resonance effect on cyclotron frequency, and 3) very small values of acting MFs, measured with tens of μT, and extremely low frequencies of AC MFs, measured with several tens of Hz. Therefore, these results evoked a suspicion in the scientific community. Afterwards, many confirmations for these data were obtained in works performed on different objects and in different experimental situations (Liboff et al., 1987; Lerchi et al., 1991; Blackman et al., 1994; Zhadin et al., 1999; and others) which convinced the scientific community of the real existence of the above effects. The specific aim of the present work concerns the effectiveness of low frequency electromagnetic fields treatment to modify biochemical properties of human keratinocytes (HaCaT). Cells exposed to a 7 Hz electromagnetic field 100 mV for one hour (twice daily), using a commercially available wave generator (Vega Select 709) showed by Scanning Microscopy modification in shape and morphology; these modifications were also associated to different actin distribution revealed by phalloidin fluorescence analysis.

Indirect immunofluorescence with fluorescent antibodies against involucrin and β catenin, both differentiation and adhesion markers, revealed an increase in involucrin and β catenin expression, supporting that exposure to electromagnetic field carries keratinocytes to an upper differentiation level.

Such study confirmed our previous observation and support the hypothesis that 7 Hz electromagnetic field, may modify cell biochemistry and interfere in differentiation and cellular adhesion of normal keratinocytes.

Temperature Induced Changes of Spontaneous Photon Emission from Human Hands

M. Cifra[1,2], **E. P. A. van Wijk**[3], **and R. van Wijk**[3,4]

[1]Dept. of Electromagnetic Field, Czech Technical University, Prague, Czech Republic
[2]Institute of Photonics and Electronics
Academy of Sciences of the Czech Republic, Prague, Czech Republic
[3]International Institute of Biophysics, Neuss, Germany
[4]Faculty of Biology, Utrecht University, Utrecht, The Netherlands

Abstract— Ultra weak spontaneous optical photon emission (UPE) arises from living organisms. It is also called biophoton emission. It can be considered as part from the broad spectrum of endogenous electromagnetic field generated by biological systems above thermal level ranging from few Hz to the optical part of the spectrum.

Although UPE may arise from relatively simple chemical reactions in biological systems, it is also supposed to play a role in long-range organization and intra- and extra cellular communication in living systems.

Exploration of the parameters of the UPE from the experiments and measurements gives a clearer view on the generation mechanisms, behavior and purpose of the UPE.

We present a report on the effect of external temperature changes on UPE intensity from human hands.

A low-noise single photon counting photomultiplier system located in a dark room was used to measure the photon emission from hands of 3 subjects in a total of 10 experimental sessions. The experimental protocol was as follows.

After dark accommodation of the subject, a baseline recording of both photon emission and skin temperature of the dominating hand was made. Then, the palm of this hand was placed on an ice block for 15 minutes and photon emission and temperature were measured from the dorsum of the hand. At the end, the ice block was removed, and both photon emission and temperature were recorded during the next 15 min, in which the hand temperature recovered, at least partially. A thermocouple device was utilized to record the changes in skin temperature.

Although there is some variability between subjects, results show a direct correlation between UPE intensity and skin temperature. The different types of explanation, which depend on both thermoregulatory principles and the origin of UPE, will be discussed.

A Microdosimetry Analysis from ELF up to MW Range for the Study of the Bioelectromagnetic Interaction

Caterina Merla, **Micaela Liberti**, **Francesca Apollonio**, **and Guglielmo D'Inzeo**
ICEmB @ Department of Electronic Engineering, "Sapienza" University of Rome, Italy

Abstract—

Introduction: In the study of the bioelectromagnetic problem, the main aim is to relate macroscopic biological effects to an electromagnetic (EM) exposure. The knowledge of the field distribution down to the single cell and sub-cellular level, known as microdosimetry, represents a fundamental issue. In fact, only such knowledge allows elucidating in a quantitative and rigorous way the chain of complex and specific events, starting at molecular level, which leads to the observed macroscopic effects [1]. Therefore an EM analysis on a single cell from DC up to microwave range has been carried out, both through an analytical quasi-static solution on a multilayered sphere, and through a numerical quasi-static solution (Comsol Multiphysics^{TM}) on different geometries (as ellipsoids, erythrocytes and neuronal cells). In this paper we present a deep analysis of the role of each parameter involved looking at cell size, shape, compartment thicknesses, and dielectric model.

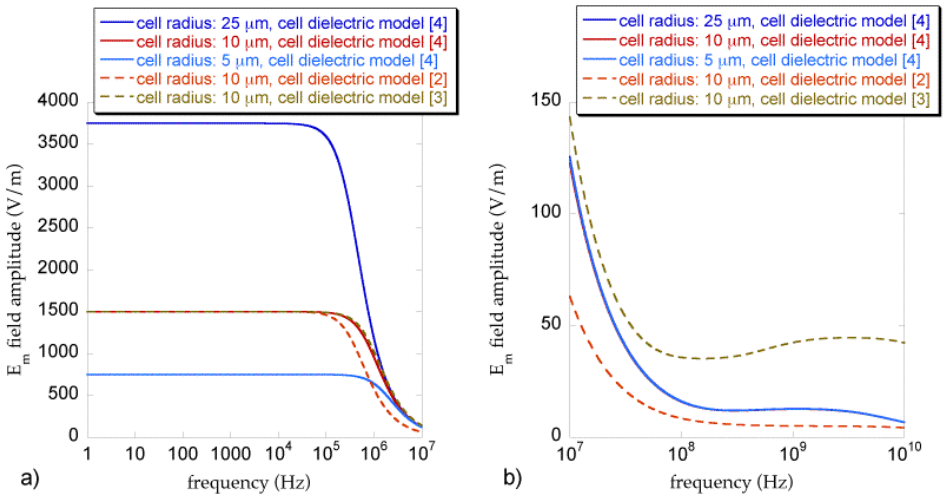

Figure 1: Membrane field amplitude obtained for three different radius and three different dielectric models in the low frequency. (a) And high frequency, (b) Range of analysis.

Results: In the low frequency range (DC ÷ 10 MHz) the cell dimensions (5, 10 and 25 μm for the radius of a spherical cell) mainly affect the membrane E field values, as from Fig. 1(a) where higher electric field within cell membrane has been obtained for a 25 μm radius. In the same frequency range the cell dielectric model adopted [2–4] has no influence on the E field determination (Fig. 1(a)). At high frequencies (from 10 MHz up to tens of GHz) otherwise the cell dielectric model [2–4] gains a fundamental role for the E field values, as presented in Fig. 1(b) where a variability of about 80% on the membrane E field values as a function of different dielectric models is shown. No variations of the field values are associated to different cell radius (Fig. 1(b)). The E field for different membrane thicknesses (5 and 10 nm) has also been calculated in the whole frequency spectrum, no differences have been observed until the thickness of the different biological compartments is maintained into a plausible morphologically range. In fact a decrease of the field has been evidenced for unrealistic membrane thickness greater than 100 nm. Moreover, membrane field values obtained in the three-layered (standard model) and five-layered (taking into account bound water) cell configurations have been compared. Similar field values have been observed in the two cases evidencing that the additional presence of the bound water layers (with different thicknesses of 0.5, 1 and 5 nm) does not alter the membrane field distribution.

Conclusion: These microdosimetric results can help the comprehension of the relationship between biological effects and the EM exposure at single cell level. Moreover these studies are also interesting in a bio-medical context, supporting the design of the EM applicators (i.e., electrodes) and the optimization of the applied field waveforms.

REFERENCES

1. Apollonio, F., et al., *IEEE Trans. Microwave Theory and Tech.*, Vol. 48, 2082–2093, 2000.
2. Liu, L. M. and S. F. Cleary, *Bioelectromagnetics*, Vol. 16, 160–171, 1995.
3. Kotnik, T. and D. Miklavcic, *Bioelectromagnetics*, Vol. 21, 385–394, 2000.
4. Merla, C., et al., *Proc. 16th International Zurich Symposium on Electromagnetic Compatibility, EMC*, Zurich, 2005.

Detection and Identifications of Biological and Artificial Materials Characterized by Their Optical Rotation and Circular Dichroism Based on Mueller Matrix Measurements

Ezekiel Bahar
Electrical Engineering Department, University of Nebraska-Lincoln, USA

Abstract— The characteristics solutions for waves propagation in biological materials, (such as human tissue and threat agents) that possess chiral properties, are the right and left circularly polarized waves with different propagation coefficients. As a result the electric field of a linearly polarized wave rotates as it propagates through biological materials. This property, which is associated with differences in the phase velocities, is referred to as Optical Rotation. The property associated with differences in the attenuation accounts for the ellipticity of the wave polarization and it is referred to as Circular Dichroism. Measurements of these properties of Optically Active materials are used to identify these biological materials. At normal incidence and grazing incidence the Optical Activity of the material does not impact on the elements of Mueller matrix since the cross polarized reflection and transmission coefficients vanishes. However at oblique incidence, the Optical Activity of the materials impacts in the eight quasi off diagonal elements of the Mueller matrix and to first order they are proportional to the chiral parameter. Since the chiral parameter for biological materials is significantly smaller than the wavelength, the eight quasi diagonal elements of the Mueller matrix are insensitive to the optical activity of the material, to the first order of the chiral parameter.

Based on the analytical expressions for the cross polarized reflection and transmission coefficients, a road map for the identification of the biological materials is presented. It includes the selection of the pair of Mueller matrix elements most suitable for this purpose as well as the optimum excitation of the optically active materials considering the electromagnetic parameters of the host media.

Artificial chiral materials characterized by negative or positive refractive incidences have novel engineering applications.

Author Index